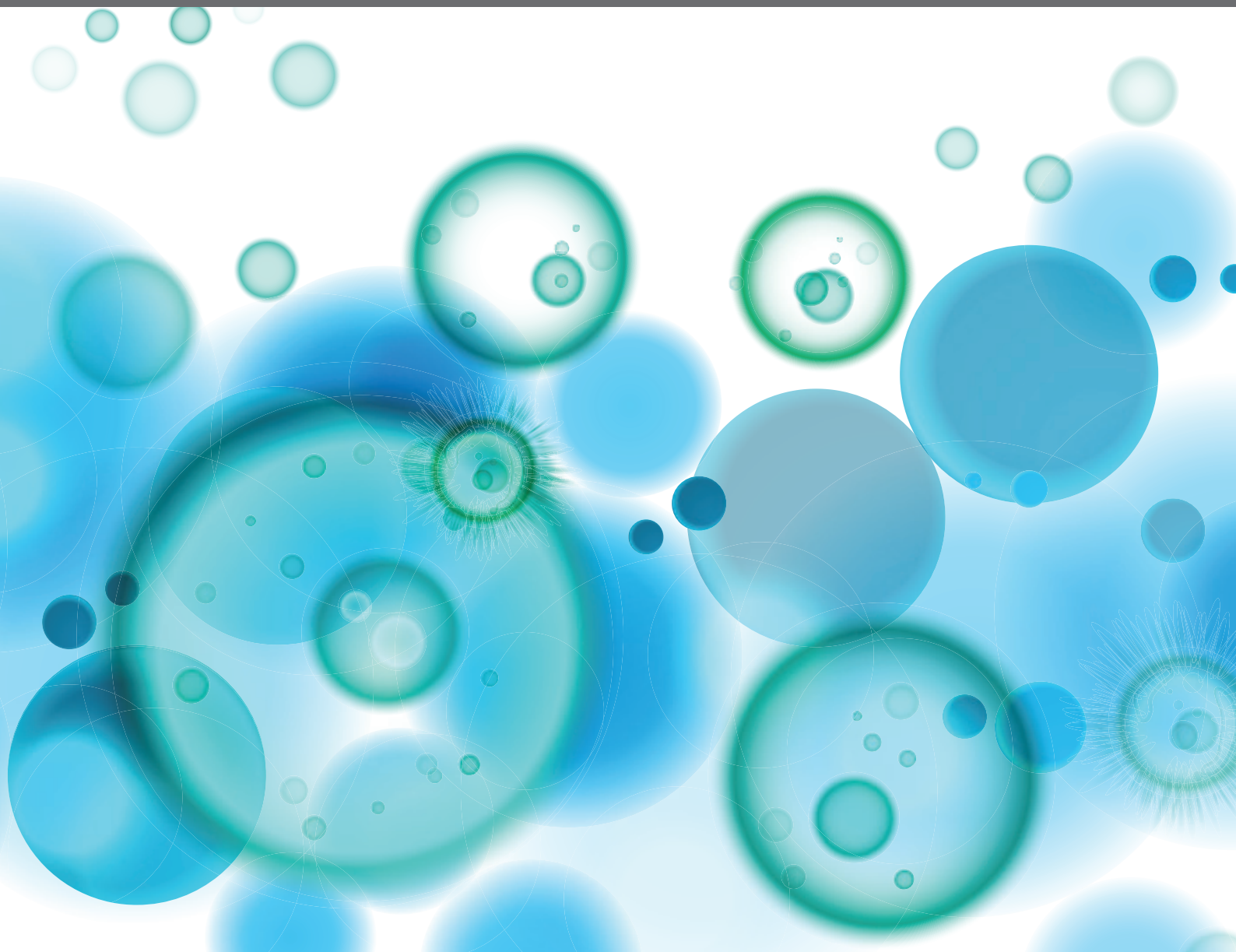


NEGATIVE REGULATORS OF INNATE IMMUNITY AND THEIR ROLE IN HOST RESPONSES TO INJURY AND INFECTION, 2nd Edition

EDITED BY: Maciej Lech and Shrikant R. Mulay
PUBLISHED IN: Frontiers in Immunology





frontiers

Frontiers eBook Copyright Statement

The copyright in the text of individual articles in this eBook is the property of their respective authors or their respective institutions or funders. The copyright in graphics and images within each article may be subject to copyright of other parties. In both cases this is subject to a license granted to Frontiers.

The compilation of articles constituting this eBook is the property of Frontiers.

Each article within this eBook, and the eBook itself, are published under the most recent version of the Creative Commons CC-BY licence.

The version current at the date of publication of this eBook is CC-BY 4.0. If the CC-BY licence is updated, the licence granted by Frontiers is automatically updated to the new version.

When exercising any right under the CC-BY licence, Frontiers must be attributed as the original publisher of the article or eBook, as applicable.

Authors have the responsibility of ensuring that any graphics or other materials which are the property of others may be included in the CC-BY licence, but this should be checked before relying on the CC-BY licence to reproduce those materials. Any copyright notices relating to those materials must be complied with.

Copyright and source acknowledgement notices may not be removed and must be displayed in any copy, derivative work or partial copy which includes the elements in question.

All copyright, and all rights therein, are protected by national and international copyright laws. The above represents a summary only. For further information please read Frontiers' Conditions for Website Use and Copyright Statement, and the applicable CC-BY licence.

ISSN 1664-8714

ISBN 978-2-8325-5204-9

DOI 10.3389/978-2-8325-5204-9

About Frontiers

Frontiers is more than just an open-access publisher of scholarly articles: it is a pioneering approach to the world of academia, radically improving the way scholarly research is managed. The grand vision of Frontiers is a world where all people have an equal opportunity to seek, share and generate knowledge. Frontiers provides immediate and permanent online open access to all its publications, but this alone is not enough to realize our grand goals.

Frontiers Journal Series

The Frontiers Journal Series is a multi-tier and interdisciplinary set of open-access, online journals, promising a paradigm shift from the current review, selection and dissemination processes in academic publishing. All Frontiers journals are driven by researchers for researchers; therefore, they constitute a service to the scholarly community. At the same time, the Frontiers Journal Series operates on a revolutionary invention, the tiered publishing system, initially addressing specific communities of scholars, and gradually climbing up to broader public understanding, thus serving the interests of the lay society, too.

Dedication to Quality

Each Frontiers article is a landmark of the highest quality, thanks to genuinely collaborative interactions between authors and review editors, who include some of the world's best academicians. Research must be certified by peers before entering a stream of knowledge that may eventually reach the public - and shape society; therefore, Frontiers only applies the most rigorous and unbiased reviews.

Frontiers revolutionizes research publishing by freely delivering the most outstanding research, evaluated with no bias from both the academic and social point of view. By applying the most advanced information technologies, Frontiers is catapulting scholarly publishing into a new generation.

What are Frontiers Research Topics?

Frontiers Research Topics are very popular trademarks of the Frontiers Journals Series: they are collections of at least ten articles, all centered on a particular subject. With their unique mix of varied contributions from Original Research to Review Articles, Frontiers Research Topics unify the most influential researchers, the latest key findings and historical advances in a hot research area! Find out more on how to host your own Frontiers Research Topic or contribute to one as an author by contacting the Frontiers Editorial Office: frontiersin.org/about/contact

NEGATIVE REGULATORS OF INNATE IMMUNITY AND THEIR ROLE IN HOST RESPONSES TO INJURY AND INFECTION, 2nd Edition

Topic Editors:

Maciej Lech, LMU Munich University Hospital, Germany

Shrikant R. Mulay, Central Drug Research Institute (CSIR), India

Publisher's note: This is a 2nd edition due to an article retraction.

Citation: Lech, M., Mulay, S. R., eds. (2024). Negative Regulators of Innate Immunity and Their Role in Host Responses to Injury and Infection, 2nd Edition. Lausanne: Frontiers Media SA. doi: 10.3389/978-2-8325-5204-9

Table of Contents

- 05 Editorial: Negative Regulators of Innate Immunity and Their Role in Host Responses to Injury and Infection**
Shrikant R. Mulay and Maciej Lech
- 08 Case Report: Successful Response to Intravenous Immunoglobulin and Steroid Pulses in a Renal Transplant Recipient With Severe Covid-19 Disease and Associated Acute Allograft Failure**
Pedro Rosa-Guerrero, Antonio Trujillo-Aguilera, Juan Molina, Ana Navas, Cristina López-Martín, Aurora Jurado, Alberto Rodríguez-Benot and Álvaro Torres-De-Rueda
- 15 Complement C4, Infections, and Autoimmune Diseases**
Hongbin Wang and Mengyao Liu
- 30 Neutrophil Extracellular Traps Exacerbate Secondary Injury via Promoting Neuroinflammation and Blood–Spinal Cord Barrier Disruption in Spinal Cord Injury**
Zhou Feng, Lingxia Min, Liang Liang, Beike Chen, Hui Chen, Yi Zhou, Weiwei Deng, Hongliang Liu and Jingming Hou
- 42 NLRC5 Deficiency Deregulates Hepatic Inflammatory Response but Does Not Aggravate Carbon Tetrachloride-Induced Liver Fibrosis**
Akouavi Julite I. Quenum, Akhil Shukla, Fjolla Rexhepi, Maryse Cloutier, Amit Ghosh, Thomas A. Kufer, Sheela Ramanathan and Subburaj Ilangumaran
- 55 Nlr1-Regulated Defense and Metabolic Responses to Aspergillus fumigatus Are Morphotype and Cell Type Specific**
Bridget Kastelberg, Tariq Ayubi, Nuria Tubau-Juni, Andrew Leber, Raquel Hontecillas, Josep Bassaganya-Riera and Shiv D. Kale
- 70 Metallothionein 3-Zinc Axis Suppresses Caspase-11 Inflammasome Activation and Impairs Antibacterial Immunity**
Debabrata Chowdhury, Jason C. Gardner, Abhijit Satpati, Suba Nookala, Santhosh Mukundan, Aleksey Porollo, Julio A. Landero Figueroa and Kavitha Subramanian Vignesh
- 94 Plasmodium berghei-Released Factor, PbTIP, Modulates the Host Innate Immune Responses**
Inderjeet Kalia, Rajesh Anand, Afshana Quadiri, Shreya Bhattacharya, Bijayalaxmi Sahoo and Agam Prasad Singh
- 111 Identification of a Novel Mutation in TNFAIP3 in a Family With Poly-Autoimmunity**
Marianna Nicoletta Rossi, Silvia Federici, Andrea Uva, Chiara Passarelli, Camilla Celani, Ivan Caiello, Valentina Matteo, Stefano Petrocchi, Eva Piano Mortari, Fabrizio De Benedetti, Giusi Prencipe and Antonella Insalaco

120 Negative Regulation of the IL-1 System by IL-1R2 and IL-1R8: Relevance in Pathophysiology and Disease

Domenico Supino, Luna Minute, Andrea Mariancini, Federica Riva, Elena Magrini and Cecilia Garlanda

138 PHLDA1 Suppresses TLR4-Triggered Proinflammatory Cytokine Production by Interaction With Tollip

Hui Peng, Juping Wang, Xuhong Song, Jiangni Huang, Haoming Hua, Fanlu Wang, Ziyun Xu, Jing Ma, Jie Gao, Jing Zhao, Anna Nong, Dongyang Huang and Bin Liang



Editorial: Negative Regulators of Innate Immunity and Their Role in Host Responses to Injury and Infection

Shrikant R. Mulay¹ and Maciej Lech^{2*}

¹ Pharmacology Division, Council of Scientific and Industrial Research (CSIR)-Central Drug Research Institute, Lucknow, India,

² LMU Klinikum, Medizinische Klinik und Poliklinik IV, Ludwig-Maximilians-Universität München, München, Germany

Keywords: homeostasis, allostasis, inflammation, infection, injury

Editorial on the Research Topic

Negative Regulators of Innate Immunity and their Role in Host Responses to Injury and Infection

INTRODUCTION

Every cell type can sense danger and at the same time display a plethora of different mechanisms that allow it to maintain or restore homeostasis. It is not surprising that immune cells that in their function per se are sensitive to danger signals play a predominant role in keeping the immune balance. Cells use various extra- and intracellular factors to regulate inflammation making it a central component of the system that orchestrates the immune responses since a tightly regulated immune system provides stability through constancy. Efficient and adequate regulation of immune responses requires various modulatory mechanisms that trigger allostasis, defined as the ability to accomplish stability through change. Defective immune responses frequently lead to severe (1) autoinflammatory or (2) autoimmune reactions that may both be systemic or tissue-specific. Autoinflammatory disorders are characterized by self-directed inflammatory responses and acute inflammation as a consequence of the unregulated innate immune system. Autoimmune diseases result from the loss of immune tolerance against self-antigens. They are characterized by the existence of autoreactive T and B cells and are often described as triggered by the impairment of adaptive immunity alone. In both cases, a lack of negative regulation of immune responses might be responsible for the onset of inflammatory disease. Conserved regulatory mechanisms modulate the immune response and bridge the gap between innate and adaptive immunity as they can terminate first inflammatory responses and initiate subsequent development of adaptive immunity. The uncontrolled influx and activation of the immune cells associated with the production of pro-inflammatory cytokines might, in consequence, lead to a prolonged presentation of intracellular antigens, and the development of autoantibodies against particular cell compartments are produced are often the cause of severe diseases. Despite a significant number of experimental studies the complex mechanisms of immune dysregulation are not well understood. This Frontiers Research Topic represents a collection of articles that focused on innate and adaptive mechanisms that contribute to local homeostasis and tissue-specific responses to the infection, injury, and inflammation.

OPEN ACCESS

Edited and reviewed by:

Francesca Granucci,
University of Milano-Bicocca, Italy

*Correspondence:

Maciej Lech
Maciej.Lech@med.uni-muenchen.de

Specialty section:

This article was submitted to
Molecular Innate Immunity,
a section of the journal
Frontiers in Immunology

Received: 08 March 2022

Accepted: 08 March 2022

Published: 28 March 2022

Citation:

Mulay SR and Lech M (2022) Editorial:
Negative Regulators of Innate
Immunity and Their Role in Host
Responses to Injury and Infection.
Front. Immunol. 13:891919.
doi: 10.3389/fimmu.2022.891919

HOMEOSTASIS, ALLOSTASIS, AND THE KEY ROLE OF NEGATIVE REGULATORS OF INFLAMMATION

Wang and Liu reviewed the role of a key molecule in the complement system C4 in infections and autoimmune diseases. The authors gave a comprehensive overview of the regulation of complement C4 activation and presented the immunomodulatory role of C4 linking microbial infections and autoimmune disorders. Supino et al. focused on the negative regulation of the IL-1 system. The IL-1 family of cytokines and receptors is associated with a broad spectrum of immunological and inflammatory responses. They discussed the hallmarks of two key regulatory receptors of the IL-1 system, IL-1R2, the first decoy receptor identified, and IL-1R8, a pleiotropic regulator of different IL-1 family members and co-receptor for IL-37, the anti-inflammatory member of the IL-1 family.

Nucleotide-binding oligomerization domain (NOD)-like receptors (NLRs) are a specialized group of cytosolic pattern recognition receptors (PRRs) that represent a crucial component of the host innate immune system. They include NLRA, NLRB, NLRC, NLRP, and NLRX superfamilies and are responsible for monitoring the intracellular microenvironment, mediating inflammation, and pathogen clearance (1). Quenum et al. demonstrated the importance of nucleotide-binding leucine-rich repeat-containing receptor (NLR) family protein-5 (NLRC5) in liver homeostasis. The authors proved that NLRC5 regulated hepatic inflammatory response upon injury but did not affect liver fibrosis. Moreover, NLRC5-deficient livers showed increased phosphorylation of the NF- κ B subunit p65 increased expression of F4/80 (Adgre1), a marker of tissue-resident macrophages. Further supporting the role of NLRs in homeostasis and inflammation, Kastelberg et al. focused on Nlrp1 as a critical regulator of immune signaling in pulmonary fungal infection using the clinically relevant fungus *Aspergillus fumigatus*. They showed that loss of Nlrp1 resulted in a decreased ability of host cells to process *A. fumigatus* conidia in a cell type-specific manner and limited ability to generate superoxide and/or generic reactive oxygen species during specific responses to fungal PAMPs. They proved that during fungal pulmonary infections Nlrp1 is responsible for the regulation of cell metabolism by affecting the glycolysis process. Besides NLRs, innate immune cells are equipped with a set of other cytosolic sensors so-called inflammasomes, which are responsible for the detection of pathogens and danger signals. Chowdhury et al. dedicated their experimental undertake to a mechanism that restricts non-canonical inflammasome activation. They elegantly demonstrated that the caspase-11 inflammasome in mouse and human macrophages (M ϕ) is negatively controlled by the zinc (Zn²⁺) regulating protein, metallothionein 3 (MT3). MT3 enhanced intracellular Zn²⁺ resulting in inhibition of the TRIF-IRF3-STAT1 pathway and restricting of caspase-11 effector function. Other regulatory mechanisms involved in controlling inflammation and immunity to pathogens refer to immune responses against viruses and parasites. Peng et al. identified pleckstrin homology-like domain, family A, member

1 (PHLDA1) as a negative regulator of LPS-induced proinflammatory response. This study evidenced that PHLDA1 suppresses TLR4/MyD88 signaling pathway using the interaction with Toll Interacting Protein (TOLLIP).

Lee et al. investigated the expression of ephrinA1/ephA2 in normal mucosa and inflamed sinonasal mucosa of chronic rhinosinusitis (CRS) patients. The authors described a novel role of ephrinA1/ephA2 signaling in antiviral innate immune response in the sinonasal epithelium. They proved that rhinovirus (RV) infection or poly (I:C) treatment induced chemokine secretion which was attenuated by ephA2 inhibitor. The production of antiviral mediators including type I and type III IFNs enhanced upon blocking ephA2 suggesting its role as a negative regulator of antiviral immunity. Kalia et al. considered an alternative approach to highlight the importance of immune modulation in fighting the disease. The authors investigated the protein PbTIP from *Plasmodium berghei*. PbTIP is a homolog of the human T cell immunomodulatory protein (TIP) that suppresses host immune responses. The shed PbTIP is a perfect example of a molecular mimic that modulates macrophage responses during the parasitic infection increasing the survival of the parasite.

Feng et al. investigated the mechanism by which neutrophil extracellular traps (NETs) affect spinal cord injury (SCI). NETs regulation is critical for neutrophils to exert their immunological activity. They showed that neutrophils promote neuroinflammation, whereas successful restriction of inflammation ease secondary damage, thus hindering scar formation and improving recovery after SCI. Both inhibitions of NETs formation by peptidylarginine deiminase 4 (PAD4) inhibitor and disruption of NETs by DNase 1 showed positive effects.

TARGETING INFLAMMATION TO REGAIN HOMEOSTASIS

Further articles in this Research Topic presented the anti-inflammatory approach as target for pharmacological intervention. Rosa-Guerrero et al. described the successful response to high-dose intravenous immunoglobulin (IVIG) combined with steroid pulses in the case of Covid-19 pneumonia in a single-kidney transplanted patient. The authors described the clinical efficacy and anti-inflammatory and immunosuppressive potential of steroids and contributed to the special issue with an interesting example of treatment of inflammatory disease.

Complementary to the above-mentioned work, Rossi et al. illustrate an example of new phenotypic abnormality in four consanguineous patients with a mutation in affecting TNFAIP3 (A20), a central negative regulator of NF- κ B signaling pathway. They identified a novel heterozygous frameshift mutation (p.His577Alafs*95) that introduced a premature stop codon in the zinc finger domain of A20/TNFAIP3, leading to putative haploinsufficiency of the protein. The authors linked the mutation to a predominantly autoimmune phenotype with recurrent fever episodes. The mutation leads to decreased

levels of A20 in blood cells and higher levels of NF- κ B phosphorylation, as well as increased production of the proinflammatory cytokines IL-1 β , IL-6, TNF- α , and hyperactivation of the IFN γ signaling pathway.

SUMMARY AND PERSPECTIVE

Various studies challenge the role of homeostasis and mechanisms of immune control in health and disease, as well as their substantial potential as a target in clinical applications.

REFERENCE

1. Chen G, Shaw MH, Kim YG, Nunez G. NOD-Like Receptors: Role in Innate Immunity and Inflammatory Disease. *Annu Rev Pathol* (2009) 4:365–98. doi: 10.1146/annurev.pathol.4.110807.092239

Conflict of Interest: SM is now an employee for AstraZeneca (Biopharmaceuticals R&D, Cambridge, UK).

The remaining authors declare that the research was conducted in the absence of any commercial or financial relationships that could be construed as a potential conflict of interest.

Allostatic load and loss of immune homeostasis might aggravate the tissue damage and affect the tissue repair during tissue injury. A better understanding of molecules that modulate immune processes could lead to the development of innovative therapies in the future.

AUTHOR CONTRIBUTIONS

SM and ML wrote the article. Both authors contributed to the article and approved the submitted version.

Publisher's Note: All claims expressed in this article are solely those of the authors and do not necessarily represent those of their affiliated organizations, or those of the publisher, the editors and the reviewers. Any product that may be evaluated in this article, or claim that may be made by its manufacturer, is not guaranteed or endorsed by the publisher.

Copyright © 2022 Mulay and Lech. This is an open-access article distributed under the terms of the Creative Commons Attribution License (CC BY). The use, distribution or reproduction in other forums is permitted, provided the original author(s) and the copyright owner(s) are credited and that the original publication in this journal is cited, in accordance with accepted academic practice. No use, distribution or reproduction is permitted which does not comply with these terms.



OPEN ACCESS

Edited by:

Shrikant R. Mulay,
Central Drug Research Institute
(CSIR), India

Reviewed by:

Trinath Jamma,
Birla Institute of Technology
and Science, India
Chack-Yung Yu,
The Ohio State University,
United States

***Correspondence:**

Álvaro Torres-De-Rueda
atorresnefro@yahoo.es;
jalvaro.torres.sspa@
juntadeandalucia.es

[†]These authors have contributed
equally to this work and share
first authorship

Specialty section:

This article was submitted to
Molecular Innate Immunity,
a section of the journal
Frontiers in Immunology

Received: 22 February 2021

Accepted: 20 April 2021

Published: 11 May 2021

Citation:

Rosa-Guerrero P, Trujillo-Aguilera A,
Molina J, Navas A, López-Martín C,
Jurado A, Rodríguez-Benot A
and Torres-De-Rueda Á
(2021) Case Report: Successful
Response to Intravenous
Immunoglobulin and Steroid Pulses
in a Renal Transplant Recipient
With Severe Covid-19 Disease and
Associated Acute Allograft Failure.
Front. Immunol. 12:671013.
doi: 10.3389/fimmu.2021.671013

Case Report: Successful Response to Intravenous Immunoglobulin and Steroid Pulses in a Renal Transplant Recipient With Severe Covid-19 Disease and Associated Acute Allograft Failure

Pedro Rosa-Guerrero^{1,2†}, Antonio Trujillo-Aguilera^{1,3†}, Juan Molina^{1,3}, Ana Navas^{1,3}, Cristina López-Martín⁴, Aurora Jurado^{1,3}, Alberto Rodríguez-Benot^{1,2} and Álvaro Torres-De-Rueda^{1,2,5*}

¹ Maimonides Biomedical Research Institute of Cordoba (IMIBIC), Reina Sofía University Hospital, University of Cordoba, Cordoba, Spain, ² Department of Nephrology, Reina Sofía University Hospital, Cordoba, Spain, ³ Department of Immunology and Allergy, Reina Sofía University Hospital, Cordoba, Spain, ⁴ Department of Intensive Care, Reina Sofía University Hospital, Cordoba, Spain, ⁵ Asociación Medicina e Investigación (A.M.I.), Cordoba, Spain

The impact of Covid-19 pneumonia caused by SARS-CoV-2 on transplanted populations under chronic immunosuppression seems to be greater than in normal population. Clinical management of the disease, particularly in those patients worsening after a cytokine storm, with or without allograft impairment and using available therapeutic approaches in the absence of specific drugs to fight against the virus, involves a major challenge for physicians. We herein provide evidence of the usefulness of high-dose intravenous immunoglobulin (IVIG) combined with steroid pulses to successfully treat a case of Covid-19 pneumonia in a single-kidney transplanted patient with mechanical ventilation and hemodialysis requirements in the setting of a cytokine storm. A rapid decrease in the serum level of inflammatory cytokines, particularly IL-6, IL-8, TNF- α , MCP-1 and IL-10, as well as of acute-phase reactants such as ferritin, D-dimer and C-reactive protein was observed after the IVIG infusion and methylprednisolone bolus administration with a parallel clinical improvement and progressive allograft function recovery, allowing the patient's final discharge 40 days after the treatment onset. The immunomodulatory effect of IVIG together with the anti-inflammatory and immunosuppressive potential of steroids could be an alternative strategy to treat severe cases of Covid-19 pneumonia associated with an uncontrolled inflammatory response in transplanted populations.

Keywords: Covid-19, SARS-CoV-2, kidney transplantation, intravenous immunoglobulin, steroids, cytokine storm, case report

INTRODUCTION

Although the majority of Covid-19 disease clinical manifestations range from asymptomatic to mild respiratory infections, an important number of patients undergo symptomatic or severe pneumonia with acute respiratory distress syndrome (ARDS) and concomitant life-threatening complications (1). Solid-organ transplanted recipients comprise a particularly vulnerable group given their increased susceptibility to infections as a consequence of chronic immunosuppression and coexisting conditions (2). In such a population, frontline adopted strategies for managing the infection, beside conventional care practice, are mainly based on the adjustment of baseline immunosuppressive regimens with the purpose of enhancing the host-response against the virus (3). Unfortunately, the time-course of Covid-19 disease is known to be highly erratic and initial therapeutic efforts are not often enough to avoid a poor progression in susceptible individuals. Importantly, successful treatments for patients undergoing a critical situation secondary to infection are urgently needed.

One of the most relevant findings amongst patients with more severe forms of the disease is the presence of high levels of circulating cytokines and subsequent acute-phase reactants (4), suggesting that an innate-immunological dysregulation characterized by a massive cytokine release (so-called *cytokine-storm*) may be associated with a worsening of the clinical syndrome involving multiple organ failure and higher rates of fatal outcomes. Accordingly, a reasonable therapeutic approach should be addressed to limit the collateral host-tissues damage promoted by the hyperinflammatory state, beyond the use of drugs specifically targeting the virus or advanced life-support measures.

CASE DESCRIPTION

During the course of the first wave of the pandemic, a 54-year-old man with end-stage renal disease of unknown etiology, recipient of a renal allograft in 2015 under combined maintenance immunosuppression with prednisone, tacrolimus (TAC) and everolimus (EVE), baseline serum creatinine of 1.2 mg/dL and estimated glomerular filtration rate of 67 mL/min, was admitted to Emergency Room on 19th March with a 5-day history of fever and dyspnea unresponsive to paracetamol and levofloxacin intake (**Figure 1**). On examination, chest-X-ray revealed multiple bilateral patchy ground-glass opacities. The nasopharyngeal SARS-CoV-2 RNA-PCR was positive and the patient was diagnosed with Covid-19 associated bilateral pneumonia. His past medical history was remarkable for left-native kidney radical nephrectomy in 2006 after a focal clear-cell adenocarcinoma diagnosis; obstructive sleep apnea syndrome managed with continuous positive airway pressure and long-

standing hypertension controlled with doxazosin, enalapril and manidipine.

On admission, piperacillin-tazobactam 4/0.5 g/8h plus azithromycin 250 mg od, and hydroxychloroquine 200 mg od were started, whilst EVE was discontinued and TAC dose was lowered. On day +4 after admission, lopinavir/ritonavir 400/100 mg/12h was added. On day +6, the patient evolved into a progressive respiratory failure, requiring mechanical ventilation in the intensive care unit (ICU). At that point, all immunosuppression was discontinued, only maintaining 6-methylprednisolone (6MP) 40 mg IV/24h. A total of 4 doses of lopinavir/ritonavir and 1 dose of β -Interferon (250 μ g on day +7) were given. In the first 48h at ICU, the patient's general condition worsened, presenting oliguric acute kidney failure with an active urine sediment, which was treated with continuous renal replacement therapy (CRRT). The global clinical course linked to radiologic deterioration and biochemical findings (ferritin > 16500 ng/mL; D-dimer 12255 ng/mL; c-reactive protein 145.6 mg/L; lactate dehydrogenase 590 U/L; IL-6 234.7 pg/mL; **Figures 2, 3**) became highly suggestive of an unbalanced systemic inflammatory response in the context of a *cytokine-storm*. In this setting, a three-day consecutive course of high-dose intravenous immunoglobulin (IVIG) 65 g/day (an accumulated 2.2 g/kg) and 125 mg/day of 6MP were administered (days +9, +10 and +11 since admission; **Figure 1**).

This cycle was followed by a rapid and significant improvement in the pro-inflammatory profile (ferritin 1949.1 ng/mL; D-dimer 1597 ng/mL; c-reactive protein 29.9 mg/L; lactate dehydrogenase 525 U/L; IL-6 4.1 pg/mL; **Figures 2, 3**) with hemodynamic stabilization and discontinuation of CRRT six days after IVIG plus corticosteroid pulses completion (having received a total course of 9 days of CRRT). The patient continued under alternative-day renal replacement therapy with hemodialysis for another 13 days and was extubated after 23 days on mechanical ventilation, remaining up-to a total of 30 days in the ICU. Diuresis and renal function progressively recovered, being restarted on oral prednisone and TAC on +36 day after admission, followed by EVE one week later. SARS-CoV-2 RNA-PCR became negative on day +41. The patient was discharged after 49 hospital days (**Figure 1**) with a serum creatinine of 2.3 mg/dL, 1200 mg/L proteinuria and resumed regular outpatient clinic reviews. The anti-HLA antibody panel determined at the time of discharge remained negative, suggesting the absence of humoral alloresponse. Current general condition remains satisfactory without clinical findings of allograft impairment (last follow-up serum creatinine was 1.65 mg/dL) or respiratory sequels.

DISCUSSION

Herein we present a case of a SARS-CoV-2 infected single-kidney transplanted patient with ARDS and acute kidney-allograft failure under a depleted immunosuppressant regimen with the hallmark of associated cytokine-storm, who was treated with high doses of IVIG and steroid pulses in an attempt mainly to reduce the excessive inflammatory response

Abbreviations: ARDS, acute respiratory distress syndrome; CRRT, continuous renal replacement therapy; EVE, everolimus; ICU, intensive care unit; IVIG, intravenous immunoglobulin; TAC, tacrolimus; 6MP, 6-methylprednisolone.

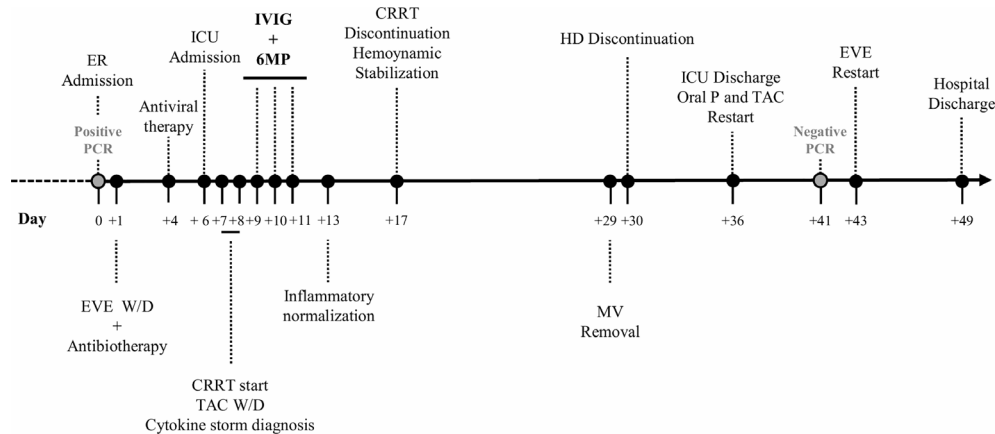


FIGURE 1 | Timeline of hospitalization. CRRT, continuous renal replacement therapy; EVE, everolimus; ER, emergency room; HD, hemodialysis; ICU, intensive care unit; IVIG, intravenous immunoglobulin; MV, mechanical ventilation; oral P, oral prednisone; TAC, tacrolimus; W/D, withdrawal; 6MP, 6-methylprednisolone.

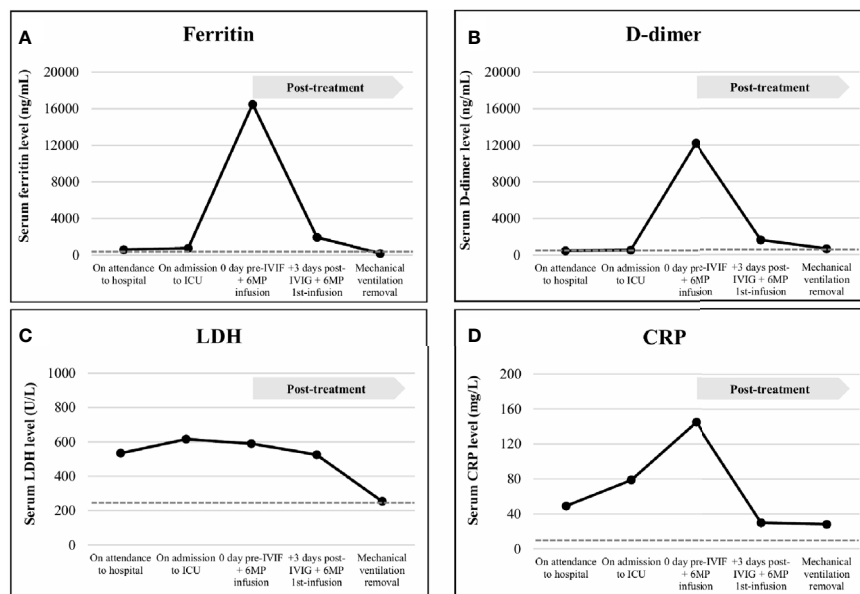


FIGURE 2 | Acute-phase reactants levels, including ferritin (A), D-dimer (B), lactate dehydrogenase (LDH, C) and C-reactive protein (CRP, D), analyzed in serum samples of the patient on attendance to hospital date, on admission to Intensive Care Unit (ICU) date, on the day of the intravenous immunoglobulin (IVIG) plus 6-methylprednisolone (6MP) infusion, early (3 days) after the IVIG plus 6MP infusion and on mechanical ventilation removal. Normal range laboratory values are displayed in broken lines. The treatment administration is indicated in a grey box. Ferritin was assessed from serum samples by sandwich immunoassay using direct chemiluminescence technology (Atellica IM Ferritin -Fer-, ref. 10995568) on an Atellica® IM Analyzer (Siemens Healthineers Diagnostics Inc.). D-dimer was determined from citrated plasma by automated latex enhanced immunoassay (ref. 0020008500, Instrumentation Laboratory, Werfen) on an ACL TOP 700 LAS (Werfen). LDH was quantified from serum samples according to the proportional increase in the absorbance at 340/310 nm of NADH (Atellica CH Lactate Dehydrogenase L-P -LDPL-, ref. 11097594) on an Atellica® CH Analyzer (Siemens Healthineers Diagnostics Inc.). CRP was measured from serum samples by latex enhanced immunoturbidimetry assay (Atellica CH Wide Range C-Reactive Protein -wrCRP-, ref. 11097645) on an Atellica® CH Analyzer (Siemens Healthineers Diagnostics Inc.). All the automatic assays were performed according to manufacturer instructions.

but also to prevent eventual rejection damage, supported by their well-known immunomodulatory and immunosuppressive effects. The compassionate use of tocilizumab, an IL-6 receptor antagonist potentially able to mitigate the cytokine release

syndrome induced by SARS-CoV-2 (5), although being considered, was finally dismissed due to a reasonable clinical suspicion of concomitant bacterial infection, which nevertheless was later discarded. Interestingly, a dramatic

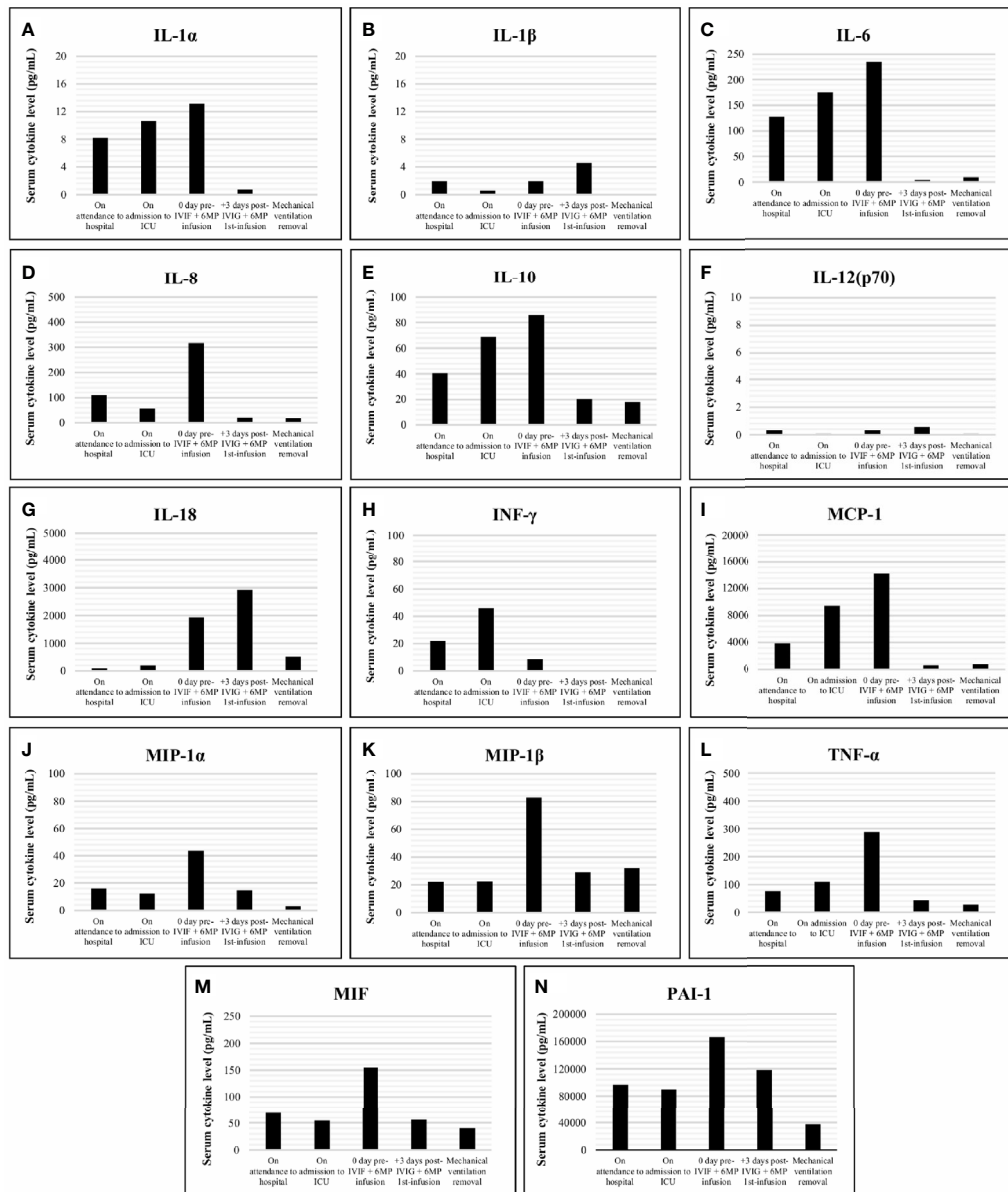


FIGURE 3 | Cytokine levels (pg/mL) including IL-1 α , IL-1 β , IL-6, IL-8, IL-10, IL-12(p70), IL-18, INF- γ , MCP-1, MIP-1 α , MIP-1 β , TNF- α , MIF and PAI-1 (A–N), analyzed in serum samples of the patient obtained on attendance to hospital date, on admission to Intensive Care Unit (ICU) date, on the day of the intravenous immunoglobulin (IVIG) plus 6-methylprednisolone (6MP) infusion, early (3 days) after the IVIG plus 6MP infusion and on mechanical ventilation removal. Cytokine measurements were retrospectively performed on -80 °C preserved samples, except for IL-6 (prospectively analyzed), using customized Milliplex[®] MAP kits (Panel A: IL-1 α , IL-1 β , IL-6, IL-8, IL-10, IL-12(p70), IL-18, INF- γ , MCP-1, MIP-1 α , MIP-1 β and TNF- α , ref. HCYTA-60K; Panel B: MIF and PAI-1, ref. HSP1MAG-63K; Merck-Millipore) according to manufacturer instructions on a Luminex platform with xPONENT vs. 4.2 as acquisition and analysis software.

clearance of the inflammatory cytokine network, as well as acute-phase reactants, was observed in a short time-frame once the treatment was administered as depicted in **Figures 2, 3** respectively, with a parallel clinical improvement of the patient, including progressive hemodynamic stabilization and gradual recovery of renal-allograft function with neither evidence of clinical rejection nor development of donor-specific anti-HLA antibodies.

Beyond the cytopathic organ injury caused by SARS-CoV-2 targeting ACE-2 expressing host-tissues (6), the clinical severity was in this case exacerbated by the extensive inflammatory damage induced by an anomalous late release of cytokines in response to the unresolved infection (7). A progressive rise since admission of IL-6, IL-8, IL-10, and TNF- α as well as other key mediators (e.g., MCP-1, PAI-I or MIF) largely related with the development of sepsis (8, 9), was found. High levels of circulating

inflammatory cytokines exert a pernicious effect on endothelium, causing the disruption of its function as a barrier with the subsequent fluid leakage to intercellular spaces and the imbalance of homeostatic equilibrium into a procoagulant and antifibrinolytic state, resulting in microvascular thrombosis and organ ischemia. Moreover, this hyperinflammatory environment promotes oxidative stress damage through an increased production of reactive oxygen species (10). Altogether, these systemic alterations could drive the progression of the infection towards ARDS and acute renal-allograft failure, major complications associated with poorer outcome in Covid-19 disease (11, 12).

Inflammatory profile normalization, before an irreversible multi-organ impairment, is expected to be critical for recovery. A reduction of plasma IL-6 level has been already associated with favorable prognosis during the septic insult, whereas the persistent overproduction of IL-10, which should act as a key negative regulator controlling the magnitude of the response, paradoxically seems to be the main fatality predictor by inducing a robust immunosuppressant state (8). From this perspective, the positive response here described was most probably linked to the rapid decrease of both pro- and anti-inflammatory cytokines mediated by the treatment. Despite the global decrease, some particular behaviors were detected, as in the case of the pro-inflammatory IL-18, which transiently increased after IVIG plus 6MP infusion (**Figure 3G**). This finding could partially be explained by the lack of negative feedback as a result of the circulating INF- γ low level at that point (**Figure 3H**), suppressing the expression of the high affinity IL-18 binding protein, a physiological IL-18 inhibitor (13). In turn, the reduction of INF- γ , whose main source of production are activated T- and NK-cells, during the first 48h in ICU before treatment, could be secondary to the functional exhaustion of these lymphocytes (14) after a prolonged unsuccessful response against SARS-CoV-2, being this fact followed by or overlapped the disease progression.

It has been suggested that the mechanism by which IVIG leads to immunomodulation depends on both the immunoglobulin Fc and F(ab')₂ regions. On one hand, high-doses of IVIG can saturate Fc γ -receptors performing an inhibitory role on innate-immune cells, decreasing their migration capacity and responsiveness to soluble mediators and also can sequester circulating complement molecules (15). On the other hand, it can neutralize inflammatory cytokines and apoptosis-inducing molecules by F(ab') regions (15). The anti-inflammatory and immunosuppressive effects of glucocorticoids are mostly mediated through their receptor, an almost ubiquitously expressed transcription factor which, upon ligand binding, translocates towards the nucleus leading major changes in inflammatory gene expression programs, typically due to its physical interaction with specific DNA sequences as well as with transcription modulators such as NF- κ B or AP-1. Particularly, on monocytes-macrophages, whose dysfunction plays a pivotal role in the physiopathology of severe inflammation, corticoids inhibit or down-regulate the expression of several pro-inflammatory cytokines, limiting an overwhelming response (16).

Regarding adaptive cellular immunity, IVIG and corticoids may alter the balance of T-cell subpopulations to favor an anti-inflammatory response by promoting the expansion and enhancement of CD4⁺FoxP3⁺ regulatory T-cells and by inhibiting the proliferation and activity of effector T-helper 1 cells (17, 18).

Further than being one of the mainstays to prevent rejection since the inception of solid-organ transplantation, corticoids have been widely used in managing inflammatory and autoimmune diseases, even showing clinical benefits to treat disseminated intravascular coagulation, sepsis or ARDS (19). In turn, IVIG is implemented in a broad spectrum of disorders, including some involving an uncontrolled immune response such as Kawasaki disease or toxic shock syndrome, which share similarities with severe Covid-19 forms (20). Despite both drugs could offer a rationale for its use in Covid-19 disease evolving towards a severe systemic inflammatory response, only the use of corticoids has been recommended when supplemental oxygen was required (21). In contrast, there is not an agreement about the feasible usefulness of IVIG to improve clinical outcomes in SARS-CoV-2 infected patients, notwithstanding a few publications support its effectiveness alone or combined with corticoids in more severe cases (22–24).

In conclusion, together with previous reports, the study of this case evinces that IVIG at immunomodulatory doses in combination with steroids could be an alternative successful strategy to control the cytokine-storm triggered by SARS-CoV-2 infection, improving the course of the disease and offering protection against immunological rejection in transplanted patients off their maintenance immunosuppression regimes. Since this is a single-case, more studies evaluating the effectiveness of this therapy would be necessary to extrapolate it to similar scenarios. Future studies designed to explore whether the administration of IVIG-6MP at early stages of the disease may provide a prophylactic effect by blocking the Covid-19 progression towards an hyperinflammatory syndrome would merit consideration, especially in view of the current lack of efficient treatments against the virus and the delicate equilibrium within the host immunity status required for both overcoming the infection and avoiding allograft rejection.

PATIENT PERSPECTIVE

Being a renal transplant patient taking immunosuppressive medication, I became very worried for my life when I was notified to have Covid-19 disease, but also for losing my kidney allograft. During my first days at the hospital, I rapidly worsened and was therefore transferred to ICU under artificial breathing. Of that horrible period, I only vaguely remember having nightmares. After regaining consciousness, I started a slow recovery, during which I often felt depressed and anxious, but I finally could leave the hospital off dialysis and with my kidney improving day by day. I am very thankful to the cooperative and multidisciplinary work that experts in different

areas of knowledge performed and the treatment and the personal attention I received, and very especially to my daughter who, being a nurse in training, stayed long days of room isolation looking after me and working towards my recovery.

DATA AVAILABILITY STATEMENT

The data analyzed in this study is subject to the following licenses/restrictions: Patient's clinical record. Requests to access these datasets should be directed to atorresnefro@yahoo.es.

ETHICS STATEMENT

Ethical review and approval was not required for the study on human participants in accordance with the local legislation and institutional requirements. The patients/participants

provided their written informed consent to participate in this study.

AUTHOR CONTRIBUTIONS

PRG, ATR, and CLM participated in the diagnosis and treatment of the patient. PRG and ATA collected clinical data. JM, AN, and ATA conducted cytokine measurements. PRG, ATA, JM, AN, and ATR wrote the draft. AJ and ARB reviewed the final version and made significant conceptual contributions to the manuscript. All authors contributed to the article and approved the submitted version.

FUNDING

The publishing of this work was financed by Asociación Medicina e Investigación (A.M.I.).

REFERENCES

- Wang D, Hu B, Hu C, Zhu F, Liu X, Zhang J, et al. Clinical Characteristics of 138 Hospitalized Patients With 2019 Novel Coronavirus-Infected Pneumonia in Wuhan, China. *JAMA* (2020) 323:1061–9. doi: 10.1001/jama.2020.1585
- Alberici F, Delbarba E, Manenti C, Econimo L, Valerio F, Pola A, et al. A Single Center Observational Study of the Clinical Characteristics and Short-Term Outcome of 20 Kidney Transplant Patients Admitted for SARS-CoV2 Pneumonia. *Kidney Int* (2020) 97:1083–8. doi: 10.1016/j.kint.2020.04.002
- Kronbichler A, Gauckler P, Windpessl M, Il Shin J, Jha V, Rovin BH, et al. COVID-19: Implications for Immunosuppression in Kidney Disease and Transplantation. *Nat Rev Nephrol* (2020) 16:365–7. doi: 10.1038/s41581-020-0305-6
- Huang C, Wang Y, Li X, Ren L, Zhao J, Hu Y, et al. Clinical Features of Patients Infected With 2019 Novel Coronavirus in Wuhan, China. *Lancet* (2020) 395:497–506. doi: 10.1016/S0140-6736(20)30183-5
- Perez-Saez MJ, Blasco M, Redondo-Pachon D, Ventura-Aguar P, Bada-Bosch T, Perez-Flores I, et al. Use of Tocilizumab in Kidney Transplant Recipients With COVID-19. *Am J Transplant* (2020) 20:3182–90. doi: 10.1111/ajt.16192
- Zou X, Chen K, Zou J, Han P, Hao J, Han Z. Single-Cell RNA-seq Data Analysis on the Receptor ACE2 Expression Reveals the Potential Risk of Different Human Organs Vulnerable to 2019-nCoV Infection. *Front Med* (2020) 14:185–92. doi: 10.1007/s11684-020-0754-0
- Tay MZ, Poh CM, Renia L, MacAry PA, Ng LFP. The Trinity of COVID-19: Immunity, Inflammation and Intervention. *Nat Rev Immunol* (2020) 20:363–74. doi: 10.1038/s41577-020-03111-8
- Chaudhry H, Zhou J, Zhong Y, Ali MM, McGuire F, Nagarkatti PS, et al. Role of Cytokines as a Double-Edged Sword in Sepsis. *In Vivo* (2013) 27:669–84.
- Schulte W, Bernhagen J, Bucala R. Cytokines in Sepsis: Potent Immunoregulators and Potential Therapeutic Targets—An Updated View. *Mediators Inflamm* (2013) 2013:165974. doi: 10.1155/2013/165974
- Ince C, Mayeux PR, Nguyen T, Gomez H, Kellum JA, Ospina-Tascon GA, et al. The Endothelium in Sepsis. *Shock* (2016) 45:259–70. doi: 10.1097/SHK.0000000000000473
- Hirsch JS, Ng JH, Ross DW, Sharma P, Shah HH, Barnett RL, et al. Acute Kidney Injury in Patients Hospitalized With COVID-19. *Kidney Int* (2020) 98:209–18. doi: 10.1016/j.kint.2020.05.006
- Robbins-Juarez SY, Qian L, King KL, Stevens JS, Husain SA, Radhakrishnan J, et al. Outcomes for Patients With COVID-19 and Acute Kidney Injury: A Systematic Review and Meta-Analysis. *Kidney Int Rep* (2020) 5:1149–60. doi: 10.1016/j.ekir.2020.06.013
- Yasuda K, Nakanishi K, Tsutsui H. Interleukin-18 in Health and Disease. *Int J Mol Sci* (2019) 20:649. doi: 10.3390/ijms20030649
- Zheng M, Gao Y, Wang G, Song G, Liu S, Sun D, et al. Functional Exhaustion of Antiviral Lymphocytes in COVID-19 Patients. *Cell Mol Immunol* (2020) 17:533–5. doi: 10.1038/s41423-020-0402-2
- Nagelkerke SQ, Kuijpers TW. Immunomodulation by IVIg and the Role of Fc-Gamma Receptors: Classic Mechanisms of Action After All? *Front Immunol* (2014) 5:674. doi: 10.3389/fimmu.2014.00674
- Ehrchen JM, Roth J, Barczyk-Kahlert K. More Than Suppression: Glucocorticoid Action on Monocytes and Macrophages. *Front Immunol* (2019) 10:2028. doi: 10.3389/fimmu.2019.02028
- Kaufman GN, Massoud AH, Dembele M, Yona M, Piccirillo CA, Mazer BD. Induction of Regulatory T Cells by Intravenous Immunoglobulin: A Bridge Between Adaptive and Innate Immunity. *Front Immunol* (2015) 6:469. doi: 10.3389/fimmu.2015.00469
- Taves MD, Ashwell JD. Glucocorticoids in T Cell Development, Differentiation and Function. *Nat Rev Immunol* (2021) 21:233–43. doi: 10.1038/s41577-020-00464-0
- Villar J, Ferrando C, Martinez D, Ambros A, Munoz T, Soler JA, et al. Dexamethasone Treatment for the Acute Respiratory Distress Syndrome: A Multicentre, Randomised Controlled Trial. *Lancet Respir Med* (2020) 8:267–76. doi: 10.1016/S2213-2600(19)30417-5
- Diorio C, Henrickson SE, Vella LA, McNerney KO, Chase J, Burudpakdee C, et al. Multisystem Inflammatory Syndrome in Children and COVID-19 are Distinct Presentations of SARS-CoV-2. *J Clin Invest* (2020) 130:5967–75. doi: 10.1172/JCI140970
- Group RC, Horby P, Lim WS, Emberson JR, Mafham M, Bell JL, et al. Dexamethasone in Hospitalized Patients With Covid-19 - Preliminary Report. *N Engl J Med* (2020) 384:693–704. doi: 10.1056/NEJMoa2021436
- Cao W, Liu X, Bai T, Fan H, Hong K, Song H, et al. High-Dose Intravenous Immunoglobulin as a Therapeutic Option for Deteriorating Patients With Coronavirus Disease 2019. *Open Forum Infect Dis* (2020) 7:ofaa102. doi: 10.1093/ofid/ofaa102
- Mohtadi N, Ghayssouri A, Shirazi S, Sara A, Shafiee E, Bastani E, et al. Recovery of Severely Ill COVID-19 Patients by Intravenous Immunoglobulin (IVIg) Treatment: A Case Series. *Virology* (2020) 548:1–5. doi: 10.1016/j.virol.2020.05.006
- Riphagen S, Gomez X, Gonzalez-Martinez C, Wilkinson N, Theocharis P. Hyperinflammatory Shock in Children During COVID-19 Pandemic. *Lancet* (2020) 395:1607–8. doi: 10.1016/S0140-6736(20)31094-1

Conflict of Interest: The authors declare that the research was conducted in the absence of any commercial or financial relationships that could be construed as a potential conflict of interest.

Copyright © 2021 Rosa-Guerrero, Trujillo-Aguilera, Molina, Navas, López-Martín, Jurado, Rodríguez-Benot and Torres-De-Rueda. This is an open-access article

distributed under the terms of the Creative Commons Attribution License (CC BY). The use, distribution or reproduction in other forums is permitted, provided the original author(s) and the copyright owner(s) are credited and that the original publication in this journal is cited, in accordance with accepted academic practice. No use, distribution or reproduction is permitted which does not comply with these terms.



Complement C4, Infections, and Autoimmune Diseases

Hongbin Wang^{1,2,3*} and Mengyao Liu¹

¹ Master Program of Pharmaceutical Sciences College of Graduate Studies, California Northstate University, Elk Grove, CA, United States, ² Department of Pharmaceutical and Biomedical Sciences College of Pharmacy, California Northstate University, Elk Grove, CA, United States, ³ Department of Basic Science College of Medicine, California Northstate University, Elk Grove, CA, United States

OPEN ACCESS

Edited by:

Maciej Lech,
LMU Munich University Hospital,
Germany

Reviewed by:

Chack-Yung Yu,
The Ohio State University,
United States
Marja-Liisa Lokki,
University of Helsinki, Finland

*Correspondence:

Hongbin Wang
hongbin.wang@cnsu.edu

Specialty section:

This article was submitted to
Molecular Innate Immunity,
a section of the journal
Frontiers in Immunology

Received: 14 April 2021

Accepted: 21 June 2021

Published: 14 July 2021

Citation:

Wang H and Liu M (2021)
Complement C4, Infections,
and Autoimmune Diseases.
Front. Immunol. 12:694928.
doi: 10.3389/fimmu.2021.694928

Complement C4, a key molecule in the complement system that is one of chief constituents of innate immunity for immediate recognition and elimination of invading microbes, plays an essential role for the functions of both classical (CP) and lectin (LP) complement pathways. Complement C4 is the most polymorphic protein in complement system. A plethora of research data demonstrated that individuals with C4 deficiency are prone to microbial infections and autoimmune disorders. In this review, we will discuss the diversity of complement C4 proteins and its genetic structures. In addition, the current development of the regulation of complement C4 activation and its activation derivatives will be reviewed. Moreover, the review will provide the updates on the molecule interactions of complement C4 under the circumstances of bacterial and viral infections, as well as autoimmune diseases. Lastly, more evidence will be presented to support the paradigm that links microbial infections and autoimmune disorders under the condition of the deficiency of complement C4. We provide such an updated overview that would shed light on current research of complement C4. The newly identified targets of molecular interaction will not only lead to novel hypotheses on the study of complement C4 but also assist to propose new strategies for targeting microbial infections, as well as autoimmune disorders.

Keywords: complement, C4, C4a, C4d, infections, autoimmune diseases

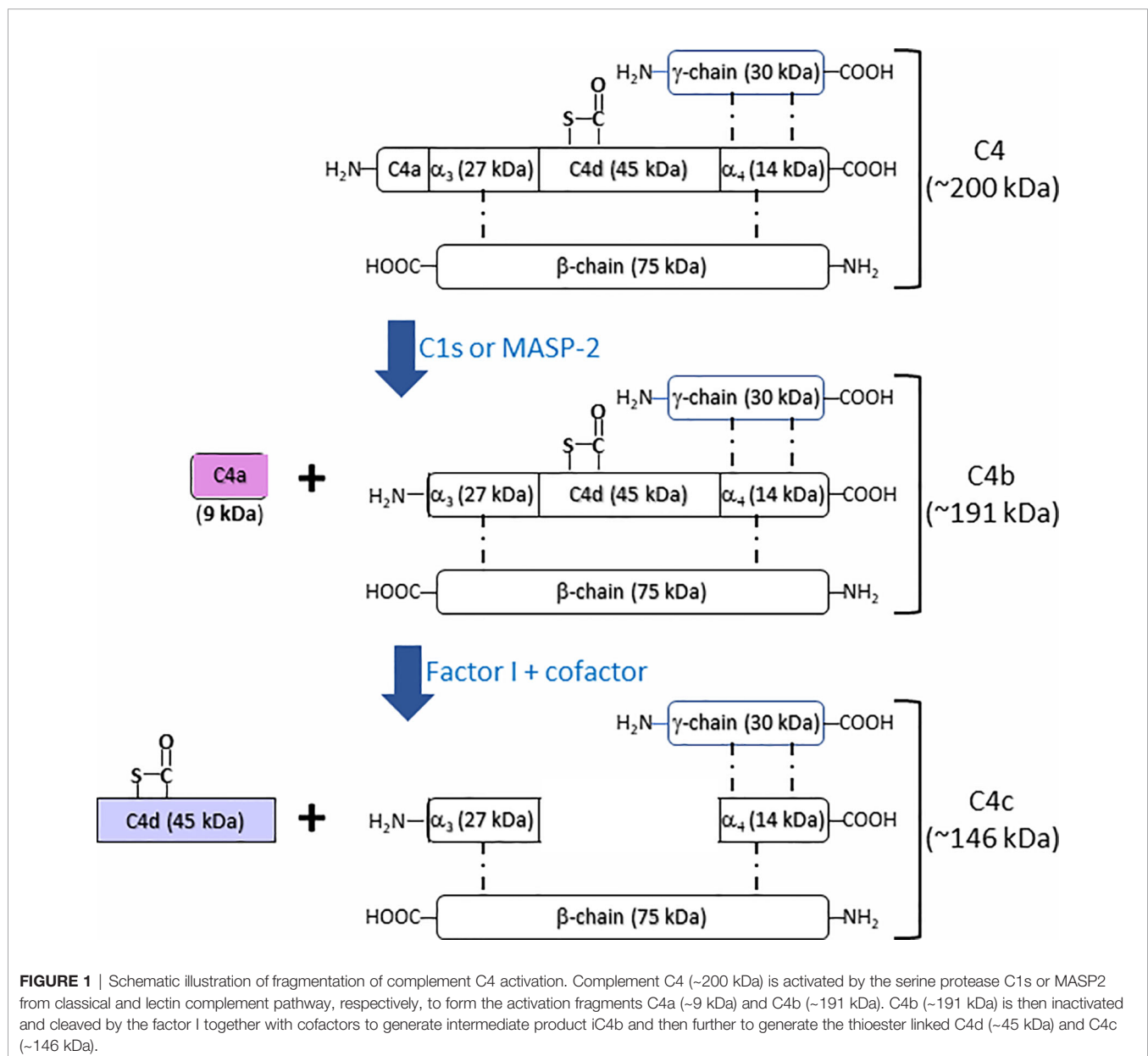
INTRODUCTION

Complement system plays a pivotal role in human innate immunity defending microbial infections, eliminating foreign pathogens, and maintaining tissue homeostasis. The activation of the complement system induces the increased production of cytokines, chemokines, and other innate defense molecules. In addition, complement activation fragments (e.g., anaphylatoxin C3a and C5a) significantly increased the recognition of antigens by follicular dendritic cells and B cells and induced the humoral adaptive immune response and production of antibodies and reactive T cells. Moreover, complement system functions as an effector on the clearance of soluble immune complexes and cell debris, which otherwise could induce an immune response against auto antigens and potentially trigger autoimmunity (1–3). Deficiency or dysfunction of the complement system could cause infections in adult patients (4) and also predispose individuals

to autoimmune diseases, such as rheumatoid arthritis (RA), systemic sclerosis, and systemic lupus erythematosus (SLE) (5).

Complement component C4 (Mw = ~200 kDa), an essential component in complement system, plays an indispensable role in the activation of classical and lectin complement cascades. It is a disulfide-bonded three-chain glycoprotein, consisting of an α -chain (95 kDa), a β -chain (75 kDa), and a γ -chain (30 kDa) (Figure 1) (6, 7). In the process of the activation of classical complement pathway, C1q from C1 complex [C1q-(C1r)₂-(C1s)₂] recognizes antigen-antibody immune complexes or certain membrane-bound structures, e.g. C-reactive protein (CRP) or lipopolysaccharides (LPS), resulting in the transition from C1s zymogen to an active C1s repositions, which would be able to interact with sulfotyrosine residues on C4 (8, 9). Similar to the

activation of classical complement pathway, the lectin complement pathway is activated by complex carbohydrate structures and mediated *via* recognition molecules as mannan binding lectin (MBL), ficolins, and collectin 10/11, leading to the activation of mannan-associated serine protease-2 (MASP-2), which relies heavily on its active sites, two complement control protein (CCP) domains, and the serine protease (SP) domain for the efficient binding and cleavage of C4 (10–12). As shown in Figure 1, the activated C1s and MASP-2 from classical and lectin pathways respectively cleaves the amino terminal part of the α -chain at a single site of complement C4 to generate C4a fragment peptide (9 kDa) and C4b (195 kDa) (13). C4b binds to target surface *via* its reactive thioester, which can be inactivated to an intermediate form iC4b by proteolytic cleavage by the serine



protease factor I together with co-factor CD46 (14, 15). iC4b is further cleaved to thioester linked C4d (45 kDa) and soluble C4c (146 kDa), which can be used as a biomarker for complement activation from classical and lectin pathways. Both classical and lectin pathways lead to further activation of C2 to generate C3 convertase C4b2a, which will activate C3 to generate C3a and C3b. C3 convertase binds to C3b to form C5 convertase that will cleave C5 to generate C5a and C5b. C5b binds to C6, C7, C8, and C9 to form membrane attack complexes (MAC) C5b-9 that are formed on the surface of pathogen cell membranes. Comparing crystal and solution structures of C4b with its paralog C3b, their conformations are shown surprisingly conserved (16). Further study revealed that the C3 convertases (C4b2a vs. C3bBb) from the classical/lectin and alternative pathways are also strikingly similar, which is in agreement with their identical functions in the cleavage of the downstream complement proteins C3 and C5 (17).

The complete or partial deficiency of complement C4 results in the increased risk of infection and autoimmune diseases. A plethora of studies demonstrated that complement C4 plays an essential role in defending microbial infection. It is also well established that the complete or partial deficiency of complement C4 is associated with the increased susceptibility to infections (18–23). In addition, the deficiency of complement C4 could lead to various autoimmune diseases (24–33). The reduced concentrations of C4 protein and the reduced serum complement activity occur with the active disease in SLE (25, 34), as well as in infections (35).

In this review, we will look into the updated studies on the role of complement C4 in infectious diseases and autoimmune disorders. In this way, we aim to elucidate and update the functions of complement C4 in infectious diseases and autoimmune disorders, trying to highlight the important role of complement C4 as a potential intervention target for the management of those disorders.

DIVERSITY OF COMPLEMENT C4 GENES AND PROTEINS

The human complement C4 gene (*C4A* and *C4B* genes) locus is located in the highly polymorphic major histocompatibility complex (MHC) class III gene region on chromosome 6, which could be a short form (C4S, 14.6 kb) or a long form (C4L, 21 kb), depending on the absence or the presence of the 6.36 kb endogenous retroviral sequence HERV-K(C4) in intron 9 of human C4 genes. Three quarters of C4 genes harbor the 6.36-kb endogenous retrovirus HERV-K (C4) (36). Each human C4 gene has 41 exons, which codes for a 5.4 kb transcript. C4 gene lies within a unit of four consecutive genes known as an RCCX module, which stands for the serine/threonine nuclear protein kinase RP, Complement component C4, steroid 21-hydroxylase CYP21, and extracellular matrix protein tenascin TNX (*RP-C4-CYP21-TNX*) (RCCX) (37–44). An elevated level of genomic copy number variations (CNV) was shown in MHC region III, supposedly to present immunologic diversity (45). The duplication of these four genes occurs as a module in the class III region of a haplotype for the MHC. The gene copy number

(GCN) of *C4A* genes varies from 0 to 5 and GCN of *C4B* genes varies from 0 to 4. The highest total C4 gene dosage reported is 7 (46). It took a long time for scientists to make it clear on the genetic diversity of human complement C4. The initial model was proposed as a single locus of codominant alleles for *C4A* and *C4B*, and later two-locus or *C4A-C4B* models dominated the complement field for about two decades. Extensive molecular and genetic studies have now provided a clear definition of genetic structures that are responsible for C4 isotypes (*C4A* and *C4B*) protein expression. Complement C4 protein exists as two isotypes, *C4A* and *C4B*, which are encoded by the C4 genes (*C4A* or *C4B* gene), and share >99% sequence identities. Five nucleotide variations located in exon 26 confer to four isotype-specific amino acid substitutions at positions 1101–1106 (PCPVLD for *C4A* and LSPVIH for *C4B*) and the major structural and functional differences between the *C4A* and *C4B* isotypes (47). *C4A* is named after its acidity and migrates faster in agarose gel electrophoresis as compared to *C4B* that is basic and migrates slower (47–51). In addition, *C4A* and *C4B* are highly polymorphic with more than 40 different alleles, gene duplications, and “null alleles” (52–55). *C4A* is generally associated with the Rodgers (Rg) blood group antigens and is more reactive with immune complex or the targets containing free amino groups, whereas *C4B* is generally associated with the Chido (Ch) blood group antigens and is more affinity to hydroxyl groups (56). It was revealed that *C4A* has a longer half-life in plasma as compared to *C4B*, suggesting a role of *C4A* in the clearance of the immune complex and a role of *C4B* for membrane attack complex formation and the defense against bacterial pathogens (57). The individuals with long C4 genes (C4L) have lower serum levels of complement C4 as compared with short C4 genes (C4S) (36). C4 gene copy number variations (CNV) are correlated to the serum levels of complement C4 protein and low C4 GCNs predisposes individuals with various disease susceptibility (58). Low copy numbers or the deficiency of C4 genes was reported to be one of the strongest risk factors associated with several immune disorders, such as SLE, chronic central serous chorioretinopathy, Behçet’s disease, and Vogt-koyanagi-Harada disease (25, 58–63). It was also reported that the deficiency of either *C4A* or *C4B* has been associated with the increased susceptibility of infections (18, 64, 65). Interestingly, it was reported by Bay et al. that low C4 gene copy numbers (< 4 total copies of C4 genes) are associated with superior graft survival in patients transplanted with a deceased donor kidney (66). A comprehensive review on the variations of C4 genetic structures and proteins was presented by Blanchong CA et al. (36).

Other causes than genetic variations also can affect the expression or the function of complement C4. Early studies by Goldman et al. in cultured guinea pig peritoneal cells demonstrated that complement component can be regulated by short-term treatment *in vivo* or *in vitro* with monospecific antibody to individual complement components can have long-term effects on the production of those components. Antibody treatment induced specific suppression of C4 in peritoneal cell monolayers. Further studies revealed that long-term C4 suppression is actively maintained by a soluble suppressor

factor (FsC4) (67–70). Most of those experiments were carried out *in vitro* cellular models from guinea pig. It is still unclear whether this observation can be replicated in human.

Dysregulation of classic and lectin complement pathways that complement C4 participates in can lead to complement-mediated autoimmune diseases. C4 nephritic factor (C4Nef), first described by Halbwachs et al. in 1980, is an autoantibody to C3 convertase (C4b2a). C4Nef can prolong the half-life of C3 convertase by stabilizing C4b2a and protects C4b2a against decay dissociation by C4 binding protein (C4BP). Multiple clinical studies demonstrated that C4Nef was associated with post-infectious acute glomerulonephritis, systemic lupus erythematosus, chronic proliferative glomerulonephritis and hypocomplementemic membranoproliferative glomerulonephritis (MPGN), and meningococcal disease (71–76).

A recent study by Battin et al. using *in vitro* binding screening demonstrated that Neuropilin-1 (NRP1) acts as a receptor for complement split products, such as C4d, C3d, and iC3b. NRP1 is a highly conserved type 1 transmembrane protein that is involved in the tumorigenesis, the development of cardiovascular, and nervous systems through the interaction with vascular endothelial growth factor (VEGF) and semaphoring 3A (Sema3A). NRP1 is also expressed in murine immune cells and serves as a marker for mouse T_{reg} cells. Interestingly, NRP1 was demonstrated to bind C4d in a concentration-dependent and saturable manner. These data demonstrated NRP1 functions as a receptor for C4d that is covalently bound to target surfaces during complement activation, suggesting that NRP1 might be involved in regulation of the process of infections and autoimmune disorders by targeting the split product from classical or lectin complement pathway (77).

REGULATION OF THE ACTIVATION OF COMPLEMENT C4

Complement C4 in Microbial Infection

Complement C4 is involved in the activation of both classical and lectin complement pathways. The classical pathway of complement system is crucial for anti-microbial defense through anti-pathogen antibody, which recruits C1 complex and initiates a cleavage cascade involving C4, C2, C3, and C5 and accomplishing microbial clearance. In addition, lectin complement pathway is also involved in the anti-microbial defense. Recent study revealed that loss of classical pathway results in rapidly progressing septicemia and impaired macrophage activation, suggesting that the classical pathway is the dominant pathway for activation of the complement system during complement innate immunity to *S. pneumoniae*. In response to microbial pathogens, lectin pathway is activated as an innate immune response through direct binding to bacterial surface sugar components. In contrast, the classical pathway was an effector of adaptive immune response through activation of antibody–antigen complexes on bacterial surfaces and plays a vital role partially targeted by the binding of natural IgM to bacteria (21).

An early research work by Schifferli et al. demonstrated that C4A isoform of complement C4 was more efficient than C4B isoform in the processing of immune complexes in humans. In contrast, hemolysis by C4B isoform was more efficient than by C4A isoform, suggesting that both C4 isoforms are complementary (78). A recent study by Liesmaa et al. demonstrated that homozygous C4A deficiency in patients was associated with the increased prevalence of lymphomas, celiac disease, and autoimmune disease SLE. In the same study, homozygous C4B deficiency in patients was documented to be linked with the drug intolerance and various post-infectious symptoms. Homozygous C4B deficiency alone is not considered as a significant factor in causing invasive infection (79). From the multiple studies from different laboratories, it seems still debatable in terms of the role of homozygous C4A or C4B deficiency in infection-proneness of an individual (64, 79–82).

Complement interfering protein (CIP) expressed on the surface of group *B. Streptococcus* (GBS) enables cell adhesion and penetration and impedes innate and adaptive immune responses. It was found that CIP was able to interact with the human C4b ligand and to interfere with the classical- and lectin-complement pathways (83). Clinical *Staphylococcus aureus* (*S. aureus*) strains can recruit complement regulator C4-binding protein (C4BP) to *S. aureus* surface to inhibit C4 complement effectors through binding significant amounts of the C4BP from serum. The complex (*S. aureus*-bound C4BP) functions as a cofactor for factor I-mediated C4b cleavage to iC4b and C4d, which was used as a strategy by *S. aureus* for immune evasion (84).

A recent study revealed that gram-negative *Bordetella pertussis* could evade the attack from the human complement system by releasing virulent protein Vag8 of *B. pertussis*. Endogenously secreted and recombinant Vag8 can inhibit complement deposition on the bacterial surface at the level of C4b. The binding of C1 inhibitor (C1-inh) to C1s, C1r, and MASP-2 was disrupted by the association of Vag8 with human C1-inh, which will free active proteases to cleave C2 and C4 away from the bacterial surface, revealing a mechanism of the unique complement evasion strategy of *B. pertussis* (85).

An alkaline protease Alp1p secreted from *A. fumigatus mycelia* can facilitate early immune evasion by deactivating the complement defense in the human host, either by directly cleaving the complement components C3, C4, and C5 or by cleaving them to a form that is further fragmented by other proteases (86, 87).

Some small organisms other than microbials are also involved in the activation or the inhibition of complement systems. For examples, complement activation-inhibition substance from maggot excretions, which splits complement proteins C3 and C4 in a cation-independent manner, could provide a novel treatment for several diseases that result from the activation of complement system (88). ES-62, a protein with an N-linked glycan linked with phosphorylcholine (PCh) produced from parasitic nematodes, was bound to C-reactive protein (CRP) in normal human serum. C1q can capture ES-62-CRP to form a larger complex ES-62-CRP-C1q in serum. Following CRP interaction, ES-62 was able to deplete early complement

component C4 and inhibit classical pathway activation (89). The immune evasion strategies used by those microorganisms aforementioned were summarized in **Table 1**.

It is now becoming apparent that microbial organisms generate various mechanisms to defend the attacks from innate immunity of complement system. Elucidation of those mechanisms will potentially provide strategies to treat microbial infectious diseases, as well as to explore the anti-complement therapeutic interventions.

Complement C4 in Viral Infection

Infection of Hepatitis B

There are extensive studies on the role of complement system in viral infections (93–95). A study by Bugdaci et al. was carried out in 143 patients on the relationship of serum complement C4 levels and chronic hepatitis B (CHB) infection with high transaminase level. Serum C4 levels in patients with CHB with high transaminase level were found significantly lower. In addition, Child score in patients with cirrhosis inversely correlated with C4 levels, suggesting that the levels of complement C4 in plasma significantly correlate with liver biopsy findings and may be a useful indicator of disease activity and/or damage in patients with CHB with high transaminase levels (96).




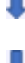







Infection of Hepatitis C

A study by the same research group of Bugdaci et al. on 100 patients with chronic hepatitis C found that complement C4 levels showed significant correlation with alanine aminotransferase but could not find any relationship between serum complement C4 level and fibrosis (97). It remains

unanswered why C4 activity was significantly lower in patients with chronic hepatitis C virus (HCV) infections. One speculation could be due to excessive activation of C4 protein by the activation of classical and lectin complement pathways during HCV infections. Several studies evaluated the expression of C4 in terms of anti-HCV therapeutic response and disease progression in chronic hepatitis C (CHC) patients. The studies revealed that mRNA and protein levels of complement C4 were significantly increased after anti-HCV treatment. A positive alteration in C4 level represents as an independent predictor for treatment response and reflects viral clearance after anti-HCV therapy in CHC patients (98–100). Further studies revealed that hepatitis C virus proteins [HCV core; non-structural (NS) 5A] render transcriptional suppression of the expression of complement C4. Liver biopsy specimens from chronic HCV patients displayed significantly lower levels of complement C4 mRNA as compared to the liver tissue samples from patients with other types of liver disease. HCV core protein was found to decrease the expression of upstream stimulating factor 1 (USF-1), a transcription factor essential for basal C4 expression. In addition, HCV NS5A protein can inhibit the expression of interferon regulatory factor 1 (IRF-1), which is important for IFN γ -induced complement C4 expression. These results highlight the roles of HCV proteins in establishing a chronic infection through the regulation of innate immunity by affecting the expression of complement C4 (90).

Another study by Mawatari et al. demonstrated that HCV NS3/4A protease could cleave the γ -chain of complement C4 in a concentration-dependent manner, suggesting that complement C4 is a novel cellular substrate of HCV NS3/4A protease,

TABLE 1 | The evasion mechanisms of microorganisms from the attack of innate immunity of complement system by targeting complement C4.

Microorganisms	Molecule(s) involved	Expression or Function of C4	Reference
Hepatitis C			
HCV Core protein	USF-1 and C4 mRNA		(90)
HCV NSSA	IRF-1 and C4 mRNA		(90)
HCV NS3/4A	Cleavage of C4 γ -chain		(91)
HCV NS2/NS5B	Disruption of the interaction of MICA/B and NKG2D		(92)
Flavivirus (DENV, WNV, YFV)			
NS1	Cleavage of C4		(93)
<i>B. Streptococcus</i>	Complement interfering protein (CIP)		(83)
<i>S. aureus</i>	C4-binding protein (C4BP)		(84)
<i>B. pertussis</i>	Vag8		(85)
<i>A. fumigatus mycelia</i>	Alkaline protease Alp1p		(86, 87)
Maggot	Inhibition substance of complement activation		(88)
Parasitic nematodes	ES-62		(89)

USF-1, upstream stimulating factor 1; IRF-1, interferon regulatory factor 1; MICA/B, major histocompatibility complex class I-related chains A and B; NKG2D, a transmembrane protein belonging to the NKG2 family of C-type lectin-like receptors.

which reveals new insight into the mechanisms underlying persistent HCV infection (91).

Natural killer (NK) cells have been revealed to contribute to regulating complement synthesis. Studies using co-culture of NK cells (NK3.3) with human hepatoma cells (Huh7.5) expressing HCV core or NS5A protein revealed a significantly increased synthesis of complement C4 and C3 *via* increased specific transcription factors. The regulatory activity is mediated through a direct interaction between the hepatocyte protein major histocompatibility complex class I-related chains A and B (MICA/B) and NKG2D on NK cells. However, when NK cells were co-cultured with Huh7.5 cells infected with cell culture-grown HCV, complement C4 and C3 synthesis was impaired. MICA/B expression in HCV-infected hepatocytes was found to be repressed during co-culture because the HCV-associated expressions of NS2 and NS5B proteins can disable a crucial receptor ligand in infected hepatoma cells, resulting in the disability of infected cells to respond to stimuli from NK cells to up-regulate the expression of complement C3 and C4 (92). This piece of data revealed that HCV synthesizes the proteins that can down-regulate complement C4 expression to evade the attack from complement systems.

Infection With Flaviviridae and Other Viruses

Flavivirus infection, such as West Nile virus (WNV) and Dengue virus (DENV), was restricted through an antibody-independent fashion. N-linked glycans on the structural proteins of flaviviruses was recognized by mannose-binding lectin (MBL), resulting in neutralization and efficient clearance *via* a C3- and C4-dependent mechanism that applied both the canonical and bypass complement lectin activation pathways, which recognizes terminal mannose-containing carbohydrates on the viruses (101). A recent study by Avirutnan et al. demonstrated that flavivirus non-structural (NS)1 protein from dengue virus (DENV), West Nile virus (WNV), and yellow fever virus (YFV) binds to C4 to enhance cleavage of C4 and reduce C4b deposition and C3 convertase (C4bC2a) activity that confers to immune evasion function for the viruses (93).

Interestingly, Puumala (PUUV) hantavirus triggers complement system activation *via* the alternative pathway, which is complement C4-independent, causing the increase of sC5b-9 and the decrease of C3. In the acute stage of PUUV infection, the level of complement activation correlates with disease severity, indicating that complement activation may contribute to the pathogenesis of acute PUUV infection (102).

A recent study by Bottermann et al. revealed a novel antiviral mechanism that is C4-dependent and late-acting complement components-independent. C4 inhibits human adenovirus infection by the deposition of cleaved C4b on capsid, which inhibits its disassembly, preventing endosomal escape and cytosolic access (103). The mechanisms that viruses applied to downregulate the expression or the function of complement C4 are summarized in **Table 1**.

Coronavirus (SARS-CoV1, SARS-CoV-2, and MERS-CoV)

In the midst of pandemic with severe acute respiratory syndrome coronavirus 2 (SARS-CoV-2)/COVID-19. The infection involves

in multiple organs and cause striking elevations in pro-inflammatory cytokines and high risk of thrombosis. Numerous postmortem studies have revealed deposits of complement fragments on interalveolar endothelial cells, high incidence of venous thromboembolism (VTE), and diffused microvascular thrombi with endothelial swelling with a thrombotic microangiopathy (TMA). Preclinical studies with SARS-CoV-1 and MERS-CoV, which have significant homology to SARS-CoV-2, confirm that complement activation is not only linked to virus related organ damage but also is possible causative (104). In mouse models with infection with MERS-CoV or SARS-CoV-1, increased tissue deposition of C5b-9, C3b, and C4d and correlation with severity of injury were observed. Given the fact that deficiency of complement C3, C4, and factor B can protect mice from virus caused by lung injury, classical, lectin, and alternative complement pathways might be involved in mediating SARS-CoV-1 or SARS-CoV-triggered lung injury (105, 106). In the few published post-mortem studies of COVID-19 patients, the increased deposits of C3b, MBL, MASP-2, C4b, and C5b-9 were observed (107, 108). It shows excessive activation of lectin pathway, which is in line with the fact that the spike protein in SARS-CoV-2 is heavily glycosylated with L-fucose and mannose, which provides recognition sites for MBL binding and causes activation of lectin pathway (109). There is no doubt that complement C4 will be hyper-activated in SARS-CoV-2 infection. Is there any relationship between the complement C4 activation and COVID-19 infection caused endothelial swelling and diffused microvascular thrombi that resemble TMA? We would speculate that the hyperactivation of lectin pathway might cause endothelial disruption that might be one of the mechanisms to induce microvascular thrombi in COVID-19 patients. It remains to be evaluated how the lectin pathway and complement C4 activations cause endothelial swelling and diffused microvascular thrombi.

Complement C4 Activation Under Other Pathological Conditions

A recent study by Romano et al. revealed that anti-interleukin-6 receptor monoclonal antibody (Tocilizumab) could dramatically decrease serum level of complement C4 in rheumatoid arthritis patients. Neither circulating immunocomplexes nor any patients ever displaying clinical features of immunocomplex diseases was found. The study concluded that C4 consumption is because of the direct action of the drug rather than immunocomplex-induced complement activation (110).

Histone H3 and H4 can be released from the damaged or lysed cells. One recent study by Qaddoori et al. revealed that histone H3 and H4 strongly bind to C4b region of complement C4, result in significant inhibition of classical and mannose-binding lectin pathways. Histone H3 and H4 did not affect the cleavage of C4 to C4a and C4b, indicating a possible natural feedback mechanism to prevent the excessive injury of host cells by the inhibition of complement activation by histones (111).

A recent study by Vogt et al., using highly specific antibody against a cleavage neoepitope in C4d, identified pigment epithelium-derived factor (PEDF) from synovial fluid of

rheumatoid arthritis patients as an activator of classical complement pathway, which belongs to the serine proteinase inhibitor family. C1q protein can bind PEDF, in particular, head regions of C1q, which is known to interact with other activators of the classical pathway. The results suggested PEDF activated classical complement and might mediate inflammatory processes in joint (112). The interactions of virus, bacteria, and some pathological conditions causing the consumption or inhibition of complement C4 through classic or lectin complement pathway are illustrated in **Figure 2**.

Using computational approach (protein-protein docking and molecular dynamics simulation), a recent study tried to understand Trypsin (Tryp)-mediated C4 activation by comparing with the co-crystallized structure of C4-MASP2. Comparative analysis of C4 alone, C4-Tryp, and C4-MASP2 discovered the impact of Tryp on C4 was like that of MASP2. These studies define the role of sessile loop in the interaction with serine domain, which could be beneficial to understand the interactions of complement C4 with other complement components (113).

C2- and C4-Bypass Lectin Pathways

It seems that sometimes the activation of three complement pathways is not clear-cut. Recent studies in mice established that the complement activation *via* the alternative pathway requires the presence of C4 and MBL proteins and the complement activation by *Cryptococcus* spp. can take place *via* multiple complement pathways (114, 115).

Although complement C4 does not directly participate in the activation of alternative complement pathway (AP), several early

studies from the 1980s to 1990s of last century demonstrated that C4b generated from classical pathway activation could trigger the alternative pathway without involvement of complement C2 (116–118). It was reported that MBL can activate complement C3 and AP without the involvement of MASP-2, C2, or C4 (119, 120). A recent study by Tateishi and Matsushita demonstrated that upon the attachment to serogroup C-specific oligosaccharide from *Salmonella*, in contrast to that MBL activates the alternative pathway *via* a C2-bypass pathway without the involvement of MASP-2, C2 or C4, mannan-bound MBL can activate the alternative pathway *via* a C2-bypass pathway that requires both MASP-2 and C4, suggesting that there may be two distinct MBL-mediated C2-bypass activation of alternative complement pathway, depending on the ligands to which MBL binds (121). It seems that there are some issues related to those *in vitro* assays. First, those MBL preparations could possibly have the trace contamination with MASP-2. Another question is how pure the serum preparations with the depleted MBL, C2, or C4 can be. The mechanism of MBL mediated C2-bypass AP activation remains to be determined and further studies are needed to elucidate the molecular base of MBL-mediated C2-bypass pathways as indicated in the paper.

Several studies suggested that MBL complement pathway could activate C3 or C5 through C4-bypass mechanisms (119, 122–125). The study in a mouse model by Schwaebler et al. demonstrated that in the absence of complement C4, *in vitro* lectin pathway-mediated activation of C3 requires MASP-2, C2, and MASP-1/3. In a model of transient myocardial postischemic reperfusion injury (IRI), comparing to their wild-type

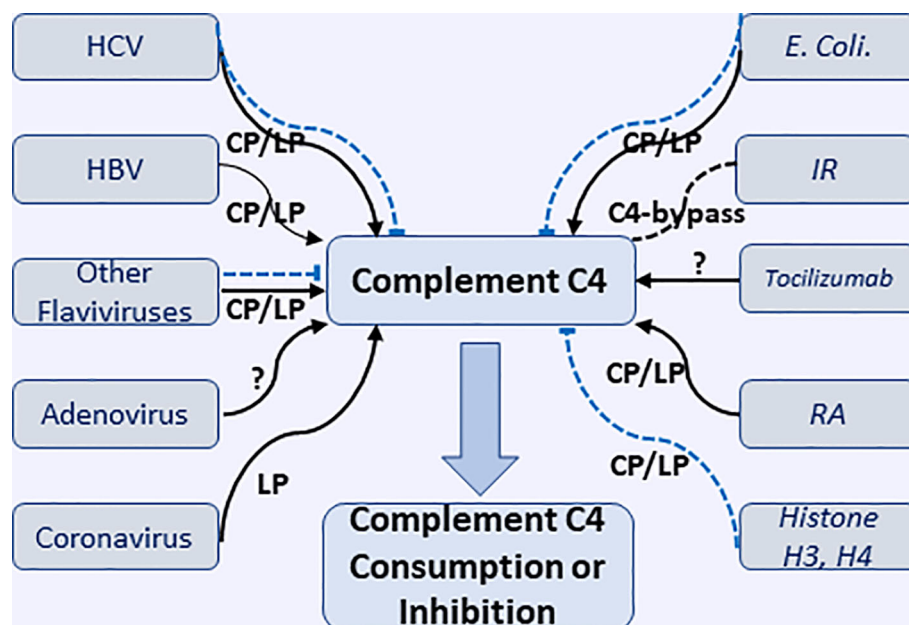


FIGURE 2 | Interactions of various microorganisms (including viruses and *E. coli.*) and pathological conditions with complement C4 to cause consumption or inhibition of complement C4 through classical, lectin, and undefined pathways. HCV, hepatitis V virus; HBV, hepatitis B virus; IR, ischemia reperfusion; RA, rheumatoid arthritis. Black solid arrow represents the activation of complement C4; Blue dash line represents the inhibition of complement C4.

littermates, infarct volumes of MASP-2-deficient mice were smaller. However, mice deficient in complement C4 were not protected, the observation implies the presence of a previously undocumented C4-bypass and lectin pathway-dependent mechanism. As monoclonal Antibody-based inhibitors of MASP-2 and MASP-2 deficiency can also protect mice from gastrointestinal IRI, suggesting the benefit of anti-MASP-2 antibody therapy in reperfusion injury and other lectin pathway-mediated disorders (126). In this study, it was unclear how the correlation between complement C3 activation by C4-bypass lectin pathway and the disease state of infarct volume. IRI may not be due to the complement C3 activation, but could be attributed by MASP-2- or MASP-1-induced direct activation of coagulation systems, leading to the formation of a fibrin clot (127, 128). Lectin pathway complement activation plays a critical role in contributing to ischemia reperfusion (IR) injury. One recent study in a mouse model corroborates the effect of MASP-2, an essential enzyme for lectin pathway, which mediates tissue injury and renal ischemia reperfusion injury independent of complement C4 (129). C2- and C4-bypass lectin pathways activation are depicted in **Figure 3**.

Although classical and the alternative pathways can still be activated, MASP-2 deficient mice fail to opsonize *Streptococcus*

pneumoniae in the none-immune host and therefore are highly susceptible to pneumococcal infection. Mouse ficolin A, human L-ficolin, and collectin 11 in both species, but not mannan-binding lectin (MBL), are the pattern recognition molecules that drive lectin pathway activation on the surface of *S. pneumoniae*. pneumococcal opsonization in the absence of complement C4. This study corroborates the crucial function of MASP-2 in the lectin pathway and underlines the prominence of MBL-independent lectin pathway activation in the host defense against pneumococci (130).

Recent study in mice demonstrated that MASP-2 deposits complement C4 onto mitochondria, revealing the potential role of the complement lectin pathway in mitochondrial immune handling. These processes are speculated to be involved either in the induction of problematic inflammatory reactions or in homeostatic clearance of mitochondria (131).

As discussed above, the complement lectin pathway has a protective function against invading pathogens and plays an essential role in ischemia/reperfusion (I/R)-injury as well. The serpin C1-inhibitor and aprotinin, a Kunitz-type inhibitor can inhibit MASP-2. Recombinant tissue factor pathway inhibitor (rTFPI) was identified as a novel selective inhibitor of MASP-2, without disturbing the activity of MASP-1 or the classical

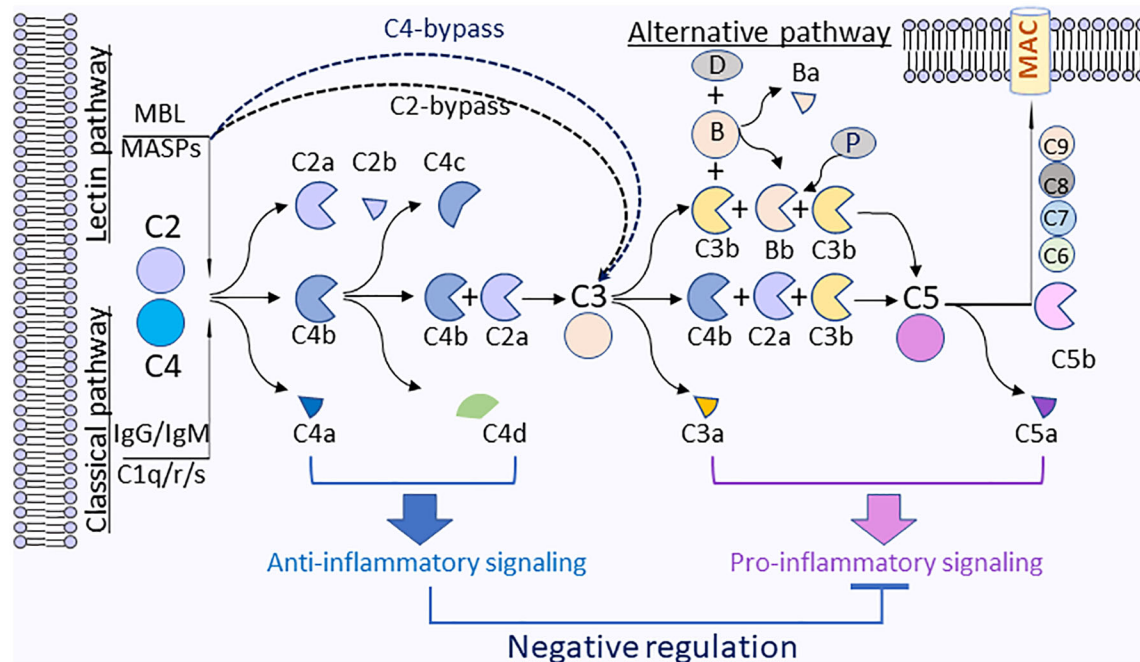


FIGURE 3 | Anti-inflammatory functions by complement C4 activation fragments C4a and C4d. On the surface of pathogens, the activation of complement C4 is triggered through classical (antibody) or lectin (sugar) pathways that will activate C1s or MASPs, which will rapidly cleave C4 to generate C4a and C4b. C4b will be further fragmented by factor I and cofactors to generate C4d and C4c. C4b will associate with C2a to form a complement C3 cleavage enzyme (C3 convertase), C4b2a, which will cleave C3 to generate C3a and C3b. C3b will be associated with C4b2a to converge to C5 convertase (C4bC2aC3b), which will cleave C5 to generate C5a and C5b. C5b will associate with C6, C7, C8, and C9 to form membrane attack complexes (MAC) C5b-9 on the surface of pathogens. For the alternative pathway, C3b is spontaneous C3 turnover or generated by classical or lectin pathways. C3b bound to factor B (B). The complex is converted by factor D (D) to C3-cleaving enzyme C3bBb that is stabilized by properdin (P) and further form C3bBbC3b, which can cleave C5 to generate C5a and C5b. Plasma membrane (blue) represents the surface of pathogen cells.

pathway proteases C1s and C1r. Ex vivo assay revealed that Kunitz-2 domain in TFPI was necessary for the inhibition of MASP-2 activity. TFPI could be a therapeutic approach to constraint the tissue injury in the conditions of cerebral stroke, myocardial infarction, or solid organ transplantation (132).

THE SIGNALING PATHWAYS OF C4 ACTIVATION FRAGMENTS

C4a, one of the activation fragments of complement C4, identified in 1979, was regarded as the third anaphylatoxin although it is still under debate (133, 134). C4a has been described to possess a strong chemotaxis inhibitory effect on monocytes at the concentration as low as 10^{-16} M (135). C4a was also reported to inhibit C3a-induced O_2^{2-} generation in guinea pig macrophages, to produce immediate erythema/edema when injected into human skin, and to induce contraction of guinea pig ileum (133, 136). It was suggested that a function for C4a is closely related to C3a due to its ability to desensitize the action of C3a-induced contraction of guinea pig ileum (133). It was later revealed that human C4a acted as an agonist for the guinea pig but not the human C3aR receptor (137). Studies using recombinant human C4a have also demonstrated that C4a can impair C5a-induced neointima formation, reduce C3a- or C5a-mediated chemoattractant and secretagogue activities in mast cells, and prevent hyperoxic lung injury *via* a macrophage-dependent signaling pathway (138–140). It remains to be established how C4a can modulate the functions of monocytes/macrophages to generate anti-inflammatory effects.

C4d, another cleavage product by complement C4 activation, has long been considered as a biomarker for disease activity in autoimmune disorders or antibody-mediated allograft rejection. A recent study identified Ig-like transcript (ILT) 4 and ITL5v2 as cellular receptors for C4d and interaction of C4d with ILT4 conferred a dose-dependent inhibition of TNF α and IL-6 secretion and attenuation of intracellular $[Ca^{2+}]$ flux in monocytes activated *via* Fc-cross-linking of up to 50% as compared to control (141). ILT4 has been involved in the control of autoreactivity (142, 143), induction of transplantation tolerance (144), and maintenance of feto-maternal tolerance during pregnancy (145). Mice lack of PIR-B, the ortholog of ILT4, suffer from autoimmune glomerulonephritis (146) and exacerbated graft versus host disease (147). It appears that the interactions of complement C4 activation cleavage fragments (such as C4a and C4d) with their respective receptors plays inhibitory roles to impede inflammatory reactions induced by cytokines, chemokines, and other anaphylatoxins (C3a, C5a). One interesting paradigm will be that upon complement activation (*i.e.*, microbial or viral infection, immunocomplex, or apoptotic debris), complement C4 activation fragments may act as regulators to maintain homeostasis and to contain downstream anaphylatoxins' proinflammatory effects, which may trigger hyper-inflammatory reactions. The activation of complement C4 and potential immune-regulation mechanisms of split products from complement C4 are illustrated in **Figure 3**.

COMPLEMENT C4 DEFICIENCY LINKS INFECTIONS AND AUTOIMMUNE DISEASES

It remains incompletely understood why total deficiencies of some complement components are associated with some autoimmune diseases (148). Complement C4 plays a vital role in the activation of classical and lectin pathways and the formation of C3 convertase, which leads to the generation of the membrane attack complex (MAC) against microbes. It was reported that complement C4 is protective for autoimmune lupus disease independent of C3 in mice (30). C4(-/-) mice have significantly more IgM anti-double-strand DNA antibodies than C4(+/+) control mice (32). Increased frequency of C4 deficiency phenotypes was reported in IgA nephropathy and Henoch-Schönlein purpura (HSP) (26), insulin-dependent diabetes mellitus (IDDM) (149), systemic lupus erythematosus (SLE) (150, 151), repeated infections (152), juvenile idiopathic arthritis patients (27), glomerulonephritis (153). The lack of complement C4 can trigger inapt clearance of apoptotic debris and stimulate chronic activation of myeloid cells. The deficiency in complement component C4 also results in a breakdown in the elimination of autoreactive B-cell clones at the transitional stage, depicted by a relative increase in their response to a series of stimuli, entering into follicles, and a higher tendency to form self-reactive germinal centers (GCs), allowing the maturation and activation of self-reactive B-cell clones (154). Using two well-defined murine models to examine complement deficiency in peripheral tolerance, the study revealed that complement C4 protein and the receptors CD21/CD35 are involved in negative selection of self-reactive B lymphocytes, suggesting an immune deficiency of complement C4 predisposes mice to SLE (29). A low serum C4 level in patients with autoimmune disease may be due to ongoing disease activity associated with the consumption caused by complement activation and or it may be due to genetic factors (155). One of the questions still remains: whether and how does infections link to autoimmune disease upon the deficiency of complement C4? It is speculated that C4 deficiency would negatively affect the efficiency and progression of complement activation, decrease phagocytes functions and the clearance of apoptotic and necrotic cells (156).

A recent study by Yammani et al. demonstrated that complement C4 deficiency is a predisposing factor for streptococcus pneumonia-induced anti-dsDNA IgA autoantibody production. In a C4KO mice model, serotype 19F and virulent serotype 3 pneumococci induce systemic anti-dsDNA IgA production; interestingly which is more pronounced in female C4KO mice. Further study revealed that pneumococci pneumococcal polysaccharide (PPS) vaccination alone induced increases in anti-dsDNA IgA levels, which can be completely blocked by TLR2/4 antagonist, OxPAPC. Pam3CSK4, a TLR2 agonist, equally stimulated anti-dsDNA IgA production in C4KO mice, suggesting complement C4 plays a role in subduing autoantibody production stimulated by cross-reactive antigens and TLR2 agonists associated with *S. pneumonia* (33).

A complete analysis of the potential Epstein-Barr virus (EBV) peptide cross-reactome has been performed to search for peptides common to SLE-EBV and human SLE autoantigens. The study found EBV proteome can act as an immunological potential. Using publicly available databases, fifty-one SLE-related proteins were analyzed for hexapeptide sharing with EBV proteome and found 34 of hexapeptides are shared between human SLE autoantigens and EBV proteins. Interestingly, the study also revealed that peptide sharing mostly occurred with complement component C4 and Interleukin-10 (IL-10). This study demonstrated that the EBV vs. SLE autoantigens peptide overlap and powerfully supports cross-reactivity as a major mechanism in EBV-associated SLE etiopathogenesis (157). Among patients with systemic lupus erythematosus (SLE), a prevalence of HPV infection has been reported. One interesting hypothesis is that immune responses caused by HPV infection may interact with proteins that associate with SLE (158).

In lymphoid tissues and peripheral blood of C4KO mice, it was discovered with the decreased frequencies of CD4⁺CD25⁺ T_{regs} and reduced expression of Foxp3 and TGF- β , which are crucial for the efficient development and function of T_{regs} cells. Thus, the study suggested that the association of the deficiency of complement C4 in the classical complement pathway with the development of autoimmune disorder might be *via* the role of T_{regs} deficiency (159). It remains to be elucidated how the fragments generated from complement C4 activation, such as C4a and C4d, are regulating T_{regs} cells functions.

CONCLUDING REMARKS

Complement system is essential for the maintenance of homeostasis by elimination of immune complexes, supporting self-tolerance and anti-inflammation, and promoting tissue repair (160, 161). While the complement activation of the downstream of complement C3 resulting in inflammatory molecules, such as C3a, C5a, and the membrane attack complex (MAC), plays a less important role, the early components of the classical pathway, such as C1q, C4, and C2, are more critical in maintaining homeostasis and lack of some of early components of classical pathway will predispose an individual to autoimmune disorders. Many studies have linked the complement C4 deficiency/partial deficiency with autoimmune disorders. In addition, C4 deficiency is clearly

linked to the susceptibility of infections. Those observations persuade us to speculate that infection-caused inflammation needs the containment that requires the immune modulation from the contribution of complement C4, otherwise it will be aggravated under the deficiency of C4. Complement C4 is reported to be chiefly expressed in hepatocytes, but the upregulation of mRNA expression of complement C4 was observed by LPS, IFN γ , and interleukin-6 in other types of cells, indicating that infection-induced cytokines could trigger the upregulation of complement C4 expression as a feedback regulatory response. Mounting evidence supports the observation that infections may initiate and/or exacerbate autoimmune reactions (162–165), which is in line with the studies in mouse models that have established the role of complement C4 as suppressing auto-antibody production (31–33, 166). Nevertheless, the mechanisms of complement C4 involved in homeostasis still have been poorly addressed. Recent studies demonstrated that complement C4 activation fragments, like C4a and C4d, can modulate cytokines generation from macrophages probably through their respective receptors. One of possible mechanisms that complement C4 mediated homeostatic process might be *via* its activation fragments, which can modulate immune reactions to restrain infection-induced hyper-inflammatory reactions induced by cytokines and anaphylatoxin C3a and C5a (**Figure 3**).

Future studies are necessary to focus on the immune regulatory functions of C4 activation fragments, which will be explored as therapeutic targets for the treatment of infections, as well as the autoimmune disorders.

AUTHOR CONTRIBUTIONS

HW contributed to the conception and idea of the work. All authors contributed to the article and approved the submitted version.

FUNDING

Research work was supported by the seed grant (to HW) from College of Pharmacy and mini-grant (to HW) from College of Medicine, California Northstate University, Elk Grove, CA 95757, United States.

REFERENCES

- Kallionpää H, Elo LL, Laajala E, Mykkanen J, Ricano-Ponce I, Vaarma M, et al. Innate Immune Activity Is Detected Prior to Seroconversion in Children With HLA-Conferred Type 1 Diabetes Susceptibility. *Diabetes* (2014) 63(7):2402–14. doi: 10.2337/db13-1775
- Dempsey PW, Allison ME, Akkaraju S, Goodnow CC, Fearon DT. C3d of Complement as a Molecular Adjuvant: Bridging Innate and Acquired Immunity. *Science* (1996) 271(5247):348–50. doi: 10.1126/science.271.5247.348
- Nauta AJ, Daha MR, van Kooten C, Roos A. Recognition and Clearance of Apoptotic Cells: a Role for Complement and Pentraxins. *Trends Immunol* (2003) 24(3):148–54. doi: 10.1016/S1471-4906(03)00030-9
- Audemard-Verger A, Descloux E, Ponard D, Deroux A, Fantin B, Fieschi C, et al. Infections Revealing Complement Deficiency in Adults: a French Nationwide Study Enrolling 41 Patients. *Med (Baltimore)* (2016) 95(19):e3548. doi: 10.1097/MD.0000000000003548
- Ballanti E, Perricone C, Greco E, Ballanti M, Di Muzio G, Chimenti MS, et al. Complement and Autoimmunity. *Immunol Res* (2013) 56(2-3):477–91. doi: 10.1007/s12026-013-8422-y
- Law SK, Dodds AW. The Internal Thioester and the Covalent Binding Properties of the Complement Proteins C3 and C4. *Protein Sci* (1997) 6(2):263–74. doi: 10.1002/pro.5560060201
- Sim RB, Sim E. Autolytic Fragmentation of Complement Components C3 and C4 and Its Relationship to Covalent Binding Activity. *Ann N Y Acad Sci* (1983) 421:259–76. doi: 10.1111/j.1749-6632.1983.tb18114.x

8. Perry AJ, Wijeyewickrema LC, Wilmann PG, Gunzburg MJ, D'Andrea L, Irving JA, et al. A Molecular Switch Governs the Interaction Between the Human Complement Protease C1s and Its Substrate, Complement C4. *J Biol Chem* (2013) 288(22):15821–9. doi: 10.1074/jbc.M113.464545
9. Duncan RC, Mohlin F, Taleski D, Coetzer TH, Huntington JA, Payne RJ, et al. Identification of a Catalytic Exosite for Complement Component C4 on the Serine Protease Domain of C1s. *J Immunol* (2012) 189(5):2365–73. doi: 10.4049/jimmunol.1201085
10. Duncan RC, Bergstrom F, Coetzer TH, Blom AM, Wijeyewickrema LC, Pike RN. Multiple Domains of MASP-2, an Initiating Complement Protease, Are Required for Interaction With Its Substrate C4. *Mol Immunol* (2012) 49(4):593–600. doi: 10.1016/j.molimm.2011.10.006
11. Drentin N, Conroy P, Gunzburg MJ, Pike RN, Wijeyewickrema LC. Investigation of the Mechanism of Interaction Between Mannose-Binding Lectin-Associated Serine Protease-2 and Complement C4. *Mol Immunol* (2015) 67(2 Pt B):287–93. doi: 10.1016/j.molimm.2015.06.011
12. Kidmose RT, Laursen NS, Dobo J, Kjaer TR, Sirotkina S, Yatime L, et al. Structural Basis for Activation of the Complement System by Component C4 Cleavage. *Proc Natl Acad Sci USA* (2012) 109(38):15425–30. doi: 10.1073/pnas.1208031109
13. Pilely K, Skjoedt MO, Nielsen C, Andersen TE, Louise Aabom A, Vitved L, et al. A Specific Assay for Quantification of Human C4c by Use of an Anti-C4c Monoclonal Antibody. *J Immunol Methods* (2014) 405:87–96. doi: 10.1016/j.jim.2014.01.011
14. Wieser M, Francisci T, Lackner D, Buerckstuemmmer T, Wasner K, Eilenberg W, et al. CD46 Knock-Out Using CRISPR/Cas9 Editing of hTERT Immortalized Human Cells Modulates Complement Activation. *PLoS One* (2019) 14(4):e0214514. doi: 10.1371/journal.pone.0214514
15. Barilla-LaBarca ML, Liszewski MK, Lambris JD, Hourcade D, Atkinson JP. Role of Membrane Cofactor Protein (CD46) in Regulation of C4b and C3b Deposited on Cells. *J Immunol* (2002) 168(12):6298–304. doi: 10.4049/jimmunol.168.12.6298
16. Mortensen S, Kidmose RT, Petersen SV, Szilagyi A, Prohaszka Z, Andersen GR. Structural Basis for the Function of Complement Component C4 Within the Classical and Lectin Pathways of Complement. *J Immunol* (2015) 194(11):5488–96. doi: 10.4049/jimmunol.1500087
17. Mortensen S, Jensen JK, Andersen GR. Solution Structures of Complement C2 and Its C4 Complexes Propose Pathway-Specific Mechanisms for Control and Activation of the Complement Proconvertases. *J Biol Chem* (2016) 291(32):16494–507. doi: 10.1074/jbc.M116.722017
18. Bishof NA, Welch TR, Beischel LS. C4B Deficiency: a Risk Factor for Bacteremia With Encapsulated Organisms. *J Infect Dis* (1990) 162(1):248–50. doi: 10.1093/infdis/162.1.248
19. Jaatinen T, Lahti M, Ruuskanen O, Kinos R, Truedsson L, Laheesmaa R, et al. Total C4B Deficiency Due to Gene Deletion and Gene Conversion in a Patient With Severe Infections. *Clin Diagn Lab Immunol* (2003) 10(2):195–201. doi: 10.1128/CDLI.10.2.195-201.2003
20. Kang YS, Do Y, Lee HK, Park SH, Cheong C, Lynch RM, et al. A Dominant Complement Fixation Pathway for Pneumococcal Polysaccharides Initiated by SIGN-R1 Interacting With C1q. *Cell* (2006) 125(1):47–58. doi: 10.1016/j.cell.2006.01.046
21. Brown JS, Russell T, Gilliland SM, Holden DW, Paton JC, Ehrenstein MR, et al. The Classical Pathway Is the Dominant Complement Pathway Required for Innate Immunity to Streptococcus Pneumoniae Infection in Mice. *Proc Natl Acad Sci USA* (2002) 99(26):16969–74. doi: 10.1073/pnas.012669199
22. Mold C, Rodic-Polic B, Du Clos TW. Protection From Streptococcus Pneumoniae Infection by C-Reactive Protein and Natural Antibody Requires Complement But Not Fc Gamma Receptors. *J Immunol* (2002) 168(12):6375–81. doi: 10.4049/jimmunol.168.12.6375
23. Rowe PC, McLean RH, Wood RA, Leggiadro RJ, Winkelstein JA. Association of Homozygous C4B Deficiency With Bacterial Meningitis. *J Infect Dis* (1989) 160(3):448–51. doi: 10.1093/infdis/160.3.448
24. Hauptmann G, Tappeiner G, Schifferli JA. Inherited Deficiency of the Fourth Component of Human Complement. *Immunodef Rev* (1988) 1(1):3–22.
25. Yang Y, Chung EK, Zhou B, Lhotka K, Hebert LA, Birmingham DJ, et al. The Intricate Role of Complement Component C4 in Human Systemic Lupus Erythematosus. *Curr Dir Autoimmun* (2004) 7:98–132. doi: 10.1159/000075689
26. McLean RH, Wyatt RJ, Julian BA. Complement Phenotypes in Glomerulonephritis: Increased Frequency of Homozygous Null C4 Phenotypes in IgA Nephropathy and Henoch-Schönlein Purpura. *Kidney Int* (1984) 26(6):855–60. doi: 10.1038/ki.1984.228
27. Gilliam BE, Wolff AE, Moore TL. Partial C4 Deficiency in Juvenile Idiopathic Arthritis Patients. *J Clin Rheumatol* (2007) 13(5):256–60. doi: 10.1097/RHU.0b013e318156b9e3
28. Wopenka U, Thysell H, Sjöholm AG, Truedsson L. C4 Phenotypes in IgA Nephropathy: Disease Progression Associated With C4A Deficiency But Not With C4 Isotype Concentrations. *Clin Nephrol* (1996) 45(3):141–5.
29. Prodeus AP, Goerg S, Shen LM, Pozdnyakova OO, Chu L, Alicot EM, et al. A Critical Role for Complement in Maintenance of Self-Tolerance. *Immunity* (1998) 9(5):721–31. doi: 10.1016/S1074-7613(00)80669-X
30. Einav S, Pozdnyakova OO, Ma M, Carroll MC. Complement C4 Is Protective for Lupus Disease Independent of C3. *J Immunol* (2002) 168(3):1036–41. doi: 10.4049/jimmunol.168.3.1036
31. Chen Z, Koralov SB, Kelsoe G. Complement C4 Inhibits Systemic Autoimmunity Through a Mechanism Independent of Complement Receptors CR1 and CR2. *J Exp Med* (2000) 192(9):1339–52. doi: 10.1084/jem.192.9.1339
32. Paul E, Pozdnyakova OO, Mitchell E, Carroll MC. Anti-DNA Autoreactivity in C4-Deficient Mice. *Eur J Immunol* (2002) 32(9):2672–9. doi: 10.1002/1521-4141(200209)32:9<2672::AID-IMMU2672>3.0.CO;2-X
33. Yammani RD, Leyva MA, Jennings RN, Haas KM. C4 Deficiency Is a Predisposing Factor for Streptococcus Pneumoniae-Induced Autoantibody Production. *J Immunol* (2014) 193(11):5434–43. doi: 10.4049/jimmunol.1401462
34. Blanchong CA, Zhou B, Rupert KL, Chung EK, Jones KN, Sotos JF, et al. Deficiencies of Human Complement Component C4A and C4B and Heterozygosity in Length Variants of RP-C4-CYP21-TNX (RCCX) Modules in Caucasians. The Load of RCCX Genetic Diversity on Major Histocompatibility Complex-Associated Disease. *J Exp Med* (2000) 191(12):2183–96. doi: 10.1084/jem.191.12.2183
35. Hovingh ES, van Gent M, Hamstra HJ, Demkes M, Mooi FR, Pinelli E. Emerging Bordetella Pertussis Strains Induce Enhanced Signaling of Human Pattern Recognition Receptors TLR2, NOD2 and Secretion of IL-10 by Dendritic Cells. *PLoS One* (2017) 12(1):e0170027. doi: 10.1371/journal.pone.0170027
36. Blanchong CA, Chung EK, Rupert KL, Yang Y, Yang Z, Zhou B, et al. Genetic, Structural and Functional Diversities of Human Complement Components C4A and C4B and Their Mouse Homologues, Slp and C4. *Int Immunopharmacol* (2001) 1(3):365–92. doi: 10.1016/S1567-5769(01)00019-4
37. Carroll MC, Palsdottir A, Belt KT, Porter RR. Deletion of Complement C4 and Steroid 21-Hydroxylase Genes in the HLA Class III Region. *EMBO J* (1985) 4(10):2547–52. doi: 10.1002/j.1460-2075.1985.tb03969.x
38. Carroll MC, Campbell RD, Bentley DR, Porter RR. A Molecular Map of the Human Major Histocompatibility Complex Class III Region Linking Complement Genes C4, C2 and Factor B. *Nature* (1984) 307(5948):237–41. doi: 10.1038/307237a0
39. Yu CY. Molecular Genetics of the Human MHC Complement Gene Cluster. *Exp Clin Immunogenet* (1998) 15(4):213–30. doi: 10.1159/000019075
40. Yung Yu C, Yang Z, Blanchong CA, Miller W. The Human and Mouse MHC Class III Region: a Parade of 21 Genes at the Centromeric Segment. *Immunol Today* (2000) 21(7):320–8. doi: 10.1016/S0167-5699(00)01664-9
41. White PC, Grossberger D, Onufer BJ, Chaplin DD, New MI, Dupont B, et al. Two Genes Encoding Steroid 21-Hydroxylase Are Located Near the Genes Encoding the Fourth Component of Complement in Man. *Proc Natl Acad Sci USA* (1985) 82(4):1089–93. doi: 10.1073/pnas.82.4.1089
42. Bristow J, Tee MK, Gitelman SE, Mellon SH, Miller WL. Tenascin-X: a Novel Extracellular Matrix Protein Encoded by the Human XB Gene Overlapping P450c21B. *J Cell Biol* (1993) 122(1):265–78. doi: 10.1083/jcb.122.1.265
43. Shen L, Wu LC, Sanlioglu S, Chen R, Mendoza AR, Dangel AW, et al. Structure and Genetics of the Partially Duplicated Gene RP Located Immediately Upstream of the Complement C4A and the C4B Genes in the HLA Class III Region. Molecular Cloning, Exon-Intron Structure, Composite Retroposon, and Breakpoint of Gene Duplication. *J Biol Chem* (1994) 269(11):8466–76. doi: 10.1016/S0021-9258(17)37217-4

44. Yang Z, Mendoza AR, Welch TR, Zipf WB, Yu CY. Modular Variations of the Human Major Histocompatibility Complex Class III Genes for Serine/Threonine Kinase RP, Complement Component C4, Steroid 21-Hydroxylase CYP21, and Tenascin TNX (the RCCX Module). A Mechanism for Gene Deletions and Disease Associations. *J Biol Chem* (1999) 274(17):12147–56. doi: 10.1074/jbc.274.17.12147
45. Olsson LM, Holmdahl R. Copy Number Variation in Autoimmunity—Importance Hidden in Complexity? *Eur J Immunol* (2012) 42(8):1969–76. doi: 10.1002/eji.201242601
46. Wu YL, Savelli SL, Yang Y, Zhou B, Rovin BH, Birmingham DJ, et al. Sensitive and Specific Real-Time Polymerase Chain Reaction Assays to Accurately Determine Copy Number Variations (CNVs) of Human Complement C4A, C4B, C4-Long, C4-Short, and RCCX Modules: Elucidation of C4 CNVs in 50 Consanguineous Subjects With Defined HLA Genotypes. *J Immunol* (2007) 179(5):3012–25. doi: 10.4049/jimmunol.179.5.3012
47. Yu CY, Belt KT, Giles CM, Campbell RD, Porter RR. Structural Basis of the Polymorphism of Human Complement Components C4A and C4B: Gene Size, Reactivity and Antigenicity. *EMBO J* (1986) 5(11):2873–81. doi: 10.1002/j.1460-2075.1986.tb04582.x
48. Belt KT, Yu CY, Carroll MC, Porter RR. Polymorphism of Human Complement Component C4. *Immunogenetics* (1985) 21(2):173–80. doi: 10.1007/BF00364869
49. Dodds AW, Law SK, Porter RR. The Purification and Properties of Some Less Common Allotypes of the Fourth Component of Human Complement. *Immunogenetics* (1986) 24(5):279–85. doi: 10.1007/BF00395532
50. Sim E, Cross SJ. Phenotyping of Human Complement Component C4, a Class-III HLA Antigen. *Biochem J* (1986) 239(3):763–7. doi: 10.1042/bj2390763
51. Awdeh ZL, Alper CA. Inherited Structural Polymorphism of the Fourth Component of Human Complement. *Proc Natl Acad Sci USA* (1980) 77(6):3576–80. doi: 10.1073/pnas.77.6.3576
52. Dangel AW, Mendoza AR, Baker BJ, Daniel CM, Carroll MC, Wu LC, et al. The Dichotomous Size Variation of Human Complement C4 Genes Is Mediated by a Novel Family of Endogenous Retroviruses, Which Also Establishes Species-Specific Genomic Patterns Among Old World Primates. *Immunogenetics* (1994) 40(6):425–36. doi: 10.1007/BF00177825
53. Yu CY. The Complete Exon-Intron Structure of a Human Complement Component C4A Gene. DNA Sequences, Polymorphism, and Linkage to the 21-Hydroxylase Gene. *J Immunol* (1991) 146(3):1057–66.
54. Ulgiati D, Abraham LJ. Comparative Analysis of the Disease-Associated Complement C4 Gene From the HLA-A1, B8, DR3 Haplotype. *Exp Clin Immunogenet* (1996) 13(1):43–54. doi: 10.1007/s002510050059
55. Schneider PM, Carroll MC, Alper CA, Rittner C, Whitehead AS, Yunis EJ, et al. Polymorphism of the Human Complement C4 and Steroid 21-Hydroxylase Genes. Restriction Fragment Length Polymorphisms Revealing Structural Deletions, Homoduplications, and Size Variants. *J Clin Invest* (1986) 78(3):650–7. doi: 10.1172/JCI112623
56. Yu CY, Campbell RD. Definitive RFLPs to Distinguish Between the Human Complement C4A/C4B Isotypes and the Major Rodgers/Chido Determinants: Application to the Study of C4 Null Alleles. *Immunogenetics* (1987) 25(6):383–90. doi: 10.1007/BF00396104
57. Dodds AW, Ren XD, Willis AC, Law SK. The Reaction Mechanism of the Internal Thioester in the Human Complement Component C4. *Nature* (1996) 379(6561):177–9. doi: 10.1038/379177a0
58. Juptner M, Flachsbart F, Caliebe A, Lieb W, Schreiber S, Zeuner R, et al. Low Copy Numbers of Complement C4 and Homozygous Deficiency of C4A may Predispose to Severe Disease and Earlier Disease Onset in Patients With Systemic Lupus Erythematosus. *Lupus* (2018) 27(4):600–9. doi: 10.1177/0961203317735187
59. Hou S, Qi J, Liao D, Fang J, Chen L, Kijlstra A, et al. High C4 Gene Copy Numbers Protects Against Vogt-Koyanagi-Harada Syndrome in Chinese Han. *Br J Ophthalmol* (2014) 98(12):1733–7. doi: 10.1136/bjophthalmol-2014-305596
60. Hou S, Qi J, Liao D, Zhang Q, Fang J, Zhou Y, et al. Copy Number Variations of Complement Component C4 Are Associated With Behcet's Disease But Not With Ankylosing Spondylitis Associated With Acute Anterior Uveitis. *Arthritis Rheum* (2013) 65(11):2963–70. doi: 10.1002/art.38116
61. Yang Y, Chung EK, Wu YL, Savelli SL, Nagaraja HN, Zhou B, et al. Gene Copy-Number Variation and Associated Polymorphisms of Complement Component C4 in Human Systemic Lupus Erythematosus (SLE): Low Copy Number Is a Risk Factor for and High Copy Number Is a Protective Factor Against SLE Susceptibility in European Americans. *Am J Hum Genet* (2007) 80(6):1037–54. doi: 10.1086/518257
62. Boteva L, Morris DL, Cortes-Hernandez J, Martin J, Vyse TJ, Fernando MM. Genetically Determined Partial Complement C4 Deficiency States Are Not Independent Risk Factors for SLE in UK and Spanish Populations. *Am J Hum Genet* (2012) 90(3):445–56. doi: 10.1016/j.ajhg.2012.01.012
63. Breukink MB, Schellevis RL, Boon CJ, Fauser S, Hoyng CB, den Hollander AI, et al. Genomic Copy Number Variations of the Complement Component C4B Gene Are Associated With Chronic Central Serous Chorioretinopathy. *Invest Ophthalmol Vis Sci* (2015) 56(9):5608–13. doi: 10.1167/iov.15-17343
64. Kainulainen L, Peltola V, Seppanen M, Viander M, He Q, Lokki ML, et al. C4A Deficiency in Children and Adolescents With Recurrent Respiratory Infections. *Hum Immunol* (2012) 73(5):498–501. doi: 10.1016/j.humimm.2012.02.015
65. Jaatinen T, Ruuskanen O, Truedsson L, Lokki ML. Homozygous Deletion of the CYP21A-TNXA-RP2-C4B Gene Region Conferring C4B Deficiency Associated With Recurrent Respiratory Infections. *Hum Immunol* (1999) 60(8):707–14. doi: 10.1016/S0198-8859(99)00047-6
66. Bay JT, Scheibel L, Madsen HO, Sorensen SS, Hansen JM, Garred P. Low C4 Gene Copy Numbers Are Associated With Superior Graft Survival in Patients Transplanted With a Deceased Donor Kidney. *Kidney Int* (2013) 84(3):562–9. doi: 10.1038/ki.2013.195
67. Goldman JN, O'Rourke KS, Goldman MB. Antibody-Induced Suppression and Postsuppression Stimulation of Complement In Vitro. III. Long-Term C4 Suppression Is Actively Maintained by a Soluble Suppressor Factor (Fsc4). *Cell Immunol* (1985) 96(1):26–37. doi: 10.1016/0008-8749(85)90337-5
68. Goldman MB, O'Rourke KS, Becker DS, Goldman JN. Antibody-Induced Suppression and Postsuppression Stimulation of Complement In Vitro. II. Intracellular and Extracellular Changes in C4 During Long-Term C4 Suppression in Guinea Pig Splenic Fragments. *J Immunol* (1985) 134(5):3298–306.
69. Goldman JN, O'Rourke KS, McMannis JD, Goldman MB. Effects of Anti-C4 Antibody on Complement Production by Splenic and Peritoneal Macrophages. *Complement* (1988) 5(1):13–26. doi: 10.1159/000463027
70. Goldman MB, Becker DS, O'Rourke KS, Goldman JN. Enhancement by Cyclic AMP of Antibody-Induced Suppression of the Fourth Component of Complement. *J Immunol* (1985) 135(4):2701–6.
71. Daha MR, van Es LA. Relative Resistance of the F-42-Stabilized Classical Pathway C3 Convertase to Inactivation by C4-Binding Protein. *J Immunol* (1980) 125(5):2051–4.
72. Garam N, Prohaszka Z, Szilagyi A, Aigner C, Schmidt A, Gaggl M, et al. C4 Nephritic Factor in Patients With Immune-Complex-Mediated Membranoproliferative Glomerulonephritis and C3-Glomerulopathy. *Orphanet J Rare Dis* (2019) 14(1):247. doi: 10.1186/s13023-019-1237-8
73. Zhang Y, Meyer NC, Fervenza FC, Lau W, Keenan A, Cara-Fuentes G, et al. C4 Nephritic Factors in C3 Glomerulopathy: a Case Series. *Am J Kidney Dis* (2017) 70(6):834–43. doi: 10.1053/j.ajkd.2017.07.004
74. Halbwachs L, Leveille M, Lesavre P, Wattel S, Leibowitch J. Nephritic Factor of the Classical Pathway of Complement: Immunoglobulin G Autoantibody Directed Against the Classical Pathway C3 Convertase Enzyme. *J Clin Invest* (1980) 65(6):1249–56. doi: 10.1172/JCI109787
75. Tanuma Y, Ohi H, Watanabe S, Seki M, Hatano M. C3 Nephritic Factor and C4 Nephritic Factor in the Serum of Two Patients With Hypocomplementaemic Membranoproliferative Glomerulonephritis. *Clin Exp Immunol* (1989) 76(1):82–5.
76. Miller EC, Chase NM, Densen P, Hintermeyer MK, Casper JT, Atkinson JP. Autoantibody Stabilization of the Classical Pathway C3 Convertase Leading to C3 Deficiency and Neisserial Sepsis: C4 Nephritic Factor Revisited. *Clin Immunol* (2012) 145(3):241–50. doi: 10.1016/j.clim.2012.09.007
77. Battin C, De Sousa Linhares A, Paster W, Isenman DE, Wahrmann M, Leitner J, et al. Neuropilin-1 Acts as a Receptor for Complement Split Products. *Front Immunol* (2019) 10:2209. doi: 10.3389/fimmu.2019.02209
78. Schifferli JA, Hauptmann G, Paccaud JP. Complement-Mediated Adherence of Immune Complexes to Human Erythrocytes. Difference in the Requirements for C4A and C4B. *FEBS Lett* (1987) 213(2):415–8. doi: 10.1016/0014-5793(87)81533-8

79. Liesmaa I, Paakkanen R, Jarvinen A, Valtonen V, Lokki ML. Clinical Features of Patients With Homozygous Complement C4A or C4B Deficiency. *PLoS One* (2018) 13(6):e0199305. doi: 10.1371/journal.pone.0199305
80. Skattum L, van Deuren M, van der Poll T, Truedsson L. Complement Deficiency States and Associated Infections. *Mol Immunol* (2011) 48(14):1643–55. doi: 10.1016/j.molimm.2011.05.001
81. Samano ES, Ribeiro Lde M, Gorescu RG, Rocha KC, Grumach AS. Involvement of C4 Allotypes in the Pathogenesis of Human Diseases. *Rev Hosp Clin Fac Med Sao Paulo* (2004) 59(3):138–44. doi: 10.1590/S0041-87812004000300009
82. Senbagavalli P, Kumar N, Kaur G, Mehra NK, Geetha ST, Ramanathan VD. Major Histocompatibility Complex Class III (C2, C4, Factor B) and C3 Gene Variants in Patients With Pulmonary Tuberculosis. *Hum Immunol* (2011) 72(2):173–8. doi: 10.1016/j.humimm.2010.11.002
83. Giussani S, Pietrocola G, Donnarumma D, Norais N, Speziale P, Fabbrini M, et al. The Streptococcus Agalactiae Complement Interfering Protein Combines Multiple Complement-Inhibitory Mechanisms by Interacting With Both C4 and C3 Ligands. *FASEB J* (2019) 33(3):4448–57. doi: 10.1096/fj.201801991R
84. Hair PS, Wagner SM, Friederich PT, Drake RR, Nyalwidhe JO, Cunnion KM. Complement Regulator C4BP Binds to Staphylococcus Aureus and Decreases Opsonization. *Mol Immunol* (2012) 50(4):253–61. doi: 10.1016/j.molimm.2012.01.010
85. Hovingh ES, van den Broek B, Kuipers B, Pinelli E, Rooijackers SHM, Jongerius I. Acquisition of C1 Inhibitor by Bordetella Pertussis Virulence Associated Gene 8 Results in C2 and C4 Consumption Away From the Bacterial Surface. *PLoS Pathog* (2017) 13(7):e1006531. doi: 10.1371/journal.ppat.1006531
86. Shende R, Wong SSW, Rapole S, Beau R, Ibrahim-Granet O, Monod M, et al. Aspergillus Fumigatus Conidial Metalloprotease Mep1p Cleaves Host Complement Proteins. *J Biol Chem* (2018) 293(40):15538–55. doi: 10.1074/jbc.RA117.001476
87. Behnsen J, Lessing F, Schindler S, Wartenberg D, Jacobsen ID, Thoen M, et al. Secreted Aspergillus Fumigatus Protease Alp1 Degrades Human Complement Proteins C3, C4, and C5. *Infect Immun* (2010) 78(8):3585–94. doi: 10.1128/IAI.01353-09
88. Cazander G, Schreurs MW, Renwarin L, Dorresteyn C, Hamann D, Jukema GN. Maggot Excretions Affect the Human Complement System. *Wound Repair Regen* (2012) 20(6):879–86. doi: 10.1111/j.1524-475X.2012.00850.x
89. Ahmed UK, Maller NC, Iqbal AJ, Al-Riyami L, Harnett W, Raynes JG. The Carbohydrate-Linked Phosphorylcholine of the Parasitic Nematode Product ES-62 Modulates Complement Activation. *J Biol Chem* (2016) 291(22):11939–53. doi: 10.1074/jbc.M115.702746
90. Mawatari S, Uto H, Ido A, Nakashima K, Suzuki T, Kanmura S, et al. Hepatitis C Virus NS3/4A Protease Inhibits Complement Activation by Cleaving Complement Component 4. *PLoS One* (2013) 8(12):e82094. doi: 10.1371/journal.pone.0082094
91. Banerjee A, Mazumdar B, Meyer K, Di Bisceglie AM, Ray RB, Ray R. Transcriptional Repression of C4 Complement by Hepatitis C Virus Proteins. *J Virol* (2011) 85(9):4157–66. doi: 10.1128/JVI.02449-10
92. Kim DW, Lee SA, Kim H, Won YS, Kim BJ. Naturally Occurring Mutations in the Nonstructural Region 5B of Hepatitis C Virus (HCV) From Treatment-Naive Korean Patients Chronically Infected With HCV Genotype 1b. *PLoS One* (2014) 9(1):e87773. doi: 10.1371/journal.pone.0087773
93. Avirutnan P, Fuchs A, Hauhart RE, Somnuk P, Youn S, Diamond MS, et al. Antagonism of the Complement Component C4 by Flavivirus Nonstructural Protein NS1. *J Exp Med* (2010) 207(4):793–806. doi: 10.1084/jem.20092545
94. Agrawal P, Nawadkar R, Ojha H, Kumar J, Sahu A. Complement Evasion Strategies of Viruses: an Overview. *Front Microbiol* (2017) 8:1117. doi: 10.3389/fmicb.2017.01117
95. Mellors J, Tipton T, Longet S, Carroll M. Viral Evasion of the Complement System and Its Importance for Vaccines and Therapeutics. *Front Immunol* (2020) 11:1450. doi: 10.3389/fimmu.2020.01450
96. Bugdaci MS, Alkim C, Karaca C, Kesici B, Bayraktar B, Sokmen M. Could Complement C4 be an Alternative to Biopsy for Chronic Hepatitis B Histopathologic Findings? *J Clin Gastroenterol* (2011) 45(5):449–55. doi: 10.1097/MCG.0b013e31820f7ee5
97. Bugdaci MS, Karaca C, Alkim C, Kesici B, Bayraktar B, Sokmen M. Serum Complement C4 in Chronic Hepatitis C: Correlation With Histopathologic Findings and Disease Activity. *Turk J Gastroenterol* (2012) 23(1):33–7. doi: 10.4318/tjg.2012.0310
98. Chowdhury SJ, Karra VK, Bharali R, Kar P. Role of Complement Component C4 in Treatment Response and Disease Progression in Chronic Hepatitis C Patients. *J Viral Hepat* (2015) 22(8):671–4. doi: 10.1111/jvh.12383
99. El-Fatah Fahmy Hanno A, Mohiedeen KM, Deghedy A, Sayed R. Serum Complements C3 and C4 in Chronic HCV Infection and Their Correlation With Response to Pegylated Interferon and Ribavirin Treatment. *Arab J Gastroenterol* (2014) 15(2):58–62. doi: 10.1016/j.ajg.2014.04.005
100. Chang ML, Tsou YK, Hu TH, Lin CH, Lin WR, Sung CM, et al. Distinct Patterns of the Lipid Alterations Between Genotype 1 and 2 Chronic Hepatitis C Patients After Viral Clearance. *PLoS One* (2014) 9(8):e104783. doi: 10.1371/journal.pone.0104783
101. Fuchs A, Lin TY, Beasley DW, Stover CM, Schwaebler WJ, Pierson TC, et al. Direct Complement Restriction of Flavivirus Infection Requires Glycan Recognition by Mannose-Binding Lectin. *Cell Host Microbe* (2010) 8(2):186–95. doi: 10.1016/j.chom.2010.07.007
102. Sane J, Laine O, Makela S, Paakkala A, Jarva H, Mustonen J, et al. Complement Activation in Puumala Hantavirus Infection Correlates With Disease Severity. *Ann Med* (2012) 44(5):468–75. doi: 10.3109/07853890.2011.573500
103. Bottermann M, Foss S, Caddy SL, Cliff D, van Tienen LM, Vaysburd M, et al. Complement C4 Prevents Viral Infection Through Capsid Inactivation. *Cell Host Microbe* (2019) 25(4):617–29 e7. doi: 10.1016/j.chom.2019.02.016
104. Conway EM, Prydzial ELG. Is the COVID-19 Thrombotic Catastrophe Complement-Connected? *J Thromb Haemost* (2020) 18(11):2812–22. doi: 10.1111/jth.15050
105. Jiang Y, Zhao G, Song N, Li P, Chen Y, Guo Y, et al. Blockade of the C5a-C5aR Axis Alleviates Lung Damage in Hdp4-Transgenic Mice Infected With MERS-CoV. *Emerg Microbes Infect* (2018) 7(1):77. doi: 10.1038/s41426-018-0063-8
106. Gralinski LE, Sheahan TP, Morrison TE, Menachery VD, Jensen K, Leist SR, et al. Complement Activation Contributes to Severe Acute Respiratory Syndrome Coronavirus Pathogenesis. *mBio* (2018) 9(5):1–15. doi: 10.1128/mBio.01753-18
107. Fox SE, Akmatbekov A, Harbert JL, Li G, Quincy Brown J, Vander Heide RS. Pulmonary and Cardiac Pathology in African American Patients With COVID-19: an Autopsy Series From New Orleans. *Lancet Respir Med* (2020) 8(7):681–6. doi: 10.1016/S2213-2600(20)30243-5
108. Magro C, Mulvey JJ, Berlin D, Nuovo G, Salvatore S, Harp J, et al. Complement Associated Microvascular Injury and Thrombosis in the Pathogenesis of Severe COVID-19 Infection: a Report of Five Cases. *Transl Res* (2020) 220:1–13. doi: 10.1016/j.trsl.2020.04.007
109. Watanabe Y, Allen JD, Wrapp D, McLellan JS, Crispin M. Site-Specific Glycan Analysis of the SARS-CoV-2 Spike. *Science* (2020) 369(6501):330–3. doi: 10.1126/science.abb9983
110. Romano C, Del Mastro A, Sellitto A, Solaro E, Esposito S, Cuomo G. Tocilizumab Reduces Complement C3 and C4 Serum Levels in Rheumatoid Arthritis Patients. *Clin Rheumatol* (2018) 37(6):1695–700. doi: 10.1007/s10067-018-3992-7
111. Qaddoori Y, Abrams ST, Mould P, Alhamdi Y, Christmas SE, Wang G, et al. Extracellular Histones Inhibit Complement Activation Through Interacting With Complement Component 4. *J Immunol* (2018) 200(12):4125–33. doi: 10.4049/jimmunol.1700779
112. Vogt LM, Talens S, Kwasniewicz E, Scavenius C, Struglics A, Enghild JJ, et al. Activation of Complement by Pigment Epithelium-Derived Factor in Rheumatoid Arthritis. *J Immunol* (2017) 199(3):1113–21. doi: 10.4049/jimmunol.1700018
113. Sinha VK, Sharma OP, Kumar MS. Insight Into the Intermolecular Recognition Mechanism Involved in Complement Component 4 Activation Through Serine Protease-Trypsin. *J Biomol Struct Dyn* (2018) 36(3):575–89. doi: 10.1080/07391102.2017.1288658
114. Mershon-Shier KL, Vasuthasawat A, Takahashi K, Morrison SL, Beenhouwer DO. In Vitro C3 Deposition on Cryptococcus Capsule Occurs via Multiple Complement Activation Pathways. *Mol Immunol* (2011) 48(15-16):2009–18. doi: 10.1016/j.molimm.2011.06.215

115. Takahashi M, Ishida Y, Iwaki D, Kanno K, Suzuki T, Endo Y, et al. Essential Role of Mannose-Binding Lectin-Associated Serine Protease-1 in Activation of the Complement Factor D. *J Exp Med* (2010) 207(1):29–37. doi: 10.1084/jem.20090633
116. Matsushita M, Okada H. Alternative Complement Pathway Activation by C4b Deposited During Classical Pathway Activation. *J Immunol* (1986) 136(8):2994–8.
117. Farries TC, Steuer KL, Atkinson JP. The Mechanism of Activation of the Alternative Pathway of Complement by Cell-Bound C4b. *Mol Immunol* (1990) 27(11):1155–61. doi: 10.1016/0161-5890(90)90104-8
118. Meri S, Pangburn MK. A Mechanism of Activation of the Alternative Complement Pathway by the Classical Pathway: Protection of C3b From Inactivation by Covalent Attachment to C4b. *Eur J Immunol* (1990) 20(12):2555–61. doi: 10.1002/eji.1830201205
119. Selander B, Martensson U, Weintraub A, Holmstrom E, Matsushita M, Thiel S, et al. Mannan-Binding Lectin Activates C3 and the Alternative Complement Pathway Without Involvement of C2. *J Clin Invest* (2006) 116(5):1425–34. doi: 10.1172/JCI25982
120. Dumestre-Perard C, Lamy B, Aldebert D, Lemaire-Vieille C, Grillot R, Brion JP, et al. Aspergillus Conidia Activate the Complement by the Mannan-Binding Lectin C2 Bypass Mechanism. *J Immunol* (2008) 181(10):7100–5. doi: 10.4049/jimmunol.181.10.7100
121. Tateishi K, Matsushita M. Activation of the Alternative Complement Pathway by Mannose-Binding Lectin via a C2-Bypass Pathway. *Microbiol Immunol* (2011) 55(11):817–21. doi: 10.1111/j.1348-0421.2011.00378.x
122. May JE, Frank MM. Hemolysis of Sheep Erythrocytes in Guinea Pig Serum Deficient in the Fourth Component of Complement. I. Antibody and Serum Requirements. *J Immunol* (1973) 111(6):1671–7.
123. Yang Y, Lhotka K, Chung EK, Eder P, Neumair F, Yu CY. Complete Complement Components C4A and C4B Deficiencies in Human Kidney Diseases and Systemic Lupus Erythematosus. *J Immunol* (2004) 173(4):2803–14. doi: 10.4049/jimmunol.173.4.2803
124. Schweinle JE, Ezekowitz RA, Tenner AJ, Kuhlman M, Joiner KA. Human Mannose-Binding Protein Activates the Alternative Complement Pathway and Enhances Serum Bactericidal Activity on a Mannose-Rich Isolate of Salmonella. *J Clin Invest* (1989) 84(6):1821–9. doi: 10.1172/JCI114367
125. Atkinson JP, Frank MM. Bypassing Complement: Evolutionary Lessons and Future Implications. *J Clin Invest* (2006) 116(5):1215–8. doi: 10.1172/JCI28622
126. Schwaible WJ, Lynch NJ, Clark JE, Marber M, Samani NJ, Ali YM, et al. Targeting of Mannan-Binding Lectin-Associated Serine Protease-2 Confers Protection From Myocardial and Gastrointestinal Ischemia/Reperfusion Injury. *Proc Natl Acad Sci USA* (2011) 108(18):7523–8. doi: 10.1073/pnas.1101748108
127. Gulla KC, Gupta K, Krarup A, Gal P, Schwaible WJ, Sim RB, et al. Activation of Mannan-Binding Lectin-Associated Serine Proteases Leads to Generation of a Fibrin Clot. *Immunology* (2010) 129(4):482–95. doi: 10.1111/j.1365-2567.2009.03200.x
128. Megyeri M, Mako V, Beinrohr L, Doleschall Z, Prohaszka Z, Cervenak L, et al. Complement Protease MASP-1 Activates Human Endothelial Cells: PAR4 Activation Is a Link Between Complement and Endothelial Function. *J Immunol* (2009) 183(5):3409–16. doi: 10.4049/jimmunol.0900879
129. Asgari E, Farrar CA, Lynch N, Ali YM, Roscher S, Stover C, et al. Mannan-Binding Lectin-Associated Serine Protease 2 Is Critical for the Development of Renal Ischemia Reperfusion Injury and Mediates Tissue Injury in the Absence of Complement C4. *FASEB J* (2014) 28(9):3996–4003. doi: 10.1096/fj.13-246306
130. Ali YM, Lynch NJ, Haleem KS, Fujita T, Endo Y, Hansen S, et al. The Lectin Pathway of Complement Activation Is a Critical Component of the Innate Immune Response to Pneumococcal Infection. *PLoS Pathog* (2012) 8(7):e1002793. doi: 10.1371/journal.ppat.1002793
131. Brinkmann CR, Jensen L, Dagnaes-Hansen F, Holm IE, Endo Y, Fujita T, et al. Mitochondria and the Lectin Pathway of Complement. *J Biol Chem* (2013) 288(12):8016–27. doi: 10.1074/jbc.M112.430249
132. Keizer MP, Pouw RB, Kamp AM, Patiwaal S, Marsman G, Hart MH, et al. TFPI Inhibits Lectin Pathway of Complement Activation by Direct Interaction With MASP-2. *Eur J Immunol* (2015) 45(2):544–50. doi: 10.1002/eji.201445070
133. Gorski JP, Hugli TE, Muller-Eberhard HJ. C4a: the Third Anaphylatoxin of the Human Complement System. *Proc Natl Acad Sci USA* (1979) 76(10):5299–302. doi: 10.1073/pnas.76.10.5299
134. Barnum SR. C4a: an Anaphylatoxin in Name Only. *J Innate Immun* (2015) 7(4):333–9. doi: 10.1159/000371423
135. Tsuruta T, Yamamoto T, Matsubara S, Nagasawa S, Tanase S, Tanaka J, et al. Novel Function of C4a Anaphylatoxin. Release From Monocytes of Protein Which Inhibits Monocyte Chemotaxis. *Am J Pathol* (1993) 142(6):1848–57.
136. Murakami Y, Yamamoto T, Imamichi T, Nagasawa S. Cellular Responses of Guinea-Pig Macrophages to C4a; Inhibition of C3a-Induced O₂- Generation by C4a. *Immunol Lett* (1993) 36(3):301–4. doi: 10.1016/0165-2478(93)90104-A
137. Lienenklaus S, Ames RS, Tornetta MA, Sarau HM, Foley JJ, Crass T, et al. Human Anaphylatoxin C4a Is a Potent Agonist of the Guinea Pig But Not the Human C3a Receptor. *J Immunol* (1998) 161(5):2089–93.
138. Jiang X, Ma Y, Yu J, Li H, Xie F. Protective Effect of C4a Against Hyperoxic Lung Injury via a Macrophage-Dependent But Not a Neutrophil/Lymphocyte-Dependent Signaling Pathway. *Mol Med Rep* (2016) 13(2):1250–6. doi: 10.3892/mmr.2015.4651
139. Xie P, Nishiura H, Semba U, Chen J, Zhao R, Kuniyasu A, et al. Inhibitory Effects of C4a on Chemoattractant and Secretagogue Functions of the Other Anaphylatoxins via Gi Protein-Adenylyl Cyclase Inhibition Pathway in Mast Cells. *Int Immunopharmacol* (2012) 12(1):158–68. doi: 10.1016/j.intimp.2011.11.006
140. Zhao Y, Xu H, Yu W, Xie BD. Complement Anaphylatoxin C4a Inhibits C5a-Induced Neointima Formation Following Arterial Injury. *Mol Med Rep* (2014) 10(1):45–52. doi: 10.3892/mmr.2014.2176
141. Hofer J, Forster F, Isenman DE, Wahrmann M, Leitner J, Holzl MA, et al. Ig-Like Transcript 4 as a Cellular Receptor for Soluble Complement Fragment C4d. *FASEB J* (2016) 30(4):1492–503. doi: 10.1096/fj.15-275594
142. Gregori S, Tomasoni D, Pacciani V, Scirpoli M, Battaglia M, Magnani CF, et al. Differentiation of Type 1 T Regulatory Cells (Tr1) by Tolerogenic DC-10 Requires the IL-10-Dependent ILT4/HLA-G Pathway. *Blood* (2010) 116(6):935–44. doi: 10.1182/blood-2009-07-234872
143. Anderson KJ, Allen RL. Regulation of T-Cell Immunity by Leucocyte Immunoglobulin-Like Receptors: Innate Immune Receptors for Self on Antigen-Presenting Cells. *Immunology* (2009) 127(1):8–17. doi: 10.1111/j.1365-2567.2009.03097.x
144. Ristich V, Zhang W, Liang S, Horuzsko A. Mechanisms of Prolongation of Allograft Survival by HLA-G/ILT4-Modified Dendritic Cells. *Hum Immunol* (2007) 68(4):264–71. doi: 10.1016/j.humimm.2006.11.008
145. Hunt JS, Petroff MG, McIntire RH, Ober C. HLA-G and Immune Tolerance in Pregnancy. *FASEB J* (2005) 19(7):681–93. doi: 10.1096/fj.04-2078rev
146. Kubo T, Uchida Y, Watanabe Y, Abe M, Nakamura A, Ono M, et al. Augmented TLR9-Induced Btk Activation in PIR-B-Deficient B-1 Cells Provokes Excessive Autoantibody Production and Autoimmunity. *J Exp Med* (2009) 206(9):1971–82. doi: 10.1084/jem.20082392
147. Nakamura A, Kobayashi E, Takai T. Exacerbated Graft-Versus-Host Disease in PIRB^{-/-} Mice. *Nat Immunol* (2004) 5(6):623–9. doi: 10.1038/ni1074
148. Ballou M, McLean RH, Yunis EJ, Awdeh ZL, O'Neill GJ, Einarson M, et al. C4 Polymorphism and HLA Linkage: Studies in a Family With Hereditary C4 Deficiency. *Clin Immunol Immunopathol* (1981) 20(3):354–60. doi: 10.1016/0090-1229(81)90146-X
149. Raum D, Awdeh Z, Alper CA. BF Types and the Mode of Inheritance of Insulin-Dependent Diabetes Mellitus (IDDM). *Immunogenetics* (1981) 12(1–2):59–74. doi: 10.1007/BF01561651
150. Fielder AH, Walport MJ, Batchelor JR, Rynes RI, Black CM, Dodi IA, et al. Family Study of the Major Histocompatibility Complex in Patients With Systemic Lupus Erythematosus: Importance of Null Alleles of C4A and C4B in Determining Disease Susceptibility. *Br Med J (Clin Res Ed)* (1983) 286(6363):425–8. doi: 10.1136/bmj.286.6363.425
151. Kjellman M, Laurell AB, Low B, Sjöholm AG. Homozygous Deficiency of C4 in a Child With a Lupus Erythematosus Syndrome. *Clin Genet* (1982) 22(6):331–9. doi: 10.1111/j.1399-0004.1982.tb01849.x
152. Mascart-Lemone F, Hauptmann G, Goetz J, Duchateau J, Delespesse G, Vray B, et al. Genetic Deficiency of C4 Presenting With Recurrent Infections and a SLE-Like Disease. Genetic and Immunologic Studies. *Am J Med* (1983) 75(2):295–304. doi: 10.1016/0002-9343(83)91208-1

153. Schaller JG, Gilliland BG, Ochs HD, Leddy JP, Agodoa LC, Rosenfeld SI. Severe Systemic Lupus Erythematosus With Nephritis in a Boy With Deficiency of the Fourth Component of Complement. *Arthritis Rheum* (1977) 20(8):1519–25. doi: 10.1002/art.1780200812
154. Chatterjee P, Agyemang AF, Alimzhanov MB, Degn S, Tsiftoglou SA, Alicot E, et al. Complement C4 Maintains Peripheral B-Cell Tolerance in a Myeloid Cell Dependent Manner. *Eur J Immunol* (2013) 43(9):2441–50. doi: 10.1002/eji.201343412
155. Castley AS, Martinez OP. Molecular Analysis of Complement Component C4 Gene Copy Number. *Methods Mol Biol* (2012) 882:159–71. doi: 10.1007/978-1-61779-842-9_9
156. Rupert KL, Moulds JM, Yang Y, Arnett FC, Warren RW, Reveille JD, et al. The Molecular Basis of Complete Complement C4A and C4B Deficiencies in a Systemic Lupus Erythematosus Patient With Homozygous C4A and C4B Mutant Genes. *J Immunol* (2002) 169(3):1570–8. doi: 10.4049/jimmunol.169.3.1570
157. Kanduc D. Proteome-Wide Epstein-BarrVirus Analysis of Peptide Sharing With Human Systemic Lupus Erythematosus Autoantigens. *Isr Med Assoc J* (2019) 21(7):444–8.
158. Segal Y, Dahan S, Calabro M, Kanduc D, Shoenfeld Y. HPV and Systemic Lupus Erythematosus: a Mosaic of Potential Crossreactions. *Immunol Res* (2017) 65(2):564–71. doi: 10.1007/s12026-016-8890-y
159. Leungwutiwong P, Ittiprasert W, Saikhun K, Tong-Ngam P, Akapirat S, Chattanadee S, et al. Impairment of CD4+CD25+ Regulatory T Cells in C4-Deficient Mice. *Asian Pac J Allergy Immunol* (2011) 29(3):220–8.
160. Ricklin D, Hajishengallis G, Yang K, Lambris JD. Complement: a Key System for Immune Surveillance and Homeostasis. *Nat Immunol* (2010) 11(9):785–97. doi: 10.1038/ni.1923
161. Nozaki M, Raisler BJ, Sakurai E, Sarma JV, Barnum SR, Lambris JD, et al. Drusen Complement Components C3a and C5a Promote Choroidal Neovascularization. *Proc Natl Acad Sci USA* (2006) 103(7):2328–33. doi: 10.1073/pnas.0408835103
162. Ercolini AM, Miller SD. The Role of Infections in Autoimmune Disease. *Clin Exp Immunol* (2009) 155(1):1–15. doi: 10.1111/j.1365-2249.2008.03834.x
163. Getts DR, Chastain EM, Terry RL, Miller SD. Virus Infection, Antiviral Immunity, and Autoimmunity. *Immunol Rev* (2013) 255(1):197–209. doi: 10.1111/imr.12091
164. Barzilai O, Ram M, Shoenfeld Y. Viral Infection can Induce the Production of Autoantibodies. *Curr Opin Rheumatol* (2007) 19(6):636–43. doi: 10.1097/BOR.0b013e3282f0ad25
165. Sfriso P, Ghirardello A, Botsios C, Tonon M, Zen M, Bassi N, et al. Infections and Autoimmunity: the Multifaceted Relationship. *J Leukoc Biol* (2010) 87(3):385–95. doi: 10.1189/jlb.0709517
166. Carroll MC. The Role of Complement in B Cell Activation and Tolerance. *Adv Immunol* (2000) 74:61–88. doi: 10.1016/S0065-2776(08)60908-6

Conflict of Interest: The authors declare that the research was conducted in the absence of any commercial or financial relationships that could be construed as a potential conflict of interest.

Copyright © 2021 Wang and Liu. This is an open-access article distributed under the terms of the Creative Commons Attribution License (CC BY). The use, distribution or reproduction in other forums is permitted, provided the original author(s) and the copyright owner(s) are credited and that the original publication in this journal is cited, in accordance with accepted academic practice. No use, distribution or reproduction is permitted which does not comply with these terms.



Neutrophil Extracellular Traps Exacerbate Secondary Injury via Promoting Neuroinflammation and Blood–Spinal Cord Barrier Disruption in Spinal Cord Injury

Zhou Feng^{1†}, Lingxia Min^{1†}, Liang Liang², Beike Chen², Hui Chen¹, Yi Zhou¹, Weiwei Deng¹, Hongliang Liu^{1*} and Jingming Hou^{1*}

OPEN ACCESS

Edited by:

Shrikant R. Mulay,
Central Drug Research Institute
(CSIR), India

Reviewed by:

Hao-Sen Chiang,
National Taiwan University, Taiwan
Violetta Borelli,
University of Trieste, Italy

*Correspondence:

Jingming Hou
jingminghou@hotmail.com
Hongliang Liu
liuhongliangkt@163.com

[†]These authors have contributed
equally to this work and share
first authorship

Specialty section:

This article was submitted to
Molecular Innate Immunity,
a section of the journal
Frontiers in Immunology

Received: 21 April 2021

Accepted: 19 July 2021

Published: 11 August 2021

Citation:

Feng Z, Min L, Liang L,
Chen B, Chen H, Zhou Y, Deng W,
Liu H and Hou J (2021) Neutrophil
Extracellular Traps Exacerbate
Secondary Injury via Promoting
Neuroinflammation and Blood–Spinal
Cord Barrier Disruption
in Spinal Cord Injury.
Front. Immunol. 12:698249.
doi: 10.3389/fimmu.2021.698249

¹ Department of Rehabilitation, Southwest Hospital, Third Military Medical University (Army Medical University), Chongqing, China, ² Department of Neurosurgery, Southwest Hospital, Third Military Medical University (Army Medical University), Chongqing, China

As the first inflammatory cell recruited to the site of spinal cord injury (SCI), neutrophils were reported to be detrimental to SCI. However, the precise mechanisms as to how neutrophils exacerbate SCI remain largely obscure. In the present study, we demonstrated that infiltrated neutrophils produce neutrophil extracellular traps (NETs), which subsequently promote neuroinflammation and blood–spinal cord barrier disruption to aggravate spinal cord edema and neuronal apoptosis following SCI in rats. Both inhibition of NETs formation by peptidylarginine deiminase 4 (PAD4) inhibitor and disruption of NETs by DNase 1 alleviate secondary damage, thus restraining scar formation and promoting functional recovery after SCI. Furthermore, we found that NETs exacerbate SCI partly via elevating transient receptor potential vanilloid type 4 (TRPV4) level in the injured spinal cord. Therefore, our results indicate that NETs might be a promising therapeutic target for SCI.

Keywords: spinal cord injury, neutrophils, neutrophil extracellular traps, blood–spinal cord barrier, neuroinflammation

INTRODUCTION

Spinal cord injury (SCI) is a devastating central nervous system (CNS) trauma due to its high mobility and tremendous social and financial burden (1). Unfortunately, current treatments for SCI are far from satisfactory (2), which should mainly be attributed to the limitations in understanding of its pathophysiological mechanisms (1). Generally, SCI consists of primary injury and subsequent secondary injury mechanisms (3). Primary injury refers to initial impact to the spinal cord caused by traumatic mechanical forces, while secondary injury is known as a series of biochemical, molecular, and cellular cascades that cause further damage (4). Since primary injury happens unexpectedly and cannot be prevented, targeting secondary injury mechanisms is crucial for SCI treatment (5).

As the first inflammatory cell recruited to the lesion site of SCI, neutrophils play significant roles in the secondary injury mechanisms of SCI (6). Neutrophils migrate to the injured spinal cord within hours and peak in 1 to 3 days after SCI (7, 8). After infiltrating, neutrophils produce and

release pro-inflammatory mediators, oxidative enzymes (such as myeloperoxidase; MPO), proteolytic enzymes (such as matrix metalloproteinase-9 and elastase), and reactive oxygen species (ROS) to promote secondary damage, thus aggravating neurological deficit (7, 9, 10). In addition to secreting cytotoxic products, neutrophils were recently revealed to contribute to diverse diseases *via* releasing neutrophil extracellular traps (NETs) (11), an extracellular fibrous network firstly described by Brinkmann et al. (12). Except for CNS infections (13, 14), NETs were also demonstrated to be implicated in ischemic stroke (15), intracerebral hemorrhage (16), traumatic brain injury (17), and even neurodegenerative diseases (18). However, whether NETs contribute to pathophysiological changes in SCI remains unclear.

Therefore, we explored whether NETs promote secondary injury following SCI, and the potential mechanisms as to how NETs exacerbate SCI in the present study.

MATERIALS AND METHODS

SCI Induction and Experimental Design

One hundred and ninety-eight female Sprague–Dawley (SD) rats (250–300 g; Army Medical University) were used in the present experimentation. All rats were maintained under a 12-h light/dark cycle condition with free access to food and water. Animal use protocols were approved by the Animal Care and Use Committee of the Army Medical University (NO. SYXK20170002).

The clip-compression SCI model was induced according to a previous method (19). Briefly, after anesthetized by pentobarbital (40 mg/kg; intraperitoneally), animals were subjected to T9 laminectomy using aseptic techniques. Then, a clip with 50-g closing force was used to compress the exposed spinal cord for 60 s to induce SCI. The same surgical procedure without compression was performed in sham-operated animals. Manual bladder emptying was carried out twice daily until the recovery of normal bladder control.

Animals were assigned to five groups: sham controls without spinal cord compression (sham group); SCI models with Cl-amidine (diluted in 5% DMSO; MedChemExpress; 50 mg/kg) treatment (Cl-amidine group); SCI models with vehicle (corresponding dose of 5% DMSO) treatment (DMSO group); SCI models with DNase1 (diluted in saline; Roche; 5 mg/kg) treatment (DNase1 group); and SCI models with vehicle (corresponding dose of saline) treatment (Saline group). For drug administration, Cl-amidine was administered through intraperitoneal injection after SCI induction, and DNase1 was administered through the tail vein 1 h after SCI induction. The dosage and timing of Cl-amidine and DNase1 administration were performed based on the previous study (17).

Immunofluorescence

Immunofluorescence labeling was performed as described previously (20). After being deeply anesthetized, animals were transcardially perfused with PBS and their spinal cords were removed. Obtained samples were fixed with 4% paraformaldehyde

and then dehydrated with 30% sucrose solution. Serial longitudinal sections (10 μ m) were prepared using a cryostat microtome. After washing in PBS containing 0.3% Triton X-100, sections were incubated with relevant primary antibodies at 4°C overnight. Then, sections were washed with PBS and incubated with appropriate secondary antibodies at 37°C for 2 h. Cell nuclei were stained using DAPI. Finally, stained sections were viewed and imaged under a confocal microscope (LSM-880; Zeiss). The following primary antibodies were used: rabbit anti-Myeloperoxidase (MPO, Abcam; 1:50), mouse anti-Histone H3 (citrulline R2+ R8 +R17) (Abcam; 1:100), mouse anti-glial fibrillary acidic protein (GFAP) (Bioss; 1:500), rabbit anti-Laminin (Dako; 1:1000), mouse anti-CD31 (Abcam; 1:100), and rabbit anti-transient receptor potential vanilloid type 4 (TRPV4) (Abcam; 1:100).

SYTOX Orange staining was performed as previous described (21). Sections were stained with SYTOX Orange (Molecular Probes, Inc.) at a concentration of 5 μ M for 10 min. Then, stained sections were viewed and imaged under a confocal microscope (LSM-880; Zeiss) after washing with PBS.

Western Blot Analysis

Western blot (WB) was performed according to a previous method (22). Briefly, after animals were anesthetized and decapitated, spinal cord tissues of the lesion site were removed and collected immediately on ice (8). Then, samples were homogenized and lysed in RIPA buffer containing protease and phosphatase inhibitors. After centrifuging at 12,000 rpm for 10 min at 4°C, protein concentrations were determined using a BCA Assay Kit (Beyotime). Equal amounts of protein lysate (20 μ g) were separated by 10% SDS-PAGE electrophoresis, followed by transferring onto PVDF membranes. After blocking in 5% fresh-non-fat skim milk prepared in TBST for 2 h at room temperature, membranes were incubated with the appropriate primary antibodies at 4°C overnight. Then, membranes were incubated with corresponding HRP-conjugated secondary antibodies for 2 h at room temperature after washing with TBST. Finally, protein bands were visualized with chemiluminescent HRP Substrate (Thermo Fisher) under Western Lightning-ECL (Bio-Rad, USA). The following primary antibodies were used: mouse anti-Histone H3 (citrulline R2+ R8 +R17) (Abcam; 1:1000), rabbit anti-ZO-1 (Abcam; 1:5000), rabbit anti-occludin (Abcam; 1:5000), rabbit anti-transient receptor potential vanilloid type 4 (TRPV4) (Abcam; 1:1000), and mouse anti-GAPDH (Zen-bio; 1:5000).

Luminex Liquid Suspension Chip Assay

Luminex liquid suspension chip assay was applied to analyze inflammatory cytokines [including tumor necrosis factor (TNF)- α , interferon (IFN)- γ , interleukin (IL)-1 β , IL-6, and IL-10], which was performed by Wayen Biotechnologies (Shanghai, China). Briefly, samples were obtained after spinal cord tissues from the same site of WB were lysed and centrifuged at 10,000 rpm for 10 min. After protein concentrations were measured, equal amount of protein (45 μ g) sample was taken to diluted to equal volume (50 μ l). Then, samples were incubated in 96-well plates embedded with

microbeads for 1 h, after which they were incubated with detection antibodies for 30 min. Finally, streptavidin-PE was added into each well to be incubated for 10 min, and values were measured by the Bio-Plex MAGPIX System (Bio-Rad).

TUNEL Staining

After washing in PBS containing 0.3% Triton X-100, sections were incubated with the primary antibody mouse anti-NeuN (Abcam; 1:200), which is used to mark neurons, at 4°C overnight and then incubated with appropriate secondary antibody at 37°C for 2 h. Subsequently, sections were incubated with TUNEL staining mixture (In Situ Cell Death Detection Kit, TMR red; Roche) at 37°C for 1 h. Cell nuclei were stained using DAPI. Finally, stained sections were imaged under a confocal microscope (LSM-880; Zeiss). TUNEL-positive cells and neurons were counted using ImageJ software (National Institutes of Health, USA).

H&E Staining

Firstly, sections were stained with hematoxylin for 1 min and washed three times in distilled water. Then, sections were stained with eosin for 2 min. Stained sections were imaged using a light microscope.

Electrophysiological Assessment

The functional integrity of spinal pathway was evaluated by motor evoked potentials (MEPs) according to a previous method (23). Briefly, after being anesthetized with 1% pentobarbital sodium (20 mg/kg; intraperitoneally), experimental animals were implanted with four monopolar needle electrodes in appropriate locations: one at the base of the nose (acting as the anode), one at the midpoint between two ears (acting as the cathode), one into the gastrocnemius muscle (recording electrode), and the last one at the base of the tail (ground electrode). The brain was excited by electrical pulse (intensity 10 mA; width 0.1 ms; rate 1 Hz), and the base-to-peak amplitude of MEPs was recorded.

Behavioral Experiments

Motor function was evaluated with the Basso, Beattie, and Bresnahan (BBB) locomotor test on days 1, 7, 14, 21, and 28 after SCI induction. Briefly, experimental animals were observed by two evaluators to move freely in an open field for 5 min in a blinded manner. Motor function was evaluated according to the 0–21 BBB scoring. The average score of two evaluators was calculated to analysis.

Blood–Spinal Cord Barrier Permeability Evaluation

Blood–spinal cord barrier (BSCB) permeability was determined using Evans blue (EB) dye extravasation as previously described with some modifications (24). Briefly, 24 h after SCI, 2% (w/v) EB dye (5 ml/kg, Sigma Aldrich) solution in saline was administered through the femoral vein. One hour later, rats were anesthetized and perfused with saline. For extravasation quantification, injured spinal cord was removed and weighed immediately. Then, samples were homogenized in 400 µl of 50%

trichloroacetic acid and centrifuged at 10,000 g for 30 min. After incubating overnight at 4°C, samples were centrifuged at 10,000 g for 30 min, and supernatants were diluted fourfold with ethanol. Finally, fluorescence intensity was measured at 620/680 nm. Results were expressed as µg dye/g tissue.

For EB fluorescence, injured spinal cord was removed, fixed with 4% paraformaldehyde overnight, and dehydrated in 30% sucrose at 4°C. Then, samples were sectioned into 10-µm slices and observed using a confocal fluorescence microscope (LSM880, Zeiss).

Statistical Analysis

Statistical analysis was performed using GraphPad Prism 8.0. Single comparison between two groups was analyzed by two-tailed Student's *t* test. Multigroup comparisons were analyzed by one-way analysis of variance (ANOVA) followed by Bonferroni *post hoc* test. Data were presented as means ± standard deviation. *p* value below 0.05 was considered statistically significant.

RESULTS

Infiltrated Neutrophils Produce NETs in the Injured Spinal Cord

We first identified the presence of neutrophils and NETs at the epicenter of the SCI. Neutrophils peaked at 24 h and remained high until 3 days after SCI (**Supplementary Figure 1A**). At 24 h after SCI, a large number of neutrophils that were marked with MPO infiltrated into the injured spinal cord and produce NETs, which was characterized by citrullinated histone H3 (CitH3)⁺ neutrophils (**Figure 1A**). Furthermore, we visualized NETs (network of cell-free DNA structure) with SYTOX Orange staining in the lesion site at 24 h after SCI (**Figure 1B**). Quantification of the CitH3 levels at different time points in the injured spinal cord confirmed the presence of NETs (**Figure 1B** and **Supplementary Figure 1B**), while level of total histone H3 expression was not changed after SCI (**Supplementary Figure 2A**).

To demonstrate the effect of Cl-amidine, an inhibitor of enzyme peptidylarginine deiminase 4 (PAD4), which is the key enzyme mediating NETs formation, and DNase1 on restricting NETs, we firstly excluded the effect of vehicles (DMSO and saline) on NETs. We found that both DMSO and saline had no significant effect on the level of CitH3 in both sham and SCI rats (**Supplementary Figures S3A, B**). Administering Cl-amidine reduced NETs significantly after SCI (**Figure 2**). Similarly, degrading NETs with DNase1 also significantly reduced the level of NETs in the lesion site (**Figure 3**). Both Cl-amidine and DNase1 administration had no significant effect on the level of total histone H3 expression in SCI rats (**Supplementary Figures S2B, C**). Although we found that the peak of NETs was observed at 3 days after SCI, early administration of both Cl-amidine and DNase1 also significantly reduced the NETs at later stage (**Supplementary Figure S4**). These results suggest that infiltrated neutrophils produce NETs at the epicenter after SCI, which were prevented by both Cl-amidine and DNase1.

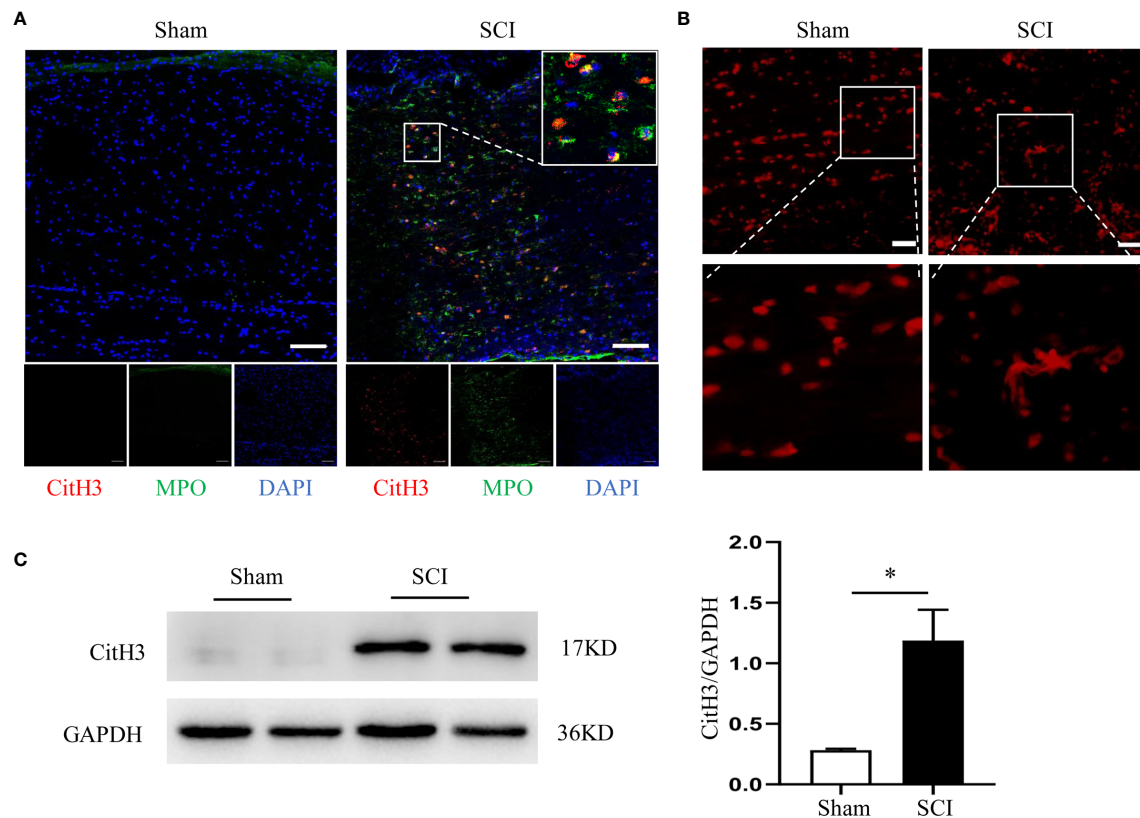


FIGURE 1 | Infiltrated neutrophils produce NETs in the injured spinal cord. **(A)** Representative images of CitH3 (red) and MPO (green) double-positive cells in spinal cord from sham-operated rats and SCI rats at 24 h after operation. Nuclear was marked with DAPI (blue). Scale bars = 100 μ m. **(B)** Representative images of network-like cell-free DNA structure by Sytox Orange staining. Scale bars = 200 μ m. **(C)** Representative immunoblots and quantification of the CitH3 levels in spinal cord of rats subjected to SCI or sham operation. GAPDH is used as a loading control. Data are presented as means \pm SD of $n = 9$ (* $p < 0.05$).

Restricting NETs Attenuates Neuroinflammation and Edema After SCI

Next, we evaluated the effect of NETs on neuroinflammation and edema after SCI. Local pro-inflammatory cytokines, including TNF- α , IFN- γ , IL-1 β , and IL-6, were increased, while anti-inflammatory cytokine IL-10 was decreased at 24 h after SCI, which are all reversed by both Cl-amidine and DNase1 treatment (**Figures 4A–E**). Moreover, SCI-induced acute edema is also attenuated by Cl-amidine and DNase1 (**Figure 4F**). Thus, restricting NETs attenuated neuroinflammation and edema after SCI.

Restricting NETs Reduces Cell Death After SCI

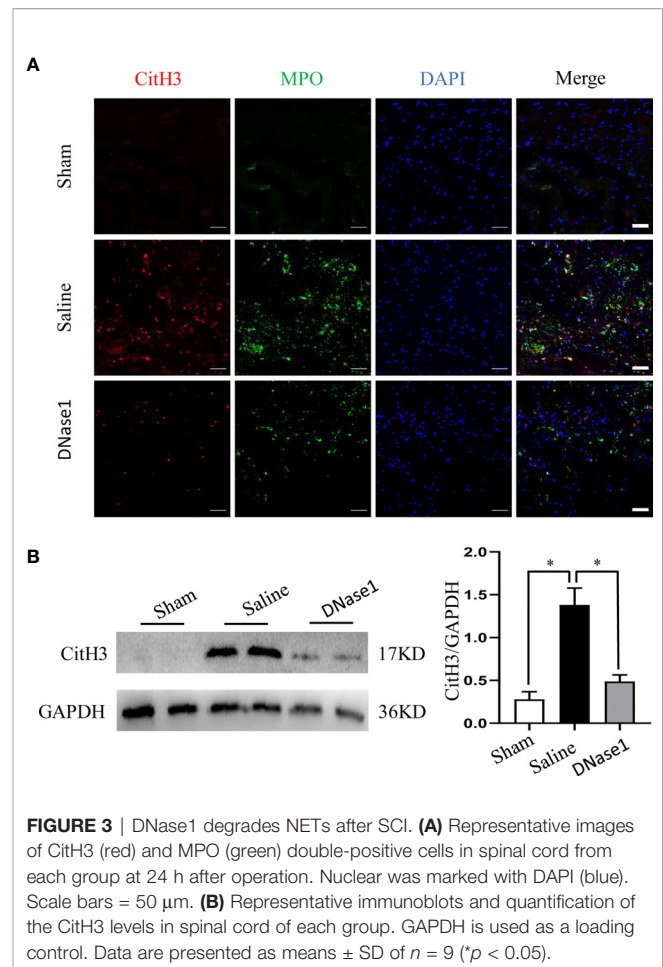
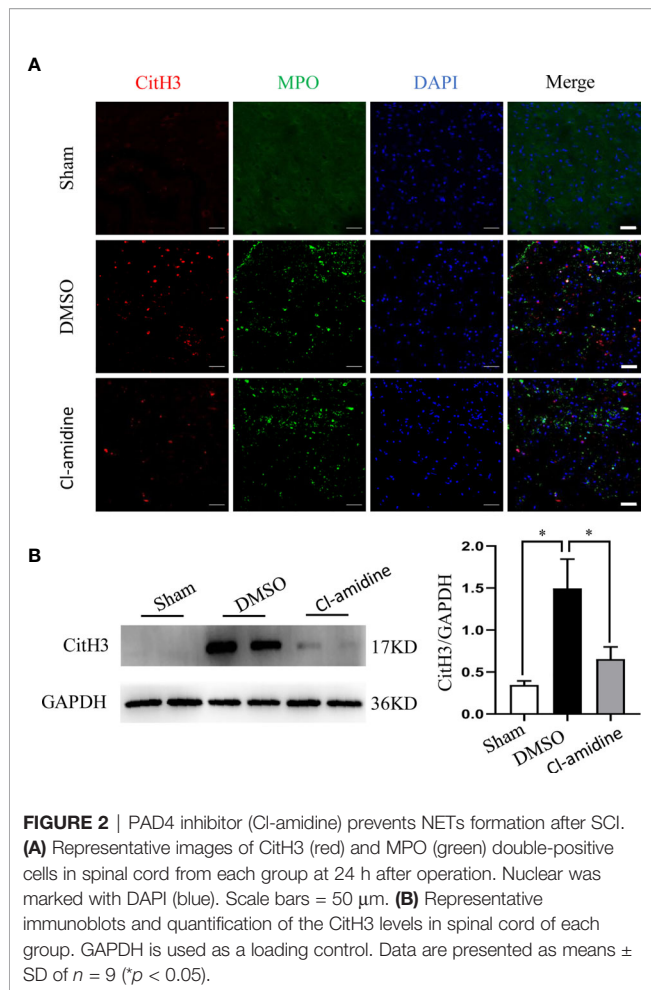
Furthermore, we evaluated the effect of NETs on cell death after SCI. SCI induced massive cell death at the epicenter of lesion at 24 h post-SCI, which was suppressed by both Cl-amidine and DNase1 (**Figures 5A, B**). Furthermore, confocal images of co-staining of NeuN and TUNEL indicate that both Cl-amidine and DNase1 reduce neuron death after SCI (**Figures 5A, C**). This finding suggests that NETs is an important cause of cell death after SCI.

Restricting NETs Reduces Scar Formation After SCI

To evaluate the effect of NETs on chronic phase of SCI, we assessed scarring (both glial and fibrotic) of lesion site at 28 days after SCI. Injury-induced glial scar formation, which is indicated by expression of GFAP, is significantly inhibited by both Cl-amidine and DNase1 administration (**Figures 6A, C**). In parallel, the amounts of laminin, which is the hallmark of the fibrotic scars hindering axon regeneration, in the lesions are significantly lower when NETs were restricted by Cl-amidine and DNase1 (**Figures 6B, D**). These results suggest that restricting NETs not only attenuates acute injury but also reduces chronic scar formation after SCI.

Restricting NETs Reduces Tissue Damage and Promotes Motor Function Recovery After SCI

To evaluate the functional consequences of NETs restriction after SCI, we assessed functional integrity of spinal pathway by MEPs and motor function by BBB locomotor test. Both restricting NETs with Cl-amidine and DNase1 reduce tissue damage in the spinal cord at 28 days after SCI (**Figure 7A**).



The representative records (**Figure 7B**) and amplitude (**Figure 7C**) of MEPs indicated that restricting NETs improve the functional integrity of motor pathway after SCI. Furthermore, motor function recovery evaluated by BBB test is significantly promoted following Cl-amidine and DNase1 treatment (**Figure 7D**). Taken together, these results suggest that restricting NETs reduced tissue damage and improved integrity of motor pathway and motor function recovery after SCI.

NETs Promote BSCB Disruption, Which May Be Partly Through Elevating TRPV4

Finally, we evaluated the effect of NETs on BSCB disruption and explored possible mechanisms. Both EB fluorescence and quantification of EB leakage indicate significant BSCB disruption at 24 h after SCI, which is ameliorated both by inhibiting NETs formation with Cl-amidine and degrading NETs with DNase1 (**Figures 8A–C**). In addition, the expression of tight junction proteins (ZO-1, occludin) that maintain the integrity of the BSCB is reduced after SCI, but prevented by Cl-amidine and DNase1 (**Figures 8D–F**). What is more, the expression of TRPV4 in CD-31-marked endothelial cells at the epicenter increases significantly after SCI, which is suppressed effectively by Cl-amidine and DNase1

(**Figures 9A–C**). Our results suggest that NETs promote BSCB disruption after SCI, which may be through, at least in part, elevating TRPV4.

DISCUSSION

In the present study, we have demonstrated that infiltrated neutrophils produce NETs in the lesion to exacerbate secondary injury *via* promoting neuroinflammation and blood–spinal cord barrier disruption after SCI. Both inhibiting NETs formation with Cl-amidine and degrading NETs with DNase1 reduce cell death, scar formation, and tissue damage, ultimately promoting motor function recovery, which benefits from alleviating neuroinflammation and blood–spinal cord barrier disruption partly by suppressing TRPV4.

In recent years, neutrophils were demonstrated to produce NETs in CNS under various pathological conditions to contribute to pathophysiology (11). In agreement with previous studies indicating the presence of NETs in stroke (15, 16) and traumatic brain injury (17), our present study demonstrated that infiltrated neutrophils produce NETs in the lesion after SCI.

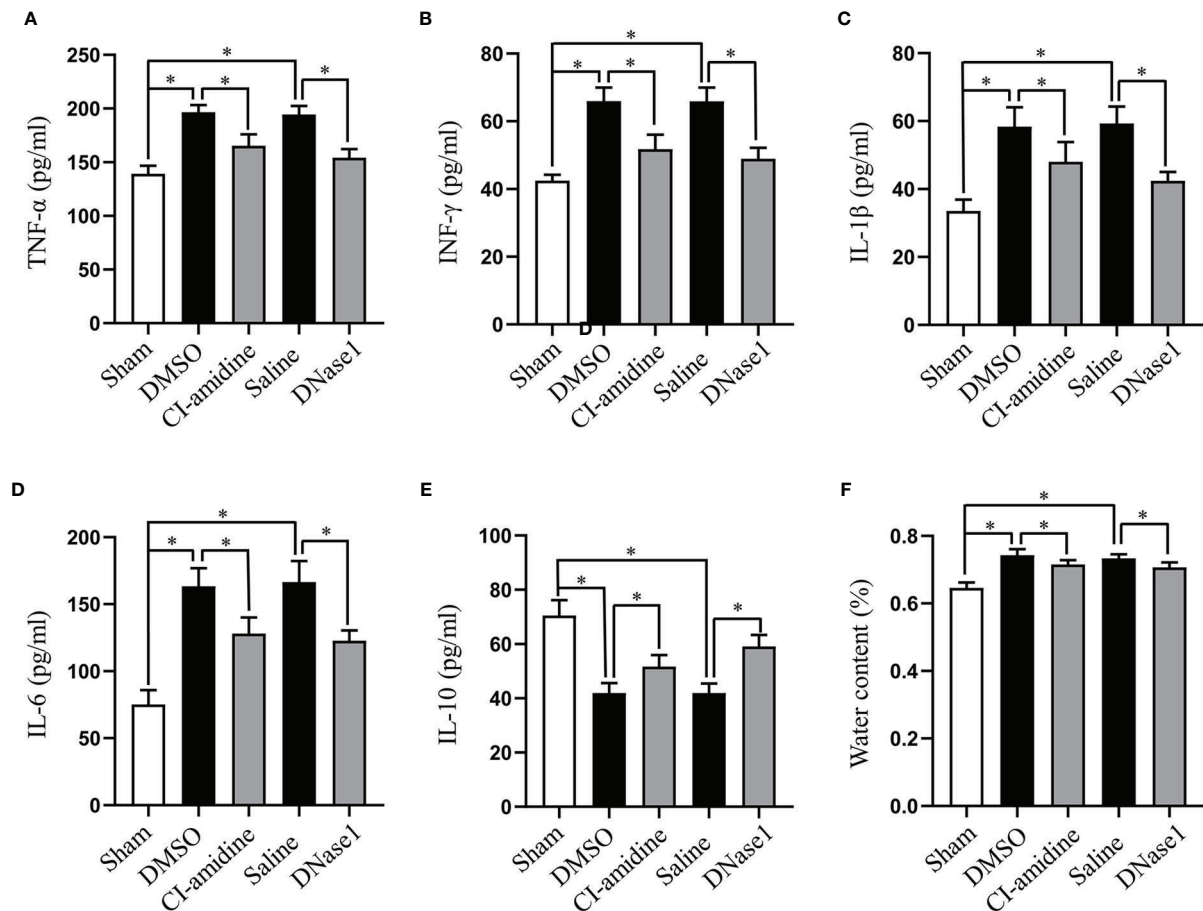


FIGURE 4 | Restricting NETs attenuates neuroinflammation and edema after SCI. Levels of (A) TNF- α , (B) IFN- γ , (C) IL-1 β , (D) IL-6, and (E) IL-10 in injured spinal cord of each group at 24 h after SCI. (F) Water contents of injured spinal cord from each group at 24 h after SCI. Data are presented as means \pm SD of $n = 6$ (* $p < 0.05$).

NETs are generally decorated with granular and cytosolic proteins, proteases, and histones (12), which are induced by the activation of PAD4 (25). The latter converts arginine to citrulline on histones to promote chromatin condensation (26); thus, it is essential for NETs formation (27). Despite the fact that neutrophil depletion is effective to block NETs formation, it is not an ideal treatment as the accompanying high risk of infection (17). Currently, inhibiting NETs formation with PAD4 inhibitor and degrading NETs with DNase1 are preferable strategies to restricting NETs (15, 17, 25). Our study corroborates the findings of previous researchers (15, 17), demonstrating that both Cl-amidine and DNase1 administration reduce NETs in CNS under pathological conditions.

Cell death, especially neuronal death, is a major pathological damage in the acute stage after SCI, which results from both primary and following secondary injury (4). Extremely preventing neuronal cell death is the goal of almost all neuroprotective therapies (2). Gratifyingly, we demonstrated that restricting NETs effectively reduces SCI-induced cell death, mainly neurons, in the present study. In addition, scar

formation at the lesion site is also a common pathological response in SCI (28). Local scar tissue consists of two components: fibrotic scar contains extracellular matrix proteins (such as laminin, fibronectin, and collagen) in the lesion core, and glial scar contains reactive astrocytes surrounding the lesion core (28, 29). Glial scar has long been considered to be a barrier to inhibit axonal regeneration and a potential therapeutic target to facilitate neural repair (30, 31). In recent years, fibrotic scar receives growing attention in CNS diseases, especially SCI (32–34). Attenuation of fibrotic scar formation has been suggested to be a therapeutic target to facilitate neurological function recovery after SCI (35, 36). In our study described here, we found that both glial and fibrotic scars are reduced *via* restricting NETs, which facilitate motor function recovery ultimately after SCI. What is more, our results indicate that NETs formation might be a potential mechanism for how infiltrated immune cells drive CNS fibrosis (37).

As the main early pathophysiological changes following SCI, local neuroinflammation and BSCB disruption reinforce mutually and promote secondary injury after SCI (1, 2, 4).

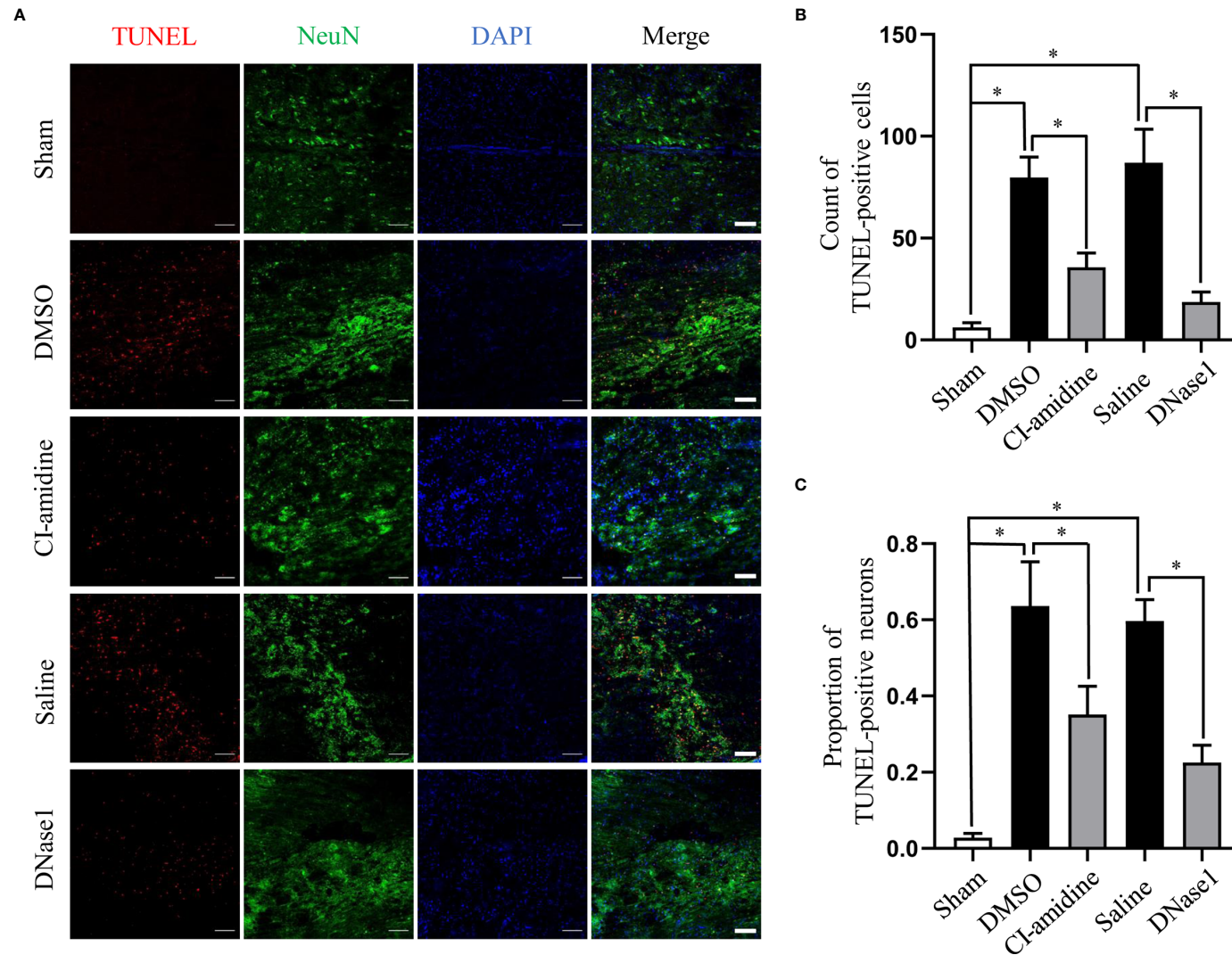


FIGURE 5 | Restricting NETs reduces cell death after SCI. **(A)** Representative images of TUNEL (red) and NeuN (green) double-positive cells in injured spinal cord of each group at 24 h after operation. Nuclear was marked with DAPI (blue). Scale bars = 100 μ m. Quantification of **(B)** TUNEL-positive cells and **(C)** double-positive cells in injured spinal cord of each group at 24 h after SCI. Data are presented as means \pm SD of $n = 6$ (* $p < 0.05$).

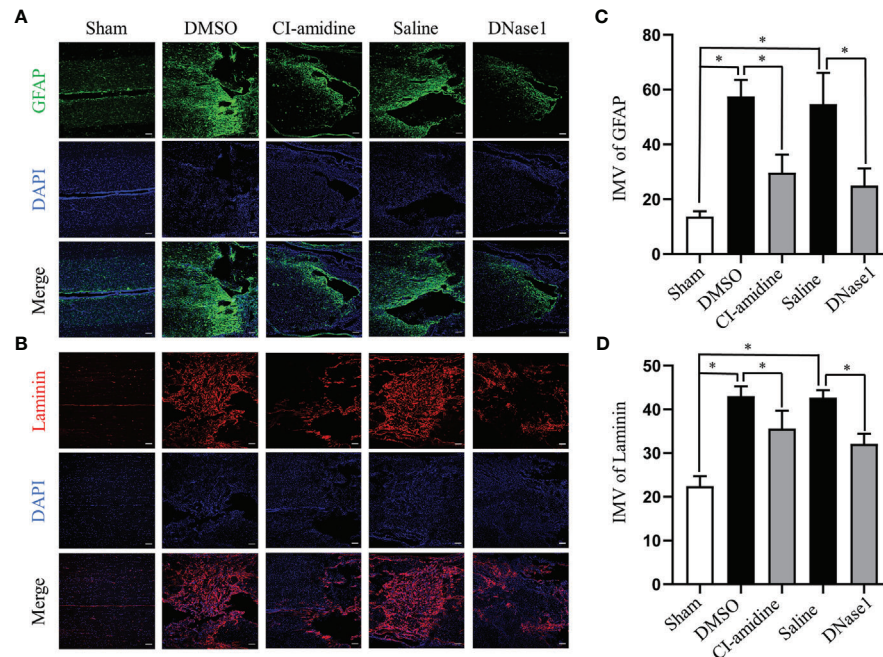


FIGURE 6 | Restricting NETs reduces both glial and fibrotic scar formation after SCI. **(A)** Representative images of GFAP (green) positive glial scar in injured spinal cord of each group at 28 days after operation. Nuclear was marked with DAPI (blue). **(B)** Representative images of Laminin (red) positive fibrotic scar in injured spinal cord of each group at 28 days after operation. Nuclear was marked with DAPI (blue). Scale bars = 100 μ m. Fluorescence intensity mean value (IMV) of **(C)** GFAP and **(D)** Laminin at the injury epicenter of each group. Data are presented as means \pm SD of $n = 6$ (* $p < 0.05$).

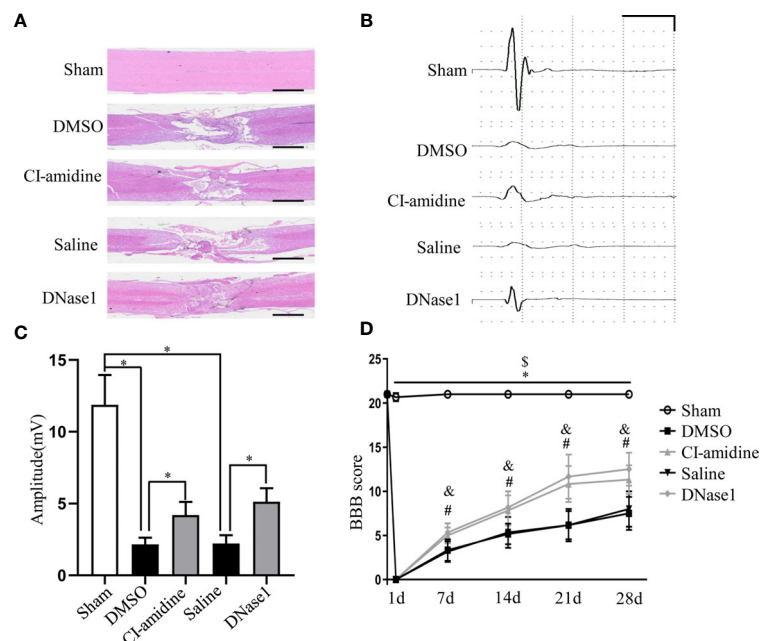


FIGURE 7 | Restricting NETs reduces tissue damage and promotes motor function recovery after SCI. **(A)** Representative images of H&E staining performed on the injured spinal cord section of each group at 28 days after operation. Scale bars = 2 mm. **(B)** Representative recording of motor evoked potentials (MEPs) of each group at 28 days after operation. Scale: 5 mV/10 ms. **(C)** Amplitudes of MEPs of each group. Data are presented as means \pm SD of $n = 6$ (* $p < 0.05$ versus vehicle). **(D)** The BBB scores at different time points of each group. Data are presented as means \pm SD of $n = 6$ (* $p < 0.05$ sham versus DMSO, $^{\$}p < 0.05$ sham versus Saline, $p < 0.05$ CI-amidine versus DMSO, $^{\$}p < 0.05$ DNase1 versus Saline).

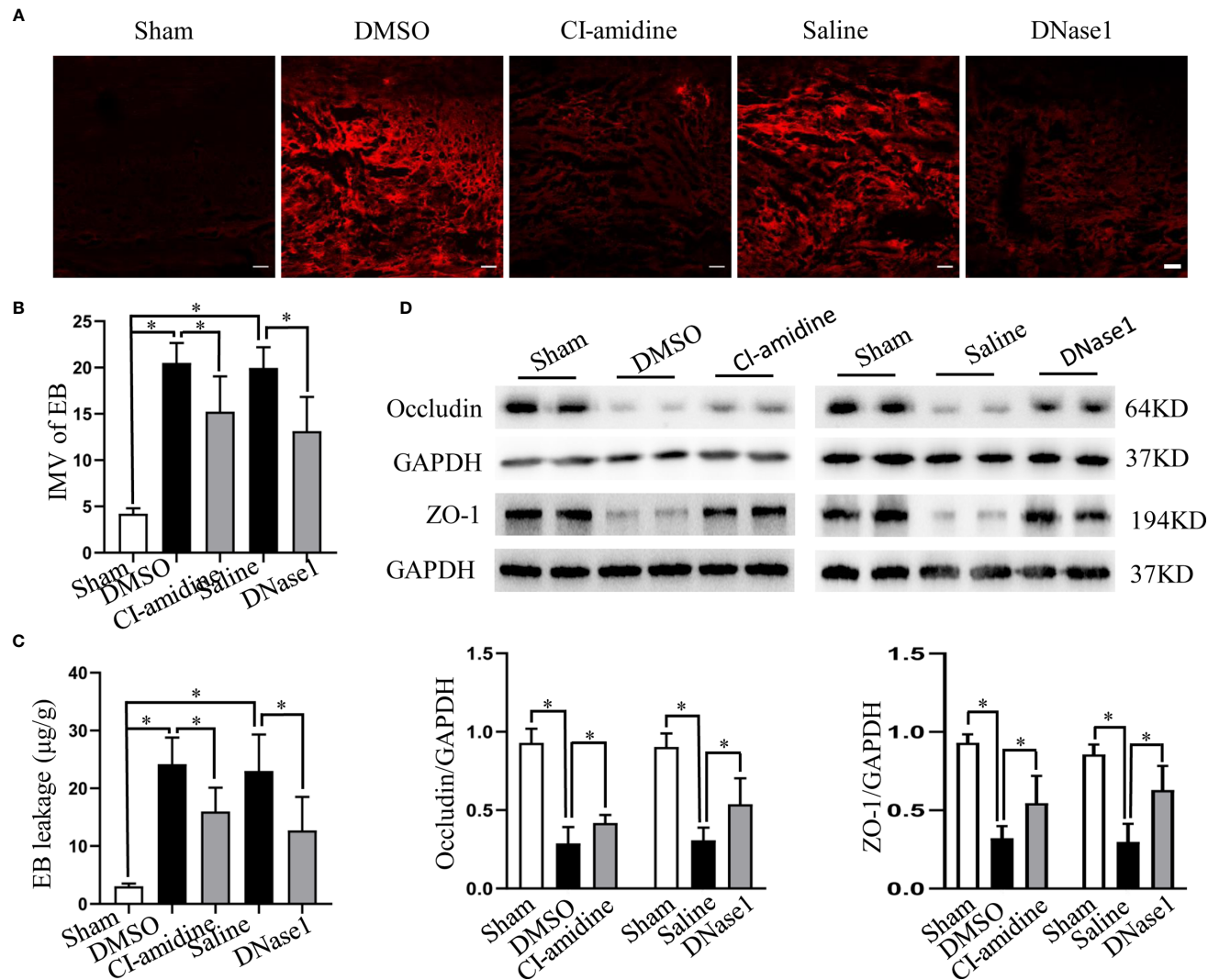


FIGURE 8 | NETs promote BSCB disruption after SCI. **(A)** Representative fluorescence images of EB (red) leakage at the injury epicenter of each group at 24 h after operation. Scale bars = 100 μ m. **(B)** Fluorescence intensity mean value (IMV) of EB at the injury epicenter of each group. **(C)** Quantification of EB leakage at the injury epicenter of each group at 24 h after operation. **(D)** Representative immunoblots and quantification of the BSCB tight junction proteins (ZO-1, occludin) levels in injured spinal cord of each group at 24 h after operation. Data are presented as means \pm SD of $n = 6$ (* $p < 0.05$).

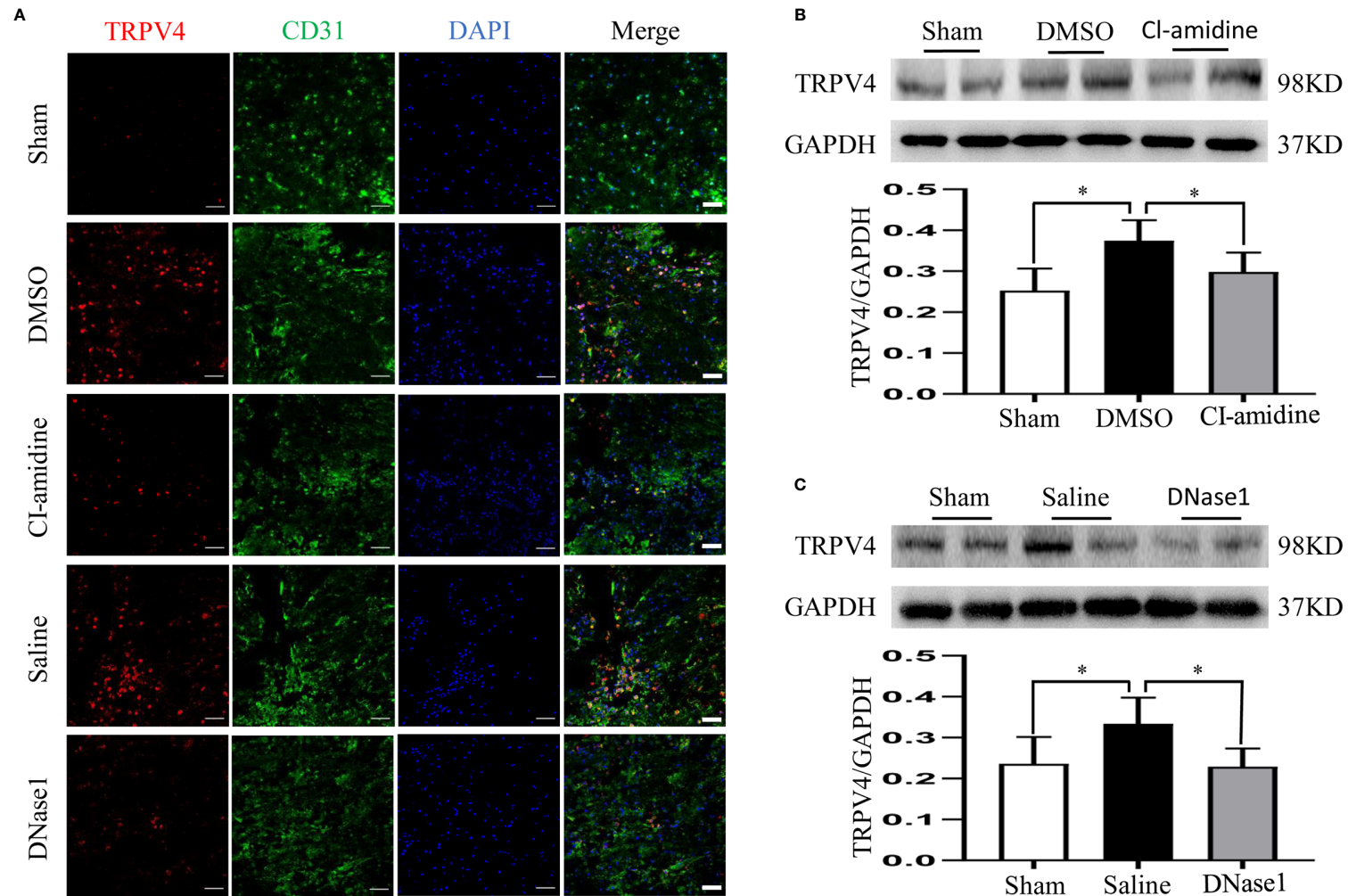
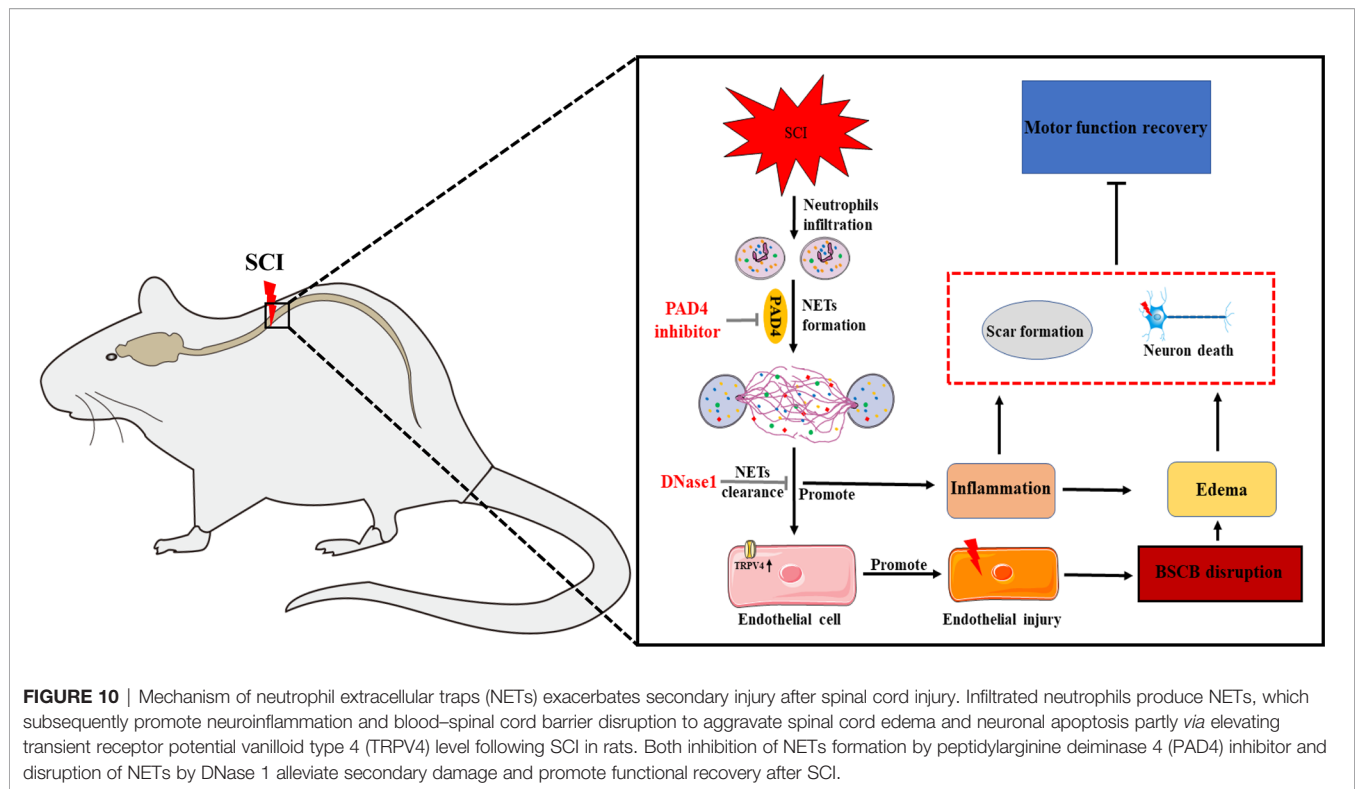


FIGURE 9 | NETs promote BSCB disruption through elevating TRPV4. **(A)** Representative images of TRPV4 (red) and CD31 (green) double-positive cells at the injury epicenter of each group at 24 h after operation. Nuclear was marked with DAPI (blue). Scale bars = 50 μ m. **(B, C)** Representative immunoblots and quantification of TRPV4 levels in injured spinal cord of each group at 24 h after operation. Data are presented as means \pm SD of $n = 6$ (* $p < 0.05$).



Preventing neuroinflammation and BSCB disruption are crucial strategies to block persistent secondary injury (38, 39). In the present study, we demonstrated that reducing NETs alleviates both neuroinflammation and BSCB disruption in injured spinal cord, hence ameliorating SCI and promoting functional recovery. Finally, we attempted to explore the potential mechanisms as to how NETs aggravate BSCB disruption and demonstrated that TRPV4 is upregulated in CD31-marked endothelial cells after SCI, which is suppressed by both Cl-amidine and DNase1. In agreement with our results, the nonselective cation channel TRPV4 was proved to contribute to endothelial and secondary damage after SCI, while inhibiting which attenuated SCI in a recent research (29). Combined with these results, we reasonably speculate that NETs aggravate BSCB disruption *via*, at least partly, elevating TRPV4 following SCI. Meanwhile, there are several limitations that require further studies in the present research. Firstly, *in vitro* study is needed to further confirm whether NETs damage endothelial cells through TRPV4 elevation. Secondly, whether NETs aggravate SCI through other mechanisms is worth investigating. Finally, all these results need to be verified in various models in the future.

In summary, our data demonstrated that NETs aggravate neuroinflammation and BSCB disruption, which may be partly *via* elevating TRPV4, to exacerbate secondary injury after SCI, while both inhibiting NETs formation and degrading NETs alleviate injury and promote motor function recovery (Figure 10). Therefore, our findings demonstrated that NETs may be a potential therapeutic target for SCI.

DATA AVAILABILITY STATEMENT

The original contributions presented in the study are included in the article/Supplementary Material. Further inquiries can be directed to the corresponding author.

ETHICS STATEMENT

The animal study was reviewed and approved by Animal Care and Use Committee of the Army Medical University.

AUTHOR CONTRIBUTIONS

ZF, LM, LL, BC, HC, YZ, and WD contributed to the implementation of the experiment. HL and JH contributed to the design and paper writing. All authors contributed to the article and approved the submitted version.

FUNDING

This work was supported by grants 81671211 (JH) and 81672251 (HL) from the National Natural Science Foundation of China and 2017MPRC-08 from the Talent Project of Southwest Hospital of China.

SUPPLEMENTARY MATERIAL

The Supplementary Material for this article can be found online at: <https://www.frontiersin.org/articles/10.3389/fimmu.2021.698249/full#supplementary-material>

REFERENCES

- Ahuja CS, Wilson JR, Nori S, Kotter MRN, Druschel C, Curt A, et al. Traumatic Spinal Cord Injury. *Nat Rev Dis Primers* (2017) 3:17018. doi: 10.1038/nrdp.2017.18
- Ahuja CS, Martin AR, Fehlings MG. Recent Advances in Managing a Spinal Cord Injury Secondary to Trauma. *F1000Research* (2016) 5:1017. doi: 10.12688/f1000research.7586.1
- Blesch A, Tuszynski MH. Spinal Cord Injury: Plasticity, Regeneration and the Challenge of Translational Drug Development. *Trends Neurosci* (2009) 32(1):41–7. doi: 10.1016/j.tins.2008.09.008
- Alizadeh A, Dyck SM, Karimi-Abdolrezaee S. Traumatic Spinal Cord Injury: An Overview of Pathophysiology, Models and Acute Injury Mechanisms. *Front Neurol* (2019) 10:282. doi: 10.3389/fneur.2019.00282
- Oyinbo CA. Secondary Injury Mechanisms in Traumatic Spinal Cord Injury: A Nugget of This Multiply Cascade. *Acta Neurobiol Exp* (2011) 71(2):281–99.
- Neirinx V, Coste C, Franzen R, Gothot A, Rogister B, Wislet S. Neutrophil Contribution to Spinal Cord Injury and Repair. *J Neuroinflamm* (2014) 11:150. doi: 10.1186/s12974-014-0150-2
- Fleming JC, Norenberg MD, Ramsay DA, Dekaban GA, Marcillo AE, Saenz AD, et al. The Cellular Inflammatory Response in Human Spinal Cords After Injury. *Brain J Neurol* (2006) 129(Pt 12):3249–69. doi: 10.1093/brain/awl296
- Devaux S, Cizkova D, Quanic J, Franck J, Nataf S, Pays L, et al. Proteomic Analysis of the Spatio-Temporal Based Molecular Kinetics of Acute Spinal Cord Injury Identifies a Time- and Segment-Specific Window for Effective Tissue Repair. *Mol Cell Proteomics* (2016) 15(8):2641–70. doi: 10.1074/mcp.M115.057794
- Yates AG, Jogle T, Gillespie ER, Couch Y, Ruitenberg MJ, Anthony DC. Acute IL-1RA Treatment Suppresses the Peripheral and Central Inflammatory Response to Spinal Cord Injury. *J Neuroinflamm* (2021) 18(1):15. doi: 10.1186/s12974-020-02050-6
- Kolaczowska E, Kubes P. Neutrophil Recruitment and Function in Health and Inflammation. *Nat Rev Immunol* (2013) 13(3):159–75. doi: 10.1038/nri3399
- Manda-Handzlik A, Demkow U. The Brain Entangled: The Contribution of Neutrophil Extracellular Traps to the Diseases of the Central Nervous System. *Cells* (2019) 8(12):1477. doi: 10.3390/cells8121477
- Brinkmann V, Reichard U, Goosmann C, Fauler B, Uhlemann Y, Weiss DS, et al. Neutrophil Extracellular Traps Kill Bacteria. *Science* (2004) 303(5663):1532–5. doi: 10.1126/science.1092385
- Mohanty T, Fisher J, Bakochi A, Neumann A, Cardoso JFP, Karlsson CAQ, et al. Neutrophil Extracellular Traps in the Central Nervous System Hinder Bacterial Clearance During Pneumococcal Meningitis. *Nat Commun* (2019) 10(1):1667. doi: 10.1038/s41467-019-09040-0
- Appelgren D, Enocsson H, Skogman BH, Nordberg M, Perander L, Nyman D, et al. Neutrophil Extracellular Traps (NETs) in the Cerebrospinal Fluid Samples From Children and Adults With Central Nervous System Infections. *Cells* (2019) 9(1):43. doi: 10.3390/cells9010043
- Kang L, Yu H, Yang X, Zhu Y, Bai X, Wang R, et al. Neutrophil Extracellular Traps Released by Neutrophils Impair Revascularization and Vascular Remodeling After Stroke. *Nat Commun* (2020) 11(1):2488. doi: 10.1038/s41467-020-16191-y
- Tan Q, Guo P, Zhou J, Zhang J, Zhang B, Lan C, et al. Targeting Neutrophil Extracellular Traps Enhanced tPA Fibrinolysis for Experimental Intracerebral Hemorrhage. *Transl Res* (2019) 211:139–46. doi: 10.1016/j.trsl.2019.04.009
- Vaibhav K, Braun M, Alverson K, Khodadadi H, Kutianawalla A, Ward A, et al. Neutrophil Extracellular Traps Exacerbate Neurological Deficits After Traumatic Brain Injury. *Sci Adv* (2020) 6(22):eaax8847. doi: 10.1126/sciadv.aax8847
- Zenaro E, Pietronigro E, Della Bianca V, Piacentini G, Marongiu L, Budui S, et al. Neutrophils Promote Alzheimer's Disease-Like Pathology and Cognitive Decline Via LFA-1 Integrin. *Nat Med* (2015) 21(8):880–6. doi: 10.1038/nm.3913
- Weaver LC, Verghese P, Bruce JC, Fehlings MG, Krenz NR, Marsh DR. Autonomic Dysreflexia and Primary Afferent Sprouting After Clip-Compression Injury of the Rat Spinal Cord. *J Neurotrauma* (2001) 18(10):1107–19. doi: 10.1089/08977150152693782
- Feng Z, Tan Q, Tang J, Li L, Tao Y, Chen Y, et al. Intraventricular Administration of Urokinase as a Novel Therapeutic Approach for Communicating Hydrocephalus. *Transl Res* (2016) 180:77–90.e2. doi: 10.1016/j.trsl.2016.08.004
- Xie F, Tan Q, Yu A, Guo P, Wang L, Zeng Z, et al. The Role of Cell-Free DNA in Fibrinolysis for Intraventricular Hemorrhage. *J Neurosurg* (2021) 8:1–8. doi: 10.3171/2020.7.jns.201429
- Feng Z, Liu S, Chen Q, Tan Q, Xian J, Feng H, et al. uPA Alleviates Kaolin-Induced Hydrocephalus by Promoting the Release and Activation of Hepatocyte Growth Factor in Rats. *Neurosci Lett* (2020) 731:135011. doi: 10.1016/j.neulet.2020.135011
- Chen B, Tan Q, Zhao W, Yang Q, Zhang H, Gao F, et al. Diffusion Tensor Imaging and Electrophysiology as Robust Assays to Evaluate the Severity of Acute Spinal Cord Injury in Rats. *BMC Neurol* (2020) 20(1):236. doi: 10.1186/s12883-020-01778-1
- Goldim MPS, Della Giustina A, Petronilho F. Using Evans Blue Dye to Determine Blood-Brain Barrier Integrity in Rodents. *Curr Protoc Immunol* (2019) 126(1):e83. doi: 10.1002/cpim.83
- Jorch SK, Kubes P. An Emerging Role for Neutrophil Extracellular Traps in Noninfectious Disease. *Nat Med* (2017) 23(3):279–87. doi: 10.1038/nm.4294
- Wang Y, Wysocka J, Sayegh J, Lee YH, Perlin JR, Leonelli L, et al. Human PAD4 Regulates Histone Arginine Methylation Levels Via Demethylation. *Science* (2004) 306(5694):279–83. doi: 10.1126/science.1101400
- Martinod K, Demers M, Fuchs TA, Wong SL, Brill A, Gallant M, et al. Neutrophil Histone Modification by Peptidylarginine Deiminase 4 Is Critical for Deep Vein Thrombosis in Mice. *Proc Natl Acad Sci USA* (2013) 110(21):8674–9. doi: 10.1073/pnas.1301059110
- O'Shea TM, Burda JE, Sofroniew MV. Cell Biology of Spinal Cord Injury and Repair. *J Clin Invest* (2017) 127(9):3259–70. doi: 10.1172/jci90608
- Kumar H, Lim CS, Choi H, Joshi HP, Kim KT, Kim YH, et al. Elevated TRPV4 Levels Contribute to Endothelial Damage and Scarring in Experimental Spinal Cord Injury. *J Neurosci* (2020) 40(9):1943–55. doi: 10.1523/JNEUROSCI.2035-19.2020
- Yiu G, He Z. Glial Inhibition of CNS Axon Regeneration. *Nat Rev Neurosci* (2006) 7(8):617–27. doi: 10.1038/nrn1956
- Bradbury EJ, Burnside ER. Moving Beyond the Glial Scar for Spinal Cord Repair. *Nat Commun* (2019) 10(1):3879. doi: 10.1038/s41467-019-11707-7
- Dias DO, Goritz C. Fibrotic Scarring Following Lesions to the Central Nervous System. *Matrix Biol* (2018) 68–69:561–70. doi: 10.1016/j.matbio.2018.02.009
- Goritz C, Dias DO, Tomilin N, Barbacid M, Shupliakov O, Frisen J. A Pericyte Origin of Spinal Cord Scar Tissue. *Science* (2011) 333(6039):238–42. doi: 10.1126/science.1203165
- Zhou T, Zheng Y, Sun L, Badea SR, Jin Y, Liu Y, et al. Microvascular Endothelial Cells Engulf Myelin Debris and Promote Macrophage Recruitment and Fibrosis After Neural Injury. *Nat Neurosci* (2019) 22(3):421–35. doi: 10.1038/s41593-018-0324-9
- Hellal F, Hurtado A, Ruschel J, Flynn KC, Laskowski CJ, Umlauf M, et al. Microtubule Stabilization Reduces Scarring and Causes Axon Regeneration After Spinal Cord Injury. *Science* (2011) 331(6019):928–31. doi: 10.1126/science.1201148
- Dias DO, Kim H, Holl D, Werne Solnestam B, Lundberg J, Carlen M, et al. Reducing Pericyte-Derived Scarring Promotes Recovery After Spinal Cord Injury. *Cell* (2018) 173(1):153–65.e22. doi: 10.1016/j.cell.2018.02.004
- Dorrier CE, Aran D, Haenelt EA, Sheehy RN, Hoi KK, Pantic L, et al. CNS Fibroblasts Form a Fibrotic Scar in Response to Immune Cell Infiltration. *Nat Neurosci* (2021) 24(2):234–44. doi: 10.1038/s41593-020-00770-9
- Kumar H, Ropper AE, Lee SH, Han I. Propitious Therapeutic Modulators to Prevent Blood-Spinal Cord Barrier Disruption in Spinal Cord Injury. *Mol Neurobiol* (2017) 54(5):3578–90. doi: 10.1007/s12035-016-9910-6
- Cox A, Varma A, Banik N. Recent Advances in the Pharmacologic Treatment of Spinal Cord Injury. *Metab Brain Dis* (2015) 30(2):473–82. doi: 10.1007/s11011-014-9547-y

Conflict of Interest: The authors declare that the research was conducted in the absence of any commercial or financial relationships that could be construed as a potential conflict of interest.

Publisher's Note: All claims expressed in this article are solely those of the authors and do not necessarily represent those of their affiliated organizations, or those of the publisher, the editors and the reviewers. Any product that may be evaluated in this article, or claim that may be made by its manufacturer, is not guaranteed or endorsed by the publisher.

Copyright © 2021 Feng, Min, Liang, Chen, Chen, Zhou, Deng, Liu and Hou. This is an open-access article distributed under the terms of the Creative Commons Attribution License (CC BY). The use, distribution or reproduction in other forums is permitted, provided the original author(s) and the copyright owner(s) are credited and that the original publication in this journal is cited, in accordance with accepted academic practice. No use, distribution or reproduction is permitted which does not comply with these terms.



OPEN ACCESS

Edited by:

Shrikant R. Mulay,
Central Drug Research Institute (CSIR),
India

Reviewed by:

Lemin Zheng,
Peking University Health Science
Center, China
Yogesh Bhaskar Narkhede,
University of Georgia, United States
Sheilla Andrade De Oliveira,
Fiocruz Pernambuco, Brazil

***Correspondence:**

Subburaj Ilangumaran
Subburaj.ilangumaran@
Usherbrooke.ca

[†]These authors have contributed
equally to this work

Specialty section:

This article was submitted to
Molecular Innate Immunity,
a section of the journal
Frontiers in Immunology

Received: 29 July 2021

Accepted: 27 September 2021

Published: 12 October 2021

Citation:

Quenum AJI, Shukla A, Rexhepi F,
Cloutier M, Ghosh A, Kufer TA,
Ramanathan S and Ilangumaran S
(2021) NLRC5 Deficiency Deregulates
Hepatic Inflammatory Response but
Does Not Aggravate Carbon
Tetrachloride-Induced Liver Fibrosis.
Front. Immunol. 12:749646.
doi: 10.3389/fimmu.2021.749646

NLRC5 Deficiency Deregulates Hepatic Inflammatory Response but Does Not Aggravate Carbon Tetrachloride-Induced Liver Fibrosis

Akouavi Julite I. Quenum^{1†}, Akhil Shukla^{1†}, Fjolla Rexhepi¹, Maryse Cloutier¹,
Amit Ghosh¹, Thomas A. Kufer², Sheela Ramanathan^{1,3} and Subburaj Ilangumaran^{1,3*}

¹ Department of Immunology and Cell Biology, Faculty of Medicine and Health Sciences, Université de Sherbrooke, Sherbrooke, Canada, ² Department of Immunology (180b), Institute of Nutritional Medicine, University of Hohenheim, Stuttgart, Germany, ³ Centre de Recherche du Centre Hospitalier Universitaire de Sherbrooke (CR-CHUS), Sherbrooke, Canada

The nucleotide-binding leucine-rich repeat-containing receptor (NLR) family protein-5 (NLRC5) controls NF- κ B activation and production of inflammatory cytokines in certain cell types. NLRC5 is considered a potential regulator of hepatic fibrogenic response due to its ability to inhibit hepatic stellate activation *in vitro*. To test whether NLRC5 is critical to control liver fibrosis, we treated wildtype and NLRC5-deficient mice with carbon tetrachloride (CCl₄) and assessed pathological changes in the liver. Serum alanine transaminase levels and histopathology examination of liver sections revealed that NLRC5 deficiency did not exacerbate CCl₄-induced liver damage or inflammatory cell infiltration. Sirius red staining of collagen fibers and hydroxyproline content showed comparable levels of liver fibrosis in CCl₄-treated NLRC5-deficient and control mice. Myofibroblast differentiation and induction of collagen genes were similarly increased in both groups. Strikingly, the fibrotic livers of NLRC5-deficient mice showed reduced expression of matrix metalloproteinase-3 (*Mmp3*) and tissue inhibitor of MMPs-1 (*Timp1*) but not *Mmp2* or *Timp2*. Fibrotic livers of NLRC5-deficient mice had increased expression of TNF but similar induction of TGF β compared to wildtype mice. CCl₄-treated control and NLRC5-deficient mice displayed similar upregulation of *Cx3cr1*, a monocyte chemoattractant receptor gene, and the *Cd68* macrophage marker. However, the fibrotic livers of NLRC5-deficient mice showed increased expression of F4/80 (*Adgre1*), a marker of tissue-resident macrophages. NLRC5-deficient livers showed increased phosphorylation of the NF- κ B subunit p65 that remained elevated following fibrosis

induction. Taken together, NLRC5 deficiency deregulates hepatic inflammatory response following chemical injury but does not significantly aggravate the fibrogenic response, showing that NLRC5 is not a critical regulator of liver fibrosis pathogenesis.

Keywords: NLRC5, NF- κ B, liver fibrosis, carbon tetrachloride, hepatic stellate cells

INTRODUCTION

Fibrotic diseases of the liver, as well as that of other organs such as lungs, kidneys, heart and pancreas, arise from chronic inflammation that causes perpetual tissue damage (1). Persistent inflammation deregulates the tissue repair process and leads to progressive replacement of the parenchymatous cells with abnormal extracellular matrix (ECM), which compromises organ functions and necessitates organ transplantation in advanced stages of disease (2). Impressive progress has been made in understanding the cellular components, their secretory products and molecular pathways of fibrogenesis with the goal of finding ways to halt disease progression as well as promote fibrosis resolution and restoration of tissue homeostasis (3–5). Despite the limited success of available treatments targeting various molecules of the fibrogenic signaling pathways, this approach remains the mainstay for finding new strategies to treat fibrotic diseases (6, 7).

Liver fibrosis often results from chronic hepatitis virus infections, alcohol abuse and from obesity-associated fatty liver disease (8–10). Chronic inflammatory stimuli that accompany these conditions induce pro-inflammatory cytokines and chemokines from injured hepatocytes and liver-resident macrophages (Kupffer cells) that promote recruitment of circulating monocytes and their differentiation towards pro-inflammatory macrophages (11, 12). This inflammatory response activates hepatic stellate cells (HSC), which are also directly activated by injured hepatocytes, resulting in HSC proliferation and differentiation towards myofibroblasts that express α -smooth muscle actin (α SMA) (13). Growth factors and the profibrogenic cytokine transforming growth factor beta (TGF β) secreted by pro-inflammatory macrophages induce fibroblast proliferation and ECM deposition to facilitate wound healing and tissue repair. Pro-resolution macrophages also produce ECM remodeling enzymes such as matrix metalloproteinases (MMP) to resolve the fibrous scar tissue. However, incessant inflammatory stimuli establish a feed forward loop of pro-inflammatory and pro-fibrogenic processes (4). Progressive replacement of the liver parenchyma with fibrous scar tissue results in an end-stage disease called cirrhosis (9, 11). In addition to being a major cause of global healthcare burden and mortality, cirrhosis promotes the development of hepatocellular carcinoma (HCC), one of the most common and lethal cancers worldwide (14–18). HCC takes decades to present clinical symptoms and is often diagnosed in late stages, for which there are very few therapeutic options (19). As most HCC cases arise from cirrhotic livers, therapeutic targeting of molecules and cells that promote hepatic fibrogenesis is considered a

promising avenue to halt HCC development and progression, in addition to improving liver functions (20–23).

Members of the nucleotide binding and oligomerization domain (NOD)-like receptors (NLRs) constitute a family of cytosolic pattern recognition receptors that play a key role in inflammatory responses (24). The NLR proteins are further classified based on their N-terminal domains into NLRA, NLRB, NLRC and NLRP subgroups, each with one or more members, and most of them harboring C-terminal leucine-rich repeats (24, 25). Whereas certain members of NLRP (NLRP1, NLRP3) and NLRC (NLRC4) subfamilies activate inflammasomes and induce production of pro-inflammatory cytokines IL-1 β and IL-18, certain members of the NLRC family (NOD-1, NOD-2) activate the nuclear factor kappa-light-chain-enhancer of activated B cells (NF- κ B) to induce the expression of genes coding for these pro-inflammatory cytokines (24, 26). NLRA and NLRC5 function as transcriptional activators of MHC class-II and class-I genes, respectively, and thus are respectively known as class-II transactivator (CIITA) and class-I transactivator (CITA) (27). NLRC5 has also been implicated in regulating inflammatory response similarly to NLRC3 and NLRX1, both of which contain poorly defined N-terminal domains (24, 28–33). Over expression and knockdown studies have shown that NLRC5 inhibited LPS-induced NF- κ B activation and induction of TNF α , IL-6, RANTES (CXCL5) genes and IL-1 β secretion (28, 29, 34).

Given the prominent role of inflammatory cytokine signaling in liver fibrosis and TNF α -induced NLRC5 expression in the human HSC cell line LX-2, Li and colleagues investigated the role of NLRC5 in modulating the fibrogenic response in HSCs (35–37). Stable NLRC5 expression in LX-2 cells was shown to increase TNF α -induced IL-6 and IL-1 β mRNA expression, whereas siRNA-mediated NLRC5 knockdown diminished this response, although these effects did not affect IL-6 or IL-1 β protein expression (35). This study also reported that NLRC5 knockdown increased TNF α -induced I κ B phosphorylation, nuclear localisation of the p65 component of NF- κ B and phosphorylation of SMAD3, a key transcription factor activated by the profibrogenic cytokine TGF β , suggesting an anti-fibrogenic role for NLRC5 (35). The same group also reported elevated NLRC5 expression in human fibrotic livers and that stable NLRC5 expression in LX-2 cells upregulated TGF β -mediated induction of α SMA and collagen 1 α 1 (36). However, knockdown of NLRC5 was shown to increase TGF β -mediated apoptosis of LX-2 cells despite increasing the phosphorylation of NF- κ B, SMAD2 and SMAD3 (36). Following experimental hepatic fibrogenesis in C57BL/6 mice, increased NLRC5 expression was observed in the fibrotic livers that coincided with collagen 1 α 1 and α SMA expression and all

Abbreviations: ALT, alanine transferase; CCl₄, carbon tetrachloride; ECM, extracellular matrix; HSC, hepatic stellate cells; MMP, matrix metalloproteinase; SMA, alpha smooth muscle actin; TIMP, tissue inhibitor of MMP.

three genes showed diminished expression during fibrosis resolution (37). Inhibition of LX-2 cell activation by a mixture of methylxanthine, dexamethasone and insulin, which inhibits TGF β -mediated upregulation of α SMA and collagen 1 α 1 also inhibited NLRC5 induction in LX-2 cells (37). Based on these findings, Li and colleagues proposed an anti-fibrogenic role for NLRC5 in a negative feedback manner, following its induction in HSCs by TNF α and TGF β . Here, we sought genetic evidence for this hypothesis by evaluating liver fibrosis induced by carbon tetrachloride (CCl₄) in NLRC5-deficient mice.

METHODS

Mice

Nlrc5^{-/-} mice in C57BL/6N background, generated by crossing *Nlrc5*-floxed mice with CMV-Cre mice, were a generous gift from Dr. Dana Philpott (38). Wildtype C57BL/6N mice were used as controls. Both groups of mice were bred and housed in ventilated cages on the same housing unit throughout the experiment. The experiments were done as and when the knockout mice became available. Therefore, the numbers of mice used per group in different experiments was variable and are indicated in the corresponding figure legends. All experimental protocols on animals were carried out with the approval of the Université de Sherbrooke Animal Ethics Committee (Protocol # 2018-2083, 359-18C).

Liver Fibrosis Induction by Carbon Tetrachloride

Liver fibrosis was induced as we have described previously (39). Male mice were used for liver fibrosis induction as female sex hormones diminish inflammatory cytokine production in the liver (40). Briefly, CCl₄ (Sigma-Aldrich, Oakville, ON) diluted in corn oil (1:3) was injected *via* intraperitoneal (i.p) route (0.5 μ L CCl₄ per gram body weight) twice a week for five weeks. Three days after the last treatment, mice were euthanized, blood collected by cardiac puncture and liver tissues resected. Serum was separated and kept frozen at -80°C. Liver pieces were snap frozen and stored at -80°C for gene and protein expression studies and hydroxyproline assay. For histopathology analyses, 3-4 cubic mm size liver pieces from 4-5 different locations of the same liver were fixed for 12-16 hours in 4% paraformaldehyde solution and embedded in paraffin on the same tissue block.

Serum ALT and Liver Hydroxyproline Assays

Serum alanine transaminase (ALT) levels were measured using a kinetic assay (Pointe Scientific Inc, Brussels, Belgium) following manufacturer's instructions. Hydroxyproline content was measured as described previously (39). Ten mg of liver tissue, homogenized in 1 mL of 6N HCl using the bead mill MM 400 (Retsch, Hann, Germany), was transferred to glass tubes, topped up with 2 mL of 6N HCl and the tubes were kept on a heat block

for 16h at 110°C to hydrolyze proteins. After filtering the hydrolysate through Whatman #1 filter paper, aliquots were evaporated on a heat block and the residues were dissolved in 50% 2-propanol. Hydroxyproline standards and samples, distributed in a 96-well microtiter plate, were oxidized by adding chloramine T (Sigma-Aldrich; dissolved in 50% isopropanol and adjusted to pH 6.5 with acetate/citrate buffer). Following incubation at room temperature for 25 min, Ehrlich reagent [*p*-dimethylaminobenzaldehyde dissolved in *n*-propanol/perchloric acid (2:1)], was added and the samples incubated at 50°C for 10 min for color development. Absorbance at 550 nm was measured using the SPECTROstar Nano (BMG Labtech, Germany) spectrophotometer.

Histology and Immunohistochemistry

Liver sections were deparaffinized, rehydrated, and stained with hematoxylin and eosin (H&E) or Sirius red following standard procedures. For immunohistochemical detection of α SMA, rehydrated liver sections immersed in citrate buffer (pH 6.0) were given intermittent microwave treatment to retrieve antigenic epitopes. Following incubation in 3% hydrogen peroxide for 10 min to inhibit endogenous peroxidase activity, sections were blocked with 5% BSA in Tris-buffered saline (TBS) containing 20% Tween-20 (TBS-T). Slides were incubated overnight at 4°C with a rabbit mAb against mouse α SMA (Cell Signaling Technology, Cat #19245S) diluted in blocking buffer, washed and then incubated with horseradish peroxidase (HRP)-conjugated secondary Ab for 1 h. After thorough washing, a substrate solution containing 3,3'-diaminobenzidine (DAB; Sigma-Aldrich; 30 μ L chromogen diluted in 1 mL of DAB liquid buffer) was added for 10 min. The sections were counterstained with hematoxylin and mounted with a coverslip. Images of the stained sections, digitized using the NanoZoomer Slide Scanner (Hamamatsu Photonics, Japan), were analyzed by the NanoZoomer Digital Pathology software NDPview2.0. Sirius red staining and α SMA-positive areas were quantified using the NIH ImageJ software (version 1.53e). Data from six randomly selected fields from different liver pieces for each of the three mice per group were used for quantification.

Gene Expression Analysis

Total RNA from frozen tissues was extracted using QIAzol Lysis Reagent (Qiagen, Toronto, Ontario, Canada), according to the manufacturer's instructions. cDNA was synthesized from 1 μ g of purified RNA using QuantiTect[®] reverse transcription kit (Qiagen, Toronto, Ontario, Canada). Quantitative RT-PCR amplification reactions were carried out in CFX Connect Real-Time PCR Detection System (Bio-Rad, Canada) or QuantStudio 3 Real-Time PCR System (Thermo Fisher Scientific, Canada) using SYBR Green Supermix (Bio-Rad, Mississauga, Ontario, Canada). The expression of indicated genes was measured using primers listed in **Supplementary Table S1**. Gene expression levels between samples were normalized based on the Cycle threshold (Ct) values compared to housekeeping gene *36B4* and

the fold induction was calculated using the vehicle (oil)-treated wildtype mice as controls.

Enzyme Linked Immunosorbent Assay (ELISA)

Serum TNF protein levels were quantified using a sandwich ELISA kit from eBioscience (Cat # 88-7324) following manufacturer's instructions. Capture Ab diluted in coating buffer was added to high protein-binding 96-well plates (Nunc Maxisorp®) and incubated overnight at 4°C. After washing with PBS-0.05% Tween-20 (wash buffer), the plates were blocked with assay diluent for 1 h at room temperature. Serum samples diluted 1:1 in assay diluent and serial dilutions of recombinant TNF standard were added in duplicates, and plates were incubated at room temperature for 2 h. After thorough washing, biotinylated detection antibody was added for 1 h followed by the addition of avidin-HRP for 30 min. After thorough washing, tetramethylbenzidine substrate solution was added for 15 min and color development was measured at 450 nm using SPECTROstar Nano. The values were plotted against the standard curve to calculate TNF protein levels in serum.

Western Blot

Mice liver tissue samples were taken in a 2 mL round bottom tube and homogenized using bead mill MM 400 (Retsch, Hann, Germany) containing TNE buffer (50mM Tris-HCl, 150mM NaCl, 1mM EDTA; pH 8.0) supplemented with phosphatase and protease inhibitor cocktails (Roche, Indianapolis, IN). TNE buffer containing detergents (0.2% SDS, 1% sodium deoxycholate and 1% Triton-X) was added in equal volumes into the homogenates and kept on rocker for 30 min at 4°C. Lysate was centrifuged for 20 min at 15,000 ×g and the supernatant collected. Protein concentration was determined using RC-DC Protein Assay Kit (Bio-Rad, Mississauga, ON). Protein samples containing 30-50 µg proteins were electrophoresed on SDS-PAGE gels and analysed by Western Blot. Primary Ab used are listed in **Supplementary Table S2**. HRP-conjugated anti-mouse or anti-rabbit secondary antibodies and enhanced chemiluminescence reagents (ECL) were from GE Healthcare Life Sciences (Pittsburg, PA). Images of western blot were captured by the VersaDOC 5000 imaging system (Bio-Rad).

Statistical Analysis

The numbers of mice in experimental and control groups for the two genotypes of mice in each experiment are indicated in corresponding figure legends. Data were analyzed using the GraphPad Prism9 (San Diego, CA). Statistical significance was calculated by two-way ANOVA with Tukey's post-hoc test. *p* values <0.05 were considered significant.

RESULTS

Loss of NLRC5 Does Not Exacerbate Liver Damage Caused by Chemical Injury

TNFα, expressed by macrophages and hepatocytes in response to toll-like receptor signaling, contributes to liver fibrosis by

activating HSC and immune cells (12). Loss of TNF receptor TNFR1 attenuates liver fibrosis induced by CCl₄ or bile duct ligation, accompanied by reduced expression of *Col1a1* and *Il6* genes and decreased NF-κB activation in liver tissues as well as in isolated HSCs (41, 42). NF-κB signaling promotes cell survival and proliferation of not only hepatocytes but also HSCs (42–44). As NLRC5 knockdown in HSCs was shown to increase NF-κB signaling (35), we examined whether NLRC5 deficiency promoted liver fibrosis *in vivo*. To this end, we induced liver fibrosis by intraperitoneal administration of CCl₄ in NLRC5-deficient and control mice for five weeks. Alterations in liver function were evaluated and histological and molecular changes were assessed. As shown in **Figure 1A**, both wildtype and *Nlrc5*^{-/-} mice showed comparable levels of liver damage as revealed by elevated serum levels of alanine transaminase (ALT). Hematoxylin and eosin-stained liver sections showed similar features of hepatocyte damage and mononuclear cell infiltration in both wildtype and *Nlrc5*^{-/-} mice (**Figure 1B**). Together these results indicated that loss of NLRC5 does not increase hepatocyte damage induced by chronic chemical injury.

CCl₄-Induced Liver Fibrosis in NLRC5-Deficient Mice Is Comparable to Wildtype Mice

Next, we compared the extent of liver fibrosis in CCl₄-treated *Nlrc5*^{-/-} and control mice. Sirius red staining of collagen fibers revealed comparable pattern and distribution of fibrotic areas in *Nlrc5*^{-/-} and wildtype mice that was also confirmed by quantification of the stained areas (**Figures 2A, B**). Moreover, measurement of hydroxyproline, which is enriched in connective tissue collagen fibers (45), was increased in CCl₄-treated wildtype mice (**Figure 2C**). Interestingly, *Nlrc5*^{-/-} mice treated with vehicle (corn oil, control) showed significantly elevated hydroxyproline content compared to wildtype mice. Because of such elevated hydroxyproline content in *Nlrc5*^{-/-} mice, the CCl₄-mediated increase in this group was not statistically significant, even though these levels are appreciably higher than in CCl₄-treated wildtype mice (**Figure 2C**). These observations suggested that NLRC5 deficiency may augment certain aspects of the hepatic fibrogenic response that is not discernible in the presence of strong fibrogenic inducers such as CCl₄.

CCl₄-Induced Hepatic Myofibroblast Differentiation Is Similar in NLRC5-Deficient and Wildtype Mice

As fibrogenesis is mainly driven by HSCs activation and their differentiation to myofibroblasts (13), we evaluated the expression of the *Acta2* gene coding for αSMA and that of *Pdgfrb* coding for platelet-derived growth factor beta, a mitogen for HSC. The induction of *Acta2* was significantly high in CCl₄-treated wildtype mice livers but showed only marginal increase in *Nlrc5*^{-/-} mice. On the other hand, *Pdgfrb* upregulation was significantly elevated in the livers of CCl₄-treated *Nlrc5*^{-/-} mice but less prominently in control mice (**Figure 3A**). However, the upregulation of *Acta2* and *Pdgfrb*

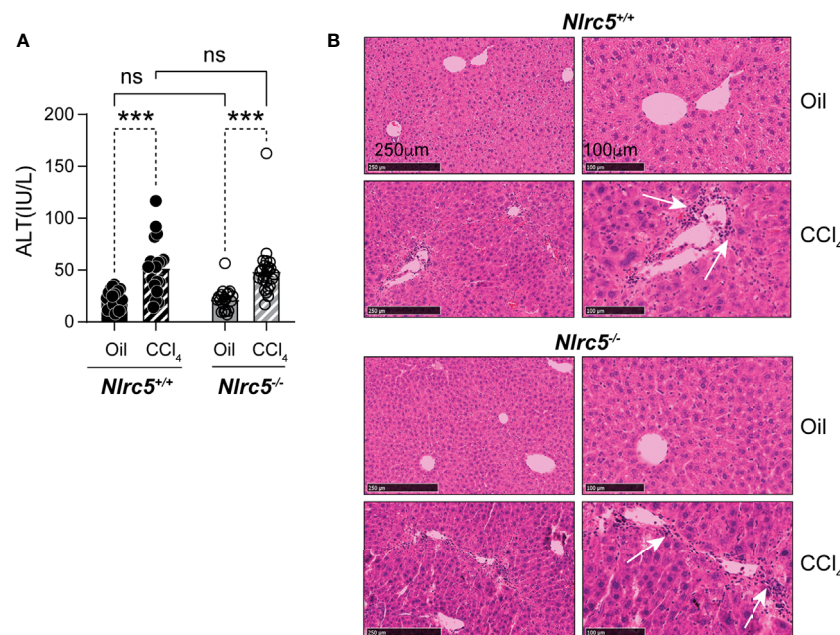


FIGURE 1 | Loss of NLRC5 does not exacerbate liver damage caused by chemical injury. **(A)** Serum ALT levels in NLRC5-deficient and control mice following 5 weeks of treatment with CCl₄ or corn oil (vehicle). Data shown are mean ± standard error of mean (SEM) from 4–5 mice per group from two separate experiments. Statistical significance was calculated by two-way ANOVA with Tukey's *post-hoc* test: ****p* < 0.001, ns, not significant. **(B)** Images of hematoxylin and eosin-stained sections of the livers, representative of 4–6 mice per group are shown. Magnified images (right) show comparable changes in hepatocyte morphology and mononuclear cell infiltration (arrows) in CCl₄-treated NLRC5-deficient and control livers.

genes was not significantly different between CCl₄-treated wildtype and *Nlrc5*^{-/-} mice. Moreover, immunohistochemical staining of αSMA in the liver sections from vehicle- or CCl₄-treated mice showed a comparable increase in pattern and staining of myofibroblast distribution in CCl₄-treated wildtype and *Nlrc5*^{-/-} mice that was also confirmed by digital quantification of the stained areas (**Figures 3B, C**). These findings indicated that NLRC5 deficiency does not markedly affect myofibroblast differentiation during chemically induced liver fibrosis.

Similar Induction of Collagens but Differential Induction of ECM Remodelling Enzymes in NLRC5-Deficient and Control Livers

Consistent with the comparable levels of myofibroblast differentiation in *Nlrc5*^{-/-} and wildtype mice livers following CCl₄ treatment, genes encoding the fibrillar collagens, collagen 1α1 and collagen 3α1 (46) were strongly induced in both groups (**Figure 4A**). Similarly, the gene coding for the ECM modifying enzyme MMP2 and tissue inhibitor of MMPs-2 (*Mmp2*, *Timp2*), which respectively exert anti- and pro-fibrogenic roles in liver fibrosis (47–49), were strongly upregulated by CCl₄ treatment in both *Nlrc5*^{-/-} and control mice livers (**Figure 4B**). However, *Mmp3* and *Timp1* genes, whose impact on liver fibrosis is controversial or unclear (49), were strongly induced in wildtype mice livers but showed significantly lower or negligible induction in NLRC5-

deficient livers (**Figure 4B**). These findings indicate that NLRC5 deficiency does not appreciably affect the induction of many fibrogenic response genes and that the observed differences caused by NLRC5 deficiency are not strong enough to influence the severity of liver fibrosis.

Fibrotic Livers of NLRC5-Deficient Mice Show Increased TNF Expression

Liver fibrosis establishes feed forward loops involving pro-inflammatory and profibrogenic cytokine gene expression by immune cells and their recruitment by chemokines (50, 51). To determine how NLRC5 deficiency affects these processes, we first evaluated the expression of candidate genes implicated in these processes. NLRC5-deficient livers displayed a significantly higher induction of the pro-fibrogenic tumor necrosis factor gene *Tnf* (**Figure 5A**). Serum TNF levels were elevated in both control and *Nlrc5*^{-/-} mice following CCl₄ treatment (**Figure 5B**). Notably, vehicle-treated *Nlrc5*^{-/-} mice displayed appreciably higher levels of TNF than control mice. The interleukin-1β gene *Il1b* did not show appreciable induction following CCl₄ treatment in control livers but was significantly elevated in NLRC5-deficient livers due to lower expression in the oil-treated group (**Figure 5A**). The transcript levels of IL-6, a survival cytokine, was appreciably lower in *Nlrc5*^{-/-} livers (**Figure 5A**). The *Tgfb* gene coding for the key fibrogenic cytokine transforming growth factor beta showed comparable upregulation in both groups following CCl₄

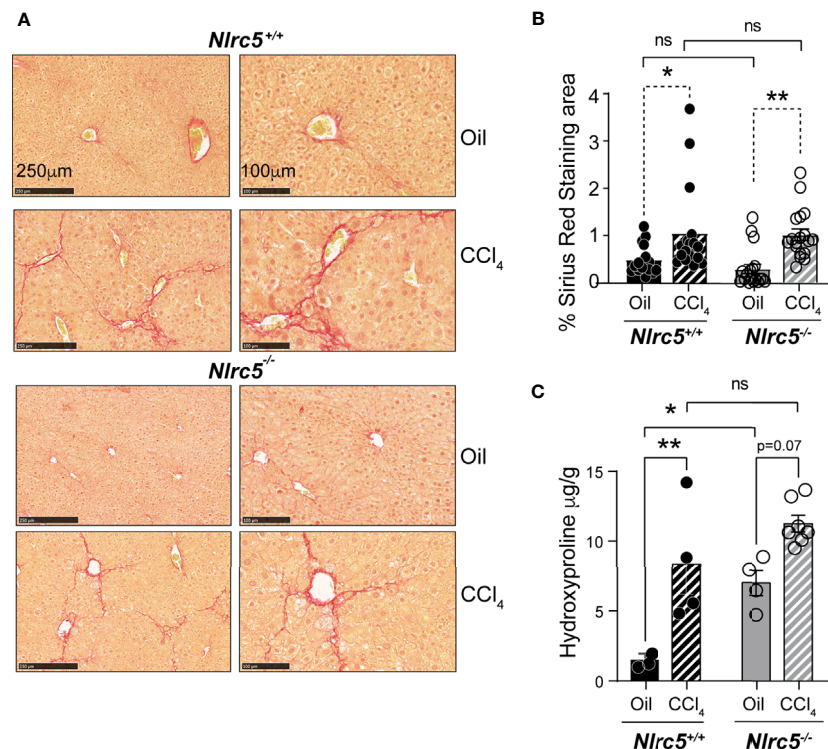


FIGURE 2 | CCl₄-induced liver fibrosis in NLRC5-deficient mice is comparable to wildtype mice. **(A)** Sirius red-stained sections of oil- or CCl₄-treated control and NLRC5-deficient livers at low (left) and high (right) magnifications. Data shown are representative of 4–5 mice per group from two independent experiments. **(B)** Quantification of Sirius red-stained area. Six randomly selected fields from liver pieces collected from different locations of each of the three mice per group were used for quantification. **(C)** Hydroxyproline content of livers from oil (n=3–4) or CCl₄-treated (n=4–7) control and NLRC5-deficient mice. Data shown in **(B, C)** are mean ± SEM. Two-way ANOVA with Tukey's *post-hoc* test: *p < 0.05, **p < 0.01, ns, not significant.

treatment (**Figure 5C**). On the other hand, the antifibrogenic interferon gamma gene *Ifng* was appreciably reduced in wildtype livers following CCl₄ treatment, whereas *Nlrc5*^{-/-} livers showed a significant upregulation (**Figure 5C**). These findings indicate that NLRC5 deficiency did cause an upregulation of hepatic *Tnf* gene expression and systemic TNF protein levels, but this did not result in increased liver fibrosis.

Increase in F4/80 Positive Cells in NLRC5-Deficient Livers

The key producer cells of TNF during liver fibrosis are activated liver-resident Kupffer cells and monocyte-derived macrophages, which are recruited by chemokines expressed in the inflamed liver (51). As NLRC5-deficient mice showed elevated TNF expression, we evaluated the gene expression of the macrophage recruiting chemokine CCL2 (macrophage chemoattractant protein-1) and the T cell chemoattractant CCL5, as well as CX3CR1, the receptor for CX3CL1 (fractalkine) expressed on monocyte-derived macrophages and required for their homeostasis (52, 53). Whereas the expression of *Ccl2* and *Ccl5* showed only marginal induction in both wildtype and *Nlrc5*^{-/-} livers, *Cx3cr1* was strongly upregulated in both groups (**Figure 6A**). Next, we examined the gene expression of macrophage markers CD68 and F4/80 (ADGRE1) and T lymphocytes markers CD3e and CD8α. As

shown in **Figure 6B**, the fibrotic livers of both control and NLRC5-deficient mice showed increased expression of *Cd68* and *Adgre1*, and the latter was significantly higher in *Nlrc5*^{-/-} livers. Whereas F4/80 is highly expressed in tissue-resident macrophages, CD68 is expressed in both tissue-resident and infiltrating macrophages (54, 55). The T cell marker transcript levels were not markedly altered by CCl₄ treatment in both groups of mice. These findings suggest that NLRC5 deficiency increases the activation of liver-resident macrophages, which presumably contributes to elevated *Tnf* expression.

NLRC5-Deficient Livers Display Elevated Levels of p65 Activation

Finally, we examined the protein expression of molecules associated with fibrosis and signaling events reported to be regulated by NLRC5 in whole liver homogenates. CCl₄-treated wildtype and *Nlrc5*^{-/-} mice livers showed increased levels of αSMA and MMP2 compared to vehicle-treated control groups (**Figure 7A**), reflecting the increased transcript levels of *Acta2* and *Mmp2* genes in the fibrotic livers (**Figures 3A, 4B**). Notably, phosphorylation of the p65 subunit of NF-κB, which occurs downstream of diverse inflammatory signaling pathways including TNF (56), was found to be elevated in vehicle-treated *Nlrc5*^{-/-} mice livers compared to wildtype control mice and this

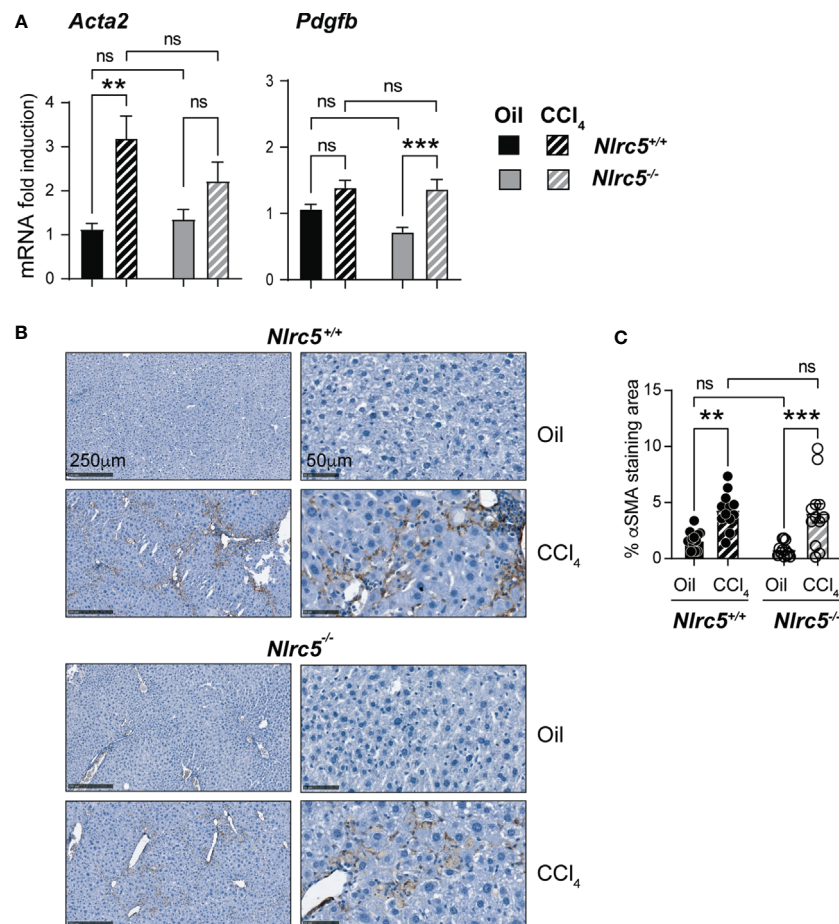


FIGURE 3 | CCl₄-induced myofibroblast differentiation is similar in NLRC5-deficient and wildtype livers. **(A)** Induction of *Acta2* and *Pdgfra* genes in fibrotic livers. Quantitative RT-PCR analysis of 8-10 mice from two independent experiments. **(B)** Immunohistochemical staining of α SMA in oil- or CCl₄-treated control and NLRC5-deficient mice livers. Representative liver sections from 4-5 mice per group from two independent experiments are shown. **(C)** Quantification of α SMA-stained areas. Six randomly selected fields from liver pieces collected from different locations of three mice per group were used for quantification. Data shown in **(A, C)** are mean \pm SEM. Two-way ANOVA with Tukey's *post-hoc* test: **p < 0.01; ***p < 0.001; ns, not significant.

p65 phosphorylation was sustained following CCl₄ treatment, with a concomitant decrease in total IκB (**Figure 7B**). This observation is consistent with the findings in the HSC cell line LX-2 following NLRC5 knockdown (37). However, phosphorylation of SMAD3, which occurs downstream of TGFβ signaling and reported to be reduced by NLRC5 knockdown in LX-2 cells (36), was reduced in *Nlr5*^{-/-} mice livers with or without CCl₄ treatment, whereas phosphorylation of SMAD2 was comparable to control mice livers (**Figure 7C**). These results indicate that NLRC5 deficiency deregulates NF-κB activation and may also modulate the SMAD signaling pathway in the liver.

DISCUSSION

The growing healthcare burden of fibrotic diseases can be partly attributed to increased lifespan and the associated inflammaging as well as various lifestyle factors such as obesity and alcohol

overuse. In addition to these factors, the limited progress in therapeutic control of the fibrogenic cascade has strengthened the efforts to understand the various molecular players with the goal of identifying potential pharmacological targets (5–7, 14, 57–60). Even though C57BL/6 mice are less susceptible than Balb/c mice to CCL₄-induced liver fibrosis, various gene knockout mice in the C57BL/6 background have immensely contributed to the molecular understanding of liver fibrosis pathogenesis (61). Inflammatory cytokines such as TNF α and the fibrogenic cytokine TGF β play key roles in the pathogenesis of liver fibrosis (41, 42, 62–64). IFN γ , which exerts antifibrogenic activity (65, 66), is a strong inducer of NLRC5 (67). The reports on NLRC5-mediated regulation of NF- κ B and SMAD activation downstream of TNF α and TGF β , respectively, in the human HSC cell line LX-2 raised the possibility that NLRC5 could be an important regulator of liver fibrosis and NLRC5-deficient mice would be useful to identify and characterize new drug targets to treat liver fibrosis. Our findings indicate that even though

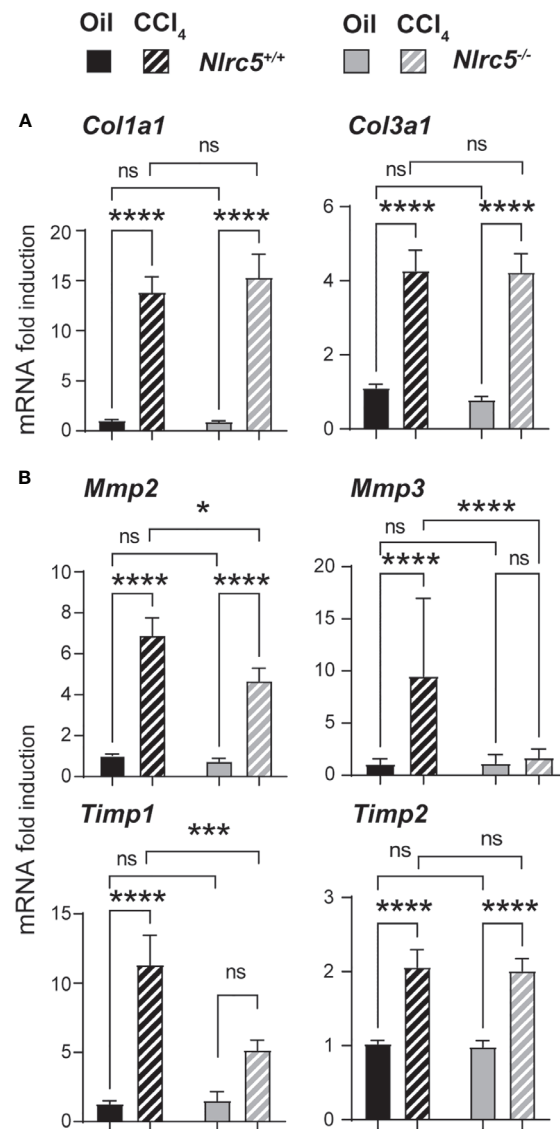


FIGURE 4 | Similar induction of collagens but differential induction ECM remodeling enzymes in NLRC5-deficient and control livers. RNA extracted from liver tissues from the indicated groups of mice were evaluated for the expression of (A) collagen (*Col1a1*, *Col3a1*) and (B) ECM remodeling enzymes (*Mmp2*, *Mmp3*, *Timp1*, *Timp2*) by qRT-PCR. Data shown are mean \pm SEM; $n = 6$ –10 mice for each group collected from 2–3 independent experiments. Two-way ANOVA with Tukey's *post-hoc* test: * $p < 0.05$; *** $p < 0.001$; **** $p < 0.0001$; ns, not significant.

NLRC5 likely regulates these signaling events in the liver at steady state and after tissue injury, loss of these NLRC5-mediated regulatory mechanisms does not exacerbate liver fibrosis.

Our finding that NLRC5-deficient livers show increased phosphorylation of p65/RelA concurs with the previous reports on the regulatory functions of NLRC5 on NF- κ B, although there are controversies about its universality (33). Initial studies showed that LPS-induced NF- κ B activation was attenuated by NLRC5 overexpression whereas an inverse effect was observed by siRNA-mediated knockdown of NLRC5 in HEK293T cells expressing TLR4, in the murine macrophage cell line RAW264.7 and in mouse embryonic fibroblasts (MEF) (28, 29, 34). Mechanistically,

NLRC5 mediated this inhibition by interacting with I κ B kinases IKK $\alpha\beta$, thereby preventing them from being activated by NEMO downstream of LPS-induced TLR4 signaling (29). This inhibition was reported to be dynamically regulated by LPS-induced K63-linked polyubiquitination of NLRC5 and its deubiquitination by USP14 (29, 68). Subsequent studies using bone marrow-derived macrophages (BMDM), dendritic cells (BMDC) and peritoneal macrophages from four independently generated *Nlrc5*^{-/-} mice showed that NLRC5 deficiency did not affect LPS-induced inflammatory cytokine production, although Tong et al., reported increased NF- κ B activation and TNF α production in MEFs and BMDM following LPS stimulation (69–72). It has been

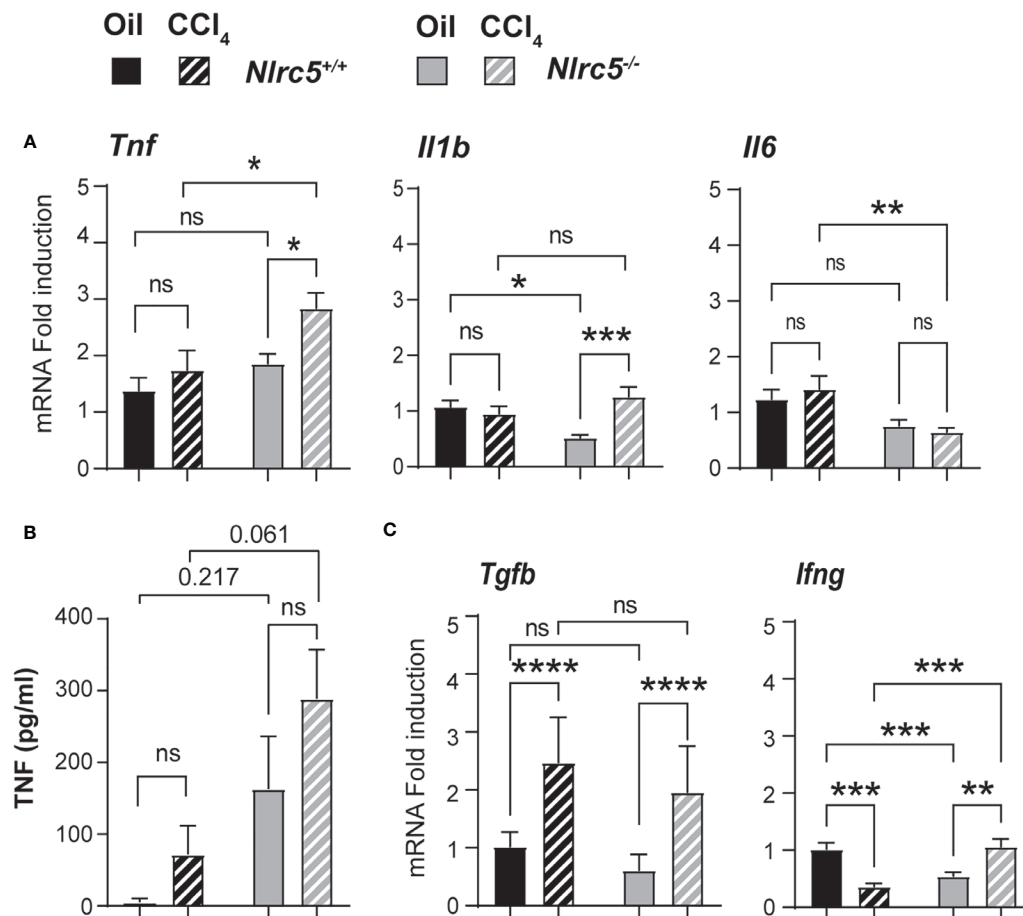


FIGURE 5 | Fibrotic livers of NLRC5-deficient mice show increased TNF expression. **(A)** Hepatic RNA from the indicated groups of mice were tested for the expression of pro-inflammatory cytokine genes *Tnf*, *Il1b* and *Il6* by qRT-PCR; n = 7–11 mice for each group from 2–3 independent experiments. **(B)** ELISA quantification of serum TNF levels; n = 4 mice per group. **(C)** Expression of pro-fibrogenic (*Tgfb*) and anti-fibrogenic (*Ifng*) cytokine genes in the liver tissue samples used in **(A)**. Data shown are mean ± SEM; Two-way ANOVA with Tukey's *post-hoc* test: **p* < 0.05; ***p* < 0.01; ****p* < 0.001; *****p* < 0.0001; ns, not significant. For certain comparisons, significance values are indicated.

suggested that differential ubiquitination of NLRC5 in different cell type may account for such differences (68). Nonetheless, elevated levels of phospho-p65 in NLRC5-deficient livers (Figure 7B) and increased expression of TNF following fibrosis induction (Figures 5A, B) confirm NLRC5-mediated regulation of NF-κB *in vivo*. This regulation may occur in hepatic macrophages, stellate cells and hepatocytes as all of them respond to TLR agonists (73). This possibility is supported by the elevated transcript levels of the tissue-resident macrophage marker F4/80 (*Adgre1*) (54) in the fibrotic livers of NLRC5-deficient mice (Figure 6B). NF-κB is also activated by TNFα (56) and both TLR and TNFα signaling pathways converge on the IKKαβγ complex regulated by NLRC5 (56, 68, 73). Thus, the elevated levels of phospho-p65 observed in NLRC5-deficient livers could result from both gut-derived TLR agonists and the resultant induction of TNFα in hepatic macrophages.

Intriguing differences were observed between NLRC5 knockout and wildtype mice livers in the induction of genes

coding for the ECM modulating enzymes. Whereas *Mmp2* and *Timp2* genes are upregulated following CCl₄ treatment in both wildtype and NLRC5-deficient livers, *Mmp3* and *Timp1* genes were not significantly induced in the absence of NLRC5 (Figure 4B). TIMP1 is an inhibitor of MMPs and thus promotes fibrogenesis but is not required to induce liver fibrosis (74). Hence, the reduced *Timp1* expression in NLRC5-deficient mouse livers is non-consequential on fibrosis development. However, *Timp1* is known to be induced by TNFα (75), and hence reduced *Timp1* transcript levels in NLRC5-deficient mouse livers despite elevated levels of TNFα and NF-κB activation is intriguing.

Even though NLRC5 does not directly activate inflammasomes, it is reported to interact with NLRP3 and contribute to inflammasome activation and IL-1β production in the human monocyte cell line THP-1 (76). However, peritoneal macrophages from NLRC5 knockout mice did not show any change in IL-1β production compared to wildtype macrophages (69, 72). Besides,

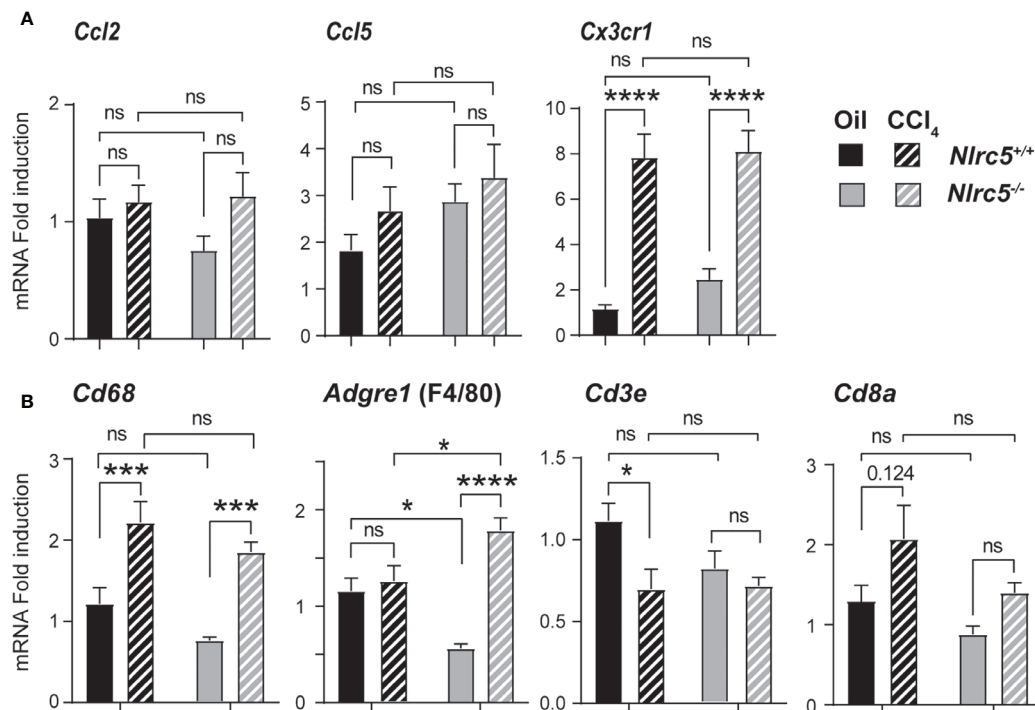


FIGURE 6 | Increased expression of F4/80 gene in the fibrotic livers of NLRC5-deficient mice. RNA extracted from liver tissues from the indicated groups of mice were evaluated for the gene expression of (A) chemokines (*Ccl2*, *Ccl5*, *Cx3cr1*) and (B) the markers of macrophages (CD68, F4/80) and T lymphocytes (CD3e, CD8a). Data shown are mean \pm SEM; $n = 7$ –11 mice for each group from 2–3 independent experiments. Two-way ANOVA with Tukey's *post-hoc* test: * $p < 0.05$; *** $p < 0.001$; **** $p < 0.0001$; ns, not significant. For certain comparisons, significance values are indicated.

IL-1 β does not figure predominantly in the pathogenesis of chronic liver diseases including liver fibrosis (77). Negligible changes in *Il1b* transcript levels (Figure 6A) and comparable level of liver fibrosis in NLRC5-deficient livers (Figure 2) suggest that NLRC5-dependent NLRP3 inflammasome activation plays little pathogenic role in liver fibrosis induced by chemically induced hepatocyte injury.

IFN γ is considered an anti-fibrogenic cytokine in the liver, but strain-dependent differences and pro-fibrogenic role in certain experimental models have been reported (65, 66, 78, 79). In the liver, IFN γ is produced by activated NK cells and T cells. Whereas IFN γ expression is significantly downmodulated following CCl₄ treatment in wildtype mice livers, and opposite trend was observed in NLRC5-deficient mice. The reduced *Ifng* transcript levels in vehicle-treated *Nlrc5*^{-/-} mice and its upregulation following fibrogenic stimuli suggest that NLRC5-dependent MHC-I expression may modulate the activation of immune cells under sterile inflammatory settings.

Li and colleagues have implicated NLRC5 in regulating signaling pathways activated by the key fibrogenic cytokine TGF β , as NLRC5 knockdown in LX-2 cells enhanced TGF β -induced phosphorylation of the activating SMADs SMAD3 and SMAD2, and increased expression of α SMA and collagen 1 α 1 genes (36). We did not find increased SMAD phosphorylation in the livers of CCl₄-treated NLRC5-deficient mice compared to wildtype mice although *Tgfb* gene was induced to a similar extent

in both groups. On the other hand, SMAD3 phosphorylation was diminished in NLRC5-deficient livers (Figure 7C). Even though the relatively high proportion of hepatocytes (60–80%) in the liver could mask any small difference in protein expression and their modification in a small proportion of HSCs, comparable levels of fibrosis induction in NLRC5-deficient and wildtype mice argues against the possibility of NLRC5-mediated modulation of TGF β response impacting hepatic fibrogenesis.

Overall, our findings support the regulatory role of NLRC5 on NF- κ B activation and TNF expression and suggest that this function may have a homeostatic role in restraining hepatic cellular activation by gut-derived TLR ligands. However, this NLRC5-mediated regulation is neither sufficient nor essential to overcome strong inflammatory and fibrogenic signaling such as the one induced by chronic chemical injury, as NLRC5-deficient and wildtype control mouse livers develop comparable levels of fibrosis. It is possible that adaptive repair mechanisms might have attenuated the increased inflammatory response in NLRC5-deficient mice, obscuring its effect after 5 weeks of CCl₄ treatment. Therefore, it will be worthwhile to evaluate the effect of NLRC5 deficiency at early stages of acute injury. As TNF signaling plays a crucial pathogenic role in obesity-associated hepatic inflammation and hepatocarcinogenesis (10), the constitutively elevated p65 phosphorylation NLRC5-deficient livers also warrants further investigations into possible regulatory functions of NLRC5 on NF- κ B activation and TNF

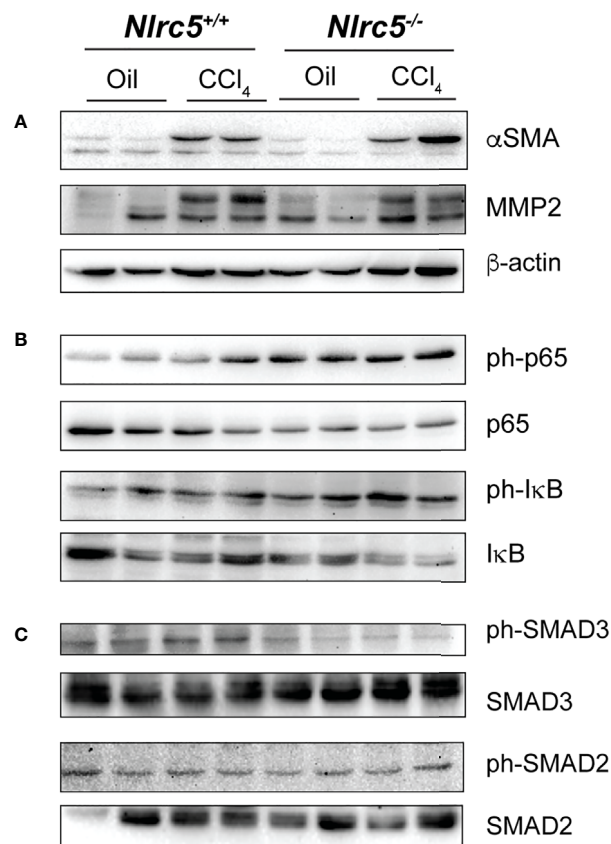


FIGURE 7 | NLRC5-deficient livers display elevated levels of phospho-p65 and diminished levels of phospho-SMAD3. Liver tissue homogenates from control and NLRC5-deficient livers following treatment with CCl₄ or corn oil were evaluated for the expression of the indicated proteins associated with liver fibrosis **(A)**, NF-κB signaling **(B)** and TGFβ signaling **(C)**. At least four samples for each group from more than two experiments were tested, and representative data for two mice per group are shown.

production under milder but chronic inflammatory conditions such as the one associated with diet-induced fatty liver disease and HCC development.

DATA AVAILABILITY STATEMENT

The original contributions presented in the study are included in the article/**Supplementary Material**. Further inquiries can be directed to the corresponding author.

ETHICS STATEMENT

The animal study was reviewed and approved by Université de Sherbrooke Animal Ethics Committee (Protocol # 2018-2083, 359-18C).

AUTHOR CONTRIBUTIONS

SI, TK, and SR conceived the idea. SI obtained funding. SI, AQ, and AS designed the experiments, analyzed data and wrote

the manuscript. FR, MC, and AG repeated certain experiments. All authors contributed to the article and approved the submitted version.

FUNDING

This work was supported by the Canadian Institutes of Health Research project grant PJT-153255 to SI. AG is a recipient of a postdoctoral fellowship from FRQS. CR-CHUS is an FRQS-funded research center.

ACKNOWLEDGMENTS

The authors thank Dr. Dana Philpott for generously sharing NLRC5 knockout mice.

SUPPLEMENTARY MATERIAL

The Supplementary Material for this article can be found online at: <https://www.frontiersin.org/articles/10.3389/fimmu.2021.749646/full#supplementary-material>

REFERENCES

- Rockey DC, Bell PD, Hill JA. Fibrosis—a Common Pathway to Organ Injury and Failure. *N Engl J Med* (2015) 372:1138–49. doi: 10.1056/NEJMra1300575
- Wynn TA. Common and Unique Mechanisms Regulate Fibrosis in Various Fibroproliferative Diseases. *J Clin Invest* (2007) 117:524–9. doi: 10.1172/JCI31487
- Wynn TA, Ramalingam TR. Mechanisms of Fibrosis: Therapeutic Translation for Fibrotic Disease. *Nat Med* (2012) 18:1028–40. doi: 10.1038/nm.2807
- Duffield JS, Lupher M, Thannickal VJ, Wynn TA. Host Responses in Tissue Repair and Fibrosis. *Annu Rev Pathol* (2013) 8:241–76. doi: 10.1146/annurev-pathol-020712-163930
- Schuppan D, Kim YO. Evolving Therapies for Liver Fibrosis. *J Clin Invest* (2013) 123:1887–901. doi: 10.1172/JCI66028
- Ratziu V, Friedman SL. Why do So Many NASH Trials Fail? *Gastroenterology* (2020). doi: 10.1053/j.gastro.2020.05.046
- Henderson NC, Rieder F, Wynn TA. Fibrosis: From Mechanisms to Medicines. *Nature* (2020) 587:555–66. doi: 10.1038/s41586-020-2938-9
- Battaller R, Brenner DA. Liver Fibrosis. *J Clin Invest* (2005) 115:209–18. doi: 10.1172/JCI24282
- Hernandez-Gea V, Friedman SL. Pathogenesis of Liver Fibrosis. *Annu Rev Pathol* (2011) 6:425–56. doi: 10.1146/annurev-pathol-011110-130246
- Park EJ, Lee JH, Yu GY, He G, Ali SR, Holzer RG, et al. Dietary and Genetic Obesity Promote Liver Inflammation and Tumorigenesis by Enhancing IL-6 and TNF Expression. *Cell* (2010) 140:197–208. doi: 10.1016/j.cell.2009.12.052
- Pellicoro A, Ramachandran P, Iredale JP, Fallowfield JA. Liver Fibrosis and Repair: Immune Regulation of Wound Healing in a Solid Organ. *Nat Rev Immunol* (2014) 14:181–94. doi: 10.1038/nri3623
- Seki E, Schwabe RF. Hepatic Inflammation and Fibrosis: Functional Links and Key Pathways. *Hepatology* (2015) 61:1066–79. doi: 10.1002/hep.27332
- Friedman SL. Mechanisms of Hepatic Fibrogenesis. *Gastroenterology* (2008) 134:1655–69. doi: 10.1053/j.gastro.2008.03.003
- Lozano R, Naghavi M, Foreman K, Lim S, Shibuya K, Aboyans V, et al. Global and Regional Mortality From 235 Causes of Death for 20 Age Groups in 1990 and 2010: A Systematic Analysis for the Global Burden of Disease Study 2010. *Lancet* (2012) 380:2095–128. doi: 10.1016/S0140-6736(12)61728-0
- Byass P. The Global Burden of Liver Disease: A Challenge for Methods and for Public Health. *BMC Med* (2014) 12:159. doi: 10.1186/s12916-014-0159-5
- Mokdad AA, Lopez AD, Shahrz S, Lozano R, Mokdad AH, Stanaway J, et al. Liver Cirrhosis Mortality in 187 Countries Between 1980 and 2010: A Systematic Analysis. *BMC Med* (2014) 12:145. doi: 10.1186/s12916-014-0145-y
- Farazi PA, DePinho RA. Hepatocellular Carcinoma Pathogenesis: From Genes to Environment. *Nat Rev Cancer* (2006) 6:674–87. doi: 10.1038/nrc1934
- Torre LA, Bray F, Siegel RL, Ferlay J, Lortet-Tieulent J, Jemal A. Global Cancer Statistics, 2012. *CA Cancer J Clin* (2015) 65:87–108. doi: 10.3322/caac.21262
- Whittaker S, Marais R, Zhu AX. The Role of Signaling Pathways in the Development and Treatment of Hepatocellular Carcinoma. *Oncogene* (2010) 29:4989–5005. doi: 10.1038/ncr.2010.236
- Schuppan D, Pinzani M. Anti-Fibrotic Therapy: Lost in Translation? *J Hepatol* (2012) 56 Suppl 1:S66–74. doi: 10.1016/S0168-8278(12)60008-7
- Trautwein C, Friedman SL, Schuppan D, Pinzani M. Hepatic Fibrosis: Concept to Treatment. *J Hepatol* (2015) 62:S15–24. doi: 10.1016/j.jhep.2015.02.039
- Higashi T, Friedman SL, Hoshida Y. Hepatic Stellate Cells as Key Target in Liver Fibrosis. *Adv Drug Delivery Rev* (2017) 121:27–42. doi: 10.1016/j.addr.2017.05.007
- Tacke F. Targeting Hepatic Macrophages to Treat Liver Diseases. *J Hepatol* (2017) 66:1300–12. doi: 10.1016/j.jhep.2017.02.026
- Motta V, Soares F, Sun T, Philpott DJ. NOD-Like Receptors: Versatile Cytosolic Sentinels. *Physiol Rev* (2015) 95:149–78. doi: 10.1152/physrev.00009.2014
- Ting JP, Lovering RC, Alnemri ES, Bertin J, Boss JM, Davis BK, et al. The NLR Gene Family: A Standard Nomenclature. *Immunity* (2008) 28:285–7. doi: 10.1016/j.immuni.2008.02.005
- Maekawa T, Kufer TA, Schulze-Lefert P. NLR Functions in Plant and Animal Immune Systems: So Far and Yet So Close. *Nat Immunol* (2011) 12:817–26. doi: 10.1038/ni.2083
- Kobayashi KS, van den Elsen PJ. NLRC5: A Key Regulator of MHC Class I-Dependent Immune Responses. *Nat Rev Immunol* (2012) 12:813–20. doi: 10.1038/nri3339
- Benko S, Magalhaes JG, Philpott DJ, Girardin SE. NLRC5 Limits the Activation of Inflammatory Pathways. *J Immunol* (2010) 185:1681–91. doi: 10.4049/jimmunol.0903900
- Cui J, Zhu L, Xia X, Wang HY, Legras X, Hong J, et al. NLRC5 Negatively Regulates the NF-kappaB and Type I Interferon Signaling Pathways. *Cell* (2010) 141:483–96. doi: 10.1016/j.cell.2010.03.040
- Conti BJ, Davis BK, Zhang J, O'Connor W Jr, Williams KL, Ting JP. CATERPILLER 16.2 (CLR16.2), a Novel NBD/LRR Family Member That Negatively Regulates T Cell Function. *J Biol Chem* (2005) 280:18375–85. doi: 10.1074/jbc.M413169200
- Schneider M, Zimmermann AG, Roberts RA, Zhang L, Swanson KV, Wen H, et al. The Innate Immune Sensor NLRC3 Attenuates Toll-Like Receptor Signaling via Modification of the Signaling Adaptor TRAF6 and Transcription Factor NF-KappaB. *Nat Immunol* (2012) 13:823–31. doi: 10.1038/ni.2378
- Xia X, Cui J, Wang HY, Zhu L, Matsueda S, Wang Q, et al. NLRX1 Negatively Regulates TLR-Induced NF-kappaB Signaling by Targeting TRAF6 and IKK. *Immunity* (2011) 34:843–53. doi: 10.1016/j.immuni.2011.02.022
- Benko S, Kovacs EG, Hezel F, Kufer TA. NLRC5 Functions Beyond MHC I Regulation—What Do We Know So Far? *Front Immunol* (2017) 8:150. doi: 10.3389/fimmu.2017.00150
- Li L, Xu T, Huang C, Peng Y, Li J. NLRC5 Mediates Cytokine Secretion in RAW264.7 Macrophages and Modulated by the JAK2/STAT3 Pathway. *Inflammation* (2014) 37:835–47. doi: 10.1007/s10753-013-9804-y
- Xu T, Ni MM, Huang C, Meng XM, He YH, Zhang L, et al. NLRC5 Mediates IL-6 and IL-1beta Secretion in LX-2 Cells and Modulated by the NF-KappaB/Smad3 Pathway. *Inflammation* (2015) 38:1794–804. doi: 10.1007/s10753-015-0157-6
- Xu T, Ni MM, Xing L, Li XF, Meng XM, Huang C, et al. NLRC5 Regulates TGF-Beta1-Induced Proliferation and Activation of Hepatic Stellate Cells During Hepatic Fibrosis. *Int J Biochem Cell Biol* (2016) 70:92–104. doi: 10.1016/j.biocel.2015.11.010
- Liu X, Wu Y, Yang Y, Li W, Huang C, Meng X, et al. Role of NLRC5 in Progression and Reversal of Hepatic Fibrosis. *Toxicol Appl Pharmacol* (2016) 294:43–53. doi: 10.1016/j.taap.2016.01.012
- Sun T, Ferrero RL, Girardin SE, Gommerman JL, Philpott DJ. NLRC5 Deficiency has a Moderate Impact on Immunodominant CD8(+) T Cell Responses During Rotavirus Infection of Adult Mice. *Immunol Cell Biol* (2019) 97:552–62. doi: 10.1111/imcb.12244
- Kandhi R, Bobbala D, Yeganeh M, Mayhue M, Menendez A, Ilangumaran S. Negative Regulation of the Hepatic Fibrogenic Response by Suppressor of Cytokine Signaling 1. *Cytokine* (2016) 82:58–69. doi: 10.1016/j.cyt.2015.12.007
- Naugler WE, Sakurai T, Kim S, Maeda S, Kim K, Elsharkawy AM, et al. Gender Disparity in Liver Cancer Due to Sex Differences in MyD88-Dependent IL-6 Production. *Science* (2007) 317:121–4. doi: 10.1126/science.1140485
- Sudo K, Yamada Y, Moriaki H, Saito K, Seishima M. Lack of Tumor Necrosis Factor Receptor Type 1 Inhibits Liver Fibrosis Induced by Carbon Tetrachloride in Mice. *Cytokine* (2005) 29:236–44. doi: 10.1016/j.cyt.2004.11.001
- Tarrats N, Moles A, Morales A, Garcia-Ruiz C, Fernandez-Checa JC, Mari M. Critical Role of Tumor Necrosis Factor Receptor 1, But Not 2, in Hepatic Stellate Cell Proliferation, Extracellular Matrix Remodeling, and Liver Fibrogenesis. *Hepatology* (2011) 54:319–27. doi: 10.1002/hep.24388
- Chaisson ML, Broiling JT, Ladiges W, Tsai S, Fausto N. Hepatocyte-Specific Inhibition of NF-kappaB Leads to Apoptosis After TNF Treatment, But Not After Partial Hepatectomy. *J Clin Invest* (2002) 110:193–202. doi: 10.1172/JCI0215295
- Gieling RG, Elsharkawy AM, Caamano JH, Cowie DE, Wright MC, Ebrahimi MR, et al. The C-Rel Subunit of Nuclear factor-kappaB Regulates Murine Liver Inflammation, Wound-Healing, and Hepatocyte Proliferation. *Hepatology* (2010) 51:922–31. doi: 10.1002/hep.23385
- Reddy GK, Enwemeka CS. A Simplified Method for the Analysis of Hydroxyproline in Biological Tissues. *Clin Biochem* (1996) 29:225–9. doi: 10.1016/0009-9120(96)00003-6

46. Gressner AM, Weiskirchen R. Modern Pathogenetic Concepts of Liver Fibrosis Suggest Stellate Cells and TGF- β as Major Players and Therapeutic Targets. *J Cell Mol Med* (2006) 10:76–99. doi: 10.1111/j.1582-4934.2006.tb00292.x
47. Radbill BD, Gupta R, Ramirez MC, DiFeo A, Martignetti JA, Alvarez CE, et al. Loss of Matrix Metalloproteinase-2 Amplifies Murine Toxin-Induced Liver Fibrosis by Upregulating Collagen I Expression. *Dig Dis Sci* (2011) 56:406–16. doi: 10.1007/s10620-010-1296-0
48. Hu YB, Li DG, Lu HM. Modified Synthetic siRNA Targeting Tissue Inhibitor of Metalloproteinase-2 Inhibits Hepatic Fibrogenesis in Rats. *J Gene Med* (2007) 9:217–29. doi: 10.1002/jgm.1009
49. Giannandrea M, Parks WC. Diverse Functions of Matrix Metalloproteinases During Fibrosis. *Dis Model Mech* (2014) 7:193–203. doi: 10.1242/dmm.012062
50. Moreno M, Battaller R. Cytokines and Renin-Angiotensin System Signaling in Hepatic Fibrosis. *Clin Liver Dis* (2008) 12:825–52. doi: 10.1016/j.cld.2008.07.013
51. Marra F, Tacke F. Roles for Chemokines in Liver Disease. *Gastroenterology* (2014) 147:577–94.e1. doi: 10.1053/j.gastro.2014.06.043
52. Landsman L, Bar-On L, Zernecke A, Kim KW, Krauthgamer R, Shagdarsuren E, et al. CX3CR1 is Required for Monocyte Homeostasis and Atherogenesis by Promoting Cell Survival. *Blood* (2009) 113:963–72. doi: 10.1182/blood-2008-07-170787
53. Yona S, Kim KW, Wolf Y, Mildner A, Varol D, Breker M, et al. Fate Mapping Reveals Origins and Dynamics of Monocytes and Tissue Macrophages Under Homeostasis. *Immunity* (2013) 38:79–91. doi: 10.1016/j.immuni.2012.12.001
54. Waddell LA, Lefevre L, Bush SJ, Raper A, Young R, Lisowski ZM, et al. ADGRE1 (EMR1, F4/80) Is a Rapidly-Evolving Gene Expressed in Mammalian Monocyte-Macrophages. *Front Immunol* (2018) 9:2246. doi: 10.3389/fimmu.2018.02246
55. Weston CJ, Zimmermann HW, Adams DH. The Role of Myeloid-Derived Cells in the Progression of Liver Disease. *Front Immunol* (2019) 10:893. doi: 10.3389/fimmu.2019.00893
56. Luedde T, Schwabe RF. NF- κ B in the Liver—Linking Injury, Fibrosis and Hepatocellular Carcinoma. *Nat Rev Gastroenterol Hepatol* (2011) 8:108–18. doi: 10.1038/nrgastro.2010.213
57. WHO. *Global Health and Aging*. World Health Organization (2011). Available at: https://www.who.int/ageing/publications/global_health.pdf.
58. Stahl EC, Haschak MJ, Popovic B, Brown BN. Macrophages in the Aging Liver and Age-Related Liver Disease. *Front Immunol* (2018) 9:2795. doi: 10.3389/fimmu.2018.02795
59. Murtha LA, Morten M, Schuliga MJ, Mabotwana NS, Hardy SA, Waters DW, et al. The Role of Pathological Aging in Cardiac and Pulmonary Fibrosis. *Aging Dis* (2019) 10:419–28. doi: 10.14336/AD.2018.0601
60. Kim IH, Xu J, Liu X, Koyama Y, Ma HY, Diggle K, et al. Aging Increases the Susceptibility of Hepatic Inflammation, Liver Fibrosis and Aging in Response to High-Fat Diet in Mice. *Age (Dordr)* (2016) 38:291–302. doi: 10.1007/s11357-016-9938-6
61. Liedtke C, Luedde T, Sauerbruch T, Scholten D, Streetz K, Tacke F, et al. Experimental Liver Fibrosis Research: Update on Animal Models, Legal Issues and Translational Aspects. *Fibrogenesis Tissue Repair* (2013) 6:19. doi: 10.1186/1755-1536-6-19
62. Yang YM, Seki E. TNF α in Liver Fibrosis. *Curr Pathobiol Rep* (2015) 3:253–61. doi: 10.1007/s40139-015-0093-z
63. Sanderson N, Factor V, Nagy P, Kopp J, Kondaiah P, Wakefield L, et al. Hepatic Expression of Mature Transforming Growth Factor β 1 in Transgenic Mice Results in Multiple Tissue Lesions. *Proc Natl Acad Sci USA* (1995) 92:2572–6. doi: 10.1073/pnas.92.7.2572
64. Dewidar B, Meyer C, Dooley S, Meindl-Beinker AN. TGF- β in Hepatic Stellate Cell Activation and Liver Fibrogenesis-Updated 2019. *Cells* (2019) 8. doi: 10.3390/cells8111419
65. Weng HL, Cai WM, Liu RH. Animal Experiment and Clinical Study of Effect of Gamma-Interferon on Hepatic Fibrosis. *World J Gastroenterol* (2001) 7:42–8. doi: 10.3748/wjg.v7.i1.42
66. Baroni GS, D'Ambrosio L, Curto P, Casini A, Mancini R, Jezequel AM, et al. Interferon Gamma Decreases Hepatic Stellate Cell Activation and Extracellular Matrix Deposition in Rat Liver Fibrosis. *Hepatology* (1996) 23:1189–99. doi: 10.1002/hep.510230538
67. Shukla A, Cloutier M, Appiya Santharam M, Ramanathan S, Ilangumaran S. The MHC Class-I Transactivator NLRC5: Implications to Cancer Immunology and Potential Applications to Cancer Immunotherapy. *Int J Mol Sci* (2021) 22:1964. doi: 10.3390/ijms22041964
68. Meng Q, Cai C, Sun T, Wang Q, Xie W, Wang R, et al. Reversible Ubiquitination Shapes NLRC5 Function and Modulates NF- κ B Activation Switch. *J Cell Biol* (2015) 211:1025–40. doi: 10.1083/jcb.201505091
69. Kumar H, Pandey S, Zou J, Kumagai Y, Takahashi K, Akira S, et al. NLRC5 Deficiency Does Not Influence Cytokine Induction by Virus and Bacteria Infections. *J Immunol* (2011) 186:994–1000. doi: 10.4049/jimmunol.1002094
70. Robbins GR, Truax AD, Davis BK, Zhang L, Brickey WJ, Ting JP. Regulation of Class I Major Histocompatibility Complex (MHC) by Nucleotide-Binding Domain, Leucine-Rich Repeat-Containing (NLR) Proteins. *J Biol Chem* (2012) 287:24294–303. doi: 10.1074/jbc.M112.364604
71. Yao Y, Wang Y, Chen F, Huang Y, Zhu S, Leng Q, et al. NLRC5 Regulates MHC Class I Antigen Presentation in Host Defense Against Intracellular Pathogens. *Cell Res* (2012) 22:836–47. doi: 10.1038/cr.2012.56
72. Tong Y, Cui J, Li Q, Zou J, Wang HY, Wang RF. Enhanced TLR-Induced NF- κ B Signaling and Type I Interferon Responses in NLRC5 Deficient Mice. *Cell Res* (2012) 22:822–35. doi: 10.1038/cr.2012.53
73. Yang L, Seki E. Toll-Like Receptors in Liver Fibrosis: Cellular Crosstalk and Mechanisms. *Front Physiol* (2012) 3:138. doi: 10.3389/fphys.2012.00138
74. Thiele ND, Wirth JW, Steins D, Koop AC, Ittrich H, Lohse AW, et al. TIMP-1 is Upregulated, But Not Essential in Hepatic Fibrogenesis and Carcinogenesis in Mice. *Sci Rep* (2017) 7:714. doi: 10.1038/s41598-017-00671-1
75. Osawa Y, Hoshi M, Yasuda I, Saibara T, Moriaki H, Kozawa O. Tumor Necrosis Factor- α Promotes Cholestasis-Induced Liver Fibrosis in the Mouse Through Tissue Inhibitor of Metalloproteinase-1 Production in Hepatic Stellate Cells. *PLoS One* (2013) 8:e65251. doi: 10.1371/journal.pone.0065251
76. Davis BK, Roberts RA, Huang MT, Willingham SB, Conti BJ, Brickey WJ, et al. Cutting Edge: NLRC5-Dependent Activation of the Inflammasome. *J Immunol* (2011) 186:1333–7. doi: 10.4049/jimmunol.1003111
77. Hammerich L, Tacke F. Interleukins in Chronic Liver Disease: Lessons Learned From Experimental Mouse Models. *Clin Exp Gastroenterol* (2014) 7:297–306. doi: 10.2147/CEG.S43737
78. Knight B, Lim R, Yeoh GC, Olynk JK. Interferon- γ Exacerbates Liver Damage, the Hepatic Progenitor Cell Response and Fibrosis in a Mouse Model of Chronic Liver Injury. *J Hepatol* (2007) 47:826–33. doi: 10.1016/j.jhep.2007.06.022
79. Shi Z, Wakil AE, Rockey DC. Strain-Specific Differences in Mouse Hepatic Wound Healing are Mediated by Divergent T Helper Cytokine Responses. *Proc Natl Acad Sci USA* (1997) 94:10663–8. doi: 10.1073/pnas.94.20.10663

Conflict of Interest: The authors declare that the research was conducted in the absence of any commercial or financial relationships that could be construed as a potential conflict of interest.

Publisher's Note: All claims expressed in this article are solely those of the authors and do not necessarily represent those of their affiliated organizations, or those of the publisher, the editors and the reviewers. Any product that may be evaluated in this article, or claim that may be made by its manufacturer, is not guaranteed or endorsed by the publisher.

Copyright © 2021 Quenum, Shukla, Rexhepi, Cloutier, Ghosh, Kufer, Ramanathan and Ilangumaran. This is an open-access article distributed under the terms of the Creative Commons Attribution License (CC BY). The use, distribution or reproduction in other forums is permitted, provided the original author(s) and the copyright owner(s) are credited and that the original publication in this journal is cited, in accordance with accepted academic practice. No use, distribution or reproduction is permitted which does not comply with these terms.



NlrX1-Regulated Defense and Metabolic Responses to *Aspergillus fumigatus* Are Morphotype and Cell Type Specific

OPEN ACCESS

Edited by:

Maciej Lech,
LMU Munich University Hospital,
Germany

Reviewed by:

Denis Gris,
Université de Sherbrooke,
Canada
Lakshna Mahajan,
University of Delhi, India

*Correspondence:

Shiv D. Kale
shiv@nimml.org

[†]These authors have contributed
equally to this work

Specialty section:

This article was submitted to
Molecular Innate Immunity,
a section of the journal
Frontiers in Immunology

Received: 29 July 2021

Accepted: 29 September 2021

Published: 01 November 2021

Citation:

Kastelberg B, Ayubi T,
Tubau-Juni N, Leber A,
Hontecillas R, Bassaganya-Riera J
and Kale SD (2021) NlrX1-
Regulated Defense and
Metabolic Responses to
Aspergillus fumigatus
Are Morphotype and
Cell Type Specific.
Front. Immunol. 12:749504.
doi: 10.3389/fimmu.2021.749504

Bridget Kastelberg[†], Tariq Ayubi[†], Nuria Tubau-Juni, Andrew Leber, Raquel Hontecillas, Josep Bassaganya-Riera and Shiv D. Kale^{*}

NIMML Institute, Blacksburg, VA, United States

The Nlr family member X1 (NlrX1) is an immuno-metabolic hub involved in mediating effective responses to virus, bacteria, fungi, cancer, and auto-immune diseases. We have previously shown that NlrX1 is a critical regulator of immune signaling and mortality in several models of pulmonary fungal infection using the clinically relevant fungus *Aspergillus fumigatus*. In the absence of NlrX1, hosts produce an enhanced Th2 response primarily by CD103+ dendritic cell populations resulting in enhanced mortality *via* immunopathogenesis as well as enhanced fungal burden. Here, we present our subsequent efforts showcasing loss of NlrX1 resulting in a decreased ability of host cells to process *A. fumigatus* conidia in a cell-type-specific manner by BEAS-2B airway epithelial cells, alveolar macrophages, bone marrow-derived macrophages, but not bone marrow-derived neutrophils. Furthermore, loss of NlrX1 results in a diminished ability to generate superoxide and/or generic reactive oxygen species during specific responses to fungal PAMPs, conidia, and hyphae. Analysis of glycolysis and mitochondrial function suggests that NlrX1 is needed to appropriately shut down glycolysis in response to *A. fumigatus* conidia and increase glycolysis in response to hyphae in BEAS-2B cells. Blocking glycolysis and pentose phosphate pathway (PPP) *via* 2-DG and NADPH production through glucose-6-phosphate dehydrogenase inhibitor resulted in significantly diminished conidial processing in wild-type BEAS-2B cells to the levels of NlrX1-deficient BEAS-2B cells. Our findings suggest a need for airway epithelial cells to generate NADPH for reactive oxygen species production in response to conidia *via* PPP. In context to fungal pulmonary infections, our results show that NlrX1 plays significant roles in host defense *via* PPP modulation of several aspects of metabolism, particularly glycolysis, to facilitate conidia processing in addition to its critical role in regulating immune signaling.

Keywords: NLRX1, *aspergillus fumigatus*, glycolysis, nod-like proteins, defense, fungi, reactive oxygen species, NADPH oxidase

INTRODUCTION

Aspergillus fumigatus is a clinically relevant, fungal pathogen that causes a wide variety of pulmonary disease manifestations. As an opportunistic pathogen, *A. fumigatus* relies on inherent deficiencies in the host immune system to facilitate disease (1). These clinically identified defects are often associated with an inability by the host to appropriately recruit innate immune cells, primarily macrophages and neutrophils, in order to identify, process, and clear the fungus (1). While much focus has been placed on macrophages and neutrophils, the importance of dendritic cell subsets, airway epithelial cells, and T cells as orchestrators of the innate and adaptive immune system has become evident (2–7). There has also been substantial effort to understand intra- and intercellular communication within and among host cell populations that facilitates these processes. Our prior work identified the host nod-like receptor X1 (Nlr1) as a critical regulator of defense and immune signaling that functioned in a cell- and context-specific manner (6). Here, we expand on aspects of that work using a variety of *in vitro* cell models and Nlr1 knockouts to unravel novel aspects of defense responses and metabolism that are fungal morphotype, host cell type, and Nlr1 dependent.

Studies to dissect defense responses to *A. fumigatus* have been primarily pursued in macrophages, neutrophils, and airway epithelial cells. Macrophages rapidly ingest *A. fumigatus* resting or swollen conidia *via* receptor-mediated phagocytosis followed by phagosome acidification and reactive oxygen species production (8–11). This process has been shown to be dependent upon LC3-associated phagocytosis, NOX2 NADPH oxidase complex, and enhancement of glycolysis (8–10). Neutrophils have also been shown to rapidly internalize and produce superoxide, hydrogen peroxide, and hypochlorous acid in response to resting and swollen conidia; however, the relative production of these defense compounds was significantly lower in resting conidia in comparison to swollen (12). Further non-oxidative responses have also been observed (13). Responses to the hyphal form of *A. fumigatus* results in the production of neutrophil extracellular traps that are thought to ensnare the fungus as well as allow for the generation of massive levels of reactive oxygen species *via* NADPH oxidases and myeloperoxidase (13, 14). Both neutrophils and macrophages provide important examples of morphotype-specific responses by critical host cell populations (13, 15).

In vitro internalization rates of *A. fumigatus* conidia by airway epithelial cells are highly variable, ranging from 10%–50%, and dependent on cell type (BEAS-2B, 16HBE14o-, A549, primary bronchial, nasal, etc.) [Reviewed in (16)]. Recognition of conidia by airway epithelial cells occurs in at least a Tlr2 manner and involves the increased expression of Dectin-1 (17). Processing of conidia has been shown to be dependent on host phosphoinositide 3-kinase, flotillin-2, caveolin, and Rab5c (11). Further several putative defensins have been identified to be expressed in response to conidia (17). A growing body of literature indicates that conidia are also processed extracellularly or made inactive though the precise mechanism(s) remaining unknown (11, 18). One study using transmission electron

microscopy did not observe internalization of *A. fumigatus* conidia by airway epithelial cells post challenge in immunosuppressed mice, but rather found conidia at junction sites between ciliated and/or goblet cells (19). Preliminary data on the generation of reactive oxygen species have been observed by airway epithelial cells after prolonged exposure to viable *A. fumigatus* resting conidia and is dependent on Dectin-1; however, this mechanism also remains unknown (17).

Nlr1 is a nod-like receptor consisting of a mitochondrial targeting signal, a nucleotide binding domain, and leucine-rich repeat domain. Nlr1 has been shown to be a critical regulator of host immune and defense responses to a variety of microbial pathogens, cancers, and auto-immune diseases [reviewed recently in (20)]. Mechanistically, Nlr1 appears to function as a multi-faceted hub. A subset of Nlr1's functions include its ability to bind TRAF6/2, thereby mitigating a variety of immune signal transduction pathways (21), interact within the inner mitochondrial membrane, thereby impacting mitochondrial function as well as forms of reactive oxygen species production (22–25), bind TUFM to facilitate autophagy and LC3-associated phagocytosis (26), and insulate the DNA sensing adaptors STING and/or MAVS to mitigate innate immune signaling to a variety of viruses (27, 28). This diversity of concurrent functions has made Nlr1 a promising therapeutic target for a variety of diseases (29, 30).

Our prior work on *Nlr1* identified the gene to be differentially expressed during models of invasive pulmonary aspergillosis (31). *In vivo* studies involving several models of invasive pulmonary aspergillosis using *Nlr1* knockout mice indicated enhanced fungal burden, mortality, and enhanced immune signaling towards a detrimental Th2 response *via* CD103+ dendritic cells in the absence of *Nlr1* that ultimately resulted in immunopathogenesis-driven mortality (6). We hypothesized that the enhanced fungal burden may function as a double detriment to the Th2-mediated immunopathogenesis. Here, we follow up on our prior observation of enhanced fungal burden by determining if the loss of *Nlr1* results in enhanced conidial survival in a variety of cell types as well as dissecting how Nlr1 mediates these processes. Results from this study provided novel insight into how Nlr1 regulates defense and metabolic responses to *A. fumigatus* in a morphotype- and cell-type-specific manner.

MATERIALS AND METHODS

Cell Extraction, Culture, and Maintenance

A. fumigatus strain Af293 was routinely cultured on glucose minimal media at 37°C for 5–7 days. Conidia were harvested in PBS + Tween 20 (0.1%) and passed through a 90-micron filter to remove hyphae and particulate prior to challenge. Fresh aliquots of *A. fumigatus* were taken after every fourth passage. Wild-type and Nlr1-deficient cells generated by CRISPR-Cas9 (Δ Nlr1) BEAS-2B cells were routinely cultured at 37°C in the presence of 5% CO₂ using RPMI base medium supplemented with 10% fetal bovine serum and 1× penicillin-streptomycin (6). Wild-type and

Δ Nlr1 BEAS-2B cells were grown to a maximum of 75% confluence and discarded after their ninth passage. Wild-type and Nlr1 knockout (*Nlr1*^{-/-}, derived from homozygous mice) bone marrow-derived macrophages (BMDMs) and bone marrow-derived neutrophils (BMDNs) were extracted from male mice between 15 and 30 weeks of age as previously described in (32). BMDNs were immediately utilized post purification. BMDMs were differentiated using 25 ng/ml M-CSF. On day 6 post incubation, BMDMs were seeded at 5×10^5 or 5×10^4 cells into 24- and 96-well plates, respectively, and utilized the following day for challenge experiments.

Challenge Assays

Freshly harvested Af293 conidia were challenged against wild-type and Nlr1-deficient BMDMs, BMDNs, alveolar macrophages, and immortalized human bronchial epithelial BEAS-2B cells (5×10^4 96-well, 5×10^5 24-well, American Type Culture Collection) for 3, 6, 9, 12, and/or 24 h at 37°C in the presence of 5% CO₂.

For the FUN-1 assay, conidia and mammalian cells were incubated with calcofluor white M2R (CFWM2R, 25 μ M) for 15 min to label conidia. Cells and conidia were incubated in NP-40 buffer (250 μ l) plus the metabolic dye FUN-1 (2.5 μ M) for 1 h at 37°C. Conidia (50,000–60,000) from independent challenges were analyzed by flow cytometry for FUN-1 and CRWM2R fluorescence. Positive gating was determined using conidia challenged onto empty tissue culture wells containing respective cell culture media. Independent experiments were run in triplicate. All experiments were independently repeated. Statistical difference was determined using the Kruskal–Wallis test followed by a Dunn's test for multiple comparisons. For challenge assays involving inhibitors, BEAS-2B cells were incubated for 3 h with the respective inhibitor prior to challenge and then washed 3 \times to remove the inhibitor.

For the XTT cell viability assay (CyQuant), cells (5×10^4 , 96-well) were challenged for 24 h with *A. fumigatus* conidia, washed with PBS, and resuspended in fresh media (100 μ l). Cells were then vigorously pipetted to lyse BEAS-2B cells as viable BEAS-2B cells masked XTT metabolism by the fungus. No PBS wash or vigorous pipetting was required for alveolar macrophage and BMDM challenges. XTT solution was made fresh as per the manufacturer's instruction and 50 μ l was added to each well. Cells were incubated for 2–4 h at 37°C and the absorbance was read at 450 and 660 nm (background correction). Corrected absorbance from media only wells was subtracted from challenges to determine specific absorbance. All experiments were independently repeated. Statistical significance was determined by Kruskal–Wallis test followed by a Dunn's test for multiple comparisons.

For the colony-forming unit assay, conidia (5×10^3) were challenged against cells (5×10^4) for 12 h and were resuspended in 250 μ l of NP-40 buffer, plated (50 μ l) onto GMM plates, and incubated for 12–24 h at 37°C. All experiments were independently repeated. Statistical significance was determined by the Kruskal–Wallis test followed by a Dunn's test for multiple comparisons.

Measurement of Reactive Oxygen Species Production and Oxidative Stress

Wild-type and Nlr1-deficient BEAS-2B airway epithelial cells, BMDMs, and BMDNs (50,000 per well, 96-well plate format) were pre-stained with ROS- and OS-specific fluorescent dyes (Enzo scientific, ROS-ID[®] ROS/RNS detection kit) for 30 min prior to challenge with fungal pathogen-associated molecular patterns (PAMPs) curdlan (100 ng/ml, InvivoGen), zymosan depleted (100 ng/ml, InvivoGen), zymosan (100 ng/ml, InvivoGen), killed hyphae (100 ng/ml, laboratory derived), and killed Af293 conidia (50,000 per well in 10 μ l). Cells were incubated at 37°C in the presence of 5% CO₂ prior to and post challenge. Fluorescence was measured for ROS production (Excitation: 490/14, Emission: 525/20) and OS production (Excitation: 550/20, Emission: 620/20) at 30, 60, 90, 180, 360, and 540 min post challenge using a Cytation 5 plate reader at 37°C in the presence of 5% CO₂. Experiments were conducted at 6 \times and repeated independently. Statistical difference was determined using the Kruskal–Wallis test followed by a Dunn's test for multiple comparisons.

Modified Mitochondrial and Glycolytic Stress Tests

Both mitochondrial and glycolytic stress tests were performed as described by the manufacturer's protocol (Agilent). Cells were plated at a density of 50,000 cells per well (24-well format) approximately 24 h prior to run. Cells were washed three times with PBS (500 μ l) and incubated for 1 h in serum and bicarbonate free DMEM in the absence of glutamine (glycolytic) or in the presence of 1 mM glutamine (mitochondrial) at 37°C. After initial baseline equilibration, fungal PAMPs curdlan (100 ng/ml) and zymosan depleted (100 ng/ml), killed conidia (50,000), killed hyphae (100 ng/ml), and control media were injected *via* port-A and allowed to mix prior to sequential addition of compounds for glycolytic and mitochondrial stress tests. For the mitochondrial stress test, basal respiration was determined by averaging the oxygen consumption rate (OCR) prior to treatment with control media. ATP production was determined by measuring the minimal OCR post oligomycin treatment and the average basal OCR. Maximal respiration was calculated based on the difference in maximal OCR post FCCP treatment and minimal OCR post oligomycin treatment. Spare capacity was determined by the difference in average basal OCR and the maximal OCR post FCCP treatment. For the glycolytic stress test, glycolytic activity was determined by the difference in basal extracellular acidification rate (ECAR) and ECAR post glucose treatment. Glycolytic capacity was determined by the difference in basal ECAR and ECAR post oligomycin treatment. Glycolytic reserve was determined by the difference in the ECAR post glucose injection and the ECAR post 2-DG injection. All experiments were independently repeated. *N* = 6. Statistical significance was assessed by the Kruskal–Wallis test followed by a Dunn's test for multiple comparisons.

RESULTS

We initially set out to determine if *Nlr1* contributes to the host cell's ability to process *A. fumigatus* conidia. Our prior efforts had indicated that loss of *Nlr1* resulted in enhanced fungal burden in immuno-competent and suppressed mice when inoculated with *A. fumigatus* (6). Loss of *Nlr1* in BEAS-2B airway epithelial cells, alveolar macrophages, and BMDMs, but not BMDNs resulted in significantly decreased conidial processing using both colony-forming units 12 h post

challenge as well as an XTT metabolism 24 h post challenge ($p < 0.05$ where denoted by an asterisk) (**Figures 1A, B, D–H**). We had previously established a flow cytometry assay to measure conidial viability through FUN-1 fluorescence at early time points post challenge (11). This assay also indicated that *Nlr1*-deficient BEAS-2B ($\Delta Nlr1$) cells processed approximately half as many viable conidia as wild-type cells 3 and 6 h post challenge ($p < 0.05$) (**Figure 1C**). Our *in vitro* results suggest that the contributions of *Nlr1* to fungal processing are relevant to airway epithelial cell and macrophages, two critical cell

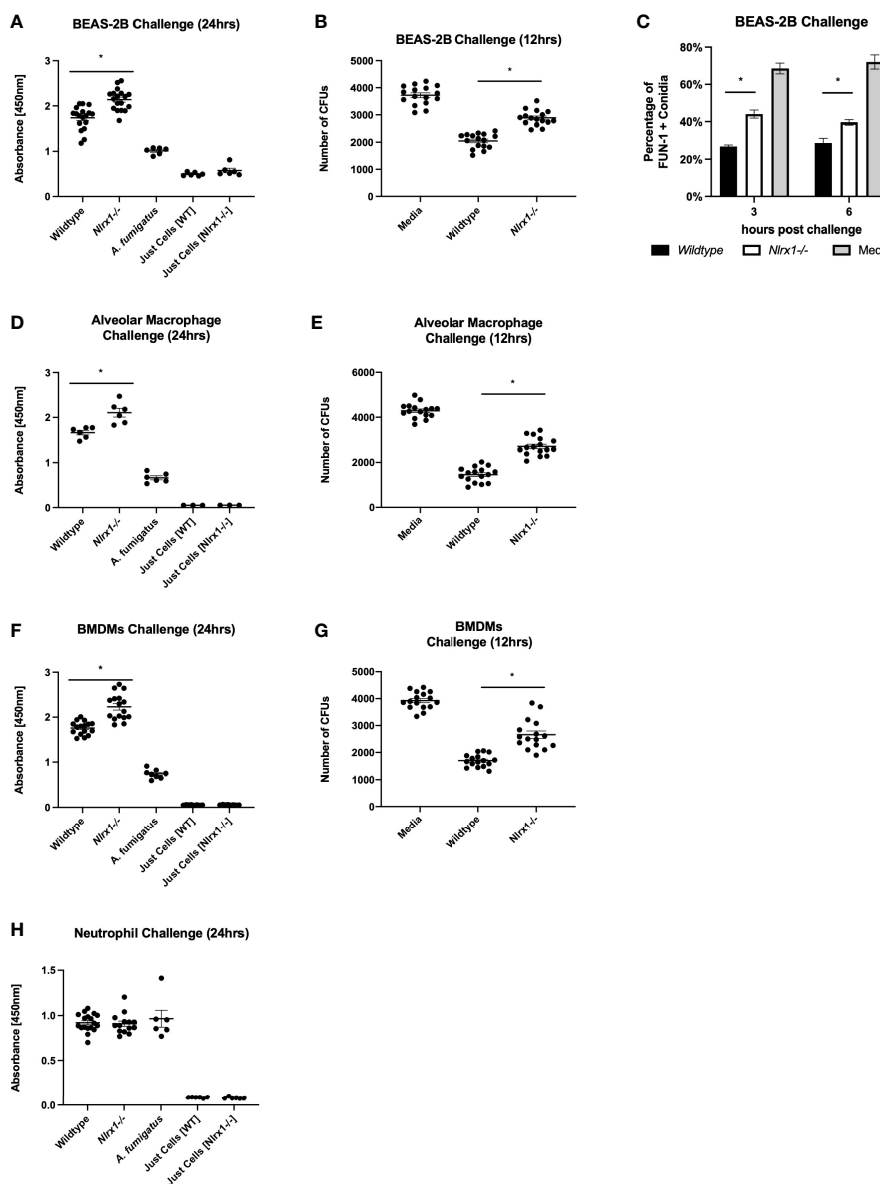


FIGURE 1 | *Nlr1* mediated *A. fumigatus* processing occurs in a cell-type-specific manner. Viable *A. fumigatus* conidia were challenged against wild-type and *Nlr1*-deficient (**A–C**) BEAS-2B airway epithelial cells, (**F, G**) bone marrow-derived macrophages, (**D, E**) alveolar macrophages, and (**H**) bone marrow-derived neutrophils. Conidial viability was assessed via (**A, D, F, H**) XTT viability assay 24 h post challenge, (**B, E, G**) the colony-forming unit assay 12 h post challenge, and (**C**) FUN-1+ fluorescence assay 3 h post challenge. $p < 0.05$, indicated by asterisk via Kruskal–Wallis test followed by a Dunn's test for multiple comparisons.

populations involved in early response to and processing of *A. fumigatus*. BMDNs did not have an altered ability to process conidia. This finding is quite relevant as enhanced mortality and fungal burden dependent on Nlr1 were greater in *in vivo* models of IPA where neutrophils were depleted or rendered ineffectual (6). It has yet to be determined if Nlr1 impacts processing of hyphae in these cell types.

Prior work of others indicates reactive oxygen species production, specifically superoxide produced by NADH and NADPH oxidases, are critical for processing *A. fumigatus* conidia by macrophages (8–10). Nlr1 has been shown to be needed for robust generation of reactive oxygen species to combat a variety of microbial pathogens (22–25). We sought to determine if Nlr1 regulated the production of general oxidative stress (ROS) as well as specific generation of superoxide (O_2^-) in response to *A. fumigatus*. We established a time course approach (measurements at 30, 60, 90, 180, 360, and 540 min post challenge) using cell-stable fluorescent dyes to measure ROS as well as specific generation of O_2^- by BEAS-2B airway epithelial cells (Figures 2A–D and Supplementary Figure 1). We challenged both WT and Δ Nlr1 cell populations over 12 h with killed *A. fumigatus* conidia, killed hyphae, control buffer, or fungal PAMPs curdlan, zymosan, and zymosan depleted. Both curdlan and zymosan depleted are thought to be recognized by C-type lectin receptors such as Dectin-1, while zymosan is recognized by both human Tlr2 and Dectin-1. These three PAMPs are also commonly associated with the hyphal form of *A. fumigatus*.

Wild-type BEAS-2B cells produced O_2^- within 30 min to the three hyphae-associated fungal PAMPs and killed hyphae, but not to killed conidia in comparison to control (Figure 2A). Concurrent measurements of ROS indicated a robust response to all five stimuli in comparison to control by 30 min, but diminished to or below baseline levels by 60–90 min, with the exception of zymosan, which remained elevated throughout (Figure 2B). Δ Nlr1 cells produced significantly decreased amounts of O_2^- and general ROS in response to all stimuli in comparison to WT cells ($p < 0.05$) (Figures 2C, D and Supplementary Figure 1). The loss of ROS in the absence of Nlr1 correlated well with a decrease in conidial processing observed during challenge assays (Figure 1). Our findings illuminate a very exciting phenomena that BEAS-2B airway cells do not produce detectable levels of O_2^- over control PBS treatment in response to conidia, but do so for hyphae and hyphae-associated PAMPs. Further elevated ROS responses, which do occur for all five stimuli are mitigated in the absence of Nlr1. The decrease in ROS in the absence of Nlr1 fit well with the decreased processing of conidia observed by BEAS-2B cells.

We then conducted cellular ROS and OS measurements in BMDMs using killed conidia, and fungal PAMPs (Figures 2E, F and Supplementary Figure 2). Elevated and significant levels of O_2^- and ROS were detected in response to all four stimuli within 30 min as expected for phagocytic cells ($p < 0.05$). Surprisingly, loss of Nlr1 resulted in similar, non-statistically significant, levels of O_2^- and ROS in comparison to wild-type ($p > 0.10$). This finding suggested that Nlr1-dependent O_2^- and ROS production does not meaningfully contribute to the diminished conidial processing observed for the absence of Nlr1 in BMDMs.

We then performed similar experiments using BMDNs using the five stimuli. BMDNs did not produce elevated O_2^- in response to killed conidia, but did to hyphae and hyphae-associated PAMPs (Figures 2G, H and Supplementary Figure 3). BMDNs did produce statistically significant levels of ROS in response to conidia ($p < 0.05$), but the amount was minuscule in comparison to killed hyphae and fungal PAMPs. Loss of Nlr1 in BMDNs did not result in meaningful changes in ROS or OS production. Our initial assessment of ROS and OS regulation in response to *A. fumigatus* conidia and hyphae suggests that cell-type (BEAS-2B, BMDMs, and BMDNs) and morphotype (conidia, hyphae) responses are often, but not always, dependent upon Nlr1 (summarized in Table 1).

Loss of Nlr1 Results in Diminished Mitochondrial Function in BEAS-2B Cells

Our results suggested that BEAS-2B cells were processing a significant amount of conidia in a manner that did not involve superoxide production, but correlated with the need to rapidly produce alternate forms of reactive oxygen species in a Nlr1-dependent manner. ROS can be generated within the mitochondria as a product of oxidative phosphorylation (OxPhos) as well as in the cytoplasm by a variety of stress- and defense-related enzymes. To determine if Nlr1 was contributing to mitochondrial ROS generation in BEAS-2B cells *via* OxPhos, we conducted standard and modified mitochondrial stress test using BEAS-2B cells pre-challenged with killed *A. fumigatus* conidia, hyphae, and fungal PAMPs curdlan, zymosan depleted, and zymosan (Figure 3).

Loss of Nlr1 resulted in a near-complete loss of mitochondrial ATP-linked respiration, a significantly diminished maximal respiration and spare capacity using the standard mitochondrial stress test ($p < 0.05$, Figures 3A–C, O–R). Our data suggest that mitochondrial respiration is what we would assume to be near the minimum possible to retain viability for Δ Nlr1 BEAS-2B cells. At first impression, this would fit with the decreased production of O_2^- and ROS. However, treatment of wild-type BEAS-2B cells with killed hyphae resulted in significantly decreased mitochondrial respiration, maximal respiration, and a complete lack of spare capacity (Figures 3I, M, O–R). This suggested that the observed increases in ROS and superoxide production in response to hyphae by WT BEAS-2B cells was not a part of mitochondrial OxPhos. Treatment of WT BEAS-2B cells with killed conidia or fungal PAMPs did not appear to modulate mitochondrial respiration, further indicating that the observed O_2^- and general ROS responses did not correlate with changes in mitochondrial function (Figures 3G, H, J–L, N–R). Though the decrease in ROS and OS as well as mitochondrial function appear to correlate in the absence of Nlr1, the significant decrease in mitochondrial function as measured by oxygen consumption by wild-type cells does not fit this hypothesis, suggesting that Nlr1 function in ROS is occurring elsewhere or indirectly associated with its role in the mitochondria. Our results additionally highlight a novel finding that BEAS-2B cells respond to hyphae, but not conidia, by immediately diminishing mitochondrial OxPhos as measured by oxygen consumption. These unique responses fit the notion of

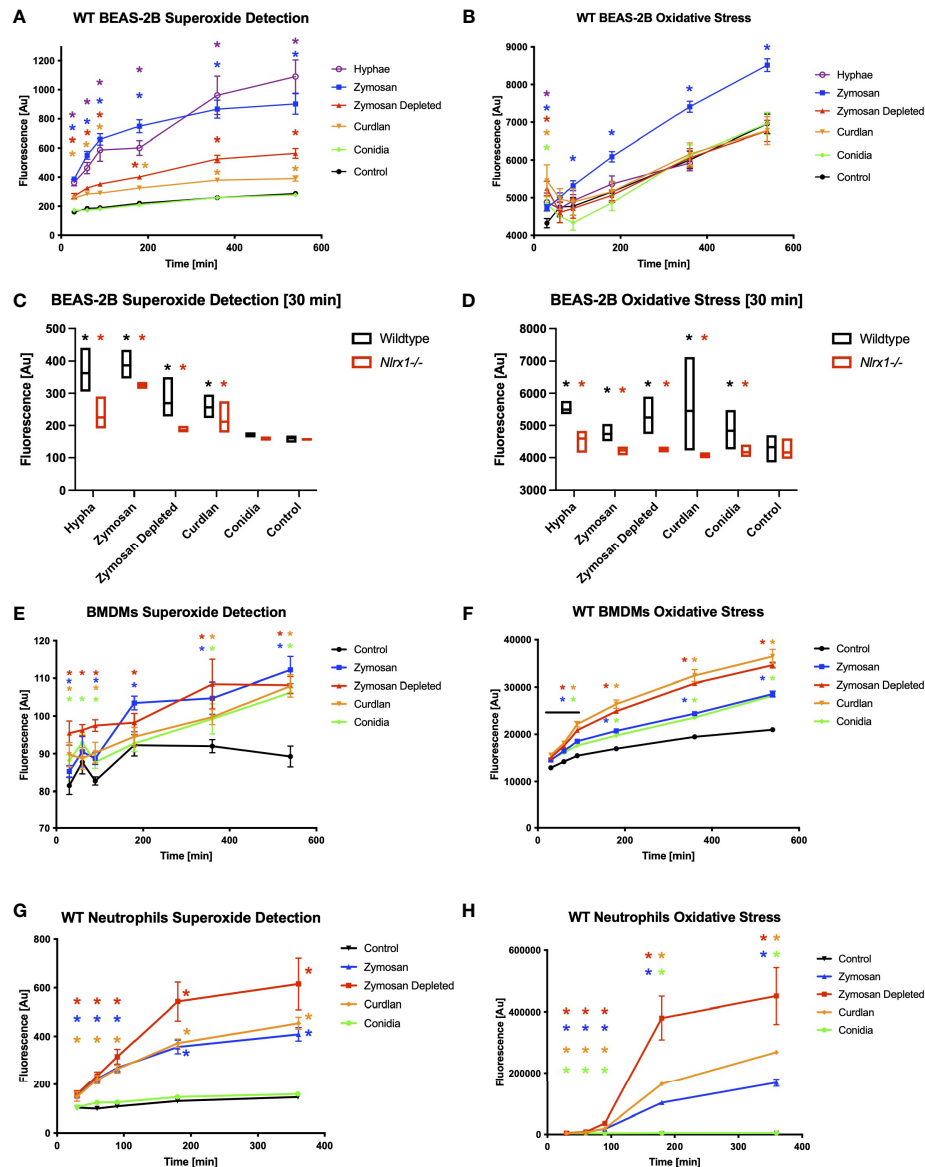


FIGURE 2 | Reactive oxygen species production and superoxide production in response to *A. fumigatus* conidia hyphae, and a subset of fungal PAMPs is dependent on Nlr1. BEAS-2B airway epithelial cells were pre-stained for 30 min with cell-permeable, stable fluorescent dyes specific for (A, C, E, G) superoxide production or (B, D, F, H) general reactive oxygen species production prior to challenge. (A, B) Wild-type BEAS-2B cells, (E, F) bone marrow-derived macrophages, and (G, H) neutrophils were challenged for 9 h with killed *A. fumigatus* conidia, hyphae, and fungal PAMPs, and fluorescence was measured 30, 60, 90, 180, 360, and 540 min post challenge. Colored asterisk (corresponding to treatment group) denotes $p < 0.05$ via Kruskal–Wallis test followed by a Dunn’s test for multiple comparisons against the control. Black asterisk denotes $p < 0.05$ via Kruskal–Wallis test followed by a Dunn’s test for multiple comparisons against the control. Red asterisk denotes $p < 0.05$ between genotypes for a given treatment group. **Supplementary Figures S1–S3** show time course data for Nlr1-deficient background compared to wild type.

morphotype-specific responses by the host cell that have been observed by our group and others.

Glycolysis Is Differentially Modulated in Response to *A. fumigatus* Conidia and Hyphae in a Nlr1-Dependent Manner

Given the novel observation of decreased mitochondrial respiration in response to hyphae and the lack of direct

correlation between mitochondrial respiration and superoxide/ROS production in response to *A. fumigatus* by BEAS-2B cells, we thought to explore if glycolysis is perturbed in response to *A. fumigatus* and if this process is dependent on Nlr1. Early aspects of glycolysis serve as a central conduit to the pentose phosphate pathway, which is a critical source of NADPH utilized by NADPH oxidases to generate ROS. When sugars are diverted to the PPP, glycolysis can also become effectively diminished.

TABLE 1 | Summary of superoxide production and ROS production and their dependency on Nlr1 in response to *A. fumigatus* and fungal PAMPs.

BEAS-2B Airway Epithelial Cells				
	Superoxide Production	Nlr1 Dependency	ROS Production	Nlr1 Dependency
Conidia Killed	-	Not Applicable	+	Yes
Hyphae Killed	+	Yes	+	Yes
Curdlan	+	Yes	+	Yes
Zymosan	+	Yes	+	Yes
Zymosan Depleted	+	Yes	+	Yes
Bone Marrow Derived Macrophages				
	Superoxide Production	Nlr1 Dependency	ROS Production	Nlr1 Dependency
Conidia Killed	+	No	+	No
Hyphae Killed	+	No	+	No
Curdlan	+	No	+	No
Zymosan	+	No	+	No
Zymosan Depleted	+	No	+	No
Bone Marrow Derived Neutrophils				
	Superoxide Production	Nlr1 Dependency	ROS Production	Nlr1 Dependency
Conidia Killed	-	Not Applicable	+	No
Hyphae Killed	+	No	+	No
Curdlan	+	No	+	No
Zymosan	+	No	+	No
Zymosan Depleted	+	No	+	No

Summarized data are from BEAS-2B airway epithelial cells, bone marrow-derived macrophages, and bone marrow-derived neutrophils.

Similarly, movement of molecules into the TCA cycle can give a false appearance that glycolysis is shut down when in fact glycolysis is occurring just not *via* lactate production as measured in the glycolytic stress test. We conducted a standard glycolytic stress test as well as the modified form where we once again pretreated cells with killed *A. fumigatus* conidia, hyphae, and fungal PAMPs. The basal glycolytic stress test indicated that Nlr1-deficient cells were statistically deficient in glycolysis and had diminished glycolytic capacity and glycolytic reserve ($p < 0.05$) (Figures 4A–C, O–Q). Thus, the absence of Nlr1 also decreases basal glycolysis function and reserve.

Surprisingly, pre-treating BEAS-2B cells with killed conidia resulted in near-complete shutdown of glycolysis, glycolytic capacity, and reserve during the glycolytic stress test. This highly novel and significant finding suggests that glycolysis is shut down in response to killed conidia (Figures 4D, E). This shutdown may be part of a process to shunt glucose into the PPP to facilitate NADPH production to be utilized for ROS production, thereby reducing lactate production, which is indirectly measured *via* decreased changes in pH over time (ECAR) by the Seahorse metabolic flux analyzer. Even more surprising, Nlr1-deficient BEAS-2B cells did not shut down glycolysis in response to conidia and had a similar response to Nlr1-deficient cells treated with control buffer (Figures 4J, N–Q). We conclude that loss of Nlr1 results in a failure to shut down glycolysis in response to conidia by BEAS-2B cells. This failure to shut down glycolysis may provide an explanation into why enhanced conidial germination and decreased ROS production is observed for Δ Nlr1 cells.

Contrastingly, treatment of BEAS-2B cells with killed hyphae prior to the stress test indicated significantly elevated glycolysis, decreased glycolytic capacity, and a near-complete depletion of the glycolytic reserve in comparison to control cells ($p < 0.05$) (Figures 4D, E, I, M, O–Q). Nlr1-deficient BEAS-2B cells treated with hyphae were also elevated in glycolysis in comparison to control treatments yet were decreased in glycolysis activation in comparison to wild type treated with hyphae. Both WT and Nlr1-deficient BEAS-2B cells were completely depleted of any glycolytic reserves, suggesting significant bioenergetics in response to stimuli.

Treatment with curdlan and zymosan did not significantly elevate glycolysis, but did significantly decrease glycolytic reserve in comparison to control BEAS-2B cells (Figures 4G, H, K, L). Ultimately, our results suggest that BEAS-2B cells activate glycolysis and deplete reserves in response to killed hyphae while turning off glycolysis in response to conidia. Nlr1-deficient cells fail to ablate glycolysis in response to conidia and can only partially elevate glycolysis in response to hyphae (Figure 4F).

Block-Aid of Pentose Phosphate Pathway Reduces ROS Production and Processing in Response to *A. fumigatus* Conidia

Our results from the modified glycolytic stress tests indicated that glycolysis is significantly diminished in response to conidia and is also controlled *via* a Nlr1-dependent process or potentially Nlr1 directly. This finding fit well with the observation of decreased ROS production by Δ Nlr1 BEAS-2B

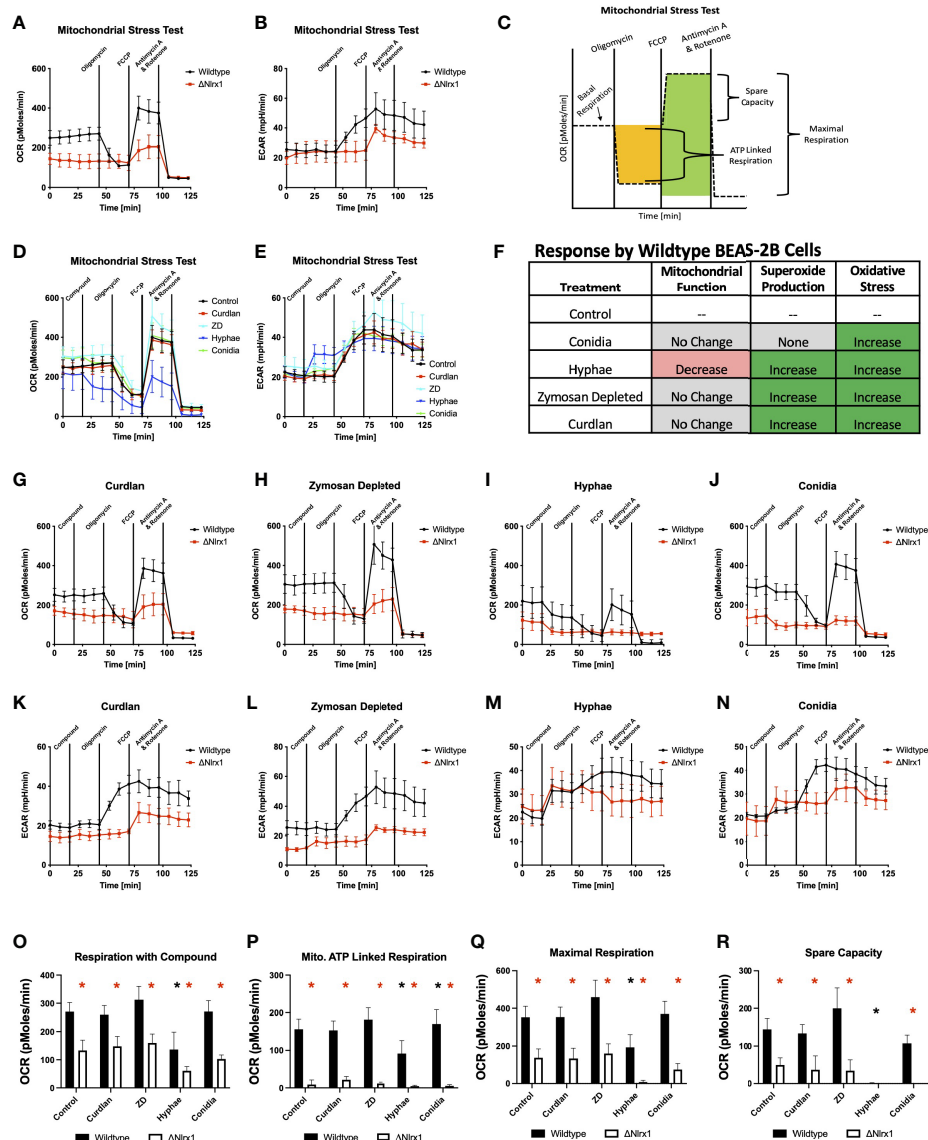


FIGURE 3 | Modulation of mitochondrial energetics within wild-type BEAS-2B cells in response to *A. fumigatus* conidia, hyphae, and a subset of fungal PAMPs is dependent on Nlr1. (A) Oxygen consumption rate (OCR, pmol/min) and (B) extracellular acidification rate (ECAR, mpH/min) for wild-type and Nlr1-deficient (Δ Nlr1) cells using a standardized mitochondrial stress test outlined in (C). Measurement of (D) OCR and (E) ECAR by wild-type BEAS-2B cells during a modified mitochondrial stress test. The modified version of the assay provides an injection of fungal PAMPs (zymosan depleted and curdlan), killed hyphae, or killed conidia prior to the standard test. (F) Summary of mitochondrial function, superoxide production, and general reactive oxygen species production by BEAS-2B cells in response to killed conidia, hyphae, and fungal PAMPs zymosan depleted, and curdlan. (G–J) OCR and (K–N) ECAR by wild-type and Δ Nlr1 BEAS-2B cells during a modified mitochondrial stress test using fungal PAMPs (zymosan depleted and curdlan), killed hyphae, or killed conidia. Calculated values for (O) respiration with compound, (P) mitochondrial ATP-linked respiration, (Q) maximal respiration, and (R) spare capacity. For (O–R), black asterisk denotes $p < 0.05$ via Kruskal–Wallis test followed by a Dunn's test for multiple comparisons against the control. Red asterisk denotes $p < 0.05$ between genotypes for a given treatment group.

cells and enhanced conidial germination. We hypothesized that the shutdown of glycolysis was occurring to facilitate a movement of energy towards the PPP to generate NADPH. To test this hypothesis, we treated wild-type BEAS-2B cells with 2-DG, an inhibitor of hexokinase and glucose-6-phosphate isomerase, thereby inhibiting glycolysis and PPP, as well as glucose-6-phosphate dehydrogenase inhibitor 1, an inhibitor of the enzyme responsible for NADPH production in PPP. We also

tested sodium oxamate, an inhibitor of lactate dehydrogenase, and a combination of Rotenone/Antimycin A, potent inhibitors of mitochondrial complex I and III, respectively.

Pre-treatment of wild-type BEAS-2B cells with either 2-DG or glucose-6-phosphate dehydrogenase inhibitor 1 resulted in a significantly increased percentage of metabolically viable conidia in comparison to control and produced similar viability levels as Δ Nlr1 ($p < 0.05$, Figure 5). Pre-treatment with sodium oxamate, a

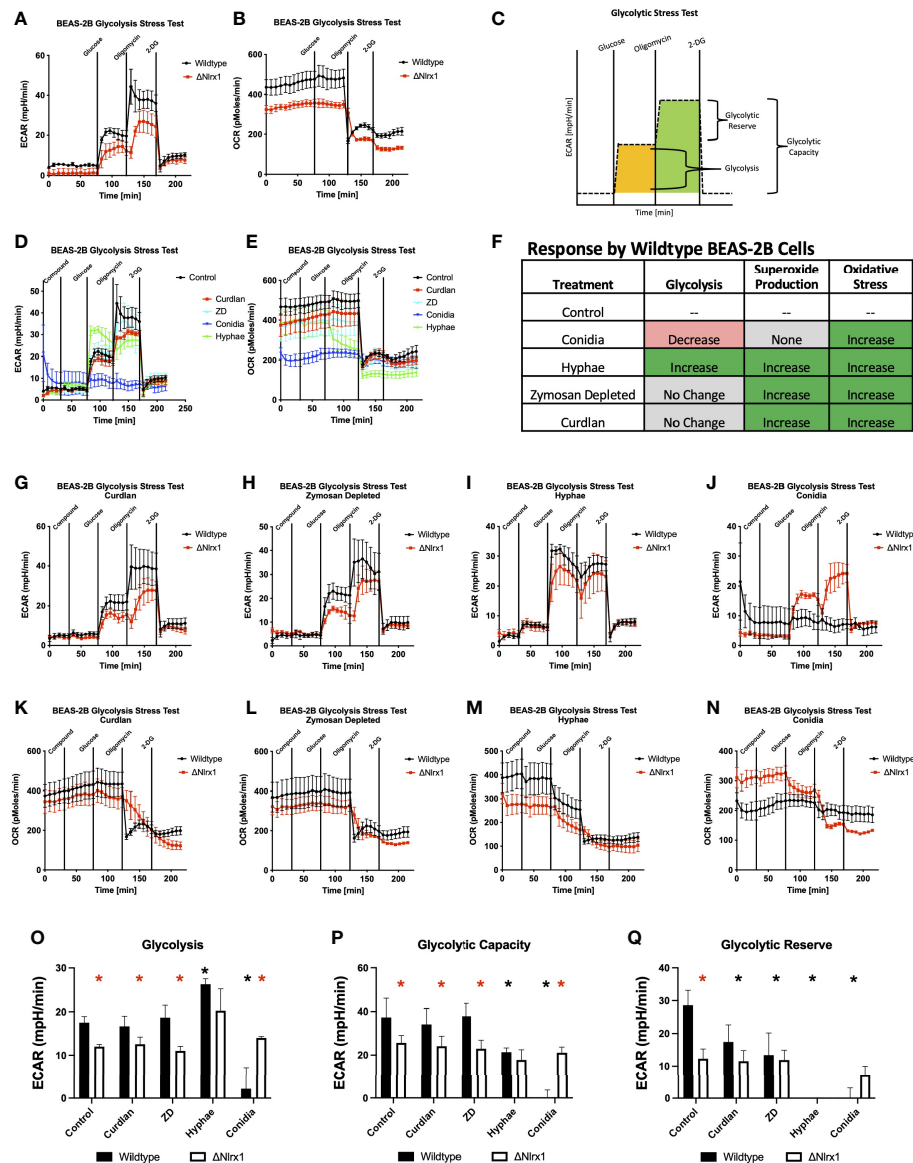


FIGURE 4 | Modulation of glycolysis within BEAS-2B in response to *A. fumigatus* conidia, hyphae, and a subset of fungal PAMPs is dependent on Nlr1. **(A)** Extracellular acidification rate (ECAR, mpH/min) and **(B)** oxygen consumption rate (OCR, pmol/min) for wild-type and Nlr1-deficient (Δ Nlr1) cells using a standardized glycolytic stress test outlined in **(C)**. Measurement of **(D)** ECAR and **(E)** OCR by wild-type BEAS-2B cells during a modified glycolytic stress test. The modified version of the assay provides an injection of fungal PAMPs (zymosan depleted and curdlan), killed hyphae, or killed conidia prior to the standard test. **(F)** Summary of glycolysis, superoxide production, and general reactive oxygen species production by BEAS-2B cells in response to killed conidia, hyphae, and fungal PAMPs zymosan depleted and curdlan. **(G–J)** ECAR and **(K–N)** OCR by wild-type and Δ Nlr1 BEAS-2B cells during a modified glycolytic stress test using fungal PAMPs (zymosan depleted and curdlan), killed hyphae, or killed conidia. Calculated values for **(O)** glycolysis, **(P)** glycolytic capacity, and **(Q)** glycolytic reserve. For **(O–Q)**, black asterisk denotes $p < 0.05$ via Kruskal–Wallis test followed by a Dunn’s test for multiple comparisons against the control. Red asterisk denotes $p < 0.05$ between genotypes for a given treatment group.

specific inhibitor of lactate dehydrogenase, did not alter conidial processing for WT or Δ Nlr1 cells ($p > 0.10$), while the treatment with Rot/AntA resulted in a statistically significant increase in conidial survival for both genotypes ($p < 0.05$, **Figure 5**). These results fit well with our working model that glycolysis is shut down in order to shunt glucose 6-phosphate to fuel the pentose phosphate pathway specifically NADPH production. While our

metabolic analysis *via* Seahorse metabolic flux analyzer did not identify a perturbation in mitochondrial function in response to killed conidia. Our inhibitor challenge assays suggest that loss of basal mitochondria function results in a Nlr1-independent decrease in conidial viability. A summary, working model is presented in **Figure 6** for how BEAS-2B cells respond to conidia and hyphae in a Nlr1-dependent manner based on our findings.

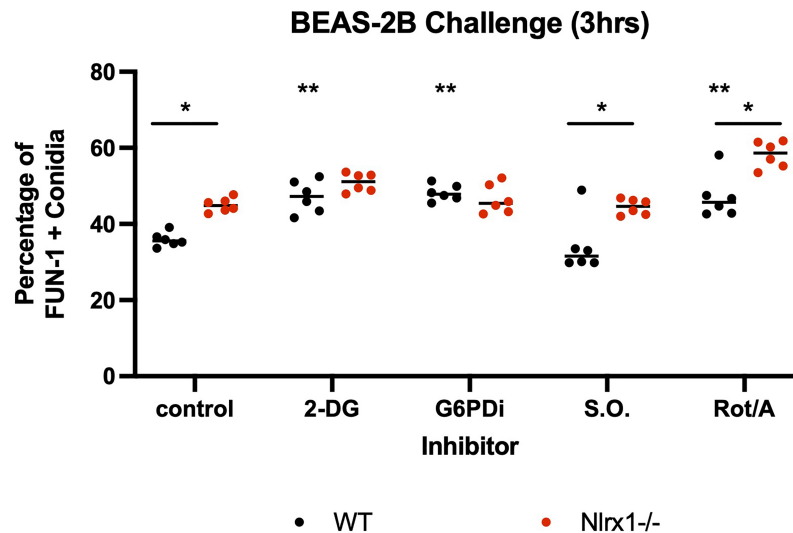


FIGURE 5 | Inhibition of glycolysis and mitochondrial function in BEAS-2B reduces early conidial processing. Wild-type and Nlr1-deficient (Δ Nlr1) BEAS-2B cells were pre-incubated with inhibitors at varying concentrations for 3 h. Cells were then washed three times with $2 \times$ PBS to remove all inhibitors. Cells were then challenged with AF293 for 3 h and a FUN-1+ fluorescence assay was subsequently conducted. Final concentration of inhibitors: 2-DG, 25 mM; G6PDi-1, 50 μ M; Sodium oxamate (S.O.), 25 mM; Rotenone/Antimycin A (Rot/Ant), 0.5 μ M. Black double asterisk denotes $p < 0.05$ via Kruskal-Wallis test followed by a Dunn's test for multiple comparisons against the control. Black single asterisk with a line across the two genotypes denotes $p < 0.05$ between genotypes for a given treatment group.

DISCUSSION

Host resistance and clearance of *A. fumigatus*, and other ubiquitous microorganisms inhaled into the respiratory system, is an inherent and evolved feature with significant selection pressure. Mucociliary clearance is thought to be a key mechanism by which conidia and fungal particulate are removed from the upper respiratory system. Beyond mucociliary clearance, there exists a highly coordinated process of inter- and intracellular signaling events leading to the appropriate recognition, processing, containment, and eventual clearance of *A. fumigatus*. Aberrations in these processes may result in a variety of disease manifestation. Our prior results using Nlr1-deficient mice in models of IPA indicated enhanced immunopathogenesis due to loss of regulation in both inter- and intracellular signaling as well as fungus burden, thereby resulting in a double detriment. Our *in vitro* studies indicate a defect in processing and killing of conidia by Nlr1-deficient airway epithelial cells, alveolar macrophages, and BMDMs. This fit well with the enhanced fungal burden observed for Nlr1-deficient mice in our prior studies on day 1 and day 3 post challenge using three different models of IPA and one of immuno-competent challenge (6).

Our results presented in this study indicate that conidia do not induce a specific production of superoxide in BEAS-2B cells, but rather induce general ROS production as an early burst that may be associated with general oxidative stress or specific production for defense purposes. The intensity of this burst was significantly lower in Δ Nlr1 cells. Reactive oxygen species can be produced as either a product or by-product of

mitochondrial function during oxidative phosphorylation (33). ROS, specifically hydrogen peroxide, can also be produced *via* NADPH-dependent DUOXs (DUOX1 and DUOX2) in a non-phagocytic manner at the cell membrane (34). Given our prior work and that of others on extracellular processing of conidia by airway epithelial cells (11, 18), DUOXs are a prime candidate for this function. DUOXs have also been previously shown to be critical in the killing and/or immune response to a number of microbes including *Helicobacter felix*, *Pseudomonas aeruginosa*, *Enterococcus faecalis*, *Candida albicans*, and influenza A virus, as well as maintaining gut and pulmonary homeostasis (35–41). Given the lack of mitochondrial perturbation in response to conidia as well as the Nlr1-independent effect of Rot/AntA on conidial processing, we suspect that the Nlr1-dependent ROS burst observed would therefore be due to NADPH oxidases such as DUOXs.

Cellular NADPH can be generated from glucose-6-phosphate dehydrogenase (G6PD) in the pentose phosphate pathway, cytoplasmic isocitrate dehydrogenase (IDH1), and cytoplasmic maleic enzyme (ME1) [Reviewed in (42)]. Our analysis of glycolysis *via* Seahorse metabolic flux analyzer indicated that glycolysis was significantly decreased in response to conidia by wild-type BEAS-2B cells. One explanation to this occurrence was the need to move molecules into the pentose phosphate pathway. Inhibition of glycolysis and the pentose phosphate pathway *via* 2-DG and the specific inhibition of G6PD *via* G6PDi resulted in significant increase in conidial survival post challenge against WT BEAS-2B cells to levels similar to the Nlr1 knockout. Our results in total suggest that the shutdown of glycolysis in response to *A. fumigatus* conidia is regulated by Nlr1 to shunt glucose towards

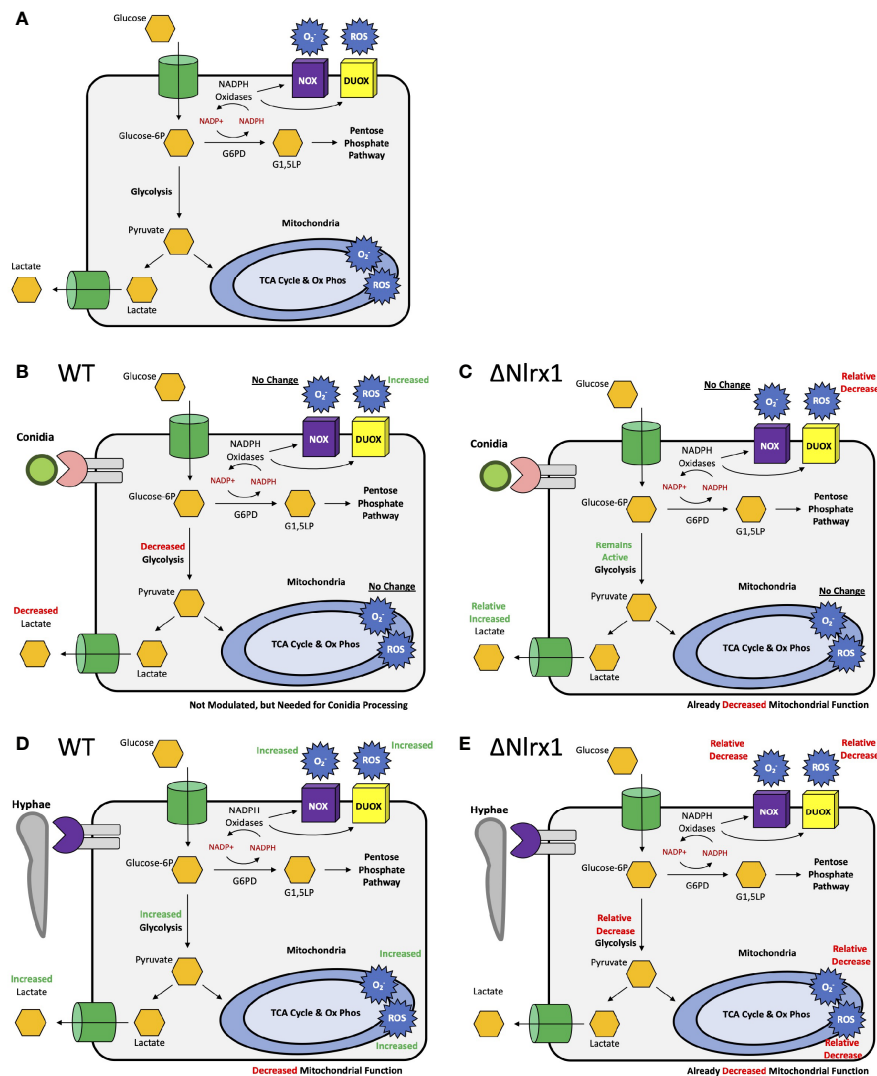


FIGURE 6 | Simplified, working models for metabolic responses to conidia and hyphae in airway epithelial cells and their dependency on Nlr1. **(A)** Simplified representation of glycolysis, the pentose phosphate pathway, oxidative phosphorylation, ROS, and superoxide production. Modulation of these pathways in response to **(B)** conidia and **(D)** hyphae by wild-type cells. Relative modulation of these pathways in response to **(C)** conidia and **(E)** hyphae by Nlr1-deficient cells in comparison to wild type.

the pentose phosphate pathway to generate NADPH. This response has not been observed for *A. fumigatus* conidia or clinically relevant fungi to the best of our knowledge. How Nlr1 shuts down glycolysis in response to *A. fumigatus* conidia is of high relevance as this cellular metabolic function is critical for processing conidia. The increase in glycolysis and depletion of reserves in response to hyphae suggest that metabolism is an important component in mediating the appropriate morphotype-specific response to *A. fumigatus*.

An increase in glycolysis in response to a bacteria, parasites, and viruses has been documented for several pathosystems (43–46). A recent study has observed enhanced glycolysis in response to *A. fumigatus* conidia by macrophage cell types (8). Our results

support this connection as we noted a robust production of superoxide and ROS by BMDMs that is Nlr1 dependent. Differences in the method of ROS generation between the cell types will be exciting to explore into the future as ample prior evidence suggests cell-specific ROS generation [reviewed in (34)]. Similarly, our work also suggests that Nlr1 plays a critical role in not only shutting down glycolysis when needed in response to conidia, but also its amplification in response to hyphae. How this contrasting modulation of glycolysis occurs will provide unique insight into the underlying differences for these signaling pathways in different cell types.

Much of our current study has centered around the role of an early ROS burst in response to *A. fumigatus* that is dependent on

Nlr1. However, it is critical to acknowledge a number of additional non-oxidative defense strategies such as secreted peptides and proteins (47–49) may also be differentially expressed in a decreasing manner in the Nlr1-deficient background. One broad conclusion of our study is that the functions and roles of Nlr1 continue to extend, and these processes, such as an absence of negative regulation of glycolysis may also impact additional processes within the cell such as gene expression of defense proteins.

Our preliminary work with BMDMs and alveolar macrophages indicated that Nlr1 is critical for conidial processing. Macrophages rapidly internalize *A. fumigatus* conidia and process conidia in a manner dependent on NADPH oxidases as shown through p47phox deficient macrophages and chemical inhibitors of NADPH oxidases (10). P47phox functions as a central organizer of the NOX2 NADPH oxidase phagocytic complex that produces superoxide (10). We observed small decreases in superoxide and ROS production by Nlr1-deficient BMDMs indicating that Nlr1 may be modulating additional non-oxidative aspects of conidial processing. Nlr1 has been shown to facilitate LC3-associated phagocytosis (LAP) of *Histoplasma capsulatum* in macrophages via cytoplasmic interactions with TUFM/ATG5-ATG12, but not Dectin-1/Syk-mediated ROS production (50). Loss of Nlr1 did not impact *H. capsulatum* replication, only LAP. It will be interesting to explore if Nlr1 regulates phagocytosis of *A. fumigatus* conidia in macrophages and neutrophils and if this process has an impact on conidial processing.

There have been a variety of reports indicating ROS production being independent or dependent on Nlr1. Overexpression and targeting of NLRX1 to the mitochondria triggered ROS production to levels similar to that produced by TNF α treatment in HeLa cells, suggesting a dependence on Nlr1 (23). Concurrent overexpression of Nlr1 and treatment of HeLa cells with either TNF α , *Shigella* infection, or the viral RNA analog polyinosinic:polycytidylic acid resulted in further enhanced ROS production (23). Similarly, Nlr1 overexpression was shown to enhance *Chlamydia trachomatis*-induced ROS production in HeLa cells (24). This ROS production could be inhibited via either DPI treatment, indicating that the source was cytoplasmic or membrane NOX and/or DUOX proteins or by siRNA targeting either DUOX1, DUOX2, or NOX4. This finding fits well with our hypothesis that Nlr1 is regulating ROS production external to the mitochondria in BEAS-2B epithelial cells.

Conversely, loss of Nlr1 has been shown to increase ROS production by BMDMs in response to *H. pylori* that correlated with decreased *H. pylori* survival post challenge (25). In animal and cell models of ischemia-reperfusion injury reactive oxygen species, specifically mitochondrial superoxide production was shown to increase in the absence of Nlr1 (51). No statistically significant or minimal decrease in ROS production was observed in *Nlr1*^{-/-} BMDMs and neutrophils in comparison to WT with a variety of PAMPs (LPS, TNF α , polyI: C, Pam3Cys, and fmlp) (28). Our results were in accord with these finding as we did not observe a Nlr1 dependency on

superoxide or ROS production by BMDMs and BMDNs in response to fungal PAMPs or killed conidia. Relatedly, Nlr1 was shown to not influence Syk/NADPH mediated ROS production in response to fungal pathogen *Histoplasma capsulatum*, but Nlr1 did modulate LC3 phagocytosis by macrophages via cytoplasmic interactions with TUFM/ATG5-ATG12 (50). In totality, the cell-type and morphotype specificity to *A. fumigatus* and fungal PAMPs observed in our work transcends to a wider scope and implies specific pathway level regulation of ROS production that is dependent on cell type and stimuli.

The function of Nlr1 in mitochondrial respiration has also been contrasting among studies, and recent meta-analysis suggests a highly cell-type-specific functionality of Nlr1 (52). Mechanistically, Nlr1 has been shown to translocate into the mitochondria where it interacts with UQCRC2, a member of complex III, and Fas-activated serine-threonine kinase family protein-5 (FASTKD5) (22, 23, 53). The Nlr1/UQCRC2/Complex III is thought to impact mitochondrial ROS as well as mitochondrial respiration (22, 23, 53). Nlr1 binding of FASTKD5 and mitochondrial RNA leads to an inhibition of maturation for transcripts encoding complex I and IV components (54). Loss of Nlr1 results in an increased rate of OxPhos in hepatocytes presumably due to maturation of these transcripts (54). In epithelial cell (HEK293) models of ischemia-reperfusion injury, loss of Nlr1 also resulted in increased oxygen consumption, oxidative stress, and downstream apoptosis (51). In CD4⁺ T cells, activation of Nlr1 leads to increased expression of markers associated with oxidative phosphorylation (29). Our results with BEAS-2B epithelial cells indicate that loss of Nlr1 resulted in decreased oxygen consumption, mitochondrial function, spare capacity, and maximal respiration during the mitochondrial stress test. We also observed a decreased oxygen consumption during the glycolytic stress test. Ultimately, these findings add the notion of Nlr1 being highly cell type specific in regards to mitochondrial function.

While our hypothesis is centered on the loss of Nlr1 resulting in a failure to modulate pathways at the protein level, an interesting hypothesis is that the loss of Nlr1 has resulted in an underlying change in gene expression that results in the loss of signal transduction pathway components from being expressed versus a failure for that pathway to transduce that signal in the absence of Nlr1. Given the observed effects of Nlr1 on maturing complex I and IV components as well as gene expression of OxPhos components, this will be an important consideration in the future (29, 54). Ongoing studies will allow us to determine if loss of Nlr1 changes the underlying transcriptome.

The interplay between host metabolism, immune signaling, and cellular defense towards microbes is an exciting field of study that presents novel therapeutic options and insight into host biology. One aspect of the intertwined and complex nature of these processes has been partially illuminated in the context of Nlr1. Why and how BEAS-2B cells decrease glycolysis in response to conidia yet increase for hyphae will be an exciting exploration for future studies. Furthermore, the physiological relevance of why glycolysis is decreased by non-hematopoietic

stem cell populations such as airway epithelial cells in response to conidia will also be important to determine.

DATA AVAILABILITY STATEMENT

The raw data supporting the conclusions of this article will be made available by the authors, without undue reservation.

ETHICS STATEMENT

The animal study was reviewed and approved by the NIMML Institute.

AUTHOR CONTRIBUTIONS

SK conceived the idea. SK, JB-R, and RH designed the experiments. BK, TA, NT-J, and SK conducted the experiments. BK, TA, NT-J, AL, and SK analyzed the results. BK and SK wrote the manuscript with input from all authors. All authors contributed to the article and approved the submitted version.

SUPPLEMENTARY MATERIAL

The Supplementary Material for this article can be found online at: <https://www.frontiersin.org/articles/10.3389/fimmu.2021.749504/full#supplementary-material>

REFERENCES

- Latge JP, Chamilos G. Aspergillus Fumigatus and Aspergillosis in 2019. *Clin Microbiol Rev* (2019) 33(1):1–75. doi: 10.1128/CMR.00140-18
- de Luca A, Bozza S, Zelante T, Zagarella S, D'Angelo C, Perruccio K, et al. Non-Hematopoietic Cells Contribute to Protective Tolerance to Aspergillus Fumigatus via a TRIF Pathway Converging on IDO. *Cell Mol Immunol* (2010) 7(6):459–70. doi: 10.1038/cmi.2010.43
- Loures FV, Rohm M, Lee CK, Santos E, Wang JP, Specht CA, et al. Recognition of Aspergillus Fumigatus Hyphae by Human Plasmacytoid Dendritic Cells Is Mediated by Dectin-2 and Results in Formation of Extracellular Traps. *PLoS Pathog* (2015) 11(2):e1004643. doi: 10.1371/journal.ppat.1004643
- Bozza S, Gaziano R, Spreca A, Bacci A, Montagnoli C, di Francesco P, et al. Dendritic Cells Transport Conidia and Hyphae of Aspergillus Fumigatus From the Airways to the Draining Lymph Nodes and Initiate Disparate Th Responses to the Fungus. *J Immunol* (2002) 168(3):1362–71. doi: 10.4049/jimmunol.168.3.1362
- Espinosa V, Jhingran A, Dutta O, Kasahara S, Donnelly R, Du P, et al. Inflammatory Monocytes Orchestrate Innate Antifungal Immunity in the Lung. *PLoS Pathog* (2014) 10(2):e1003940. doi: 10.1371/journal.ppat.1003940
- Kastelberg B, Tubau-Juni N, Ayubi T, Leung A, Leber A, Hontecillas R, et al. NLRX1 Is a Key Regulator of Immune Signaling During Invasive Pulmonary Aspergillosis. *PLoS Pathog* (2020) 16(9):e1008854. doi: 10.1371/journal.ppat.1008854
- Carvalho A, De Luca A, Bozza S, Cunha C, D'Angelo C, Moretti S, et al. TLR3 Essentially Promotes Protective Class I-Restricted Memory CD8(+) T-Cell Responses to Aspergillus Fumigatus in Hematopoietic Transplanted Patients. *Blood* (2012) 119(4):967–77. doi: 10.1182/blood-2011-06-362582
- Goncalves SM, Duarte-Oliveira C, Campos CF, Aimaniananda V, Ter Horst R, Leite L, et al. Phagosomal Removal of Fungal Melanin Reprograms Macrophage Metabolism to Promote Antifungal Immunity. *Nat Commun* (2020) 11(1):2282. doi: 10.1038/s41467-020-16120-z
- Kyrmizi I, Ferreira H, Carvalho A, Figueroa JAL, Zampas P, Cunha C, et al. Calcium Sequestration by Fungal Melanin Inhibits Calcium-Calmodulin Signalling to Prevent LC3-Associated Phagocytosis. *Nat Microbiol* (2018) 3(7):791–803. doi: 10.1038/s41564-018-0167-x
- Philippe B, Ibrahim-Granet O, Prevost MC, Gougerot-Pocidalo MA, Sanchez Perez M, van der Meeren A, et al. Killing of Aspergillus Fumigatus by Alveolar Macrophages Is Mediated by Reactive Oxidant Intermediates. *Infect Immun* (2003) 71(6):3034–42. doi: 10.1128/IAI.71.6.3034-3042.2003
- Clark HR, Powell AB, Simmons KA, Ayubi T, Kale SD. Endocytic Markers Associated With the Internalization and Processing of Aspergillus Fumigatus Conidia by BEAS-2b Cells. *mSphere* (2019) 4(1). doi: 10.1128/mSphere.00663-18
- Levitz SM, Diamond RD. Mechanisms of Resistance of Aspergillus Fumigatus Conidia to Killing by Neutrophils *In Vitro*. *J Infect Dis* (1985) 152(1):33–42. doi: 10.1093/infdis/152.1.33
- Gazendam RP, van Hamme JL, Tool AT, Hoogenboezem M, van den Berg JM, Prins JM, et al. Human Neutrophils Use Different Mechanisms To Kill Aspergillus Fumigatus Conidia and Hyphae: Evidence From Phagocyte Defects. *J Immunol* (2016) 196(3):1272–83. doi: 10.4049/jimmunol.1501811
- Bruns S, Knemeyer O, Hasenberg M, Aimaniananda V, Nietzsche S, Thywissen A, et al. Production of Extracellular Traps Against Aspergillus Fumigatus *In Vitro* and in Infected Lung Tissue Is Dependent on Invading Neutrophils and

Supplementary Figure 1 | Reactive oxygen species and oxidative stress production by wild type and Δ Nlr1 BEAS-2B airway epithelial in response to fungal PAMPs and *A. fumigatus*. Wild type and Δ Nlr1 BEAS-2B cells were pre-incubated with (A–F) a fluorescent dye specific for superoxide production or (G–L) a fluorescent oxidative stress (OS) indicator. Cells were then treated with (A, G) control PBS buffer, (B, H) killed hyphae, (C, I) zymosan, (D, J) curdlan, (E, K) zymosan depleted, or (F, L) killed conidia for 9hrs. Fluorescence was measured at 30, 60, 90, 180, 360, 540 min post treatment. N=6–8. Error bars denote standard deviation. All experiments were independently repeated. $P < 0.05$, indicated by asterisk via Kruskal-Wallis test followed up by a Dunn's test for multiple comparisons.

Supplementary Figure 2 | Reactive oxygen species and oxidative stress production by wild type and Nlr1 deficient bone marrow derived macrophages in response to fungal PAMPs and *A. fumigatus*. Wild type and Nlr1 deficient bone marrow derived macrophages (BMDMs) were pre-incubated with (A–F) a fluorescent dye specific for superoxide production or (G–L) a fluorescent oxidative stress (OS) indicator. Production of (A) superoxide and (B) reactive oxygen species by wildtype BMDMs to stimuli (killed conidia, zymosan depleted, zymosan, curdlan, and control PBS) over 9 hours. Wildtype and Nlr1-/- BEAS-2B cells were then treated with either (B, H) curdlan, (C, I) zymosan depleted, (D, J) zymosan, (E, K) killed conidia or (F, L) control PBS buffer over 9hrs. Fluorescence was measured at 30, 60, 90, 180, 360, 540 min post treatment. N=8. Error bars denote standard deviation. All experiments were independently repeated. $P < 0.05$, indicated by asterisk via Kruskal-Wallis test followed by a Dunn's test for multiple comparisons.

Supplementary Figure 3 | Reactive oxygen species and oxidative stress production by wild type and Nlr1 deficient bone marrow derived neutrophils in response to fungal PAMPs and *A. fumigatus*. Wild type and Nlr1 deficient bone marrow derived neutrophils (BMDNs) were pre-incubated with (A–G) a fluorescent dye specific for superoxide production or (H–N) a fluorescent oxidative stress (OS) indicator. Production of (A, B) superoxide and (H, I) reactive oxygen species by wildtype BMDNs to stimuli (killed conidia, zymosan depleted, zymosan, curdlan, and control PBS) over 6 hours. Cells were then treated with (C, J) curdlan, (D, K) zymosan depleted, (E, L) zymosan, (F, M) killed conidia or (G, N) control PBS buffer for 6hrs. Fluorescence was measured at 30, 60, 90, 180, 360 min post treatment. N=8. Error bars denote standard deviation. All experiments were independently repeated. $P < 0.05$, indicated by asterisk via Kruskal-Wallis test followed by a Dunn's test for multiple comparisons.

- Influenced by Hydrophobin RodA. *PLoS Pathog* (2010) 6(4):e1000873. doi: 10.1371/journal.ppat.1000873
15. Netea MG, Warris A, van der Meer JW, Fenton MJ, Verver-Janssen TJ, Jacobs LE, et al. *Aspergillus Fumigatus* Evades Immune Recognition During Germination Through Loss of Toll-Like Receptor-4-Mediated Signal Transduction. *J Infect Dis* (2003) 188(2):320–6. doi: 10.1086/376456
 16. Bigot J, Guillot L, Guitard J, Ruffin M, Corvol H, Balloy V, et al. Bronchial Epithelial Cells on the Front Line to Fight Lung Infection-Causing *Aspergillus Fumigatus*. *Front Immunol* (2020) 11:1041. doi: 10.3389/fimmu.2020.01041
 17. Sun WK, Lu X, Li X, Sun QY, Su X, Song Y, et al. Dectin-1 Is Inducible and Plays a Crucial Role in *Aspergillus*-Induced Innate Immune Responses in Human Bronchial Epithelial Cells. *Eur J Clin Microbiol Infect Dis* (2012) 31(10):2755–64. doi: 10.1007/s10096-012-1624-8
 18. Richard N, Marti L, Varrot A, Guillot L, Guitard J, Hennequin C, et al. Human Bronchial Epithelial Cells Inhibit *Aspergillus Fumigatus* Germination of Extracellular Conidia via FLeA Recognition. *Sci Rep* (2018) 8(1):15699. doi: 10.1038/s41598-018-33902-0
 19. Rammaert B, Jouvion G, de Chaumont F, Garcia-Hermoso D, Szczepaniak C, Renaudat C, et al. Absence of Fungal Spore Internalization by Bronchial Epithelium in Mouse Models Evidenced by a New Bioimaging Approach and Transmission Electronic Microscopy. *Am J Pathol* (2015) 185(9):2421–30. doi: 10.1016/j.ajpath.2015.04.027
 20. Pickering RJ, Booty LM. NLR in Exile: Emerging Roles of NLRX1 in Immunity and Human Disease. *Immunology* (2021) 162(3):268–80. doi: 10.1111/imm.13291
 21. Xia X, Cui J, Wang HY, Zhu L, Matsueda S, Wang Q, et al. NLRX1 Negatively Regulates TLR-Induced NF-kappaB Signaling by Targeting TRAF6 and IKK. *Immunity* (2011) 34(6):843–53. doi: 10.1016/j.immuni.2011.02.022
 22. Arnoult D, Soares F, Tattoli I, Castanier C, Philpott DJ, Girardin SE. An N-Terminal Addressing Sequence Targets NLRX1 to the Mitochondrial Matrix. *J Cell Sci* (2009) 122(Pt 17):3161–8. doi: 10.1242/jcs.051193
 23. Tattoli I, Carneiro LA, Jehanno M, Magalhaes JG, Shu Y, Philpott DJ, et al. NLRX1 Is a Mitochondrial NOD-Like Receptor That Amplifies NF-kappaB and JNK Pathways by Inducing Reactive Oxygen Species Production. *EMBO Rep* (2008) 9(3):293–300. doi: 10.1038/sj.embor.7401161
 24. Abdul-Sater AA, Said-Sadier N, Lam VM, Singh B, Pettengill MA, Soares F, et al. Enhancement of Reactive Oxygen Species Production and Chlamydial Infection by the Mitochondrial Nod-Like Family Member NLRX1. *J Biol Chem* (2010) 285(53):41637–45. doi: 10.1074/jbc.M110.137885
 25. Philipson CW, Bassaganya-Riera J, Viladomiu M, Kronsteiner B, Abedi V, Hoops S, et al. Modeling the Regulatory Mechanisms by Which NLRX1 Modulates Innate Immune Responses to *Helicobacter Pylori* Infection. *PLoS One* (2015) 10(9):e0137839. doi: 10.1371/journal.pone.0137839
 26. Lei Y, Wen H, Yu Y, Taxman DJ, Zhang L, Widman DG, et al. The Mitochondrial Proteins NLRX1 and TUFM Form a Complex That Regulates Type I Interferon and Autophagy. *Immunity* (2012) 36(6):933–46. doi: 10.1016/j.immuni.2012.03.025
 27. Guo H, König R, Deng M, Riess M, Mo J, Zhang L, et al. NLRX1 Sequesters STING to Negatively Regulate the Interferon Response, Thereby Facilitating the Replication of HIV-1 and DNA Viruses. *Cell Host Microbe* (2016) 19(4):515–28. doi: 10.1016/j.chom.2016.03.001
 28. Allen IC, Moore CB, Schneider M, Lei Y, Davis BK, Scull MA, et al. NLRX1 Protein Attenuates Inflammatory Responses to Infection by Interfering With the RIG-I-MAVS and TRAF6-NF-kappaB Signaling Pathways. *Immunity* (2011) 34(6):854–65. doi: 10.1016/j.immuni.2011.03.026
 29. Leber A, Hontecillas R, Zoccoli-Rodriguez V, Bienert C, Chauhan J, Bassaganya-Riera J. Activation of NLRX1 by NX-13 Alleviates Inflammatory Bowel Disease Through Immunometabolic Mechanisms in CD4(+) T Cells. *J Immunol* (2019) 203(12):3407–15. doi: 10.4049/jimmunol.1900364
 30. Leber A, Hontecillas R, Zoccoli-Rodriguez V, Ehrich M, Chauhan J, Bassaganya-Riera J. Exploratory Studies With NX-13: Oral Toxicity and Pharmacokinetics in Rodents of an Orally Active, Gut-Restricted First-in-Class Therapeutic for IBD That Targets NLRX1. *Drug Chem Toxicol* (2019) 25:1–6. doi: 10.1080/01480545.2019.1679828
 31. Kale SD, Ayubi T, Chung D, Tubau-Juni N, Leber A, Dang HX, et al. Modulation of Immune Signaling and Metabolism Highlights Host and Fungal Transcriptional Responses in Mouse Models of Invasive Pulmonary Aspergillosis. *Sci Rep* (2017) 7(1):17096. doi: 10.1038/s41598-017-17000-1
 32. Swamydas M, Lionakis MS. Isolation, Purification and Labeling of Mouse Bone Marrow Neutrophils for Functional Studies and Adoptive Transfer Experiments. *J Vis Exp* (2013) 77:e50586. doi: 10.3791/50586
 33. Zorov DB, Juhaszova M, Sollott SJ. Mitochondrial Reactive Oxygen Species (ROS) and ROS-Induced ROS Release. *Physiol Rev* (2014) 94(3):909–50. doi: 10.1152/physrev.00026.2013
 34. Rada B, Leto TL. Oxidative Innate Immune Defenses by Nox/Duox Family NADPH Oxidases. *Contrib Microbiol* (2008) 15:164–87. doi: 10.1159/000136357
 35. Rada B, Lekstrom K, Damian S, Dupuy C, Leto TL. The *Pseudomonas* Toxin Pyocyanin Inhibits the Dual Oxidase-Based Antimicrobial System as It Imposes Oxidative Stress on Airway Epithelial Cells. *J Immunol* (2008) 181(7):4883–93. doi: 10.4049/jimmunol.181.7.4883
 36. Grasberger H, El-Zaatari M, Dang DT, Merchant JL. Dual Oxidases Control Release of Hydrogen Peroxide by the Gastric Epithelium to Prevent *Helicobacter Felis* Infection and Inflammation in Mice. *Gastroenterology* (2013) 145(5):1045–54. doi: 10.1053/j.gastro.2013.07.011
 37. Brothers KM, Gratacap RL, Barker SE, Newman ZR, Norum A, Wheeler RT. NADPH Oxidase-Driven Phagocyte Recruitment Controls *Candida Albicans* Filamentous Growth and Prevents Mortality. *PLoS Pathog* (2013) 9(10):e1003634. doi: 10.1371/journal.ppat.1003634
 38. Hoeven R, McCallum KC, Cruz MR, Garsin DA. Ce-Duox1/BLI-3 Generated Reactive Oxygen Species Trigger Protective SKN-1 Activity via P38 MAPK Signaling During Infection in *C. Elegans*. *PLoS Pathog* (2011) 7(12):e1002453. doi: 10.1371/journal.ppat.1002453
 39. Kim HJ, Kim CH, Kim MJ, Ryu JH, Seong SY, Kim S, et al. The Induction of Pattern-Recognition Receptor Expression Against Influenza A Virus Through Duox2-Derived Reactive Oxygen Species in Nasal Mucosa. *Am J Respir Cell Mol Biol* (2015) 53(4):525–35. doi: 10.1165/rcmb.2014-0334OC
 40. Xiao X, Yang L, Pang X, Zhang R, Zhu Y, Wang P, et al. A Mesh-Duox Pathway Regulates Homeostasis in the Insect Gut. *Nat Microbiol* (2017) 2:17020. doi: 10.1038/nmicrobiol.2017.20
 41. Fischer H. Mechanisms and Function of DUOX in Epithelia of the Lung. *Antioxid Redox Signal* (2009) 11(10):2453–65. doi: 10.1089/ARS.2009.2558
 42. Xiao W, Wang RS, Handy DE, Loscalzo J. NAD(H) and NADP(H) Redox Couples and Cellular Energy Metabolism. *Antioxid Redox Signal* (2018) 28(3):251–72. doi: 10.1089/ars.2017.7216
 43. Eisenreich W, Heesemann J, Rudel T, Goebel W. Metabolic Host Responses to Infection by Intracellular Bacterial Pathogens. *Front Cell Infect Microbiol* (2013) 3:24. doi: 10.3389/fcimb.2013.00024
 44. Goodwin CM, Xu S, Munger J. Stealing the Keys to the Kitchen: Viral Manipulation of the Host Cell Metabolic Network. *Trends Microbiol* (2015) 23(12):789–98. doi: 10.1016/j.tim.2015.08.007
 45. Eisenreich W, Heesemann J, Rudel T, Goebel W. Metabolic Adaptations of Intracellular Bacterial Pathogens and Their Mammalian Host Cells During Infection (“Pathometabolism”). *Microbiol Spectr* (2015) 3(3). doi: 10.1128/microbiolspec.MBP-0002-2014
 46. Caradonna KL, Engel JC, Jacobi D, Lee CH, Burleigh BA. Host Metabolism Regulates Intracellular Growth of *Trypanosoma Cruzi*. *Cell Host Microbe* (2013) 13(1):108–17. doi: 10.1016/j.chom.2012.11.011
 47. Ballard E, Yucel R, Melchers WJG, Brown AJP, Verweij PE, Warris A. Antifungal Activity of Antimicrobial Peptides and Proteins Against *Aspergillus Fumigatus*. *J Fungi (Basel)* (2020) 6(2). doi: 10.3390/jof6020065
 48. Lupetti A, van Dissel JT, Brouwer CP, Nibbering PH. Human Antimicrobial Peptides’ Antifungal Activity Against *Aspergillus Fumigatus*. *Eur J Clin Microbiol Infect Dis* (2008) 27(11):1125–9. doi: 10.1007/s10096-008-0553-z
 49. Simon A, Kullberg BJ, Tripet B, Boerman OC, Zeeuwen P, van der Ven-Jongekrijg J, et al. Drosomycin-Like Defensin, A Human Homologue of *Drosophila Melanogaster* Drosomycin With Antifungal Activity. *Antimicrob Agents Chemother* (2008) 52(4):1407–12. doi: 10.1128/AAC.00155-07

50. Huang JH, Liu CY, Wu SY, Chen WY, Chang TH, Kan HW, et al. NLRX1 Facilitates Histoplasma Capsulatum-Induced LC3-Associated Phagocytosis for Cytokine Production in Macrophages. *Front Immunol* (2018) 9:2761. doi: 10.3389/fimmu.2018.02761
51. Stokman G, Kors L, Bakker PJ, Rampanelli E, Claessen N, Teske GJD, et al. NLRX1 Dampens Oxidative Stress and Apoptosis in Tissue Injury via Control of Mitochondrial Activity. *J Exp Med* (2017) 214(8):2405–20. doi: 10.1084/jem.20161031
52. Fekete T, Bencze D, Biro E, Benko S, Pazmandi K. Focusing on the Cell Type Specific Regulatory Actions of NLRX1. *Int J Mol Sci* (2021) 22(3). doi: 10.3390/ijms22031316
53. Rebsamen M, Vazquez J, Tardivel A, Guarda G, Curran J, Tschopp J. NLRX1/NOD5 Deficiency Does Not Affect MAVS Signalling. *Cell Death Differ* (2011) 18(8):1387. doi: 10.1038/cdd.2011.64
54. Kors L, Rampanelli E, Stokman G, Butter LM, Held NM, Claessen N, et al. Deletion of NLRX1 Increases Fatty Acid Metabolism and Prevents Diet-Induced Hepatic Steatosis and Metabolic Syndrome. *Biochim Biophys Acta Mol Basis Dis* (2018) 1864(5 Pt A):1883–95. doi: 10.1016/j.bbadis.2018.03.003

Conflict of Interest: The authors declare that the research was conducted in the absence of any commercial or financial relationships that could be construed as a potential conflict of interest.

Publisher's Note: All claims expressed in this article are solely those of the authors and do not necessarily represent those of their affiliated organizations, or those of the publisher, the editors and the reviewers. Any product that may be evaluated in this article, or claim that may be made by its manufacturer, is not guaranteed or endorsed by the publisher.

Copyright © 2021 Kastelberg, Ayubi, Tubau-Juni, Leber, Hontecillas, Bassaganya-Riera and Kale. This is an open-access article distributed under the terms of the Creative Commons Attribution License (CC BY). The use, distribution or reproduction in other forums is permitted, provided the original author(s) and the copyright owner(s) are credited and that the original publication in this journal is cited, in accordance with accepted academic practice. No use, distribution or reproduction is permitted which does not comply with these terms.



Metallothionein 3-Zinc Axis Suppresses Caspase-11 Inflammasome Activation and Impairs Antibacterial Immunity

OPEN ACCESS

Edited by:

Maciej Lech,
LMU Munich University Hospital,
Germany

Reviewed by:

Amal O. Amer,
The Ohio State University,
United States
Djalma Souza Lima-Junior,
National Institutes of Health (NIH),
United States

*Correspondence:

Kavitha Subramanian Vignesh
Kavitha.Subramanian@uc.edu

Specialty section:

This article was submitted to
Molecular Innate Immunity,
a section of the journal
Frontiers in Immunology

Received: 09 August 2021

Accepted: 15 October 2021

Published: 12 November 2021

Citation:

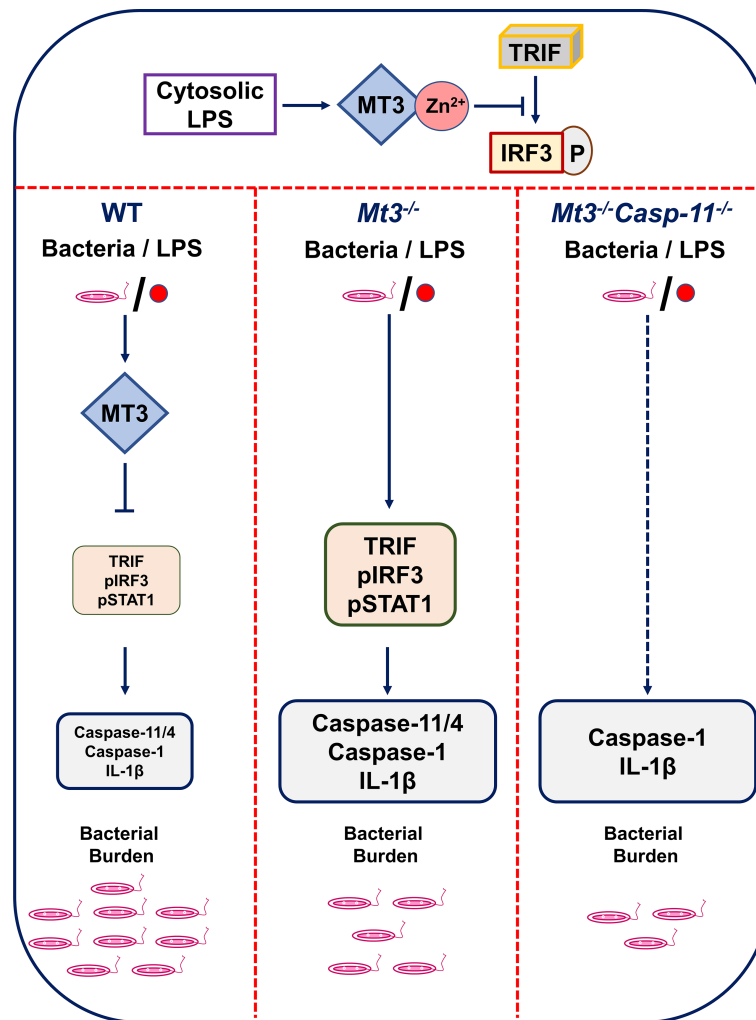
Chowdhury D, Gardner JC, Satpati A,
Nookala S, Mukundan S, Porollo A,
Landerio Figueroa JA and
Subramanian Vignesh K (2021)
Metallothionein 3-Zinc Axis
Suppresses Caspase-11
Inflammasome Activation and Impairs
Antibacterial Immunity.
Front. Immunol. 12:755961.
doi: 10.3389/fimmu.2021.755961

Debabrata Chowdhury¹, Jason C. Gardner², Abhijit Satpati³, Suba Nookala³,
Santhosh Mukundan³, Aleksey Porollo^{4,5,6}, Julio A. Landerio Figueroa⁷
and Kavitha Subramanian Vignesh^{1*}

¹ Division of Infectious Diseases, College of Medicine, University of Cincinnati, Cincinnati, OH, United States, ² Department of Internal Medicine, Division of Pulmonary, Critical Care, and Sleep Medicine, University of Cincinnati College of Medicine, Cincinnati, OH, United States, ³ Department of Biomedical Sciences, School of Medicine and Health Sciences, University of North Dakota, Grand Forks, ND, United States, ⁴ Center for Autoimmune Genomics and Etiology, Cincinnati Children's Hospital Medical Center, Cincinnati, OH, United States, ⁵ Division of Biomedical Informatics, Cincinnati Children's Hospital Medical Center, Cincinnati, OH, United States, ⁶ Department of Pediatrics, University of Cincinnati, Cincinnati, OH, United States, ⁷ University of Cincinnati/Agilent Technologies Metallomics Center of the Americas, Department of Chemistry, University of Cincinnati, Cincinnati, OH, United States

Non-canonical inflammasome activation by mouse caspase-11 (or human CASPASE-4/5) is crucial for the clearance of certain gram-negative bacterial infections, but can lead to severe inflammatory damage. Factors that promote non-canonical inflammasome activation are well recognized, but less is known about the mechanisms underlying its negative regulation. Herein, we identify that the caspase-11 inflammasome in mouse and human macrophages (M ϕ) is negatively controlled by the zinc (Zn²⁺) regulating protein, metallothionein 3 (MT3). Upon challenge with intracellular lipopolysaccharide (iLPS), M ϕ increased MT3 expression that curtailed the activation of caspase-11 and its downstream targets caspase-1 and interleukin (IL)-1 β . Mechanistically, MT3 increased intramacrophage Zn²⁺ to downmodulate the TRIF-IRF3-STAT1 axis that is prerequisite for caspase-11 effector function. *In vivo*, MT3 suppressed activation of the caspase-11 inflammasome, while caspase-11 and MT3 synergized in impairing antibacterial immunity. The present study identifies an important yin-yang relationship between the non-canonical inflammasome and MT3 in controlling inflammation and immunity to gram-negative bacteria.

Keywords: macrophage, non-canonical inflammasome, zinc, metallothionein, innate immunity, caspase-11 non-canonical inflammasome, MT3



GRAPHICAL ABSTRACT | The MT3- Zn^{2+} axis suppresses TRIF signaling resulting in decreased IRF3 phosphorylation. When MT3 is absent, TRIF-IRF3-STAT1 signaling and non-canonical inflammasome activation are exaggerated. A lack of MT3 augments immunity to gram-negative bacteria, an effect, that is further enhanced by the combined absence of MT3 and caspase-11 *in vivo*. Thus, while MT3 curtails caspase-11 activation, the two molecules act together in compromising antibacterial immunity.

INTRODUCTION

Gram-negative bacteria that cause more than 30% of the total healthcare-associated infections worldwide remain a global concern of morbidity and mortality (1). Assembly of inflammasome complexes during bacterial pathogenesis drives robust inflammation and shapes antibacterial immune responses. The non-canonical inflammasome is activated when innate immune cells such as M ϕ sense bacterial ligands in the cytosol (2). LPS from bacterial cell walls enters the cytosol during bacterial escape from vacuoles or *via* rupture of outer membrane vesicles (OMV) (3). iLPS directly binds caspase-11, triggering the non-canonical inflammasome cascade, followed by activation of pro-caspase-1 to caspase-1, processing of pro-IL-1 β to mature IL-1 β and pyroptosis, a lytic form of programmed cell death. Activation of gasdermin D (GSDMD) by caspase-11 and caspase-1, leads to pore

formation on the cell membrane facilitating the exit of IL-1 β from M ϕ (4). Unrestricted activation of this inflammatory cascade is a major underlying cause of tissue damage and sepsis-associated mortality (2). Thus, it is crucial to thoroughly understand the molecular cues that guard against excessive activation of the caspase-11 inflammasome. Although factors that promote non-canonical inflammasome activation have been extensively studied, less is known about the mechanisms that negatively regulate it.

MTs are Zn^{2+} regulating proteins induced by endogenous and exogenous stimuli including cytokines, infection, oxidative stress and heavy metals (5, 6). Intracellular availability of total Zn^{2+} , exchangeable Zn^{2+} and Zn^{2+} redistribution among proteins is tightly regulated by MTs (7). Mice have 4 MT isoforms (MT1-4), whereas more than 16 MT isoforms are present in humans (8). Our knowledge on the role of the MT family in immune responses largely emerges from studies on MT1 and MT2. We

and others have shown that MT1 and MT2 promote antifungal and antibacterial immunity in M ϕ primarily *via* Zn²⁺ sequestration (9, 10). MT3, on the other hand, suppresses manifestation of proinflammatory phenotypic and metabolic changes and impairs antifungal immunity *in vitro* in M ϕ and *in vivo*. M ϕ expression of MT3 is inducible by IL-4 stimulation. In these cells, MT3 increases intracellular free-Zn²⁺, promotes Zn²⁺ uptake by a prototypic intracellular pathogen and favors microbial survival (11). Thus, MTs and their ability to regulate Zn²⁺ homeostasis intricately ties M ϕ inflammatory responses to antimicrobial defense.

Zn²⁺ is indispensable in many biochemical processes due to its role in structural and catalytic functions of enzymes and macromolecules. Zn²⁺ excess or deficiency compromises the development and function of immune cells including monocytes and M ϕ , leading to increased risk of infection (12). Zn²⁺ also has a profound role as a signaling ion attributable to the transient changes in intracellular exchangeable Zn²⁺. LPS triggers increased Zn²⁺ import in leukocytes, monocytes and M ϕ (13, 14). In peripheral blood mononuclear cells (PBMCs) and human M ϕ (hM ϕ), LPS-induced Zn²⁺ influx promotes IL-1 β production (14). In contrast, exogenous exposure to Zn²⁺ in human monocytes may reduce IL-1 β production due to inhibition of nucleotide phosphodiesterases (15). Thus, the effects of Zn²⁺ on signaling and cytokine production are context and Zn²⁺ concentration-dependent. Changes in ion flux, specifically K⁺ and Cl⁻ egress and intracellular mobilization of Ca²⁺ underlie canonical nod-like receptor pyrin domain containing-3 (NLRP3) inflammasome activation (16). Intriguingly, Zn²⁺ exerts disparate effects on activation of this cascade. Long-term Zn²⁺ depletion disrupts lysosomal integrity leading to increased activation of the canonical NLRP3 inflammasome (17). On the other hand, short-term chelation of Zn²⁺ attenuates the canonical pathway due to impaired function of the pannexin-1 receptor (18).

The importance of Zn²⁺ regulation by MTs in the non-canonical inflammasome pathway remain unexplored. Given the suppressive role of MT3 in M ϕ inflammatory responses (19), we hypothesized that MT3 negatively regulates the highly inflammatory caspase-11 activation cascade. Bioinformatics analysis predicted the involvement of MT3 in regulating non-canonical inflammasome-associated pathways. Using a combination of protein-protein interaction network analysis, immunological and mass-spectrometric approaches, we demonstrate that triggering caspase-11 activation results in a profound, gradual increase in the M ϕ Zn²⁺ pool mediated by MT3. The increase in Zn²⁺ attenuates signaling *via* toll/interleukin-1 receptor (TIR) domain containing adaptor-inducing interferon (IFN) β - interferon regulatory factor 3 - signal transducer and activator of transcription factor 1 (TRIF-IRF3-STAT1), a pathway that is prerequisite for caspase-11 inflammasome activation (20). Zn²⁺ deficiency augments, whereas Zn²⁺ supplementation suppresses the non-canonical inflammasome in M ϕ . Using whole-body *Mt3*^{-/-} and myeloid-MT3-deficient mice, we elucidate that MT3 blunts non-canonical inflammasome activation *in vitro* and *in vivo* upon challenge with iLPS or gram-negative bacteria but not gram-positive bacteria. Importantly, this function of MT3 is conserved

in hM ϕ . Although caspase-11 and MT3 form a negative regulatory loop, we find that these two molecules synergize in compromising antibacterial immunity. Our data uncover a previously unknown yin-yang relationship whereby the MT3-Zn²⁺ axis exerts a brake on non-canonical inflammasome activation but the functions of MT3 and caspase-11 converge in crippling immunity to invading bacteria (see **Graphical Abstract**).

RESULTS

MT3 Suppresses Activation of the Non-Canonical Inflammasome *In Vitro*

MT3 attenuates cell death in neuronal and glial cells, but the precise underlying mechanisms are not fully understood (21). As non-canonical inflammasome activation leads to pyroptotic cell death, we investigated if MT3 effector function is related to caspase-11 activation in M ϕ . We explored whether MT3 is involved in inflammatory and cell-death processes using functional enrichment analysis. We assessed protein-protein interaction networks of MT3 in *Mus musculus* and *Homo sapiens* using the STRING database (22). The MT3 interaction partners significantly enriched 15 mouse and 43 human gene ontology categories for biological processes (GO BP) related to programmed cell death (PCD), LPS responses, signaling *via* TRIF, IL-1 and type-I IFN, cytokine responses and several immune processes. A complete network of MT3 interactions and GO BP categories is in **Table 1**, **Supplementary Table S1**, **Supplementary Files S1** and **S2**. PCD and LPS responses are linked to inflammasome activation and more specifically, TRIF and type-I IFN signaling are tied to the non-canonical inflammasome pathway. A lack of TRIF signaling ablates non-canonical inflammasome activation in response to iLPS without impacting M ϕ response to canonical NLRP3 triggers such as ATP and nigericin (20). Thus, our bioinformatics analysis together with our previously reported role for MT3 in suppressing proinflammatory responses in M ϕ led us to investigate whether MT3 negatively regulates the non-canonical inflammasome pathway.

In M ϕ , exposure to iLPS triggers caspase-11 activation and cell death by pyroptosis (2). We directly assessed if MT3 regulates non-canonical inflammasome activation using WT and *Mt3*^{-/-} mice. BMDM ϕ were exposed to iLPS or vehicle control and time-dependent changes in the gene expression of *Mt1*, *Mt2* and *Mt3* were examined. *Mt3* expression increased gradually from 1 hour (h) and peaked at 48h in WT BMDM ϕ challenged with iLPS (**Figure 1A**). The expression of *Mt1* and *Mt2* peaked at 6h, but receded over time in both WT and *Mt3*^{-/-} BMDM ϕ (**Supplementary Figures S1A, B**). To determine whether exogenous LPS had an effect on MT3, we stimulated WT BMDM ϕ with extracellular LPS (exLPS) for 48h. While iLPS increased *Mt3* expression by 10-fold, the fold increase observed with exLPS challenge was much lower (**Figure 1B**).

Next, we examined if MT3 regulated non-canonical inflammasome activation by assessing pro- and active forms of caspase-11, caspase-1 and IL-1 β in cell lysates and supernatants

TABLE 1 | See also **Supplementary Table S1** and **Files S1, S2** | Protein interaction network of *Mus musculus* MT3 to determine functionally enriched GO BP categories using the STRING database.**Protein-Protein Interaction Network of *Homo sapiens* MT3**

Sl. No	Term ID	Term Description	FDR	Protein Labels
1	GO:0060548	Negative regulation of cell death	2.30E-10	NGFR,MT3,RIPK2,CAT,TRAF2,RIPK1,SLC40A1,SOD1,RPS27A,EGFR,APP,ALB,SNCB,FAIM2,ERBB4,GPX4,SLC30A10,TXN,MAG,UBA52,GPX1,TRAF6,UBC,SOD2,AKT1,IKBK
2	GO:0043069	Negative regulation of programmed cell death	6.51E-09	NGFR,MT3,RIPK2,CAT,TRAF2,RIPK1,SLC40A1,SOD1,RPS27A,EGFR,ALB,SNCB,FAIM2,ERBB4,GPX4,SLC30A10,MAG,UBA52,GPX1,TRAF6,UBC,SOD2,AKT1
3	GO:0043066	Negative regulation of apoptotic process	2.32E-08	NGFR,MT3,RIPK2,CAT,TRAF2,RIPK1,SLC40A1,SOD1,RPS27A,EGFR,ALB,SNCB,FAIM2,ERBB4,SLC30A10,MAG,UBA52,GPX1,TRAF6,UBC,SOD2,AKT1
4	GO:0010941	Regulation of cell death	2.59E-08	TNFRSF1A,NGFR,MT3,RIPK2,CAT,TRAF2,RIPK1,SLC40A1,SOD1,RPS27A,EGFR,APP,ALB,SNCB,FAIM2,RTN4,ERBB4,GPX4,SLC30A10,TXN,MAG,FOXO3,UBA52,CYLD,GPX1,TRAF6,UBC,SOD2,AKT1,IKBK
5	GO:0043067	Regulation of programmed cell death	8.35E-08	TNFRSF1A,NGFR,MT3,RIPK2,CAT,TRAF2,RIPK1,SLC40A1,SOD1,RPS27A,EGFR,APP,ALB,SNCB,FAIM2,RTN4,ERBB4,GPX4,SLC30A10,MAG,FOXO3,UBA52,CYLD,GPX1,TRAF6,UBC,SOD2,AKT1
6	GO:0042981	Regulation of apoptotic process	2.74E-07	TNFRSF1A,NGFR,MT3,RIPK2,CAT,TRAF2,RIPK1,SLC40A1,SOD1,RPS27A,EGFR,APP,ALB,SNCB,FAIM2,RTN4,ERBB4,SLC30A10,MAG,FOXO3,UBA52,CYLD,GPX1,TRAF6,UBC,SOD2,AKT1
7	GO:0010942	Positive regulation of cell death	1.84E-06	TNFRSF1A,NGFR,MT3,RIPK2,TRAF2,RIPK1,SOD1,RPS27A,APP,ERBB4,FOXO3,UBA52,CYLD,TRAF6,UBC,SOD2,AKT1
8	GO:0035666	TRIF-dependent toll-like receptor signaling pathway	8.19E-06	RIPK1,RPS27A,UBA52,UBC,IKBK
9	GO:0070498	Interleukin-1-mediated signaling pathway	1.00E-05	RIPK2,RPS27A,UBA52,TRAF6,UBC,IKBK
10	GO:0045089	Immune response-activating signal transduction	2.38E-05	RIPK2,EREG,RIPK1,RPS27A,DDX58,UBA52,CYLD,TRAF6,UBC,IKBK
11	GO:0071345	Cellular response to cytokine stimulus	3.60E-05	RTN4R,TNFRSF1A,NGFR,MT3,RIPK2,EREG,TRAF2,RIPK1,SOD1,RPS27A,AQP4,FOXO3,UBA52,TRAF6,UBC,SOD2,AKT1,IKBK
12	GO:1903209	Positive regulation of oxidative stress-induced cell death	4.97E-05	RIPK1,SOD1,APP,FOXO3
13	GO:0045088	Regulation of innate immune response	5.35E-05	RIPK2,EREG,RIPK1,RPS27A,APP,DDX58,UBA52,CYLD,TRAF6,UBC,IKBK
14	GO:0002757	Immune response-activating signal transduction	0.00015	RIPK2,EREG,RIPK1,RPS27A,DDX58,UBA52,CYLD,TRAF6,UBC,IKBK
15	GO:0002684	Positive regulation of immune system process	0.00017	RIPK2,EREG,TRAF2,RIPK1,RPS27A,APP,RNF31,RBP4,DDX58,FOXO3,UBA52,CYLD,TRAF6,UBC,AKT1,IKBK
16	GO:0001959	Regulation of cytokine-mediated signaling pathway	0.00022	TNFRSF1A,RIPK2,TRAF2,RIPK1,RNF31,CYLD,IKBK
17	GO:0006915	apoptotic process	0.00025	TNFRSF1A,NGFR,MT3,RIPK2,TRAF2,RIPK1,APP,FAIM2,RTN4,ERBB4,FOXO3,GPX1,SOD2,AKT1,GNB1,IKBK
18	GO:0012501	Programmed cell death	0.00031	TNFRSF1A,NGFR,MT3,RIPK2,TRAF2,RIPK1,APP,FAIM2,RTN4,ERBB4,FOXO3,CYLD,GPX1,SOD2,AKT1,GNB1,IKBK
19	GO:1902175	Regulation of oxidative stress-induced intrinsic apoptotic signaling pathway	0.00032	SOD1,GPX1,SOD2,AKT1
20	GO:1902042	Negative regulation of extrinsic apoptotic signaling pathway <i>via</i> death domain receptors	0.00056	TRAF2,RIPK1,FAIM2,GPX1
21	GO:0050778	Positive regulation of immune response	0.00064	RIPK2,EREG,TRAF2,RIPK1,RPS27A,RNF31,DDX58,UBA52,CYLD,TRAF6,UBC,IKBK
22	GO:1903202	Negative regulation of oxidative stress-induced cell death	0.0011	TXN,GPX1,SOD2,AKT1
23	GO:2001236	Regulation of extrinsic apoptotic signaling pathway	0.0018	TRAF2,RIPK1,FAIM2,CYLD,GPX1,AKT1
24	GO:0002376	Immune system process	0.0029	TNFRSF1A,NGFR,RIPK2,TTR,CAT,NTS,HNF1A,RIPK1,SLC40A1,PRDX1,SOD1,RPS27A,APP,RNF31,ATP7A,DDX58,AQP4,MAG,UBA52,CYLD,SERPINA1,TRAF6,UBC,AKT1,IKBK
25	GO:0097300	Programmed necrotic cell death	0.0034	TRAF2,RIPK1,CYLD
26	GO:0071356	Cellular response to tumor necrosis factor	0.0045	TNFRSF1A,NGFR,TRAF2,RIPK1,FOXO3,AKT1
27	GO:0032743	Positive regulation of interleukin-2 production	0.0046	RIPK2,TRAF2,TRAF6
28	GO:0032755	Positive regulation of interleukin-6 production	0.0049	RIPK2,EREG,DDX58,TRAF6
29	GO:0010940	Positive regulation of necrotic cell death	0.0062	MT3,RIPK1
30	GO:0097190	Apoptotic signaling pathway	0.0063	TNFRSF1A,NGFR,TRAF2,RIPK1,FOXO3,GPX1,SOD2
31	GO:2001233	Regulation of apoptotic signaling pathway	0.0066	TRAF2,RIPK1,SOD1,FAIM2,CYLD,GPX1,SOD2,AKT1
32	GO:2001234	Negative regulation of apoptotic signaling pathway	0.0068	TRAF2,RIPK1,FAIM2,GPX1,SOD2,AKT1
33	GO:0050852	T cell receptor signaling pathway	0.0096	RIPK2,RNF31,TRAF6,IKBK
34	GO:0097191	Extrinsic apoptotic signaling pathway	0.0096	TNFRSF1A,TRAF2,RIPK1,FOXO3
35	GO:2001242	Regulation of intrinsic apoptotic signaling pathway	0.0096	SOD1,CYLD,GPX1,SOD2,AKT1
36	GO:0070673	Response to interleukin-18	0.01	RIPK2,AKT1

(Continued)

TABLE 1 | Continued

Protein-Protein Interaction Network of *Homo sapiens* MT3

Sl. No	Term ID	Term Description	FDR	Protein Labels
37	GO:2001238	Positive regulation of extrinsic apoptotic signaling pathway	0.0145	TRAF2,RIPK1,CYLD
38	GO:0060760	Positive regulation of response to cytokine stimulus	0.0152	RIPK2,TRAF2,DDX58
39	GO:0001819	Positive regulation of cytokine production	0.0215	RIPK2,EREG,TRAF2,RIPK1,SOD1,DDX58,TRAF6
40	GO:0002824	Positive regulation of adaptive immune response based on somatic recombination of immune receptors built from immunoglobulin superfamily domains	0.0476	RIPK2,TRAF2,TRAF6
41	GO:0045639	Positive regulation of myeloid cell differentiation	0.0476	RIPK1,FOXO3,TRAF6
42	GO:0031663	Lipopolysaccharide-mediated signaling pathway	0.0493	RIPK2,AKT1
43	GO:2001235	Positive regulation of apoptotic signaling pathway	0.05	TRAF2,RIPK1,SOD1,CYLD

of WT and *Mt3*^{-/-} BMDM ϕ challenged with iLPS. A lack of MT3 exacerbated activation of caspase-11 in cell lysates, and caspase-1 and IL-1 β in culture supernatants. Pro-caspase-11, pro-caspase-1 and pro-IL-1 β proteins in cell lysates were similar between iLPS treated WT and *Mt3*^{-/-} BMDM ϕ (Figure 1C). We further examined combined lysate and supernatant samples and found increased caspase-11 activation in *Mt3*^{-/-} BMDM ϕ challenged with iLPS (Figure 1D). Thus, the differences observed were not merely a result of reduced release of the active forms from cells, but an increase in non-canonical inflammasome activation in *Mt3*^{-/-} BMDM ϕ . Intracellular transfection of LPS at two different concentrations (2 and 10 μ g/ml) yielded similar results (Figures 1C, D). We then examined the levels of IL-1 α in supernatants of WT and *Mt3*^{-/-} BMDM ϕ challenged with iLPS. In contrast to IL-1 β , IL-1 α was moderately reduced in the supernatants of *Mt3*^{-/-} BMDM ϕ (Supplementary Figures S1C, D). We note that although IL-1 α is activated by caspase-11, it is characteristically different from IL-1 β , as it exists in both membrane-bound and secreted forms that are differentially regulated, and both pro- and cleaved IL-1 α are bioactive (23–25).

MT3 Represses CASPASE-4 Activation and Antibacterial Resistance in Human M ϕ

Gram-negative bacteria activate the non-canonical inflammasome via CASPASE-4 in hM ϕ (26). We investigated whether human MT3, similar to mouse MT3, suppressed non-canonical inflammasome activation and antibacterial immunity. Human monocyte-derived M ϕ obtained from PBMCs were transfected with scramble siRNA or MT3 siRNA followed by transfection with iLPS. To assess siRNA specificity, we analyzed the expression of MT3 and MT2A genes. MT3, but not MT2A expression was silenced in MT3 siRNA transfected hM ϕ (Figure 2A). MT3 deficiency resulted in elevated activation of CASPASE-4 and heightened release of IL-1 β from hM ϕ (Figures 2B, C). We previously showed that a lack of MT3 increased resistance of mouse BMDM ϕ to *Escherichia coli* (19). We therefore queried whether silencing MT3 in hM ϕ impaired bacterial clearance *in vitro*. hM ϕ treated with scramble siRNA or MT3 siRNA were infected with *E. coli* K12 for 24h. MT3-deficient hM ϕ exerted a sharp decline in intracellular bacterial survival compared to control hM ϕ (Figure 2D).

MT3 Dampens Antibacterial Resistance and Caspase-11 Inflammasome Activation *In Vitro* and *In Vivo*

We examined whether MT3 regulated antibacterial immunity and non-canonical inflammasome activation *in vitro* and *in vivo*. WT and *Mt3*^{-/-} BMDM ϕ were infected with *E. coli*. After 24h, bacterial survival was reduced in *Mt3*^{-/-} BMDM ϕ (Figure 2E). Next, we infected WT and *Mt3*^{-/-} mice *in vivo* intraperitoneally (*i.p.*) with *E. coli* for 6h. Compared to WT mice, MT3 deficiency bolstered bacterial elimination from the blood and moderately improved bacterial clearance in the kidney and peritoneal lavage (Figure 2F). Caspase-11, GSDMD (N-terminal) and caspase-1 activation were heightened in kidney homogenates of infected *Mt3*^{-/-} mice compared to infected WT mice (Figure 2G). The decrease in pro-GSDMD of *Mt3*^{-/-} mice may be explained by increased conversion of pro- to active-GSDMD form (Figure 2G). IL-1 β in the peritoneal lavage was significantly elevated ($p < 0.01$) and serum IL-1 β exhibited a trend towards increase in infected *Mt3*^{-/-} mice compared to WT controls (Figure 2H). To determine if this response is consistent upon LPS challenge *in vivo*, we primed mice *i.p.* with poly(I:C) for 6h and challenged them *i.p.* with ultrapure LPS. After 18h, IL-1 β was elevated in the peritoneal lavage and serum of *Mt3*^{-/-} mice compared to WT mice (Figure 2I). We further queried the impact of MT3 on LPS-induced sepsis. WT and *Mt3*^{-/-} mice were challenged with ultrapure LPS (20 mg/kg) and assayed for weight loss, murine sepsis scores (MSS) as reported previously (27) and survival. MT3 deficiency resulted in greater weight loss and increased sepsis scores, but both genotypes similarly succumbed to septic shock (Supplementary Figures S2A–C).

We then investigated whether MT3 increased susceptibility to other gram-negative bacteria. WT and *Mt3*^{-/-} mice were infected intranasally (*i.n.*) with a virulent, heavily encapsulated strain of *Klebsiella pneumoniae* (KP2 2-70). MT3 deficiency significantly ($p < 0.05$) improved *K. pneumoniae* clearance in the spleen, but no changes were observed in the lung and kidney (Figure 2J). Gram-positive bacteria activate caspase-11 via the NLRP6 inflammasome (28). We determined whether the increased non-canonical inflammasome activation and antibacterial resistance observed in *Mt3*^{-/-} mice extended to gram-positive bacterial infection. WT and *Mt3*^{-/-} mice were challenged subcutaneously (*s.q.*) with a clinical

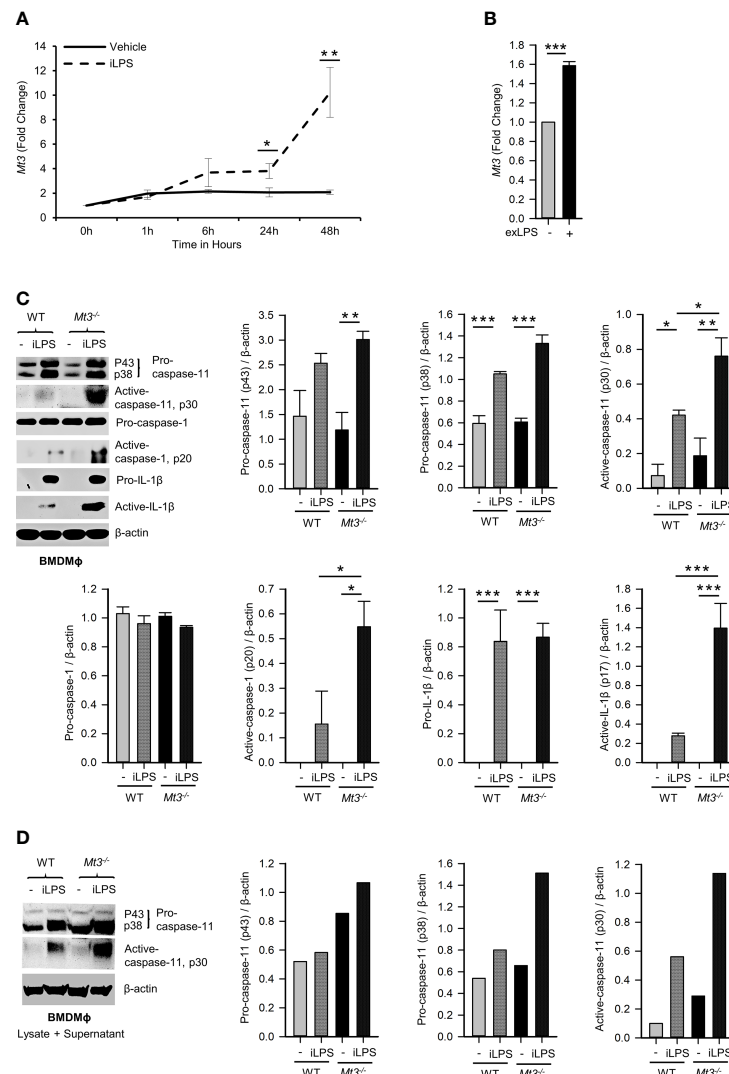


FIGURE 1 | See also **Supplementary Figure S1** MT3 suppresses caspase-11 inflammasome activation in BMDMφ. qRT-PCR analysis of *Mt3* expression in WT BMDMφ stimulated with (A) iLPS (2 μg/ml) or vehicle control, 3-5 independent experiments and (B) exLPS (10 μg/ml) for 48h, 3 independent experiments, two-tailed t-test. (C) Western Blots of pro- and active-caspase-11, pro-caspase-1, pro-IL1β and β-actin in cell lysates and active-caspase-1 and active-IL-1β in supernatants of WT and *Mt3*^{-/-} BMDMφ stimulated with iLPS (10 μg/ml) or vehicle for 48h. Bar graphs are densitometric analysis of targets normalized to β-actin, 3-4 independent experiments, one-way ANOVA, data are mean ± SEM. (D) Western Blots of pro- and active-caspase-11 and β-actin in lysate + supernatant samples from WT and *Mt3*^{-/-} BMDMφ stimulated with iLPS (2 μg/ml) or vehicle for 48h. Bar graphs are densitometric analysis of targets normalized to β-actin. *p < 0.05, **p < 0.01, ***p < 0.001.

isolate of Group-A-Streptococcus GAS5448 (29). After 72h, *Mt3*^{-/-} mice manifested significantly ($p < 0.05$) reduced GAS burden in the kidney and spleen compared to WT mice. Bacterial CFUs in the blood exhibited a similar trend (**Supplementary Figure S2D**). Importantly, although *Mt3*^{-/-} mice exhibited higher activation of caspase-1 and IL-1β, the levels of active caspase-11 and pro-caspase-11 were diminished in GAS-infected *Mt3*^{-/-} mice compared to WT mice (**Supplementary Figure S2E**). Thus, although MT3 compromises resistance to both gram-negative and gram-positive bacteria, it specifically suppresses non-canonical inflammasome signaling in response to gram-negative microbial triggers.

Caspase-11 Synergizes With MT3 in Impairing *E. coli* Clearance In Vivo

Caspase-11 is crucial in antibacterial defenses particularly against gram-negative bacteria, although some studies have suggested a detrimental role for caspase-11 in bacterial elimination (30–35). MT3 suppressed antibacterial immunity as well as non-canonical inflammasome activation. Thus, we investigated whether the heightened immunity to *E. coli* in *Mt3*^{-/-} mice was due to increased non-canonical inflammasome activation. We infected WT, *Casp-11*^{-/-}, *Mt3*^{-/-}, and *Mt3*^{-/-}*Casp-11*^{-/-} mice (**Supplementary Figure S3A**) *i.p.* with *E. coli* and assessed bacterial burden 6h post-infection. Compared to WT mice, bacterial elimination was

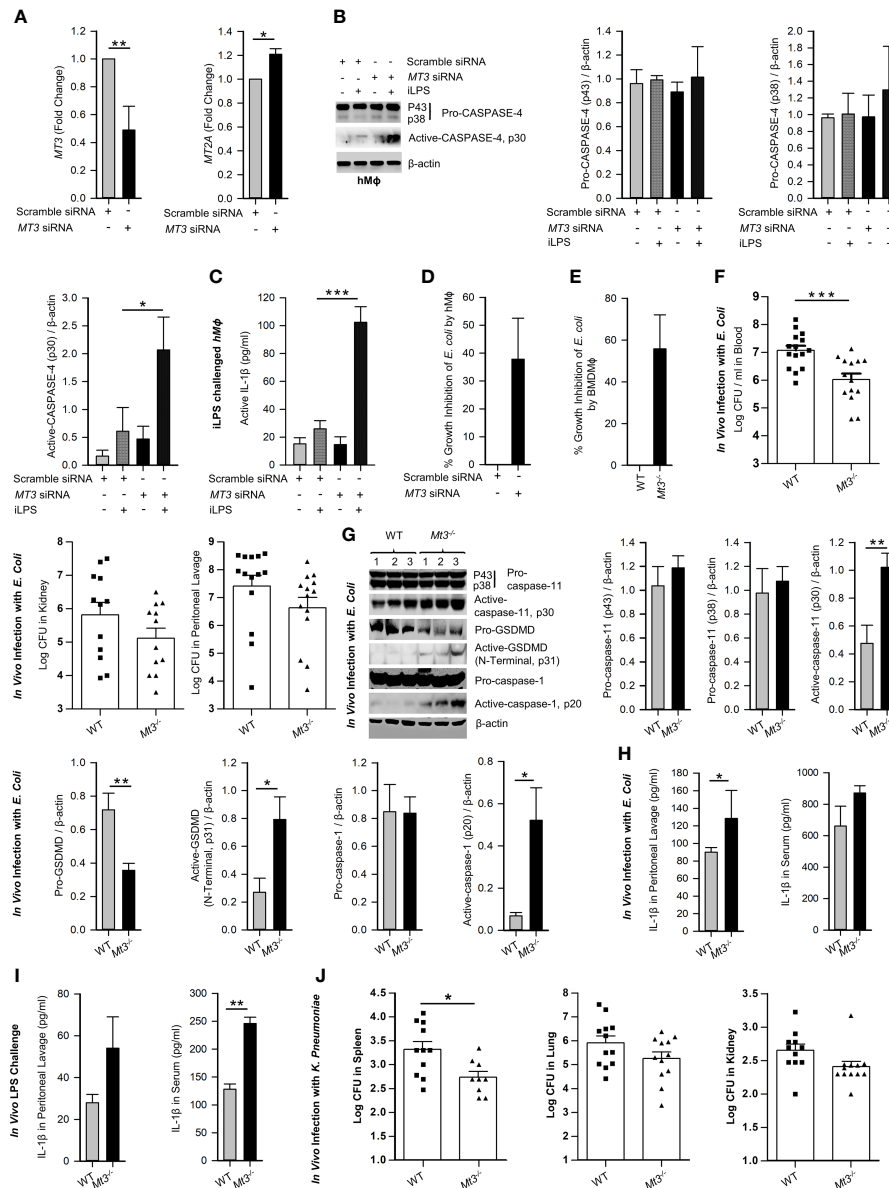


FIGURE 2 | See also **Supplementary Figure S2**. MT3 curtails CASPASE-4 and caspase-11 signaling and antibacterial immunity in hMφ and *in vivo*. **(A)** MT3 and MT2A expression analyzed by qRT-PCR in hMφ transfected with scramble siRNA or MT3 siRNA for 24h, 3 independent experiments, two-tailed t-test. **(B)** Scramble siRNA or MT3 siRNA treated hMφ stimulated with ILPS (10 μg/ml) or vehicle for 48h. Immunoblots of pro-CASPASE-4 and active-CASPASE-4 in cell extracts, 3 independent experiments, one-way ANOVA. **(C)** Active-IL-1β measured by ELISA in supernatants of hMφ treated as above, 3 independent experiments, one-way ANOVA. **(D)** *E. coli* growth inhibition in hMφ transfected with MT3 siRNA and infected with 25 *E. coli* (K12): 1 hMφ for 24h compared to scramble siRNA treated hMφ, 3 independent experiments, two-tailed t-test. **(E)** *E. coli* growth inhibition in WT and *Mt3*^{-/-} BMDMφ infected with 25 *E. coli* (K12):1 hMφ for 24h, 4 independent experiments, two-tailed t-test. **(F)** WT and *Mt3*^{-/-} mice infected *i.p.* with 1X10⁹ *E. coli* for 6h, log CFUs of *E. coli* in blood, kidney and peritoneal lavage samples, n = 12-15 per group, two-tailed t-test. **(G)** Western blots of inflammasome mediators in kidney homogenates of WT and *Mt3*^{-/-} mice infected as above, n = 6 per group, two-tailed t-test. **(H)** WT and *Mt3*^{-/-} mice infected *i.p.* with 1 X10⁹ *E. coli* for 1h and IL-1β measured in peritoneal lavage and serum by ELISA. n = 3 per group, two-tailed t-test. **(I)** WT and *Mt3*^{-/-} mice primed *i.p.* with poly(I:C) (10 mg/kg) for 6h and challenged with LPS (2 mg/kg) *i.p.* After 18h, IL-1β was measured in peritoneal lavage and serum by ELISA, n = 3/group, two-tailed t-test. **(J)** Bacterial growth in spleen, lung and kidney of WT and *Mt3*^{-/-} mice infected *i.n.* with *K. pneumoniae* (4 X10⁴ CFUs/mouse) for 48h, n = 8-12 per group, two-tailed t-test, data are mean ± SEM. *p < 0.05, **p < 0.01, ***p < 0.001.

enhanced in *Mt3*^{-/-} and *Casp-11*^{-/-} mice but this response was further exacerbated in *Mt3*^{-/-} mice lacking caspase-11 (**Figure 3A**). These data indicate that the combined absence of MT3 and caspase-11 improves resistance to gram-negative bacterial

infection. We then analyzed caspase-11 inflammasome mediators in kidney homogenates harvested 6h post-infection. Mice lacking MT3, or caspase-11, exhibited elevated activation of GSDMD (N-terminal), caspase-1 and IL-1β compared to WT mice (**Figure 3B**).

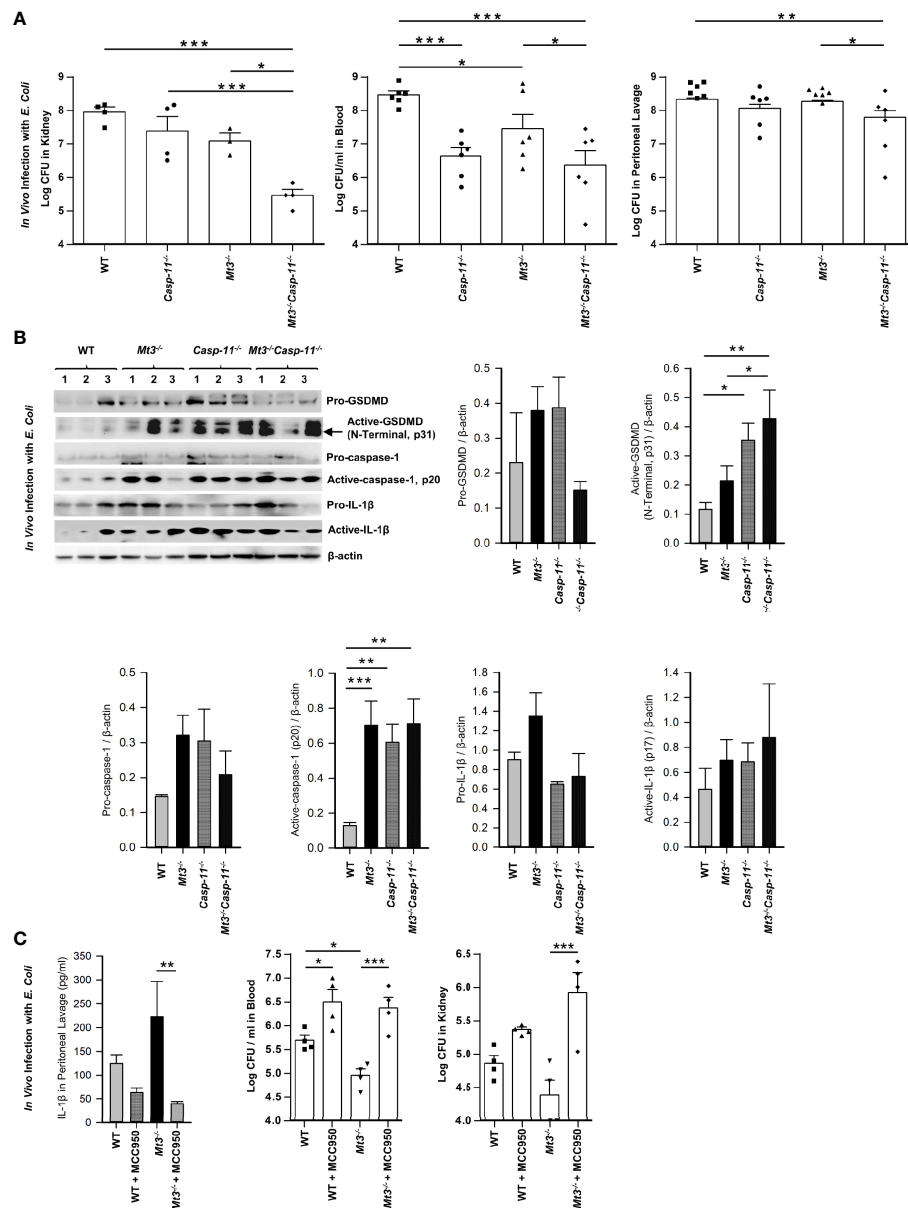


FIGURE 3 | See also **Supplementary Figure S3** Caspase-11 synergizes with MT3 in impairing bacterial clearance. WT, *Casp-11*^{-/-}, *Mt3*^{-/-} and *Casp-11*^{-/-}*Mt3*^{-/-} mice were infected *i.p.* with *E. coli* (1 × 10⁹ CFUs/mouse) for 6h. **(A)** Bacterial CFUs measured in kidney, blood and peritoneal lavage, n = 3-6 per group, one-way ANOVA. **(B)** Western blots of pro-GSDMD, active-GSDMD (p31), pro-caspase-1, active-caspase-1, pro-IL-1β and active-IL-1β in kidney homogenates, n = 3-6 per group, one-way ANOVA, data are mean ± SEM. **(C)** WT and *Mt3*^{-/-} mice treated *i.p.* with MCC950 (1 mg/mouse) or PBS and infected *i.p.* with *E. coli* (1 × 10⁹ CFUs/mouse) for 6h. IL-1β was measured by ELISA in peritoneal lavage, n = 6 per group, one-way ANOVA, data are mean ± SEM. Bacterial CFUs in whole blood and kidney, n = 4 per group, one-way ANOVA, data are mean ± SEM. *p < 0.05, **p < 0.01, ***p < 0.001.

These changes were also observed in the *Mt3*^{-/-}*Casp-11*^{-/-} mice. Since GSDMD is a target of caspase-11 as well as caspase-1 (36), an elevation in active GSDMD may result from higher caspase-1 activation observed in mice lacking MT3, caspase-11 or both. Caspase-8, a pro-apoptotic caspase, collaborates with caspase-11 to mediate systemic inflammation and septic shock (37, 38). Moreover, caspase-8, in addition to caspase-1 can directly cleave IL-1β. We therefore analyzed caspase-8 in kidney homogenates

from *E. coli* infected WT, *Mt3*^{-/-}, *Casp-11*^{-/-} and *Mt3*^{-/-}*Casp-11*^{-/-} mice. Caspase-11 negatively influenced the activation of caspase-8 (**Supplementary Figure S3B**).

The above data demonstrate that even when caspase-11 is absent, *Mt3*^{-/-} mice exert heightened levels of active caspase-1, active IL-1β and antibacterial immunity. We therefore queried whether improved bacterial elimination in the absence of MT3 was facilitated by the canonical NLRP3 inflammasome. WT and

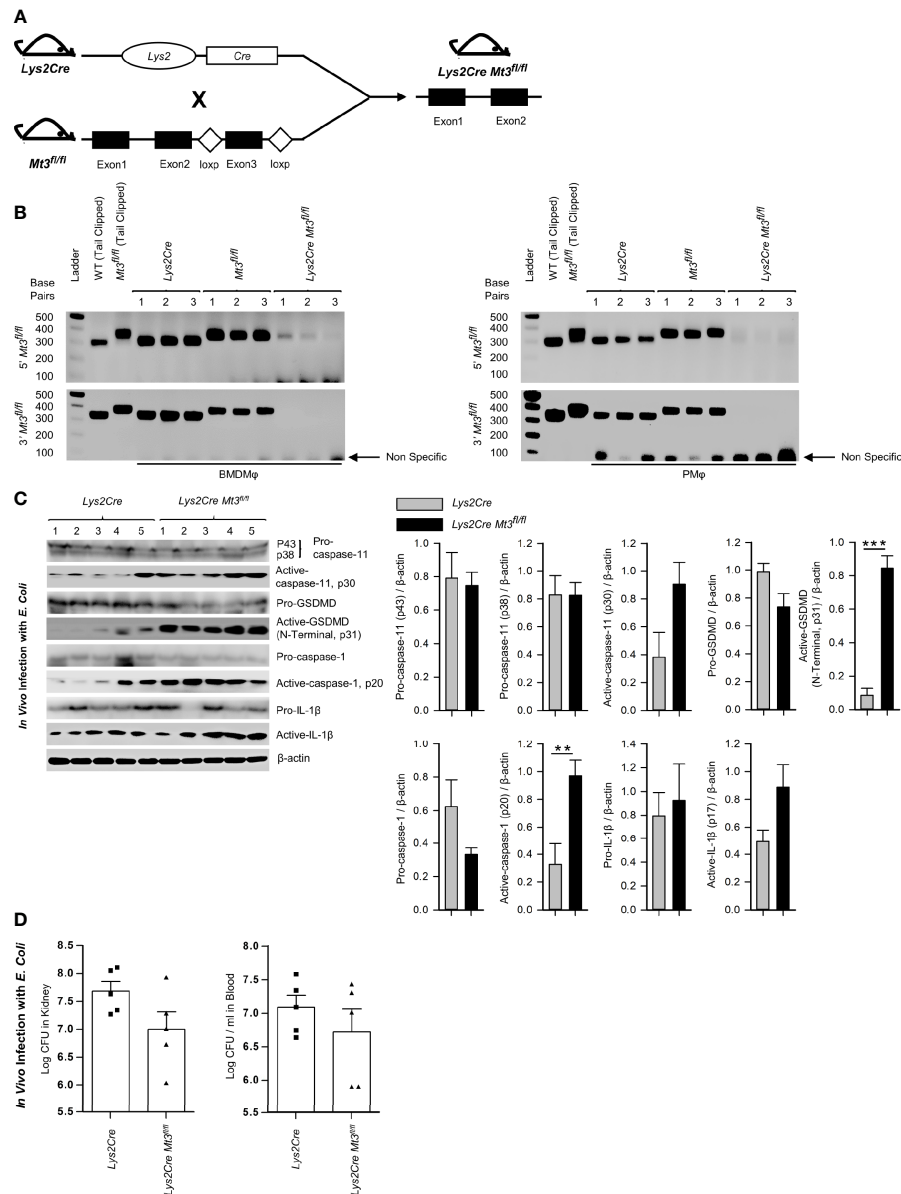


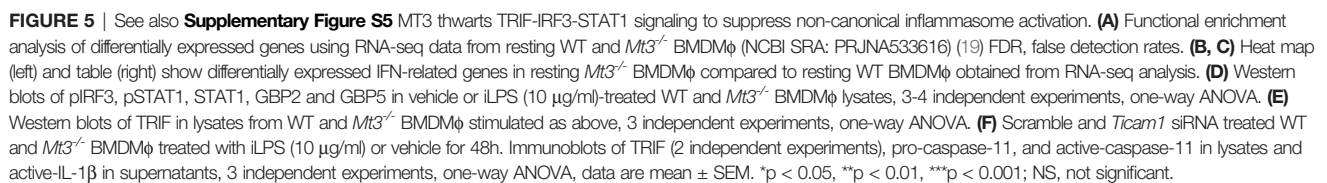
FIGURE 4 | See also **Supplementary Figure S4** Myeloid-MT3 suppresses non-canonical inflammasome activation and blunts gram-negative bacterial clearance *in vivo*. **(A)** Generation of *Mt3^{fl/fl}* mice by inserting loxP sites flanking exon 3 of the *Mt3* gene using the CRISPR-Cas9 gene targeting approach. *Mt3^{fl/fl}* mice crossed with *Lys2Cre* mice to obtain *Lys2Cre Mt3^{fl/fl}* mice. **(B)** Efficacy of myeloid *Mt3* deletion assessed by genotyping peritoneal Mφ (PMφ) and BMDMφ from *Lys2Cre*, *Mt3^{fl/fl}* and *Lys2Cre Mt3^{fl/fl}* mice. Gel electrophoresis analysis demonstrating efficient deletion of the *Mt3* gene from BMDMφ and PMφ of *Lys2Cre Mt3^{fl/fl}* mice. **(C)** Western blots of pro-caspase-11, active-caspase-11, pro-GSDMD, active-GSDMD (p31), pro-caspase-1, active-caspase-1, pro-IL-1β and active-IL-1β in whole kidney homogenates of mice infected as above, n = 3-5 per group, two-tailed t-test. **(D)** Bacterial CFUs in kidney and whole blood of *Lys2Cre* and *Lys2Cre Mt3^{fl/fl}* mice infected *i.p.* with *E. coli* (1 X10⁹ CFUs/mouse) for 6h, n = 3-5 per group, two-tailed t-test, data are mean ± SEM. **p < 0.01, ***p < 0.001.

Mt3^{-/-} mice were treated *i.p.* with MCC950 (NLRP3 inhibitor) followed by infection *i.p.* with *E. coli*. Treatment with MCC950 reduced IL-1β levels and sharply blunted antibacterial resistance in the blood and kidney of *Mt3^{-/-}* mice compared to vehicle-treated controls. Bacterial burdens were also elevated in WT mice by NLRP3 inhibition (**Figure 3C**). Collectively, these data demonstrate that MT3 negatively controls activation of the

non-canonical inflammasome and that both MT3 and caspase-11 cripple resistance to bacterial infection.

Myeloid MT3 Orchestrates Negative Control of the Non-Canonical Inflammasome

To affirm that the effects on caspase-11 inflammasome activation observed in the *Mt3^{-/-}* mice were dependent on myeloid-MT3, we



caspase-11 inflammasome targets and bacterial burden were examined in kidney and blood. *Lys2Cre Mt3^{fl/fl}* mice exerted increased activation of caspase-11, GSDMD (N-terminal), caspase-1, and IL-1 β in kidney homogenates and improved bacterial elimination compared to *Lys2Cre* control mice (**Figures 4C, D**). Thus, myeloid MT3 facilitates subversion of non-canonical inflammasome activation and contributes to antibacterial immunity *in vivo*.

MT3 Exerts a Brake on the TRIF-IRF3-STAT1 Axis to Curtail Caspase-11 Signaling

Signaling via the TRIF pathway is crucial for caspase-11 activation and synergistic engagement of the NLRP3 inflammasome leading to activation of caspase-1 and IL-1 β (20). Downstream of TRIF, IRF3 and IRF7 induce IFN β production that activates STAT1 signaling and promotes transcription of inflammasome components including caspase-11 and guanylate binding proteins (GBPs). GBP2 and GBP5 facilitate LPS release into the cytosol from intracellular vacuoles containing bacteria (39, 40). Our functional enrichment data based on protein-protein interaction network analyses revealed a potential involvement of MT3 in LPS, TRIF, type-I IFN and IL-1 signaling (Table 1, Supplementary Table S1 and Supplementary Files S1, S2). We further examined our published RNA-seq data (NCBI SRA: PRJNA533616) to determine differentially expressed genes by comparing resting WT and *Mt3*^{-/-} BMDM ϕ (19). The derived list of differentially expressed genes significantly enriched 12 GO BP categories directly related to cytokine and chemokine signaling and regulation of inflammatory responses based on DAVID functional enrichment analysis (Figure 5A) (41). These analyses suggested that MT3 deficiency perturbed the expression of immune-related genes even at the resting state. We reported that a lack of MT3 augments IFN γ responsiveness (19). Herein, from our RNA-seq analysis, we identified 20 genes related to IFN-signaling that were upregulated in resting *Mt3*^{-/-} BMDM ϕ compared to resting WT BMDM ϕ (p adj <0.05) (Figures 5B, C). Among these, *Isg15*, *Mx1* and *Ifit* (*Ifit1bl1*, *Ifit3*, *Ifit3b*, *Ifit2*, *Ifit1*, *Ifit1bl2*) family of genes are known targets of type-I IFNs (42–45). These observations led us to posit that MT3 regulated the cellular response to LPS challenge by modulating the TRIF-IRF3-STAT1 axis upstream of non-canonical inflammasome activation. LPS engages the TRIF-IRF3-STAT1 axis via toll-like receptor 4 (TLR4) signaling in M ϕ . To address this hypothesis, we challenged WT and *Mt3*^{-/-} BMDM ϕ with iLPS or vehicle and examined activation of the TRIF-IRF3-STAT1 pathway. M ϕ lacking MT3 exerted increased activation of phospho-IRF3 (pIRF3), pSTAT1, GBP2 and GBP5 (Figure 5D). TRIF protein levels were unaltered by MT3 deficiency (Figure 5E). Type-I IFN signaling is required for activation of the caspase-11 inflammasome cascade by gram-negative bacteria (20). As MT3 deficiency augmented the expression of genes involved in IFN signaling (Figures 5B, C), we blocked the interferon- α/β receptor (IFNAR) 1 using a monoclonal antibody prior to iLPS challenge in WT and *Mt3*^{-/-} M ϕ . IFNAR1 blockade resulted in decreased pro-caspase-11 (p43 subunit). Total STAT1 and pro-caspase-1 (p38 subunit) were not greatly affected (Supplementary Figure S5). We found robust attenuation of pSTAT1, active-caspase-11 and active-caspase-1, but secretion of active-IL-1 β in both WT and *Mt3*^{-/-} M ϕ was increased upon blockade of IFNAR1 signaling. This finding corresponded with high pro-IL-1 β levels in M ϕ treated with the IFNAR1 antibody (Supplementary Figure S5). These data indicate that although IFNAR1 signaling is required for fueling the non-canonical inflammasome cascade and activation of caspase-1, pro-IL-1 β and its activation are suppressed by IFNAR1.

We queried if MT3 exerted a brake on TRIF signaling to downmodulate non-canonical inflammasome activation. WT

and *Mt3*^{-/-} BMDM ϕ were treated with scramble or *Ticam1* (gene encoding TRIF) siRNA, and challenged with iLPS (Figure 5F). *Ticam1* silencing reversed the effects of MT3 deficiency resulting in a sharp reduction in caspase-11 and IL-1 β activation in M ϕ (Figure 5F). These data reveal a central role for MT3 in attenuating the crosstalk between TRIF signaling and the caspase-11 activation cascade.

Zn²⁺ Flux by MT3 Drives Suppression of the Non-Canonical Inflammasome in M ϕ

MTs are master regulators of intracellular Zn²⁺ availability and distribution (46, 47). We determined if negative control of the non-canonical inflammasome by MT3 was Zn²⁺-dependent. First, we systematically assessed Zn²⁺ changes in WT and *Mt3*^{-/-} BMDM ϕ upon challenge with iLPS over time using SEC-ICP-MS. Activation of the non-canonical inflammasome in WT M ϕ was associated with profound changes in the intracellular Zn²⁺ pool. iLPS exposure led to a gradual increase in total Zn²⁺ largely associated with the chromatogram peak(s) between 18–21 min. that we previously identified as MTs (Figures 6A, B) (9, 11). The time-dependent elevation in Zn²⁺ corresponded with kinetics of *Mt3* induction (Figures 1A and 6A, B). M ϕ lacking MT3 failed to elevate total Zn²⁺ and MT-associated Zn²⁺ in response to iLPS (Figure 6B). In contrast to the increase in Zn²⁺ pool observed in WT M ϕ challenged with iLPS, resting *Mt3*^{-/-} M ϕ harbored higher Zn²⁺ content that reduced over time post iLPS challenge (Figure 6B). These data indicate that MT3 drives an elevation in intracellular Zn²⁺ in M ϕ during non-canonical inflammasome activation.

Zn²⁺ chelation in human monocytes increases IRF3 activation (48). We reasoned that if the effects of MT3 were Zn²⁺ dependent, altering the intracellular Zn²⁺ concentration will at least in part reverse the heightened non-canonical inflammasome signaling observed in *Mt3*^{-/-} cells. To test this postulate, we exposed WT and *Mt3*^{-/-} BMDM ϕ to increasing amounts of ZnSO₄ and challenged them with iLPS *in vitro*. Exogenous ZnSO₄ supplementation remarkably reduced the ability of *Mt3*^{-/-} M ϕ to respond to iLPS. pIRF3, pSTAT1 and activation of caspase-11 were reduced in ZnSO₄-supplemented *Mt3*^{-/-} M ϕ (Supplementary Figure S6A). A similar effect of Zn²⁺ was also observed in WT M ϕ (Supplementary Figure S6A). We investigated if exposing WT M ϕ to a Zn²⁺-deficient environment would mimic the effects MT3 deficiency on the non-canonical inflammasome. WT BMDM ϕ were cultured in Zn²⁺-sufficient or Zn²⁺-deficient Opti-MEM media prior to iLPS exposure. WT M ϕ exposed to a Zn²⁺-deficient milieu manifested higher pIRF3 and caspase-11 activation accompanied by increased activation and release of IL-1 β (Figure 6C). The amount of TRIF, pro-caspase-11 and pro-IL-1 β were not affected by Zn²⁺ deficiency (Figures 6C and Supplementary Figure S6B).

Next, we directly addressed whether Zn²⁺ is required for the suppressive function of MT3 on the caspase-11 inflammasome. We first overexpressed the MT3 gene in *Mt1*^{-/-}*Mt2*^{-/-} M ϕ and isolated the protein. *Mt1*^{-/-}*Mt2*^{-/-} BMDM ϕ were transfected with the *Mt3* overexpressing vector (pCMV6-Ac-MT3-GFP) or an empty vector (pCMV6-Ac-GFP) control. *Mt1*^{-/-}*Mt2*^{-/-} M ϕ were

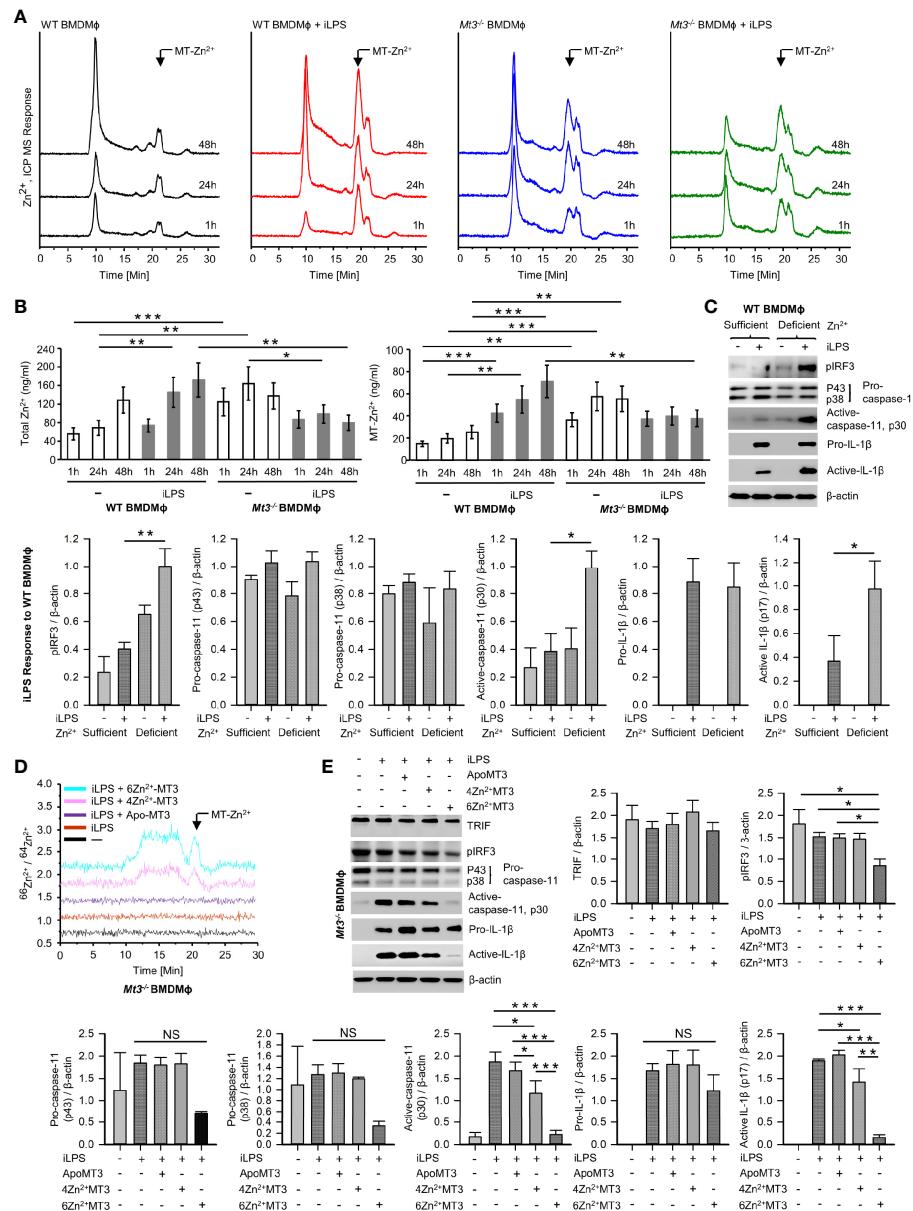


FIGURE 6 | See also **Supplementary Figures S6, 7** MT3-Zn²⁺ axis drives negative regulation of the non-canonical inflammasome. **(A)** SEC-ICP-MS of WT and *Mt3*^{-/-} BMDMφ exposed to vehicle or iLPS (10 μg/ml) for the indicated time points, chromatograms depict Zn²⁺ distribution in cell lysates across various molecular masses, arrow indicates Zn²⁺ associated with the MT-peak (18–21 min.) on the chromatogram, Y axis is off-set to allow easy comparison under the same scale. **(B)** Bar graphs of total Zn²⁺ and MT-Zn²⁺ in WT and *Mt3*^{-/-} BMDMφ post iLPS (10 μg/ml) or vehicle exposure. Two-way t-test against respective BMDMφ controls at each time point, 3 independent experiments, data are mean ± SD. **(C)** WT BMDMφ treated with iLPS (10 μg/ml) or vehicle for 24h in Zn²⁺ sufficient or Zn²⁺ deficient Opti-MEM media, immunoblots of pIRF3, pro-caspase-11, active-caspase-11 and pro-IL-1β in lysates and active-IL-1β in media supernatants, one-way ANOVA, data are mean ± SEM. **(D, E)** *Mt3*^{-/-} BMDMφ transfected with Pro-Ject™ or Pro-Ject™ complexed with apo-MT3, 4Zn²⁺MT3 or 6Zn²⁺MT3 and treated with iLPS (10 μg/ml) or vehicle for 24h in Zn²⁺ deficient Opti-MEM media. **(D)** Chromatograms depict Zn²⁺ distribution in cell lysates across various molecular masses, arrow indicates Zn²⁺ signal associated with the MT-peak (18–21 min.) on the chromatogram, Y axis is off-set to allow easy comparison under the same scale. **(E)** Western blots of pIRF3, pro-caspase-11, active-caspase-11 and pro-IL-1β in lysates and active-IL-1β in supernatants, 3 independent experiments, one-way ANOVA, data are mean ± SEM. *p < 0.05, **p < 0.01, ***p < 0.001; NS, not significant.

used so as to exclude any contribution of these MTs in the MT3 purification process. The MT-associated peak from MT3-overexpressed Mφ was identified by SEC-ICP-MS (**Supplementary Figure S7**) and collected. We complexed

MT3 with the ⁶⁶Zn²⁺ isotope to acquire an MT3-Zn²⁺ saturation of 4 Zn²⁺ ions per MT3 (MT3-4Zn²⁺) and 6 Zn²⁺ ions per MT3 (MT3-6Zn²⁺). The ⁶⁶Zn²⁺ isotope was used to monitor changes in the ratio of ⁶⁶Zn²⁺/⁶⁴Zn²⁺ post-transfection

of the MT3- $^{66}\text{Zn}^{2+}$ complexes in M ϕ . We transfected apo-MT3, MT3-4Zn $^{2+}$ or MT3-6Zn $^{2+}$ into *Mt3* $^{-/-}$ BMDM ϕ in Zn $^{2+}$ -deficient media. The use of *Mt3* $^{-/-}$ BMDM ϕ and Zn $^{2+}$ -deficient media enabled exclusion of any possible contribution from endogenous MT3 and exogenous Zn $^{2+}$ in our analysis. Post-transfection of apo-MT3 or MT3-Zn $^{2+}$ complexes, M ϕ were challenged with iLPS to activate the non-canonical inflammasome. To confirm that intracellular Zn $^{2+}$ changes occurred upon transfection of the MT3- $^{66}\text{Zn}^{2+}$ complexes, we analyzed BMDM ϕ lysates by SEC-ICP-MS. *Mt3* $^{-/-}$ cells transfected with MT3-4Zn $^{2+}$ and MT3-6Zn $^{2+}$ but not apo-MT3 exhibited an increase in the $^{66}\text{Zn}^{2+}/^{64}\text{Zn}^{2+}$ ratio in the MT-peak region at 18–21 mins. in the chromatogram indicating an elevation in the intracellular $^{66}\text{Zn}^{2+}$ isotope (**Figure 6D**). These data confirm that transfection of the MT3-Zn $^{2+}$ complexes resulted in an increase in intracellular $^{66}\text{Zn}^{2+}$ in M ϕ . In parallel, we isolated cell lysates and supernatants proteins from these M ϕ to determine whether apo-MT3 or the MT3-Zn $^{2+}$ complexes modulated the non-canonical inflammasome pathway. Transfection of MT3-4Zn $^{2+}$ and MT3-6Zn $^{2+}$ but not apo-MT3, dampened pIRF3, active caspase-11 and active IL-1 β in response to iLPS (**Figure 6E**). TRIF levels were unaffected by MT3 transfection (**Figure 6E**). Pro-caspase-11 and pro-IL-1 β were modestly diminished by MT3-4Zn $^{2+}$ and MT3-6Zn $^{2+}$ exposure, but these changes were not significant (**Figure 6E**). The effect of MT3-6Zn $^{2+}$ was more profound than that of MT3-4Zn $^{2+}$ indicating that a higher Zn $^{2+}$ saturation on MT3 corresponded with a stronger suppressive effect on the non-canonical inflammasome (**Figure 6E**).

Taken together, these findings reveal a previously undescribed interplay between the non-canonical inflammasome and its negative regulator, whereby the MT3-Zn $^{2+}$ axis suppresses caspase-11 inflammasome, but the two molecules concur in compromising immunological fitness of the host during bacterial pathogenesis.

DISCUSSION

Human CASPASE-4 or mouse caspase-11 are inflammatory caspases that drive cell death *via* pyroptosis. These caspases directly recognize bacterial LPS in the cytosol resulting in CASPASE-4 or caspase-11 auto-processing and synergistic activation of the NLRP3 inflammasome that culminates in caspase-1 activation, processing and release of IL-1 β and IL-18 (2, 32). While the non-canonical inflammasome boosts host immunological fitness to some bacterial infections, heightened activation of this cascade poses the danger of tissue injury and organ failure. Thus far, negative regulation of IFN β production by prostaglandin E2, immunity-related GTPases M clade, cyclic-adenosine monophosphate, and low dose oxidized phospholipid oxPAPC have been shown to thwart activation of the non-canonical inflammasome (49–52). The role of MTs in regulating inflammasome activation pathways has largely been unknown. Herein, we identify a previously undescribed function

of MT3 in curtailing the highly inflammatory non-canonical inflammasome activation cascade *via* Zn $^{2+}$ regulation. We demonstrate that while MT3 orchestrates negative regulation of the caspase-11 inflammasome, the combined presence of MT3 and caspase-11 blunts resistance to *E. coli* infection *in vivo*. These studies illuminate a central role for the MT3-Zn $^{2+}$ axis in shaping the intricate balance between host antibacterial immunity and unrestrained inflammation.

MT1 and MT2 are ubiquitously expressed and can be induced by infection (53–56). Initial studies on MT3 revealed tissue-restricted expression with high levels predominantly found in the brain tissue where it inhibits neuronal cell death (21, 57). The immunological functions of MT3, particularly in the innate arm have only recently been investigated (11, 19, 21). We reported that *Mt3* is inducible by the pro-resolving cytokines IL-4 and IL-13 in M ϕ . One inducer of *Mt3* expression is STAT6 signaling, and this MT is crucial in shaping the phenotypic and metabolic attributes of M ϕ stimulated with type-2 cytokines (11, 19). Studies on MTs in response to exogenous LPS stimulation have largely focused on MT1 and MT2. Monocytes and M ϕ induce MT1 and MT2 upon extracellular LPS exposure (58, 59). We found that iLPS challenge also induced *Mt1* and *Mt2* in M ϕ , although their expression receded to baseline over time. In contrast, *Mt3* expression gradually increased as non-canonical inflammasome activation progressed. Subversion of inflammatory responses in M ϕ by MT3 and the delayed expression pattern in response to a non-canonical inflammasome trigger are reminiscent of waning inflammation after the initial peak of inflammasome activation has subsided (19). In line with this hypothesis, protein interaction network analysis predicted the involvement of MT3 in cellular responses related to non-canonical inflammasome activation. M ϕ lacking MT3 exerted robust activation of caspase-11, caspase-1 and IL-1 β . Similar to our observations with mouse MT3, a lack of human MT3 exacerbated the activation of CASPASE4 and IL-1 β in hM ϕ . Human and mouse MT3 proteins that share 86% identity thus have consistent roles that culminate in negative regulation of the non-canonical inflammasome cascade in M ϕ (60). As non-canonical inflammasome activation progressed, MT3 guarded against its unrestrained activation to avert potential inflammatory damage. Together, these observations reveal a pivotal role for MT3 in curtailing the vigor of the caspase-11 activation cascade. Although *Mt3* $^{-/-}$ mice exerted higher sepsis scores and weight loss, they succumbed to septic shock similar to WT controls, suggesting that a threshold level of caspase-11 activation may be sufficient to promote sepsis-associated mortality.

In vivo, LPS released from OMV of gram-negative bacteria triggers caspase-11 activation (2, 3). Myeloid-MT3 contributed to averting excessive activation of caspase-11 and synergistic activation of the canonical inflammasome in response to gram-negative microbial triggers. MT3 compromised antibacterial resistance to *E. coli* and *K. pneumoniae*, but this was not due to its suppressive action on the caspase-11 inflammasome *in vivo*. Instead, *Mt3* $^{-/-}$ and *Casp-11* $^{-/-}$ mice manifested improved antibacterial immunity, an effect that was further augmented when *Mt3* $^{-/-}$ mice lacked caspase-11. The synergism between MT3 and caspase-11 may result from

independent or combined effects of MT3 and caspase-11 *in vivo*. Of note, the activation of caspase-1 and caspase-8 in the absence of MT3 and caspase-11 reveal that canonical inflammasome activation was operational and both caspase-1 and caspase-8 may contribute to IL-1 β activation *in vivo* (38).

M ϕ utilize Zn²⁺ deprivation and Zn²⁺ intoxication mechanisms as strategies for antimicrobial defense (56, 61, 62). We previously showed that ablation of MT3 in M ϕ augments immunity to *Histoplasma capsulatum* as well as *E. coli*. The increased antimicrobial resistance in *Mt3*^{-/-} M ϕ is at least partially attributable to a decrease in the M ϕ exchangeable Zn²⁺ pool and exaggerated IFN γ responsiveness (11, 19). Myeloid and non-myeloid cells may together contribute to bacterial elimination in whole-body MT3-deficient mice. Nonetheless, the augmented bacterial elimination observed in *Lys2Cre Mt3*^{fl/fl} mice indicates that myeloid-MT3 contributes to the suppression of antibacterial defenses *in vivo*. The finding that MT3 deficiency dually bolstered inflammasome activation and antibacterial immunity underpins a role for this protein in suppressing the emergence of a proinflammatory phenotype in M ϕ . Our data unveil a unique crosstalk between caspase-11 and its negative regulator, whereby although MT3 keeps caspase-11 activation under control, the two synergistically compromise host immunological fitness to gram-negative bacterial infection.

Caspase-11 activation can have opposing effects on clearance of different bacteria. It improves resistance to *Burkholderia thailandensis*, *B. pseudomallei*, *Brucella abortus*, and *Legionella pneumophila* but may compromise immunity to *B. cenocepacia*, *Salmonella typhimurium*, *E. coli*, *Shigella flexneri*, *K. pneumoniae* and gram-positive infections including *Streptococcus pyogenes*, *Staphylococcus aureus* and *Listeria monocytogenes* (28, 31–33, 35, 63–69). Lipoteichoic acid from gram-positive bacteria engages the caspase-11 inflammasome *via* NLRP6 (28). Likewise, GAS infection led to caspase-11 activation *in vivo*. Although MT3 exerted disparate effects on caspase-11 activation in gram-positive and gram-negative infections, caspase-1 and IL-1 β activation was suppressed by MT3 in both infection settings. In the context of GAS infection, both the host and the pathogen contribute to canonical inflammasome activation. Surface and secreted GAS virulence factor *emm*, and the streptococcal pyrogenic exotoxin B (SpeB) proteins act as second signals to activate caspase-1 signaling (70–72). Our data do not exclude the role of pathogen-derived factors in contributing to the increased canonical inflammasome activation observed in *Mt3*^{-/-} mice infected with GAS. Nonetheless, our findings indicate that MT3 exerted a suppressive effect on the canonical caspase-1 pathway activated by gram-positive bacteria, while sparing negative regulation of the upstream non-canonical inflammasome activation *in vivo*.

The TRIF pathway is a central node in activation of the caspase-11 inflammasome in response to gram-negative infection (20). Targeting TRIF, but not IFNAR1, completely reversed the inflammatory cascade, including IL-1 β activation. Blockade of IFNAR1 attenuated downstream activation of STAT1, caspase-11 and caspase-1, but both pro-IL-1 β and

active IL-1 β levels were dramatically enhanced. This finding contrasts with the previously reported requirement of both TRIF and IFNAR1 in this pathway (20). Although that study utilized BMDM ϕ from *IFNAR1*^{-/-} mice and we used an anti-IFNAR1 monoclonal antibody, both approaches resulted in attenuation of targets downstream of IFNAR1. Emerging evidence points to an indirect inhibitory effect of type-I IFNs on inflammasome activation by decreasing pro-IL-1 β transcription *via* IL-10 or 25-hydroxycholesterol (73, 74). The subdued activation of caspase-1 and heightened active IL-1 β levels suggests that IL-1 β activation occurs *via* a caspase-1 independent pathway when IFNAR is blocked. Interfering with IFNAR1 signaling can therefore subdue activation of critical inflammasome components including caspase-11 and caspase-1 but sustain IL-1 β production and activation.

The crucial function of Zn²⁺ as a signaling molecule is well documented (13, 75–77). Changes in plasma and cellular Zn²⁺ levels regulate the production of various cytokines *via* NF- κ B signaling (78, 79). Specifically, Zn²⁺ deficiency in humans increases the production of tumor necrosis factor (TNF) α and IL-1 β by LPS-treated PBMCs *ex vivo*, whereas Zn²⁺ supplementation reduces it (80, 81). Therefore, a shift from physiological Zn²⁺ concentrations at the systemic or cellular level can impact proinflammatory cytokine responses and inflammation. To our knowledge, modulation of M ϕ Zn²⁺ homeostasis during non-canonical inflammasome activation has not been previously demonstrated. Our data show that caspase-11 activation is accompanied by a gradual expansion of the intracellular Zn²⁺ pool driven by MT3. Zn²⁺ deficiency did not augment pro- forms of caspase-11 (p43 and p38), but specifically increased their activation. Zn²⁺ diminishes signaling *via* IRF3 by limiting its nuclear localization (48). Accordingly, MT3 interfered with signaling *via* the TRIF-IRF3-STAT1 axis by shaping the M ϕ Zn²⁺ pool. The MT3-Zn²⁺ axis dampened IRF3 phosphorylation and downstream mediators without impacting TRIF levels. Although we cannot rule out the direct effect of Zn²⁺ on inflammasome components downstream of IRF3, the suppressive action of MT3 on the non-canonical inflammasome was Zn²⁺ dependent. Our data demonstrate that by manipulating the M ϕ Zn²⁺ milieu, caspase-11 activation can either be triggered or averted. This finding has important implications in defining a role for Zn²⁺ in subverting caspase-11 driven hyperinflammation. Developing therapeutic strategies that temper activation of the caspase-11/4 inflammasome have garnered tremendous interest to alleviate endotoxemia. In light of this, the MT3-Zn axis emerges as a fresh and vital candidate that guards the vigor of a caspase-11 fueled inflammatory response. In the context of gram-negative bacterial pathogenesis, our data indicate that strategies aimed at combined targeting of MT3 and the caspase-11 inflammasome may be more beneficial in infection control than targeting caspase-11 alone.

Taken together, our studies illuminate a double-edged phenomenon in inflammasome regulation whereby the MT3-Zn²⁺ axis is a sentinel of the caspase-11 inflammasome but MT3 and the non-canonical inflammasome function in concert to compromise host antibacterial resistance.

MATERIAL AND METHODS

Reagents and Resources

Reagents and resources can be found in **Table 2**.

TABLE 2 | Reagents and resources.

Name	Source	Identifier
Antibodies		
anti-TRIF	Proteintech	Cat#23288-1-AP
anti-pIRF3 (Ser396)	BIOSS	Cat#bs-3195R
anti-STAT1	Abcam	Cat#ab99415
anti-pSTAT1 (pY701) [M135]	Abcam	Cat#ab29045
anti-GBP5	Proteintech	Cat#13220-1-AP
anti-GBP2	Proteintech	Cat#11854-1-AP
anti-Caspase 11 (17D9)	eBioscience™	Cat#14-9935-82
anti-Caspase-11	Abcam	Cat# ab180673
anti-CASPASE-4	MBL	Cat#M029-3
anti-GSDMD	Proteintech	Cat#20770-1-AP
anti-Caspase-1	AdipoGen Life Sciences	Cat#AG-20B-0042-C100
anti-Caspase-1 (14F468)	Santa Cruz	Cat#sc-56036
anti-IL-1β/IL-1F2	Biotechnology	
anti-IL-1β/IL-1F2	R&D Systems	Cat#AF-401-NA
anti-IL-1β (B122)	R&D Systems	Cat#MAB4011
	Santa Cruz	Cat#sc-12742
	Biotechnology	
anti-Caspase-8 (1G12)	Enzo Life Sciences	Cat#ALX-804-447-C100
anti-β-actin	Cell Signaling Technology	Cat#4967s
anti-β-actin	ThermoFisher Scientific	Cat#PA1-183
anti-β-actin	R&D Systems	Cat#MAB-8929
Mouse anti-armenian hamster	Santa Cruz	Cat#sc-2789
IgG-HRP	Biotechnology	
Goat anti-rabbit IgG(H+L), HRP conjugate	Proteintech	Cat#SA00001-2
IRDye® 800CW goat anti-rabbit IgG	LI-COR Biosciences	Cat#926-32211
IRDye® 680RD goat anti-rabbit IgG	LI-COR Biosciences	Cat#926-68071
Goat anti-mouse IgG(H+L), HRP conjugate	Proteintech	Cat#SA00001-1
IRDye® 680RD goat anti-mouse IgG	LI-COR Biosciences	Cat#926-68070
Mouse IgG (H&L) secondary antibody peroxidase conjugated pre-adsorbed	Rockland	Cat#610-1319-0500
Rabbit anti-goat IgG(H+L), HRP conjugate	Immunochemicals	
Goat anti-Rat IgG(H+L), HRP conjugate	Proteintech	Cat#SA00001-4
IRDye® 800CW goat anti-rat IgG	Proteintech	Cat#SA00001-15
anti-IFNAR1 (Clone: MAR1-5A3)	LI-COR Biosciences	Cat#926-32219
anti-IgG1 (Clone: MOPC-21)	BioLegend	Cat#127302
Bacterial Strains		
<i>Escherichia coli</i> (K12)	BioLegend	Cat#400102
<i>Klebsiella pneumoniae</i> (KP2 2-70)	Dr. Jason Gardner (gardnejr@ucmail.uc.edu)	N/A
Group A <i>Streptococcus</i> (<i>Streptococcus pyogenes</i>)	Dr. Jason Gardner (gardnejr@ucmail.uc.edu)	N/A
	Dr. Suba Nookala (suba.nookala@und.edu)	N/A

(Continued)

TABLE 2 | Continued

Name	Source	Identifier
Primers		
<i>Mt3</i>	Applied Biosystems	Mm00496661_g1
<i>Mt2</i>	Applied Biosystems	Mm00809556_s1
<i>Mt1</i>	Applied Biosystems	Mm00496660_g1
<i>Hprt</i>	Applied Biosystems	Mm00446968_m1
<i>MT3</i>	Applied Biosystems	Hs00359394_g1
<i>MT2A</i>	Applied Biosystems	HS02379661_g1
<i>HPRT1</i>	Applied Biosystems	Hs99999909_m1
Genotyping Primers	IDT	N/A
siRNA and expression vector		
<i>MT3</i>	Ambion	Cat#AM16708
<i>Ticam1</i>	Dharmacon™	Cat#L-055987-00-0005
ON-TARGETplus™ Control Pool (Non-Targeting pool)	Dharmacon™	Cat#D-001810-10-20
pCMV6-AC-GFP (PS100010)	ORIGENE	Cat#MG200059
pCMV6-AC-GFP	ORIGENE	Cat# PS100010
Chemicals and accessories		
RPMI 1640	CORNING	REF#10-041-CV
Opti-MEM® I	GIBCO	REF#31985-070
FBS	HyClone	Cat#SH30396.03
DPBS	CORNING	REF#21-031-CV
PBS without calcium and magnesium	CORNING	REF#21-040-CV
HBSS	CORNING	REF#21-021-CM
HEPES	Sigma	Cat#H3375
Mouse M-CSF	PEPROTECH	Cat#315-02
Human M-CSF	PEPROTECH	Cat#300-25
Trypsin-EDTA	CORNING	REF#25-053-CI
LPS-B5 Ultrapure	InVivoGen	Cat#tlrl-pb5lps
Glycerol	Fisher Bioreagents	Cat#BP229-1
LB Broth	Fisher Bioreagents	Cat#BP1427-500
BBL™ Brain Heart Infusion Broth	Becton Dickinson	Cat#22182
Agar	BD Bacto™	Cat#214010
BD Bacto™ Dehydrated Culture Media: Todd Hewitt Broth	BD	Cat#249240
Gibco™ Bacto™ Yeast Extract	Gibco	Cat#212750
BD BBL™ RODAC™ Trypticase™ Soy Agar with 5% Sheep Blood (TSA II)	BD	Cat#221261
EZ Pack™ Agarose	ASi	Item No.#AG2501
MCC950	ApexBio	B7946-50
ZnSO ₄	Sigma	Cat#z-4750
Sodium Chloride	Sigma	Cat#S1679-1KG
Ethyl Alcohol	Fisher Scientific	Cat#A407-4
Methanol	Fisher Scientific	Cat#A434-20
Methanol	BDH	Cat#BDH1135-4LP
Dimethyl Sulfoxide	Sigma	Cat#D8418-1L
Chloroform	Fisher Scientific	Cat#C5312
Hydrochloric Acid	Fisher Scientific	Cat#A508-212
Sulfuric Acid	Fisher Scientific	Cat#A300 ^{SL} -212
Sodium Hydroxide	Fisher Scientific	Cat#S318-3
Precise Protein Gels	Invitrogen	REF#XP04205BOX
SurePAGE™, Bis-Tris, 10x8 gels (4-20%, 15 wells)	GenScript	Cat#M00657
Tris-MOPS-SDS Running Buffer Powder	GenScript	Cat#M00138
Nitrocellulose membranes	BIO-RAD	Cat#162-0112

(Continued)

TABLE 2 | Continued

Name	Source	Identifier
Protease & Phosphatase Inhibitor Cocktail	Thermo Scientific	Cat#78442
Denaturing Cell Extraction Buffer	Invitrogen	Cat#FNN0091
XCell II™ Blot Module	ThermoFisher Scientifics	Cat#EI9051
Glycine	Fisher Scientific	Cat#BP381
Tris-base	Fisher Scientific	Cat#BP152
SDS	Fisher Scientific	Cat#BP166
Tween 20	Acros Organics	Cat#23336-0010
Tween 20	Sigma	Cat#P-1379
Triton X100	Fisher Scientific	Cat#BP151
Bovine serum albumin	Sigma	Cat#A7030
Intercept® (TBS) Blocking Buffer	LI-COR Biosciences	Cat#927-60001
Non-fat dry milk	Nash Finch Co.	N/A
Isoflurane	Covetrus	NDC Code(s) #11695-6777-2
Nair	Chuech & Dwight Co. inc	N/A
Gauze	Medline	REF#PRM25444
Puritan cotton tipped applicator	Puritan	SKU#836-WC
Insulin injection syringe (1mL)	Exelint international co.	Cat#26029
10 ml plastic Syringe	Fisherbrand	Cat#14955459
1 ml plastic Syringe	Fisherbrand	Cat#14955456
BioLite12 well multidish	Thermo Scientific	Lot# H4XA4RE106
24 well tissue culture plates	CellPro	Lot# 072219BA03
48 well cell culture plate	NEST	Lot# 121717A004
Tissue culture plate 96 well, flat bottom	Fisherbrand	Cat#FB012931
96 well ELISA plate	NEST	Lot#04291818A007
Petri dish	NEST	Lot#753001
15 ml Centrifuge tube	Fisher Scientific	Cat#14-955-237
50 ml Centrifuge tube	Fisher Scientific	Cat#14-955-239
Cell scraper	SPL Life Sciences	Cat#90030
Golden Rod animal Lancet (4mm)	Medipoint Inc	N/A
Omni homogenizer Th-01 and tips	Omni International	Model Number#THP115
GeneArt Platinum Cas9 Nuclease	ThermoFisher	Cat# B25641
Nuclease	ThermoFisher	Cat# 1074181
Alt-R SpCas9 Nuclease 3NLS sgRNA	CCHMC transgenic core	N/A
TSK gel 3000SW gel filtration column	TOSOH BIOSCIENCE	Cat#05789
DreamTaq DNA Polymerase	Thermo Scientific	REF#EP0702
Commercial Assays		
TransIT®-TKO	Mirus Bio LLC	Prod. No.#MIR 2150
TransIT®-LT1	Mirus Bio LLC	Prod. No.#MIR 2300
Pierce Protein Transfection Reagent Kit	Thermo Scientific	REF#89850
Human IL-1β/IL-1F2 DuoSet ELISA	R&D Systems	Cat#DY201-05
Mouse IL-1β	BioLegend	Cat# 432601
IL-1α	BioLegend	Cat# 433401
RNeasy Mini Kit	Qiagen	Cat# 74104
QUICK-RNA™ MINIPREP KIT	Denville Scientific	Cat# R1055
Reverse Transcription System	Promega	REF#A3500
Probe Lo-Rox 2X qPCR Mix	RADIANT™	Cat#QP9020
CytoTox 96® NonRadioactive Cytotoxicity Assay kit	Promega	REF#G1781

(Continued)

TABLE 2 | Continued

Name	Source	Identifier
SuperSignal™ West Femto Maximum Sensitivity Substrate	Thermo Scientific	Cat#34096
NEBNext Poly(A) mRNA Magnetic Isolation Module	New England BioLabs	Cat#E7490L
NEBNext Ultra Directional RNA Library Prep Kit	New England BioLabs	Cat# E7420L
NEBNext Library Quant Kit	New England BioLabs	Cat# E7630L
MEGAshorscript T7 Kit	Thermo Fisher	Cat#AM1354
MEGAclear Kit	Thermo Fisher	Cat# AM1908
Quick-DNA™ Miniprep Plus Kit	ZYMO RESEARCH	Cat#D4069
Radiant™ Taq DNA Polymerase	RADIANT™	Cat#C101
Experimental Models: Organisms/Strains		
C57BL/6 Mice	Jackson Laboratory	Stock#00064
C57BL/6 <i>Mt3</i> ^{-/-} deletion of Exon 3	Transgenic Animal and Genome editing core facility at CCHMC	N/A
C57BL/6 <i>Mt1</i> ^{-/-} <i>Mt2</i> ^{-/-}	Dr. George S. Deepe (deepegs@ucmail.uc.edu)	N/A
C57BL/6 <i>Casp4</i> ^{tm1Yuan/J} (<i>Casp-11</i> ^{-/-})	Jackson Laboratory	Stock#024698
<i>Mt3</i> ^{-/-} <i>Casp-11</i> ^{-/-}	Crossed and bred in-house	N/A
C57BL/6 <i>Lys2Cre</i>	Dr. George S. Deepe (deepegs@ucmail.uc.edu)	N/A
C57BL/6 <i>Lys2Cre Mt3</i> ^{fl/fl}	Crossed and bred in-house	N/A
Instrument, Software and Algorithms		
FluorChem® HD2	Cell Biosciences	S/N#FC HD2 Imager
Odyssey CLx Imaging system	LI-COR	N/A
7500 Fast Real Time PCR System	Applied Biosystems	S/N#275013253
RNA-seq data analysis - DAVID Bioinformatics Resources v.6.8	NIAID/NIH	(https://david.ncifcrf.gov/summary.jsp)
Protein-protein interaction networks- STRING v.11.0	ELIXIR	(https://string-db.org/)
NIH ImageJ Fiji	NIH	(https://imagej.nih.gov/ij/)

Microbes

E. coli (K12) and *K. pneumoniae* were kindly provided by Dr. Jason Gardner at the University of Cincinnati. Group A Streptococcus (GAS 5448) was kindly provided by Dr. Suba Nookala at the University of North Dakota.

Mice

All mice used in this study were on the C57BL/6 background. WT and *Casp4*^{tm1Yuan/J} (*Casp-11*^{-/-}) mice were acquired from the Jackson Laboratory. *Lys2Cre* mice were kindly provided by Dr. George S. Deepe, Jr. (University of Cincinnati). *Mt3*^{-/-} (exon 3 deleted) and *Mt3*^{fl/fl} mice were generated using clustered regularly interspaced short palindromic repeats (CRISPR) by the Transgenic Animal and Genome Editing Core facility at the Cincinnati Children's Hospital Medical Center (CCHMC). In mice, the *Mt* gene cluster is located on chromosome 8. The *Mt3*

gene consists of 3 exons and is preceded by *Mt1* and *Mt2* genes. We targeted exon 3 of *Mt3* by flanking it with loxp sites (*Mt3^{fl/fl}*) using the CRISPR-Cas9 gene targeting approach. *Lys2Cre Mt3^{fl/fl}* mice that exhibit myeloid *Mt3* deficiency were generated by crossing *Lys2Cre* mice to *Mt3^{fl/fl}* mice. Deletion of the *Mt3* gene was confirmed in BMDM ϕ and PM ϕ of *Lys2Cre Mt3^{fl/fl}* mice by genotyping as detailed in the CRISPR/Cas9 generation of *Mt3^{fl/fl}* mice section. To confirm 3' loxp site insertion or deletion, genomic DNA amplified using forward (5' TAG GCT TCC CAC CTG TTT GG 3') and reverse (5' GCC AAG ATA AAG TCC GGG GT 3') primers. To confirm 5' loxp site insertion or deletion, genomic DNA amplified using forward (5' TCG AAC TAC CTC CAA ACA GAG AAC 3') and reverse (5' TCA GTT TGG TCC AAA CGG GAT G 3') primers. To confirm *Lys2Cre* gene insertion, genomic DNA amplified using mutant (5' CCC AGA AAT GCC AGA TTA CG 3'), common (5' CTT GGG CTG CCA GAA TTT CTC 3') and WT (5' TTA CAG TCG GCC AGG CTG AC 3') primers. *Casp-11^{-/-}Mt3^{-/-}* mice were generated by crossing *Casp-11^{-/-}* mice to *Mt3^{-/-}* mice. *Casp-11* was amplified using tail genomic DNA by mutant reverse (5' CGC TTC CTC GTG CTT TAC GGT AT 3'), common forward (5' ACA ATT GCC ACT GTC CAG GT 3') and WT reverse (5' CAT TGC TGA CCT TAT TTC TGT ATG G 3') primers. *Mt3* was amplified using tail genomic DNA by forward (5' TTG GGG TGA GGT GTA GAG GT 3') and reverse (5' GCC AAG ATA AAG TCC GGG GT 3') primers. Mice used in this study had ad-libitum access to food and water. All mice were housed in the Department of Laboratory Animal Medicine, University of Cincinnati, accredited by American Association for Accreditation of Laboratory Animal Care (Frederick, MD) and experiments were conducted in accordance with Animal Welfare Act guidelines of the National Institutes of Health.

CRISPR/Cas9 Generation of *Mt3^{fl/fl}* Mice

The methods for the design of sgRNAs, donor oligos and the production of *Mt3^{fl/fl}* (loxP sites surrounding exon 3 of the murine *Mt3* gene) animals were as described previously (82). The sgRNAs were selected according to the on- and off-target scores from the CRISPR design web tool (<http://genome-engineering.org>) as well as CRISPOR (<http://crispor.tefor.net>) (83). The selected sgRNA target sequences were cloned, according to the published method (84), into the pX458 vector (addgene #48138) that was modified by us to contain an optimized sgRNA scaffold (85) and a Cas9-2A-GFP. Their editing activity were validated by the T7E1 assay in mouse mK4 cells (86), compared side-by-side with Tet2 sgRNA that was known to work in mouse embryos efficiently (87). Validated sgRNA was transcribed *in vitro* using the MEGAscript T7 kit (ThermoFisher) and purified by the MEGAclear Kit (ThermoFisher), and stored at -80°C. To prepare the injection mix, we incubated sgRNA and Cas9 protein (ThermoFisher) at 37°C for 5 mins. to form the ribonucleoprotein complex and then added the donor oligos to it. The initial attempt was to insert both loxP sites simultaneously *via* piezo-driven cytoplasmic injection (88) of 100 ng/ul Cas9 protein, 50 ng/ul 5' sgRNA, 50 ng/ul 3' sgRNA, 50 ng/ul 5' donor,

and 50 ng/ul 3' donor into fertilized eggs. Injected eggs were transferred into the oviductal ampulla of pseudo-pregnant CD-1 females on the same day. Pups were born and genotyped by PCR and Sanger sequencing. However, only 3' loxP-containing mice were obtained from this attempt. After breeding them to homozygosity for the 3' loxP, a new set of 5' sgRNA and the donor oligo was designed and injected into the zygotes with the mix containing 150 ng/ul Cas9 protein, 75 ng/ul 5' sgRNA, and 100 ng/ul ssDNA donor oligo. Injected eggs were transferred into the oviductal ampulla of pseudopregnant CD-1 females on the same day. Pups were born and genotyped by PCR and Sanger sequencing. Founder mice carrying both 5' and 3' loxP sites in cis were finally obtained. Animals were housed in a controlled environment with a 12-h light/12-h dark cycle, with free access to water and a standard chow diet. All animal procedures were carried out in accordance with the Institutional Animal Care and Use Committee-approved protocol of Cincinnati Children's Hospital and Medical Center.

M ϕ Culture

hM ϕ were prepared from peripheral blood mononuclear cells (PBMCs). Briefly, human blood obtained from the Hoxworth Blood Center, University of Cincinnati was diluted (1:2) with calcium- and magnesium-free 1X Dulbecco's phosphate-buffered saline (DPBS) and inverted gently to mix. Ficoll-Paque (10 ml for the total volume of 40 ml diluted blood) was layered at the bottom of the tube. The tubes were centrifuged at 400 X g for 30 mins. without break at 20°C. The PBMC interface was transferred to sterile tubes and washed three times using 40 ml of DPBS containing 2mM EDTA and centrifuged at 120 X g for 10 mins. without break at 4°C. A final wash was performed with DPBS (without EDTA). Isolated PBMCs were resuspended in complete RPMI 1640 medium. PBMCs (5×10^6) were plated in 24 well plates containing complete RPMI medium. After 24h, adherent monocytes were washed three times with DPBS and plated in complete RPMI 1640 medium (Corning®) containing 10 ng/ml macrophage-colony stimulating factor (M-CSF), 10%FBS, 10 μ g/ml gentamycin sulfate (Alkali Scientific Inc.) and 2-mercaptoethanol. Cells were differentiated by exposure to human recombinant M-CSF on days 0, 2 and 4. After 6 days, hM ϕ were washed with DPBS prior to use for the experiment.

Mouse BMDM ϕ were prepared by differentiating bone marrow cells in complete RPMI 1640 medium containing 10 ng/ml mouse M-CSF, 10% fetal bovine serum (FBS) (HyClone Laboratories, Utah), gentamycin sulfate (10 μ g/ml) and 2-mercaptoethanol. BMDM ϕ were fed on days 0, 2 with complete RPMI 1640 medium containing 10 ng/ml M-CSF and were supplemented on day 4 with M-CSF. After 6 days, adherent M ϕ were harvested by washing with DPBS followed by trypsinization and centrifuged at 1600 rpm for 5 mins. at 4°C. M ϕ were washed again with DPBS at 1600 rpm for 5 mins. at 4°C and counted under the microscope. Dead cells were excluded from enumeration using Trypan Blue stain. BMDM ϕ (0.5×10^6 in 24 well or 1×10^6 in 12 well plate) were seeded.

Bioinformatics Analysis

The STRING database was used to review the protein-protein interaction networks of MT3 in *Mus musculus* and *Homo sapiens* (22). A full network analysis was conducted based on text mining, experiments, databases, co-expression, neighborhood, gene fusion and co-occurrence data with a minimum required interaction score of 0.4 and a maximum of 50 interactors in the first shell and 50 interactors in the second shell. Statistical significance of the enriched biological processes (GO BP categories) in the MT3 network was set with a false discovery rate (FDR) <0.05.

Identification of differentially expressed genes in resting WT compared to resting *Mt3^{-/-}* M ϕ was based on our previously published RNA-seq data (NCBI SRA: PRJNA533616) (19). The number of biological replicates used in the analysis was 3 per group. Genes differentially expressed with a fold change FC>2 and adjusted p value $q < 0.05$ were considered significant. The Benjamini-Hochberg correction was used to adjust p values for multiple hypothesis testing. Differentially expressed genes in *Mt3^{-/-}* BMDM ϕ compared to WT BMDM ϕ with $q < 0.05$ were queried using the functional annotation clustering tool DAVID to identify statistically enriched GO categories (using the GO terms, BP direct, CC direct and MF direct) in *Mt3^{-/-}* BMDM ϕ compared to WT BMDM ϕ (41). Significance of enrichment was set to FDR <0.05.

Gene Silencing

For gene silencing, M ϕ were transfected with the transfection complex (50 μ l) of siRNA and TransIT-TKO[®] (0.5%) transfection reagent (Mirus Bio[™]) in 500 μ l of complete RPMI 1640 medium without antibiotics as per the manufacturer's instructions. Concentration of siRNAs used for gene silencing were 100 nM each of the non-targeting pool (ON-TARGETplus[™] scramble siRNA), human MT3 (MT3 Silencer[®] Pre-designed siRNA) and mouse *Ticam1* (ON-TARGETplus SMARTpool). All siRNAs were purchased from Dharmacon (GE Healthcare). Both BMDM ϕ and hM ϕ were incubated with the siRNA containing transfection complexes for 24h in RPMI medium and washed prior to transfection with LPS in Opti-MEM medium. TRIF silencing was assessed by protein expression using Western blots. Human MT3 silencing was assessed by gene expression using qRT-PCR.

IFNAR1 Neutralization

IFNAR1 on WT and *Mt3^{-/-}* BMDM ϕ was neutralized using 10 μ g/ml monoclonal anti-IFNAR1 antibody (BioLegend; Clone: MAR1-5A3) 1h prior and 24h after iLPS (10 μ g/ml) stimulation. Negative control groups were treated with the same dose of isotype control IgG antibody (BioLegend; Clone: MOPC-21). After a total 48h, cell lysates and supernatants were harvested for the molecular analysis.

Non-Canonical Inflammasome Activation in M ϕ

To activate the non-canonical inflammasome, 1×10^6 M ϕ were transfected with a transfection complex (50 μ l) of 0.3% TransIT[™]-LT1 (Mirus Bio[™]) transfection reagent (vehicle) and 2 μ g/ml or 10 μ g/ml ultrapure LPS-B5 (*In vivo* Gen)

prepared from *E. coli* 055:K59(B5) in 500 μ l Opti-MEM medium (Thermo Fisher Scientific-US) as per manufacturer's instructions for 24h.

Preparation of Zn²⁺-Sufficient and Zn²⁺-Deficient Opti-MEM Media

Molecular biology grade chelex-100 resin (BioRad) was washed three times with metal free ddiH₂O prior to use. To prepare Zn²⁺-deficient Opti-MEM medium, washed Chelex-100 resin (3 g per 100 ml) was added to Opti-MEM media and vigorously shaken for 1h on an orbital shaker at room temperature. After this time, media was filtered using a 0.22 μ m filter and mixed with fresh washed chelex-100 resin and the same procedure was repeated for a total of 3 times to eliminate metals from Opti-MEM media. Chelex was removed from the media by a final filtration step. During each of these stages, an aliquot of the media was saved to monitor the efficiency of Ca²⁺, Mg²⁺, Mn²⁺, Co²⁺, Zn²⁺, Cu²⁺, Ni²⁺ and Fe²⁺ elimination by ICP-MS. The amount of Zn²⁺ in Opti-MEM media was decreased by 95% by the above chelation method. To prepare Zn²⁺-sufficient media, chelexed Opti-MEM was reconstituted with Ca²⁺, Mg²⁺, Mn²⁺, Co²⁺, Cu²⁺ and Zn²⁺ at the original concentrations as measured by ICP-MS. To prepare Zn²⁺-deficient media, all measured elements except Zn²⁺ were added to the chelexed Opti-MEM media at the original measured concentrations. Finally, the pH of Zn²⁺-sufficient and Zn²⁺-deficient Opti-MEM media was adjusted to 7.4 and filtered prior to use.

MT3 Overexpression and Purification

The pCMV6-Ac-GFP vector containing the mouse *Mt3* gene (pCMV6-Ac-MT3-GFP) and empty pCMV6-Ac-GFP vectors were acquired from Origene and dissolved in nuclease-free sterile H₂O. Plasmid DNA (5 ng) was added to 50 μ l of thawed Novablue competent *E. coli* cells (EMD Millipore) and transformation was performed as per manufacturer's instructions. *E. coli* cells were serially diluted in S. O. C media (ThermoFisher Scientific) and plated onto Luria-Bertani (LB) plates with 50 μ g/ml carbenicillin and grown for 24h at 37°C. A single colony was isolated and inoculated in LB media containing carbenicillin and grown at 37°C for 5h in a shaker. The culture was further amplified by passaging for another 24h. *E. coli* cells were then harvested by centrifugation at 2000 rpm for 10 mins. and plasmid was extracted using the EndoFree plasmid MAXI kit (Qiagen) as per the manufacturer's instructions. The plasmid was reconstituted in endotoxin-free TE buffer and OD readings obtained were in the range of 1.8-1.9. The resulting endotoxin-free plasmid DNA was set to a concentration of 1 mg/ml in filter-sterilized EndoFree TE buffer and frozen into aliquots until further use.

Mt1^{-/-}Mt2^{-/-} BMDM ϕ were transfected with pCMV6-Ac-GFP control vector or pCMV6-Ac-MT3-GFP vector using the LT1 transfection reagent (Mirus Bio) in RPMI media containing 10% serum without antibiotics as per the manufacturer's instructions. After 48h, BMDM ϕ cultures were lysed with 250 μ l of 0.1% SDS prepared in double-deionized (ddi) H₂O for 20 min. on ice with intermittent mixing. Cell lysates were transferred to 0.22 μ m

filter tubes and centrifuged at 13000 rpm for 5 mins. Filtered cell lysates were subjected to SEC-ICP-MS to isolate the MT3 protein as described below.

Preparation of apo-MT3, 4Zn²⁺-MT3 or 6Zn²⁺-MT3

Cell lysates from above were analyzed by SEC-ICP-MS to detect the MT3-associated peak, followed by collection of the fraction of interest (18–21 mins.). The collected fraction was concentrated by freeze drying in Millrock lyophilizer (Millrock, NY). The concentrated fraction was treated with 1 g of Chelex X-100 resin to remove the divalent metals associated to the protein. The total MT concentration was calculated by the total sulfur concentration in the sample with a 1:20 stoichiometry. The sample was divided into 3 fractions, and each fraction was incubated for 2 h in 50 mM Tris-HCl with the appropriate concentration of ⁶⁶Zn²⁺ nitrate to obtain an MT3-Zn²⁺ saturation of 0, 4 or 6 Zn²⁺ ions per MT3 molecule. After incubation, samples were filtered using a 3 kDa MWCO filter to remove the unbound Zn²⁺ and reconstituted in 1X PBS.

Transfection of Apo, Zn²⁺-MT3 Complexes Into BMDMφ

In a 24 well plate, 5 × 10⁵ *Mt3*^{-/-} BMDMφ were transfected with the transfection complex (10 μl) containing 500 ng of apo-MT3, 4Zn²⁺-MT3 or 6Zn²⁺-MT3 and Pro-JectTM (1.75 μl) protein transfection reagent (ThermoScientific-US) in 250 μl of 2% FBS containing antibiotic free RPMI 1640 medium. Control *Mt3*^{-/-} BMDMφ were treated with Pro-JectTM alone. Cells were incubated with the transfection complexes for 3.5h and washed two times using HBSS prior to challenge with iLPS in Zn²⁺ free Opti-MEM medium. At the experiment end point, cell lysates were either prepared for SEC-ICP-MS analysis or both cell lysates and supernatants were collected for the analysis of non-canonical inflammasome activation.

SEC-ICP-MS-MS Analysis and Normalization of Data

SEC-ICP-MS-MS analysis of WT and *Mt3*^{-/-} BMDMφ was performed as described previously (11). Mφ were plated in Opti-MEM media, and either left untreated or transfected with 10 μg/ml LPS for 1, 24 and 48h. After this time, Mφ were washed twice in HBSS and cells were lysed with 0.1% SDS on ice for 20 mins. Cell lysates were then centrifuged in 0.22 mm filter tubes at 13000 rpm for 10 mins. Filtered cell lysates were frozen at -80°C until further analysis by SEC-ICP-MS. 50–80 μl of cell lysates were injected to the HPLC-ICP-MS system according to protein concentration. To normalize the response of ICP-MS-MS signal from SEC separations on different days, 50 μl of 0.5 mg/ml carbonic anhydrase was injected into the liquid chromatography system, and area of Zn²⁺ signals from samples was normalized to area of the carbonic anhydrase peak from each day. The absorbance of carbonic anhydrase at 280 nm was followed to ensure protein integrity.

The instrumentation consisted of an Agilent 1100 HPLC equipped with a degasser, a binary pump, a thermostated auto sampler, a column oven compartment and a diode array

detector. For the Mφ lysates, a TSK gel 3000SW gel filtration column (TSK Tokyo Japan) 7.8 × 300 mm, 10 mm particle size was used. The mobile phase was ammonium acetate pH 7.4, 0.05% MeOH at 0.5 ml/minute. The HPLC system was coupled to the ICP-MS-MS nebulizer via a short polyether ether ketone capillary of 0.17 mm internal diameter. An Agilent 7500ce ICP-MS system equipped with a micromist quartz nebulizer, a chilled double pass Scott spray chamber and a standard 2 mm insert quartz torch with shield torch was used for all experiments. The ICP-MS was operated by the Agilent Mass Hunter integrated chromatographic software in the helium collision mode as reported previously (11). The isotope dilution experiments were processed by exporting the chromatographic data to Origin (Origin labs, CA) and the signal, in the form of counts per second, was used to calculate the ratio of ⁶⁶Zn²⁺/⁶⁴Zn²⁺ at every point in the chromatograms. This was used to generate a new chromatogram that reflected the input of ⁶⁶Zn²⁺ from the MT3-Zn²⁺ complex at every molecular mass region in the chromatogram. The total area under the chromatograms was used to calculate the concentration of total Zn²⁺ (⁶⁴Zn²⁺) and ⁶⁶Zn²⁺ from the MT3-⁶⁶Zn²⁺ complexes (⁶⁶Zn²⁺/⁶⁴Zn²⁺) against a calibration curve of Zn²⁺ based on carbonic anhydrase.

ICP-MS-MS and SEC-ICP-MS-MS Quality Control to Avoid External Zn²⁺ Contamination

All metal analysis experiments were performed using trace metal grade reagents with acid washed plastic vials. Reagent blanks were used to correct the background signal. The analysis was performed through a metal free encased auto sampler. The concentration of Zn²⁺ in the blanks was always below 100 parts per trillion (ppt), the blank estimate concentration on the calibration curves was always below 50 ppt, while the detection limits were below 30 ppt.

For chromatographic analysis, the mobile phase was cleaned using a Chelex 100 resin, using the batch method. In brief, 3 g of Chelex-100 was added to a liter of mobile phase, stirred for 30 mins. and passed through a 0.45 mm membrane. This decreased the Zn²⁺ concentration below 200 ppt (measured as total). By this method, the base line ICP-MS-MS ⁶⁶Zn²⁺ signal was below 1000 counts per second, which represents sub-ppb levels. The SEC column was cleaned using 10 volumes of 0.2 M NaCl and equilibrated with the mobile phase, followed by injection of 50 μl of 2% HNO₃ three times to remove any accumulated Zn²⁺ in the column. With this procedure, Zn²⁺ distribution in the samples never deviated more than 10% compared to the theoretical natural Zn²⁺ isotope distribution in the control Mφ samples. Four blanks and four carbonic anhydrase standards were injected after the cleaning procedure for monitoring Zn²⁺ signal by ICP-MS-MS to ensure optimal column performance. Typically, the column was cleaned every 30–40 samples.

LPS Treatment *In Vivo*

Thirteen-week-old WT and *Mt3*^{-/-} mice were primed with *i.p.* injection of 10 mg/kg poly(I:C) for 6h followed by 2 mg/kg ultrapure LPS-B5 (*In vivo*Gen) prepared from *E. coli* 055:K59 (B5) (*i.p.* injection) for 18h. At the experiment end point, blood

was collected by cardiac puncture, allowed to clot, and centrifuged at 2000 rpm for 30 mins. at 4°C to isolate serum. Serum was used to measure cytokines by enzyme-linked immunosorbent assay (ELISA).

In Vitro and In Vivo Infection With Gram-Negative Bacteria

For *in vitro* infection, *E. coli* (K12) was grown in LB broth at 37°C overnight in an orbital shaker. The culture was pelleted, washed and resuspended with ice-cold DPBS. Optical Density (OD) of the culture was measured at 600nm using a spectrophotometer. To analyze *E. coli* burden in *in vitro*, hMφ were transfected with scramble siRNA or *MT3* siRNA as described above. hMφ, WT and *Mt3*^{-/-} BMDMφ were infected with a multiplicity of infection (MOI) of 25 *E. coli*: 1 hMφ for 3.5h in Opti-MEM media. Mφ were washed 3 times with 10 µg/ml gentamycin sulfate containing DPBS to kill extracellular bacteria and incubated in Opti-MEM media with antibiotic for 24h. Mφ were again washed 3 times with antibiotic-free DPBS, diH₂O was added and cells were incubated for 30 min. to induce osmotic lysis. Cells were scraped and lysates were diluted in DPBS followed by plating on LB agar plates and incubated at 37°C for 24h. Colonies were enumerated as above. Intracellular bacterial burden was represented as percent inhibition of bacterial growth in *MT3*-silenced hMφ compared to scramble siRNA treated hMφ and in *Mt3*^{-/-} BMDMφ compared to WT BMDMφ.

To analyze antibacterial immunity *in vivo*, 10 to 12 week-old mice were used. Mice were infected with *E. coli* 1 X 10⁹ CFUs *via i.p.* injection (300 µl/mouse) for 1h or 6h. To investigate the role of NLRP3 inflammasome in antibacterial immunity, mice were treated with 1 mg/mouse MCC950 (an inhibitor of NLRP3 inflammasome) *via i.p.* injection (100 µl/mouse) for 1h followed by *E. coli* 1 X 10⁹ CFUs *via i.p.* injection (300 µl/mouse) for 6h. *K. pneumoniae* KP2 2-70, a virulent, heavily encapsulated gram-negative bacterial strain (89, 90), was grown overnight in brain heart infusion (BHI) broth. The following morning bacteria were washed with DPBS, and administered at 4 x 10⁴ CFUs in 50 µl per mouse by the *i.n.* to isoflurane-anesthetized mice for 48h. At the infection end point, blood was collected by cardiac puncture. A portion of the blood sample was acquired in anticoagulant (3% Na-citrate or EDTA) containing tubes to determine bacterial CFUs in blood. The remaining blood was allowed to clot, and centrifuged at 2000 rpm for 30 mins. at 4°C to isolate serum. Peritoneal lavage was collected using ice-cold 10 ml DPBS. Kidney, lung, and spleen were collected after perfusion with 3 ml of DPBS, indicated organs and skin was rinsed in DPBS and ground with 5 ml DPBS using a glass grinder. Bacterial growth was measured in blood, peritoneal lavage, kidney, lung, skin and spleen samples. Serum and peritoneal lavage were used to measure cytokines by enzyme-linked immunosorbent assay (ELISA).

LPS-Induced Septic Shock

Septic shock was induced in mice *via i.p.* injection with ultrapure LPS-B5 (20 mg/kg) (*In vivo*Gen) prepared from *E. coli* 055:K59 (B5). Mice were weighed and sepsis scores were determined at

various intervals. The MSS scoring method assesses sepsis severity with scores ranging from 1-4 based on 7 parameters (appearance, consciousness, activity, stimulus (sounds/touch), eyes aspect, respiration rate and respiration quality) (27). Survival analysis was conducted using the Kaplan-Meier analysis method and log-rank (Mantel-Cox test) was used to determine statistical differences in survival.

In Vivo Infection With Gram-Positive Bacteria

A representative MIT1 clonal Group-A-Streptococcus GAS5448 was used for subcutaneous infections (91). GAS was grown at 37°C under static conditions in Todd-Hewitt broth (BD, MD, USA) supplemented with 1.5% yeast extract (BD Biosciences, MD, USA) and *in vivo* infections were performed as described previously (29, 92). WT and *Mt3*^{-/-} mice (n=8/group) were used in this study as a model for subcutaneous GAS infections. One day prior to infection, the hair on the back of the mice was depilated (using Nair cream) and mice were infected subcutaneously with 0.1 ml of GAS suspension prepared in sterile DPBS (Ca²⁺/Mg²⁺ free, low endotoxin, Mediatech, VA, USA, DPBS) (OD₆₀₀ adjusted to yield ~1-5x10⁸ (8) CFUs). Actual inoculum was determined by plating on trypticase soy agar containing 5% sheep blood (BD Biosciences, MD, USA). Mice were monitored twice daily for body weight, lesions, and mortality. To determine GAS dissemination and load, mice were humanely euthanized 72h post-infection. Blood was drawn through cardiac puncture; necrotic skin, kidney, and spleen were recovered aseptically and weighed. One ml of DPBS was added per 100 mg tissue and homogenized (Omni International, Marietta, GA) followed by plating of ten-fold dilutions on blood agar plates. GAS burden was calculated as colony-forming units (CFUs) per ml (blood) or per mg of tissue. The remaining homogenates were centrifuged for 15 mins. at 12,000 x g at 4°C, and supernatants were stored at -80°C for western blot analysis.

Gene Expression

RNA was isolated from Mφ after elimination of genomic DNA using RNeasy Plus Mini kit (Qiagen) or QUICK-RNA™ MINIPREP KIT (Thomas Scientific). cDNA was prepared using Reverse Transcription Systems Kit (Promega, WI) or rAmp First Strand cDNA Synthesis Flex Kit (Thomas Scientific). Taqman primer/probe sets (Applied Biosystems, CA) were used for real-time gene expression analysis using ABI Prism 7500. For time course analysis of expression of murine *Mt* genes, Mφ were left unstimulated or stimulated with 2 µg/ml iLPS for 0h, 1h, 6h, 24h and 48h. Data are presented as fold change in gene expression normalized to unstimulated Mφ at the 0h time point. To examine the effects of extracellular ultrapure LPS (exLPS) on murine *Mt3* gene expression, BMDMφ were left unstimulated or stimulated with 10 µg/ml exLPS. Data are presented as fold change in gene expression normalized to unstimulated Mφ at the 48h time point. For *MT2A* gene expression analysis in *MT3* silenced hMφ, cells were treated with either *MT3* siRNA or scramble siRNA as mentioned above. Data are presented as fold change in gene expression normalized to control siRNA treated hMφ.

Hypoxanthine guanine phosphoribosyl transferase (*Hprt*) was used as an internal control to compare target gene expression.

Western Blotting

TRIF (Proteintech), pIRF3 (BIOSS), STAT1, pSTAT1 (Abcam), GBP2, GBP5 (Proteintech), caspase-11 (Abcam and eBioscience™), CASPASE-4 (MBL), Gasdermin D (Proteintech and Cell Signaling Technologies), caspase-1 (AdipoGen Life Sciences), IL-1 β (R&D Systems) and caspase-8 (Enzo Life Sciences) were assessed in kidney homogenates of *E. coli* infected mice. Cell lysates were prepared using Denaturing Cell Extraction Buffer (Invitrogen) containing protease & phosphatase inhibitor cocktail (ThermoScientific). Culture supernatants were frozen at -80°C until use and processed using methanol-chloroform protein extraction method. Briefly, supernatants were mixed with equal volume of 100% ice-cold methanol and 0.25 times of the total volume of chloroform followed by gentle vortexing and centrifugation at 20,000 X g at 4°C for 10 min. Upper-phase was discarded without disturbing inter-phase proteins. Ice-cold methanol (500 μ l) was added to the tube, gently vortexed and centrifuged at 20,000 X g at 4°C for 10 mins. Supernatants were discarded and pellet was dried at 37°C for 3-5 mins. Urea (8 M, pH-8.0) was used to dissolve the pellet and extracted proteins were stored at -80°C. Total cell lysates, supernatants proteins, cell lysates + supernatants and kidney homogenates were boiled in SDS-PAGE 1X sample buffer at 95°C for 5 mins. Kidney homogenates were centrifuged at 20,000 X g at 4°C for 15 mins. Supernatants were collected for protein analysis. Reduced proteins were run on 8%, 10% or 12% SDS-PAGE gels and transferred on to 0.22 μ m nitrocellulose membranes (GE Healthcare Life Sciences). Membranes were blocked using 5% skim milk in 1X Tris-buffered saline and 0.1% Tween 20 (1XTBST) and probed overnight with primary antibodies at 4°C. Membranes were washed 3 times for 10 mins. each with 1XTBST and probed with corresponding HRP conjugated or IRDyes (LI-COR) secondary antibodies, washed and developed using BrightStar™ Femto HRP Chemiluminescent 2-Component Substrate Kit (Alkali Scientific Inc). β -actin was used as an internal loading control. Western blots were analyzed using ImageJ software and densitometry data were normalized to β -actin.

ELISA

Human and mouse IL-1 β (BioLegend) concentration in media supernatants, serum and in peritoneal lavage and mouse IL-1 α (BioLegend) in media supernatants were determined using commercial ELISA kits according to the manufacturer's instructions.

Quantification and Statistical Analysis

Data were analyzed using Sigma plot or GraphPad Prism by one-way ANOVA for multiple comparisons using the indicated *ad-hoc* methods with at least 3 or more independent biological replicates. Where two groups were compared, two-tailed t-test was used. For *in vivo* infection, bacterial CFUs were log-transformed for statistical analysis. p values were calculated, *p < 0.05, **p < 0.01, ***p < 0.001; NS, not significant, ND, not detected.

DATA AVAILABILITY STATEMENT

The original contributions presented in the study are included in the article/Supplementary Material, further inquiries can be directed to the corresponding author.

ETHICS STATEMENT

All animal studies were reviewed and approved by the Institutional Animal Care and Use Committee (IACUC) at the University of Cincinnati and were conducted within the Department of Laboratory Animal Medicine accredited by American Association for Accreditation of Laboratory Animal Care (Frederick, MD). All animal experiments were conducted in accordance with Animal Welfare Act guidelines of the National Institutes of Health.

AUTHOR CONTRIBUTIONS

DC and KSV planned and conducted molecular and biochemical *in vitro* and *in vivo* experiments, generated *Casp-11^{-/-}Mt3^{-/-}* and *Lys2Cre Mt3^{fl/fl}* mice, analyzed data, and wrote the manuscript. JG conducted *in vivo* infections with *K. pneumoniae*. AS, SN, and SM conducted *in vivo* experiments with GAS infection and analyzed data. AP assisted with bioinformatics analysis. JL conducted chromatographic and mass spectrometric analysis using ICP-MS and SEC-ICP-MS and MT3-Zn²⁺ complex preparations, and analyzed data. KSV designed and supervised the project. All authors contributed to the article and approved the submitted version.

FUNDING

This work was supported by a Junior Faculty Pilot Project Award, American Heart Association 19CDA34770022 Award, American Association of Immunology Careers in Immunology Fellowship Awards to KSV and NIAIDR01 AI106269-06 awarded in part to KSV. GAS studies were supported by the UND CoBRE Host-Pathogen Interactions Pilot Award - NIH/NIGMS award P20GM113123, UND SMHS funds (SN), and UND VPRED Postdoctoral funding support (AS).

ACKNOWLEDGMENTS

We thank Transgenic Animal and Genome Editing Core at Cincinnati Children's Hospital Medical (CCHMC) Center for production of *Mt3^{fl/fl}* mice.

SUPPLEMENTARY MATERIAL

The Supplementary Material for this article can be found online at: <https://www.frontiersin.org/articles/10.3389/fimmu.2021.755961/full#supplementary-material>

REFERENCES

1. Haque M, Sartelli M, McKimm J, Abu Bakar M. Health Care-Associated Infections - an Overview. *Infect Drug Resist* (2018) 11:2321–33. doi: 10.2147/IDR.S177247
2. Kayagaki N, Kagawa S, Hamada H, Ariyoshi T. Non-Canonical Inflammasome Activation Targets Caspase-11. *Nature* (2011) 479:117–21. doi: 10.1038/nature10558
3. Vanaja SK, Russo AJ, Behl B, Banerjee I, Yankova M, Deshmukh SD, et al. Bacterial Outer Membrane Vesicles Mediate Cytosolic Localization of LPS and Caspase-11 Activation. *Cell* (2016) 165:1106–19. doi: 10.1016/j.cell.2016.04.015
4. Liu X, Zhang Z, Ruan J, Pan Y, Magupalli VG, Wu H, et al. Inflammasome-Activated Gasdermin D Causes Pyroptosis by Forming Membrane Pores. *Nature* (2016) 535:153–8. doi: 10.1038/nature18629
5. Davis SR, Cousins RJ. Metallothionein Expression in Animals: A Physiological Perspective on Function. *J Nutr* (2000) 130:1085–8. doi: 10.1093/jn/130.5.1085
6. Kimura T, Kambe T. The Functions of Metallothionein and ZIP and ZnT Transporters: An Overview and Perspective. *Int J Mol Sci* (2016) 17:336. doi: 10.3390/ijms17030336
7. Krezel A, Maret W. The Functions of Metamorphic Metallothioneins in Zinc and Copper Metabolism. *Int J Mol Sci* (2017) 18:1237. doi: 10.3390/ijms18061237
8. Palmer RD. The Elusive Function of Metallothioneins. *Proc Natl Acad Sci U S A* (1998) 95:8428–30. doi: 10.1073/pnas.95.15.8428
9. Subramanian Vignesh K, Landero Figueroa JA, Porollo A, Caruso JA, Deepe GS Jr. Granulocyte Macrophage-Colony Stimulating Factor Induced Zn Sequestration Enhances Macrophage Superoxide and Limits Intracellular Pathogen Survival. *Immunity* (2013) 39:697–710. doi: 10.1016/j.immuni.2013.09.006
10. Wu A, Tymoszyk P, Haschka D, Heeke S, Dichtl S, Petzer V, et al. Salmonella Utilizes Zinc To Subvert Antimicrobial Host Defense of Macrophages via Modulation of NF-kappaB Signaling. *Infect Immun* (2017) 85:e00418–17. doi: 10.1128/IAI.00418-17
11. Subramanian Vignesh K, Landero Figueroa JA, Porollo A, Divanovic S, Caruso JA, Deepe GS Jr. IL-4 Induces Metallothionein 3- and SLC30A4-Dependent Increase in Intracellular Zn(2+) That Promotes Pathogen Persistence in Macrophages. *Cell Rep* (2016) 16:3232–46. doi: 10.1016/j.celrep.2016.08.057
12. Shankar AH, Prasad AS. Zinc and Immune Function: The Biological Basis of Altered Resistance to Infection. *Am J Clin Nutr* (1998) 68:447S–63S. doi: 10.1093/ajcn/68.2.447S
13. Pyle CJ, Akhter S, Bao S, Dodd CE, Schlesinger LS, Knoell DL. Zinc Modulates Endotoxin-Induced Human Macrophage Inflammation Through ZIP8 Induction and C/EBPbeta Inhibition. *PLoS One* (2017) 12:e0169531. doi: 10.1371/journal.pone.0169531
14. Haase H, Ober-Blöbaum JL, Engelhardt G, Hebel S, Heit A, Heine H, et al. Zinc Signals are Essential for Lipopolysaccharide-Induced Signal Transduction in Monocytes. *J Immunol* (2008) 181:6491–502. doi: 10.4049/jimmunol.181.9.6491
15. von Bulow V, Rink L, Haase H. Zinc-Mediated Inhibition of Cyclic Nucleotide Phosphodiesterase Activity and Expression Suppresses TNF-Alpha and IL-1 Beta Production in Monocytes by Elevation of Guanosine 3',5'-Cyclic Monophosphate. *J Immunol* (2005) 175:4697–705. doi: 10.4049/jimmunol.175.7.4697
16. Gong T, Yang Y, Jin T, Jiang W, Zhou R. Orchestration of NLRP3 Inflammasome Activation by Ion Fluxes. *Trends Immunol* (2018) 39:393–406. doi: 10.1016/j.it.2018.01.009
17. Summersgill H, England H, Lopez-Castejon G, Lawrence CB, Luheshi NM, Pahle J, et al. Zinc Depletion Regulates the Processing and Secretion of IL-1beta. *Cell Death Dis* (2014) 5:e1040. doi: 10.1038/cddis.2013.547
18. Brough D, Pelegrin P, Rothwell NJ. Pannexin-1-Dependent Caspase-1 Activation and Secretion of IL-1beta is Regulated by Zinc. *Eur J Immunol* (2009) 39:352–8. doi: 10.1002/eji.200838843
19. Chowdhury D, Alrfai H, Landero Figueroa JA, Candor K, Porollo A, Fecher R, et al. Metallothionein 3 Controls the Phenotype and Metabolic Programming of Alternatively Activated Macrophages. *Cell Rep* (2019) 27:3873–86.e3877. doi: 10.1016/j.celrep.2019.05.093
20. Rathinam VA, Vanaja SK, Waggoner L, Sokolovska A, Becker C, Stuart LM, et al. TRIF Licenses Caspase-11-Dependent NLRP3 Inflammasome Activation by Gram-Negative Bacteria. *Cell* (2012) 150:606–19. doi: 10.1016/j.cell.2012.07.007
21. Lee SJ, Koh JY. Roles of Zinc and Metallothionein-3 in Oxidative Stress-Induced Lysosomal Dysfunction, Cell Death, and Autophagy in Neurons and Astrocytes. *Mol Brain* (2010) 3:30. doi: 10.1186/1756-6606-3-30
22. Szklarczyk D, Gable AL, Lyon D, Junge A, Wyder S, Huerta-Cepas J, et al. STRING V11: Protein-Protein Association Networks With Increased Coverage, Supporting Functional Discovery in Genome-Wide Experimental Datasets. *Nucleic Acids Res* (2019) 47:D607–13. doi: 10.1093/nar/gky1131
23. Kim B, Lee Y, Kim E, Kwak A, Ryoo S, Bae SH, et al. The Interleukin-1alpha Precursor is Biologically Active and is Likely a Key Alarmin in the IL-1 Family of Cytokines. *Front Immunol* (2013) 4:391. doi: 10.3389/fimmu.2013.00391
24. Kurt-Jones EA, Beller DI, Mizel SB, Unanue ER. Identification of a Membrane-Associated Interleukin 1 in Macrophages. *Proc Natl Acad Sci U S A* (1985) 82:1204–8. doi: 10.1073/pnas.82.4.1204
25. Fettelschoss A, Kistowska M, Leibundgut-Landmann S, Beer HD, Johansen P, Senti G, et al. Inflammasome Activation and IL-1beta Target IL-1alpha for Secretion as Opposed to Surface Expression. *Proc Natl Acad Sci U S A* (2011) 108:18055–60. doi: 10.1073/pnas.1109176108
26. Casson CN, Yu J, Reyes VM, Taschuk FO, Yadav A, Copenhaver AM, et al. Human Caspase-4 Mediates Noncanonical Inflammasome Activation Against Gram-Negative Bacterial Pathogens. *Proc Natl Acad Sci U S A* (2015) 112:6688–93. doi: 10.1073/pnas.1421699112
27. Shrum B, Anantha RV, Xu SX, Donnelly M, Haeryfar SM, McCormick JK, et al. A Robust Scoring System to Evaluate Sepsis Severity in an Animal Model. *BMC Res Notes* (2014) 7:1–11. doi: 10.1186/1756-0500-7-233
28. Hara H, Seregin SS, Yang D, Fukase K, Chamillard M, Alnemri ES, et al. The NLRP6 Inflammasome Recognizes Lipoteichoic Acid and Regulates Gram-Positive Pathogen Infection. *Cell* (2018) 175:1651–1664 e1614. doi: 10.1016/j.cell.2018.09.047
29. Chella Krishnan K, Mukundan S, Alagarsamy J, Hur J, Nookala S, Siemens N, et al. Genetic Architecture of Group A Streptococcal Necrotizing Soft Tissue Infections in the Mouse. *PLoS Pathog* (2016) 12:e1005732. doi: 10.1371/journal.ppat.1005732
30. Wang J, Shao Y, Wang W, Li S, Xin N, Xie F, et al. Caspase-11 Deficiency Impairs Neutrophil Recruitment and Bacterial Clearance in the Early Stage of Pulmonary Klebsiella Pneumoniae Infection. *Int J Med Microbiol* (2017) 307:490–6. doi: 10.1016/j.ijmm.2017.09.012
31. Aachoui Y, Leaf IA, Hagar JA, Fontana MF, Campos CG, Zak DE, et al. Caspase-11 Protects Against Bacteria That Escape the Vacuole. *Science* (2013) 339:975–8. doi: 10.1126/science.1230751
32. Broz P, Ruby T, Belhocine K, Bouley DM, Kayagaki N, Dixit VM, et al. Caspase-11 Increases Susceptibility to Salmonella Infection in the Absence of Caspase-1. *Nature* (2012) 490:288–91. doi: 10.1038/nature11419
33. Krause K, Daily K, Estfanous S, Hamilton K, Badr A, Abu Khweek A, et al. Caspase-11 Counteracts Mitochondrial ROS-Mediated Clearance of Staphylococcus Aureus in Macrophages. *EMBO Rep* (2019) 20:e48109. doi: 10.15252/embr.201948109
34. Kovacs SB, Oh C, Maltez VI, McGlaughon BD, Verma A, Miao EA, et al. Neutrophil Caspase-11 Is Essential to Defend Against a Cytosol-Invasive Bacterium. *Cell Rep* (2020) 32:107967. doi: 10.1016/j.celrep.2020.107967
35. Cerqueira DM, Gomes MTR, Silva ALN, Rungue M, Assis NRG, Guimarães ES, et al. Guanylate-Binding Protein 5 Licenses Caspase-11 for Gasdermin-D Mediated Host Resistance to Brucella Abortus Infection. *PLoS Pathog* (2018) 14:e1007519. doi: 10.1371/journal.ppat.1007519
36. Wang K, Sun Q, Zhong X, Zeng M, Zeng H, Shi X, et al. Structural Mechanism for GSDMD Targeting by Autoprocessed Caspases in Pyroptosis. *Cell* (2020) 180:941–955 e920. doi: 10.1016/j.cell.2020.02.002
37. Mandal P, Feng Y, Lyons JD, Berger SB, Otani S, DeLaney A, et al. Caspase-8 Collaborates With Caspase-11 to Drive Tissue Damage and Execution of Endotoxic Shock. *Immunity* (2018) 49:42–55 e46. doi: 10.1016/j.immuni.2018.06.011
38. Antonopoulos C, Russo HM, El Sanadi C, Martin BN, Li X, Kaiser WJ, et al. Caspase-8 as an Effector and Regulator of NLRP3 Inflammasome Signaling. *J Biol Chem* (2015) 290:20167–84. doi: 10.1074/jbc.M115.652321

39. Santos JC, Dick MS, Lagrange B, Degrandi D, Pfeffer K, Yamamoto M, et al. LPS Targets Host Guanylate-Binding Proteins to the Bacterial Outer Membrane for non-Canonical Inflammasome Activation. *EMBO J* (2018) 37:e98089. doi: 10.15252/embj.201798089
40. Lagrange B, Benaoudia S, Wallet P, Magnotti F, Provost A, Michal F, et al. Human Caspase-4 Detects Tetra-Acylated LPS and Cytosolic Francisella and Functions Differently From Murine Caspase-11. *Nat Commun* (2018) 9:242. doi: 10.1038/s41467-017-02682-y
41. Huang da W, Sherman BT, Lempicki RA. Systematic and Integrative Analysis of Large Gene Lists Using DAVID Bioinformatics Resources. *Nat Protoc* (2009) 4:44–57. doi: 10.1038/nprot.2008.211
42. Durfee LA, Huibregtse JM. Identification and Validation of ISG15 Target Proteins. *Subcell Biochem* (2010) 54:228–37. doi: 10.1007/978-1-4419-6676-6_18
43. Pletneva LM, Haller O, Porter DD, Prince GA, Blanco JCG. Induction of Type I Interferons and Interferon-Inducible Mx Genes During Respiratory Syncytial Virus Infection and Reinfection in Cotton Rats. *J Gen Virol* (2008) 89:261–70. doi: 10.1099/vir.0.83294-0
44. Varela M, Diaz-Rosales P, Pereiro P, Forn-Cuni G, Costa MM, Dios S, et al. Interferon-Induced Genes of the Expanded IFIT Family Show Conserved Antiviral Activities in non-Mammalian Species. *PLoS One* (2014) 9:e100015. doi: 10.1371/journal.pone.0100015
45. Tirumurugan KG, Pawar RM, Dhinakar Raj G, Thangavelu A, Hammond JA, Parida S. RNAseq Reveals the Contribution of Interferon Stimulated Genes to the Increased Host Defense and Decreased PPR Viral Replication in Cattle. *Viruses* (2020) 12:463. doi: 10.3390/v12040463
46. Hojyo S, Fukada T. Roles of Zinc Signaling in the Immune System. *J Immunol Res* (2016) 2016:6762343. doi: 10.1155/2016/6762343
47. Maret W. Metals on the Move: Zinc Ions in Cellular Regulation and in the Coordination Dynamics of Zinc Proteins. *BioMetals* (2011) 24:411–8. doi: 10.1007/s10534-010-9406-1
48. Brieger A, Rink L, Haase H. Differential Regulation of TLR-Dependent MyD88 and TRIF Signaling Pathways by Free Zinc Ions. *J Immunol* (2013) 191:1808–17. doi: 10.1049/jimmunol.1301261
49. Zaslon Z, Flis E, Wilk MM, Carroll RG, Palsson-McDermott EM, Hughes MM, et al. Caspase-11 Promotes Allergic Airway Inflammation. *Nat Commun* (2020) 11:1055. doi: 10.1038/s41467-020-14945-2
50. Finethy R, Dockerman J, Kutsch M, Orench-Rivera N, Wallace GD, Piro AS, et al. Dynamin-Related Irgm Proteins Modulate LPS-Induced Caspase-11 Activation and Septic Shock. *EMBO Rep* (2020) 21:e50830. doi: 10.15252/embr.202050830
51. Chen R, Zeng L, Zhu S, Liu J, Zeh HJ, Kroemer G, et al. cAMP Metabolism Controls Caspase-11 Inflammasome Activation and Pyroptosis in Sepsis. *Sci Adv* (2019) 5:eav5562. doi: 10.1126/sciadv.aav5562
52. Chu LH, Indramohan M, Ratsimandresy RA, Gangopadhyay A, Morris EP, Monack DM, et al. The Oxidized Phospholipid oxPAPC Protects From Septic Shock by Targeting the non-Canonical Inflammasome in Macrophages. *Nat Commun* (2018) 9:996. doi: 10.1038/s41467-018-03409-3
53. Subramanian Vignesh K, Deepe GS Jr. Metallothioneins: Emerging Modulators in Immunity and Infection. *Int J Mol Sci* (2017) 18:2197. doi: 10.3390/ijms18102197
54. Dalton T, Palmiter RD, Andrews GK. Transcriptional Induction of the Mouse Metallothionein-I Gene in Hydrogen Peroxide-Treated Hepa Cells Involves a Composite Major Late Transcription Factor/Antioxidant Response Element and Metal Response Promoter Elements. *Nucleic Acids Res* (1994) 22:5016–23. doi: 10.1093/nar/22.23.5016
55. Chowdhury D, Deepe GS, Subramanian Vignesh K. The Metallothionein-Zinc Landscape: How It Shapes Antimicrobial Immunity. In: *Zinc Signaling*. Singapore: Springer (2019). p. 57–77.
56. Botella H, Peyron P, Levillain F, Poincloux R, Poquet Y, Brandl I, et al. Mycobacterial P(1)-Type ATPases Mediate Resistance to Zinc Poisoning in Human Macrophages. *Cell Host Microbe* (2011) 10:248–59. doi: 10.1016/j.chom.2011.08.006
57. Palmiter RD, Findley SD, Whitmore TE, Durnam DM. MT-III, a Brain-Specific Member of the Metallothionein Gene Family. *Proc Natl Acad Sci U S A* (1992) 89:6333–7. doi: 10.1073/pnas.89.14.6333
58. Leibbrandt ME, Koropatnick J. Activation of Human Monocytes With Lipopolysaccharide Induces Metallothionein Expression and is Diminished by Zinc. *Toxicol Appl Pharmacol* (1994) 124:72–81. doi: 10.1006/taap.1994.1010
59. Arizono K, Kagawa S, Hamada H, Ariyoshi T. Nitric Oxide Mediated Metallothionein Induction by Lipopolysaccharide. *Res Commun Mol Pathol Pharmacol* (1995) 90:49–58.
60. Coordinators NR. Database Resources of the National Center for Biotechnology Information. *Nucleic Acids Res* (2016) 44:D7–19. doi: 10.1093/nar/gkx1095
61. Stocks CJ, von Pein JB, Curson JEB, Rae J, Phan MD, Foo D, et al. Frontline Science: LPS-Inducible SLC30A1 Drives Human Macrophage-Mediated Zinc Toxicity Against Intracellular Escherichia Coli. *J Leukoc Biol* (2021) 109:287–97. doi: 10.1002/JLB.2HI0420-160R
62. Stocks CJ, Phan MD, Achard MES, Nhu NTK, Condon ND, Gawthorne JA, et al. Uropathogenic Escherichia Coli Employs Both Evasion and Resistance to Subvert Innate Immune-Mediated Zinc Toxicity for Dissemination. *Proc Natl Acad Sci U S A* (2019) 116:6341–50. doi: 10.1073/pnas.1820870116
63. Case CL, Kohler LJ, Lima JB, Strowig T, de Zoete MR, Flavell RA, et al. Caspase-11 Stimulates Rapid Flagellin-Independent Pyroptosis in Response to Legionella Pneumophila. *Proc Natl Acad Sci U S A* (2013) 110:1851–6. doi: 10.1073/pnas.1211521110
64. Akhter A, Caution K, Abu Khweek A, Tazi M, Abdulrahman BA, Abdelaziz DH, et al. Caspase-11 Promotes the Fusion of Phagosomes Harboring Pathogenic Bacteria With Lysosomes by Modulating Actin Polymerization. *Immunity* (2012) 37:35–47. doi: 10.1016/j.immuni.2012.05.001
65. Knodler LA, Crowley SM, Sham HP, Yang H, Wrande M, Ma C, et al. Noncanonical Inflammasome Activation of Caspase-4/Caspase-11 Mediates Epithelial Defenses Against Enteric Bacterial Pathogens. *Cell Host Microbe* (2014) 16:249–56. doi: 10.1016/j.chom.2014.07.002
66. Kobayashi T, Ogawa M, Sanada T, Mimuro H, Kim M, Ashida H, et al. The Shigella OspC3 Effector Inhibits Caspase-4, Antagonizes Inflammatory Cell Death, and Promotes Epithelial Infection. *Cell Host Microbe* (2013) 13:570–83. doi: 10.1016/j.chom.2013.04.012
67. Codo AC, Saraiva AC, Dos Santos LL, Visconde MF, Gales AC, Zamboni DS, et al. Inhibition of Inflammasome Activation by a Clinical Strain of Klebsiella Pneumoniae Impairs Efferocytosis and Leads to Bacterial Dissemination. *Cell Death Dis* (2018) 9:1182. doi: 10.1038/s41419-018-1214-5
68. Krause K, Caution K, Badr A, Hamilton K, Saleh A, Patel K, et al. CASP4/caspase-11 Promotes Autophagosome Formation in Response to Bacterial Infection. *Autophagy* (2018) 14:1928–42. doi: 10.1080/15548627.2018.1491494
69. Mueller NJ, Wilkinson RA, Fishman JA. Listeria Monocytogenes Infection in Caspase-11-Deficient Mice. *Infect Immun* (2002) 70:2657–64. doi: 10.1128/IAI.70.5.2657-2664.2002
70. LaRock CN, Nizet V. Inflammasome/IL-1 β Responses to Streptococcal Pathogens. *Front Immunol* (2015) 6:518. doi: 10.3389/fimmu.2015.00518
71. Hancz D, Westerlund E, Bastiat-Sempe B, Sharma O, Valfridsson C, Meyer L, et al. Inhibition of Inflammasome-Dependent Interleukin 1 β Production by Streptococcal NAD(+) Glycohydrolase: Evidence for Extracellular Activity. *mBio* (2017) 8:e00756–17. doi: 10.1128/mBio.00756-17
72. Valderrama JA, Riestra AM, Gao NJ, LaRock CN, Gupta N, Ali SR, et al. Group A Streptococcal M Protein Activates the NLRP3 Inflammasome. *Nat Microbiol* (2017) 2:1425–34. doi: 10.1038/s41564-017-0005-6
73. Reboldi A, Dang EV, McDonald JG, Liang G, Russell DW, Cyster JG. Inflammation. 25-Hydroxycholesterol Suppresses Interleukin-1-Driven Inflammation Downstream of Type I Interferon. *Science* (2014) 345:679–84. doi: 10.1126/science.1254790
74. Guarda G, Braun M, Staehli F, Tardivel A, Mattmann C, Förster I, et al. Type I Interferon Inhibits Interleukin-1 Production and Inflammasome Activation. *Immunity* (2011) 34:213–23. doi: 10.1016/j.immuni.2011.02.006
75. Sayadi A, Nguyen AT, Bard FA, Bard-Chapeau EA. Zip14 Expression Induced by Lipopolysaccharides in Macrophages Attenuates Inflammatory Response. *Inflamm Res* (2013) 62:133–43. doi: 10.1007/s00011-012-0559-y
76. Wessels I, Maywald M, Rink L. Zinc as a Gatekeeper of Immune Function. *Nutrients* (2017) 9:1286. doi: 10.3390/nu9121286
77. Maywald M, Wessels I, Rink L. Zinc Signals and Immunity. *Int J Mol Sci* (2017) 18:2222. doi: 10.3390/ijms18102222
78. Foster M, Samman S. Zinc and Regulation of Inflammatory Cytokines: Implications for Cardiometabolic Disease. *Nutrients* (2012) 4:676–94. doi: 10.3390/nu4070676
79. Prasad AS, Beck FW, Grabowski SM, Kaplan J, Mathog RH. Zinc Deficiency: Changes in Cytokine Production and T-Cell Subpopulations in Patients With

- Head and Neck Cancer and in Noncancer Subjects. *Proc Assoc Am Physicians* (1997) 109:68–77.
80. Beck FW, Li Y, Bao B, Prasad AS, Sarkar FH. Evidence for Reprogramming Global Gene Expression During Zinc Deficiency in the HUT-78 Cell Line. *Nutrition* (2006) 22:1045–56. doi: 10.1016/j.nut.2006.08.001
 81. Prasad AS. Zinc: Mechanisms of Host Defense. *J Nutr* (2007) 137:1345–9. doi: 10.1093/jn/137.5.1345
 82. Yuan CL, Hu YC. A Transgenic Core Facility's Experience in Genome Editing Revolution. *Adv Exp Med Biol* (2017) 1016:75–90. doi: 10.1007/978-3-319-63904-8_4
 83. Haeussler M, Schönig K, Eckert H, Eschstruth A, Mianné J, Renaud JB, et al. Evaluation of Off-Target and on-Target Scoring Algorithms and Integration Into the Guide RNA Selection Tool CRISPOR. *Genome Biol* (2016) 17:148. doi: 10.1186/s13059-016-1012-2
 84. Ran FA, Hsu PD, Wright J, Agarwala V, Scott DA, Zhang F. Genome Engineering Using the CRISPR-Cas9 System. *Nat Protoc* (2013) 8:2281–308. doi: 10.1038/nprot.2013.143
 85. Chen B, Gilbert LA, Cimini BA, Schnitzbauer J, Zhang W, Li GW, et al. Dynamic Imaging of Genomic Loci in Living Human Cells by an Optimized CRISPR/Cas System. *Cell* (2013) 155:1479–91. doi: 10.1016/j.cell.2013.12.001
 86. Valerius MT, Patterson LT, Witte DP, Potter SS. Microarray Analysis of Novel Cell Lines Representing Two Stages of Metanephric Mesenchyme Differentiation. *Mech Dev* (2002) 112:219–32. doi: 10.1016/S0925-4773(02)00008-4
 87. Wang H, Yang H, Shivalila CS, Dawlaty MM, Cheng AW, Zhang F, et al. One-Step Generation of Mice Carrying Mutations in Multiple Genes by CRISPR/Cas-Mediated Genome Engineering. *Cell* (2013) 153:910–8. doi: 10.1016/j.cell.2013.04.025
 88. Yang H, Wang H, Jaenisch R. Generating Genetically Modified Mice Using CRISPR/Cas-Mediated Genome Engineering. *Nat Protoc* (2014) 9:1956–68. doi: 10.1038/nprot.2014.134
 89. Domenico P, Diedrich DL, Straus DC. Extracellular Polysaccharide Production by *Klebsiella Pneumoniae* and its Relationship to Virulence. *Can J Microbiol* (1985) 31:472–8. doi: 10.1139/m85-088
 90. Wei RQ, Yee JB, Straus DC, Hutson JC. Bactericidal Activity of Testicular Macrophages. *Biol Reprod* (1988) 38:830–5. doi: 10.1095/biolreprod.38.4.830
 91. Chatellier S, Ihendyane N, Kansal RG, Khambaty F, Basma H, Norrby-Teglund A, et al. Genetic Relatedness and Superantigen Expression in Group A Streptococcus Serotype M1 Isolates From Patients With Severe and Nonsevere Invasive Diseases. *Infect Immun* (2000) 68:3523–34. doi: 10.1128/IAI.68.6.3523-3534.2000
 92. Nookala S, Mukundan S, Fife A, Alagarsamy J, Kotb M. Heterogeneity in FoxP3- and GARP/LAP-Expressing T Regulatory Cells in an HLA Class II Transgenic Murine Model of Necrotizing Soft Tissue Infections by Group A Streptococcus. *Infect Immun* (2018) 86:e00432–18. doi: 10.1128/IAI.00432-18

Conflict of Interest: The authors declare that the research was conducted in the absence of any commercial or financial relationships that could be construed as a potential conflict of interest.

Publisher's Note: All claims expressed in this article are solely those of the authors and do not necessarily represent those of their affiliated organizations, or those of the publisher, the editors and the reviewers. Any product that may be evaluated in this article, or claim that may be made by its manufacturer, is not guaranteed or endorsed by the publisher.

Copyright © 2021 Chowdhury, Gardner, Satpati, Nookala, Mukundan, Porollo, Landero Figueroa and Subramanian Vignesh. This is an open-access article distributed under the terms of the Creative Commons Attribution License (CC BY). The use, distribution or reproduction in other forums is permitted, provided the original author(s) and the copyright owner(s) are credited and that the original publication in this journal is cited, in accordance with accepted academic practice. No use, distribution or reproduction is permitted which does not comply with these terms.



***Plasmodium berghei*-Released Factor, *PbTIP*, Modulates the Host Innate Immune Responses**

OPEN ACCESS

Edited by:

Shrikant R. Mulay,
Central Drug Research Institute (CSIR),
India

Reviewed by:

Yunhao Tan,
AbbVie, United States
Surendra Kumar Prajapati,
Henry M. Jackson Foundation for the
Advancement of Military Medicine
(HJF), United States
Hardik Patel,
Seattle Children's Research Institute,
United States

*Correspondence:

Agam Prasad Singh
singhap@nii.ac.in

[†]Present address:

Rajesh Anand,
Department of Biotechnology,
Guru Ghasidas Vishwavidyalaya, Koni,
Bilaspur, India
Afshana Quadiri,
Host-Parasite Biology Lab, National
Institute of Malaria Research, New
Delhi, India
Bijayalaxmi Sahoo,
Department of Biotechnology and
Medical Engineering, National Institute
of Technology, Rourkela, India

Specialty section:

This article was submitted to
Molecular Innate Immunity,
a section of the journal
Frontiers in Immunology

Received: 24 April 2021

Accepted: 01 November 2021

Published: 07 December 2021

Citation:

Kalia I, Anand R, Quadiri A,
Bhattacharya S, Sahoo B and
Singh AP (2021) *Plasmodium berghei*-
Released Factor, *PbTIP*, Modulates
the Host Innate Immune Responses.
Front. Immunol. 12:699887.
doi: 10.3389/fimmu.2021.699887

**Inderjeet Kalia¹, Rajesh Anand^{1†}, Afshana Quadiri^{1†}, Shreya Bhattacharya¹,
Bijayalaxmi Sahoo^{2†} and Agam Prasad Singh^{1*}**

¹ Infectious Diseases Laboratory, National Institute of Immunology, New Delhi, India, ² Department of Biological Sciences and Engineering, Maulana Azad National Institute of Technology, Bhopal, India

The *Plasmodium* parasite has to cross various immunological barriers for successful infection. Parasites have evolved mechanisms to evade host immune responses, which hugely contributes to the successful infection and transmission by parasites. One way in which a parasite evades immune surveillance is by expressing molecular mimics of the host molecules in order to manipulate the host responses. In this study, we report a *Plasmodium berghei* hypothetical protein, *PbTIP* (PbANKA_124360.0), which is a *Plasmodium* homolog of the human T-cell immunomodulatory protein (TIP). The latter possesses immunomodulatory activities and suppressed the host immune responses in a mouse acute graft-versus-host disease (GvHD) model. The *Plasmodium berghei* protein, *PbTIP*, is expressed on the merozoite surface and exported to the host erythrocyte surface upon infection. It is shed in the blood circulation by the activity of an uncharacterized membrane protease(s). The shed *PbTIP* could be detected in the host serum during infection. Our results demonstrate that the shed *PbTIP* exhibits binding on the surface of macrophages and reduces their inflammatory cytokine response while upregulating the anti-inflammatory cytokines such as TGF- β and IL-10. Such manipulated immune responses are observed in the later stage of malaria infection. *PbTIP* induced Th2-type gene transcript changes in macrophages, hinting toward its potential to regulate the host immune responses against the parasite. Therefore, this study highlights the role of a *Plasmodium*-released protein, *PbTIP*, in immune evasion using macrophages, which may represent the critical strategy of the parasite to successfully survive and thrive in its host. This study also indicates the human malaria parasite TIP as a potential diagnostic molecule that could be exploited in lateral flow-based immunochromatographic tests for malaria disease diagnosis.

Keywords: immunomodulation, immune evasion, T cell immunomodulatory protein, malaria, macrophages altered phenotype, M2 macrophages, immune-tolerance

INTRODUCTION

Malaria is a debilitating infectious disease in vertebrates, including humans, and is transmitted through the bites of the *Plasmodium* carrier *Anopheles* mosquitoes. In 2019, approximately 229 million malaria cases were reported, with about 409,000 deaths, and these figures will likely shoot up due to the recent coronavirus outbreak, restricting mosquitoes and parasite control measures (1, 2).

Natural immunity against malaria is crucial to protect the host from the severe form of the disease and anemia (3). Natural immunity develops in a population of a malaria-endemic area by repeated *Plasmodium* exposure for many years through mosquito bites. However, it does not provide sterile protection against the disease; also, it is short lived and fades away quickly (3, 4). Immune responses against blood-stage parasites are complex and possibly initiated when parasite-derived glycosylphosphatidylinositol (GPI), DNA, and metabolic products (e.g., hemozoin and uric acid) are released during the blood stage of malaria infection (5–8). These parasite-derived products are sensed by Toll-like receptors (TLRs) and nucleotide-binding oligomerization domain (NOD)-like receptors containing pyrin domain 3 on dendritic cells (DCs) and macrophages and lead to the activation of CD4⁺ and CD8⁺ T cells, as well as parasite-specific antibodies to contain the blood-stage infection (9–11). However, observational studies have suggested that the human malaria parasite always persists for several weeks or months and that immunity to malaria develops slowly, indicating that the parasite may have developed strategies to suppress the host immune responses in order to thrive in the host (12). Previous studies have suggested that the malaria parasite can inhibit the activation of parasite-specific CD4⁺ T-cell responses by inducing the apoptosis of DCs, downregulating co-stimulatory molecules, and/or suppressing antigen presentation by DCs (13–15). The *Plasmodium* parasite also induces apoptosis and anergy of the activated CD4⁺ T and B cells (16–18). Observational studies in mice and humans have suggested the role of natural regulatory T cells (Tregs) in malaria infection and the presence of increased Tregs during the infection (19, 20). However, the mechanisms of host immune manipulation by the parasite remain poorly understood.

The manipulation of host immune pathways by parasites involving active discharge of molecules, analogous to host cytokines, has recently been reported during malaria infection (21). The *Plasmodium* parasite-released homolog of the mammalian migration inhibitory factor (MIF) induces antigen-experienced CD4⁺ T cells into short-lived effector cells rather than memory cells through binding on its CD74 receptor in DCs and macrophages during blood-stage malaria (22, 23). Such ability of pathogens to circumvent the host defense mechanisms is also evident in bacterial infection and chronic infection of filarial worms and schistosomes (24, 25). In nematodes, immune evasion strategies promote the survival of parasites within the host by altering the activation of the host immune responses during infection. The worm-secreted/excreted products such as serpins, miRNA, and proteases are capable of mimicking host molecules to carry out immune modulation in the host (25, 26). Various reports highlight such ability of the parasites to circumvent the host anti-parasitic responses, and this understanding is critical in designing therapeutic interventions.

Here, we report that the malaria parasite expresses a T-cell immunomodulatory protein (*PbTIP*) on the surface of merozoites that is homologous to human T-cell immunomodulatory protein (TIP). TIP was shown to have a protective role in a mouse model of

graft-versus-host disease (GvHD) by manipulating T-cell responses (27). The *Plasmodium berghei* homolog of TIP, *PbTIP*, is exported on the infected erythrocyte surface upon infection by merozoites. Fragmentation of the surface-expressed *P. berghei* *PbTIP*, likely by protease(s), resulted in its shedding from the red blood cell (RBC) surface into host circulation. Once in circulation, *PbTIP* exhibited binding on host macrophages and reduced the expressions of their inflammatory cytokine genes while upregulating the expressions of the Th2-type/anti-inflammatory cytokine genes. *PbTIP* also helps in parasite growth *in vivo*.

RESULTS

A *Plasmodium* Hypothetical Protein Is Homologous to Human T-Cell Immunomodulatory Protein

BLAST searches of human TIP (Q8TB96) across species showed homology with a hypothetical *Plasmodium falciparum* protein, Q8I3H7, and both proteins shared 29.6% homology along the protein length (28). SMART domain analysis (Simple Modular Architecture Research Tool; <http://smart.embl-heidelberg.de/>) (29) revealed a conserved domain organization in human TIP and Q8I3H7, both containing transmembrane (TM) helices at similar locations. It also revealed the presence of the VCBS domain (pfam13517) (**Figure 1A**), which is found in several copies in long proteins in many species of *Vibrio*, *Colwellia*, *Bradyrhizobium*, and *Shewanella*, hence named VCBS. The suggested role of the VCBS domain is in cellular adhesion (30, 31). Through homology searches, we also found that *P. falciparum* Q8I3H7 is orthologous to an uncharacterized *P. berghei* protein, sharing 71.9% homology (query cover = 92%, *e*-value = 0.0). Human TIP also shares 27.88% homology with this *P. berghei* protein; hence, we called it *PbTIP* (**Figure 1B**). *PbTIP* also shares 28.33% homology with mouse TIP (Q99KW9.2). *P. falciparum* Q8I3H7 is not only an ortholog of *PbTIP*; rather, other orthologs of this protein are present across all *Plasmodium* species. No paralogs of this protein could be found in respective *Plasmodium* species (32).

The adhesion property of human TIP and *PbTIP* is envisaged by the presence of seven FG-GAP repeats, which is characteristic of integrin- α . The FG-GAP repeats also contained a conserved calcium-binding motif (D-x-N/D-x-D-xxx-D), and these repeats were shown to have importance in ligand binding (33, 34) (**Figure 1B**). A putative epidermal growth factor (EGF)-like domain is also present in *PbTIP*, which aligned well with mouse EGF and the EGF-like domain of the *P. berghei* protein, MSP1 (merozoite surface protein 1) (**Figure 1C**). *Plasmodium* proteins containing an EGF-like domain have already been shown to mediate adhesion through this domain. The RGD motif (arginine-glycine-aspartic acid, a tripeptide motif that mediates adhesion in extracellular matrix proteins such as fibronectin, vitronectin, and laminin) in the EGF-like domain also strongly correlates with its role in adhesion (35). The existence of a VCBS domain in *PbTIP* further strengthens

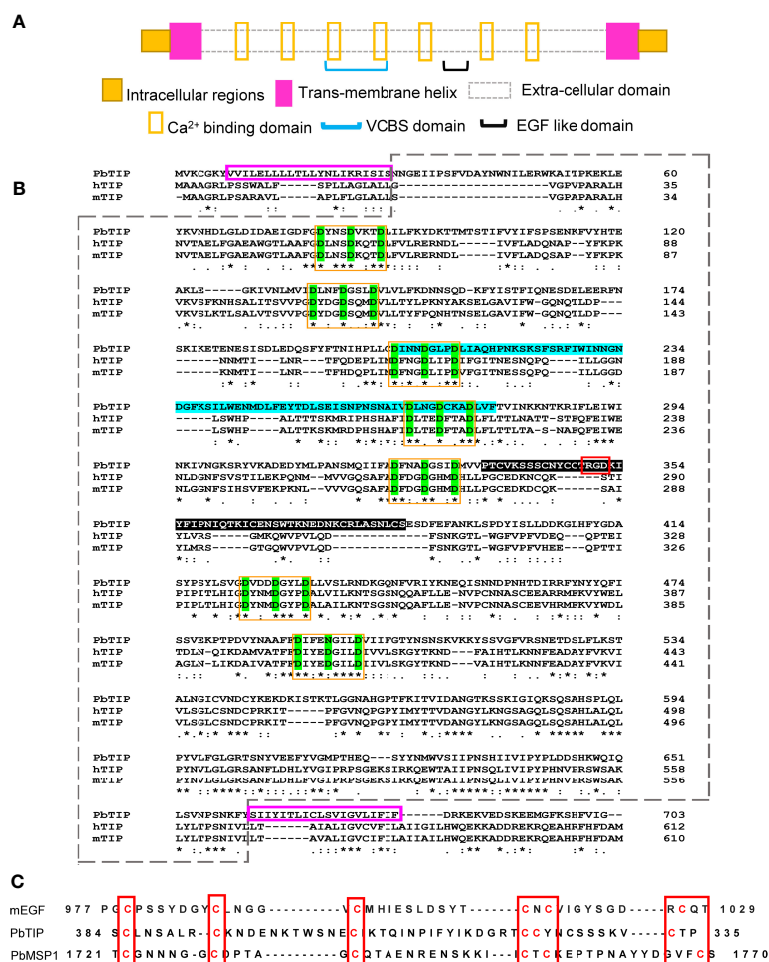


FIGURE 1 | A hypothetical *Plasmodium* protein is homologous to human T-cell immunomodulatory protein (TIP) and is predicted to contain various putative adhesion domains. **(A)** Summary of the various putative domains in the *Plasmodium berghei* TIP. **(B)** The PbANKA_124360.0 encoded protein designated as PbTIP shared 27.88% and 28.33% homology with human TIP and mouse TIP, respectively, along their lengths. PbTIP is predicted to contain two transmembrane (TM) helices [7–29 and 662–681 amino acid (AA) positions, outlined in pink], leaving behind small intracellular stretches at both ends, and most part of the protein is extracellular (enclosed in a dashed box). Seven atypical calcium-binding motifs (yellow boxes) were present at regular intervals in the extracellular part of the PbTIP containing the conserved D-x/N/D-x-D-xxx-D sequence. The VCBS (*Vibrio*, *Colwellia*, *Bradyrhizobium*, and *Shewanella*) domain was also present and encompassed the third and fourth calcium binding motifs (highlighted in blue). “*” indicates perfect alignment. Multiple stars “*”, “***”, “****”, “*****” are repetition of same marking and has same meaning as the single star. “.” indicates a site belonging to a group exhibiting strong similarity. “.” indicates a site belonging to a group exhibiting weak similarity. A putative epidermal growth factor (EGF)-like domains (shaded black) containing the RGD (arginine–glycine–aspartic acid) motif was also present between the fifth and sixth calcium-binding motifs. **(C)** The PbTIP putative EGF-like domain aligns well with the mouse EGF and MSP1 of *P. berghei*, and these domains are well known to play an adhesion role in many *Plasmodium* proteins. The RGD motif further strengthens its role in adhesion.

its role in adhesion as the VCBS domain is implicated in cellular surface binding, as reported in various bacteria (30) (Figure 1B and Supplementary Figure S1). All the predicted domains of PbTIP are summarized in Figure 1A.

PbTIP Localizes to the Surface of Infected Erythrocytes

TMHMM 2.0 (the transmembrane helix prediction tool; <http://www.cbs.dtu.dk/services/TMHMM/>) (36) analysis of the *P. berghei* TIP (PbANKA_124360.0) amino acid sequence revealed the presence of two TM helices, one at each terminus (Figure 2A). Moreover,

Parker's hydrophilicity tool also predicted two hydrophobic stretches in PbTIP that correspond to two predicted TM helices at both termini (Figure 2B). The intervening part of the protein between two TM regions is likely extracellular and represents the ectodomain part of the protein (Figure 1B, dashed box).

Bacterially expressed recombinant PbTIP was used for mouse and rat immunizations in order to raise immune sera against the protein. Immune serum was used to localize PbTIP in the parasite by performing immunofluorescence assays (IFAs). Our results suggest that PbTIP was expressed on the surface of merozoites. Immunostaining images demonstrated that the

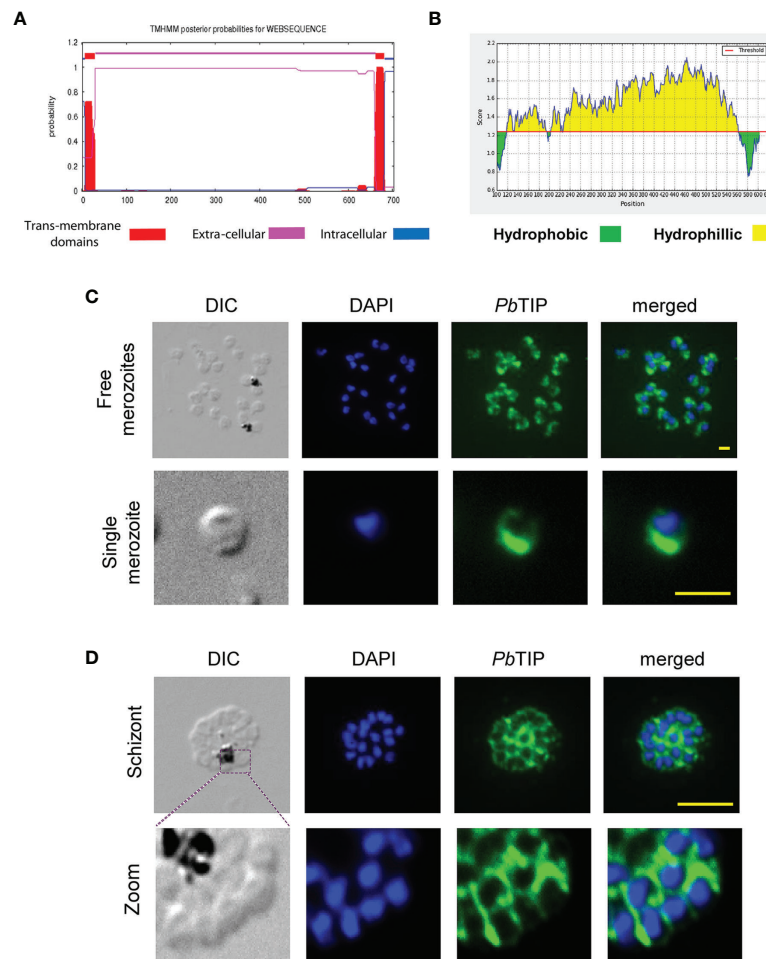


FIGURE 2 | The *Plasmodium berghei* T-cell immunomodulatory protein (*PbTIP*) is likely a membrane-anchored protein of merozoites. **(A)** The TMHMM server 2.0 predicts the presence of two transmembrane (TM) regions at both termini of this protein, while the intervening part between these TM helices is predicted as extracellular, suggesting that *PbTIP* could be an extracellular membrane-anchored protein. **(B)** Parker's hydrophilicity prediction showing two hydrophobic regions (green) at both termini corresponding to the TM helices, while the hydrophilic region (yellow) represents the extracellular part of the protein (window size = 200 amino acids, threshold = 1.243, center position = 100). **(C)** *PbTIP* localization on the surface of *Plasmodium* merozoites as revealed by immunostaining against the target protein of formaldehyde-fixed free merozoites. The protein is abundant at one end of merozoites. Scale bar, 1 μ m. **(D)** *PbTIP* immunolocalization on the surface of mature schizont and around the merozoites packed within it. Scale bar, 10 μ m.

protein localized to the merozoite surface, similar to MSP1, which is a known merozoite surface protein. Although its surface expression was not uniform like MSP1, it was abundant at the one end of merozoites (**Figure 2C** and **Supplementary Figure S2**). *PbTIP* was also expressed in packed merozoites inside a schizont as a surface protein, clearly marking boundaries (**Figure 2D**).

Immunostaining of parasitized blood smear upon its permeabilization revealed that *PbTIP* was localized to the parasitophorous vacuolar (PV) membrane and within the infected erythrocyte cytosol. *PbTIP* was exported from the parasite into the host cell cytoplasm and surface, as exhibited by the immunostaining assay (**Figures 3A, B**). Intra-erythrocytic staining revealed the punctate pattern of *PbTIP* in the ring and trophozoite stages of *P. berghei*. *PbTIP* was also expressed in the

gametocyte stage, and its expression was much higher in gametocytes compared to that in the asexual blood stages of *P. berghei* (**Figure 3A**, bottom panel).

When immunostaining was performed on a non-permeabilized infected blood smear, it showed *PbTIP* expression on the surface of infected RBCs. The co-localization of band 3 (a RBC membrane marker) and *PbTIP* indicated that this protein decorated the surface of infected host cells (**Figure 3B**). To be localized on the surface of erythrocytes, *PbTIP* would have been exported across parasite confinement within the cell. The protein traversed the PV membrane and the host cytoplasm in order to reach the surface (**Supplementary Figure S3**). However, the amino acid sequence of *PbTIP* did not show any identifiable *Plasmodium* export element (PEXEL) motif to facilitate its export, suggesting that it may be a PEXEL-negative exported protein (PNEP) (37).

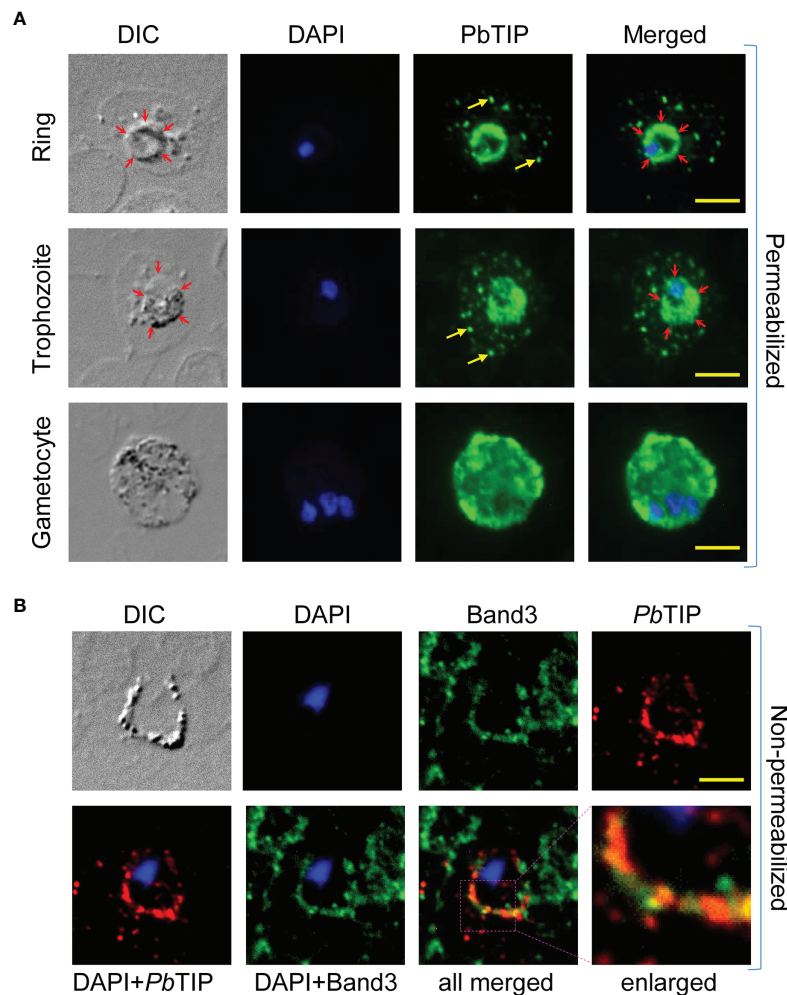


FIGURE 3 | *Plasmodium berghei* T-cell immunomodulatory protein (*PbTIP*) was exported across the parasitophorous vascular membrane (PVM) and into the infected surface of host erythrocytes. **(A)** Immunostaining of permeabilized *P. berghei* blood stages with antibodies (polyclonal sera) against the target protein revealed *PbTIP* expression in its various forms. Intra-erythrocytic *PbTIP* staining revealed its presence in the cytoplasm of host cell. Yellow arrows represent the *PbTIP* in the cytosol of host cell in a punctate pattern. To demonstrate the export here, PVM is marked with red arrows (DIC panels) and the presence of *PbTIP* beyond the PVM marked as the exported protein. Moreover, EXP1 (a known parasite PVM protein) and *PbTIP* co-staining clearly demonstrated its export across the PVM in infected red blood cells (RBCs) (**Supplementary Figure S3**). *PbTIP* is also localized to the PVM in the ring and trophozoite stages. *PbTIP* expression in mature gametocytes was much higher compared to that in the ring and trophozoite stages. Permeabilization of blood smears was performed with 0.2% saponin, as described in *Materials and Methods*. **(B)** The export of *PbTIP* into the surface of infected RBCs was demonstrated by performing immunostaining on non-permeabilized cells. *PbTIP* (red fluorescence) can be seen clearly displayed on the infected surface of RBCs as a ring that co-localizes with band 3 (green fluorescence), which is one of the most abundant membrane proteins of erythrocytes. Band 3 antibodies were used to mark the surface of erythrocytes. This representative image was taken from more than 50 similar images. DAPI staining was used to locate the nucleus of the parasite. Scale bar, 5 μ m.

***PbTIP* Is Processed and Shed From the RBC Surface**

Immunostaining of parasitized red blood cells demonstrated the occurrence of *PbTIP* in the cell surroundings, indicating that it is probably shed from the infected RBC surface. A mature schizont and gametocyte shedding of this protein are shown in **Figure 4A**. MSP1 (a merozoite surface protein) did not exhibit protein shedding, indicating that only some surface proteins were shed, which included *PbTIP* (**Supplementary Figure S4**). However, the mechanism of this shedding is unknown, and it is possibly

executed by the cleavage of the membrane-anchored *PbTIP* by proteases similar to rhomboid protease (38, 39). The shedding of *PbTIP* into host circulation is likely executed by its fragmentation, as multiple fragments of protein were detected in the parasite blood-stage lysate when subjected to electrophoresis and Western blotting. Uncleaved *PbTIP* was detected at ~77 kDa, while multiple fragments of it were detected at various sizes, viz. ~70, ~50, and ~25 kDa (**Figure 4B**). Recombinant *PbTIP* also exhibited cleavage and resulted in protein fragments of similar sizes in *Escherichia coli*

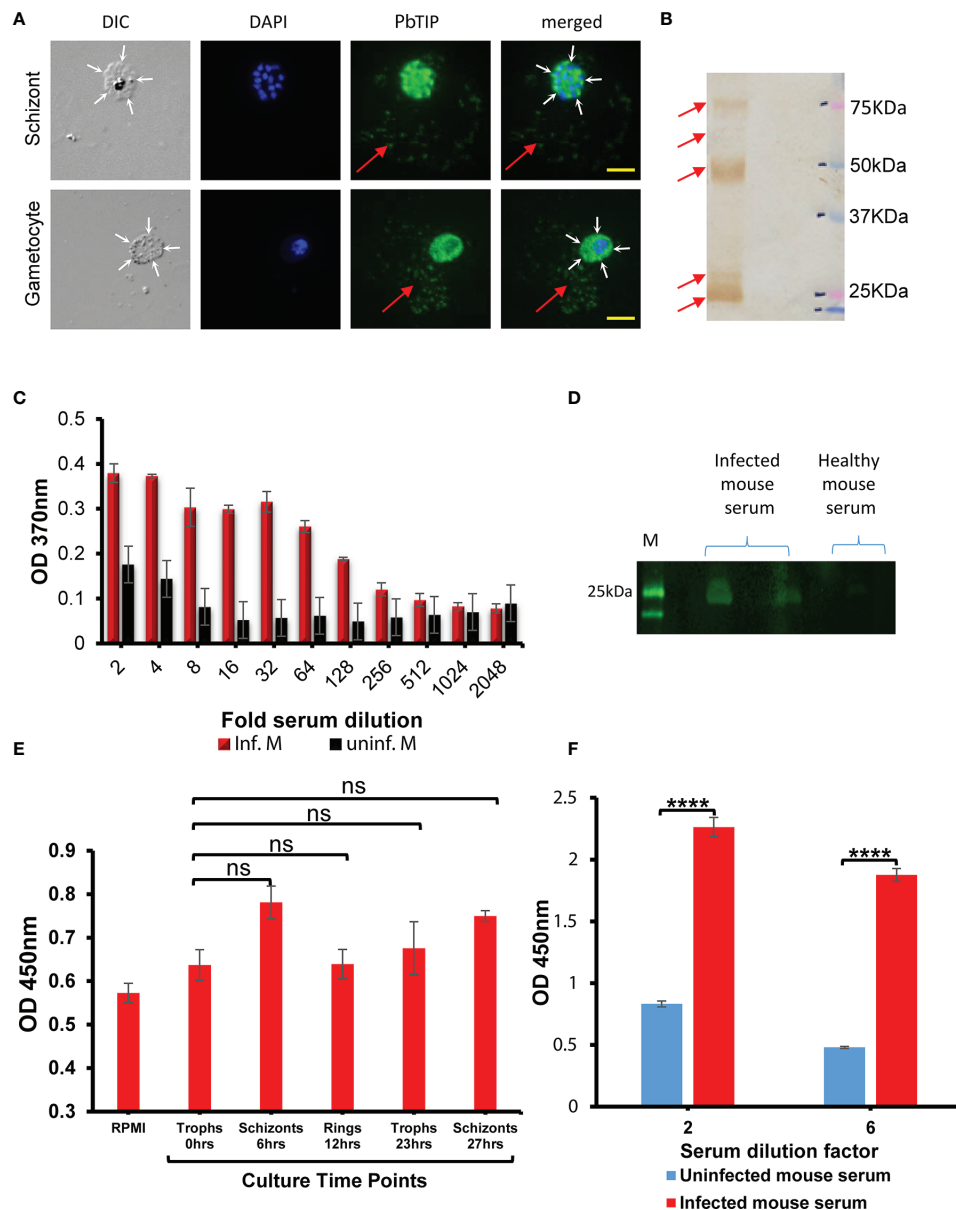


FIGURE 4 | Parasitized erythrocyte surface-exported *Plasmodium berghei* T-cell immunomodulatory protein (*PbTIP*) cleavage likely caused the shedding of this protein into host circulation. **(A)** Immunostaining of various forms of blood-stage parasites showed *PbTIP* staining in their immediate surroundings. Immunostaining of the schizont and gametocyte stages showed shed *PbTIP* in their surroundings. Red arrow represents the shed *PbTIP* in the surroundings of these parasitic forms. The boundaries of infected host cells are marked with white arrows. These representative images were taken from more than 30 similar microscopy images. Scale bar, 10 μm. **(B)** Probing with anti-*PbTIP* antibodies in the blood-stage parasite lysate revealed the fragmentation of *PbTIP* into multiple smaller fragments. This fragmentation, by an uncharacterized process, is likely responsible for the shedding of the protein from the surface of erythrocytes. Full-length *PbTIP* was observed at ~75 kDa, and its two major fragments were observed at ~50 and ~25 kDa. **(C)** Shed *PbTIP* was detected in the infected host blood sera using sandwich ELISA, with healthy mouse sera as a negative control (black bars). *PbTIP* could be detected in the host circulation up to 128-fold dilution of the blood sera (red bars). Error bars represent the standard deviation of the mean absorption at 370 nm optical density (OD). The data presented are from three replicates performed. **(D)** Fragments of shed *PbTIP* (~25–30 kDa) detected by Western blotting of infected mouse serum, with healthy mouse serum as a negative control. **(E)** Detection of the released *PbTIP* in the *P. berghei* culture medium harvested at various time points. Parasite culture was set from infected mouse blood containing mostly trophozoite stages, and the spent culture medium was harvested at various time points as described in the figure and sandwich ELISA performed as described in the *Materials and Methods*. In *in vitro* conditions, *PbTIP* shedding was not optimum. Only a non-significant (ns) increase in the shed *PbTIP* levels post-schizont bursting (at 6 and 27 h) was observed. Fresh culture medium, RPMI, was used as the negative control in the ELISA. Schizont bursting was ascertained by Giemsa staining of a cultured schizont smear. **(F)** For comparison purposes, we detected shed *PbTIP* in infected mouse serum again using sandwich ELISA and observed that shedding was significantly higher in *in vivo* conditions ($p = 0.00014$ and 4.39×10^{-5} , respectively). The x-axis represents the dilution of serum used in the ELISA, i.e., at 1:2 and 1:6 ratios. Uninfected mouse serum was used as the negative control in ELISA. The mice used for both studies had identical parasitemia. **** denotes the P value less than 0.00005 to 0.00001 and ns means not significant.

(**Supplementary Figure S5A**), and *PbTIP* cleavage was not due to a proteolytic cleavage during the purification process. However, the mechanism of *PbTIP* cleavage and the protease(s) involved are still unknown. Protein sequencing of one of the major *E. coli*-expressed *PbTIP* fragments (~55 kDa) pointed at the presence of one of the cleavage sites near its N-terminus (**Supplementary Figure S6** and **Table S1**).

Shed *PbTIP* was also detected in the serum collected from malaria-infected mouse with indirect sandwich ELISA using antibodies against this protein. We detected *PbTIP* even up to a 128-fold dilution of the infected mouse serum (**Figure 4C**). Serum from uninfected mice was taken as a negative control in the ELISA. Moreover, the infected host sera, when subjected to electrophoresis followed by immunoblotting with antibodies against *PbTIP*, showed ~25- to 30-kDa sized fragments of *PbTIP*, while no band was observed in healthy mouse serum (**Figure 4D**). These bands likely originate from the cleaved fragments of the surface-anchored extracellular domain of the *PbTIP*. To address the critical aspect of *PbTIP* shedding, which is the time of its release, we interrogated by culturing *P. berghei* *in vitro* and collecting the spent medium at various time points in order to detect shed *PbTIP* in it using ELISA. Our results indicated that, in culture conditions, the *PbTIP* level did not significantly change over the entire time course (one complete cycle of growth), suggesting that *PbTIP* shedding is not optimal in the *in vitro* conditions (**Figure 4E**). A non-significant enhancement in shed *PbTIP* in the culture medium was observed during the schizont stage (6 and 27 h post-culture). However, the *in vitro* results significantly differed from our *in vivo* data, where we detected a significant amount of shed *PbTIP* in the serum collected from infected mice (**Figure 4F**), indicating that, somehow, shedding has a comparatively high feasibility *in vivo* than in *in vitro* conditions.

In brief, our results indicated that *PbTIP* shedding is not optimal in culture conditions, while a significant amount of *PbTIP* could be detected in *in vivo* conditions. Our immunostaining images also indicated that schizont rupture events did not contribute significantly to the release of *PbTIP* into the surroundings (**Supplementary Figure S7**).

PbTIP* Binding on Macrophages Downregulate Th1 Cytokines While Inducing Th2 Responsive Genes *In Vitro

The adhesion properties of *PbTIP* in host circulation were evident *in vitro* by incubating recombinant *PbTIP* (10 µg/ml) with murine origin macrophages, RAW 264.7 cells (**Figure 5A**, top panel). This binding is in concordance with various adhesion domains in *PbTIP* (FG-GAP domains, RGD motif, VCBS domain, and EGF-like domain), which may affect binding on host cells (30, 35). *PbTIP* binding on the surface of macrophages was further confirmed by incubating the sera of infected mice containing parasite-shed *PbTIP* with RAW 264.7 cells (**Figure 5A**, middle panel). Parasite blood-stage lysate (obtained by freeze-thaw lysis) containing various fragments of *PbTIP* also displayed binding on macrophages (**Figure 5A**, bottom panel). The binding was further confirmed using mouse peritoneal macrophages that demonstrated the surface

binding of *PbTIP* on macrophages (**Figure 5B**). Pre-immune serum of mice was used in negative controls while performing IFAs.

To study the immunomodulatory effect of *PbTIP* upon its binding to host macrophages, we stimulated RAW 264.7 cells with *E. coli* lipopolysaccharide (LPS) in the presence and absence of recombinant *PbTIP*. LPS is a well-known immune stimulus recognized through TLR4 present on the surface of macrophages leading to the activation of multiple signalling components, such as NF-κB and IRF3, and the subsequent production of Th1-type pro-inflammatory cytokines. In this section, the LPS-elicited immune responses of RAW 264.7 cells are described in the presence and absence of recombinant *PbTIP*. We stimulated RAW 264.7 cells with *E. coli* LPS (100 ng/ml) alone or in combination with recombinant *PbTIP*, and buffer (50 mM Tris, 150 mM NaCl, and 10% glycerol) alone was used as a negative control. LPS stimulation of RAW 264.7 cells for 9 h resulted in increased messenger RNA (mRNA) expression levels of the pro-inflammatory cytokines, which included interleukin 1β (IL-1β), IL-12, interferon gamma (IFN-γ), and tumor necrosis factor alpha (TNF-α). However, the levels of pro-inflammatory cytokines were reduced significantly when RAW 264.7 cells were treated with a combination of LPS and *PbTIP* (10 µg/ml). The expression levels of cytokines were validated with quantitative PCR (qPCR) (performed in triplicate) at the transcript level, and the C_t values obtained were analyzed to calculate the relative fold change using the $2^{-\Delta\Delta C_t}$ method. The transcript levels of IL-1β, TNF-α, IFN-γ, and IL-12p40 were reduced by 6-, 15-, 2.6-, and 3-fold, respectively (**Figure 5C**).

Furthermore, the stimulation of RAW 264.7 cells in a similar fashion for a longer duration, i.e., 20 h (40), resulted in the upregulation of Th2-type/anti-inflammatory cytokine transcripts while suppressing the inflammatory cytokine transcripts. The mRNA expression levels of TGF-β and IL-10 were upregulated by five and ninefold, respectively (**Figure 5D**). The cytokine transcript levels were validated by qPCR and analyzed in a similar manner (as in **Figure 5C**) to calculate the relative fold change. Details of the primers and their references are provided in **Supplementary Table S2**.

Furthermore, cytokines were also estimated in the cell culture medium (spent medium) of the LPS-elicited RAW 264.7 cells in the presence and absence of recombinant *PbTIP* at respective time points through ELISA. Our results indicated that the expressions of the pro-inflammatory cytokines were suppressed significantly while those of the anti-inflammatory cytokines were found significantly upregulated in the study, conveying the same notion of immunosuppression and inducing Th2 responses in macrophages upon exposure to *PbTIP* (**Supplementary Figure S8**).

PbTIP* Accelerates Parasite Growth While Inducing Key Immunosuppressive Genes *In Vivo

The *in vivo* effect of recombinant *PbTIP* on parasite growth was established by injecting this protein (2 mg/kg, day 1 onwards). The experimental design, number of doses, and the amount injected were all similar to those published by Fiscella et al. (27).

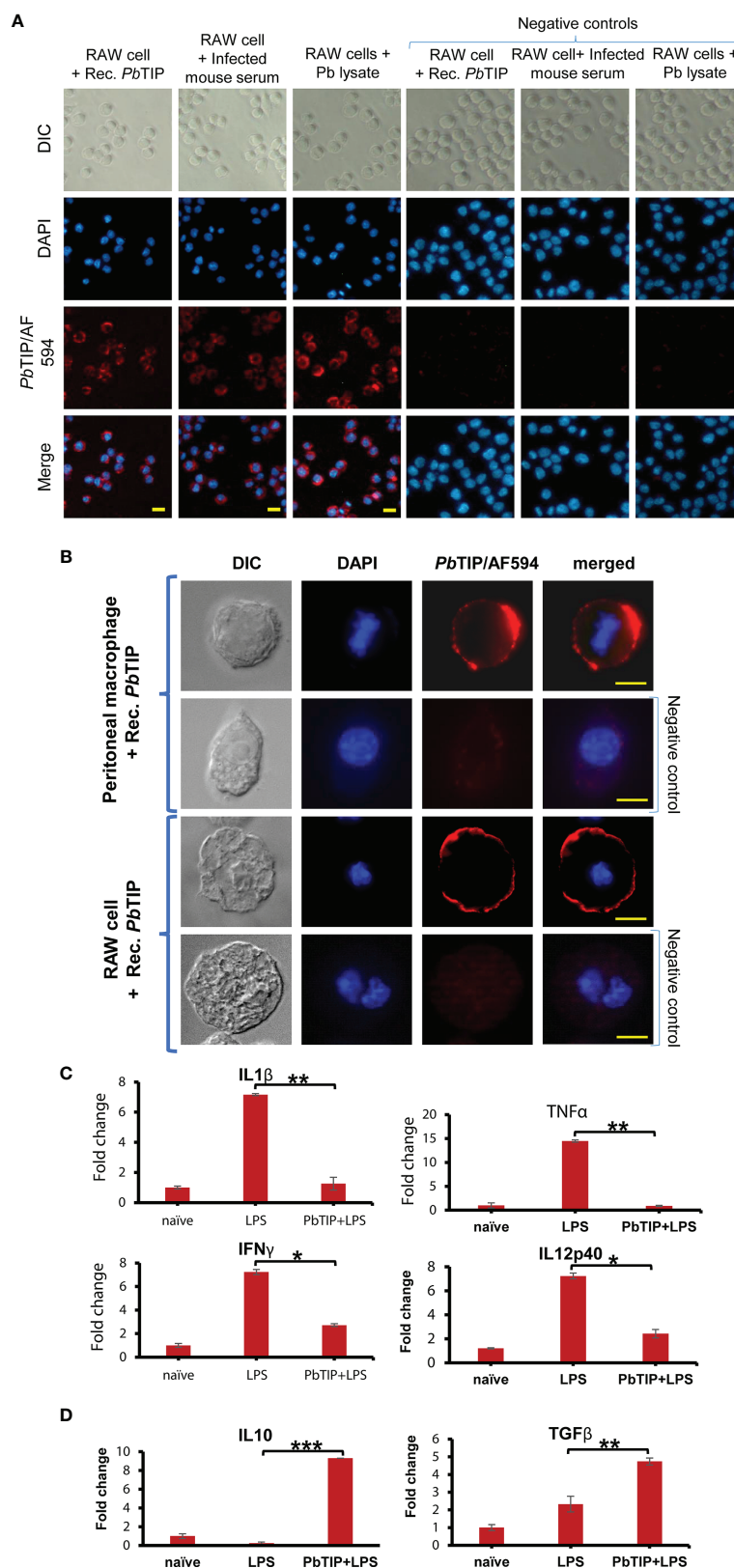


FIGURE 5 | Continued

FIGURE 5 | Shed *Plasmodium berghei* T-cell immunomodulatory protein (*PbTIP*) in host circulation exhibited binding on macrophages and reduced their inflammatory responses while upregulating the Th2-type/anti-inflammatory responses *in vitro*. **(A)** Brief incubation of recombinant *PbTIP* (10 µg/ml) with RAW 264.7 cells followed by immunostaining against the protein revealed its binding on the cell surface (*top left panels*). The shed *PbTIP* in malaria-infected mouse serum also displayed binding on RAW 264.7 cells *in vitro* (*middle left panel*). No binding on RAW 264.7 cells was observed with healthy mouse serum (*right control panel*). Parasite blood-stage lysate (obtained from parasite free-thaw lysis) containing various fragments of *PbTIP* also exhibited binding on RAW 264.7 cells (*bottom left panel*). Images were taken at $\times 200$ magnification on a Zeiss Axio imager M2 microscope. DAPI was used to stain the nuclei of cells. *Scale bar*, 10 µm. **(B)** Recombinant *PbTIP* binding upon incubation with murine peritoneal macrophages and RAW 264.7 cells. Images were taken at a higher magnification to unveil surface binding of *PbTIP*. *Scale bar*, 10 µm (*top panel*) and 5 µm. Glutathione S-transferase (GST) protein was used as a negative control for binding. **(C)** *PbTIP* surface binding reduced the ability of macrophages to mount inflammatory responses upon lipopolysaccharide (LPS) stimulation: (i) IL-1 β was reduced by sixfold; (ii) TNF- α was reduced by 15-fold; (iii) IFN- γ was reduced by 2.6-fold; (iv) IL-12p40 was reduced by threefold. **(D)** The levels of anti-inflammatory cytokines such as TGF- β and IL-10, however, increased by five and ninefold, respectively, with longer exposure to *PbTIP* (20 h). The experiment was repeated more than three times, and C_t values obtained from quantitative PCR (qPCR) were used to calculate the relative fold change using the $2^{-\Delta\Delta C_t}$ method. Statistical significance values (p -values) of the transcript fold change between the LPS-stimulated and LPS+*PbTIP* RAW 264.7 cells were given for various cytokine genes: for IL-1 β , TNF- α , IFN- γ , and IL12p40, 0.0032, 0.008, 0.01, and 0.04, respectively. For the anti-inflammatory cytokines, such as IL-10 and TGF- β , the p -values were 0.0002 and 0.004, respectively. Student's t -test was performed to calculate the statistical significance of the data. *, ** and *** signifies p values in the range of 0.05 to 0.01, 0.005 to 0.001 and 0.0005 to 0.0001, respectively.

Mice ($n = 8$ per group) were infected with 2×10^5 *P. berghei*-infected RBCs given intravenously on day 2. After four consecutive daily doses of recombinant *PbTIP*, we observed accelerated parasite growth in treated mice when compared with the control group (**Figure 6A** (ii)). Parasitemia was determined by staining thin blood smears with Giemsa stain and counting the parasites per 100 RBCs using a light microscope. At least 2,000 RBCs were counted for each slide. On day 5, the parasitemia in the treated group was almost twofold higher than that in the control group. Moreover, recombinant *PbTIP*-injected mice died 1 day earlier, as shown in **Figure 6A** (iii).

The immunosuppressive effects of *PbTIP*, as evident *in vitro* on host macrophages (**Figures 5C, D**), was further explored *in vivo*. The systemic effect of *PbTIP* on various host responses was studied by treating healthy C57BL/6 mice with recombinant *PbTIP* (2 mg/kg) for four consecutive days, followed by peripheral blood mononuclear cell (PBMC) isolation and transcriptome analysis. Glutathione S-transferase (GST) protein-injected mice were taken as control. Next-generation sequencing (NGS) data analysis revealed 51 upregulated and 3 downregulated genes (**Supplementary Table S3**).

Many of the differentially expressed genes have direct relevance to this study, and some of them are described here (**Figure 6B** (ii) and **Supplementary Figure S9**). Upon *PbTIP* exposure, *Arl5b*, which is a negative regulator of MDA5-dependent immune response, was upregulated, and its overexpression repressed the MDA5-induced activation of the interferon- β promoter (41). The B- and T-lymphocyte attenuator (BTLA) was another upregulated gene upon *PbTIP* exposure, which behaved like PD1 and CTLA-4. BTLA displayed T-cell inhibition and was also a negative regulator of B-cell proliferation (42). Upregulation of ATM (serine-threonine kinase) in immune cells may cause apoptosis of monocytes. *Atrx* and *Caprin2* were also upregulated and reported to be linked with apoptotic pathways (43, 44). Genes such as *Cacna1e* and *FLT1* were also significantly upregulated under cancerous conditions, and evidence suggests that these genes could be crucial factors for the macrophage M2 phenotype in the tumor microenvironment (45, 46). Such macrophages display skewed immune responses toward M2-type/anti-inflammatory response. Conversely, *Ece1*, involved in

the proteolytic processing of endothelin 1 peptide and produced by the macrophages in response to microbial stimulation, was downregulated. Another downregulated gene, *Arhgap22* (a rho GTPase), has been reported essential in lamellipodia formation in macrophages, and its downregulation may affect the migration of macrophages upon *PbTIP* exposure (47). A few of the differentially regulated genes selected based on transcriptome data were validated by qPCR (**Supplementary Figure S10**). The qPCR results concur with the transcriptome data. Primer details are provided in **Supplementary Table S2**.

DISCUSSION

The real success of parasites in their host is majorly attributed to their ability to subvert the anti-parasitic host immune responses (48). In higher vertebrates, the immune system has evolved to recognize a vast array of foreign invaders in order to facilitate their elimination (49). On the other hand, pathogens have developed various immunomodulation strategies to effectively manipulate host responses and thrive successfully in their host (12, 25). For example, mouse malaria is characterized by the production of pro-inflammatory cytokines in the early phase of the infection and a reduced cytokine response in the face of continuing infection. Dendritic cells has also become less responsive to TLR-mediated IL-12 and TNF- α production while enhancing their ability to produce the immunosuppressive cytokine IL-10 (14). During the later stages of malaria infection, host immunity becomes refractory not only to *Plasmodium* antigens but also to unrelated antigens (50). Immunomodulation by host molecular mimics has been reported during viral infections and is crucial during *Plasmodium* infection (51). *Plasmodium*-released host-like molecules, such as PMIF (*Plasmodium* macrophage migration inhibitory factor) and TCTP (translationally controlled tumor protein homolog of host histamine-releasing factor), have already been proven to manipulate the host immune responses for the benefit of the parasite (22, 52).

In the search of parasite molecules homologous to their host, we came across a T-cell immunomodulatory protein (TIP) that is conserved in *Plasmodium* species and shares homology with human TIP in its topology and domain structures (28). The

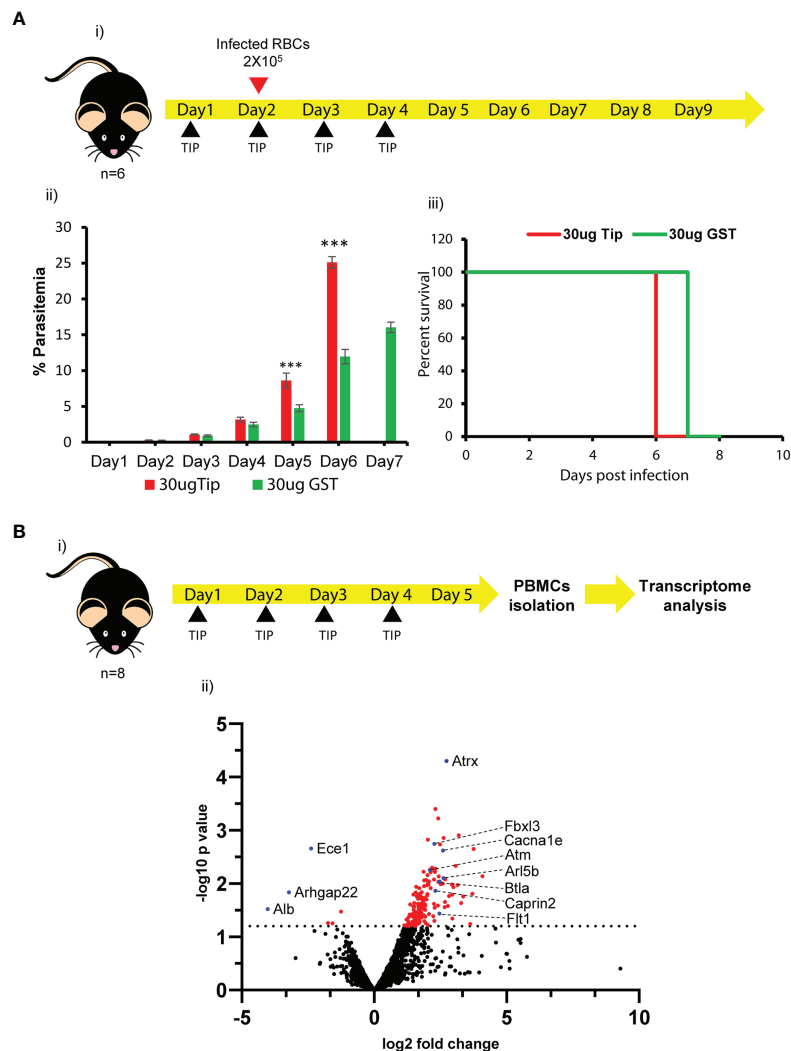


FIGURE 6 | Recombinant *Plasmodium berghei* T-cell immunomodulatory protein (*PbTIP*) treatment caused accelerated parasite growth in mice and systemic effect on host immune cells. **(A)** (i) Experimental workflow showing treatment of mice with recombinant *PbTIP* to study its effect on parasite growth. The recombinant *P. berghei* protein was intraperitoneally injected (2 mg/kg) into C57BL/6J mice ($n = 8$) for four consecutive days. Infection was initiated on day 2 and daily parasitemia was followed post-infection. (ii) Injection of recombinant *PbTIP* in malaria-infected mice accelerated parasite growth, as estimated by monitoring daily parasitemia. On day 6 post-infection, parasitemia was approximately twofold higher in *PbTIP*-treated mice. Glutathione S-transferase (GST) protein-injected mice were taken as the control since recombinant *TIP* has a GST fusion partner. The experiment was repeated more than three times. Student's *t*-test was performed to evaluate the significance of the data (the *p*-values on days 3, 4, 5, and 6 were 0.038, 0.01, 0.0003, and 2.91×10^{-8} , respectively, suggesting significant differences in parasitemia between the two groups). (iii) Recombinant *PbTIP*-treated mice also showed early death compared to control-treated mice. However, it was not found to be statistically significant using the log-rank test ($p > 0.05$). **(B)** (i) Systemic effect of *PbTIP* on host responses was studied by treating C57BL/6J mice with recombinant *PbTIP* (2 mg/kg) for four consecutive days, followed by peripheral blood mononuclear cell (PBMC) isolation and transcriptome analysis. (ii) Volcano plot displaying the differentially expressed genes revealed in the transcriptome analysis, and the genes that may have direct relevance in our study are highlighted as blue dots. Various upregulated genes upon *PbTIP* exposure are reported to be negative regulators of immune responses (*Arl5B*, *BTLA*, and *Fbxl3*), mediators of apoptosis (*ATM*, *Atrx*, and *Caprin2*), and induced in cancerous conditions (*Cacna1e* and *Fli1*). Of the downregulated genes, *Arhgap22* may affect the migration of macrophages upon *PbTIP* exposure. GST protein-treated mouse PBMCs were used as the control in the transcriptome analysis. Black dots represent genes that were not significantly changed in the study ($-\log_{10} p < 1.2$), while red dots represent the significantly upregulated/downregulated genes ($-\log_{10} p > 1.2$). The dashed line denotes the cutoff mark for the significance level ($-\log_{10} p = 1.2$). We used unpaired *t*-tests assuming unequal variances to calculate the significance values of the genes in the study. *** means p value < 0.0004.

presence of seven loosely conserved FG-GAP domains, including the conserved Ca^{2+} -binding motifs such as integrins of metazoans, suggests its role in adhesion. Reports suggested that these seven FG-GAP domains may fold into a seven-bladed beta-propeller structure that serves as its ligand-binding domain.

PbTIP is also conserved in metazoans from placozoa to vertebrates, including humans (53). All its orthologs across the species in *Homo sapiens* (ITFG1/TIP, 612AA), *Mus musculus* (ITFG2, 610AA), *Drosophila melanogaster* (CG7739, 596AA), and *Caenorhabditis elegans* (LNKIN1, 599AA) have similar

domain organization and protein lengths. However, considering the relatively low homology between *Plasmodium* TIP and its natural host's mosquito vector and human, the possibility of a recent horizontal gene transfer seems highly unlikely. It could be an old conserved protein that has undergone gradual changes, yet showing homology across the species. As described earlier, *PbTIP* is conserved among all *Plasmodium* species; however, no paralogs have been reported, contrary to its host homolog integrins that are organized in multigene families with multiple paralogs (54).

Here, we report that *PbTIP* is a surface protein of merozoites in *P. berghei* similar to MSP1; however, its expression was not uniform all over the surface of merozoites. It was localized abundantly at one end of the merozoites. The presence of two putative TM helices at each terminus further strengthens the *PbTIP* membrane localization potential. *PbTIP* was decorated on the surface of infected erythrocytes when merozoites developed into the ring and trophozoite stages. Our data indicated that *PbTIP* was exported across the PV membrane, although it does not contain any recognizable PEXEL motif to facilitate export. Possibly, it is a PEXEL-negative exported protein, like many other *Plasmodium* proteins such as MAHRP1, SBP1, and REX2, where the N-terminal TM helix along with the few proximal amino acids are implicated in the export (37). The *PbTIP* N-terminal TM helix along with a few amino acids may have facilitated its export in a PEXEL-negative manner. In the ring and trophozoite stages, *PbTIP* decorated the parasite PV membrane within the infected RBCs, and it was also observed in the host cell cytosol. It could be possible that *PbTIP* has become part of the PV membrane during its export to the host cell surface. Immunostaining of various asexual stages against *PbTIP* further revealed that this protein was somehow shed from the surface of parasitized host cells, as we detected it in their surroundings. Protein shedding was seen significantly higher in the mature gametocyte stages. A few well-characterized *Plasmodium* proteins were shed by protease processing at the cellular surface, and these included AMA1, CSP1, and MSP1 (55, 56). CSP is known to undergo protease processing and shed during the gliding motility of sporozoites, leaving behind its trails (57). *PbTIP* also sheds from the infected host cell surface as its multiple cleaved fragments were observed in the blood-stage parasite lysate with immunoblotting. Fragments of the same size were detected by immunoblotting in every independent experiment, suggesting that fragmentation did not result due to random protease processing. It is possibly cleaved by specific protease(s) that produces the same sized fragments every time.

There could be a variety of proteases involved in *PbTIP* proteolytic processing and its subsequent shedding; however, the involvement of *Plasmodium* intramembrane rhomboid proteases is highly anticipated. Various intramembrane proteases have been characterized in Apicomplexa, including *Plasmodium* species that are implicated in the proteolytic cleavage of integral membrane proteins (58). The role of rhomboid protease in the shedding of TRAP during sporozoite motility and infectivity has been reported (38). Similarly, the shedding of AMA1 and MSP1 through the proteolytic activity of

rhomboid proteases has been reported earlier. The existence of loosely conserved helix destabilizing residues in the N-terminal TM helix of *PbTIP* also strengthens our prediction regarding the involvement of parasite rhomboid(s) in its cleavage and the subsequent shedding from the cellular surface (59). However, some of our findings unveiled that *PbTIP* shedding is comparatively more feasible *in vivo* than in cultured conditions, suggesting the involvement of host origin factors in the shedding process. However, no direct evidence is available to support this; the mechanism of proteolysis and the proteases involved remain to be explored.

PbTIP could also be detected in host circulation by immunoassays. In circulation, 25- to 30-kDa protein fragments were more abundant than were other fragments. Furthermore, the presence of TIP (from human malaria parasites) in host circulation could be exploited in the development of malaria rapid antigen testing kits. *Plasmodium* histidine-rich protein 2 (HRP2), lactate dehydrogenase (pLDH), and aldolase are extensively used for this purpose and pose few advantages over conventional microscopic testing of malaria besides sensitivity (60). Among all, HRP2 is predominantly used for rapid detection test (RDT) worldwide, but recent reports of HRP2 and HRP3 mutant *P. falciparum* parasites raised alarm over the search for alternative candidates for the purpose of RDT. The use of purified monoclonal antibodies against *PfTIP*/*PvTIP* will surely improve the ELISA sensitivity and bring the detection limit better than that of the present standards.

As described earlier, *PbTIP* possesses integrin- α domains and various other adhesion domains (VCBS domain, EGF-like domain, and RGD motif). The presence of *PbTIP* in host circulation directed us to look for the host cells on which it can possibly bind. We tested immune cells firstly as its homolog has already been proven to possess an immune modulation function. *PbTIP* exhibited binding on macrophages; upon further analysis, we found that it was binding to macrophages of murine origin only. No binding was observed in cells of human origin, suggesting species specificity (data not shown). Furthermore, the *PbTIP* receptor on macrophages was still elusive and out of the various adhesion domains, which one has affected the binding is still not clear. The receptor for the mammalian TIP is also not yet reported, therefore making it difficult to predict any strong candidate for *PbTIP* binding.

Since we were more interested in the downstream effects of *PbTIP* binding on macrophages to establish its possible role in immunomodulation, we tested the inflammatory responses of murine macrophages in the presence of recombinant *PbTIP*. Exposure of macrophages to recombinant *PbTIP* suppressed the inflammatory response while it upregulated the Th2-type/anti-inflammatory response. Inflammatory cytokines such as IL-1 β , IL-6, IL-12p40, TNF- α , and IFN- γ were downregulated manifold. On the other hand, the anti-inflammatory cytokines such as IL-10 and TGF- β were upregulated manifold upon protein exposure to *PbTIP* presence along with *E. coli* LPS. However, the fold change in cytokines at the transcript level (by qPCR) should not be compared with the corresponding ELISA data (protein level) as the qPCR data displayed the

transcript profile of RAW 264.7 cells at the time of harvest while ELISA estimated the total accumulated protein in the spent media. The effect of parasite protein on macrophages leading to altered immune response may have direct relevance to the survival of parasites in the host. *EmTIP*, a homolog of human TIP in the tapeworm *Echinococcus multilocularis*, was also present in the excretory/secretory products of the parasite, and it has been shown to stimulate CD4⁺ T cells *in vitro* (61).

It is well established that enhanced levels of TGF- β and IL-10 lead to the increased number of Tregs. In malaria patients, higher levels of Tregs have been reported, which eventually developed tolerance in the host (62). *PbTIP* may induce Tregs through IL-10 and TGF- β response by macrophages upon its binding, although it is too early to make such a statement. In the infection setting, macrophages and DCs are the primary cells that detect parasites mounting a pro-inflammatory cytokine response. Inflammation plays three major roles: phagocytosis, antigen presentation, and initiation of immune responses through the production of various cytokines and growth factors (6). A reduced inflammatory potential upon *PbTIP* exposure may affect several aspects of macrophages, as explained, although we have not looked into their altered phagocytic activities or antigen presentation, if any. It appears that *PbTIP* might have affected the NF κ B and MAP kinase pathways that LPS activates through TLR-mediated binding to mount an inflammatory response. Reduced inflammatory responses from DCs and macrophages have been reported in murine malaria during the later stage of infection, as described earlier. Such responses from macrophages upon *PbTIP* exposure seem to cause less Th1-type response while enhancing the ability of target cells to produce Th2-type cytokines. This may induce tolerance in the host in the long term, and the host becomes tolerant not only to parasite antigens but also to unrelated antigens. Recently, two groups [Guha et al., human field data (63), and Nahrendorf et al., mouse model data (64)] have shown that monocytes from malaria-exposed individuals differentiate into anti-inflammatory M2-type macrophages. Although their views differed on the locations where monocytes changed to the M2 phenotype, both groups agreed that these changes occurred through epigenetic modifications (a decrease in H3K4me3) at the inflammatory cytokine gene loci. The cytokine profile of malaria-infected RBC-exposed monocytes, described by Guha et al., largely matches with our data on *PbTIP* protein-exposed macrophages. Therefore, it is likely that, among the many factors causing monocyte reprogramming by infected RBC, *Plasmodium*-released *PbTIP* could be a leading cause.

The *in vivo* systemic effect of *PbTIP* on various immune cells was studied in mice treated with recombinant *PbTIP*, followed by PBMC isolation from the peripheral circulation and transcriptome analysis. The *in vitro* response of recombinant *PbTIP* on macrophages should not be compared with its systemic *in vivo* effect. The interplay of various immune cells and their immune responses cannot be replicated *in vitro*; hence these studies cannot be directly correlated. Our analysis suggests that *PbTIP* exposure upregulated the various immune inhibition genes or immune checkpoint pathway genes. Various apoptotic

genes were found upregulated, which may have caused apoptosis of responsive immune cells. A few genes that skewed macrophages toward the M2 phenotype were also found differentially expressed upon *PbTIP* exposure. Mice treated with recombinant *PbTIP* have enhanced daily parasitemia, suggesting that this protein may affect parasite survival *in vivo*. Overall, this study suggests an immunosuppressive role of *PbTIP* in host responses, as evident in the *in vitro* and *in vivo* studies. The function of mammalian TIP is still elusive for us to state that parasite *PbTIP* anyhow mimics the host's TIP function similar to the host MIF mimicked by the *Plasmodium*-released PMIF. To the best of our knowledge, genetic manipulation in mice has revealed the role of mouse TIP (ITFG2) in the development of B- and T-cell responses. Deficient mice showed retention of B cells in the spleen and a lower concentration of immunoglobulin G (IgG) in plasma. It was found essential for the development of a normal germinal center and for adequate humoral response (33). Hence, as of now, it is very early to make a statement that denotes *PbTIP* as a functional mimic of host TIP.

In summary, our data suggest that a host-like protein in *P. berghei* was expressed on the surface of merozoites and exported to the surface of parasitized host cells in the blood-stage infection. By an uncharacterized mechanism, it was cleaved in multiple short fragments that are likely responsible for its shedding from the host cell surface. Shed protein was detected in infected host circulation, and it can be pursued in the development of rapid testing of malaria. The *PbTIP* shed into host circulation also possessed adhesion properties, exhibited binding on the surface of macrophages, and modulated their inflammatory responses. We report macrophages with reduced inflammatory responses upon *PbTIP* exposure and the upregulation of Th2 cytokines such as IL-10 and TGF- β . Our *in vivo* studies also conveyed the same effect of *PbTIP* on various immune cells. The limitations of our results are that we need to replicate our finding with human malaria parasites and test the TIP of human malaria parasites in order to develop a RDT kit.

MATERIALS AND METHODS

Animals and Parasite Strains

Six- to 8-week-old male/female C57BL/6J mice were used in all the animal experiments. All experimental procedures were carried out following Institutional Animal Ethical Committee (IAEC) guidelines (IAEC project approval no. NII/IAEC 535/19). To carry out experiments, the animals were first intraperitoneally injected with 150 μ l of a ketamine-xylazine mix to induce short-term anesthesia. The *P. berghei* strains used in this study were obtained from The Malaria Research and Reference Reagent Resource Centre (MR4). Frozen stocks of Pb_ANKA (MRA-671, BEI Resources) or Pb_ANKA-GFPcon (MRA-867, BEI Resources) strains were injected into 6- to 8-week-old mice to infect them with malaria. *Anopheles stephensi* mosquitoes were reared in a humid chamber maintained at 27°C, 70% humidity, and fed on sucrose (20%)-soaked cotton pads. Young female mosquitoes were fed on *P. berghei*-infected

C57BL/6J mice and afterwards maintained at 19–21°C, 70% humidity. On the 18th day after blood feeding, infected mosquitoes again fed on healthy mice to complete the cycle. Sporozoites were obtained by dissecting the salivary glands on the 20th day and then used for *in vivo* and *in vitro* infection experiments.

Overexpression, Purification of *PbTIP*, and Antibody Generation

A codon-optimized *PbTIP* gene fragment (corresponding to 29–660 amino acids) omitting two terminal TM domains was cloned into the *E. coli* expression vector pGEX6p1, and ligation was facilitated using the *Bam*HI and *Sal*I restriction enzymes (NEB, Ipswich, MA, USA). Details of the primers used for cloning are given in **Supplementary Table S3**. The protein was overexpressed in BL21 cells (Stratagene, La Jolla, CA, USA) at 16°C for 15 h with 0.3 mM isopropyl β -D-1-thiogalactopyranoside (IPTG) at OD₆₀₀ = 0.8. The recombinant protein was isolated from inclusion bodies by lysing the IPTG-induced bacterial pellet in lysis buffer (50 mM Tris–HCl, pH 8.0, 150 mM NaCl, 5 mM EDTA, 1 mM PMSF, and 10 μ g/ml DNase), followed by sonication (amplitude = 30, pulse on = 5 s, pulse off = 10 s) and centrifugation. The supernatant was discarded and the pellet washed three times with wash buffer I (100 mM Tris–HCl, pH 8.0, 5 mM EDTA, 1 mM DTT, 2 M urea, and 2% Triton X-100); the pellet was finally resuspended in solubilization buffer II (50 mM Tris–HCl, pH 8.0, 150 mM NaCl, 1 mM DTT, and 8 M urea) at room temperature for 3–4 h. The clear supernatant was collected and passed through a 0.45- μ m syringe filter, followed by sodium dodecyl sulfate polyacrylamide gel electrophoresis (SDS-PAGE) to check the purity of the protein. Urea was removed by stepwise dialysis, gradually decreasing the urea concentration in the dialysis buffer. No precipitate was observed during dialysis. No columns or purification matrix was used as the inclusion bodies itself gave highly pure protein. Purified protein treatment with Pierce™ High Capacity Endotoxin Removal Spin Columns (Thermo Scientific, Waltham, MA, USA) resulted in a protein preparation where the endotoxin level was below the recommended limit for animal use. Mice and rats were immunized with recombinant *PbTIP* as per the standard immunization regimen given in **Supplementary Table S4**. A week after the final immunization, mouse sera were collected and the antibody titer was determined with direct ELISA (**Supplementary Figure S7**).

Immunofluorescence Assays

Cells fixed on glass slides were permeabilized (if needed) with 0.2% saponin (Sigma, St. Louis, MO, USA) for 30 min, followed by blocking with 3% bovine serum albumin (BSA). The cells were incubated with primary antibodies (rat anti-*PbTIP* or mouse anti-*PbTIP* immune sera) at 500 dilutions overnight, followed by secondary antibodies (anti-rat AF594 or anti-mouse AF488; Abcam, Cambridge, UK) used at 2,000 dilution. Three phosphate-buffered saline (PBS) washes for 5 min each were given after incubations with the primary and secondary antibodies. Slides were mounted in anti-fade (50% glycerol and

2% DABCO; Sigma) and the images taken with a Zeiss AxioImager M2 fluorescence microscope.

Western Blotting

Parasite pellets (obtained upon saponin lysis of infected RBCs) were resuspended in 1× PBS and sonicated to separate the soluble and insoluble fractions. The resulting pellet was solubilized in 0.1% SDS containing PBS and centrifuged to obtain the lysate. For Western blot of mouse serum, the excess of albumin protein was removed with AlbuminOut (G-Biosciences, New Delhi, India), followed by SDS-PAGE. The protein from the gel was transferred into a nitrocellulose membrane (Bio-Rad, Hercules, CA, USA), followed by overnight incubation with a blocking buffer (Odyssey). The membrane was probed with a primary antibody (rat anti-*PbTIP* immune sera, 1/1,000 dilution) for 3 h, followed by an IR-labeled secondary antibody (rabbit anti-rat IR800, 1/10,000 dilution; Invitrogen, Carlsbad, CA, USA) for 2 h. The blot was imaged using the Licor Odyssey imager. For the horseradish peroxidase (HRP)-labeled secondary antibodies, the membrane was incubated with 10 ml of 0.1% 3,3'-diaminobenzidine tetrahydrochloride (DAB; Sigma) containing 12 μ l of 30% H₂O₂ until the band developed.

Sandwich ELISA

A high-protein-binding 96-well ELISA plate (Corning, NY, USA) was coated with mouse anti-*PbTIP* immune sera in coating buffer overnight at 4°C. Serial dilutions of the *Plasmodium*-infected mouse sera were incubated overnight for binding in cold conditions, followed by incubation with the rat anti-*PbTIP* immune sera (primary antibodies, 1,000 dilution) for 2 h the next day. The rabbit anti-rat HRP secondary antibody (Novus Biologicals, Englewood, CO, USA) was used at 5,000 dilution for 1 h and developed by adding 100 μ l/well of the TMB substrate (Sigma–Thermo Fisher, India), and the absorbance was measured at 370 nm in a Tecan M200 (Theale, Reading, UK) plate reader. In the direct ELISA for estimating the antibody titer, 0.2–0.5 μ g/well of the recombinant *PbTIP* was coated; the rest of the process remained the same.

For cytokine estimation using ELISA, the spent culture medium was collected at 9 and 20 h and 50 μ l of the spent medium was used for ELISA following the manufacturer's protocol (BioLegend cat. nos. 432604, 431604, 436707, and 431411; Becton Dickinson cat nos. 560478 and 555138).

Parasite Culture for Schizonts

C57BL/6J mice infected with *P. berghei* parasite were humanely sacrificed at 8%–10% parasitemia (mostly trophozoites); the infected blood was collected in heparinized vials. Blood was centrifuged to remove plasma, resuspended in complete RPMI1640 [20% fetal bovine serum (FBS) and 50 mg/L hypoxanthine] media, keeping the hematocrit at 4%–6%, and incubated at 37°C. The culture flasks were flushed with the excess of mixed gas (90% N₂, 5% CO₂, and 5% O₂) and capped tightly. At regular intervals, the spent culture medium was collected, centrifuged, and kept for ELISA. Schizont formation and their

bursting were monitored with Giemsa staining of thin smears of blood culture collected at regular intervals.

Macrophage Binding Assay

Thioglycolate elicited mouse peritoneal macrophages were isolated in ice-cold Dulbecco's PBS and allowed to adhere onto sterile coverslips on a 24-well cell culture plate containing complete RPMI medium (Lonza, Basel, Switzerland). One hour later, the cells were washed with PBS to remove non-adherent cells. Similarly, RAW 264.7 cells were also seeded in a cell culture plate and 10 µg/ml of the recombinant *PbTIP* was incubated with peritoneal macrophages and RAW 264.7 cells for 1 h. After incubation, the cells were washed with an excess of PBS and fixed with 4% paraformaldehyde (PFA), followed by IFAs to decipher the surface binding of *PbTIP*.

Macrophage LPS Stimulation *In Vitro*

RAW 264.7 cells were cultured in complete Dulbecco's modified Eagle's medium (DMEM; Lonza) containing 10% FBS (Gibco, Waltham, MA, USA) and seeded into a 24-well cell culture plate. The cells were stimulated with 100 ng/ml of *E. coli* LPS (Thermo Fisher, India) in the presence and absence of 10 µg/ml recombinant *PbTIP* for recommended hours. Post-incubation, the RNA was isolated from each well with Trizol (Thermo Fisher, India) following the recommended procedure and 2 µg of the RNA was converted into complementary DNA (cDNA) with an iScript reverse transcription kit (BioRad). qPCR was performed with the gene-specific primers of the various cytokines and a high-efficiency qPCR mix (cat no. 18114R1074; GCC Biotech, West Bengal, India) to calculate the relative fold change (**Supplementary Table S3**). The primers used in the study are given in **Supplementary Table S3**.

Transcriptome Analysis

A group of eight C57BL/6J mice were given four consecutive doses of 2 mg/kg of recombinant *PbTIP* and their blood collected. An equivalent group of control-treated (GST protein-treated) mice were included in the experiment. PBMCs were isolated with Percoll-based density gradient centrifugation and total RNA was isolated from the purified PBMCs. Briefly, Trizol-preserved samples were stored in -80°C deep freezer until use and then thawed once at the time of RNA extraction. Chilled chloroform was added to one-fifth volume of the Trizol, mixed well, and centrifuged to collect the upper aqueous phase. RNA was precipitated with an equal volume of chilled isopropanol and retrieved by centrifugation at full speed. The RNA pellet was washed with chilled 70% ethanol, air dried, and dissolved in an appropriate volume of nuclease-free water. The RNA integrity number (RIN) was >7 for each sample. A TruSeq (Illumina, San Diego, CA, USA) stranded mRNA library was made using 5 µg total RNA and was sequenced with the Illumina NovaSeq 6000 platform. The paired-end read length was 150 bases. A total of 6 Gb data was collected per sample.

Initial RNA sequence quality assessment was carried out on raw reads using FastQC v0.11. Adapter contamination and low-quality reads ($Q < 30$) were trimmed out using the NGSQC

Toolkit v2.3.3. If 70% of the reads had average good quality ($Q \geq 30$), then it was kept and was considered as high-quality (HQ) data. In the next step, HQ reads were assembled using a *de novo* transcriptome assembly method. The total reads obtained were 37,546,250 and 37,546,250 for the control and 33,346,685 and 33,346,685 for the *TIP*-treated samples. Differential gene expression analysis was carried out using Cuffdiff v2.2.1. The obtained blast hits were then used to annotate the transcripts at different levels, such as pathway and Gene Ontology (GO) annotation, using the Retrieve/ID mapping utility provided by the UniProt database.

Giemsa Staining

Thin blood smears fixed on glass slides (methanol fixed) were stained with a 1:10 times diluted Giemsa staining solution (48900-1L-F; Sigma) in a staining buffer (8 mM KH_2PO_4 , 6 mM Na_2HPO_4 , pH 7.0). The Giemsa stain was kept on slides for 30 min, followed by washing the slides under running tap water to remove excess of the stain, and then the slides were air dried for some time. Blood smears were observed under $\times 100$ magnification using oil immersion lens fitted in a Nikon 80i microscope.

Statistical Analysis

Data are presented as the mean and SDs. Statistical analyses were performed using Student's *t*-test. Statistically significant differences compared with the control are indicated by asterisks: * $p < 0.05$, ** $p < 0.01$, *** $p < 0.001$. All the statistical analysis was done in Excel or GraphPad Prism. Survival curve was analyzed by the log-rank test to evaluate its statistical significance.

DATA AVAILABILITY STATEMENT

The datasets presented in this study can be found in online repositories. The names of the repository and accession number can be found below: <https://www.ncbi.nlm.nih.gov/>, GSE173309.

ETHICS STATEMENT

The animal study was reviewed and approved by the Animal Ethics Committee of the National Institute of Immunology, New Delhi, India.

AUTHOR CONTRIBUTIONS

AS and RA conceived the project. IK and AS designed all the experiments and analyzed the data. IK performed the experiments. RA, SB, and BS generated the reagents for the study. AQ helped in transcriptome data collection and manuscript editing. All authors contributed to the article and approved the submitted version.

ACKNOWLEDGMENTS

The *Plasmodium berghei* strain ANKA, MRA-671, contributed by Mark F. Wiser, and strain (ANKA) 507m6cl1, MRA-867, contributed by Chris J. Janse and Andrew P. Waters, were obtained through BEI Resources, NIAID, NIH. This work was financially supported by Science and Engineering Research Board (SERB), Government of India grant (EMR/2015/001546) sanctioned to AS. IK received fellowships from National Institute of Immunology (NII) core grant and SERB, Government of India.

SUPPLEMENTARY MATERIAL

The Supplementary Material for this article can be found online at: <https://www.frontiersin.org/articles/10.3389/fimmu.2021.699887/full#supplementary-material>

Supplementary Material | Gene ontology (GO) analysis. Gene ontology (GO) analyses revealed that following cellular components were enriched; Plasma membrane (GO:0005886), Cytoplasm (GO:0005737), nucleus (GO:0005634) and integral components of membrane (GO:0016021). Similarly enriched molecular components include, identical protein binding (GO:0042802), ATP binding (GO:0005524), signalling receptor binding (GO:0005102) Calcium ion binding (GO:0005509) and Zinc ion binding (GO:0008270). The biological processes that were majorly affected included cell surface receptor signalling (GO:0007166), cAMP biosynthetic process (GO:0006171), negative regulation of angiogenesis (GO:0016525), intracellular signal transduction (GO:0035556) and cellular response to LPS (GO:0071222). Detailed analysis further revealed that up-regulated genes inhibit immune response; by negative regulation of i) antigen processing and presentation of endogenous peptide antigen via MHC class I via ER pathway, TAP-independent [GO:0002486], ii) CD4⁺ alpha-beta T cell proliferation [GO:2000562], iii) CD8⁺ alpha-beta T cell proliferation [GO:2000565], iv) IFN-gamma production [GO:0032689], v) IL-17 production [GO:0032700], vi) TNF production [GO:0032720], and by positive regulation of i) I-kappaB kinase/NF-kappaB signaling [GO:0043123], ii) IL-10 production [GO:0032733] iii) isotype switching [GO:0045830] iv) regulatory T cell differentiation [GO:0045591], v) protein ubiquitination [GO:0031398] vi) TGF beta receptor signaling pathway [GO:0007179] Upregulated genes are also involved in immune checkpoint blockade pathways as evident by enrichment of GO terms i) negative regulation of cell population proliferation [GO:0008285] ii) intracellular signal transduction [GO:0035556], iii) immune response-regulating cell surface receptor signalling pathway [GO:0002768] iv) extrathymic T cell selection [GO:0045062] and v) cell population proliferation [GO:0008283]

Supplementary Table 1 | Peptides detected in MS/MS analysis of ~55kDa fragment of the recombinant *PbTIP*. Peptide sequences revealed that 55kDa fragment is a cleavage product of full-length protein, hence it is the part of the protein.

Supplementary Table 2 | Primers used in this study.

Supplementary Table 3 | List of differentially expressed genes in mouse PBMC upon recombinant *PbTIP* treatment. GST protein treated PBMCs was taken as control here.

Supplementary Table 4 | Mouse or rat immunization regime to raise antibodies against *PbTIP*.

Supplementary Figure 1 | Smart domain analysis (<http://smart.embl-heidelberg.de/>) of *PbTIP* amino acid sequence revealed the presence of VCBS domain positioned between 196 to 277 amino acid residues. The suggested role of VCBS domain is in the adhesion and it is present in multiple copies in the long proteins of many bacteria.

Supplementary Figure 2 | Antibodies against the MSP1 stain the merozoites surface uniformly unlike *PbTIP*. Anti-MSP1 primary antibody staining (secondary antibody was labelled with Alexa 594) showed that MSP1 was present uniformly all over the merozoites surface while *PbTIP* expression was uneven on the merozoites surface. *PbTIP* is localized more at one end of the merozoites rather than distribution all over the surface as MSP1. Scale bar 1µm.

Supplementary Figure 3 | *PbTIP* is exported across the PV membrane and localized to the surface of host cells. *Plasmodium PbTIP* is exported out of PVM and become the part of erythrocytes membrane. Here, the PV membrane is marked in red by staining against the EXP1 protein (secondary antibody was labelled with Alexa 594) and *PbTIP* expression (green, secondary antibody with Alexa 488) is shown beyond it. Scale bar 5µm.

Supplementary Figure 4 | MSP1 is not shed from schizonts surface. MSP1 protein was used as a negative control to show shedding of *PbTIP* from the *Plasmodium* schizonts and other stages of parasite. *PbTIP* was shown to shed from various parasitic stages while MSP1 gives the typical staining on merozoites and schizonts. Scale bar 5µm.

Supplementary Figure 5 | Expression and purification of recombinant *PbTIP* in *E. coli*. (A) Inclusion bodies from IPTG induced bacterial pellet was solubilized in 8M urea buffer and protein recovered from inclusion bodies was refolded by step-wise removal of urea by dialysis. No precipitation was observed during dialysis and high purity (>95%) protein was recovered from inclusion bodies. Refolded protein was run on an acrylamide gel. Two lanes represent protein loading in duplicates.

(B) Overexpressed recombinant *PbTIP* was confirmed with western blotting using antibodies against the GST and detected the full-length *PbTIP* along with GST at ~95kDa (right panel). A major fragment was observed at ~55kDa which is a cleaved fragment of the full-length *PbTIP* and explained below. Two lanes represent the protein loading in duplicates.

Supplementary Figure 6 | N-terminal sequence analysis of the ~55kDa fragment recovered along with full-length recombinant *PbTIP* revealed one of the cleavage sites near its N-terminus. Inclusion bodies purified *PbTIP* was subjected to electrophoresis and transferred onto the PVDF membrane. After Ponceau staining *PbTIP* fragment ~55kDa (TF55) was cut from the membrane and processed for N-terminal amino acid sequencing by Edman's degradation method. The first 10 amino acids of this *PbTIP* fragment revealed a cleavage between 128-129 amino acids position in the full-length protein.

Supplementary Figure 7 | Schizonts burst do not contribute to the shed *PbTIP* in the host circulation. Shedding of *PbTIP* from a gametocyte (FITC signal) while signals were not detected from the merozoites upon schizonts burst. These two independent events were captured in the same field suggesting that schizonts burst does not contribute significantly to shed *PbTIP*.

Supplementary Figure 8 | Pro-inflammatory and anti-inflammatory cytokines profile of LPS elicited RAW 264.7 cells upon exposure of recombinant *PbTIP*. RAW 264.7 cells were stimulated with LPS (100ng/ml) alone and LPS+recombinant *PbTIP* (10µg/ml) keeping the untreated cells as naïve. The level of various cytokines was measured in the culture medium (spent medium) by ELISA following the manufacturers protocol (Biolegend and BD). ELISA results indicate that *PbTIP* significantly suppressed the pro-inflammatory cytokines (IL-1β, TNF-α, IFN-γ and IL-12p40) expression in LPS elicited macrophages *in-vitro*, suggesting immunosuppressive effect of *PbTIP* on macrophages. P-values for IL-1β, TNF-α, IFN-γ and IL-12p40 respectively are 0.0017, 0.0032, 0.0203, and 0.0026. Pro-inflammatory cytokines were measured upon 9hours of stimulation. Anti-inflammatory cytokines (IL-10 and TGF-β) were also measured by ELISA however upon longer incubation (20hours) and found to be significantly over-expressed in *PbTIP* exposed LPS-elicited macrophages. These results demonstrate the *PbTIP* potential to favour anti-inflammatory responses in macrophages while suppressing the pro-inflammatory responses. P-values for IL-10 and TGF-β respectively are 0.00504 and 0.0005. P-values were calculated by applying t-test.

Supplementary Figure 9 | Volcano plot displaying differentially expressed genes of PBMCs upon *PbTIP* treatment. The volcano plot displaying differentially expressed genes of mouse PBMCs upon treatment with *PbTIP* as described in (i).

Here the x-axis represents the \log_2 fold change while the y-axis denotes $-\log_{10}$ (q-value) or $-\log_{10}$ (false discovery rate). All significantly up-regulated/down-regulated genes are highlighted in red dots while genes that were validated by qPCR are in blue dots. Black dots denote non-significant genes in the study (adjusted $-\log_{10}$ q-value < 0.05). Most of the genes in the study were found to be up-regulated hence giving a skewed appearance to the volcano plot.

Supplementary Figure 10 | Transcriptome data validation by RT-qPCR. Primers were designed against the few genes that were significantly changed in the transcriptome data. Primers list is given in the **Table S3**. RT-qPCR was performed on cDNA from RNA samples that were given for transcriptome analysis. The genes

transcripts that were found up-regulated in transcriptome analysis were also found up-regulated when tested by qPCR.

Supplementary Figure 11 | Estimation of antibody titre of anti-PbTIP immune sera. Antibody titre of anti-PbTIP antibodies collected from recombinant PbTIP immunized mice, was estimated by ELISA. ELISA plate was coated with purified recombinant PbTIP and ELISA was performed as discussed earlier in the method section. OD370nm was plotted against different dilutions of immune sera. Antibodies against PbTIP were able to recognize antigen up to ~0.25 million dilutions. Control immunized (sham-treated) mice were taken as a negative control in ELISA.

REFERENCES

- World Health Organization. *World Malaria Report*. Geneva, Switzerland: WHO (2020). ISBN 978 92 4 1564403.
- Wimberly M, Bayabil E, Beyene B, Henebry G, Liu Y, Mihretie A, et al. EPIDEMIA-An EcoHealth Informatics System for Integrated Forecasting of Malaria Epidemics. *Malar J* (2020) 13(1):92–92. doi: 10.1186/1475-2875-13-S1-P92
- Doolan DL, Dobaño C, Baird JK. Acquired Immunity to Malaria. *Clin Microbiol Rev* (2009) 22:13–36. doi: 10.1128/CMR.00025-08
- Hoffman SL, Goh LML, Luke TC, Schneider I, Le TP, Doolan DL, et al. Protection of Humans Against Malaria by Immunization With Radiation-Attenuated Plasmodium Falciparum Sporozoites. *J Infect Dis* (2002) 185 (8):1155–64. doi: 10.1086/339409
- Krishnegowda G, Hajjar AM, Zhu J, Douglass EJ, Uematsu S, Akira S, et al. Induction of Proinflammatory Responses in Macrophages by the Glycosylphosphatidylinositols of Plasmodium Falciparum: Cell Signaling Receptors, Glycosylphosphatidylinositol (GPI) Structural Requirement, and Regulation of GPI Activity. *J Biol Chem* (2005) 280:8606–16. doi: 10.1074/jbc.M413541200
- Buçan AN, Williamson KC. Setting the Stage: The Initial Immune Response to Blood-Stage Parasites. *Virulence* (2020) 11:88–103. doi: 10.1080/21505594.2019.1708053
- Griffith JW, Sun T, McIntosh MT, Bucala R. Pure Hemozoin Is Inflammatory *In Vivo* and Activates the NALP3 Inflammasome via Release of Uric Acid. *J Immunol* (2009) 183:5208–20. doi: 10.4049/jimmunol.0713552
- Coban C, Ishii KJ, Kawai T, Hemmi H, Sato S, Uematsu S, et al. Toll-Like Receptor 9 Mediates Innate Immune Activation by the Malaria Pigment Hemozoin. *J Exp Med* (2005) 201:19–25. doi: 10.1084/jem.20041836
- Imai T, Ishida H, Suzue K, Taniguchi T, Okada H, Shimokawa C, et al. Cytotoxic Activities of CD8+ T Cells Collaborate With Macrophages to Protect Against Blood-Stage Murine Malaria. *Elife* (2015) 2015:1–49. doi: 10.7554/eLife.04232
- René Rachou I, Oswaldo Cruz F, Horizonte B, Junqueira C, R Barbosa CR, Costa PA, et al. Cytotoxic CD8 + T Cells Recognize and Kill Plasmodium vivax-Infected Reticulocytes. *Nat Med* (2018) 24:1330–6. doi: 10.1038/s41591-018-0117-4
- Meding SJ, Langhorne J. CD4+ T Cells and B Cells Are Necessary for the Transfer of Protective Immunity To Plasmodium Chabaudi Chabaudi. *Eur J Immunol* (1991) 21:1433–8. doi: 10.1002/eji.1830210616
- Stanisic DI, Barry AE, Good MF. Escaping the Immune System: How the Malaria Parasite Makes Vaccine Development a Challenge. *Trends Parasitol* (2013) 29:612–22. doi: 10.1016/j.pt.2013.10.001
- Urban BC, Ferguson DJP, Pain A, Willcox N, Magdalena Plebanski JMA, DJ R. Plasmodium Falciparum-Infected Erythrocytes Modulate the Maturation of Dendritic Cells. *Nature* (1999) 400:73–7. doi: 10.1038/21900
- Perry JA, Olver CS, Burnett RC, Avery AC. Cutting Edge: The Acquisition of TLR Tolerance During Malaria Infection Impacts T Cell Activation. *J Immunol* (2005) 174:5921–5. doi: 10.4049/jimmunol.174.10.5921
- Wilson NS, Behrens GMN, Lundie RJ, Smith CM, Waithman J, Young L, et al. Systemic Activation of Dendritic Cells by Toll-Like Receptor Ligands or Malaria Infection Impairs Cross-Presentation and Antiviral Immunity A R T I C L E S. *Nat Immunol* (2006) 7:165–72. doi: 10.1038/ni1300
- Illingworth J, Butler NS, Roetynck S, Mwacharo J, Pierce SK, Bejon P, et al. Chronic Exposure to Plasmodium Falciparum Is Associated With Phenotypic Evidence of B and T Cell Exhaustion. *J Immunol* (2013) 190:1038–47. doi: 10.4049/JIMMUNOL.1202438
- Pinzon-Charry A, Woodberry T, Kienle V, McPhun V, Minigo G, Lampah DA, et al. Apoptosis and Dysfunction of Blood Dendritic Cells in Patients With Falciparum and Vivax Malaria. *J Exp Med* (2013) 210:1635–46. doi: 10.1084/jem.20121972
- Horne-Debets JM, Faleiro R, Karunaratne DS, Liu XQ, Lineburg KE, Poh CM, et al. PD-1 Dependent Exhaustion of CD8+ T Cells Drives Chronic Malaria. *Cell Rep* (2013) 5:1204–13. doi: 10.1016/j.celrep.2013.11.002
- Hisaeda H, Maekawa Y, Iwakawa D, Okada H, Himeno K, Kishihara K, et al. Escape of Malaria Parasites From Host Immunity Requires CD4 + CD25+ Regulatory T Cells. *Nat Med* (2004) 10:29–30. doi: 10.1038/nm975
- Mackroth MS, Malhotra I, Mungai P, Koech D, Muchiri E, King CL. Human Cord Blood CD4 + CD25 Hi Regulatory T Cells Suppress Prenatally Acquired T Cell Responses to Plasmodium Falciparum Antigens. *J Immunol* (2011) 186:2780–91. doi: 10.4049/jimmunol.1001188
- Mahanta A, Ganguli P, Barah P, Sarkar RR, Sarmah N, Phukan S, et al. Integrative Approaches to Understand the Mastery in Manipulation of Host Cytokine Networks by Protozoan Parasites With Emphasis on Plasmodium and Leishmania Species. *Front Immunol* (2018) 9:296. doi: 10.3389/fimmu.2018.00296
- Sun T, Holowka T, Song Y, Zierow S, Leng L, Chen Y, et al. A Plasmodium-Encoded Cytokine Suppresses T-Cell Immunity During Malaria. *Proc Natl Acad Sci USA* (2012) 109:E2117–26. doi: 10.1073/pnas.1206573109
- Holowka T, Castilho TM, Garcia AB, Sun T, McMahon-Pratt D, Bucala R. Leishmania-Encoded Orthologs of Macrophage Migration Inhibitory Factor Regulate Host Immunity to Promote Parasite Persistence. *FASEB J* (2016) 30:2249–65. doi: 10.1096/fj.201500189R
- Bhavsar AP, Guttman JA, Finlay BB. Manipulation of Host-Cell Pathways by Bacterial Pathogens. *Nature* (2007) 449:827–34. doi: 10.1038/nature06247
- Cooper D, Eleftherianos I. Parasitic Nematode Immunomodulatory Strategies: Recent Advances and Perspectives. *Pathogens* (2016) 5:58–58. doi: 10.3390/pathogens5030058
- Hewitson JP, Grainger JR, Maizels RM. Helminth Immunoregulation: The Role of Parasite Secreted Proteins in Modulating Host Immunity. *Mol Biochem Parasitol* (2009) 167:1–11. doi: 10.1016/j.molbiopara.2009.04.008
- Fiscella M, Perry JW, Teng B, Bloom M, Zhang C, Leung K, et al. TIP, a T-Cell Factor Identified Using High-Throughput Screening Increases Survival in a Graft-Versus-Host Disease Model. *Nat Biotechnol* (2003) 21:302–7. doi: 10.1038/nbt797
- Kaczanowski S, Zielenkiewicz P. A TIP on malaria (genomics) To the editor. *Nat Biotechnol* (2003) 21:733–733.
- Schultz J, Milpetz F, Bork P, Ponting CP. SMART, a Simple Modular Architecture Research Tool: Identification of Signaling Domains. *Proc Natl Acad Sci USA* (1998) 95:5857–64. doi: 10.1073/pnas.95.11.5857
- Oliveira P, Pinto F, Pacheco CC, Mota R, Tamagnini P. An Exoprotein Required for Filament Adhesion and Aggregation in *A. Nabaena* sp PCC 7120. *Environ Microbiol* (2015) 17:1631–48. doi: 10.1111/1462-2920.12600
- Duperthuy M, Sjöström AE, Sabharwal D, Damghani F, Uhlin BE, Wai SN. Role of the Vibrio Cholerae Matrix Protein Bap1 in Cross-Resistance to Antimicrobial Peptides. *PloS Pathog* (2013) 9:e1003620. doi: 10.1371/journal.ppat.1003620
- Aurrecoechea C, Brestelli J, Brunk BP, Dommer J, Fischer S. PlasmoDB: A Functional Genomic Database for Malaria Parasites. *Nucleic Acids Res* (2009) 37:D539–3. doi: 10.1093/NAR/GKN814

33. Al-Shami A, Crisostomo J, Wilkins C, Xu N, Humphries J, Chang WC, et al. Integrin- α FG-GAP Repeat-Containing Protein 2 Is Critical for Normal B Cell Differentiation and Controls Disease Development in a Lupus Model. *J Immunol* (2013) 191:3789–98. doi: 10.4049/jimmunol.1203534
34. Oxvig C, Springer TA. *Experimental Support for a-Propeller Domain in Integrin-Subunits and a Calcium Binding Site on its Lower Surface*. (1998). Available at: www.pnas.org (Accessed January 6, 2021).
35. Via A, Uyar B, Brun C, Zanzoni A. How Pathogens Use Linear Motifs to Perturb Host Cell Networks. *Trends Biochem Sci* (2015) 40:36–48. doi: 10.1016/j.tibs.2014.11.001
36. Krogh A, Larsson B, von Heijne G, Sonhammer ELL. Predicting Transmembrane Protein Topology With a Hidden Markov Model: Application to Complete Genomes. *J Mol Biol* (2001) 305:567–80. doi: 10.1006/jmbi.2000.4315
37. Spielmann T, Gilberger TW. Protein Export in Malaria Parasites: Do Multiple Export Motifs Add Up to Multiple Export Pathways? *Trends Parasitol* (2010) 26:6–10. doi: 10.1016/j.pt.2009.10.001
38. Ejigiri I, Ragheb DRT, Pino P, Coppi A, Bennett BL, Soldati-Favre D, et al. Shedding of TRAP by a Rhomboid Protease From the Malaria Sporozoite Surface Is Essential for Gliding Motility and Sporozoite Infectivity. *PLoS Pathog* (2012) 8:e1002725. doi: 10.1371/journal.ppat.1002725
39. Baker RP, Wijetilaka R, Urban S. Two Plasmodium Rhomboid Proteases Preferentially Cleave Different Adhesins Implicated in All Invasive Stages of Malaria. *PLoS Pathog* (2006) 2(10):e113. doi: 10.1371/journal.ppat.0020113
40. Hobbs S, Reynoso M, Geddis AV, Mitrophanov AY, Matheny RW. LPS-Stimulated NF- κ B P65 Dynamic Response Marks the Initiation of TNF Expression and Transition to IL-10 Expression in RAW 264.7 Macrophages. *Physiol Rep* (2018) 6:e13914. doi: 10.14814/PHY2.13914
41. Kitai Y, Takeuchi O, Kawasaki T, Ori D, Sueyoshi T, Murase M, et al. Negative Regulation of Melanoma Differentiation-Associated Gene 5 (MDA5)-Dependent Antiviral Innate Immune Responses by Arf-Like Protein 5b *. *J Biol Chem* (2014) 290:1269–80. doi: 10.1074/jbc.M114.611053
42. Watanabe N, Gavrieli M, Sedy JR, Yang J, Fallarino F, Loftin SK, et al. BTLA is a Lymphocyte Inhibitory Receptor With Similarities to CTLA-4 and PD-1. *Nat Immunol* (2003) 4:670–9. doi: 10.1038/ni944
43. Conte D, Huh M, Goodall E, Delorme M, Parks RJ, Picketts DJ. Loss of Atrx Sensitizes Cells to DNA Damaging Agents Through P53-Mediated Death Pathways. *J Infect Dis* (2012) 7(12):e52167. doi: 10.1371/journal.pone.0052167
44. Bauer M, Goldstein M, Heylmann D, Kaina B. Human Monocytes Undergo Excessive Apoptosis Following Temozolomide Activating the ATM/ATR Pathway While Dendritic Cells and Macrophages Are Resistant. *PLoS One* (2012) 7:39956. doi: 10.1371/journal.pone.0039956
45. Natrajan R, Little SE, Reis-Filho JS, Hing L, Messahel B, Grundy PE, et al. Amplification and Overexpression of CACNA1E Correlates With Relapse in Favorable Histology Wilms' Tumors. *Clin Cancer Res* (2006) 12:7284–93. doi: 10.1158/1078-0432.CCR-06-1567
46. Incio J, Tam J, Rahbari NN, Suboj P, Mcmanus DT, Chin SM, et al. Cancer Therapy: Preclinical PlGF/VEGFR-1 Signaling Promotes Macrophage Polarization and Accelerated Tumor Progression in Obesity. *Clin Cancer Res* (2016) 22(12):2993–3004. doi: 10.1158/1078-0432.CCR-15-1839
47. Königs V, Jennings R, Vogl T, Horsthemke M, Bachg AC, Xu Y, et al. Mouse Macrophages Completely Lacking Rho Subfamily GTPases (RhoA, RhoB, and RhoC) Have Severe Lamellipodial Retraction Defects, But Robust Chemotactic Navigation and Altered Motility. *J Biol Chem* (2014) 289:30772–84. doi: 10.1074/jbc.M114.563270
48. Schmid-Hempel P. Immune Defence, Parasite Evasion Strategies and Their Relevance for "Macroscopic Phenomena" Such as Virulence. *Philos Trans R Soc Lond B: Biol Sci* (2009) 364:85–98. doi: 10.1098/rstb.2008.0157
49. Riley M, Artavanis-Tsakonas K, Tongren JE, Riley EM. Correspondence: Dr E The War Between the Malaria Parasite and the Immune System: Immunity, Immunoregulation and Immunopathology. *Clin Exp Immunol* (2003) 133(2):145–52. doi: 10.1046/j.1365-2249.2003.02174.x
50. Williamson WA, Greenwood BM. IMPAIRMENT OF THE IMMUNE RESPONSE TO VACCINATION AFTER ACUTE MALARIA. *Lancet* (1978) 311:1328–9. doi: 10.1016/S0140-6736(78)92403-0
51. Lucas A, Mcfadden G. As Novel Biotherapeutics Secreted Immunomodulatory Viral Proteins. *J Immunol Ref* (2004) 173:4765–74. doi: 10.4049/jimmunol.173.8.4765
52. MacDonald SM, Bhisutthibhan J, Shapiro TA, Rogerson SJ, Taylor TE, Tembo M, et al. Immunostimulation in Malaria: Plasmodium Falciparum Secretes a Functional Histamine-Releasing Factor Homolog *In Vitro* and *In Vivo*. *Proc Natl Acad Sci USA* (2001) 98:10829–32. doi: 10.1073/pnas.201191498
53. Kato M, Chou TF, Yu CZ, DeModena J, Sternberg PW. LINKIN, a New Transmembrane Protein Necessary for Cell Adhesion. *Elife* (2014) 3:e04449. doi: 10.7554/eLife.04449
54. Takada Y, Ye X, Simon S. The Integrins. *Genome Biol* (2007) 8:1–9. doi: 10.1186/gb-2007-8-5-215
55. Blackman MJ, Holder AA. Secondary Processing of the Plasmodium Falciparum Merozoite Surface Protein-1 (MSP1) by a Calcium-Dependent Membrane-Bound Serine Protease: Shedding of MSP133 as a Noncovalently Associated Complex With Other Fragments of the MSP1. *Mol Biochem Parasitol* (1992) 50:307–15. doi: 10.1016/0166-6851(92)90228-C
56. Howell SA, Wells I, Fleck SL, Kettleborough C, Collins CR, Blackman MJ. A Single Malaria Merozoite Surface Protein Mediates Shedding of Multiple Surface Proteins by Juxtamembrane Cleavage. *J Biol Chem* (2003) 278:23890–8. doi: 10.1074/jbc.M302160200
57. Stewart MJ, Vanderberg JP. Malaria Sporozoites Release Circumsporozoite Protein From Their Apical End and Translocate It Along Their Surface. *J Protozool* (1991) 38:411–21. doi: 10.1111/j.1550-7408.1991.tb01379.x
58. Rawson RB. Intriguing Parasites and Intramembrane Proteases. *Genes Dev* (2008) 22:1561–6. doi: 10.1101/gad.1686808
59. Urban S, Freeman M. Substrate Specificity of Rhomboid Intramembrane Proteases Is Governed by Helix-Breaking Residues in the Substrate Transmembrane Domain. *Mol Cell* (2003) 11:1425–34. doi: 10.1016/S1097-2765(03)00181-3
60. Bisoffi Z, Gobbi F, Van Den Ende J. Rapid Diagnostic Tests for Malaria. *BMJ* (2014) 348:66–78. doi: 10.1136/bmj.g3846
61. Nono JK. EmTIP, a T-Cell Immunomodulatory Protein Secreted by the Tapeworm Echinococcus Multilocularis Is Important for Early Metacystode Development. *PLoS Negl Trop Dis* (2014) 8:54. doi: 10.1371/JOURNAL.PNTD.0002632
62. Couper KN, Blount DG, Wilson MS, Hafalla JC, Belkaid Y. IL-10 From CD4 + CD25 2 Foxp3 2 CD127 2 Adaptive Regulatory T Cells Modulates Parasite Clearance and Pathology During Malaria Infection. *PLoS Pathog* (2008) 4:1000004. doi: 10.1371/journal.ppat.1000004
63. Nahrendorf W, Ivens A, Spence PJ. Inducible Mechanisms of Disease Tolerance Provide an Alternative Strategy of Acquired Immunity to Malaria. *Elife* (2021) 10:e1000004. doi: 10.7554/ELIFE.63838
64. Guha R, Mathioudaki A, Doumbo S, Doumbo D, Skinner J, Arora G, et al. Plasmodium Falciparum Malaria Drives Epigenetic Reprogramming of Human Monocytes Toward a Regulatory Phenotype. *PLoS Pathog* (2021) 17: e1009430. doi: 10.1371/JOURNAL.PPAT.1009430

Conflict of Interest: The authors declare that the research was conducted in the absence of any commercial or financial relationships that could be construed as a potential conflict of interest.

Publisher's Note: All claims expressed in this article are solely those of the authors and do not necessarily represent those of their affiliated organizations, or those of the publisher, the editors and the reviewers. Any product that may be evaluated in this article, or claim that may be made by its manufacturer, is not guaranteed or endorsed by the publisher.

Copyright © 2021 Kalia, Anand, Quadiri, Bhattacharya, Sahoo and Singh. This is an open-access article distributed under the terms of the Creative Commons Attribution License (CC BY). The use, distribution or reproduction in other forums is permitted, provided the original author(s) and the copyright owner(s) are credited and that the original publication in this journal is cited, in accordance with accepted academic practice. No use, distribution or reproduction is permitted which does not comply with these terms.



Identification of a Novel Mutation in *TNFAIP3* in a Family With Poly-Autoimmunity

Marianna Nicoletta Rossi^{1†}, Silvia Federici^{2†}, Andrea Uva², Chiara Passarelli³, Camilla Celani², Ivan Caiello¹, Valentina Matteo¹, Stefano Petrocchi³, Eva Piano Mortari⁴, Fabrizio De Benedetti^{1,2}, Giusi Prencipe^{1*†} and Antonella Insalaco^{2‡}

OPEN ACCESS

Edited by:

Maciej Lech,
LMU Munich University Hospital,
Germany

Reviewed by:

Barbara A. Malynn,
University of California, San Francisco,
United States
Tiphane Phillips Vogel,
Baylor College of Medicine,
United States

*Correspondence:

Giusi Prencipe
giusi.prencipe@opbg.net

[†]These authors have contributed
equally to this work

[‡]These authors have contributed
equally to this work

Specialty section:

This article was submitted to
Molecular Innate Immunity,
a section of the journal
Frontiers in Immunology

Received: 29 October 2021

Accepted: 11 January 2022

Published: 26 January 2022

Citation:

Rossi MN, Federici S, Uva A, Passarelli C, Celani C, Caiello I, Matteo V, Petrocchi S, Mortari EP, De Benedetti F, Prencipe G and Insalaco A (2022) Identification of a Novel Mutation in *TNFAIP3* in a Family With Poly-Autoimmunity. *Front. Immunol.* 13:804401. doi: 10.3389/fimmu.2022.804401

¹ Laboratory of Immuno-Rheumatology, Bambino Gesù Children's Hospital, IRCCS, Roma, Italy, ² Division of Rheumatology, Bambino Gesù Children's Hospital, IRCCS, Roma, Italy, ³ Translational Cytogenomics Research Unit, Bambino Gesù Children's Hospital, IRCCS, Roma, Italy, ⁴ Diagnostic Immunology Research Unit, Multimodal Medicine Research Area, Bambino Gesù Children's Hospital, IRCCS, Roma, Italy

Haploinsufficiency of A20 (HA20) is an inflammatory disease caused by mutations in the *TNFAIP3* gene classically presenting with Behcet's-like disease. A20 acts as an inhibitor of inflammation through its effect on NF- κ B pathway. Here we describe four consanguineous patients (three sisters and their mother) with a predominantly autoimmune phenotype, including thyroiditis, type I diabetes, hemolytic anemia and chronic polyarthritis. All patients had recurrent oral ulcers, with only 1 patient presenting also recurrent fever episodes, as a classical autoinflammatory feature. Next generation sequencing identified a novel heterozygous frameshift mutation (p.His577Alafs*95) that causes a premature stop codon in the zinc finger domain of A20, leading to a putative haploinsufficiency of the protein. Functional analyses confirmed the pathogenicity of the mutation. The variant was associated with decreased levels of A20 in blood cells. Accordingly, *ex-vivo* lipopolysaccharide (LPS)-stimulated patients' peripheral blood mononuclear cells (PBMCs) showed higher levels of p65 NF- κ B phosphorylation, as well as increased production of the proinflammatory cytokines IL-1 β , IL-6 and TNF- α . Moreover, in agreement with recent observations, demonstrating a role for A20 in inhibiting STAT1 and IFN γ pathways, markedly higher circulating levels of the two IFN γ -inducible chemokines CXCL9 and CXCL10 were detected in all patients. Supporting the findings of a hyperactivation of IFN γ signaling pathway in HA20 patients, patients' monocytes showed higher levels of STAT1 without stimulation, as well as higher phosphorylated (active) STAT1 levels following IFN γ stimulation. In conclusion, our study show that in the clinical spectrum of HA20 autoimmune features may predominate over autoinflammatory features and demonstrate, from a molecular point of view, the involvement of A20 in modulating not only the NF- κ B, but also the IFN γ pathway.

Keywords: *TNFAIP3*, poly-autoimmunity, NF- κ B, IFN γ , HA20

INTRODUCTION

A20 haploinsufficiency (HA20) has been described as an autosomal-dominant-inheritance autoinflammatory disease characterized by Behcet's-like disease symptoms, such as recurrent oral and genital ulcers and inflammatory bowel disease (IBD)-like pattern (1). It is caused by loss of function mutations in the *tumour necrosis factor- α -inducible protein 3* (TNFAIP3) gene that encodes for the A20 protein. A20 is a highly conserved protein composed of two domains: the amino-terminal OTU (ovarian tumour) domain, with a de-ubiquitinase activity, and seven carboxyl-terminal zinc finger domains, with ubiquitin ligase and binding activities. It is involved in the negative regulation of the canonical nuclear factor- κ B (NF- κ B) signaling pathway, which plays fundamental roles in inflammation, immune responses and development. Since Zhou et al. first described HA20 in 2016 (1), several frameshift and nonsense mutations, in both the OTU and zinc fingers domains, have been described (2, 3).

Although HA20 has been first described as an early-onset autoinflammatory disease, recent studies described patients with late-onset presenting with autoimmune features, such as juvenile idiopathic arthritis, rheumatoid arthritis, inflammatory bowel diseases, systemic lupus erythematosus, type 1 diabetes, psoriasis and coeliac disease. To date, the predominant autoimmune phenotype associated with HA20 is not clearly identifiable, as it also varies in family members carrying the same mutation (4).

In this study, we report a novel mutation in the TNFAIP3 gene leading to a predominantly autoimmune phenotype in four subjects (three sisters and their mother) from an Italian family.

PATIENTS AND METHODS

Patients

Patient 1 (Pt1, the index patient) is a 17 years old girl who was seen in our hospital at the age of 5, because of an autoimmune thyroiditis requiring replacement therapy. The history included recurrent oral ulcers, most often minor, since early childhood. At the age of 7 years she presented at the Emergency Room of another hospital due to worsening fatigue and shortness of breath. Hematochemistry revealed severe hemolytic anemia with positive Coombs test (5.3 g/dl) requiring blood transfusion. She was treated with intravenous (IV) immunoglobulin and subsequently with glucocorticoids because of lack of response. Three years later, she presented five relapses of hemolytic anaemia treated again with IV immunoglobulin and glucocorticoids. Because of the frequent relapses in January 2015 she was treated with rituximab. One year after the CD20 depletion treatment, asymptomatic hypogammaglobulinemia was found. Immunoglobulin replacement therapy was started, still ongoing.

When she was 9 year she developed an antinuclear-antibody (ANA) negative polyarthritis (with involvement of wrists, ankles, fingers joints and ankles tendons), treated with intra-articular glucocorticoids and methotrexate. Etanercept was added when

she was 17 age for unsatisfactory disease control after a polyarticular flare affecting the two wrists, the left ankle and several tendons, with good response. After 6 months of therapy she presented an arthritis flare involving only the left ankle treated with glucocorticoid intra-articular injection and no further relapse.

Patient 2 (Pt2) is a 20 years old girl who was admitted to our hospital at the age of 9 because of Type 1 diabetes. Her medical history included, similar to her sister, recurrent oral ulcers since early childhood. In the same hospitalization, autoimmune thyroiditis was diagnosed. She was evaluated for short stature (3° centile for height at that time): a GH secretion test was normal. At the age of 19 she presented with arthritis of both wrists and tenosynovitis of ankles. Treatment with methotrexate and etanercept was started. After 9 months, she does not show signs of active arthritis.

Patient 3 (Pt3) is a 13 year-old girl. She presented oral ulcers since childhood, like her sisters, and reports recurrent febrile episodes associated with cervical lymphadenopathy, not related to infections, between the age of 6 and 8. She had an episode of pneumonia at the age 7 years that resolved with standard therapy. She was evaluated for short stature (3° centile for height); GH secretion test was normal.

Patient 4 (Pt4) is a 46 years old woman, the mother of the three girls described above. She presented recurrent oral and genital painful ulcers since childhood, along with recurrent episode of acute abdominal pain, requiring occasional evaluations at the emergency department, with no definitive interpretation. An asymptomatic autoimmune thyroiditis was diagnosed at the age of 41 following the diagnosis in two of her daughters. She started replacement therapy. Her adult height is 10-20° centile.

The study was approved by the Bambino Gesù Children's Hospital Ethical committee. Written informed consent was obtained from the individual(s) and/or minor(s)' legal guardian/next of kin for the publication of any potentially identifiable images or data included in this article.

Genetics Analysis

DNA was extracted from peripheral blood with QIAgen columns (QIA-symphony DNA minikit, Qiagen, Hilden, Germany) according to the manufacturer's instructions. Concentration and purity of DNA samples were quantified by ND-1000 spectrophotometer (NanoDrop; Thermo Scientific, Waltham, MA, USA) and by FLx800 Fluorescence Reader (BioTek, Winooski, VT, USA).

Trio-based whole-exome sequencing (WES) was performed on genomic DNA by using the Twist Human Core Exome Kit (Twist Bioscience) according to the manufacturer's protocol on a NovaSeq6000 platform (Illumina). The reads were aligned to human genome build GRCh37/UCSC hg19. The BWA Enrichment application of BaseSpace (Illumina) and the TGen software (LifeMap Sciences, Inc.) were used for the variant calling and annotating variants, respectively. Sequence data were carefully analyzed and the presence of all suspected variants was checked in the public databases (dbSNP and Genome Aggregation Database (gnomAD)). Putative disease-

associated sequence variants were distinguished from polymorphisms using the following filtering criteria: an allele frequency below 1% in gnomAD, species conservation of the underlying amino acid and a change in the protein's primary structure. The variants were evaluated by VarSome (5) and categorized in accordance with the ACMG recommendations (6). Variants were examined for coverage and Qscore (minimum threshold of 30) and visualized by the Integrative Genome Viewer (IGV). The datasets presented in this study can be found in online repository (ClinVar: <https://www.ncbi.nlm.nih.gov/clinvar/>). The accession numbers is SUB10618687.

PBMC Isolation

PBMCs were freshly isolated by lymphocyte separation Ficoll centrifugation and cultured in complete RPMI 1640 medium. For ELISA 5×10^5 cells were cultured in 96 well in 200 μ l complete medium. For mRNA and western blotting analyses 1×10^6 cells were cultured in 24 well in 1 ml of complete medium.

Western Blotting

PBMCs isolated from patients and HDs were starved for 2h in RPMI with 0,5% fetal bovine serum (FBS) and then collected for western blotting or stimulated for 30 minutes with lipopolysaccharide (LPS) 0.01 μ g/ml. PBMCs were then washed and lysed with RIPA buffer (Cell Signaling) and protein concentration was measured with BCA Protein assay (Pierce). 30 μ g protein extracts were resolved by TGX precast mini Gels (4568084 BioRAD), transferred to nitrocellulose membranes (Amersham Life Sciences) and probed with antibody to A20 (D13H3), pS536- NF- κ B (3033S), NF- κ B (8242) and GAPDH (5174s), all from Cell Signaling Technology. Blots were developed with the ECL system (Amersham Biosciences) according to the manufacturer's protocol. Band intensity were analyzed with Image LAB software.

RNA Isolation and Quantitative Real-Time PCR

PBMCs were stimulated for 3, 6 and 12 hours with 0.01 μ g/ml of LPS or for 2 hours with 10 ng/ml of Interferon- γ (IFN γ) and mRNA expression levels of the genes of interest were analyzed by Quantitative Real-Time PCR. Total RNA was extracted using Trizol Reagent (Ambion), and cDNAs were obtained using the Superscript Vilo kit (Invitrogen). Real-time PCR assays were performed using TaqMan Universal PCR Master Mix and gene expression assays from Applied Biosystems. Gene expression was normalized using human *HPRT1* as endogenous control. Data were analyzed with the $2^{-\Delta\Delta C_t}$ method and are expressed as arbitrary units (AU).

Enzyme-Linked Immunosorbent Assays (ELISA)

PBMCs were stimulated for 24 hours with 0.01, 0.1 and 1 μ g/ml of LPS and cytokine release in the conditioned media were analyzed by Enzyme-Linked Immunosorbent Assays (ELISAs), with commercially available kits accordingly to manufacturer instructions. Plasma from patients or healthy donors were

analyzed by ELISA. IL-6 (DY206), IL-1 β (DY201), TNF- α (DY210), CXCL9 (DY392) and CXCL10 (DY266) ELISA kits were all purchased from R&D Systems. The detection limits of the assays were 9,38 pg/ml (IL-6), 3,91 pg/ml (IL-1 β), 15,6 pg/ml (TNF- α), 62,5 pg/ml (CXCL9) and 31,25 pg/ml (CXCL10).

Flow Cytometry

PBMCs were treated and analyzed as previously reported (7). Briefly, PBMCs were left unstimulated or stimulated with 10 ng/ml of human recombinant IFN γ (R&D Systems) for 10 minutes at 37°C. Anti-CD3, anti-CD14 and anti-CD16 (all from Becton Dickinson) staining was performed for 20 minutes at 4°C, in order to discriminate the monocyte, neutrophil, natural killer and T cell subpopulations. Whole blood cells were then fixed with Lyse/Fix Buffer 10 min at 37°C and further incubated 10 min at RT with FcBlock 1:200 in Stain Buffer (all from Becton Dickinson). After permeabilization with Perm Buffer II (BD PhosFlow) 20 min at 4°C, samples were stained with antibodies against phosphorylated Tyrosine (701) STAT1 (pSTAT1) and total STAT1 (all from Becton Dickinson) for 20 min at 4°C. Isotype-matched control mAbs were used to determine non-specific background staining. Samples were run on a BD LSRFortessa X-20 instrument (BD Biosciences). Results were expressed as mean fluorescence intensity (MFI) or % of positive monocytes.

Statistical Analysis

Differences between groups were analyzed by the nonparametric Mann-Whitney U test. Significance level for statistical tests was at ** $p < 0.01$ and *** $p < 0.001$ values. Graphpad Prism 9 software was used for statistical analysis and graphs.

RESULTS

We studied an Italian family (**Figure 1A**) carrying a previously unreported mutation in the *TNFAIP3* gene leading to A20 haplo-insufficiency. Disease onset occurred in early childhood in four female members of the same family. Among autoimmune manifestations, thyroiditis and chronic arthritis were present in 3/4 and 2/4 patients, respectively, and diabetes and hemolytic anemia in 1 patient. All patients presented recurrent oral aphthosis, that in 1 patient were associated to genital ulcers; Pt3 was the only with a classical, albeit mild, autoinflammatory phenotype (transient recurrent episodes of fevers) and no autoimmune manifestation up to the age of 14. Patients had stunted growth with final height below or slightly above 3rd percentile. Finally, Pt1 developed hypogammaglobinemia, not associated with recurrent infection, following rituximab administration (**Table 1**).

Next generation sequencing (NGS) analysis was performed first on Pt1 and her parents. A heterozygous c.1727dupC variant in the *TNFAIP3* gene (NM_006290), introducing the frameshift variant p.His577Alafs*95, was identified in the Pt1 and her mother (Pt 4) (**Figures 1B, C**). The variant, located between the zinc finger domains 3 and 4 of the A20 protein (**Figure 1B**),

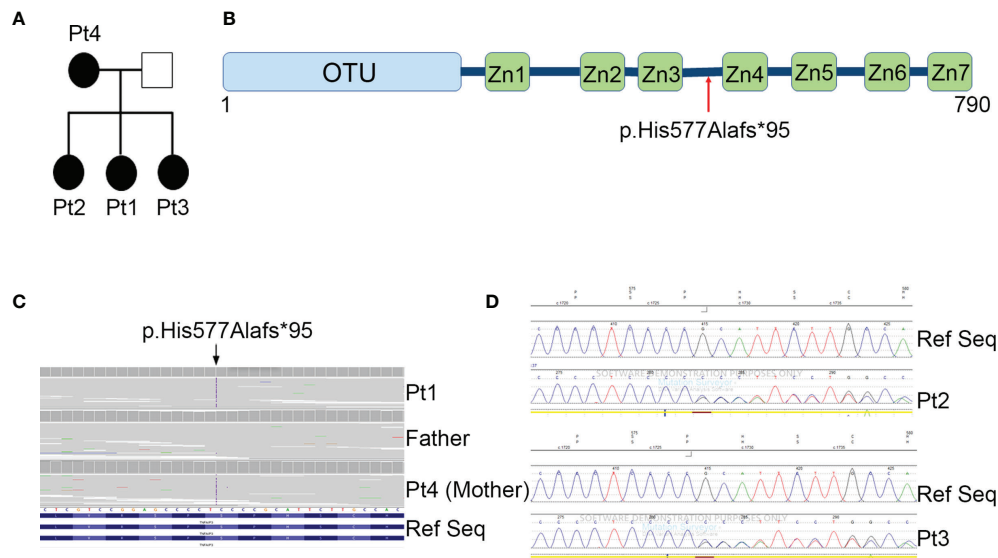


FIGURE 1 | Family pedigree and genetic analyses. **(A)** Pedigree of the family with the heterozygous mutation in *TNFAIP3* gene. **(B)** Schematic diagram of A20 protein and the location of the new identified mutation. OTU, ovarian tumor domain; ZnF 1-7, zinc finger domains. **(C)** Whole exome sequencing identified a novel heterozygous mutation p.His577Alafs*95 in the *TNFAIP3* gene. **(D)** Confirmation of the presence of the mutation in Pt2 and Pt3 by Sanger Sequencing.

was predicted to be damaging by *in silico* tools, since it introduces a premature stop codon leading to a putative haploinsufficiency of the protein. The same frameshift mutation was also present in the two sisters, Pt2 and Pt3, of our proband, as confirmed by Sanger sequencing (**Figure 1D**).

Since this mutation has not been reported before, we determined its functional relevance. We first analyzed by western blot the expression levels of A20 in peripheral blood mononuclear cells (PBMCs). Compared to healthy donors, all the patients showed a strongly reduced expression of A20 in PBMCs (**Figure 2A**).

TABLE 1 | Clinical and laboratory characteristics and treatment of the patients.

Gender	Age at Onset	Autoantibody Positivity	Clinical Manifestations	Therapy
Pt 1 F	Early childhood (less than 2 years)	Ab anti-TG: 1153 U/ml Ab anti-TPO: >3000 U/ml ANA negative	Recurrent oral ulcers Short stature (<3° centile) Autoimmune thyroiditis Polyarthrits Haemolytic anemia	None None L-Thyroxine Intra-articular glucocorticoid injections, methotrexate, etanercept High dose IV Immunoglobulin, high dose glucocorticoids, Rituximab
Pt 2 F	Early childhood (less than 2 years)	Ab anti-TG: 1956 U/ml Ab anti-TPO: >3000 U/ml ANA negative dsDNA negative ENA negative	Hypogammaglobulinemia Recurrent oral ulcers Short stature (3°-25° centile) Autoimmune thyroiditis Oligoarthritis	Substitutive IV immunoglobulin None None L-Thyroxine Intra-articular glucocorticoid injections, methotrexate, etanercept
Pt 3 F	Early childhood (less than 2 years)		Type I diabetes mellitus Recurrent oral ulcers Short stature (<3° centile) Recurrent fever in childhood	Insuline None None None
Pt 4 F	Early childhood (less than 2 years)	Ab anti-TG: 77 U/ml Ab anti-TPO: 1016 U/ml	Recurrent oral and genital ulcers Short stature (10-25°) Autoimmune thyroiditis Recurrent episodes of abdominal pain	None None L-Thyroxine None

Ab anti-TG, anti-thyroglobulin antibodies (normal value <100 U/ml); Ab anti-TPO, anti-thyroperoxidase antibodies (normal value <40 U/ml); IV, intravenous.

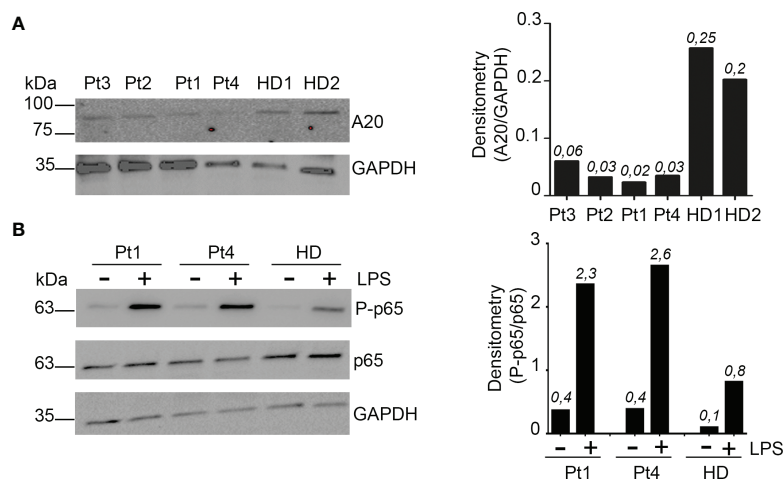


FIGURE 2 | Reduced A20 function *in vivo*. **(A)** Western Blot and densitometric analysis of A20 protein levels in PBMCs isolated from patients (Pt1-4) and 2 healthy donors (HD). GAPDH was used as loading control. Densitometric quantification of A20 was reported (right graph). **(B)** PBMCs isolated from Pt1, Pt4 and one healthy subject (HD) were starved for 2 h in media with 0.5% of FBS and lysed or stimulated for 30 minutes with 0.01 μ g/ml LPS and then lysed. Phosphorylated (S536) p65 NF-kB (P-p65) and total p65 NF-kB protein levels were assessed by Western blot analyses. GAPDH was used as loading control. The phosphorylated-p65 NF-kB/total p65 NF-kB densitometry comparative ratio was also reported (right graph). Similar results were obtained in two independent experiments.

Since A20 is a known critical negative regulator of NF-kB signaling (8), we investigated if A20 decreased levels were associated with a dysregulation of NF-kB activation, by assessing the phosphorylation status of the p65 NF-kB subunit (Serine 536, S536) in unstimulated and LPS-stimulated PBMCs from Pt1 and Pt4. Higher p65 NF-kB (S536) phosphorylation levels were detected in PBMCs isolated from these patients compared to healthy donors (HD), both in unstimulated and LPS-stimulated cells (**Figure 2B**).

To investigate the effects of the upregulation of NF-kB signaling in patients' PBMCs, we analyzed the kinetics of mRNA accumulation of three cytokines known to be induced by NF-kB (9), such as IL-1 β , IL-6 and TNF- α . As shown in **Figure 3A**, we observed that, compared to healthy donors, PBMCs from patients expressed markedly higher mRNA levels of all cytokines analyzed, particularly at shorter times (3 hours) following LPS stimulation. Consistent with these results, when we measured the cytokine levels released in conditioned media of PBMCs stimulated for 24 hours with increasing amount of LPS, we found that patients' PBMCs produced markedly higher levels of IL-1 β , IL-6 and TNF- α , compared to control PBMCs (**Figure 3B**). Interestingly, while in PBMCs from healthy donors there were no substantial differences in the cytokine levels produced following stimulation with increasing concentrations of LPS, in patients' PBMCs we observed a progressive and marked increase in cytokine production, suggesting a persistent NF-kB activation, probably secondary to a defective A20-mediated NF-kB inhibition.

Consistent with observations in the literature, demonstrating a role for A20 in inhibiting STAT1 and showing higher circulating levels of IFN γ inducible chemokines in patients with HA20 and in A20 genetically deficient mice (10, 11), all our patients showed markedly higher circulating levels of CXCL9

and CXCL10 compared to healthy donors (**Figure 4A**). Notably, although high levels of both CXCL9 and CXCL10 were detected in all four patients compared to healthy subjects, Pt1 showed lower levels compared to other family mutated members, possibly due to the ongoing treatments with methotrexate and hydroxychloroquine. The other patients were not receiving any immunomodulatory treatment at time of sampling. To further investigate the activation of the IFN γ signaling pathway, PBMCs of patients were unstimulated or stimulated *ex vivo* with IFN γ and total STAT1 and phosphorylated STAT1 (Tyrosine-701) were evaluated in monocytes. We found markedly high levels of total STAT1 in unstimulated monocytes of all four patients, compared to healthy donors (**Figure 4B**). In addition, following *ex vivo* stimulation with IFN γ , the percentage of monocytes positive for phosphorylated STAT1 (pSTAT1) was marked increase in 3 out of 4 patients, compared to that observed in healthy donors (**Figure 4C**). Accordingly, in *ex vivo* experiments, PBMCs from patients showed markedly higher mRNA expression levels of CXCL9 and CXCL10 in unstimulated condition as well as following stimulation with IFN γ (**Figure 4D**), further supporting the hyperactivation of the IFN γ signaling pathway in HA20 patients.

DISCUSSION

Herein, we describe the clinical features of four family members carrying a novel mutation in the *TNFAIP3* gene leading to HA20. HA20 is an autosomal dominant genetic disease in which an insufficient production of A20 results in a decreased inhibition of the NF-kB signaling pathway. It classically presents with autoinflammatory features, particularly with a Behcet-like disease, often characterized by severe early-onset IBD.

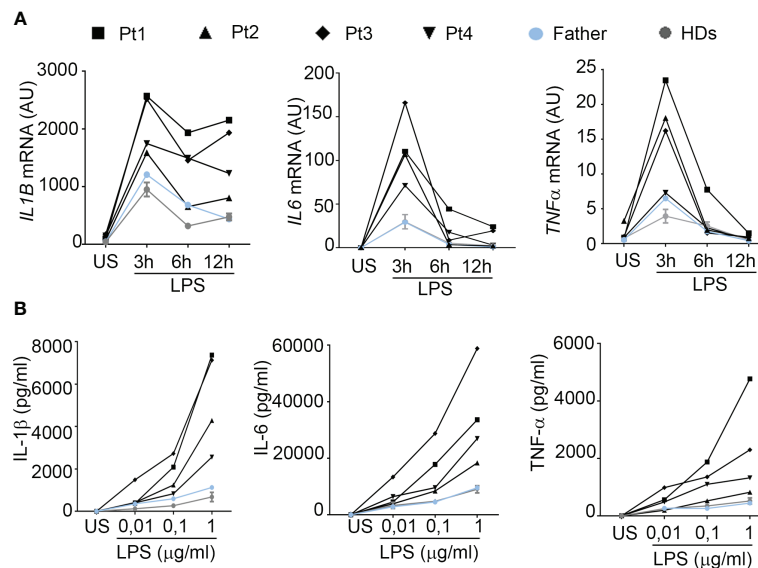


FIGURE 3 | PBMCs from HA20 patients express markedly higher levels of pro-inflammatory cytokines. **(A)** The mRNA expression levels of *IL1B*, *IL6* and *TNF* were evaluated by qPCR analysis in PBMCs from patients (Pt1-4), a relative (father) and 2 healthy donors (HDs) unstimulated (US) or stimulated for the indicated hours h with 0.01 μg/ml of LPS. Results were obtained after normalization with the housekeeping gene *HPR1* and were expressed as arbitrary units (AU). **(B)** PBMCs isolated from patients (Pt1-4), a relative (father) and 4 healthy donors (HDs) were unstimulated (US) or stimulated for 24 hours with 0.01, 0.1 and 1 μg/ml of LPS and IL-1β, IL-6 and TNF-α protein levels were measured in the conditioned media by ELISA.

In addition to gastrointestinal manifestations, muscle-skeletal disorders with arthralgia and arthritis, ocular and skin involvement and recurrent fever are often present.

In contrast, in our family, the clinical picture is predominantly characterized by autoimmune features with the following manifestations: thyroiditis in 3 patients and chronic arthritis in 2 patients. In addition, Pt1 presented with recurrent hemolytic anemia and Pt2 with diabetes mellitus. Only Pt3 presented with recurrent episodes of fevers in childhood. It should be noted that all patients complained of oral ulcers since early childhood, and one patient presented genital ulcers, a typical features of HA20. A short stature is a common characteristic of all affected members.

The association of HA20 with autoimmunity is known in humans, as well as in animal models. Indeed, findings in mice models indicate that A20 plays a crucial role in the development and function of B cells (12). Indeed, loss of A20 in B cells leads to autoimmune pathology in old mice and defects in the generation and/or localization of the mature B cell subsets (13). In humans, the presence of autoantibodies at varying degrees has been described in patients with HA20 (14). Because of the co-occurrence of autoinflammatory and/or autoimmune features in HA20, several patients received a variety of initial diagnoses including autoimmune diseases, such as rheumatoid arthritis, juvenile idiopathic arthritis, autoimmune thyroiditis, systemic lupus erythematosus, inflammatory bowel disease (i.e. Crohn's disease), as well as of autoinflammatory diseases including Behcet's disease and periodic fever with aphthous stomatitis, pharyngitis and adenitis (PFAPA). Indeed, in three out of 4 of our patients anti-thyroid autoantibodies were also found and an initial diagnosis of autoimmune thyroiditis was made.

A20 negatively regulates NF-κB signaling through two mechanisms: a de-ubiquitination activity performed by the N-terminal OTU domain, and an ubiquitin ligation activity performed through its C-terminal Zn finger domains (8). Even if OTU and Zn finger domains of A20 have different biochemical functions and act on different proteins and pathways, their action converges on the inhibition of NF-κB activity. An increase of cytokines production, as well as of phosphorylation levels of NF-κB has been described in patients carrying mutations in both OTU and Zn finger domain (1, 15). Due to the great heterogeneity of clinical and prognostic presentation of HA20 (4), there has been an attempt to associate specific clinical manifestation with the positions of mutations (3). Autoimmune thyroid disorders and musculoskeletal disorders appear to be associated with mutation in the Zn finger domains and patients with Zn finger domain mutations usually present an early onset of the disease (3). However, a clear cut genotype/phenotype correlation has not been established, also due to the fact that most patients with OTU mutations described to date express truncated TNFAIP3 proteins that eliminate all the Zn finger domains.

Several studies highlighted that the spectrum of HA20 clinical manifestations can vary even among patients carrying the same mutation and/or belonging to the same family (15, 16) and that patients with the same pathogenic variant even respond differently to the same treatment regimen (4). Not surprisingly, our patients presented different clinical manifestations of variable degree of severity ranging from a mild (Pt3 and Pt4), moderate (Pt2) to a severe phenotype (Pt1). These data support the obvious hypothesis that additional genetic/environmental mechanisms may have a role in the pathogenesis of HA20.

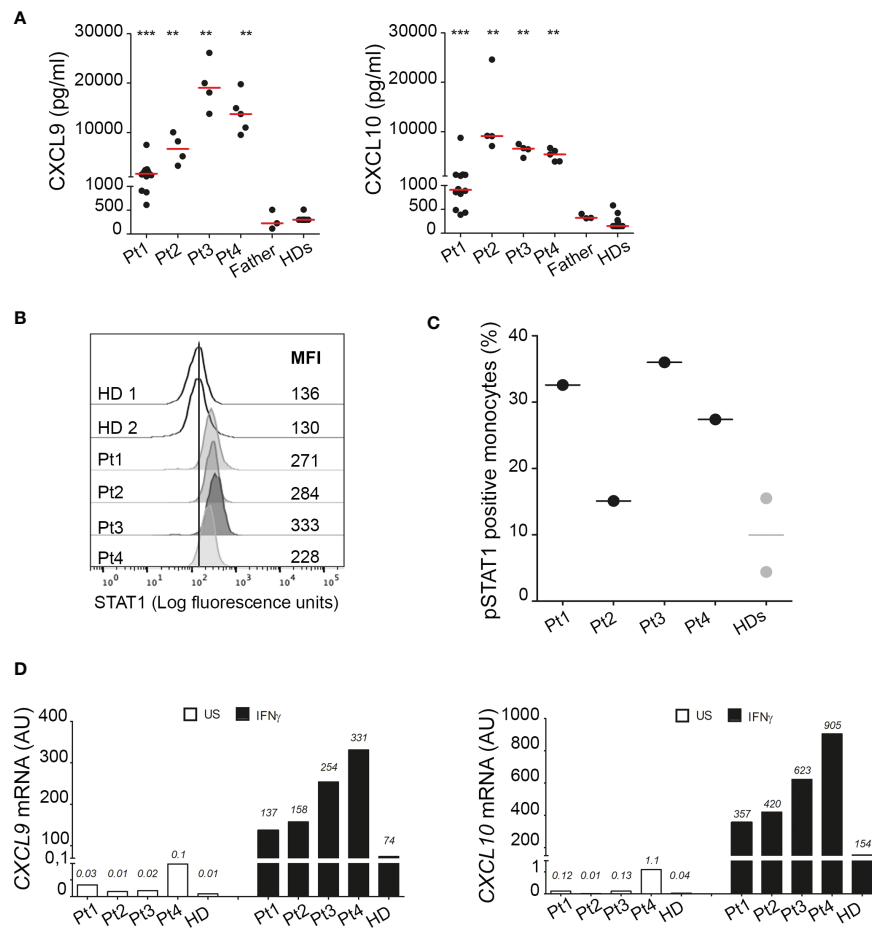


FIGURE 4 | Interferon gamma pathway is upregulated in HA20 patients. **(A)** CXCL9 and CXCL10 levels were measured in plasma samples collected from patients (Pt1-4) during different hospitalizations, from the father and from healthy donors (HD; $n=15$) by ELISA. Red bars indicate sample median. Statistical analyses were performed with Mann-Whitney test comparing each patient with HDs. $**p<0,01$; $***p<0,001$. **(B)** Unstimulated PBMCs from patients (Pt1-4) and two healthy donors (HDs) were stained for total STAT1 levels. Results are reported as STAT1 mean fluorescence intensity (MFI) in monocytes (CD14+ cells). **(C)** PBMCs from patients (Pt1-4) and two healthy donors (HDs) were stimulated for 10 minutes with 10 ng/ml of IFN γ and phosphorylated STAT1 (pSTAT1) levels were detected by flow cytometry. Results were reported as % of pSTAT1 positive monocytes (CD14+ cells). **(D)** PBMCs from patients (Pt1-4) and one healthy donor (HD) were left unstimulated (US, white columns) or stimulated for 2 hours with 10 ng/ml of IFN γ (IFN γ , black columns) and CXCL9 and CXCL10 mRNA levels were analyzed by qPCR. Results were obtained after normalization with the housekeeping gene *HPRT1* and were expressed as arbitrary units (AU). Similar results were obtained in two independent experiments.

No standard treatment has been established for the disease. Most cases seem to respond to glucocorticoids (3), but this therapy is burdened by severe side effects in the long term. The choice of treatment appears to be based on the patient's dominant clinical phenotype. Colchicine, has been reported to be effective in some cases and reports with use of several immunosuppressants, such as methotrexate, cyclosporine-A, hydroxychloroquine and mycophenolate mofetil are present with variable response (3, 17). Because of the excessive production of inflammatory cytokines, cytokine inhibitors (anti-TNF, anti-IL-1, and anti-IL-6) are variably used as second-line treatments (3, 17). In our 2 patients with arthritis, a very satisfactory response to etanercept was observed.

The novel mutation identified in our patients (p.His577Alafs*95) causes the deletion of the A20 C-terminus,

starting from Zn finger 4 domain and including Zn finger domains 4 and 7, which have been reported to be functionally relevant for A20 (18, 19). Consistent with previous observations, PBMCs isolated from our patients also showed higher levels of NF- κ B phosphorylation that are associated with markedly higher production of IL-1 β , IL-6 and TNF- α .

In agreement with recent evidence demonstrating a role for A20 in the inhibition of STAT1 expression in murine myeloid cells and in modulating IFN γ downstream genes (11), we found a marked increase in the circulating levels of the IFN γ -inducible chemokines CXCL9 and CXCL10 in all the patients studied, further supporting the functional relevance of this novel mutation. Consistent with data in mice, (11) we also showed that in circulating monocytes of HA20 patients the levels of total STAT1 are markedly higher than those observed in healthy subjects.

Moreover, we also found that, following *ex vivo* stimulation with IFN γ , the percentage of monocytes expressing phosphorylated STAT1 is higher in patients than in healthy subjects, further demonstrating the hyperactivation of the IFN γ signaling pathway in our HA20 patients. Our results are consistent with recent data showing increased phosphorylation levels of STAT1 and STAT3 (20) and an elevation of the Type I IFN score in the whole blood of some patients with HA20 (21). Altogether, these evidence further support the role of A20 in regulating IFNs signaling pathways and provide the rationale for the therapeutic use of JAK1/2 inhibitors in HA20 patients unresponsive to the conventional treatments (20, 21).

In conclusion, we report a novel pathogenic mutation in *TNFAIP3* leading to HA20. We confirm its functional relevance and demonstrate, that HA20 leads not only to increased NF- κ B activation, but also to hyperactivation of the IFN γ pathway. We confirm that a significant clinical heterogeneity exists even among patients carrying the same mutation. The spectrum of HA20 clinical manifestations is expanding and, as highlighted by our report, autoimmune features may predominate over classical autoinflammatory Behcet-like features. It is tempting to suggest that organ and non-organ specific autoimmunity in the presence of early-onset recurrent oral ulcers should elicit suspicion for HA20.

DATA AVAILABILITY STATEMENT

The original contributions presented in the study are publicly available. This data can be found here: ClinVar: SUB10618687, <https://www.ncbi.nlm.nih.gov/clinvar/>, SUB10618687.

REFERENCES

- Zhou Q, Wang H, Schwartz DM. Loss-Of-Function Mutations in *TNFAIP3* Leading to A20 Haploinsufficiency Cause an Early-Onset Autoinflammatory Disease. *Nat Genet* (2016) 48:67–73. doi: 10.1038/ng.3459
- Ma A, Malynn BA. A20: Linking a Complex Regulator of Ubiquitylation to Immunity and Human Disease. *Nat Rev Immunol* (2012) 12:774–85. doi: 10.1038/nri3313
- Chen Y, Ye Z, Chen L, Qin T, Seidler U, Tian D, et al. Association of Clinical Phenotypes in Haploinsufficiency A20 (HA20) With Disrupted Domains of A20. *Front Immunol* (2020) 11:574992. doi: 10.3389/fimmu.2020.574992
- Yu MP, Xu XS, Zhou Q, Deutch N, Lu MP. Haploinsufficiency of A20 (HA20): Updates on the Genetics, Phenotype, Pathogenesis and Treatment. *World J Pediatr* (2020) 16:575–84. doi: 10.1007/s12519-019-00288-6
- Kopanos C, Tsiolkas V, Kouris A, Chapple CE, Albarca Aguilera M, Meyer R, et al. VarSome: The Human Genomic Variant Search Engine. *Bioinformatics* (2019) 35:1978–80. doi: 10.1093/bioinformatics/bty897
- Richards S, Aziz N, Bale S, Bick D, Das S, Gastier-Foster J, et al. Standards and Guidelines for the Interpretation of Sequence Variants: A Joint Consensus Recommendation of the American College of Medical Genetics and Genomics and the Association for Molecular Pathology. *Genet Med* (2015) 17:405–24. doi: 10.1038/gim.2015.30
- Pascarella A, Bracaglia C, Caiello I, Arduini A, Moneta GM, Rossi MN, et al. Monocytes From Patients With Macrophage Activation Syndrome and Secondary Hemophagocytic Lymphohistiocytosis Are Hyperresponsive to Interferon Gamma. *Front Immunol* (2021) 12:663329. doi: 10.3389/fimmu.2021.663329

ETHICS STATEMENT

The study was approved by the Bambino Gesù Children's Hospital Ethical committee. Written informed consent was obtained from the individual(s) and/or minor(s)' legal guardian/next of kin for the publication of any potentially identifiable images or data included in this article. Written informed consent to participate in this study was provided by the participants' legal guardian/next of kin.

AUTHOR CONTRIBUTIONS

MNR, SF, FB, GP, and AI conceived and designed the work. MNR, IC, VM, CP, SP, and EP performed the experiments. SF, AU, CC, and AI enrolled patients and collected clinical data. MNR, SF, FB, GP, and AI wrote the manuscript. All authors read and approved the final manuscript.

FUNDING

This study was supported by Ricerca Corrente funding from Italian Ministry of Health to FB and GP.

ACKNOWLEDGMENTS

IRCCS Ospedale Pediatrico Bambino Gesù is part of the European Reference Network for Rare Immunodeficiency, Autoinflammatory and Autoimmune Diseases (Project ID 739543).

- Wertz IE, O'Rourke KM, Zhou H, Eby M, Aravind L, Seshagiri S, et al. De-Ubiquitination and Ubiquitin Ligase Domains of A20 Downregulate NF- κ B Signaling. *Nature* (2004) 430:694–9. doi: 10.1038/nature02794
- Liu T, Zhang L, Joo D, Sun SC. NF- κ B Signaling in Inflammation. *Signal Transduct Target Ther* (2017) 2:17023. doi: 10.1038/sigtrans.2017.23
- Moll HP, Lee A, Minussi DC, Da Silva CG, Csizmadia E, Bhasin M, et al. A20 Regulates Atherogenic Interferon (IFN)- γ Signaling in Vascular Cells by Modulating Basal Ifn β Levels. *J Biol Chem* (2014) 289:30912–24. doi: 10.1074/jbc.M114.591966
- De Wilde K, Martens A, Lambrecht S, Jacques P, Drennan MB, Debusschere K, et al. A20 Inhibition of STAT1 Expression in Myeloid Cells: A Novel Endogenous Regulatory Mechanism Preventing Development of Enthesitis. *Ann Rheum Dis* (2017) 76:585–92. doi: 10.1136/annrheumdis-2016-209454
- Das T, Chen Z, Hendriks RW, Kool M. A20/Tumor Necrosis Factor α -Induced Protein 3 in Immune Cells Controls Development of Autoinflammation and Autoimmunity: Lessons From Mouse Models. *Front Immunol* (2018) 9:104. doi: 10.3389/fimmu.2018.00104
- Chu Y, Vahl JC, Kumar D, Heger K, Bertossi A, Wójtowicz E, et al. B Cells Lacking the Tumor Suppressor *TNFAIP3/A20* Display Impaired Differentiation and Hyperactivation and Cause Inflammation and Autoimmunity in Aged Mice. *Blood* (2011) 117:2227–36. doi: 10.1182/blood-2010-09-306019
- Shaheen ZR, Williams SJA, Binstadt BA. Case Report: A Novel *TNFAIP3* Mutation Causing Haploinsufficiency of A20 With a Lupus-Like Phenotype. *Front Immunol* (2021) 12:629457. doi: 10.3389/fimmu.2021.629457
- He T, Huang Y, Luo Y, Xia Y, Wang L, Zhang H, et al. Haploinsufficiency of A20 Due to Novel Mutations in *TNFAIP3*. *J Clin Immunol* (2020) 40:741–51. doi: 10.1007/s10875-020-00792-9

16. Kadowaki T, Ohnishi H, Kawamoto N, Hori T, Nishimura K, Kobayashi C, et al. Haploinsufficiency of A20 Causes Autoinflammatory and Autoimmune Disorders. *J Allergy Clin Immunol* (2018) 141:1485–8.e1411. doi: 10.1016/j.jaci.2017.10.039
17. Berteau F, Rouviere B, Delluc A, Nau A, Le Berre R, Sarabay G, et al. Autosomic Dominant Familial Behçet Disease and Haploinsufficiency A20: A Review of the Literature. *Autoimmun Rev* (2018) 17:809–15. doi: 10.1016/j.autrev.2018.02.012
18. Bosanac I, Wertz IE, Pan B, Yu C, Kusam S, Lam C, et al. Ubiquitin Binding to A20 ZnF4 is Required for Modulation of NF-kappaB Signaling. *Mol Cell* (2010) 40:548–57. doi: 10.1016/j.molcel.2010.10.009
19. Skaug B, Chen J, Du F, He J, Ma A, Chen ZJ. Direct, Noncatalytic Mechanism of IKK Inhibition by A20. *Mol Cell* (2011) 44:559–71. doi: 10.1016/j.molcel.2011.09.015
20. Mulhern CM, Hong Y, Omoyinmi E, Jacques TS, D'arco F, Hemingway C, et al. Janus Kinase 1/2 Inhibition for the Treatment of Autoinflammation Associated With Heterozygous TNFAIP3 Mutation. *J Allergy Clin Immunol* (2019) 144:863–6.e865. doi: 10.1016/j.jaci.2019.05.026
21. Schwartz DM, Blackstone SA, Sampaio-Moura N, Rosenzweig S, Burma AM, Stone D, et al. Type I Interferon Signature Predicts Response to JAK

Inhibition in Haploinsufficiency of A20. *Ann Rheum Dis* (2020) 79:429–31. doi: 10.1136/annrheumdis-2019-215918

Conflict of Interest: The authors declare that the research was conducted in the absence of any commercial or financial relationships that could be construed as a potential conflict of interest.

Publisher's Note: All claims expressed in this article are solely those of the authors and do not necessarily represent those of their affiliated organizations, or those of the publisher, the editors and the reviewers. Any product that may be evaluated in this article, or claim that may be made by its manufacturer, is not guaranteed or endorsed by the publisher.

Copyright © 2022 Rossi, Federici, Uva, Passarelli, Celani, Caiello, Matteo, Petrocchi, Mortari, De Benedetti, Prencipe and Insalaco. This is an open-access article distributed under the terms of the Creative Commons Attribution License (CC BY). The use, distribution or reproduction in other forums is permitted, provided the original author(s) and the copyright owner(s) are credited and that the original publication in this journal is cited, in accordance with accepted academic practice. No use, distribution or reproduction is permitted which does not comply with these terms.



Negative Regulation of the IL-1 System by IL-1R2 and IL-1R8: Relevance in Pathophysiology and Disease

Domenico Supino¹, Luna Minute^{1,2}, Andrea Mariancini^{1,2}, Federica Riva³, Elena Magrini¹ and Cecilia Garlanda^{1,2*}

¹ Department of Immunology and Inflammation, IRCCS Humanitas Research Hospital, Rozzano, Italy, ² Department of Biomedical Science, Humanitas University, Pieve Emanuele, Italy, ³ Department of Veterinary Medicine, University of Milan, Milan, Italy

OPEN ACCESS

Edited by:

Shrikant R. Mulay,
Central Drug Research Institute (CSIR),
India

Reviewed by:

Murray Charles Henry Clarke,
University of Cambridge,
United Kingdom
Bangwei Wu,
Fudan University, China

*Correspondence:

Cecilia Garlanda
cecilia.garlanda@humanitasresearch.it

Specialty section:

This article was submitted to
Molecular Innate Immunity,
a section of the journal
Frontiers in Immunology

Received: 29 October 2021

Accepted: 03 January 2022

Published: 08 February 2022

Citation:

Supino D, Minute L, Mariancini A,
Riva F, Magrini E and Garlanda C
(2022) Negative Regulation
of the IL-1 System by IL-1R2
and IL-1R8: Relevance in
Pathophysiology and Disease.
Front. Immunol. 13:804641.
doi: 10.3389/fimmu.2022.804641

Interleukin-1 (IL-1) is a primary cytokine of innate immunity and inflammation. IL-1 belongs to a complex family including ligands with agonist activity, receptor antagonists, and an anti-inflammatory cytokine. The receptors for these ligands, the IL-1 Receptor (IL-1R) family, include signaling receptor complexes, decoy receptors, and negative regulators. Agonists and regulatory molecules co-evolved, suggesting the evolutionary relevance of a tight control of inflammatory responses, which ensures a balance between amplification of innate immunity and uncontrolled inflammation. IL-1 family members interact with innate immunity cells promoting innate immunity, as well as with innate and adaptive lymphoid cells, contributing to their differentiation and functional polarization and plasticity. Here we will review the properties of two key regulatory receptors of the IL-1 system, IL-1R2, the first decoy receptor identified, and IL-1R8, a pleiotropic regulator of different IL-1 family members and co-receptor for IL-37, the anti-inflammatory member of the IL-1 family. Their complex impact in pathology, ranging from infections and inflammatory responses, to cancer and neurologic disorders, as well as clinical implications and potential therapeutic exploitation will be presented.

Keywords: inflammation, toll-like-receptors, negative regulation, innate immunity, interleukin 1

INTRODUCTION

The pro-inflammatory cytokine interleukin-1 (IL-1) was discovered during the 1970s and recognised for its functions in inflammation, in particular in fever, lymphocyte activation, and hematopoiesis (1). Gene cloning and molecular identification of IL-1- and IL-1-receptor-related molecules allowed the identification of the entire IL-1 family, which is now considered a “system” comprising evolutionarily conserved ligands and receptors. A new nomenclature of the family receptors has been recently proposed and reported here, followed by previously used names. The IL-1 system includes ligands endowed with agonist activity (IL-1 α , IL-1 β , IL-18, IL-33, IL-36 α , IL-36 β , and IL-36 γ), receptor antagonists (IL-1Ra, IL-36Ra, and IL-38) and an anti-inflammatory cytokine (IL-37), and receptors acting as signalling molecules (IL-1R1, IL-1R4/ST2, IL-1R5/IL-18R α , IL-1R6/

IL-1Rrp2/IL-36R), accessory proteins (IL-1R3/IL-1RAcP, IL-1R7/IL-18R β), decoy or negative regulatory receptors (IL-1R2, IL-1R8/SIGIRR/TIR8). Finally, the system includes receptors which are still considered orphan or whose function is poorly defined (IL-1R9/TIGIRR-2, IL-1R10/TIGIRR-1).

After gene transcription and translation in response to inflammatory signals or tissue damage, ligands of the IL-1 family, in particular IL-1 β and IL-18, remain in the cytoplasm as precursors, and are then cleaved intracellularly by the inflammasome and Caspase-1 (2), or processed extracellularly by proteases, such as neutrophil protease proteinase-3, elastase, matrix metalloprotease 9 and granzyme B, reaching their optimal biological activity. In contrast with other members of the family, IL-1 α is constitutively expressed by several cell types, and can act as an alarmin also in its precursor form, when released upon tissue damage or exposed as an integral membrane protein (3–5).

IL-1-family receptors have a structure comprising a ligand-binding extracellular portion consisting of three Ig-like domains, and an intracellular TIR domain (originally an acronym for Toll/IL-1-resistance and now for Toll/IL-1R domain), which is essential for signaling via the MyD88 adaptor and shared by TLRs. Upon ligand-binding, the main receptor chain and the accessory protein chain assemble in a heterodimer and the TIR domains activate a phylogenetically conserved signaling cascade. The signaling pathway includes the TIR-containing adaptor molecule MyD88, downstream protein kinases (e.g. IL-1R associated kinases (IRAKs), and tumor necrosis factor receptor-associated factor 6 (TRAF6)) and leads to NF- κ B translocation to the nucleus and activation of mitogen-activated protein kinases (MAPKs), such as p38, c-Jun N-terminal kinases (JNKs) and extracellular signal-regulated kinases (ERKs), resulting in amplification of innate immunity and inflammation (6).

Five signaling receptor complexes, constituted by a main receptor chain and an accessory receptor chain, are responsible of cell activation after the interaction with IL-1 family members: the IL-1 receptor (IL-1R1 and IL-1R3/IL-1RAcP) which binds IL-1 α and IL-1 β ; the IL-33 receptor (IL-1R4/ST2 and IL-1R3/IL-1RAcP); the IL-18 receptor (IL-1R5/IL-18R α and IL-1R7/IL-18R β); the IL-36 receptor (IL-1R6/IL-1Rrp2 and IL-1R3/IL-1RAcP) which binds IL-36 α , β and γ ; and the recently identified IL-37 receptor (IL-1R5/IL-18R α and IL-1R8).

The IL-1 system is generally associated with inflammation and innate immunity. However, the members of this family, in particular IL-1, IL-33 and IL-18, are now known to play broader and complex roles, which include orienting innate immunity and inflammation in response to microbial or environmental challenges, and promoting differentiation and polarization of myeloid cells and innate or adaptive lymphoid cells.

Phylogenetic analysis showed that agonists, receptor antagonists, anti-inflammatory molecules and IL-1 receptor family members coevolved, since most of them (IL-1 β , IL-1Ra, the IL-36 subgroup, IL-38 and IL-37, IL-18) are present in all vertebrates (7). This suggests the relevance in evolution of IL-1 system regulation, mediated by antagonists and anti-inflammatory cytokines, as well as by decoy or regulatory

receptors. Among these, IL-1Ra and IL-36Ra are receptor antagonists that compete with the agonists IL-1 and IL-36 for the interaction with IL-1R1 and IL-1R6, respectively, thus reducing their activity (2), whereas IL-18BP is a soluble molecule that binds IL-18, preventing the interaction with its receptor (8). IL-1R2 lacks a signaling TIR domain and acts in a membrane or soluble form as a decoy receptor for IL-1 (9). IL-1R8, also known as TIR8 or SIGIRR, behaves as a negative regulator of the signal transduction by other members of the family, by interfering with the association of TIR-containing adaptor molecules to the receptor complex (10). In addition, in association with IL-1R5/IL-18R α , IL-1R8 has been shown to act as co-receptor for the anti-inflammatory cytokine IL-37 (11), thus opening several new lines of research on the role of IL-1R8 in immunopathology.

Decoy receptors are also strategies of immune evasion adopted by pathogens. For instance, DNA viruses encode proteins homologous to mammal decoy receptors; in particular, Poxviruses express a soluble version of IL-1R (12). In addition, several bacteria (e.g. *Brucella melitensis*, *Escherichia coli*, *Salmonella enterica*, *Pseudomonas denitrificans* and *Pseudomonas aeruginosa*) have evolved TIR-containing proteins (Tcps) that dampen TIR-related pathways (13–16). These data suggest that genomic recombination events originated pathogens endowed with anti-inflammatory molecules from the host genome, which may favor infection and pathogen persistence.

Here we review the regulatory roles of IL-1 receptor family members, focusing on IL-1R2, the first “decoy” receptor identified, and IL-1R8, which being expressed by different cell types and acting as negative regulator of several IL-1 family members, as well as of TLRs, has pleiotropic functions in several pathophysiological contexts involving inflammation and innate and adaptive immune responses.

THE DECOY RECEPTOR IL-1R2

IL-1R2 Mode of Action

The *IL-1R2* gene is located in chromosome 2, in the locus including the IL-1R cluster, e.g. IL-33, IL-18, and IL-36 receptors. Like other IL-1R family members, IL-1R2 protein is composed of an extracellular portion containing three extensively glycosylated immunoglobulin (Ig)-like domains, and showing 28% amino-acid homology with IL-1R1 extracellular portion. But in contrast with the other members of the family, IL-1R2 lacks the characteristic intracellular TIR domain, that is replaced by a 29 amino acid-long tail. Due to this peculiarity, this receptor is unable to initiate signal transduction following the interaction with its ligands (9, 17).

IL-1R2 affects several steps along the IL-1-mediated signaling cascade (**Figure 1**). First, IL-1R2 acts as dominant negative molecule since it prevents the formation of IL-1R1//IL-1R3 complex by sequestering IL-1R3 (9, 18, 19). Then, IL-1R2//IL-1R3 competes with IL-1R1//IL-1R3 for the interaction with the

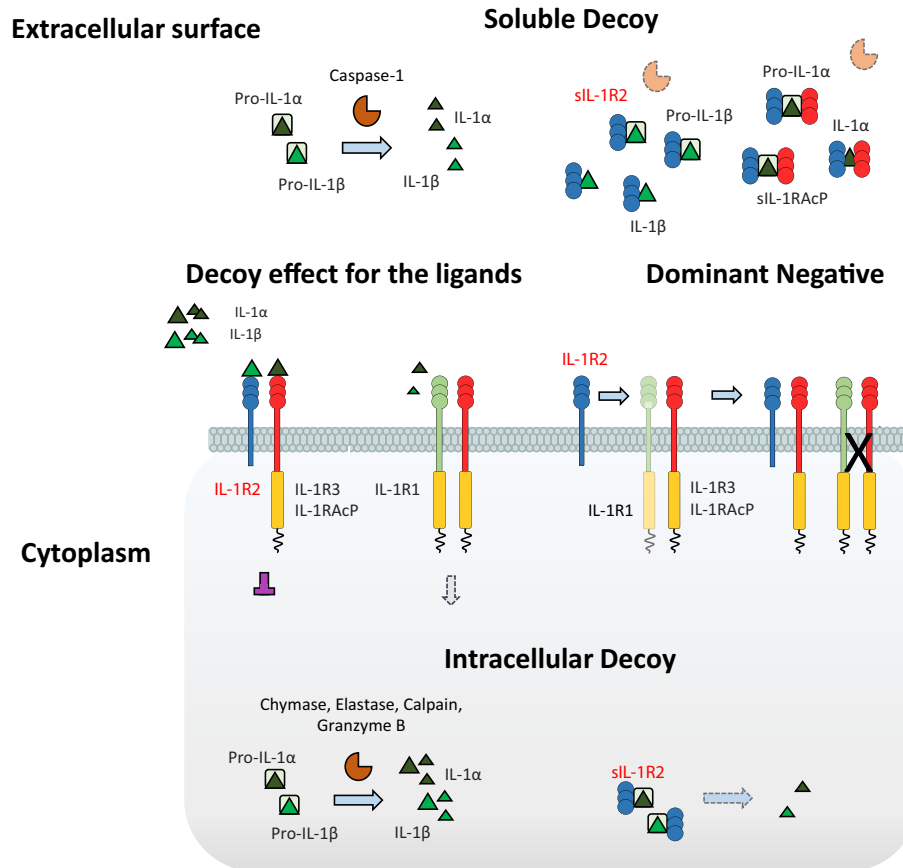


FIGURE 1 | Negative regulation of IL-1-mediated pathways by IL-1R2. IL-1R2 differs from the other ILRs for the absence of the characteristic intracellular TIR domain, thus being incapable of signaling. IL-1R2 influences several mechanisms involved in the IL-1-mediated signaling cascade. IL-1R2 interacts with IL-1R3, acting as a dominant negative and impeding the formation of the IL-1R1/IL-1R3 signaling receptor complex; then, IL-1R2/IL-1R3 prevents the interaction between the ligands and the IL-1R1/IL-1R3 complex, by competitive binding to the pro-inflammatory cytokines IL-1α and IL-1β, thus acting as a decoy for the ligands. In addition, sIL-1R2 acts as a soluble decoy by binding IL-1α and IL-1β, as well as pro-IL-1β, blocking its enzymatic cleavage by caspase-1. The interaction of sIL-1R2 with the soluble form of IL-1R3 further increases the affinity for the ligands. Finally, in cytosol soluble form, IL-1R2 regulates the pro-inflammatory activity of IL-1α by preventing the enzymatic cleavage of pro-IL-1α, acting as an intracellular decoy.

ligands, since both receptor complexes recognize the pro-inflammatory cytokines IL-1α and IL-1β (20, 21). In addition, the enzymatic cleavage of IL-1R2 or alternative splicing generate a soluble form of the receptor (sIL-1R2) that exhibits anti-inflammatory activity by sequestering IL-1 (22–25). The enzymatic cleavage of IL-1R2 is mediated by the metalloproteinase ADAM17, which is activated by pro-inflammatory stimuli such as TNFα, LPS, leukotriene B4 and fMLF (26–28). sIL-1R2 is physiologically released into the bloodstream, where it binds IL-1α and IL-1β (18, 29), as well as pro-IL-1β preventing its enzymatic cleavage by caspase-1 (30). The interaction of sIL-1R2 with the soluble form of IL-1R3 (detectable at high circulating concentration, 300ng/ml) further increases the binding affinity for pro-IL-1β. In addition, cytosolic IL-1R2 interacts with pro-IL-1α preventing its enzymatic cleavage by calpain and other inflammatory proteases, thus tuning IL-1α-dependent sterile inflammation (31). This complex is abrogated by caspase-1 which cleaves IL-1R2,

allowing cleavage and secretion of IL-1α and restoration of its activities. Low intracytoplasmic expression of IL-1R2 was described in vascular smooth muscle cell (VSMC) and activated macrophages and was considered implicated in necrosis-associated inflammation (31).

Recently, a cell-surface pro-form of IL-1α (csIL-1α) was identified in macrophages (32). IL-1R2 and glycosylphosphatidylinositol (GPI) were reported to anchor csIL-1α on the plasma membrane restraining its activation and release. IL-1R2-deficient Bone Marrow-Derived Macrophages (BMDMs) displayed low levels of csIL-1α, highlighting the contribution of IL-1R2 in tethering IL-1α. Moreover, IL-1α trafficking from the cytoplasm to the plasma membrane was specifically inhibited by the stimulation with IFNγ, suggesting that macrophage polarization plays a crucial role in the regulation of csIL-1α (32).

Collectively, these studies show that IL-1R2 may regulate IL-1 through different mechanisms, acting at the cell membrane level, intracellularly or as a soluble molecule.

IL-1R2 Expression

IL-1R2 was first identified on neutrophils, monocytes, macrophages, dendritic cells (DCs) and B cells in both human and mice (26, 33). Polarization of myeloid cells strongly influences the expression of IL-1R2, emphasizing its relevance in immune response orientation. In particular, “M2” anti-inflammatory stimuli such as IL-4, IL-13, IL-10, IL-27, glucocorticoid hormones, prostaglandins and aspirin up-regulate IL-1R2 (9, 34–38). In contrast, stimulation with “M1” pro-inflammatory molecules (e.g. LPS, IFN γ and TNF α), chemoattractants and reactive oxygen intermediates leads to down-regulation of IL-1R2 (22, 28).

Regulation of IL-1R2 expression has been described in different cell types as a mechanism which counterbalances exacerbated inflammation in response to exogenous stimuli. For instance, up-regulation of IL-1R2 in microglial cells and brain endothelial cells attenuated central nervous system (CNS) inflammation in experimental models of IL-1 β -induced-neurotoxicity (e.g. central administration of IL-1 β , kainic acid administration, cerebral ischemia) (39–41). Human atherosclerotic vessels and monocytes/macrophages were reported to express low levels of IL-1R2 in hyperlipidemic patients (42). Moreover, IL-1R2 was down-regulated in THP-1 cells stimulated with acetylated low density (ac-LDL) and very low density (VLDL) lipoproteins, suggesting a mechanistic link between familial hyperlipidemia and susceptibility to IL-1 β -mediated inflammation (42).

In the context of inflammation-dependent bone remodeling, IL-1R2 was poorly expressed by large osteoclasts, a cell population involved in exacerbation of bone loss in response to IL-1, compared to small osteoclasts (43). Similar observations have been reported in osteoarthritis (OA), a disease in which IL-1 β contributes to joint inflammation and progressive tissue destruction. Human OA chondrocytes, synovial and epithelial cells express low levels of IL-1R2 on the cell membrane. However, sIL-1R2 significantly inhibited the pro-inflammatory activity of endogenous IL-1 β , thus influencing proteoglycan biosynthesis, as well as nitric oxide (NO) and prostaglandin E2 (PGE2) production in immortalized cell lines and chondrocytes from OA patients (44), confirming its anti-inflammatory role.

Complex and sometimes conflicting results have been reported on IL-1R2 expression by lymphocytes. Regulatory T cells (Tregs) have been shown to express IL-1R2 following TCR stimulation (45). In the mouse, IL-1R2⁺ was expressed by a subset of activated Tregs which recirculate from thymus to tissues. By inhibiting IL-1 β , this subset contributed to thymus-derived FOXP3⁺ Treg maturation (46). Ritvo et al. showed that IL-1R2 is expressed by a subset of FOXP3⁺ Follicular regulatory T (Tfr) cells and that it contributed in tuning IL-1 β -dependent activation of Follicular helper T (Tfh) cells, as well as their proliferation and cytokine production, thus limiting the germinal center (GC) reaction. Flow cytometric analysis confirmed that Tfr cells of human lymphoid tissues express IL-1R2, which in contrast with previous studies, was not detected in Treg (47).

In association with IL-23, IL-1 promotes IL-17 production by human and murine T cells, contributing to Th17-related diseases

(10). IL-1R2 was shown in a subset of TCR-stimulated IL-1R1⁺ CD4⁺ T cells, and to regulate Th17 functional activation by limiting IL-1 β responsiveness. In this context, IL-1R2 expression is regulated by the NFAT/FOXP3 complex which binds to the IL-1R2 promoter (48). Since IL-1R2 may be expressed by both Th17 cells and Tregs, based on these results, IL-1R2 has been proposed to be involved in the plasticity of these cells, in particular in the trans-differentiation of Th17 into Treg and contributing to the resolution of inflammation (48, 49).

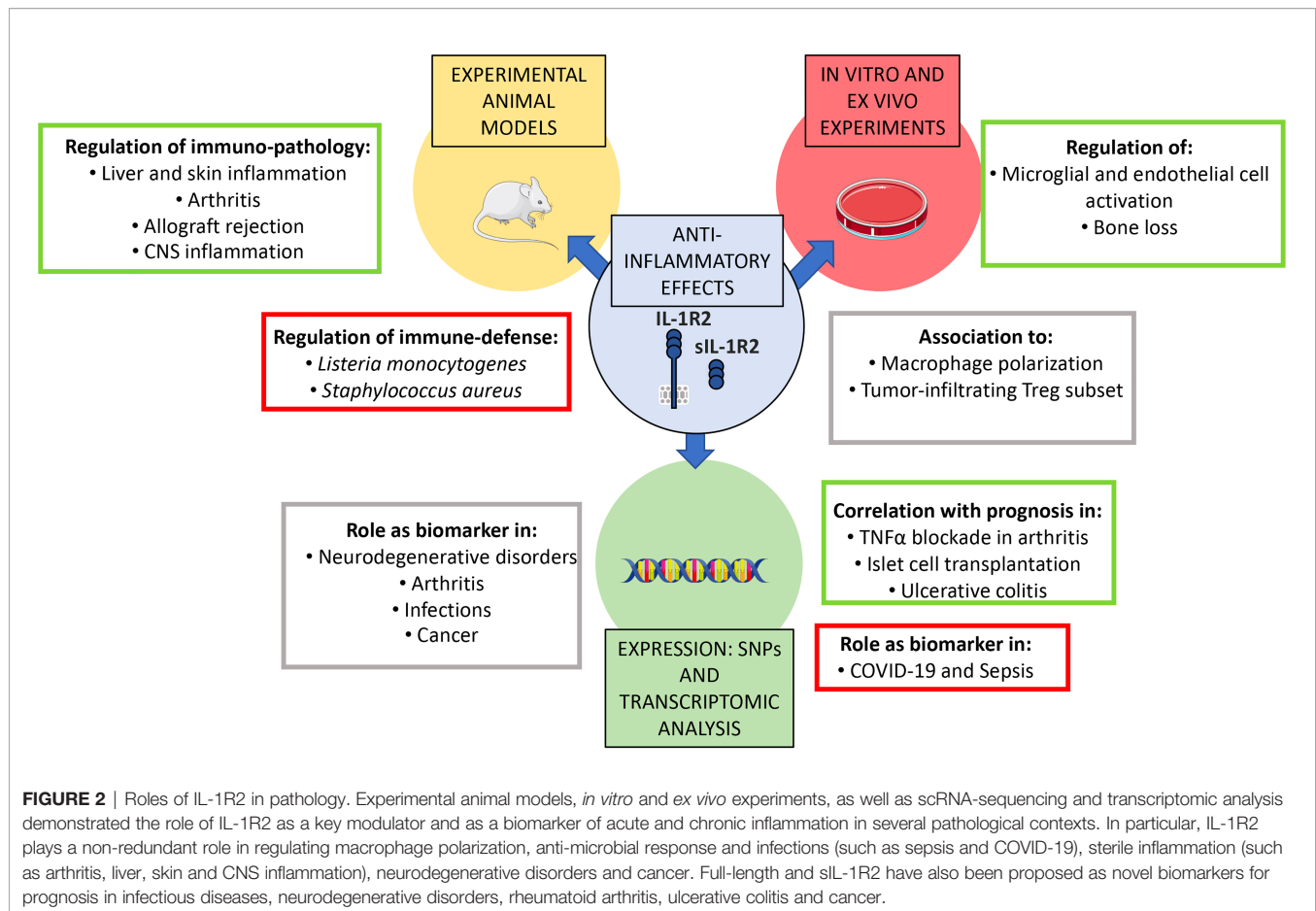
Taking advantage of single cell-RNA (scRNA) sequencing, it has been shown that tumor-infiltrating Tregs express high levels of IL-1R2 compared to other lymphocytes, in particular in breast, colorectal or non-small-cell lung cancers (50, 51). Conversely, low percentage of IL-1R2⁺ Treg cells was reported among circulating CD45RO⁺ lymphocytes from colorectal cancer patients (52). IL-1R2⁺ Treg clonality was investigated by combining scRNA-sequencing with TCR sequencing in an experimental model of skin graft, mimicking human papillomavirus (HPV)-associated epithelial hyperplasia (53). This inflammatory condition was associated with increased recruitment of non-antigen specific Tregs, which displayed two major functional states characterized by high expression of *Il1r2* or *Klrg1*, and associated with a tumor-infiltrating and a tissue-resident signature, respectively (53). Analysis of Treg heterogeneity by scRNA-sequencing revealed a subset of potent immunosuppressive cells governed by the transcription factor IRF-4 in non-small-cell lung cancer (NSCLC), which expressed high levels of IL-1R2 (54). Along the same line, in another scRNA-sequencing study of NSCLC, IL-1R2 was one of the most upregulated gene in a cluster of tumor antigen experienced Treg cells characterized by the expression of TNFRSF9⁺ (4-1BB) and was associated with poor prognosis (55). Collectively, these results suggest that IL-1R2 expression is associated with specific Treg cell clusters, representing differential maturation or activation states, developed in pathological conditions, in particular in cancer. However, the stimuli that promote IL-1R2 expression in tumor-infiltrating Treg cells and the function of IL-1R2 in this subset are still to be identified.

Finally, IL-1R2 was induced by IL-33 in Group 2 Innate lymphoid cells (ILC2s) and was associated with decreased *Il5* and *Il13* transcripts following IL-33 stimulation, suggesting it acts as an activation-induced negative regulatory feedback mechanism that decreases ILC2 responsiveness to IL-33 (56).

IL-1R2 in Infections

Even though inflammation is necessary to fight infections, deregulated immune reactions contribute to infection severity leading to tissue damage and spreading of pathogens from compartmentalized anatomical sites to circulation (57). Indeed, contrasting results emphasize the context-dependent role of IL-1 β -mediated inflammation and regulation by IL-1R2 in different infective conditions, as described below (Figure 2).

In an experimental model of *Listeria monocytogenes* infection, higher frequency of bone marrow (BM) CD115^{dim}IL-1R2⁺ monocytes was reported in lethal versus sub-lethal infections (58). In particular, up-regulation of IL-1R2 was associated with



reduced production of IL-6 and ROS after stimulation with LPS, suggesting IL-1R2 contributes to the behavior of monocytes, which act as Trojan horses rather than bactericidal effector cells in this infection (58). In addition, *Staphylococcus aureus* was reported to evade from the immune surveillance by affecting the circulating levels of sIL-1R2 protein (59). Indeed, the virulence factor protein A triggered IL-1R2 shedding from monocytes and neutrophils through the activation of ADAM17. High levels of sIL-1R2 attenuated IL-1 β -mediated inflammation and the anti-microbial response, including the production of IFN γ and TNF α (59). *Porphyromonas gingivalis* infection, which is associated with oral squamous cell carcinoma (OSCC), influenced myeloid polarization favoring the “M2”-like phenotype in macrophages and the upregulation of IL-1R2 and protumor molecules in cancer cells (60).

A scRNA-sequencing study of urinary-tract infection (UTI) patients identified IL-1R2 as one of the markers of a subset of CD14⁺, HLA-DR^{low} monocytes, which expand in different sepsis cohorts (61). In addition, IL-1R2⁺ cells were functionally exhausted as suggested by poor TNF α production upon stimulation with LPS. By mimicking sepsis-induced myelopoiesis, it was shown that IL-1R2⁺ monocytes originate from bone marrow mononuclear cells differentiated/activated by pathogen associated molecular patterns (PAMPs) (61). Along the same line, analysis of immune cells collected from COVID-19 patients indicated that “sepsis-

associated” myeloid cells significantly increased in COVID-19 patients (62). As described in sepsis, HLA-DR^{low} IL-1R2⁺ cells showed impaired activation upon stimulation with LPS, suggesting that monocytes underwent function exhaustion as a consequence of the viral infection (62). Whether IL-1R2 is only a marker of monocyte dysfunction or is functionally implicated in this cell state, is still to be defined.

IL-1R2 in Sterile Inflammation

Over the past decade, the biological role of IL-1R2 in the regulation of inflammation has been investigated by taking advantage of IL-1R2-deficient or overexpressing mice and experimental models of inflammatory diseases (Figure 2). Pioneering experiments demonstrated that transplantation of sIL-1R2-secreting keratinocytes ameliorated collagen-induced arthritis in mice (63). In agreement with this observation, increased susceptibility to arthritis was confirmed in *Il1r2*^{-/-} mice, which was associated with increased production of inflammatory mediators such as IL-6, CXCL2, NOS2, and IL-1 β by IL-1R2-deficient macrophages (64). The relevance of IL-1R2 in tuning inflammation was further highlighted in the K/BxN serum transfer arthritis model (65). Neutrophils express high levels of IL-1R2, but no significant difference in the effector functions of IL-1R2-deficient neutrophils was reported. However, neutrophils were shown to act in trans by releasing

sIL-1R2, which in turn inhibited IL-1 β -mediated activation of fibroblasts, thus regulating the expression of inflammatory molecules (e.g. IL-1 β , IL-6, CXCL-1 and CXCL-2) in ankles. In contrast, IL-1R2-deficiency did not affect severity and mortality following acute administration of IL-1 β or LPS, suggesting that IL-1R2 is primarily involved in regulating local inflammation (65). In support of this concept, IL-1R2 was described as a critical molecule in resolving liver inflammation (66). In particular, neutrophils up-regulated IL-1R2 in a liver injury model and contributed to protecting mice from hepatic deterioration, as confirmed by the adoptive transfer of this subset in the early stage of liver damage (66).

In experimental models of skin inflammation, constitutive expression of IL-1R2 by transgenic keratinocytes was associated with reduced production of granulocyte/macrophage colony-stimulating factor (GM-CSF) upon stimulation with IL-1 β (67). Moreover, PMA-induced vascular permeability was reduced in IL-1R2 transgenic mice (67). In an experimental model of endometriosis, sIL-1R2 inhibited the expression of adhesion molecules (e.g. α v and β 3 integrins), vascularization and tissue growth of transplanted human endometrium in nude mice (68).

Overexpression of IL-1R2 in the heart ameliorated cardiac allograft survival by controlling the production of pro-inflammatory mediators (e.g. IL-1 β , TNF α , prostaglandin E2 synthase, cyclooxygenase, and CCL1) and Th17 polarization (69, 70). Recently, the transcription factor PAX6 was demonstrated to regulate IL-1R2 in cardiac fibroblasts. PAX6 promoted the expression of the anti-fibrotic factors IL-1R2 and CXCL10 and downregulated the pro-fibrotic molecule TGF β 1. In contrast, angiotensin II repressed PAX6/IL-1R2 thus triggering differentiation of fibroblast and cardiac fibrosis (71).

IL-1R2 in Human Cancer

IL-1 is involved in carcinogenesis and metastasis, contributing to oncogene-driven and microenvironment-driven cancer related inflammation (72). Several studies investigated IL-1R2 expression in cancer cells or in the tumor microenvironment, to elucidate whether the IL-1R2 could be involved in tuning IL-1-dependent cancer-related inflammation. Data generated until now show that IL-1R2 is generally up-regulated in tumor tissue (Figure 2). In particular, *IL1R2* gene was up-regulated in pancreatic ductal adenocarcinoma (PDAC) and was proposed to protect cancer cells from apoptosis induced by IL-1 (73). In addition, *IL1R2* was included in a signature consisting of 9 genes that predicted tumor stages and survival of PDAC patients (74). In acute myeloid leukemia (AML), *IL1R2* gene expression was associated with bad prognosis (75), in ovarian cancer, *IL1R2* was upregulated in recurrent compared to primary cancer (76) and in prostate the molecule was expressed in prostatic cancer cells but not in normal cells (77). In gastric cancer, high expression of IL-1R2 in tumor tissue and increased levels of sIL-1R2 in plasma were associated with poor prognosis (78). Moreover, gastric cancer ascites scRNA-seq analysis suggested that IL-1R2-expressing tumor cells contributed in tuning tumor-associated macrophage-dependent IL-1 β -mediated inflammation (79).

In addition, as reported above, IL-1R2 recently emerged as a tumor-infiltrating Treg associated marker in scRNA sequencing

studies, in breast, colorectal or non-small-cell lung cancers, together with several immune-checkpoints (50, 51). However, further studies are needed to elucidate the functional role of IL-1R2 in tumor-infiltrating Treg cells and other immune cells.

Collectively, these results suggest that IL-1R2 is induced in cancer cells, often correlating with bad prognosis, and in tumor infiltrating leukocytes. However, genetic analyses in mouse or humans formally proving the actual role of IL-1R2 in cancer are still lacking. In particular, functional studies are needed to address whether IL-1R2 is part of a signature associated with immunosuppression as suggested by data on Tregs, or whether its induction reflects cancer-related inflammation, thus explaining the link with poor prognosis.

IL-1R2 as a Potential Prognostic Biomarker

The soluble form of IL-1R2 is released from the cells in inflammatory conditions. For this reason, sIL-1R2 has been investigated as a potential biomarker of inflammatory disease. Results collected over the last years show that several inflammatory diseases are associated with increased release of sIL-1R2 (Figure 2). In particular, high concentration of circulating sIL-1R2 was reported in necrotizing enterocolitis (80), acute respiratory distress syndrome (81), acute meningococcal infection (82), Dengue (83) and sepsis (84). In these conditions, sIL-1R2 often reflected the severity of the condition.

In other contexts, such as rheumatoid arthritis, sIL-1R2 concentration negatively correlated with the severity of the condition, indicating that endogenous sIL-1R2 may constitute a natural anti-inflammatory factor in chronic polyarthritis (85). In agreement, monocyte production of sIL-1R2 correlated with favorable prognosis and efficacy of TNF α blockade with Etanercept in arthritis (86). Similarly, in multiple sclerosis, sIL-1R2 concentration increased in cerebrospinal fluid in response to steroid therapy, suggesting a beneficial effect of the molecule (87). Finally, islet transplantation outcome and insulin independency positively correlated with IL-1R2 expression (88).

At the transcriptional level, *IL1R2* was part of a signature related to myeloid cell activation which was highly expressed in non-responder Kawasaki patients following immunoglobulin infusion (89), and of a signature associated with immune infiltrate in acute myocardial infarction (90). Finally, transcriptional and protein analysis showed that IL-1R2 was a favorable prognostic marker in ulcerative colitis, being up-regulated in intestinal mucosal cells from ulcerative colitis patients in remission phase (91).

Collectively, these studies indicate that IL-1R2 is induced in several conditions, but that the link with prognosis or severity of the disease is variable, possibly depending on the underlying pathogenetic mechanisms, the cell type involved and the mechanisms of induction. For these reasons, the development of IL-1R2 as biomarker or prognostic tool seems unlikely.

IL-1R8 (TIR8/SIGIRR)

IL-1R8 Mode of Action

IL-1R8 is a well conserved gene among vertebrates, including fish, located on human chromosome 11 and on mouse chromosome 7. The protein differs from other members of the family since IL-1R8

has a single Ig domain in the extracellular region which is N- and O-glycosylated, an unconventional intracellular TIR domain with two amino-acid substitutions in Ser447 and Tyr536, replaced by Cys222 and Leu305, influencing IL-1R8 signalling activity, and a long tail of 95 residues (**Figure 3**).

IL-1R8 is expressed by several cell types, in particular epithelial cells of the liver and kidney, and in lymphoid organs. Among leukocytes, IL-1R8 is highly expressed by DC, NK cells and T lymphocytes, and it is also expressed in platelets (92–95). In general, inflammatory conditions, such as treatment with LPS, are associated with downregulation of IL-1R8 expression (95–99) through the inhibition of SP1 binding on IL-1R8 promoter (96, 100).

Different IL-1R8 isoforms have been described, but their function is unknown. A longer isoform called IL-1R8L1 was characterized in tumor epithelial cell lines, in a neuroblastoma cell line, in leukemic cell lines, and in human healthy tissues (101).

The first functional roles described for IL-1R8 concern the inhibition of the signalling pathways downstream ILRs and TLRs (e.g. IL-1R1, IL-1R5/IL-18R α , IL-1R4/ST2, TLR1, TLR2, TLR4, TLR7, TLR9, TLR3), leading to the reduction of NF- κ B and JNK activation (94, 95, 102–107), (**Figure 3**). The molecular

mechanism proposed indicates that IL-1R8 is recruited to the ligand-receptor complex, and the BB-loop structure of IL-1R8 TIR domain inhibits the dimerization of MyD88 (92, 93, 102, 104, 108, 109), or causes retention of the Myddosome complex on receptors without driving the pro-inflammatory cascade (110). In addition, the IL-1R8 extracellular domain has been shown to inhibit the interaction between IL-1R1 and IL-1R3 (104). In the case of TLR3 signalling, IL-1R8 blocked TRAM homodimerization and TLR4-TRAM and TRIF-TRAM interactions (110–112). IL-1R8 is also involved in the regulation of the mTOR pathway in lymphoid and not lymphoid cells (e.g. Th17, NK cells and intestinal epithelium) (94, 113, 114).

In addition, IL-1R8 is part with IL-1R5 of the signalling receptor of IL-37, an anti-inflammatory molecule of the IL-1 family, inducing an immunosuppressive pathway, inhibiting MAPK, NF- κ B, mTOR, TAK1 and Fyn, and activating STAT3, Mer, PTEN and p62(dok) signaling (11, 115) (**Figure 3**). Upon ligation, IL-37 induced activation of glycogen synthase kinase 3 β which promoted IL-1R8 phosphorylation, internalization, and degradation by the ubiquitin-proteasome system (116). Several studies showed that IL-1R8 is necessary for the anti-inflammatory potential of IL-37 in different pathologic conditions, including LPS-induced endotoxemia, *Aspergillus*

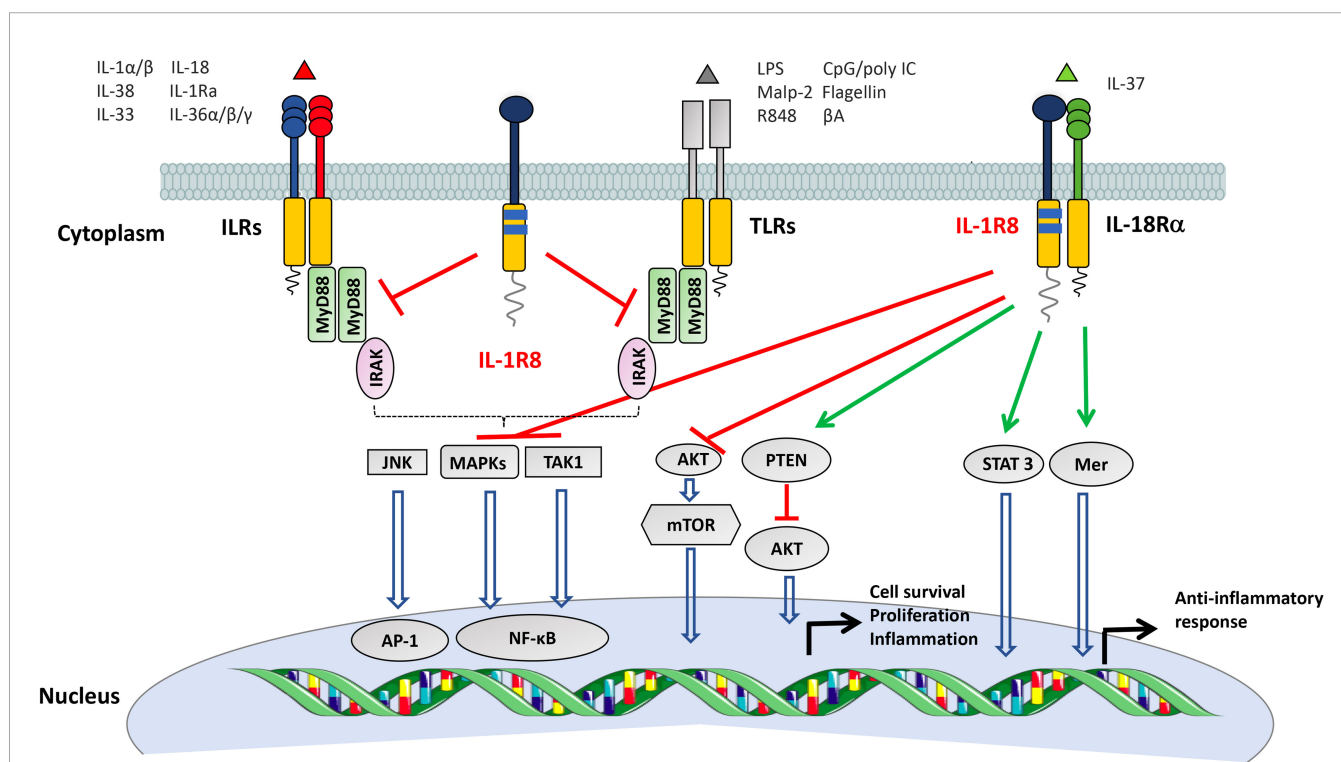


FIGURE 3 | Mechanisms of negative regulation mediated by IL-1R8. IL-1R8 is characterized by a single extracellular Ig domain, a transmembrane domain, an intracellular TIR domain and an unusually long tail of 95 residues. The IL-1R8 TIR domain differs from the TIR domains of other ILRs for the substitution of two conserved residues (Ser447 and Tyr536 with Cys222 and Leu305), suggesting unconventional signaling. IL-1R8 inhibits the signalling pathways downstream ILRs and TLRs by competing with the recruitment of MyD88 and IRAK at the TIR domain, thus dampening the signaling pathways involved in NF- κ B and JNK activation. In addition, in T, NK and epithelial cells, IL-1R8 negatively regulates the activation of the mTOR pathway. IL-1R8, together with IL-1R5, is part of the signaling receptor of the anti-inflammatory molecule IL-37. The IL-37/IL-1R5/IL-1R8 tripartite complex inhibits MAPK, NF- κ B, mTOR, TAK1 and Fyn, and activates STAT3, Mer, PTEN and p62(dok) signaling, thus leading to an anti-inflammatory pathway.

fumigatus pulmonary infection (11, 117), allergic responses (118), neuroinflammatory diseases, such as multiple sclerosis (119) or spinal cord injury (120), and DSS-induced colitis (121). Further, IL-37 inhibited β -glucan-dependent trained innate immunity, an innate immune memory program induced in monocytes/macrophages by exposure to pathogens or vaccines, associated with protection against infections. In this context, IL-1R8 was required for the inhibitory role of IL-37 in the production of inflammatory mediators by monocytes (122). Finally, IL-37 alleviated endothelial cell apoptosis and inflammation *via* IL-1R8, by inhibiting ERK and NF- κ B activation (123).

Activation of the IL-1R5//IL-1R8 receptor complex by IL-37 was also involved in tuning of mTOR signaling and activation of STAT6 and Foxo transcription factor family, with effects on metabolism, insulin response and glucose tolerance (11, 124). IL-1R8 was finally necessary for the activity of IL-37 in muscle cells, where it orchestrated the AMPK pathway and improved exercise performance and fatigue tolerance (125).

The regulatory role of IL-1R8 is conserved in evolution: for instance, in zebrafish IL-1R8 sequesters TRIF competing with its recruitment at the TLR3/TLR22 receptor complex, thus contributing to the maintenance of liver homeostasis under inflammatory conditions (126). In veterinary medicine, several reports show the expression and relevance of IL-1R8 in inflammatory and infectious conditions, including infection by porcine circovirus 2 in pigs (127) and *Staphylococcus aureus* mastitis in goat (128), inflammation in forestomach wall and mammary cells of ruminants (129–131), or intestinal epithelial cells and APCs from Peyer's patches in pigs (132–134).

IL-1R8 in Infections

IL-1R8 plays dual roles in different infections. Depending on the type of infection, IL-1R8 deficient mice developed more severe inflammation and tissue damage in several models of experimental infections, or on the other hand showed increased protective innate immune responses leading to higher resistance to the infection (**Table 1** and **Figure 4**). In a model of *Mycobacterium tuberculosis* infection, IL-1R8 deficient animals presented an increased mortality mainly due to an exaggerated inflammatory response with enhanced leukocyte infiltration in lung and higher levels of proinflammatory cytokines. The phenotype was rescued by the preventive administration of IL-1 and TNF α blocking antibodies (135). A genome wide association study aimed at identifying genetic variants associated with resistance to tuberculosis in bovine, an infection representing a risk to public health, identified IL-1R8 among genes associated with resistance to the infection (154). In line with these results, a strong association between 3 *IL1R8* SNPs (rs10902158, rs7105848, rs7111432) and tuberculosis infections was described in a study involving more than 600 patients and negative controls (155).

In *Pseudomonas aeruginosa* lung infection IL-1R8 deficient mice showed higher mortality, bacterial load and systemic and local levels of cytokines (IFN γ , IL-1 β , TNF α , IL-6) compared to wild type mice. The phenotype was reverted by IL-1R1-deficiency, demonstrating that IL-1R8 prevented *P. aeruginosa*

associated inflammation by negatively regulating IL-1R1, the major signaling pathway involved in the pathogenesis of this infection (98). In a model of *E. coli* pneumonia, the pro-resolving mediator 15-epi-lipoxin A₄ induced the expression of A20 and IL-1R8 through a lipoxin A₄ receptor/formyl peptide receptor 2 dependent mechanism, dampening lung inflammation and promoting pathogen clearance (156).

In fungal infections by *Candida albicans* and *Aspergillus fumigatus*, IL-1R8 deficient mice showed an increased susceptibility in terms of pathogen dissemination in tissues, mortality, and increased Th17 cell activation mediated by IL-1 signaling (136). Furthermore, as stated above, IL-1R8 was essential for the anti-inflammatory role of IL-37 in pulmonary aspergillosis.

On the other hand, in a model of *E. coli* pyelonephritis, the stronger inflammatory response of kidney epithelial cells to bacteria and PAMPs (LPS) protected IL-1R8 deficient mice from renal dysfunction, thanks to an increased recruitment of neutrophils in the early phase of infection (137). Along the same line, IL-1R8 deficiency protected mice from mortality in *Streptococcus pneumoniae* pneumonia and sepsis, and was associated with reduced bacterial load and dissemination (138).

IL-1R8 is highly expressed in gut epithelium and this has been linked to tuning of TLR reactivity against commensal bacteria; IL-1R8-deficiency in mice infected with *Citrobacter rodentium* was associated with exaggerated IL-1R1 signaling-dependent gut inflammation, causing a severe loss of commensal bacteria and facilitated secondary infection by *Salmonella typhimurium* (139). Along the same line, some probiotic bacteria used in the treatment of gut infections and diseases, beneficially regulated host immune responses by modulating TLR negative regulators, including IL-1R8 (157, 158).

An *in vitro* study demonstrated that IL-1R8 acts as a negative regulator of the immune response to *Chlamydia trachomatis*, by reducing the expression of IL-8 in infected epithelial cells (159).

In HIV infection, a significant correlation between TLR4 and IL-1R8 gene expression in brain and HIV-associated neurodegeneration was observed (160). Moreover, the IL-37/IL-1R8 axis was impaired in HIV infected subjects and associated with increased inflammation and viral replication, thus suggesting the therapeutic potential of the IL-37/IL-1R8 axis in HIV infection (140).

Thus, IL-1R8 emerges as a tuner of innate and inflammatory responses, and depending on specific infections, its role results in protection from immunopathology or limitation of protective immune responses against the pathogen.

IL-1R8 in Sterile Inflammation: Autoimmunity, Graft Rejection and Allergy

IL-1R8 is involved in the regulation of TLR-dependent sterile inflammation associated with autoimmunity, in several models (**Table 1** and **Figure 4**). In C57BL/6-lpr/lpr mice, that develop a progressive lymphoproliferative syndrome followed by severe autoimmune disease and lupus nephritis, IL-1R8 deficiency was associated with higher activation of DCs and expression of IL-6, IFN β , TNF, IL-12, and B cell survival factors Baff/BlyS and Bcl-2, as well as production of lupus autoantibodies (141). In the

TABLE 1 | Pathophysiological roles of IL-1R8 in disease.

Pathological context	Disease*	Role of IL-1R8	Modulated target**	Selected ref.
Infection	<i>Mycobacterium tuberculosis</i>	Prevention of liver necrosis, IL-1 β /TNF mediated inflammation	IL-1R	(135)
	<i>Pseudomonas aeruginosa</i> (lung infection)	Prevention of high bacterial load and excessive inflammation	IL-1R	(98)
	<i>Candida albicans</i> / <i>Aspergillus fumigatus</i>	Prevention of Th17 response and pathogen dissemination	IL-1R	(136)
	<i>Escherichia coli</i> (pyelonephritis)	Susceptibility to renal dysfunction	TLR4	(137)
	<i>Streptococcus pneumoniae</i>	Susceptibility to mortality induced by pneumonia and sepsis	Unknown	(138)
	<i>Citrobacter rodentium</i>	Prevention of commensal bacteria loss and gut inflammation	IL-1R	(139)
Autoimmunity	Human Immunodeficiency Virus (HIV)	Regulation of inflammation by IL-37 in HIV infected cells	IL-37	(140)
	Lupus Nephritis/Systemic Lupus Erythematosus (SLE)	Prevention of autoantigen presentation and lupus autoantibodies production/Control of Th17 response	TLRs (TLR7)	(141)
	Rheumatoid Arthritis (RA)	Control of activation of myeloid and synovial cells	IL-1R TLRs	(112)
	Psoriatic Arthritis (PsA)	Prevention of IL-17A $\gamma\delta$ T cell –mediated inflammation and IL-36	IL-1R and IL-36R	(142, 143)
	Multiple Sclerosis (MS)	Control of Th17 polarization, leukocyte infiltration in the brain and spinal cord	IL-1R	(113)
	Myasthenia Gravis (MG)	Control of Th and B cells proliferation and autoantibody secretion	IL-37	(144)
	Graft rejection	Control of donor antigen presentation, Th1 and Th17 responses	IL-1R	(145, 146)
Allergy	Hyperallergic pulmonary inflammation	Control of Th2 responses and prevention of severe disease	IL-33R; IL-37	(106, 118)
	House dust mite (HDM) asthma	Stimulation of Th2 responses, eosinophilic inflammation, mucus and HDM-specific IgG1 production	TLR-4	(147)
Thrombosis		Prevention of platelet and neutrophil-platelet aggregation	TLRs/IL-1R/ IL-18R	(95)
Neurological Dysfunctions		Regulation of neuron synapse morphology, plasticity and functions.	IL-1R/TLR4/ TLR2	(107, 148)
		Regulation of hippocampal function		
Colitis		Modulation of gut microflora and prevention of intestinal inflammation	TLRs	(103, 149)
Cancer	Colitis-associated cancer	Prevention of intestinal inflammation-associated cancer	TLRs	(114, 149, 150)
	Breast Cancer	Negative regulation of a protective tumor immune infiltrate	Unknown	(151)
	Hepatocellular carcinoma/Sarcoma lung metastasis/Colon Cancer metastasis	Immunocheckpoint in NK cells	IL-18R	(94)
	Chronic Lymphocytic leukemia/Diffuse large B-cell lymphoma	Prevention of monoclonal B cell expansion	Unknown	(152, 153)

*Selected.

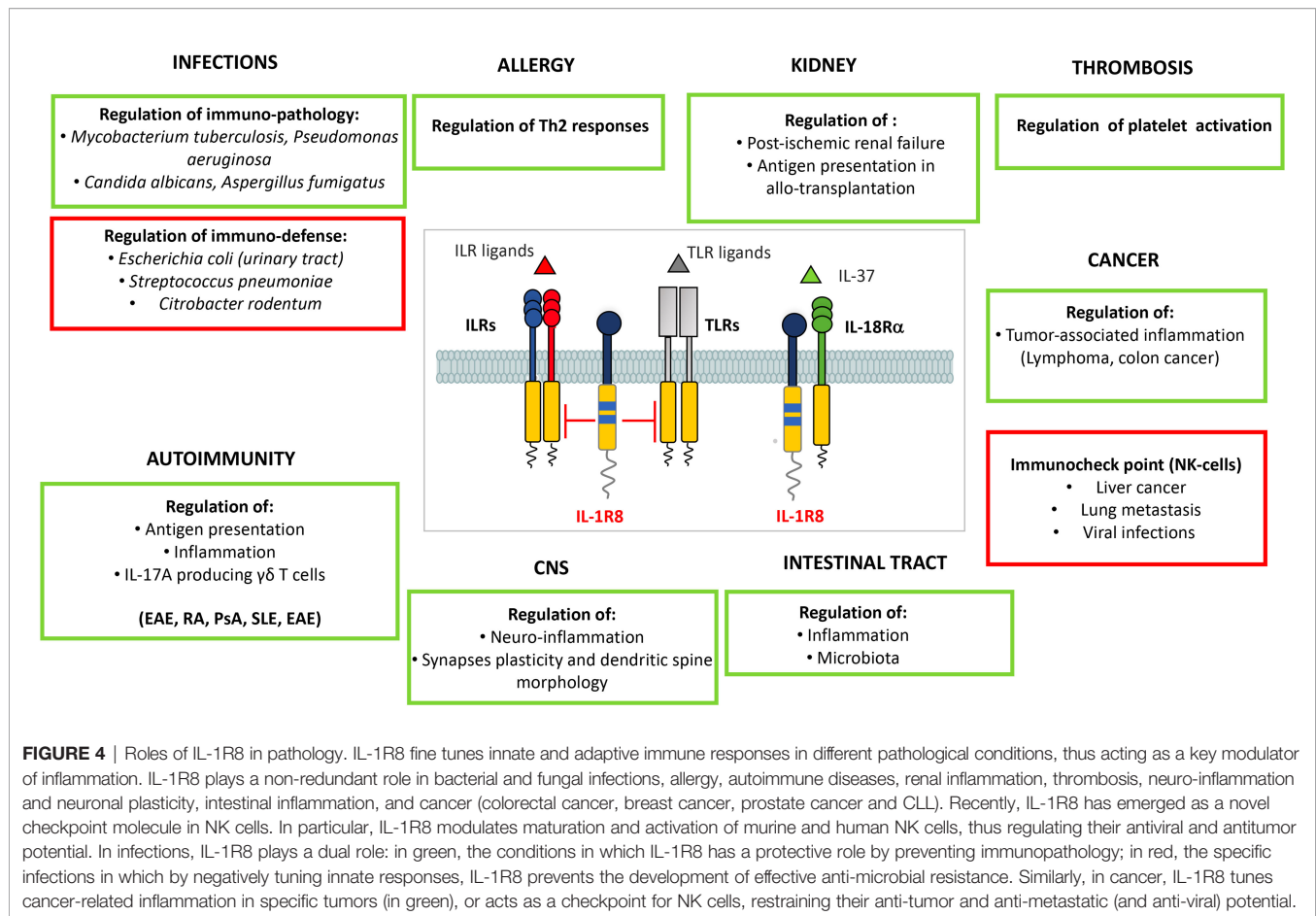
**Demonstrated or proposed.

hydrocarbon oil-induced systemic lupus erythematosus (SLE) murine model, IL-1R8-deficiency was associated with unleashed TLR-7-mediated activation of DCs and consequent more severe autoimmune tissue injury (161). In SLE patients, the percentage of circulating IL-1R8⁺CD4⁺ cells inversely correlated with SLE severity and nephritis biomarkers concentration (162), and with the percentage of Th17 circulating cells, which proportionally increase with SLE severity (163).

In two different rheumatoid arthritis (RA) mouse models, IL-1R8-deficiency was associated with overactivation of myeloid and synovial cells, leading to a more severe disease in terms of clinical score or joint cellular infiltration (112). Based on the high expression of the IL-37//IL-1R5//IL-1R8 complex in CD4⁺ cells of RA patients, IL-37 has been proposed as a promising therapeutic target in RA (164, 165).

In psoriatic arthritis (PsA), a gene expression profile of PBMCs from patients and healthy controls showed that negative regulators of innate responses, including IL-1R8, are

the genes that undergo the greatest reduction in expression (166). In line with these data, IL-1R8-deficient mice developed severe psoriatic inflammation in both chemical and cytokine-induced psoriasis mouse models, compared to wild type mice. These models depend on high IL-17A-expressing $\gamma\delta$ T cells, whose activity was suppressed by IL-1R8 (142). In addition, IL-1R8 negatively regulated IL-36-dependent psoriatic inflammation in humans and mice, acting in particular in dendritic cells and keratinocytes and modulating neutrophil chemo-attractants (143). The deficiency of IL-1R8 resulted in enhanced Th17 cell polarization *in vivo* in a multiple sclerosis (MS) mouse model (experimental autoimmune encephalomyelitis, EAE) and increased disease severity, characterized by higher leukocyte activation and infiltration in the brain and spinal cord (113). In this model, IL-1R8 was involved in the regulation of Th17 cell differentiation, expansion and functions, due to its inhibitory effects on IL-1 signaling leading to JNK and mTOR activation (113).



Recombinant IL-37 has been proposed as a novel therapeutic strategy for MS, since patients, despite the low production of endogenous IL-37, still present the receptor complex IL-1R5//IL-1R8 on their PBMCs and brain lesions (119). Along the same line, patients affected by myasthenia gravis (MG) presented lower IL-37 serum levels compared with healthy controls, which were associated with high follicular T helper and B cell numbers. Both populations express high levels of IL-1R8 and their stimulation with IL-37 results in reduced proliferation, cytokine production and secretion of autoantibodies, suggesting its therapeutic potential in MG (144).

In a model of kidney allotransplantation, IL-1R8-deficiency was associated with graft rejection, in contrast with IL-1R8-competent grafts which were spontaneously accepted. In this context, a major role was played by graft-resident DCs, which, when deficient of IL-1R8, exerted improved donor antigen presentation and stimulated the production of higher amounts of IFN γ by allogenic T cells (145). IL-1R8 overexpressing DCs also contributed to prolonged survival of allografts in an islet transplantation mouse model, by inducing weak systemic Th1 and Th17 responses that were counterbalanced by a strong Treg-mediated immunoregulation, leading to allografts survival (146).

The involvement of IL-1R8 in allergy appears at the moment controversial. Bulek K. et al. originally showed that IL-1R8-

deficiency is associated with more severe hyperallergic pulmonary inflammation and that IL-1R8 is involved in T cell-mediated type 2 response by negatively regulating the IL-33/ST2 complex (106). In a mouse model of acute asthma, intranasal administration of rIL-37 ablated allergic airway inflammation, cytokine production, mucus hyperproduction and airway hyper-responsiveness, and these benefits were completely lost in IL-1R8 or IL-18R α deficient mice (118). In contrast with these results, in a house dust mite (HDM) asthma model, which relies on the activation of TLR4 on epithelial cells and subsequent exacerbated Th2 specific response, IL-1R8-deficiency was associated with decreased production of Th2 cytokines in lung and draining lymph nodes, reduced eosinophilic inflammation, mucus production by goblet cells, HDM-specific IgG1 and airway hyperreactivity compared with wild type mice. The mechanism proposed was the up-regulation upon HDM sensitization of IL-1F5, a putative IL-1R8 ligand, an IL-4 inducer (147). Finally, a human genetic study based on exome sequencing on a cohort of Japanese patients with asthma excluded any association with IL-1R8 alleles or haplotypes (167).

Collectively, these studies in mouse underline the involvement of IL-1R8 in tuning inflammatory and immune responses activated in sterile conditions through engagement of TLRs or IL-1R family members. Even if fragmentary, evidence in human suggests the

conservation in evolution of the regulatory functions of this molecule.

IL-1R8 in Platelet Activation and Thromboembolism

IL-1R8 is expressed on different blood leukocytes, but platelets show the highest level of expression, both in humans and mice. High levels were also observed in megakaryocytes of both species (95). IL-1R8 deficiency was associated with platelet hyperactivation in basal conditions, increased platelet aggregation after prothrombotic stimulation and increased neutrophil-platelet aggregation induced by LPS, IL-1 β and IL-18 *in vitro*. Indeed, platelets also express TLRs and IL-1 family members and IL-1R8 can regulate their signaling (95). In a model of ADP-induced pulmonary thromboembolism, IL-1R8 deficient mice were more susceptible mainly due to deregulated IL-1 signaling (95). Platelets from patients affected by SIRS/sepsis showed reduced IL-1R8 surface expression compared to platelets from healthy donors, reflecting the severity of the disease. Interestingly, expression of IL-1R8 in microvesicles released from platelets *in vitro* or found in plasma of sepsis patients suggests that IL-1R8 may be rapidly shed by the release of microvesicles in inflammatory conditions, contributing to platelet dysfunction observed in this inflammatory condition (95).

IL-1R8 in the Central Nervous System

IL-1R8 is expressed in different types of cells in the brain such as neurons, astrocytes, and microglia. IL-1R8 deficient mice demonstrated impaired CNS development, leading to altered hippocampal capacity: difficulties in novel objective recognition, spatial reference memory and long-term potentiation (148) (Table 1 and Figure 4). Neurological dysfunctions were associated to increased activation of IRAK1, JNK and NF- κ B via IL-1R1 and TLR4 signaling after binding respectively to IL-1 α and HMGB1 (148). Moreover, IL-1R8-deficiency and the consequent hyperactivation of the IL-1R pathway affected neuron synapse morphology, plasticity and function (107). IL-1R8-deficient hippocampal neurons displayed an increased number of immature, thin spines and a decreased number of mature, mushroom spines, along with a significant reduction of spine width, and reduced amplitude of miniature excitatory postsynaptic currents. The phenotype of IL-1R8-deficient neurons was associated with IL-1R1-driven hyperactivation of the PI3K/AKT/mTOR pathway, and increased expression of methyl-CpG-binding protein 2 (MeCP2), a synaptopathy protein involved in neurological diseases, such as Rett syndrome and MeCP2 duplication syndrome (168). Deficiency of IL-1R1 or treatment with IL-1Ra (Anakinra) normalized MeCP2 expression and cognitive deficits in IL-1R8-deficient mice, demonstrating that IL-1R8 fine tunes IL-1R1 signalling, is involved in synaptopathies and is required for correct long-term potentiation (107). In line with these results, the treatment with Anakinra of patients with cryopyrin-associated periodic syndrome (CAPS), in addition to reduce signs and symptoms of IL-1-dependent inflammation, reversed mental defects in

patients (169). A further evidence of the relevance of IL-1R8 in the brain is provided by genetic studies on schizophrenia, which identified *SIGIRR* as one of the genes associated with genetic alterations in this psychiatric condition (170).

Finally, IL-1R8 also regulated β -amyloid peptide-dependent TLR2 activation in microglial cells and the release of the pro-inflammatory cytokines TNF α and IL-6 (171).

IL-1R8 in Cancer

Intestinal Inflammation and Cancer

IL-1R8 plays an important role in gut homeostasis, intestinal inflammation and tumorigenesis (Table 1 and Figure 4). In healthy mice, IL-1R8 was shown to modulate gut microflora-mediated activation of ILRs and TLRs, which regulated the proliferation and survival of intestinal epithelial cells in colonic crypts. IL-1R8-deficient mice showed constitutive activation of NF- κ B and JNK and increased expression of Cyclin D1 and Bcl-xL (149). The phenotype has not been confirmed by all the studies performed in healthy mice, probably due to animal house-dependent microflora variation (103, 150).

In a murine model of dextran sulfate sodium (DSS)-induced colitis, IL-1R8 deficiency is associated with increased local leukocyte infiltration and higher levels of proinflammatory cytokines (TNF α , IL-6, IL-1 β , IL-12p40, IL-17), chemokines (CXCL1, CCL2), and prostaglandins, leading to an exacerbated intestinal inflammation. At the mechanistic level, this phenotype appears to be primarily due to the regulatory function of IL-1R8 in epithelial cells. These changes result in increased weight loss, intestinal bleeding, local tissue damage and reduced mice survival (103, 149), and susceptibility to Ulcerative Colitis-associated *E. coli* pathobionts (172). In addition, as reported above, IL-1R8 was essential for the anti-inflammatory role of IL-37 in this model *in vivo*, as well as in colonic organoids (173). In agreement with results obtained in mice, *SIGIRR* genetic variants and reduced expression of IL-1R8 as well as of IL-37 were shown to be associated with necrotizing enterocolitis in human (174, 175). In particular, a *SIGIRR* stop mutation (p.Y168X) was observed in an infant who died of severe necrotizing enterocolitis (174) and its functional effect was identified (176). The study showed that the p.Y168X mutation disrupted IL-1R8-mediated STAT3-dependent expression of miR-146a and miR-155, leading to deregulated IRAK1 activation and inflammation (176), thus identifying a new molecular mechanism underlying the regulatory role of IL-1R8.

In agreement with the concept that cancer-related inflammation contributes to cancer development and progression, IL-1R8 has been described to protect from cancer development in different murine tumor models. In a model that mimics intestinal cancer developed in Ulcerative Colitis patients, IL-1R8 deficiency was associated with increased intestinal inflammation and enhanced susceptibility to cancer development. IL-1R8 reduces the expression of NF- κ B-induced genes critical for cell survival and proliferation (Bcl-xL and Cyclin D1), the local production of proinflammatory cytokines, chemokines and prostaglandin E₂, and intestinal permeability. Interestingly, the expression of IL-1R8 solely in gut epithelial

cells rescues the phenotype of IL-1R8-deficient mice, reducing their susceptibility to colitis-associated cancer development and suggesting that the activity of IL-1R8 on tumorigenesis is mainly through its function on gut epithelial cells (149, 150).

In the genetic *Apc^{min/+}* model, which resembles the Familial Adenomatous Polyposis syndrome (177), IL-1R8 deficiency led to increased tumorigenesis. IL-1R8-deficient mice show more sustained activation of the Akt/mTOR pathway in response to TLR or IL-1R ligands, leading to increased proliferation and chromosomal instability in cells of the colon crypts (114).

In human colorectal cancer, it has been shown that IL-1R8 expression is reduced compared with non-tumor tissues. Zhao et al. identified a dominant-negative isoform of IL-1R8 (IL-1R^{ΔE8}), originated from a transcript lacking the exon 8, which is not modified by complex glycans and is retained in the cytoplasm. This isoform acts as a dominant-negative on IL-1R8, inhibiting its glycosylation, localization to the surface of colon epithelial cells and function. Indeed, in human colon cancer tissues IL-1R8 is cytoplasmic while in non-tumor tissue it has been found at the cell membrane. Importantly, transgenic mice expressing this mutant form of IL-1R8 in the colonic epithelium are more susceptible to colon cancer development in the colitis-associated tumor model, presenting higher local levels of inflammatory cytokines (IL-17A and IL-6) and the activation of transcription factors STAT3 and NF-κB. Taken together, these results suggest that complex glycan modifications and cell surface expression are required for IL-1R8 to reduce intestinal inflammation and tumorigenesis *in vivo* (178).

Breast Cancer

In breast cancer, the immunomodulatory role of IL-1R8 resulted in inhibition of IL-1-dependent NF-κB activation and production of pro-inflammatory cytokines *in vitro* and *in vivo*. In the genetic MMTVneu mouse model of breast cancer, IL-1R8-deficiency was associated with reduced mammary tumor growth and lung metastasis (151), protective tumor immune infiltrate characterized by higher frequency of DCs, NK cells and CD8⁺ T cells and reduced frequency of TAMs. According to these results, RNAseq analysis in 1102 clinical samples of breast tumors revealed that high IL-1R8 expression was associated with a non-T cell inflamed molecular signature, lower expression level of proinflammatory cytokines and chemokines, DC and NK cell metagenes, components of the peptide presenting machinery, cytolytic enzymes and type I interferon (IFN)-induced genes (151). Taken together these results suggest that IL-1R8 expression in breast tumors negatively regulates the mobilization and activation of immune cells and therefore promotes tumor growth and metastasis.

IL-1R8 as a Novel Checkpoint in NK Cells

Our group recently demonstrated that IL-1R8 is expressed by murine and human NK cells and its expression increases during NK cell differentiation. IL-1R8-deficiency was associated with increased frequency of mature NK cells in blood, spleen, bone marrow and liver. IL-1R8 deficiency resulted in enhanced expression of activating NK cell receptors and increased IFNγ, granzyme B, Fas ligand expression and degranulation. IL-1R8

directly acted on NK cells regulating responsiveness to IL-18, a key cytokine involved in NK cell activation, since the phenotype of IL-1R8 deficient mice was abrogated upon depletion of IL-18 or in IL-1R8/IL-18 double deficient mice. From a molecular point of view, IL-1R8 regulated IL-18-dependent activation of mTOR and JNK pathways. In agreement with these results, RNASeq and protein phosphorylation analysis showed that the response to IL-18 was affected in IL-1R8-deficient cells, in particular in the pathways involved in NK cell activation, degranulation, cytokine production and antiviral response. The relevance of these data was shown in models of hepatocellular carcinoma, sarcoma lung metastasis and colon cancer-derived liver metastasis, where IL-1R8 deficiency was associated with reduced liver disease severity, and lung and liver metastases. Further, in a model of murine cytomegalovirus (MCMV) infection, IL-1R8 deficient mice were more protected from the viral infection thanks to enhanced NK cell degranulation and IFNγ production. Importantly, the adoptive transfer of IL-1R8 deficient NK cells was protective in the tumor metastasis and viral infection models. In human primary NK cells, IL-1R8 expression inversely correlated with IFNγ production, while IL-1R8 silencing resulted in increased IFNγ production and CD69 expression (94). Taken together, these results suggest that IL-1R8 blockade in NK cells, by tuning IL-18 signaling, may represent a novel therapeutic approach to unleash NK cell activity and strengthen NK cell antitumor and antiviral potential (Table 1 and Figure 4).

Leukemia and Lymphoma

Deregulated TLR signaling has been associated with different B cell malignancies. In a mouse model of spontaneous chronic lymphocytic leukemia (CLL), IL-1R8 deficiency was associated with early onset of the monoclonal B cell expansion and reduced life span (152). In agreement, CLL cells expressed lower levels of IL-1R8 compared to B cells from healthy donors (101).

Chronic inflammation and in particular autoimmune disorders are linked with B-cell lymphoma development. In addition to inducing more severe autoimmunity in *lpr* mice (lupus prone strain), IL-1R8 deficiency increased the onset of DLBCL in aging mice due to a constitutive activation of NF-κB in splenocytes (153). Interestingly, IL-1R8 was downregulated in DLBCL compared to normal B cells, and its expression was positively associated with overall survival (153).

Contribution of IL-1R8 in the Antitumor Potential of IL-37

IL-37 has been shown to exert several inhibitory functions on tumor angiogenesis, migration and progression. As reported above, IL-37 interacts with IL-1R5/IL-18Rα and IL-1R8 to exert its anti-inflammatory activity (11). Further, IL-37 has been shown to compete with IL-18 for IL-1R5/IL-18Rα. For instance, in Oral Squamous Cell carcinoma (OSCC), IL-37 inhibited the proinflammatory effects of IL-18 and the increased IL-18/IL-37 ratio in serum predicted shorter overall and disease-free survival (179). In other contexts where IL-37 exerts an antitumor effect, it has not been proven yet whether it acts through IL-1R8. These include hepatocellular carcinoma,

where IL-37 exerted an antiangiogenic role (180) or modulated the phenotype of TAMs by suppressing M2 polarization and regulating proinflammatory cytokine production (181), and Acute Myeloid Leukemia where IL-37 regulated IL-6 expression (182).

CONCLUDING REMARKS

In the last 50 years, since the discovery of IL-1, the complexity of this cytokine family has been investigated and dissected, leading to the identification of a large number of molecules acting as accelerators and others acting as brakes (receptor antagonists, decoy receptors, negative regulatory receptors, anti-inflammatory ligands). This complexity underlines the relevance of fine tuning of IL-1 family-dependent functions both in homeostasis and disease. Further, unexpected functions for this family have emerged, demonstrating that its involvement is not restricted to infections and inflammation, but also impact degenerative conditions and cancer. Finally, the therapeutic potential of some members of the IL-1 system or, on the opposite, of their targeting, has been demonstrated in the last years, suggesting that fine dissection of their role, regulation and genetic variants may lead to the development of novel intervention strategies. In this general context, IL-1R2 and IL-1R8 emerge as tuners in various physiological and pathological

conditions, which play essential functions to prevent immunopathology. On the other hand, their regulatory role may be exploited by escape mechanisms developed by pathogens and tumors, suggesting that their cell- and context-specific function must be dissected for the development of innovative therapeutic strategies.

AUTHOR CONTRIBUTIONS

All authors concurred in writing the manuscript. AM, LM, and DS prepared the figures. CG wrote and revised manuscript and figures. All authors contributed to the article and approved the submitted version.

ACKNOWLEDGMENTS

The contribution of the European Commission (H2020-MSCA-ITN-2015-676129), Ministero dell'Istruzione, dell'Università e della Ricerca (MIUR) (project PRIN 2015YYKPNN and 20174T7NXL), Associazione Italiana Ricerca sul Cancro (AIRC IG 21714, AIRC IG 23465 and AIRC 5x1000 21147), and the Italian Ministry of Health (Ricerca Finalizzata, RF-2013-02355470) is gratefully acknowledged.

REFERENCES

- Dinarello CA, Goldin NP, Wolff SM. Demonstration and Characterization of Two Distinct Human Leukocytic Pyrogens. *J Exp Med* (1974) 139:1369–81. doi: 10.1084/jem.139.6.1369
- Dinarello CA. Overview of the IL-1 Family in Innate Inflammation and Acquired Immunity. *Immunol Rev* (2018) 281:8–27. doi: 10.1111/imr.12621
- Garlanda C, Dinarello CA, Mantovani A. The Interleukin-1 Family: Back to the Future. *Immunity* (2013) 39:1003–18. doi: 10.1016/j.immuni.2013.11.010
- Voronov E, Dinarello CA, Apte RN. Interleukin-1alpha as an Intracellular Alarmin in Cancer Biology. *Semin Immunol* (2018) 38:3–14. doi: 10.1016/j.smim.2018.10.006
- Burzynski LC, Humphry M, Pyrrillou K, Wiggins KA, Chan JNE, Figg N, et al. The Coagulation and Immune Systems Are Directly Linked Through the Activation of Interleukin-1alpha by Thrombin. *Immunity* (2019) 50:1033–42.e6. doi: 10.1016/j.immuni.2019.03.003
- Dinarello CA. Immunological and Inflammatory Functions of the Interleukin-1 Family. *Annu Rev Immunol* (2009) 27:519–50. doi: 10.1146/annurev.immunol.021908.132612
- Rivers-Auty J, Daniels MJD, Colliver I, Robertson DL, Brough D. Redefining the Ancestral Origins of the Interleukin-1 Superfamily. *Nat Commun* (2018) 9:1156. doi: 10.1038/s41467-018-03362-1
- Novick D, Kim SH, Fantuzzi G, Reznikov LL, Dinarello CA, Rubinstein M. Interleukin-18 Binding Protein: A Novel Modulator of the Th1 Cytokine Response. *Immunity* (1999) 10:127–36. doi: 10.1016/s1074-7613(00)80013-8
- Colotta F, Re F, Muzio M, Bertini R, Polentarutti N, Sironi M, et al. Interleukin-1 Type II Receptor: A Decoy Target for IL-1 That Is Regulated by IL-4. *Science* (1993) 261:472–5. doi: 10.1126/science.8332913
- Mantovani A, Dinarello CA, Molgora M, Garlanda C. Interleukin-1 and Related Cytokines in the Regulation of Inflammation and Immunity. *Immunity* (2019) 50:778–95. doi: 10.1016/j.immuni.2019.03.012
- Nold-Petry CA, Lo CY, Rudloff I, Elgass KD, Li S, Gantier MP, et al. IL-37 Requires the Receptors IL-18Ralpha and IL-1r8 (SIGIRR) to Carry Out Its Multifaceted Anti-Inflammatory Program Upon Innate Signal Transduction. *Nat Immunol* (2015) 16:354–65. doi: 10.1038/ni.3103
- Alcami A, Koszinowski UH. Viral Mechanisms of Immune Evasion. *Trends Microbiol* (2000) 8:410–8. doi: 10.1016/s0966-842x(00)01830-8
- Patterson NJ, Werling D. To Con Protection: TIR-Domain Containing Proteins (TcP) and Innate Immune Evasion. *Vet Immunol Immunopathol* (2013) 155:147–54. doi: 10.1016/j.vetimm.2013.06.017
- Newman RM, Salunkhe P, Godzik A, Reed JC. Identification and Characterization of a Novel Bacterial Virulence Factor That Shares Homology With Mammalian Toll/interleukin-1 Receptor Family Proteins. *Infect Immun* (2006) 74:594–601. doi: 10.1128/IAI.74.1.594-601.2006
- Low LY, Mukasa T, Reed JC, Pascual J. Characterization of a TIR-Like Protein From *Paracoccus denitrificans*. *Biochem Biophys Res Commun* (2007) 356:481–6. doi: 10.1016/j.bbrc.2007.03.003
- Imbert PR, Louche A, Luizet JB, Grandjean T, Bigot S, Wood TE, et al. A *Pseudomonas aeruginosa* TIR Effector Mediates Immune Evasion by Targeting UBAP1 and TLR Adaptors. *EMBO J* (2017) 36:1869–87. doi: 10.15252/embj.201695343
- McMahan CJ, Slack JL, Mosley B, Cosman D, Lupton SD, Brunton LL, et al. A Novel IL-1 Receptor, Cloned From B Cells by Mammalian Expression, Is Expressed in Many Cell Types. *EMBO J* (1991) 10:2821–32. doi: 10.1002/j.1460-2075.1991.tb07831.x
- Re F, Sironi M, Muzio M, Matteucci C, Introna M, Orlando S, et al. Inhibition of Interleukin-1 Responsiveness by Type II Receptor Gene Transfer: A Surface "Receptor" With Anti-Interleukin-1 Function. *J Exp Med* (1996) 183:1841–50. doi: 10.1084/jem.183.4.1841
- Wang D, Zhang S, Li L, Liu X, Mei K, Wang X. Structural Insights Into the Assembly and Activation of IL-1beta With Its Receptors. *Nat Immunol* (2010) 11:905–11. doi: 10.1038/ni.1925
- Laye S, Lundkvist J, Bartfai T. Human/mouse Interleukin-1 Receptor/Receptor Accessory Protein Interactions in IL-1beta-Induced NFkappaB Activation. *FEBS Lett* (1998) 429:307–11. doi: 10.1016/S0014-5793(98)00537-7

21. Malinowsky D, Lundkvist J, Laye S, Bartfai T. Interleukin-1 Receptor Accessory Protein Interacts With the Type II Interleukin-1 Receptor. *FEBS Lett* (1998) 429:299–302. doi: 10.1016/S0014-5793(98)00467-0
22. Orlando S, Sironi M, Bianchi G, Drummond AH, Boraschi D, Yates D, et al. Role of Metalloproteases in the Release of the IL-1 Type II Decoy Receptor. *J Biol Chem* (1997) 272:31764–9. doi: 10.1074/jbc.272.50.31764
23. Lorenzen I, Lokau J, Dusterhoft S, Trad A, Garbers C, Scheller J, et al. The Membrane-Proximal Domain of A Disintegrin and Metalloprotease 17 (ADAM17) Is Responsible for Recognition of the Interleukin-6 Receptor and Interleukin-1 Receptor II. *FEBS Lett* (2012) 586:1093–100. doi: 10.1016/j.febslet.2012.03.012
24. Uchikawa S, Yoda M, Tohmonda T, Kanaji A, Matsumoto M, Toyama Y, et al. ADAM17 Regulates IL-1 Signaling by Selectively Releasing IL-1 Receptor Type 2 From the Cell Surface. *Cytokine* (2015) 71:238–45. doi: 10.1016/j.cyto.2014.10.032
25. Liu C, Hart RP, Liu XJ, Clevenger W, Maki RA, De Souza EB. Cloning and Characterization of an Alternatively Processed Human Type II Interleukin-1 Receptor mRNA. *J Biol Chem* (1996) 271:20965–72. doi: 10.1074/jbc.271.34.20965
26. Martin P, Palmer G, Vigne S, Lamacchia C, Rodriguez E, Talbot-Ayer D, et al. Mouse Neutrophils Express the Decoy Type 2 Interleukin-1 Receptor (IL-1R2) Constitutively and in Acute Inflammatory Conditions. *J Leukoc Biol* (2013) 94:791–802. doi: 10.1189/jlb.0113035
27. Giri JG, Wells J, Dower SK, McCall CE, Guzman RN, Slack J, et al. Elevated Levels of Shed Type II IL-1 Receptor in Sepsis. Potential Role for Type II Receptor in Regulation of IL-1 Responses. *J Immunol* (1994) 153:5802–9.
28. Colotta F, Orlando S, Fadlon EJ, Sozzani S, Matteucci C, Mantovani A. Chemoattractants Induce Rapid Release of the Interleukin 1 Type II Decoy Receptor in Human Polymorphonuclear Cells. *J Exp Med* (1995) 181:2181–6. doi: 10.1084/jem.181.6.2181
29. Smith DE, Hanna R, Della F, Moore H, Chen H, Farese AM, et al. The Soluble Form of IL-1 Receptor Accessory Protein Enhances the Ability of Soluble Type II IL-1 Receptor to Inhibit IL-1 Action. *Immunity* (2003) 18:87–96. doi: 10.1016/S1074-7613(02)00514-9
30. Symons JA, Young PR, Duff GW. Soluble Type II Interleukin 1 (IL-1) Receptor Binds and Blocks Processing of IL-1 Beta Precursor and Loses Affinity for IL-1 Receptor Antagonist. *Proc Natl Acad Sci USA* (1995) 92:1714–8. doi: 10.1073/pnas.92.5.1714
31. Zheng Y, Humphry M, Maguire JJ, Bennett MR, Clarke MC. Intracellular Interleukin-1 Receptor 2 Binding Prevents Cleavage and Activity of Interleukin-1alpha, Controlling Necrosis-Induced Sterile Inflammation. *Immunity* (2013) 38:285–95. doi: 10.1016/j.immuni.2013.01.008
32. Chan JNE, Humphry M, Kitt L, Krzyzanska D, Filbey KJ, Bennett MR, et al. Cell Surface IL-1alpha Trafficking Is Specifically Inhibited by Interferon-Gamma, and Associates With the Membrane via IL-1R2 and GPI Anchors. *Eur J Immunol* (2020) 50:1663–75. doi: 10.1002/eji.201948521
33. Martinez FO, Gordon S, Locati M, Mantovani A. Transcriptional Profiling of the Human Monocyte-to-Macrophage Differentiation and Polarization: New Molecules and Patterns of Gene Expression. *J Immunol* (2006) 177:7303–11. doi: 10.1049/jimmunol.177.10.7303
34. Colotta F, Saccani S, Giri JG, Dower SK, Sims JE, Introna M, et al. Regulated Expression and Release of the IL-1 Decoy Receptor in Human Mononuclear Phagocytes. *J Immunol* (1996) 156:2534–41.
35. Dickensheets HL, Donnelly RP. IFN-Gamma and IL-10 Inhibit Induction of IL-1 Receptor Type I and Type II Gene Expression by IL-4 and IL-13 in Human Monocytes. *J Immunol* (1997) 159:6226–33.
36. Kalliolias GD, Gordon RA, Ivashkiv LB. Suppression of TNF-Alpha and IL-1 Signaling Identifies a Mechanism of Homeostatic Regulation of Macrophages by IL-27. *J Immunol* (2010) 185:7047–56. doi: 10.1049/jimmunol.1001290
37. Daun JM, Ball RW, Burger HR, Cannon JG. Aspirin-Induced Increases in Soluble IL-1 Receptor Type II Concentrations *In Vitro* and *In Vivo*. *J Leukoc Biol* (1999) 65:863–6. doi: 10.1002/jlb.65.6.863
38. Re F, Muzio M, De Rossi M, Polentarutti N, Giri JG, Mantovani A, et al. The Type II "Receptor" as a Decoy Target for Interleukin 1 in Polymorphonuclear Leukocytes: Characterization of Induction by Dexamethasone and Ligand Binding Properties of the Released Decoy Receptor. *J Exp Med* (1994) 179:739–43. doi: 10.1084/jem.179.2.739
39. Pinteaux E, Parker LC, Rothwell NJ, Luheshi GN. Expression of Interleukin-1 Receptors and Their Role in Interleukin-1 Actions in Murine Microglial Cells. *J Neurochem* (2002) 83:754–63. doi: 10.1046/j.1471-4159.2002.01184.x
40. McNamee EN, Ryan KM, Kilroy D, Connor TJ. Noradrenaline Induces IL-1ra and IL-1 Type II Receptor Expression in Primary Glial Cells and Protects Against IL-1beta-Induced Neurotoxicity. *Eur J Pharmacol* (2010) 626:219–28. doi: 10.1016/j.ejphar.2009.09.054
41. Docagne F, Campbell SJ, Bristow AF, Poole S, Vignes S, Guaza C, et al. Differential Regulation of Type I and Type II Interleukin-1 Receptors in Focal Brain Inflammation. *Eur J Neurosci* (2005) 21:1205–14. doi: 10.1111/j.1460-9568.2005.03965.x
42. Pou J, Martinez-Gonzalez J, Rebollo A, Rodriguez C, Rodriguez-Calvo R, Martin-Fuentes P, et al. Type II Interleukin-1 Receptor Expression Is Reduced in Monocytes/Macrophages and Atherosclerotic Lesions. *Biochim Biophys Acta* (2011) 1811:556–63. doi: 10.1016/j.bbalt.2011.05.014
43. Trebec DP, Chandra D, Gramoun A, Li K, Heersche JN, Manolson MF. Increased Expression of Activating Factors in Large Osteoclasts Could Explain Their Excessive Activity in Osteolytic Diseases. *J Cell Chem* (2007) 101:205–20. doi: 10.1002/jcb.21171
44. Attur MG, Dave M, Cipolletta C, Kang P, Goldring MB, Patel IR, et al. Reversal of Autocrine and Paracrine Effects of Interleukin 1 (IL-1) in Human Arthritis by Type II IL-1 Decoy Receptor. Potential for Pharmacological Intervention. *J Biol Chem* (2000) 275:40307–15. doi: 10.1074/jbc.M002721200
45. Mercer F, Kozhaya L, Unutmaz D. Expression and Function of TNF and IL-1 Receptors on Human Regulatory T Cells. *PLoS One* (2010) 5:e8639. doi: 10.1371/journal.pone.0008639
46. Nikolouli E, Elfaki Y, Herppich S, Schelmbauer C, Delacher M, Falk C, et al. Recirculating IL-1r2(+) Tregs Fine-Tune Intrathymic Treg Development Under Inflammatory Conditions. *Cell Mol Immunol* (2021) 18:182–93. doi: 10.1038/s41423-019-0352-8
47. Ritvo PG, Churlaud G, Quiniou V, Florez L, Brimaud F, Fourcade G, et al. Tfr Cells Lack IL-2Ralpha But Express Decoy IL-1R2 and IL-1Ra and Suppress the IL-1-Dependent Activation of Th Cells. *Sci Immunol* (2017) 2:eaan0368. doi: 10.1126/sciimmunol.aan0368
48. Kim DH, Kim HY, Cho S, Yoo SJ, Kim WJ, Yeon HR, et al. Induction of the IL-1RII Decoy Receptor by NFAT/FOXO3 Blocks IL-1beta-Dependent Response of Th17 Cells. *Elife* (2021) 10:e61841. doi: 10.7554/eLife.61841
49. Gagliani N, Amezcua Vesely MC, Iseppon A, Brockmann L, Xu H, Palm NW, et al. Th17 Cells Transdifferentiate Into Regulatory T Cells During Resolution of Inflammation. *Nature* (2015) 523:221–5. doi: 10.1038/nature14452
50. De Simone M, Arrighi A, Rossetti G, Gruarin P, Ranzani V, Politano C, et al. Transcriptional Landscape of Human Tissue Lymphocytes Unveils Uniqueness of Tumor-Infiltrating T Regulatory Cells. *Immunity* (2016) 45:1135–47. doi: 10.1016/j.immuni.2016.10.021
51. Plitas G, Konopacki C, Wu K, Bos PD, Morrow M, Putintseva EV, et al. Regulatory T Cells Exhibit Distinct Features in Human Breast Cancer. *Immunity* (2016) 45:1122–34. doi: 10.1016/j.immuni.2016.10.032
52. Lam JH, Hong M, Koo SL, Chua CWL, Lim KL, Wee F, et al. CD30(+)OX40(+) Treg Is Associated With Improved Overall Survival in Colorectal Cancer. *Cancer Immunol Immunother* (2021) 70:2353–65. doi: 10.1007/s00262-021-02859-x
53. Zhou C, Tuong ZK, Lukowski SW, Chandra J, Frazer IH. Antigen Nonspecific Induction of Distinct Regulatory T Cell States in Oncogene-Driven Hyperproliferative Skin. *Immunohorizons* (2021) 5:102–16. doi: 10.4049/immunohorizons.2100006
54. Alvisi G, Brummelman J, Puccio S, Mazza EM, Tomada EP, Losurdo A, et al. IRF4 Instructs Effector Treg Differentiation and Immune Suppression in Human Cancer. *J Clin Invest* (2020) 130:3137–50. doi: 10.1172/JCI130426
55. Guo X, Zhang Y, Zheng L, Zheng C, Song J, Zhang Q, et al. Global Characterization of T Cells in Non-Small-Cell Lung Cancer by Single-Cell Sequencing. *Nat Med* (2018) 24:978–85. doi: 10.1038/s41591-018-0045-3
56. Lownik JC, Conrad DH, Martin RKA. Disintegrin and Metalloproteinase 17 Is Required for ILC2 Responses to IL-33. *Biochem Biophys Res Commun* (2019) 512:723–28. doi: 10.1016/j.bbrc.2019.03.120
57. Chen L, Deng H, Cui H, Fang J, Zuo Z, Deng J, et al. Inflammatory Responses and Inflammation-Associated Diseases in Organs. *Oncotarget* (2018) 9:7204–18. doi: 10.18632/oncotarget.23208

58. Drevets DA, Schawang JE, Mandava VK, Dillon MJ, Leenen PJ. Severe *Listeria Monocytogenes* Infection Induces Development of Monocytes With Distinct Phenotypic and Functional Features. *J Immunol* (2010) 185:2432–41. doi: 10.4049/jimmunol.1000486
59. Giai C, Gonzalez CD, Sabbione F, Garofalo A, Ojeda D, Sordelli DO, et al. *Staphylococcus Aureus* Induces Shedding of IL-1RII in Monocytes and Neutrophils. *J Innate Immun* (2016) 8:284–98. doi: 10.1159/000443663
60. Liu J, Yang Y, Li H, Liu Y, Sun Y, Wu J, et al. IL1R2 Polymorphisms Are Associated With Increased Risk of Esophageal Cancer. *Curr Mol Med* (2020) 20:379–87. doi: 10.2174/1566524019666191025091204
61. Reyes M, Filbin MR, Bhattacharyya RP, Billman K, Eisenhaure T, Hung DT, et al. An Immune-Cell Signature of Bacterial Sepsis. *Nat Med* (2020) 26:333–40. doi: 10.1038/s41591-020-0752-4
62. Schulte-Schrepping J, Reusch N, Paclik D, Bassler K, Schlickeiser S, Zhang B, et al. Severe COVID-19 Is Marked by a Dysregulated Myeloid Cell Compartment. *Cell* (2020) 182:1419–40 e23. doi: 10.1016/j.cell.2020.08.001
63. Bessis N, Guery L, Mantovani A, Vecchi A, Sims JE, Fradelizi D, et al. The Type II Decoy Receptor of IL-1 Inhibits Murine Collagen-Induced Arthritis. *Eur J Immunol* (2000) 30:867–75. doi: 10.1002/1521-4141(200003)30:3<867::AID-IMMU867>3.0.CO;2-M
64. Shimizu K, Nakajima A, Sudo K, Liu Y, Mizoroki A, Ikarashi T, et al. IL-1 Receptor Type 2 Suppresses Collagen-Induced Arthritis by Inhibiting IL-1 Signal on Macrophages. *J Immunol* (2015) 194:3156–68. doi: 10.4049/jimmunol.1402155
65. Martin P, Palmer G, Rodriguez E, Seemayer CA, Palomo J, Talbot-Ayer D, et al. Deficiency in IL-1 Receptor Type 2 Aggravates K/BxN Serum Transfer-Induced Arthritis in Mice But Has No Impact on Systemic Inflammatory Responses. *J Immunol* (2017) 198:2916–26. doi: 10.4049/jimmunol.1600855
66. Mattos MS, Lopes ME, de Araujo AM, Alvarenga DM, Nakagaki BN, Mafra K, et al. Prolonged Neutrophil Survival at Necrotic Sites Is a Fundamental Feature for Tissue Recovery and Resolution of Hepatic Inflammation. *J Leukoc Biol* (2020) 108:1199–213. doi: 10.1002/JLB.1MA0420-634R
67. Rauschmayr T, Groves RW, Kupper TS. Keratinocyte Expression of the Type 2 Interleukin 1 Receptor Mediates Local and Specific Inhibition of Interleukin 1-Mediated Inflammation. *Proc Natl Acad Sci USA* (1997) 94:5814–9. doi: 10.1073/pnas.94.11.5814
68. Khoufache K, Bondza PK, Harir N, Daris M, Leboeuf M, Mailloux J, et al. Soluble Human IL-1 Receptor Type 2 Inhibits Ectopic Endometrial Tissue Implantation and Growth: Identification of a Novel Potential Target for Endometriosis Treatment. *Am J Pathol* (2012) 181:1197–205. doi: 10.1016/j.ajpath.2012.06.022
69. Simeoni E, Dudler J, Fleury S, Li J, Pagnotta M, Pascual M, et al. Gene Transfer of a Soluble IL-1 Type 2 Receptor-Ig Fusion Protein Improves Cardiac Allograft Survival in Rats. *Eur J Cardiothorac Surg* (2007) 31:222–8. doi: 10.1016/j.ejcts.2006.10.042
70. Chang H, Wang Y, Wu W, Li G, Hanawa H, Zou J. Hydrodynamics-Based Delivery of an Interleukin-1 Receptor II Fusion Gene Ameliorates Rat Autoimmune Myocarditis by Inhibiting IL-1 and Th17 Cell Polarization. *Int J Mol Med* (2013) 31:833–40. doi: 10.3892/ijmm.2013.1276
71. Feng Y, Li M, Wang S, Cong W, Hu G, Song Y, et al. Paired Box 6 Inhibits Cardiac Fibroblast Differentiation. *Biochem Biophys Res Commun* (2020) 528:561–66. doi: 10.1016/j.bbrc.2020.05.146
72. Garlanda C, Mantovani A. Interleukin-1 in Tumor Progression, Therapy, and Prevention. *Cancer Cell* (2021) 39:1023–27. doi: 10.1016/j.ccell.2021.04.011
73. Ruckert F, Dawelbait G, Winter C, Hartmann A, Denz A, Ammerpohl O, et al. Examination of Apoptosis Signaling in Pancreatic Cancer by Computational Signal Transduction Analysis. *PLoS One* (2010) 5:e12243. doi: 10.1371/journal.pone.0012243
74. Khatri I, Bhasin MKA. Transcriptomics-Based Meta-Analysis Combined With Machine Learning Identifies a Secretory Biomarker Panel for Diagnosis of Pancreatic Adenocarcinoma. *Front Genet* (2020) 11:572284. doi: 10.3389/fgene.2020.572284
75. Yan H, Qu J, Cao W, Liu Y, Zheng G, Zhang E, et al. Identification of Prognostic Genes in the Acute Myeloid Leukemia Immune Microenvironment Based on TCGA Data Analysis. *Cancer Immunol Immunother* (2019) 68:1971–78. doi: 10.1007/s00262-019-02408-7
76. Laios A, O'Toole SA, Flavin R, Martin C, Ring M, Gleeson N, et al. An Integrative Model for Recurrence in Ovarian Cancer. *Mol Cancer* (2008) 7:8. doi: 10.1186/1476-4598-7-8
77. Ricote M, Garcia-Tunon I, Bethencourt FR, Fraile B, Paniagua R, Royuela M. Interleukin-1 (IL-1alpha and IL-1beta) and Its Receptors (IL-1RI, IL-1RII, and IL-1Ra) in Prostate Carcinoma. *Cancer* (2004) 100:1388–96. doi: 10.1002/cncr.20142
78. Yuan M, Wang L, Huang H, Li Y, Zheng X, Shao Q, et al. IL-1R2 Expression in Human Gastric Cancer and Its Clinical Significance. *Biosci Rep* (2021) 41: BSR20204425. doi: 10.1042/BSR20204425
79. Eum HH, Kwon M, Ryu D, Jo A, Chung W, Kim N, et al. Tumor-Promoting Macrophages Preval in Malignant Ascites of Advanced Gastric Cancer. *Exp Mol Med* (2020) 52:1976–88. doi: 10.1038/s12276-020-00538-y
80. Chan KY, Leung FW, Lam HS, Tam YH, To KF, Cheung HM, et al. Immunoregulatory Protein Profiles of Necrotizing Enterocolitis Versus Spontaneous Intestinal Perforation in Preterm Infants. *PLoS One* (2012) 7:e36977. doi: 10.1371/journal.pone.0036977
81. Kovach MA, Stringer KA, Bunting R, Wu X, San Mateo L, Newstead MW, et al. Microarray Analysis Identifies IL-1 Receptor Type 2 as a Novel Candidate Biomarker in Patients With Acute Respiratory Distress Syndrome. *Respi Res* (2015) 16:29. doi: 10.1186/s12931-015-0190-x
82. van Deuren M, van der Ven-Jongekrijg J, Vannier E, van Dalen R, Pesman G, Bartelink AK, et al. The Pattern of Interleukin-1beta (IL-1beta) and Its Modulating Agents IL-1 Receptor Antagonist and IL-1 Soluble Receptor Type II in Acute Meningococcal Infections. *Blood* (1997) 90:1101–8. doi: 10.1182/blood.V90.3.1101.1101_1101_1108
83. Puc I, Ho TC, Yen KL, Vats A, Tsai JJ, Chen PL, et al. Cytokine Signature of Dengue Patients at Different Severity of the Disease. *Int J Mol Sci* (2021) 22:2879. doi: 10.3390/ijms22062879
84. Muller B, Peri G, Doni A, Perruchoud AP, Landmann R, Pasqualini F, et al. High Circulating Levels of the IL-1 Type II Decoy Receptor in Critically Ill Patients With Sepsis: Association of High Decoy Receptor Levels With Glucocorticoid Administration. *J Leukoc Biol* (2002) 72:643–9.
85. Jouvenne P, Vannier E, Dinarello CA, Miossec P. Elevated Levels of Soluble Interleukin-1 Receptor Type II and Interleukin-1 Receptor Antagonist in Patients With Chronic Arthritis: Correlations With Markers of Inflammation and Joint Destruction. *Arthritis Rheum* (1998) 41:1083–9. doi: 10.1002/1529-0131(199806)41:6<1083::AID-ART15>3.0.CO;2-9
86. Meusch U, Klingner M, Baerwald C, Rossol M, Wagner U. Deficient Spontaneous *In Vitro* Apoptosis and Increased tmTNF Reverse Signaling-Induced Apoptosis of Monocytes Predict Suboptimal Therapeutic Response of Rheumatoid Arthritis to TNF Inhibition. *Arthritis Res Ther* (2013) 15: R219. doi: 10.1186/ar4416
87. Dujmovic I, Mangano K, Pekmezovic T, Quattrocchi C, Mesaros S, Stojasavljevic N, et al. The Analysis of IL-1 Beta and Its Naturally Occurring Inhibitors in Multiple Sclerosis: The Elevation of IL-1 Receptor Antagonist and IL-1 Receptor Type II After Steroid Therapy. *J Neuroimmunol* (2009) 207:101–6. doi: 10.1016/j.jneuroim.2008.11.004
88. van der Torren CR, Verrijn Stuart AA, Lee D, Meerding J, van de Velde U, Pipeleers D, et al. Serum Cytokines as Biomarkers in Islet Cell Transplantation for Type 1 Diabetes. *PLoS One* (2016) 11:e0146649. doi: 10.1371/journal.pone.0146649
89. Geng Z, Liu J, Hu J, Wang Y, Tao Y, Zheng F, et al. Crucial Transcripts Predict Response to Initial Immunoglobulin Treatment in Acute Kawasaki Disease. *Sci Rep* (2020) 10:17860. doi: 10.1038/s41598-020-75039-z
90. Zhao E, Xie H, Zhang Y. Predicting Diagnostic Gene Biomarkers Associated With Immune Infiltration in Patients With Acute Myocardial Infarction. *Front Cardiovasc Med* (2020) 7:586871. doi: 10.3389/fcvm.2020.586871
91. Mora-Buch R, Dotti I, Planell N, Calderon-Gomez E, Jung P, Masamunt MC, et al. Epithelial IL-1R2 Acts as a Homeostatic Regulator During Remission of Ulcerative Colitis. *Mucosal Immunol* (2016) 9:950–9. doi: 10.1038/mi.2015.108
92. Thomassen E, Renshaw BR, Sims JE. Identification and Characterization of SIGIRR, a Molecule Representing a Novel Subtype of the IL-1R Superfamily. *Cytokine* (1999) 11:389–99. doi: 10.1006/cyto.1998.0452
93. Polentarutti N, Rol GP, Muzio M, Bosio D, Camnasio M, Riva F, et al. Unique Pattern of Expression and Inhibition of IL-1 Signaling by the IL-1 Receptor Family Member TIR8/SIGIRR. *Eur Cytokine Netw* (2003) 14:211–8.
94. Molgora M, Bonavita E, Ponzetta A, Riva F, Barbagallo M, Jaillon S, et al. IL-1R8 Is a Checkpoint in NK Cells Regulating Anti-Tumour and Anti-Viral Activity. *Nature* (2017) 551:110–14. doi: 10.1038/nature24293

95. Anselmo A, Riva F, Gentile S, Soldani C, Barbagallo M, Mazzon C, et al. Expression and Function of IL-1r8 (TIR8/SIGIRR): A Regulatory Member of the IL-1 Receptor Family in Platelets. *Cardiovasc Res* (2016) 111:373–84. doi: 10.1093/cvr/cvw162
96. Kadota C, Ishihara S, Aziz MM, Rumi MA, Oshima N, Mishima Y, et al. Down-Regulation of Single Immunoglobulin Interleukin-1R-Related Molecule (SIGIRR)/TIR8 Expression in Intestinal Epithelial Cells During Inflammation. *Clin Exp Immunol* (2010) 162:348–61. doi: 10.1111/j.1365-2249.2010.04254.x
97. Khan MA, Steiner TS, Sham HP, Bergstrom KS, Huang JT, Assi K, et al. The Single IgG IL-1-Related Receptor Controls TLR Responses in Differentiated Human Intestinal Epithelial Cells. *J Immunol* (2010) 184:2305–13. doi: 10.4049/jimmunol.0900021
98. Veliz Rodriguez T, Moalli F, Polentarutti N, Paroni M, Bonavita E, Anselmo A, et al. Role of Toll Interleukin-1 Receptor (IL-1R) 8, a Negative Regulator of IL-1r/Toll-Like Receptor Signaling, in Resistance to Acute Pseudomonas Aeruginosa Lung Infection. *Infect Immun* (2012) 80:100–9. doi: 10.1128/IAI.05695-11
99. Li D, Zhang X, Chen B. SIGIRR Participates in Negative Regulation of LPS Response and Tolerance in Human Bladder Epithelial Cells. *BMC Immunol* (2015) 16:73. doi: 10.1186/s12865-015-0137-5
100. Ueno-Shuto K, Kato K, Tasaki Y, Sato M, Sato K, Uchida Y, et al. Lipopolysaccharide Decreases Single Immunoglobulin Interleukin-1 Receptor-Related Molecule (SIGIRR) Expression by Suppressing Specificity Protein 1 (Sp1) via the Toll-Like Receptor 4 (TLR4)-P38 Pathway in Monocytes and Neutrophils. *J Biol Chem* (2014) 289:18097–109. doi: 10.1074/jbc.M113.532093
101. Vilia MG, Fonte E, Veliz Rodriguez T, Tocchetti M, Ranghetti P, Scarfo L, et al. The Inhibitory Receptor Toll Interleukin-1R 8 (TIR8/IL-1r8/SIGIRR) Is Downregulated in Chronic Lymphocytic Leukemia. *Leuk Lymphoma* (2017) 58:2419–25. doi: 10.1080/10428194.2017.1295142
102. Wald D, Qin J, Zhao Z, Qian Y, Naramura M, Tian L, et al. SIGIRR, a Negative Regulator of Toll-Like Receptor-Interleukin 1 Receptor Signaling. *Nat Immunol* (2003) 4:920–7. doi: 10.1038/ni968
103. Garlanda C, Riva F, Polentarutti N, Buracchi C, Sironi M, De Bortoli M, et al. Intestinal Inflammation in Mice Deficient in Tir8, an Inhibitory Member of the IL-1 Receptor Family. *Proc Natl Acad Sci USA* (2004) 101:3522–6. doi: 10.1073/pnas.0308680101
104. Qin J, Qian Y, Yao J, Grace C, Li X. SIGIRR Inhibits Interleukin-1 Receptor- and Toll-Like Receptor 4-Mediated Signaling Through Different Mechanisms. *J Biol Chem* (2005) 280:25233–41. doi: 10.1074/jbc.M501363200
105. Lech M, Garlanda C, Mantovani A, Kirschning CJ, Schlondorff D, Anders HJ. Different Roles of Tir8/Sigirr on Toll-Like Receptor Signaling in Intrarenal Antigen-Presenting Cells and Tubular Epithelial Cells. *Kidney Int* (2007) 72:182–92. doi: 10.1038/sj.ki.5002293
106. Bulek K, Swaidani S, Qin J, Lu Y, Gulen MF, Herjan T, et al. The Essential Role of Single Ig IL-1 Receptor-Related Molecule/Toll IL-1R8 in Regulation of Th2 Immune Response. *J Immunol* (2009) 182:2601–9. doi: 10.4049/jimmunol.0802729
107. Tomasoni R, Morini R, Lopez-Atalaya JP, Corradini I, Canzi A, Rasile M, et al. Lack of IL-1R8 in Neurons Causes Hyperactivation of IL-1 Receptor Pathway and Induces MECP2-Dependent Synaptic Defects. *Elife* (2017) 6:e21735. doi: 10.7554/eLife.21735
108. Li X, Qin J. Modulation of Toll-Interleukin 1 Receptor Mediated Signaling. *J Mol Med (Berl)* (2005) 83:258–66. doi: 10.1007/s00109-004-0622-4
109. Gong J, Wei T, Stark RW, Jamitzky F, Heckl WM, Anders HJ, et al. Inhibition of Toll-Like Receptors TLR4 and 7 Signaling Pathways by SIGIRR: A Computational Approach. *J Struct Biol* (2010) 169:323–30. doi: 10.1016/j.jsb.2009.12.007
110. Guven-Maiorov E, Keskin O, Gursoy A, Nussinov RA. Structural View of Negative Regulation of the Toll-Like Receptor-Mediated Inflammatory Pathway. *Biophys J* (2015) 109:1214–26. doi: 10.1016/j.bpj.2015.06.048
111. Garlanda C, Anders HJ, Mantovani A. TIR8/SIGIRR: An IL-1r/TLR Family Member With Regulatory Functions in Inflammation and T Cell Polarization. *Trends Immunol* (2009) 30:439–46. doi: 10.1016/j.it.2009.06.001
112. Drexler SK, Kong P, Inglis J, Williams RO, Garlanda C, Mantovani A, et al. SIGIRR/TIR-8 Is an Inhibitor of Toll-Like Receptor Signaling in Primary Human Cells and Regulates Inflammation in Models of Rheumatoid Arthritis. *Arthritis Rheum* (2010) 62:2249–61. doi: 10.1002/art.27517
113. Gulen MF, Kang Z, Bulek K, Youzhong W, Kim TW, Chen Y, et al. The Receptor SIGIRR Suppresses Th17 Cell Proliferation via Inhibition of the Interleukin-1 Receptor Pathway and mTOR Kinase Activation. *Immunity* (2010) 32:54–66. doi: 10.1016/j.immuni.2009.12.003
114. Xiao H, Yin W, Khan MA, Gulen MF, Zhou H, Sham HP, et al. Loss of Single Immunoglobulin Interleukin-1 Receptor-Related Molecule Leads to Enhanced Colonic Polyposis in Apc(min) Mice. *Gastroenterology* (2010) 139:574–85. doi: 10.1053/j.gastro.2010.04.043
115. Li S, Neff CP, Barber K, Hong J, Luo Y, Azam T, et al. Extracellular Forms of IL-37 Inhibit Innate Inflammation *In Vitro* and *In Vivo* But Require the IL-1 Family Decoy Receptor IL-1r8. *Proc Natl Acad Sci USA* (2015) 112:2497–502. doi: 10.1073/pnas.1424626112
116. Li L, Wei J, Suber TL, Ye Q, Miao J, Li S, et al. IL-37-Induced Activation of Glycogen Synthase Kinase 3 β Promotes IL-1r8/Sigirr Phosphorylation, Internalization, and Degradation in Lung Epithelial Cells. *J Cell Physiol* (2021) 236:5676–85. doi: 10.1002/jcp.30253
117. Moretti S, Bozza S, Oikonomou V, Renga G, Casagrande A, Iannitti RG, et al. IL-37 Inhibits Inflammasome Activation and Disease Severity in Murine Aspergillosis. *PLoS Pathog* (2014) 10:e1004462. doi: 10.1371/journal.ppat.1004462
118. Lunding L, Webering S, Vock C, Schroder A, Raedler D, Schaub B, et al. IL-37 Requires IL-18R α and SIGIRR/IL-1R8 to Diminish Allergic Airway Inflammation in Mice. *Allergy* (2015) 70:366–73. doi: 10.1111/all.12566
119. Sanchez-Fernandez A, Zandee S, Amo-Aparicio J, Charabati M, Prat A, Garlanda C, et al. IL-37 Exerts Therapeutic Effects in Experimental Autoimmune Encephalomyelitis Through the Receptor Complex IL-1r5/IL-1r8. *Theranostics* (2021) 11:1–13. doi: 10.7150/thno.47435
120. Amo-Aparicio J, Sanchez-Fernandez A, Li S, Eisenmesser EZ, Garlanda C, Dinarello CA, et al. Extracellular and Nuclear Roles of IL-37 After Spinal Cord Injury. *Brain Behav Immun* (2021) 91:194–201. doi: 10.1016/j.bbi.2020.09.026
121. Li Y, Chu H, Zhao M, Li C, Guan Y, Guo C, et al. IL-37d Negatively Regulates NLRP3 Transcription via Receptor-Mediated Pathway and Alleviates DSS-Induced Colitis. *Inflamm Bowel Dis* (2021) 27:84–93. doi: 10.1093/ibd/izaa124
122. Cavalli G, Tengesdal IW, Gresnigt M, Nemkov T, Arts RJW, Dominguez-Andres J, et al. The Anti-Inflammatory Cytokine Interleukin-37 Is an Inhibitor of Trained Immunity. *Cell Rep* (2021) 35:108955. doi: 10.1016/j.celrep.2021.108955
123. Jia C, Zhuge Y, Zhang S, Ni C, Wang L, Wu R, et al. IL-37b Alleviates Endothelial Cell Apoptosis and Inflammation in Kawasaki Disease Through IL-1R8 Pathway. *Cell Death Dis* (2021) 12:575. doi: 10.1038/s41419-021-03852-z
124. Ballak DB, van Diepen JA, Moschen AR, Jansen HJ, Hijmans A, Groenhouf GJ, et al. IL-37 Protects Against Obesity-Induced Inflammation and Insulin Resistance. *Nat Commun* (2014) 5:4711. doi: 10.1038/ncomms5711
125. Cavalli G, Justice JN, Boyle KE, D'Alessandro A, Eisenmesser EZ, Herrera JJ, et al. Interleukin 37 Reverses the Metabolic Cost of Inflammation, Increases Oxidative Respiration, and Improves Exercise Tolerance. *Proc Natl Acad Sci USA* (2017) 114:2313–18. doi: 10.1073/pnas.1619011114
126. Feng W, Gu YF, Nie L, Guo DY, Xiang LX, Shao JZ. Characterization of SIGIRR/IL-1R8 Homolog From Zebrafish Provides New Insights Into Its Inhibitory Role in Hepatic Inflammation. *J Immunol* (2016) 197:151–67. doi: 10.4049/jimmunol.1502334
127. Yang S, Liu B, Yin S, Shang Y, Zhang X, Khan MUZ, et al. Porcine Circovirus Type 2 Induces Single Immunoglobulin Interleukin-1 Related Receptor (SIGIRR) Downregulation to Promote Interleukin-1 β Upregulation in Porcine Alveolar Macrophage. *Viruses* (2019) 11:1021. doi: 10.3390/v11111021
128. Filipe J, Bronzo V, Curone G, Castiglioni B, Vigo D, Smith B, et al. Staphylococcus Aureus Intra-Mammary Infection Affects the Expression Pattern of IL-1R8 in Goat. *Comp Immunol Microbiol Infect Dis* (2019) 66:101339. doi: 10.1016/j.cimid.2019.101339
129. Riva F, Rahman MM, Turin L, Cecilian F, Russo S, Tribbioli G, et al. TIR8 Receptor Expression in Bovine Tissues. *Vet Immunol Immunopathol* (2010) 136:65–70. doi: 10.1016/j.vetimm.2010.02.009
130. Trevisi E, Amadori M, Riva F, Bertoni G, Bani P. Evaluation of Innate Immune Responses in Bovine Forestomachs. *Res Vet Sci* (2014) 96:69–78. doi: 10.1016/j.rvsc.2013.11.011

131. Fukuyama K, Islam MA, Takagi M, Ikeda-Ohtsubo W, Kurata S, Aso H, et al. Evaluation of the Immunomodulatory Ability of Lactic Acid Bacteria Isolated From Feedlot Cattle Against Mastitis Using a Bovine Mammary Epithelial Cells *In Vitro* Assay. *Pathogens* (2020) 9:410. doi: 10.3390/pathogens9050410
132. Wu Y, Zhu C, Chen Z, Chen Z, Zhang W, Ma X, et al. Protective Effects of *Lactobacillus Plantarum* on Epithelial Barrier Disruption Caused by Enterotoxigenic *Escherichia Coli* in Intestinal Porcine Epithelial Cells. *Vet Immunol Immunopathol* (2016) 172:55–63. doi: 10.1016/j.vetimm.2016.03.005
133. Hosoya S, Villena J, Chiba E, Shimazu T, Suda Y, Aso H, et al. Advanced Application of Porcine Intestinal Epithelial Cells for the Selection of Immunobiotics Modulating Toll-Like Receptor 3-Mediated Inflammation. *J Microbiol Immunol Infect* (2013) 46:474–81. doi: 10.1016/j.jmii.2012.04.005
134. Villena J, Suzuki R, Fujie H, Chiba E, Takahashi T, Tomosada Y, et al. Immunobiotic *Lactobacillus Jensenii* Modulates the Toll-Like Receptor 4-Induced Inflammatory Response via Negative Regulation in Porcine Antigen-Presenting Cells. *Clin Vaccine Immunol* (2012) 19:1038–53. doi: 10.1128/CI.00199-12
135. Garlanda C, Di Liberto D, Vecchi A, La Manna MP, Buracchi C, Caccamo N, et al. Damping Excessive Inflammation and Tissue Damage in Mycobacterium Tuberculosis Infection by Toll IL-1 Receptor 8/Single Ig IL-1-Related Receptor, a Negative Regulator of IL-1/TLR Signaling. *J Immunol* (2007) 179:3119–25. doi: 10.4049/jimmunol.179.5.3119
136. Bozza S, Zelante T, Moretti S, Bonifazi P, DeLuca A, D'Angelo C, et al. Lack of Toll IL-1R8 Exacerbates Th17 Cell Responses in Fungal Infection. *J Immunol* (2008) 180:4022–31. doi: 10.4049/jimmunol.180.6.4022
137. Leemans JC, Butter LM, Teske GJ, Stroo I, Pulsens WP, Florquin S. The Toll Interleukin-1 Receptor (IL-1R) 8/Single Ig Domain IL-1R-Related Molecule Modulates the Renal Response to Bacterial Infection. *Infect Immun* (2012) 80:3812–20. doi: 10.1128/IAI.00422-12
138. Blok DC, van Lieshout MH, Hoogendijk AJ, Florquin S, de Boer OJ, Garlanda C, et al. Single Immunoglobulin Interleukin-1 Receptor-Related Molecule Impairs Host Defense During Pneumonia and Sepsis Caused by *Streptococcus Pneumoniae*. *J Innate Immun* (2014) 6:542–52. doi: 10.1159/000358239
139. Sham HP, Yu EY, Gulen MF, Bhinder G, Stahl M, Chan JM, et al. SIGIRR, a Negative Regulator of TLR/IL-1r Signalling Promotes Microbiota Dependent Resistance to Colonization by Enteric Bacterial Pathogens. *PLoS Pathog* (2013) 9:e1003539. doi: 10.1371/journal.ppat.1003539
140. Samarani S, Abulkhair A, Amre D, Mehrj V, Tremblay C, Routy JP, et al. The Anti-Inflammatory IL-37/SIGIRR Axis Is Functionally Compromised in HIV Infection. *AIDS* (2019) 33:1693–703. doi: 10.1097/QAD.0000000000002271
141. Lech M, Kulkarni OP, Pfeiffer S, Savarese E, Krug A, Garlanda C, et al. Tir8/Sigirr Prevents Murine Lupus by Suppressing the Immunostimulatory Effects of Lupus Autoantigens. *J Exp Med* (2008) 205:1879–88. doi: 10.1084/jem.20072646
142. Russell SE, Stefanska AM, Kubica M, Horan RM, Mantovani A, Garlanda C, et al. Toll IL-1r8/Single Ig IL-1-Related Receptor Regulates Psoriasiform Inflammation Through Direct Inhibition of Innate IL-17a Expression by Gammadelta T Cells. *J Immunol* (2013) 191:3337–46. doi: 10.4049/jimmunol.1300828
143. Giannoudaki E, Stefanska AM, Lawler H, Leon G, Hernandez Santana YE, Hassan N, et al. SIGIRR Negatively Regulates IL-36-Driven Psoriasiform Inflammation and Neutrophil Infiltration in the Skin. *J Immunol* (2021) 207:651–60. doi: 10.4049/jimmunol.2100237
144. Liu X, Zhu L, Lu Z, Chen H, Fan L, Xue Q, et al. IL-37 Represses the Autoimmunity in Myasthenia Gravis via Directly Targeting Follicular Th and B Cells. *J Immunol* (2020) 204:1736–45. doi: 10.4049/jimmunol.1901176
145. Noris M, Cassis P, Azzollini N, Cavinato R, Cugini D, Casiraghi F, et al. The Toll-IL-1R Member Tir8/SIGIRR Negatively Regulates Adaptive Immunity Against Kidney Grafts. *J Immunol* (2009) 183:4249–60. doi: 10.4049/jimmunol.0803549
146. Xue Z, Zhang X, Chen M, Lu X, Deng R, Ma Y. Dendritic Cells Transduced With Single Immunoglobulin IL-1-Related Receptor Exhibit Immature Properties and Prolong Islet Allograft Survival. *Front Immunol* (2017) 8:1671. doi: 10.3389/fimmu.2017.01671
147. Barry J, Loh Z, Collison A, Mazzone S, Lalwani A, Zhang V, et al. Absence of Toll-IL-1 Receptor 8/Single Immunoglobulin IL-1 Receptor-Related Molecule Reduces House Dust Mite-Induced Allergic Airway Inflammation in Mice. *Am J Respir Cell Mol Biol* (2013) 49:481–90. doi: 10.1165/rcmb.2012-0425OC
148. Costello DA, Watson MB, Cowley TR, Murphy N, Murphy Royal C, Garlanda C, et al. Interleukin-1alpha and HMGB1 Mediate Hippocampal Dysfunction in SIGIRR-Deficient Mice. *J Neurosci* (2011) 31:3871–9. doi: 10.1523/JNEUROSCI.6676-10.2011
149. Xiao H, Gulen MF, Qin J, Yao J, Bulek K, Kish D, et al. The Toll-Interleukin-1 Receptor Member SIGIRR Regulates Colonic Epithelial Homeostasis, Inflammation, and Tumorigenesis. *Immunity* (2007) 26:461–75. doi: 10.1016/j.immuni.2007.02.012
150. Garlanda C, Riva F, Veliz T, Polentarutti N, Pasqualini F, Radaelli E, et al. Increased Susceptibility to Colitis-Associated Cancer of Mice Lacking TIR8, an Inhibitory Member of the Interleukin-1 Receptor Family. *Cancer Res* (2007) 67:6017–21. doi: 10.1158/0008-5472.CAN-07-0560
151. Campesato LF, Silva APM, Cordeiro L, Correa BR, Navarro FCP, Zanin RF, et al. High IL-1R8 Expression in Breast Tumors Promotes Tumor Growth and Contributes to Impaired Antitumor Immunity. *Oncotarget* (2017) 8:49470–83. doi: 10.18632/oncotarget.17713
152. Bertilaccio MT, Simonetti G, Dagklis A, Rocchi M, Rodriguez TV, Apollonio B, et al. Lack of TIR8/SIGIRR Triggers Progression of Chronic Lymphocytic Leukemia in Mouse Models. *Blood* (2011) 118:660–9. doi: 10.1182/blood-2011-01-329870
153. Riva F, Ponzone M, Supino D, Bertilaccio MTS, Polentarutti N, Massara M, et al. IL1R8 Deficiency Drives Autoimmunity-Associated Lymphoma Development. *Cancer Immunol Res* (2019) 7:874–85. doi: 10.1158/2326-6066.CIR-18-0698
154. Gonzalez-Ruiz S, Strillacci MG, Duran-Aguilar M, Canto-Alarcon GJ, Herrera-Rodriguez SE, Bagnato A, et al. Genome-Wide Association Study in Mexican Holstein Cattle Reveals Novel Quantitative Trait Loci Regions and Confirms Mapped Loci for Resistance to Bovine Tuberculosis. *Animals (Basel)* (2019) 9:636. doi: 10.3390/ani9090636
155. Horne DJ, Randhawa AK, Chau TT, Bang ND, Yen NT, Farrar JJ, et al. Common Polymorphisms in the PKP3-SIGIRR-TMEM16J Gene Region Are Associated With Susceptibility to Tuberculosis. *J Infect Dis* (2012) 205:586–94. doi: 10.1093/infdis/jir785
156. Sham HP, Walker KH, Abdunnour RE, Krishnamoorthy N, Douda DN, Norris PC, et al. 15-Epi-Lipoxin A4, Resolvin D2, and Resolvin D3 Induce NF-kappaB Regulators in Bacterial Pneumonia. *J Immunol* (2018) 200:2757–66. doi: 10.4049/jimmunol.1602090
157. Kanmani P, Kim H. Beneficial Effect of Immunobiotic Strains on Attenuation of Salmonella Induced Inflammatory Response in Human Intestinal Epithelial Cells. *PLoS One* (2020) 15:e0229647. doi: 10.1371/journal.pone.0229647
158. Gupta T, Kaur H, Kapila S, Kapila R. *Lactobacillus Fermentum* (MTCC-5898) Alleviates *Escherichia Coli*-Induced Inflammatory Responses in Intestinal Epithelial Cells by Modulating Immune Genes and NF-kappaB Signalling. *J Appl Microbiol* (2021) 31:3008–17. doi: 10.1111/jam.15153
159. Al-Kuhlani M, Lambert G, Pal S, de la Maza L, Ojcius DM. Immune Response Against Chlamydia Trachomatis via Toll-Like Receptors Is Negatively Regulated by SIGIRR. *PLoS One* (2020) 15:e0230718. doi: 10.1371/journal.pone.0230718
160. Salazar S, Badkoobehi H, Rockenstein E, Crews L, Chana G, Masliah E, et al. Toll-Like Receptor Pathway Gene Expression Is Associated With Human Immunodeficiency Virus-Associated Neurodegeneration. *J Neurovirol* (2007) 13:496–503. doi: 10.1080/13550280701558616
161. Lech M, Skuginna V, Kulkarni OP, Gong J, Wei T, Stark RW, et al. Lack of SIGIRR/TIR8 Aggravates Hydrocarbon Oil-Induced Lupus Nephritis. *J Pathol* (2010) 220:596–607. doi: 10.1002/path.2678
162. Wang DY, Su C, Chen GM, Pan HF, Wang FM, Liu GL, et al. The Decreased Frequency of SIGIRR-Positive CD4+ T Cells in Peripheral Blood of Patients With SLE and Its Correlation With Disease Activity. *Mol Biol Rep* (2015) 42:423–30. doi: 10.1007/s11033-014-3783-4
163. Xiao JP, Wang DY, Wang XR, Yuan L, Hao L, Wang DG. Increased Ratio of Th17 Cells to SIGIRR(+)CD4(+) T Cells in Peripheral Blood of Patients With SLE Is Associated With Disease Activity. *BioMed Rep* (2018) 9:339–44. doi: 10.3892/br.2018.1139
164. Wang L, Wang Y, Xia L, Shen H, Lu J. Elevated Frequency of IL-37- and IL-18-Ralphal-Positive T Cells in the Peripheral Blood of Rheumatoid Arthritis Patients. *Cytokine* (2018) 110:291–97. doi: 10.1016/j.cyto.2018.02.015

165. Cavalli G, Koenders M, Kalabokis V, Kim J, Tan AC, Garlanda C, et al. Treating Experimental Arthritis With the Innate Immune Inhibitor Interleukin-37 Reduces Joint and Systemic Inflammation. *Rheumatology (Oxford)* (2016) 55:2220–29. doi: 10.1093/rheumatology/kew325
166. Batliwalla FM, Li W, Ritchlin CT, Xiao X, Brenner M, Laragione T, et al. Microarray Analyses of Peripheral Blood Cells Identifies Unique Gene Expression Signature in Psoriatic Arthritis. *Mol Med* (2005) 11:21–9. doi: 10.2119/2006-00003.Gulko
167. Nakashima K, Hirota T, Obara K, Shimizu M, Jodo A, Kameda M, et al. An Association Study of Asthma and Related Phenotypes With Polymorphisms in Negative Regulator Molecules of the TLR Signaling Pathway. *J Hum Genet* (2006) 51:284–91. doi: 10.1007/s10038-005-0358-1
168. Na ES, Nelson ED, Kavalali ET, Monteggia LM. The Impact of MeCP2 Loss-or Gain-of-Function on Synaptic Plasticity. *Neuropsychopharmacology* (2013) 38:212–9. doi: 10.1038/npp.2012.116
169. Goldbach-Mansky R, Dailey NJ, Canna SW, Gelabert A, Jones J, Rubin BI, et al. Neonatal-Onset Multisystem Inflammatory Disease Responsive to Interleukin-1beta Inhibition. *N Engl J Med* (2006) 355:581–92. doi: 10.1056/NEJMoa055137
170. Wagh VV, Vyas P, Agrawal S, Pachpor TA, Paralikar V, Khare SP. Peripheral Blood-Based Gene Expression Studies in Schizophrenia: A Systematic Review. *Front Genet* (2021) 12:736483. doi: 10.3389/fgene.2021.736483
171. Costello DA, Carney DG, Lynch MA. Alpha-TLR2 Antibody Attenuates the Abeta-Mediated Inflammatory Response in Microglia Through Enhanced Expression of SIGIRR. *Brain Behav Immun* (2015) 46:70–9. doi: 10.1016/j.bbi.2015.01.005
172. Yang H, Mirsepasi-Lauridsen HC, Struve C, Allaire JM, Sivignon A, Vogl W, et al. Ulcerative Colitis-Associated E. Coli Pathobionts Potentiate Colitis in Susceptible Hosts. *Gut Microbes* (2020) 12:1847976. doi: 10.1080/19490976.2020.1847976
173. Allaire JM, Poon A, Crowley SM, Han X, Sharafian Z, Moore N, et al. Interleukin-37 Regulates Innate Immune Signaling in Human and Mouse Colonic Organoids. *Sci Rep* (2021) 11:8206. doi: 10.1038/s41598-021-87592-2
174. Sampath V, Menden H, Helbling D, Li K, Gastonguay A, Ramchandran R, et al. SIGIRR Genetic Variants in Premature Infants With Necrotizing Enterocolitis. *Pediatrics* (2015) 135:e1530–4. doi: 10.1542/peds.2014-3386
175. Cho SX, Rudloff I, Lao JC, Pang MA, Goldberg R, Bui CB, et al. Characterization of the Pathoimmunology of Necrotizing Enterocolitis Reveals Novel Therapeutic Opportunities. *Nat Commun* (2020) 11:5794. doi: 10.1038/s41467-020-19400-w
176. Yu W, Haque I, Venkatraman A, Menden HL, Mabry SM, Roy BC, et al. SIGIRR Mutation in Human Necrotizing Enterocolitis (NEC) Disrupts STAT3-Dependent microRNA Expression in Neonatal Gut. *Cell Mol Gastroenterol Hepatol* (2021) 13:425–40. doi: 10.1016/j.jcmgh.2021.09.009
177. Yamada Y, Hata K, Hirose Y, Hara A, Sugie S, Kuno T, et al. Microadenomatous Lesions Involving Loss of Apc Heterozygosity in the Colon of Adult Apc(Min/+) Mice. *Cancer Res* (2002) 62:6367–70.
178. Zhao J, Bulek K, Gulen MF, Zepp JA, Karagkounis G, Martin BN, et al. Human Colon Tumors Express a Dominant-Negative Form of SIGIRR That Promotes Inflammation and Colitis-Associated Colon Cancer in Mice. *Gastroenterology* (2015) 149:1860–71.e8. doi: 10.1053/j.gastro.2015.08.051
179. Ding L, Zhao X, Zhu N, Zhao M, Hu Q, Ni Y. The Balance of Serum IL-18/IL-37 Levels Is Disrupted During the Development of Oral Squamous Cell Carcinoma. *Surg Oncol* (2020) 32:99–107. doi: 10.1016/j.suronc.2019.12.001
180. Mei Y, Zhu Y, Teo HY, Liu Y, Song Y, Lim HY, et al. The Indirect Antiangiogenic Effect of IL-37 in the Tumor Microenvironment. *J Leukoc Biol* (2020) 107:783–96. doi: 10.1002/JLB.3MA0220-207RR
181. Zhang Z, Zhang J, He P, Han J, Sun C. Interleukin-37 Suppresses Hepatocellular Carcinoma Growth Through Inhibiting M2 Polarization of Tumor-Associated Macrophages. *Mol Immunol* (2020) 122:13–20. doi: 10.1016/j.molimm.2020.03.012
182. Wei X, Li Y, Zhang G, Wang N, Mi M, Xin Y, et al. IL-37 Was Involved in Progress of Acute Myeloid Leukemia Through Regulating IL-6 Expression. *Cancer Manag Res* (2021) 13:3393–402. doi: 10.2147/CMAR.S303017

Conflict of Interest: The authors declare that the research was conducted in the absence of any commercial or financial relationships that could be construed as a potential conflict of interest.

Publisher's Note: All claims expressed in this article are solely those of the authors and do not necessarily represent those of their affiliated organizations, or those of the publisher, the editors and the reviewers. Any product that may be evaluated in this article, or claim that may be made by its manufacturer, is not guaranteed or endorsed by the publisher.

Copyright © 2022 Supino, Minute, Mariancini, Riva, Magrini and Garlanda. This is an open-access article distributed under the terms of the Creative Commons Attribution License (CC BY). The use, distribution or reproduction in other forums is permitted, provided the original author(s) and the copyright owner(s) are credited and that the original publication in this journal is cited, in accordance with accepted academic practice. No use, distribution or reproduction is permitted which does not comply with these terms.



PHLDA1 Suppresses TLR4-Triggered Proinflammatory Cytokine Production by Interaction With Tollip

Hui Peng^{1,2†}, Juping Wang^{3†}, Xuhong Song¹, Jiangni Huang³, Haoming Hua³, Fanlu Wang³, Ziyun Xu³, Jing Ma³, Jie Gao³, Jing Zhao³, Anna Nong³, Dongyang Huang^{1*†} and Bin Liang^{1*†}

OPEN ACCESS

Edited by:

Shrikant R. Mulay,
Central Drug Research Institute (CSIR),
India

Reviewed by:

Javeed Ali Shah,
University of Washington,
United States
Vishal Khairnar,
Dana-Farber Cancer Institute,
United States

*Correspondence:

Bin Liang
bliang@stu.edu.cn
Dongyang Huang
huangdy@stu.edu.cn

[†]These authors have contributed
equally to this work

Specialty section:

This article was submitted to
Molecular Innate Immunity,
a section of the journal
Frontiers in Immunology

Received: 27 June 2021

Accepted: 17 January 2022

Published: 14 February 2022

Citation:

Peng H, Wang J, Song X,
Huang J, Hua H, Wang F, Xu Z,
Ma J, Gao J, Zhao J, Nong A,
Huang D and Liang B (2022) PHLDA1
Suppresses TLR4-Triggered
Proinflammatory Cytokine Production
by Interaction With Tollip.
Front. Immunol. 13:731500.
doi: 10.3389/fimmu.2022.731500

¹ Department of Cell Biology and Genetics, Key Laboratory of Molecular Biology in High Cancer Incidence Coastal Chao Shan Area of Guang Dong Higher Education Institutes, Shantou University Medical College, Shantou, China, ² Department of Clinical Laboratory, Affiliated Hospital of Youjiang Medical University for Nationalities, Baise, China, ³ Department of Pathophysiology, School of Basic Medical Sciences, Youjiang Medical University for Nationalities, Baise, China

Pleckstrin homology-like domain, family A, member 1 (PHLDA1) has been reported to be expressed in many mammalian tissues and cells. However, the functions and exact mechanisms of PHLDA1 remain unclear. In this study, we found that PHLDA1 expression was significantly altered in macrophages after exposure to lipopolysaccharide (LPS) *in vitro*, suggesting that PHLDA1 may be involved in the regulation of TLR4 signaling pathway activated by LPS. PHLDA1 attenuated the production of LPS-stimulated proinflammatory cytokines (TNF- α , IL-6, and IL-1 β). Further research showed that the phosphorylation levels of some important signal molecules in TLR4/MyD88-mediated MAPK and NF- κ B signaling pathways were reduced by PHLDA1, which in turn impaired the transcription factors NF- κ B and AP1 nuclear translocation and their responsive element activities. Furthermore, we found that PHLDA1 repressed LPS-induced proinflammatory cytokine production *via* binding to Tollip which restrained TLR4 signaling pathway. A mouse model of endotoxemia was established to confirm the above similar results. In brief, our findings demonstrate that PHLDA1 is a negative regulator of LPS-induced proinflammatory cytokine production by Tollip, suggesting that PHLDA1 plays an anti-inflammatory role through inhibiting the TLR4/MyD88 signaling pathway with the help of Tollip. PHLDA1 may be a novel therapeutic target in treating endotoxemia.

Keywords: PHLDA1, TLR4, suppress, proinflammatory cytokine, Tollip

INTRODUCTION

Pleckstrin homology-like domain, family A, member 1 (PHLDA1), which is also called T-cell death-associated gene 51 (TDAG51), was first found to induce apoptosis through cross-linking T-cell receptor (TCR) signaling pathway to Fas expression (1). The PHLDA1 family consists of three members, including PHLDA1, PHLDA2, and PHLDA3. PHLDA1, which contains pleckstrin

homology-like domain, polyglutamine tract, proline-glutamine tract, and proline-histidine-rich tract (2, 3), has three splice variants (PHLDA1-201, 202, and 203) and encodes a protein with 401 amino acids (45 kDa) or 260 amino acids (29.7 kDa) in length. Numerous studies have confirmed PHLDA1 expression at the protein and mRNA levels in many mammalian tissues, including the brain, endocrine tissues, and proximal digestive tract. PHLDA1 was also found to express in many types of cancer, such as brain, liver, bladder, and lung cancer (2, 4, 5). Studies have suggested that PHLDA1 is involved in many biological processes, such as cell proliferation, cell differentiation, cell death, cancer metastasis, epithelial-mesenchymal transition, and cancer stem cell properties (6–9). Although PHLDA1 has gotten increasing attention over the past 20 years, its role in endotoxemia remains to be elucidated.

The innate immune response eliminates invading microorganisms by inducing proinflammatory molecules (cytokines, chemokines, antibiotics, etc.) (10, 11). Toll-like receptors (TLRs) are an important component of innate immune response. The discovery of TLRs promoted the development of innate immunity. The first human homolog of the *Drosophila* Toll protein, now known as TLR4, was discovered by Janeway and colleagues in 1997 (12, 13). TLR4 is widely distributed in a variety of tissues such as the liver, colon, kidney, and spleen. TLR4 is also expressed in various cells such as Kupffer cells, monocytes, macrophages, neutrophils, Hofbauer cells, and cancer cells (14–16). Upon LPS stimulation, TLR4 forms the MD2/TLR4/CD14 complex (17–20) and causes the release of proinflammatory mediators by two classical signaling pathways, namely, MyD88-dependent signaling pathway and MyD88-independent signaling pathway, and then induces an immune response eventually (21–25).

In this study, the kinetics of PHLDA1 expression was first confirmed upon stimulation with LPS *in vitro*, which prompted us to focus on the role of PHLDA1 in the modulation of the TLR4 signaling pathway. We further found that PHLDA1 markedly reduced the phosphorylation levels of some signal molecules (ERK, JNK, p38, IKK α / β , I κ B α , and NF- κ B subunit p65) in TLR4/MyD88-mediated MAPK and NF- κ B signaling pathways, which in turn decreased the production of proinflammatory cytokines (TNF- α , IL-6, and IL-1 β). Finally, we verified that LPS induced the increased interaction between PHLDA1 with Tollip. In short, our study reveals a new function of PHLDA1 as a negative regulator of LPS-induced proinflammatory cytokine production.

MATERIALS AND METHODS

Reagents, Antibodies, Plasmids, and Mice

LPS-EK (LPS from *Escherichia coli* K12) was purchased from InvivoGen (San Diego, CA, USA). Transfection reagents, including Lipofectamine 2000 and Lipofectamine RNAiMAX, were ordered from Invitrogen (Camarillo, CA, USA). EZ Cell Transfection Reagent II was ordered from Life-iLab Biotech (Shanghai, China). 4,6-Diamino-2-phenylindole (DAPI) was

ordered from Beyotime Biotechnology (Shanghai, China). Mouse macrophage colony-stimulating factor (M-CSF) was ordered from PeproTech (East Windsor, NJ, USA). Protein G PLUS-Agarose was ordered from Santa Cruz Biotechnology Inc. (Santa Cruz, CA, USA), and 10 \times RIPA lysis buffer was ordered from Merck Millipore (Bedford, MA, USA). NF- κ B and Renilla luciferase reporter plasmids were gifts from Professor Y. Eugene Chin (Institute of Biology and Medical Sciences, Soochow University Medical College). AP1 luciferase reporter plasmid was obtained from Beyotime Biotechnology (Shanghai, China). The PHLDA1 plasmid was obtained from Genechem (Shanghai, China). The primary and second antibodies are shown in **Supplementary Table 1**. BALB/c mice and C57BL/6J (4–6 weeks old) were purchased from Vital River Laboratory Animal Technology (Beijing, China). All animal experiments were performed in accordance with the guidelines of Youjiang Medical University for Nationalities.

Cell Culture

RAW264.7, 293T, and L-929 cells were cultured in Dulbecco's modified Eagle's medium (DMEM, Invitrogen, Carlsbad, CA, USA) with 10% (v/v) fetal bovine serum (FBS, Gemini Bio-Products, Woodland, CA, USA), 1% streptomycin-penicillin mixtures (Beyotime Biotechnology, Shanghai, China), and 0.03% L-glutamine at 37°C in a humidified atmosphere with 5% CO₂. Bone marrow-derived macrophages (BMDM) were isolated from the femurs of C57BL/6J mice and cultured in DMEM with 10% (v/v) FBS and M-CSF (10 ng/ml). A total of 4×10^4 cells were seeded into 96-well plates for luciferase reporter activity assay, 2×10^5 cells were cultured in 24-well plates for enzyme-linked immunosorbent assay (ELISA), and 8×10^5 cells were cultured in a 3.5-cm dish for Western blot analysis.

RNA Interference and Plasmid Transfection

Small interfering RNA (siRNA) for PHLDA1 and Tollip were designed and synthesized by GenePharma (Shanghai, China). The above siRNA fragments were transfected into RAW264.7, BMDM, or L-929 cells using jetPEI[®]-Macrophage transfection reagent (Polyplus Transfection, Illkirch, France) or Lipofectamine RNAiMAX according to the manuals of the manufacturer. The above cells were further analyzed at 72 h after transfection. PHLDA1 and Tollip siRNA sequences are listed in **Supplementary Table 2**. Plasmids were transfected into RAW264.7, BMDM, L-929, or 293T cells using Lipofectamine 2000, jetPEI[®]-Macrophage transfection reagent, or EZ Cell Transfection Reagent II according to the manuals of the manufacturer. The above cells were further analyzed at 48 h after transfection.

Measurement of Proinflammatory Cytokines

RAW264.7 cells or BMDM were seeded into 24-well plates and transfected as described above after incubation overnight. After 48 h, the above cells were stimulated with LPS for the different time periods. IL-6, TNF- α , and IL-1 β in the supernatants were

measured with ELISA kits (Elabscience Biotechnology, Wuhan, Hubei, China) according to the instructions of the manufacturer.

Dual-Luciferase Reporter Assay

293T cells were seeded into 96-well plates and transfected as described above after incubation overnight. After 24 h, the above cells were stimulated with LPS for 20 h. After the above cells were lysed with 1× passive lysis buffer (PLB), the levels of NF- κ B, AP1, and Renilla luciferase activity were detected with the Dual-Luciferase[®] Reporter (DLR[™]) Assay System (Promega Biotech, Madison, WI, USA) according to the protocol of the manufacturer.

Real-Time Quantitative Reverse Transcription PCR

Total RNA was extracted from RAW264.7 cells and BMDM with RNAiso Plus reagent according to the instructions of the manufacturer (TaKaRa, Japan) and reverse transcribed with PrimeScript[™] RT reagent Kit (Perfect Real Time) (TaKaRa, Japan). Reverse transcription products of different samples were amplified using a LightCycler 96 system (Roche, Basel, Switzerland) with TB Green[®] Premix Ex Taq[™] (Tli RNaseH Plus) (TaKaRa, Japan) according to the instructions of the manufacturer. The $2^{-\Delta\Delta C_t}$ method was used to calculate the relative mRNA levels normalized to GAPDH or β -actin. The mouse primer sequences were as follows: PHLDA1—forward primer, 5'-GAAGATGGCCCATTCAAAAGCG-3', reverse primer, 5'-GAGGAGGCTAACACGCAGG-3'; GAPDH—forward primer, 5'-GGTTGTCTCCTGCGACTTCA-3', reverse primer, 5'-TGGTCCAGGGTTTCTTACTCC-3'.

Immunoprecipitation and Western Blot

The protein concentration was tested after cell lysis and centrifugation of the whole-cell lysates. Fifty micrograms of protein samples were used as input, and the rest of them were incubated with primary antibodies at 4°C overnight. Then, 20 μ l Protein G PLUS-Agarose beads were added into the supernatant containing the above antigen-antibody complex and incubated at room temperature for 4 h. After the above immune complexes were centrifuged and washed, 20 μ l 2× loading buffer was added to each sample. Bound proteins were eluted by boiling at 100°C for 10 min and transferred to nitrocellulose membranes after separation of these proteins by sodium dodecyl sulfate-polyacrylamide gel electrophoresis. After the above membranes were incubated with primary antibodies and second antibodies, respectively, a Tanon 5200 Multi Chemiluminescent Imaging System (Tanon, Shanghai, China) was used to detect the protein bands.

Immunofluorescence

Cells (5×10^5) were seeded into a 3.5-cm dish with glass coverslips. When the cell density reached 80%, cells were fixed with 4% paraformaldehyde for 30 min and then incubated with blocking buffer for 30 min. Cells were incubated with primary antibodies and secondary antibodies, respectively. After the nuclei were stained with DAPI for 15 min, images were taken

using the FluoView[™] FV1000 Confocal Laser Scanning Microscope (Olympus, Tokyo, Japan).

Immunohistochemistry

Mouse lung tissues were fixed with 4% formalin buffer and paraffin-embedded after excising. Lung tissues were cut into 4 μ m sections, deparaffinized with xylene, and rehydrated with ethanol. The above sections were boiled in antigenic repair solution using a microwave for 20 min. Part of the sections was stained with H&E, the others were incubated 50 μ l diluted primary antibodies at 4°C overnight and 50 μ l diluted secondary antibodies at room temperature for 30 min. Finally, diaminobenzidine staining was performed. The above sections were imaged under a Leica DMIL FL fluorescent inverted microscope (Leica, Wetzlar, Germany) after hematoxylin redyeing, alcohol dehydration, and clearing in xylene.

Establishment of a Mouse Model of Endotoxemia

Eighteen BALB/c mice (weight 20–22 g) were randomly divided into three groups, with six mice per group. Groups 2 and 3, as the experimental groups, were intraperitoneally injected with LPS (8 mg/kg), and they were then sacrificed at 1 or 6 h after injection, respectively. Group 1, as the control group, was also sacrificed at 1 h after intraperitoneal injection of the same amount of phosphate buffer saline (PBS). Serums from the above groups of mice were collected and used to detect the levels of proinflammatory cytokines (TNF- α , IL-6, and IL-1 β) using ELISA. Lung tissues from the above groups of mice were removed and used to examine PHLDA1 expression using immunohistochemistry (IHC) and Western blot.

Statistical Analysis

SPSS software (version 16.0; SPSS, Inc., Chicago, IL, USA) was used for statistical analysis. All experiments were repeated at least three times. The data were expressed as mean \pm SD and compared with independent-samples *t*-test and one-way ANOVA. *P*-values <0.05 were considered to be statistically significant.

RESULTS

Kinetics of LPS-Induced PHLDA1 Expression

To investigate the role of PHLDA1 in the response of macrophages to LPS stimulation, we tested whether PHLDA1 expression could be induced by LPS. The results showed that different concentrations of LPS increased significantly PHLDA1 expression in RAW264.7 cells, but two higher concentrations (1 and 10 μ g/ml) of LPS did not increase further the expression level of PHLDA1 after PHLDA1 expression reached the peak level with 0.1 μ g/ml of LPS treatment for 12 h (**Figure 1A**). Therefore, 0.1 μ g/ml was regarded as the concentration at which LPS was used to stimulate RAW264.7 cells. To explore the kinetics of the regulation of PHLDA1 expression in RAW264.7 cells induced by LPS, we tested PHLDA1 expression in RAW264.7 cells treated with LPS for different time periods with Western blot. The results indicated that PHLDA1

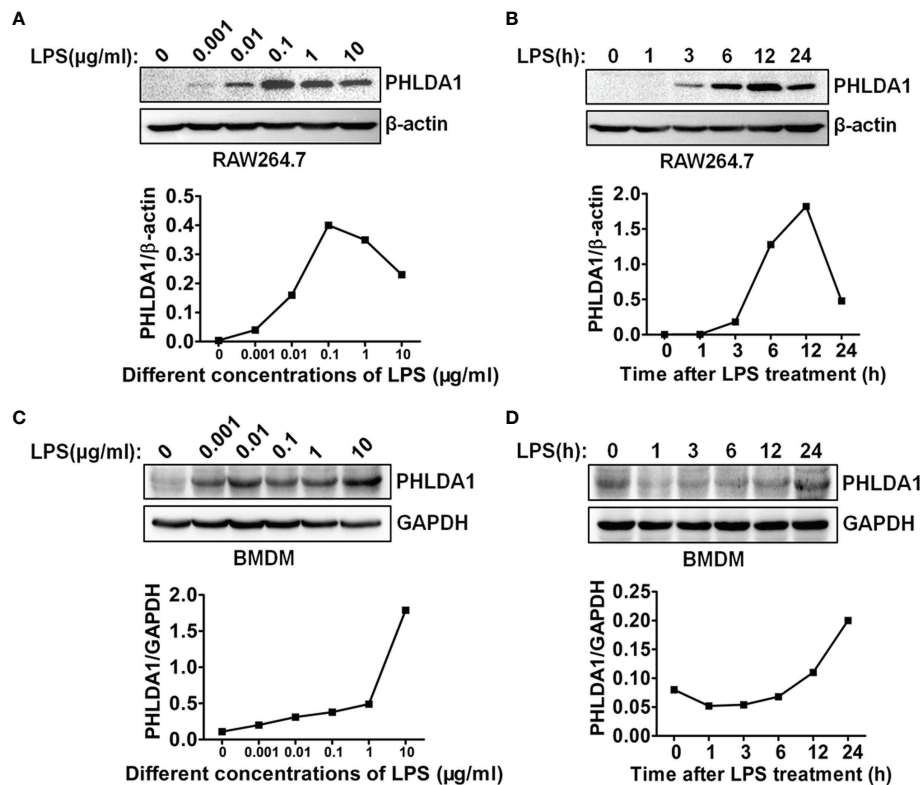


FIGURE 1 | LPS regulates PHLDA1 expression in macrophages. RAW264.7 cells (A) and BMDM (C) were treated with the different concentrations (0.001, 0.01, 0.1, 1, and 10 µg/ml) of LPS for 24 h. Western blot was used to measure PHLDA1 expression. RAW264.7 cells (B) and BMDM (D) were treated with LPS (0.1 µg/ml) for 0, 1, 3, 6, 12, and 24 h. Western blot was used to measure PHLDA1 expression. β-Actin or GAPDH was used as a loading control. The data are representative of three independent experiments. The quantified results of PHLDA1 expression are shown in the lower panel.

expression reached the peak level after 0.1 µg/ml of LPS treatment for 12 h and then gradually decreased (Figure 1B). The same experiments were performed in BMDM. The results showed that different concentrations of LPS increased sustainably PHLDA1 expression in BMDM, unlike RAW264.7 cells (Figure 1C). In addition, after LPS treatment for different time periods, PHLDA1 expression decreased firstly and then sustainably increased after LPS treatment for 1 h, which was different from that of RAW264.7 cells (Figure 1D). In summary, PHLDA1 expression displayed an increasing trend regardless of LPS treatment for different time periods or at different concentrations in both RAW264.7 cells and BMDM. To explore the effect of LPS on proinflammatory cytokine production, we explored LPS concentration- and time-dependent effects on TNF-α production in RAW264.7 cells and BMDM. The results indicated that different concentrations of LPS increased significantly TNF-α production in RAW264.7 cells and BMDM. TNF-α production reached the peak level after 0.1 or 0.01 µg/ml of LPS treatment for 12 h in RAW264.7 cells or BMDM, respectively, and then gradually decreased (Supplementary Figure 1A). In addition, LPS also markedly enhanced TNF-α production in RAW264.7 cells and BMDM at different time periods. TNF-α production simultaneously reached

the peak level after LPS treatment for 12 h in RAW264.7 cells and BMDM and then gradually decreased (Supplementary Figure 1B).

PHLDA1 Negatively Regulates LPS-Induced Proinflammatory Cytokine Production

To test whether PHLDA1 was involved in the regulation of TLR4 signaling pathway, we overexpressed PHLDA1 using plasmid transfection in RAW264.7 cells and BMDM and then detected the efficiency of PHLDA1 overexpression with Western blot and real-time quantitative reverse transcription PCR (RT-qPCR). The results demonstrated that PHLDA1 expressions were significantly upregulated at both protein (Figure 2A, left panel) and mRNA (Figures 2A, right panel, and 2B) levels in the above cells. It should be pointed out that PHLDA1 expression was not detected at the protein level using Western blot after PHLDA1 overexpression in BMDM because of limited number of cells. To determine the effect of PHLDA1 overexpression on the production of proinflammatory cytokines including TNF-α, IL-6, and IL-1β, RAW264.7 cells were overexpressed with empty vector (EV) or PHLDA1 plasmid, and then treated with or without LPS for 12 h. The results demonstrated that the production of the proinflammatory cytokines in PHLDA1-overexpressed RAW264.7 cells was significantly decreased after LPS treatment, compared with that of control cells transfected with EV

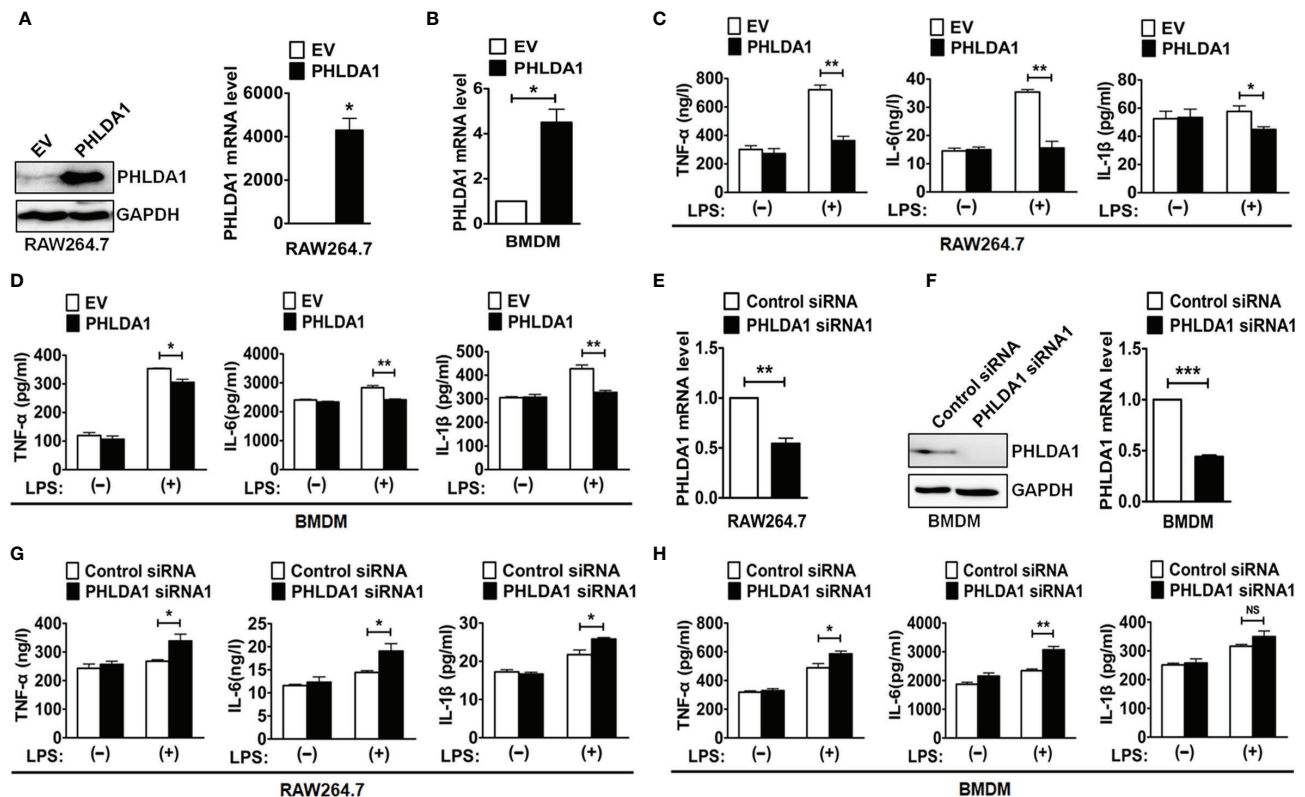


FIGURE 2 | PHLDA1 attenuates LPS-initiated production of proinflammatory cytokines. RAW264.7 cells (A) and BMDM (B) were transfected with EV or PHLDA1 plasmid. PHLDA1 expression was measured at the protein and mRNA levels with Western blot (left panel) and/or RT-qPCR (right panel). RAW264.7 cells (C) and BMDM (D), which were transfected with EV or PHLDA1 plasmid, were treated with or without LPS (0.1 μ g/ml) for 12 h. ELISA was performed to measure the production of proinflammatory cytokines (TNF- α , IL-6, and IL-1 β). RAW264.7 cells (E) and BMDM (F) were transfected with Control siRNA and PHLDA1 siRNA1, and PHLDA1 expression was measured at the protein and mRNA levels with Western blot (left panel) and/or RT-qPCR (right panel). RAW264.7 cells (G) and BMDM (H), which were transfected with Control siRNA and PHLDA1 siRNA1, were treated with or without LPS (0.1 μ g/ml) for 12 h. ELISA was performed to measure the production of proinflammatory cytokines (TNF- α , IL-6, and IL-1 β). Data are shown as means \pm SD of three independent experiments (NS means no significance, * P < 0.05; ** P < 0.01; *** P < 0.001).

(Figure 2C). Similar results were obtained in BMDM after PHLDA1 overexpression (Figure 2D). Subsequently, we screened the efficient siRNA fragments for downregulation of PHLDA1 expression. We tested LPS-induced PHLDA1 expression at the protein level with Western blot after transfection of Control siRNA and two PHLDA1 siRNAs (PHLDA1 siRNA1 and siRNA2) because our previous results confirmed that PHLDA1 expression was not detected at the protein level without LPS treatment or in 60 min after LPS treatment. The result demonstrated that both PHLDA1 siRNA1 and PHLDA1 siRNA2 reduced PHLDA1 expression, respectively, compared with Control siRNA in RAW264.7, and the PHLDA1 siRNA1 efficiency of downregulation of PHLDA1 expression was more significant than that of PHLDA1 siRNA2 (Supplementary Figure 2). For this reason, we used PHLDA1 siRNA1 to complete the follow-up experiments. To determine the effect of PHLDA1 knockdown on the production of proinflammatory cytokines, we reduced PHLDA1 expression by siRNA interference in RAW264.7 cells and BMDM, and then treated RAW264.7 cells with or without LPS for 12 h. The results demonstrated that the production of

proinflammatory cytokines was significantly increased in PHLDA1-deficient RAW264.7 cells after LPS treatment, compared with that of control cells transfected with Control siRNA (Figures 2E–G). Similar results were obtained in BMDM after the reduction of PHLDA1 expression (Figure 2H).

PHLDA1 Inhibits the Phosphorylation of Important Signal Molecules in TLR4/MyD88-Mediated Downstream MAPK and NF- κ B Signaling Pathways

We explored the effect of PHLDA1 on the activation of downstream MAPK and NF- κ B signaling pathways. The results showed that PHLDA1 overexpression significantly decreased the phosphorylation levels of some protein molecules (ERK, JNK, p38, IKK α / β , I κ B α , and NF- κ B subunit p65) in the MAPK and NF- κ B signaling pathways at different time points (0, 15, 30, 45, and 60 min) in RAW264.7 cells after LPS treatment, compared with that of control cells (Figure 3A). Then, we further solidified the above findings by including early time point such as 2 and 5 min of LPS

stimulation. Similar results were obtained in PHLDA1-upregulated RAW264.7 cells treated with LPS (**Supplementary Figure 3A**). Furthermore, we examined the effect of PHLDA1 knockdown on phosphorylation levels of the above signal molecules, and reverse results were obtained in PHLDA1-deficient RAW264.7 cells treated with LPS (**Figure 3B** and **Supplementary Figure 3B**).

PHLDA1 Impairs LPS-Induced NF- κ B and AP1 Nuclear Translocation and Their Responsive Element Activities

To further explore the underlying mechanism of PHLDA1-affected TLR4/MyD88 signaling pathway, we detected the nuclear

translocation of transcription factors NF- κ B subunit p65 and AP1 subunit c-jun with immunofluorescence (IF) after upregulation of PHLDA1 expression in RAW264.7 and L-929 cells. The results showed that PHLDA1 overexpression, which was established with IF (**Supplementary Figures 4A, B**), suppressed the translocations of p65 and c-jun from the cytoplasm to nuclear, compared with that of control RAW264.7 and L-929 cells (**Figures 4A, B, E**). The reverse results were obtained in PHLDA1-deficient RAW264.7 and L-929 cells (**Figures 4C, D, F** and **Supplementary Figure 4B**). We then tested the effect of PHLDA1 overexpression on NF- κ B and AP1 luciferase activities in 293T cells with or without LPS treatment. The results indicated that PHLDA1 overexpression decreased LPS-induced transcriptional activities of NF- κ B and AP1 (**Figures 4G, H**).

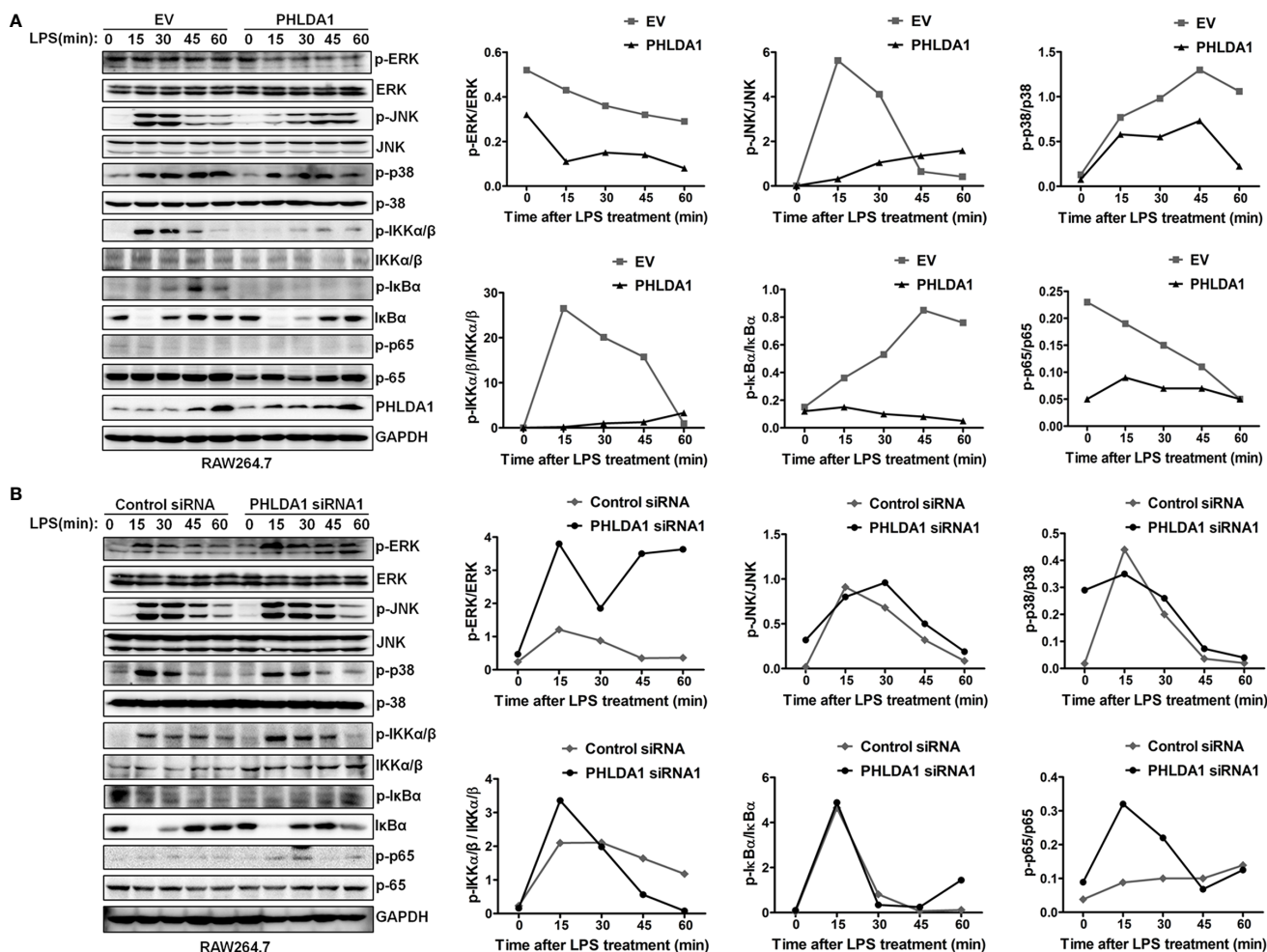


FIGURE 3 | PHLDA1 attenuates the activation of some signal molecules in MyD88-dependent TLR4 signaling pathway. **(A)** RAW264.7 cells were transfected with EV or PHLDA1 plasmid, and then stimulated with LPS (0.1 μ g/ml) for the indicated times. Phosphorylation levels and total protein expressions of important signal molecules (ERK, JNK, p38, IKK α / β , IkB α and p65) in cell lysates were analyzed using Western blot. **(B)** RAW264.7 cells were transfected with Control siRNA or PHLDA1 siRNA1, and then stimulated with LPS (0.1 μ g/ml) for the indicated times. Phosphorylation levels and total protein expressions of the above molecules were analyzed using Western blot. Data shown are representative of three independent experiments. Phosphorylation levels of the above molecules were quantitated and shown in the right panel. GAPDH was used as a loading control.

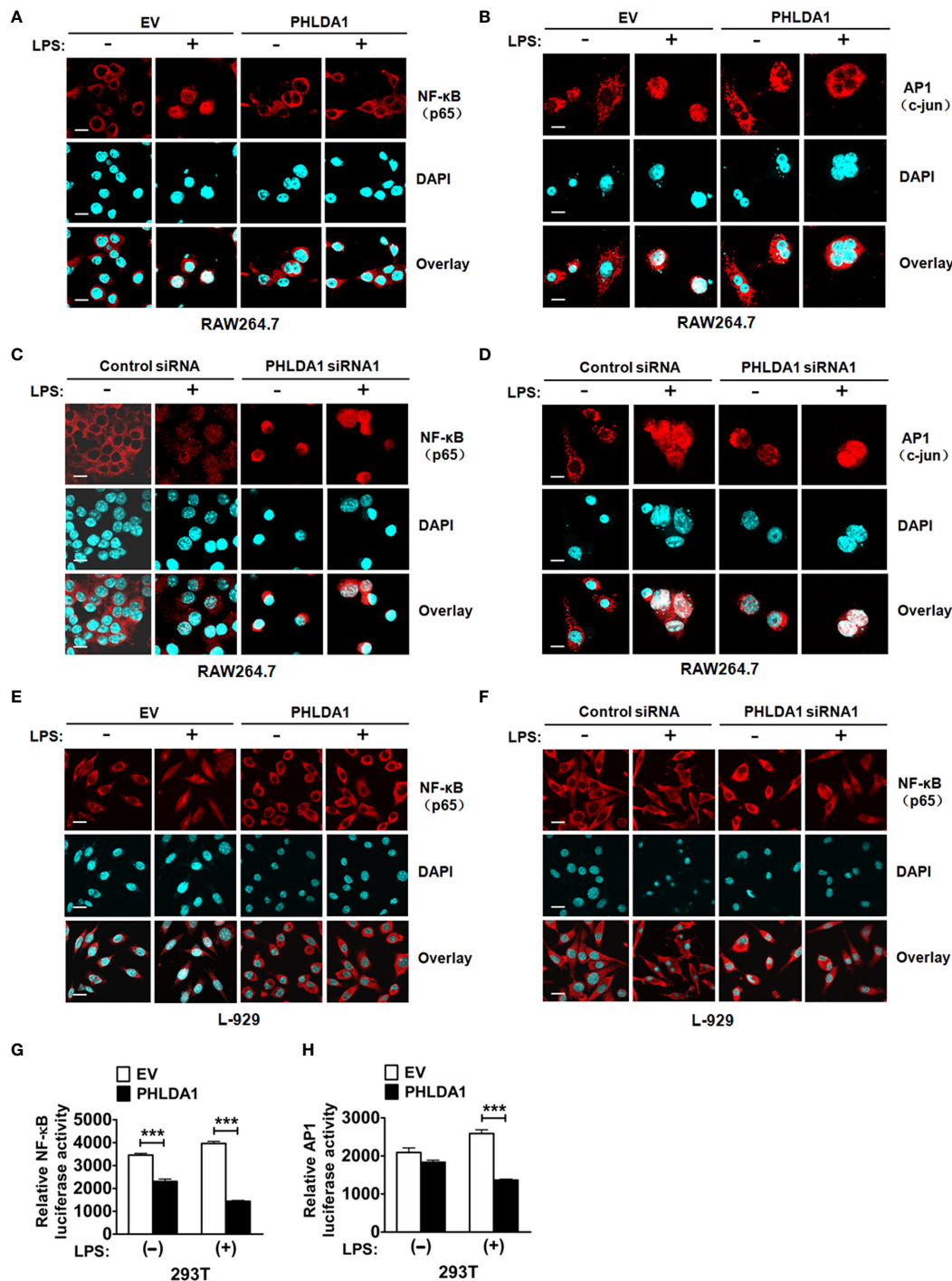


FIGURE 4 | PHLDA1 attenuates LPS-initiated nuclear translocations and responsive element activities of NF- κ B and AP1. RAW264.7 cells (**A, B**) and L-929 cells (**E**) were transfected with EV or PHLDA1 plasmid, and then stimulated with or without LPS (0.1 μ g/ml) for 1 h. Cells were immunostained with anti-NF- κ B (p65) antibody or anti-AP1 (c-jun) antibody and Alexa-594-labeled secondary antibodies. The nuclei were stained with DAPI for 15 min. The merged images were captured with a confocal microscope (scale bar, 20 μ m). RAW264.7 cells (**C, D**) and L-929 cells (**F**) were transfected with Control siRNA or PHLDA1 siRNA1, and then stimulated with or without LPS (0.1 μ g/ml) for 1 h. Cells were immunostained with anti-NF- κ B (p65) antibody or anti-AP1 (c-jun) antibody and Alexa-594-labeled secondary antibodies. The nuclei were stained with DAPI for 15 min. The merged images were captured with a confocal microscope (scale bar, 20 μ m). (**G, H**) EV or PHLDA1 plasmid was transfected into 293T cells together with pTK-Renilla luciferase and NF- κ B luciferase reporter plasmids. After 24 h of culture, the cells were incubated with LPS (0.1 μ g/ml) for 20 h. The Dual-Luciferase[®] Reporter (DLR[™]) Assay System was performed to measure NF- κ B or AP1 luciferase activity. Data are presented as mean \pm SD of three independent experiments (** P < 0.001).

PHLDA1 Inhibits TLR4-Mediated NF- κ B Nuclear Translocation and Proinflammatory Cytokine Production Through Binding to Tollip

Tollip, an important negative regulator of innate immunity, suppresses TLR signaling pathway through impairing the activity of interleukin-1 receptor-associated kinase (IRAK) (26–28). To investigate the role of Tollip which played in PHLDA1-impaired proinflammatory cytokine production induced by LPS, we completed the following *in-vitro* experiments. We found that Tollip expression presented an increasing trend as a whole in RAW264.7 treated with LPS for different time periods (Figure 5A). Co-IP assay was used to examine the effect of LPS treatment on the interaction between PHLDA1 and Tollip. The results showed that the above interaction gradually strengthened along with the increase of LPS treatment time (Figures 5B, C). Furthermore, we tested NF- κ B nuclear translocation induced by LPS based on PHLDA1 overexpression and Tollip downregulation. IF results confirmed that PHLDA1 overexpression restrained LPS-induced NF- κ B translocation from the cytoplasm to nuclear, compared with that of control RAW264.7 and L-929 cells. On the contrary, knockdown of Tollip reversed the above biological phenomenon (Figures 5D–F). The same experiments were performed with L-929 cells and similar results were obtained (Figures 5G–I). Then, we tested the production of proinflammatory cytokines (TNF- α , IL-6, and IL-1 β) induced by LPS based on PHLDA1 overexpression and Tollip downregulation. The results demonstrated that PHLDA1 overexpression restrained LPS-induced proinflammatory cytokine production, while knockdown of Tollip reversed the above biological phenomenon (Figure 5J). The same experiments were performed with L-929 cells and similar results were obtained (Figure 5K).

Verification of the Anti-Inflammatory Effect of PHLDA1 *In Vivo*

We used an endotoxemia mouse model to further confirm the above action mechanism of PHLDA1 in innate immunity after a series of *in-vitro* experiments. First of all, we screened the optimum LPS-treated time for constructing the above mouse model by detecting the kinetics of TNF- α concentration in serum from mice treated by LPS for different time periods. The results demonstrated that TNF- α concentration increased originally and reached the peak level after LPS treatment for 1 h, and then gradually decreased. TNF- α concentration is close to zero (Figure 6A). So 1 and 6 h were used as LPS treatment time to construct the above mouse model. We then examined PHLDA1 expressions of lung tissues from different groups of mice injected by LPS. IHC results showed that PHLDA1 expressions of lung tissues from group 2 (mice treated with LPS for 1 h) were more than those from group 1 (mice treated with PBS for 1 h), and PHLDA1 expressions of lung tissues from group 3 (mice treated with LPS for 6 h) were more than those from group 2 (Figure 6B). Similar results were obtained in the

lung tissues from mice by Western blot analysis (Figure 6C). ELISA analysis indicated that the levels of proinflammatory cytokines (TNF- α , IL-6, and IL-1 β) of serum from group 2 were higher than those from group 1, while the levels of proinflammatory cytokines from group 3 were lower than those from group 2 (Figure 6D).

DISCUSSION

In this study, we found that PHLDA1 expression was low and showed time- and dose-dependent changes after being exposed to LPS, suggesting that it was potentially involved in the regulation of TLR4 signaling pathway. Further studies demonstrated that overexpression of PHLDA1 attenuated LPS-induced proinflammatory cytokine production and vice versa. PHLDA1 impaired the phosphorylation levels of some important molecules (ERK, JNK, p38, IKK α/β , I κ B α , and NF- κ B subunit p65) in TLR4/MyD88-dependent signaling pathway, which in turn restrained the translocations of NF- κ B and AP1 from the cytoplasm to nuclear and their responsive element activities. Finally, we found that PHLDA1 recruited Tollip to restrain LPS-induced proinflammatory cytokine production. Similar results were obtained *in vivo*. These findings demonstrate that PHLDA1 has a pivotal role in regulating LPS-induced proinflammatory cytokine production. The proposed mechanism is depicted in Figure 7.

Previous studies have explored the role of PHLDA1 in inflammation. PHLDA1 was reported to positively regulate TLR2 signaling pathway to enhance lung contusion (29). Han et al. found that PHLDA1 directly interacted with TRAF6 and augmented K63-linked ubiquitination to activate the NF- κ B signaling pathway, which in turn promoted the production of LPS-induced proinflammatory cytokines (TNF- α and IL-1 β) and associated genes (iNOS and COX-2) in microglia cells. These findings indicated that PHLDA1 may be a potent regulator for neuroinflammation (30, 31). It was reported that PHLDA1 upregulation was dependent of RAW264.7 cell proliferation and cell cycle progression induced by LPS (32). Pam3CSK4, as a TLR2 ligand, induced PHLDA1 expression which was modulated *via* the JAK2–ERK1/2–STAT3 signaling pathway (33). Hossain et al. reported that PHLDA1 knockout significantly impaired LPS-induced expression of MCP-1 but not TNF- α (9), which is different from our results. In our study, the results showed that PHLDA1 knockdown enhanced LPS-induced production of the proinflammatory cytokines (TNF- α , IL-6, and IL-1 β). The possible reasons are as follows: 1) cells used in the experiments were different. RAW264.7 cell lines and BMDM isolated from C57BL/6J mice were used in our study, while peritoneal macrophages isolated from C57BL/6J mice were used in the report mentioned above; 2) gene regulation was different. RNA interference technology was used to downregulate PHLDA1 expression in our study, while gene knockout technology was used to delete PHLDA1 gene in the report mentioned above.

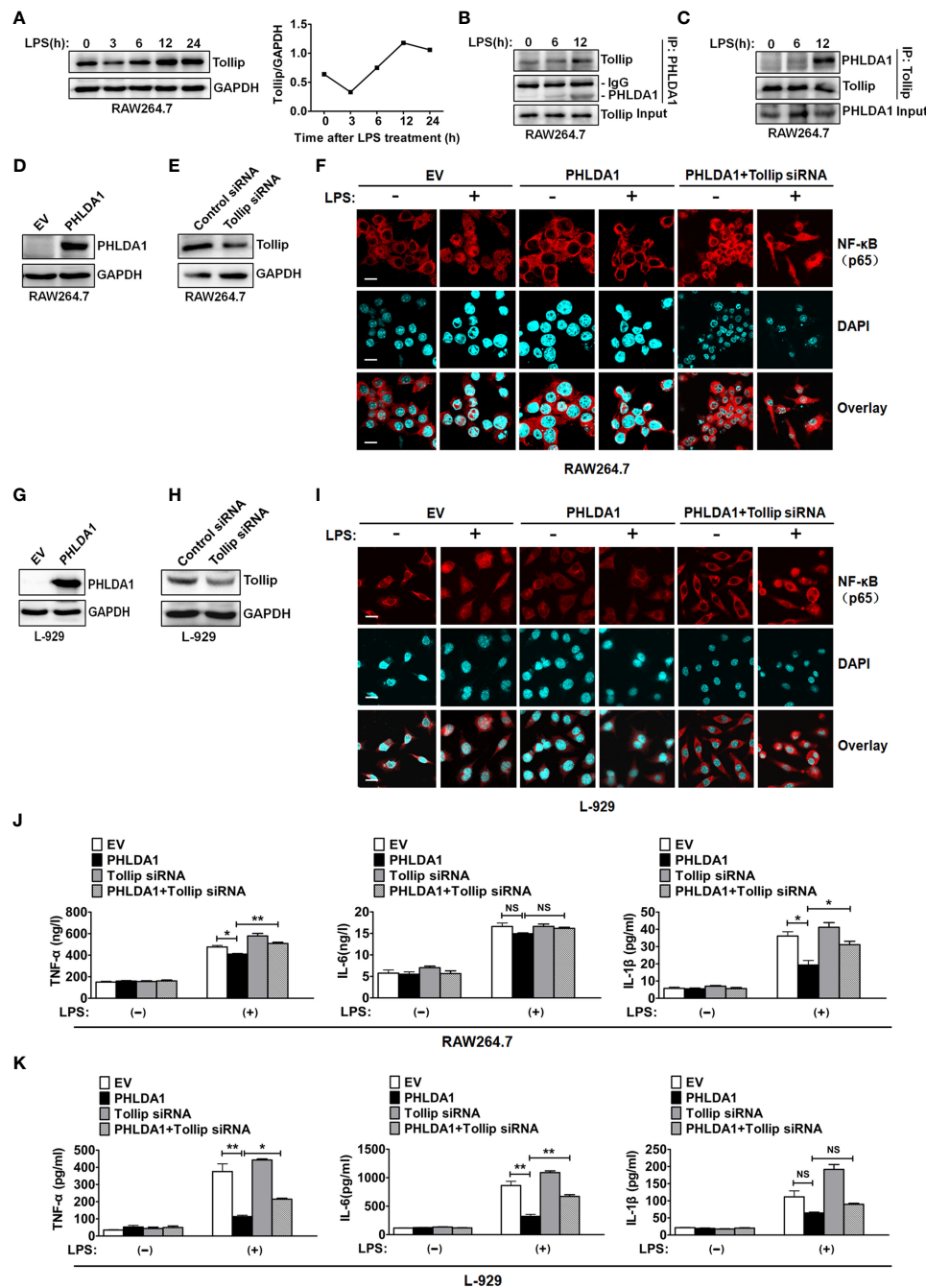


FIGURE 5 | PHLDA1 recruits Tollip to attenuate LPS-initiated NF-κB nuclear translocation and proinflammatory cytokine production. **(A)** RAW264.7 cells were treated with LPS (0.1 μg/ml) for 0, 3, 6, 12, and 24 h. Tollip expression was detected with Western blot. GAPDH was used as loading control. The quantified result of Tollip expression is shown in the right panel. **(B, C)** RAW264.7 cells were treated with 0.1 μg/ml LPS for 0, 6, and 12 h. Co-IP and Western blot analysis were used to measure the interaction between PHLDA1 and Tollip. RAW264.7 cells **(D, E)** and L-929 cells **(G, H)** were transfected with EV or PHLDA1 plasmid, Control siRNA, or Tollip siRNA, respectively. Protein expressions of PHLDA1 and Tollip were measured with Western blot. GAPDH was used as an internal control for gene expression analysis. RAW264.7 cells **(F)** and L-929 cells **(I)** were transfected with EV, PHLDA1 plasmid, and PHLDA1 plasmid plus Tollip siRNA and then treated with LPS (0.1 μg/ml) for 1 h. The above cells were fixed and stained for NF-κB (p65). Nuclei were stained with DAPI. The merged images were captured with a confocal microscope (scale bar, 20 μm). RAW264.7 cells **(J)** and L-929 cells **(K)** were transfected with EV, PHLDA1 plasmid, Tollip siRNA, and PHLDA1 plasmid plus Tollip siRNA and then treated with LPS (0.1 μg/ml) for 12 h. ELISA was performed to measure the production of proinflammatory cytokines (TNF-α, IL-6, and IL-1β). Data are shown as mean ± SD of three independent experiments (NS means no significance, * $P < 0.05$; ** $P < 0.01$). Western blot data are representative of three independent experiments.

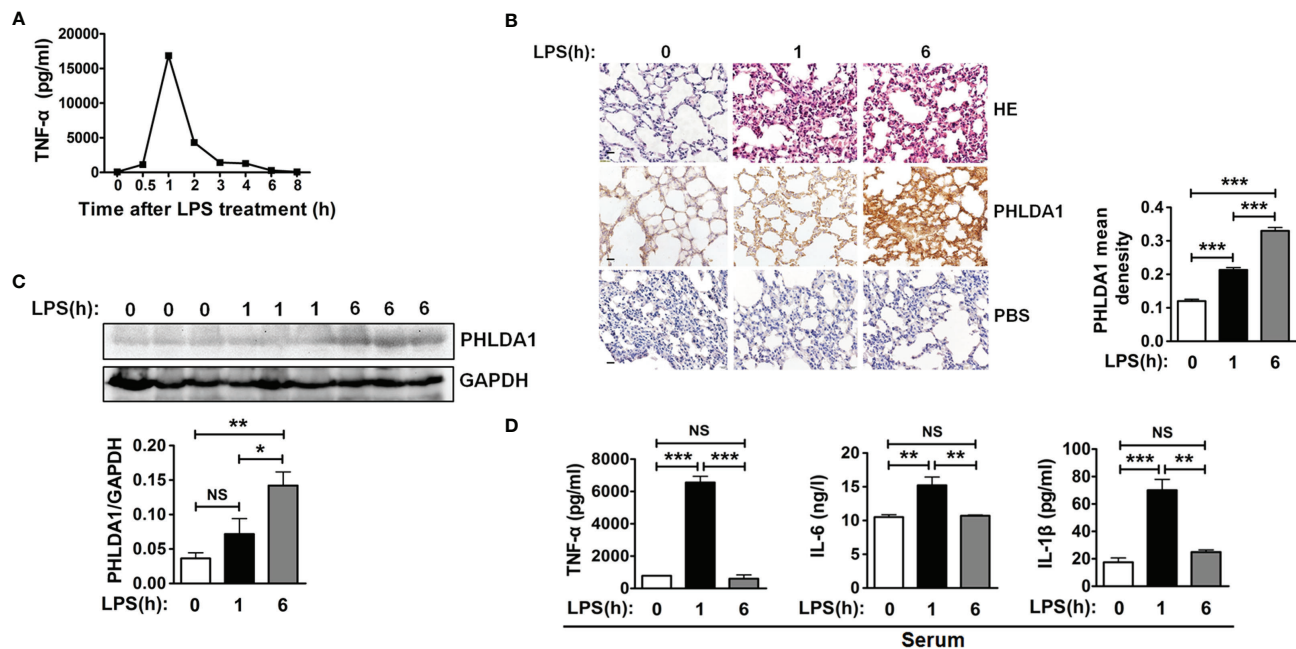


FIGURE 6 | PHLDA1 alleviates LPS-initiated proinflammatory cytokine production in a mouse model of endotoxemia. **(A)** ELISA was performed to measure TNF- α level in serum from mice treated with LPS (8 mg/kg) for 0, 0.5, 1, 2, 3, 4, 6, and 8 h, respectively. **(B)** H&E and PHLDA1 staining (scale bar, 20 μ m) of lung tissues from three groups of mice, including group 1 (control group), group 2 (treatment with LPS for 1 h), and group 3 (treatment with LPS for 6 h). PHLDA1 mean density was analyzed and shown in the right panel. **(C)** Western bolt analysis of PHLDA1 in the lung tissues from the above different groups of mice. The quantified result of PHLDA1 expression is shown in the lower panel. **(D)** ELISA analysis of proinflammatory cytokines (TNF- α , IL-6, and IL-1 β) in serum from the above different groups of mice. The data, including quantitative analysis of PHLDA1 expression, PHLDA1 mean density, and ELISA, are expressed as mean \pm SD from three independent experiments. (NS means no significance, * P < 0.05; ** P < 0.01; *** P < 0.001).

Tollip, one of the important adaptor molecules, contains three different domains including Tom1-binding domain, conserved 2 domain, and coupling of ubiquitin to ER degradation domain (34). In human, Tollip has four isoforms, namely, isoform A, isoform B, isoform C, and isoform D (35). Tollip plays a critical role in regulating TLR-mediated innate immune responses (36, 37). It was reported that Tollip interacted directly with TLR2 or TLR4 with its C-terminal domain (179–273 aa). Tollip impaired TLR-mediated cell activation and the production of proinflammatory cytokines through suppressing phosphorylation and kinase activity of IRAK in inflammation. In addition, the C-terminal region of Tollip was phosphorylated by IRAK after LPS stimulation (26, 38). Liu et al. found that lysine histone methyltransferase EZH1 enhanced the production of inflammatory cytokines (IL-6, TNF- α , and IFN- β) by inhibiting Tollip (39). Tollip knockout increased the ability of clear *Legionella pneumophila* (Lp) and proinflammatory cytokine production by affecting TLR2 activity in Lp-infected mice (40). Monophosphoryl lipid A inhibited the LPS-triggered signaling pathway via the PI3K-dependent induction of Tollip, which in turn reduced the phosphorylation and activation of IRAK-1 to impair TLR4–MyD88 signaling pathway (41–43). The above results suggested that Tollip inhibited TLR2 and TLR4 signaling pathways.

In this study, we established that PHLDA1 negatively regulated the TLR4/MyD88-dependent signaling pathway. Then, we explored the relationship between Tollip and PHLDA1. We found that PHLDA1 interacted with Tollip, and the LPS-induced interaction between the above molecules gradually increased in a time-dependent manner. To investigate whether PHLDA1 suppressed TLR4/MyD88-dependent signaling pathway through Tollip, we detected LPS-induced production of proinflammatory cytokines after PHLDA1 overexpression and Tollip downregulation, and the results showed that PHLDA1 overexpression reduced LPS-induced proinflammatory cytokine production, while Tollip deficiency rescued the above biological phenomenon. These findings confirmed our hypothesis.

In summary, PHLDA1 recruited Tollip to negatively modulate the phosphorylation levels of some important molecules (ERK, JNK, p38, IKK α / β , I κ B α , and NF- κ B subunit p65) in the TLR4/MyD88 signaling pathway, which in turn suppressed NF- κ B and AP1 nuclear translocation and their responsive element activities. Finally, LPS-induced proinflammatory cytokine production was diminished. Our study provides a new vision for exploring the function of PHLDA1 and a new therapeutic target for endotoxemia. Further studies should be conducted to investigate the following aspects: 1) the effect of PHLDA1 on TLR4, Tollip, and adaptor proteins (TIRAP, MyD88, IRAK1, IRAK4,

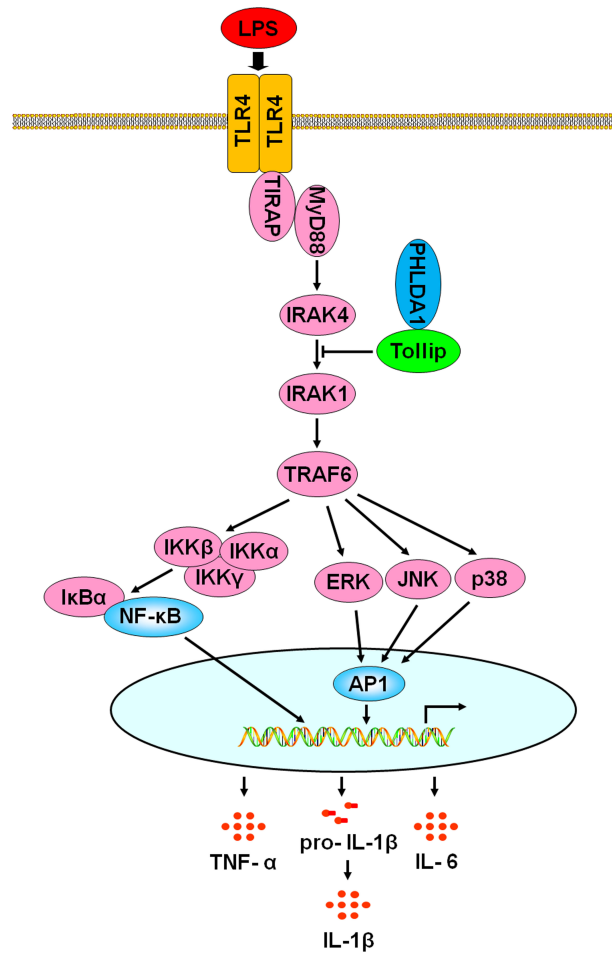


FIGURE 7 | A schematic representation of the role of PHLDA1 in modulating TLR4-mediated proinflammatory cytokine production *via* Tollip. After LPS-induced TLR4 activation, PHLDA1 recruited Tollip to inhibit IRAK phosphorylation, which further decreased the phosphorylation levels of some signal molecules (ERK, JNK, p38, IKK α / β , I κ B α , and NF- κ B subunit p65), the abilities of NF- κ B and AP1 nuclear translocations, and their responsive element activities. Eventually, LPS-initiated proinflammatory cytokine production was repressed.

and TRAF6); 2) the role of PHLDA1 in downstream TRIF-dependent signaling pathway; 3) the effect of PHLDA1 on the phagocytosis of macrophage; and 4) the discovery and development of effective adenovirus-mediated PHLDA1 injection.

DATA AVAILABILITY STATEMENT

The original contributions presented in the study are included in the article/**Supplementary Material**. Further inquiries can be directed to the corresponding authors.

ETHICS STATEMENT

The animal study was reviewed and approved by the Ethics Committee of Youjiang Medical University for Nationalities.

AUTHOR CONTRIBUTIONS

JW conceived the research and designed the experiments. HP, JH, HH, FW, ZX, JM, JG, JZ and NN performed the experiments. HP wrote the manuscript. BL, XS and DH analyzed the data. All authors revised the manuscript and approved its final version.

FUNDING

This work was supported by grants of the National Natural Science Foundation of China (81760513 and 82060528), the Guangxi Natural Science Foundation of China (2019JJA140532), the National and Provincial Natural Science Foundation Cultivation Special Project (210719166884337 and 210719166884340), Li Ka-Shing Foundation Cross-Disciplinary Research Grant (2020LKSFG09B).

SUPPLEMENTARY MATERIAL

The Supplementary Material for this article can be found online at: <https://www.frontiersin.org/articles/10.3389/fimmu.2022.731500/full#supplementary-material>

Supplementary Figure 1 | Kinetics of TNF- α level in the culture supernatants of LPS-stimulated RAW264.7 cells and BMDM. **(A)** RAW264.7 cells and BMDM were treated with various concentrations of LPS (0, 0.001, 0.01, 0.1, 1 and 10 μ g/ml) for 12 h. TNF- α in cell culture supernatants was detected using ELISA. **(B)** RAW264.7 cells and BMDM were treated with LPS (0.1 μ g/ml) for 0, 1, 3, 6, 12 and 24 h. TNF- α in cell culture supernatants was detected using ELISA.

Supplementary Figure 2 | Screening of PHLDA1 siRNA fragments. RAW264.7 cells were transfected with Control siRNA or 2 PHLDA1 siRNA fragments (PHLDA1 siRNA1, 2) and stimulated with LPS (0.1 μ g/ml) for 12 h. PHLDA1 protein expression was detected with Western blot. The quantified result of PHLDA1 expression was shown in the right panel.

REFERENCES

- Park CG, Lee SY, Kandala G, Lee SY, Choi Y. A Novel Gene Product That Couples Tcr Signaling to Fas (Cd95) Expression in Activation-Induced Cell Death. *Immunity* (1996) 4:583–91. doi: 10.1016/S1074-7613(00)80484-7
- Nagai MA. Pleckstrin Homology-Like Domain, Family A, Member 1 (PHLDA1) and Cancer. *BioMed Rep* (2016) 4:275–81. doi: 10.3892/br.2016.580
- Kuske MD, Johnson JP. Assignment of the Human PHLDA1 Gene to Chromosome 12q15 by Radiation Hybrid Mapping. *Cytogenet Cell Genet* (2000) 89:1. doi: 10.1159/000015575
- Gomes I, Xiong W, Miki T, Rosner MR. A Proline- and Glutamine-Rich Protein Promotes Apoptosis in Neuronal Cells. *J Neurochem* (1999) 73:612–22. doi: 10.1046/j.1471-4159.1999.0730612.x
- Hossain GS, van Thienen JV, Werstuck GH, Zhou J, Sood SK, Dickhout JG, et al. TDAG51 Is Induced by Homocysteine, Promotes Detachment-Mediated Programmed Cell Death, and Contributes to the Development of Atherosclerosis in Hyperhomocysteinemia. *J Biol Chem* (2003) 278:30317–27. doi: 10.1074/jbc.M212897200
- Joo JH, Liao G, Collins JB, Grissom SF, Jetten AM. Farnesol-Induced Apoptosis in Human Lung Carcinoma Cells Is Coupled to the Endoplasmic Reticulum Stress Response. *Cancer Res* (2007) 67:7929–36. doi: 10.1158/0008-5472.CAN-07-0931
- Dickhout JG, Hossain GS, Pozza LM, Zhou J, Lhotak S, Austin RC. Peroxynitrite Causes Endoplasmic Reticulum Stress and Apoptosis in Human Vascular Endothelium: Implications in Atherogenesis. *Arterioscler Thromb Vasc Biol* (2005) 25:2623–9. doi: 10.1161/01.ATV.0000189159.96900.d9
- Basseri S, Lhotak S, Fullerton MD, Palanivel R, Jiang H, Lynn EG, et al. Loss of TDAG51 Results in Mature-Onset Obesity, Hepatic Steatosis, and Insulin Resistance by Regulating Lipogenesis. *Diabetes* (2013) 62:158–69. doi: 10.2337/db12-0256
- Hossain GS, Lynn EG, Maclean KN, Zhou J, Dickhout JG, Lhotak S, et al. Deficiency of TDAG51 Protects Against Atherosclerosis by Modulating Apoptosis, Cholesterol Efflux, and Peroxiredoxin-1 Expression. *J Am Heart Assoc* (2013) 2:e000134. doi: 10.1161/JAHA.113.000134
- O'Neill LA, Golenbock D, Bowie AG. The History of Toll-Like Receptors: Redefining Innate Immunity. *Nat Rev Immunol* (2013) 13:453–60. doi: 10.1038/nri3446
- Thaiss CA, Zmora N, Levy M, Elinav E. The Microbiome and Innate Immunity. *Nature* (2016) 535:65–74. doi: 10.1038/nature18847
- Medzhitov R, Preston Hurlburt P, Janeway CA Jr. A Human Homologue of the Drosophila Toll Protein Signals Activation of Adaptive Immunity. *Nature* (1997) 388:394–97. doi: 10.1038/41131
- Akira S. Immunological Mechanism in Man Against Infection. *Nihon Naika Gakkai Zasshi* (2001) 90:2360–5.
- Gururajan M, Jacob J, Pulendran B. Toll-Like Receptor Expression and Distinct Murine Splenic and Mucosal B-Cell Subsets. *PLoS One* (2007) 2:e863. doi: 10.1371/journal.pone.0000863
- Zarembek KA, Godowski PJ. Tissue Expression of Human Toll Like Receptors and Differential Regulation of Toll-Like Receptor mRNAs in Leukocytes in Response to Microbes, Their Products, and Cytokines. *J Immunol* (2002) 168:554–61. doi: 10.4049/jimmunol.168.2.554
- Babu S, Blauvelt CP, Kumaraswami V, Nutman TB. Cutting Edge: Diminished T Cell TLR Expression and Function Modulates the Immune Response in Human Filarial Infection. *J Immunol* (2006) 176:3885–9. doi: 10.4049/jimmunol.176.7.3885
- Gioannini TL, Teghanemt A, Zhang D, Coussens NP, Dockstader W, Ramaswamy S, et al. Isolation of Anendotoxin-MD-2 Complex That Produces Toll-Like Receptor 4-Dependent Cell Activation at Picomolar Concentrations. *Proc Natl Acad Sci USA* (2004) 101:4186–91.
- Gioannini TL, Teghanemt A, Zhang D, Levis EN, Weiss JP. Monomeric Endotoxin: Protein Complexes Are Essential for TLR4-Dependent Cell Activation. *J Endotoxin Res* (2005) 11:117–23. doi: 10.1177/09680519050110020801
- Plociennikowska A, Hromada-judycka A, Borzecka K, Kwiatkowska K. Co-Operation of TLR4 and Raft Proteins in LPS-Induced Pro-Inflammatory Signaling. *Cell Mol Life Sci* (2015) 72:557–81. doi: 10.1007/s00018-014-1762-5
- Fu YJ, Xu B, Huang SW, Luo X, Deng XL, Luo S, et al. Baicalin Prevents LPS-Induced Activation of TLR4/NF-Kappa B P65 Pathway and Inflammation in Mice via Inhibiting the Expression of CD14. *Acta Pharmacol Sin* (2021) 42:88–96. doi: 10.1038/s41401-020-0411-9
- Miyake K, Ogata H, Nagai Y, Akashi S, Kimoto M. Innate Recognition of Lipopolysaccharide by Toll-Like Receptor 4/MD-2 and RP105/MD-1. *J Endotoxin Res* (2000) 6:389–91. doi: 10.1177/09680519000060051001
- Tanimura N, Saitoh S, Matsumoto F, Akashi-Takamura S, Miyake K. Roles for LPS-Dependent Interaction and Relocation of TLR4 and TRAM in TRIF-Signaling. *Biochem Biophys Res Commun* (2008) 368:94–9. doi: 10.1016/j.bbrc.2008.01.061
- Chandrasekaran CV, Sundarajan K, Edwin JR, Gururaja GM, Mundkinajeddu D, Agarwal A. Immune-Stimulatory and Anti-Inflammatory Activities of Curcuma Longa Extract and Its Polysaccharide Fraction. *Pharmacog Res* (2013) 5:71–9. doi: 10.4103/0974-8490.110527
- Shang L, Wang L, Shi X, Wang N, Zhao L, Wang J, et al. HMGB1 was Negatively Regulated by HSF1 and Mediated the TLR4/MyD88/NF-Kappa B Signal Pathway in Asthma. *Life Sci* (2020) 241:117120. doi: 10.1016/j.lfs.2019.117120
- O'Neill LA, Bowie AG. The Family of Five: TIR-Domain-Containing Adaptors in Toll-Like Receptor Signaling. *Nat Rev Immunol* (2007) 7:353–64. doi: 10.1038/nri2079
- Zhang G, Ghosh S. Negative Regulation of Toll-Like Receptor-Mediated Signaling by Tollip. *J Biol Chem* (2002) 277:7059–65. doi: 10.1074/jbc.M109537200
- Humbert-claude M, Duc D, Dwir D, Thieren L, Begka C, Legueux F, et al. Tollip, an Early Regulator of the Acute Inflammatory Response in the Substantia Nigra. *J Neuroinflamm* (2016) 13:303. doi: 10.1186/s12974-016-0766-5

28. Burns K, Clatworthy J, Martin L, Martinon F, Plumpton C, Maschera B, et al. Tollip, a New Component of the IL-1RI Pathway, Links IRAK to the IL-1 Receptor. *Nat Cell Biol* (2000) 2:346–51. doi: 10.1038/35014038
29. Wang S, Zhang H, Wang A, Huang D, Fan J, Lu L, et al. PHLDA1 Promotes Lung Contusion by Regulating the Toll-Like Receptor 2 Signaling Pathway. *Cell Physiol Biochem* (2016) 40:1198–206. doi: 10.1159/000453173
30. Han C, Yan P, He T, Cheng J, Zheng W, Zheng L, et al. PHLDA1 Promotes Microglia-Mediated Neuroinflammation via Regulating K63-Linked Ubiquitination of TRAF6. *Brain Behav Immun* (2020) 88:640–53. doi: 10.1016/j.bbi.2020.04.064
31. Luo Y, Huang Z, Zong K, Cao Z, Peng D, Zhou B, et al. miR-194 Ameliorates Hepatic Ischemia/Reperfusion Injury via targeting PHLDA1 in a TRAF6-dependent manner. *Int Immunopharmacol* (2021) 96:107604. doi: 10.1016/j.intimp.2021.107604
32. Jiao H, Jia X, Zhao T, Rong H, Zhang J, Cheng Y, et al. Up-Regulation of TDAG51 Is a Dependent Factor of LPS-Induced RAW264.7 Macrophages Proliferation and Cell Cycle Progression. *Immunopharmacol Immunotoxicol* (2016) 38:124–30. doi: 10.3109/08923973.2016.1138968
33. Lyu J, Huang B, Park D, Baek S. Regulation of PHLDA1 Expression by JAK2-ERK1/2-STAT3 Signaling Pathway. *J Cell Biochem* (2016) 117:483–90. doi: 10.1002/jcb.25296
34. Capelluto DG. Tollip: A Multitasking Protein in Innate Immunity and Protein Trafficking. *Microbes Infect* (2012) 14:140–7. doi: 10.1016/j.micinf.2011.08.018
35. Lo YL S, Beckhouse AG, Boulus SL, Wells CA. Diversification of TOLLIP Isoforms in Mouse and Man. *Mamm Genome* (2009) 20:305–14. doi: 10.1007/s00335-009-9188-3
36. Dakhana A, Mubarak RA, Pavelka N, Voelker D, Seibold M, Ledford JG, et al. Tollip Inhibits ST2 Signaling in Airway Epithelial Cells Exposed to Type 2 Cytokines and Rhinovirus. *J Innate Immun* (2020) 12:103–15. doi: 10.1159/000497072
37. Zheng Q, Zhao H, Jia D, Han X, Liu Z, Zhao M. Overexpression of Tollip Protects Against Acute Kidney Injury After Paraquat Intoxication Through Inhibiting NLRP3 Inflammasome Activation Modulated by Toll-Like Receptor 2/4 Signaling. *Mediators Inflamm* (2021) 2021:5571272.
38. Bulut Y, Faure E, Thomas L, Equils O, Arditi M. Cooperation of Toll-Like Receptor 2 and 6 for Cellular Activation by Soluble Tuberculosis Factor and *Borrelia burgdorferi* Outer Surface Protein A Lipoprotein: Role of Toll-Interacting Protein and IL-1 Receptor Signaling Molecules in Toll-Like Receptor 2 Signaling. *J Immunol* (2001) 167:987–94. doi: 10.4049/jimmunol.167.2.987
39. Liu Y, Zhang Q, Ding Y, Li X, Zhao D, Zhao K, et al. Histone Lysine Methyltransferase Ezh1 Promotes TLR-Triggered Inflammatory Cytokine Production by Suppressing Tollip. *J Immunol* (2015) 194:2838–46. doi: 10.4049/jimmunol.1402087
40. Shah JA, Emery R, Lee B, Venkatasubramanian S, Simmons JD, Brown M, et al. TOLLIP Deficiency Is Associated With Increased Resistance to *Legionella Pneumophila* Pneumonia. *Mucosal Immunol* (2019) 12:1383–90. doi: 10.1038/s41385-019-0196-7
41. Watts BA3rd, Tamayo E, Sherwood ER, Good DW. Monophosphoryl Lipid A Induces Protection Against LPS in Medullary Thick Ascending Limb Through Induction of Tollip and Negative Regulation of IRAK-1. *Am J Physiol Renal Physiol* (2019) 317:F705–19. doi: 10.1152/ajprenal.00170.2019
42. Wu S, Liu X, Chen L, Wang Y, Zhang M, Wang M, et al. Polymorphisms of TLR2, TLR4 and TOLLIP and Tuberculosis in Two Independent Studies. *Biosci Rep* (2020) 40:BSR20193141.
43. Ito Y, Schaefer N, Sanchez A, Francisco D, Alam R, Martin RJ, et al. Toll-Interacting Protein, Tollip, Inhibits IL-13-Mediated Pulmonary Eosinophilic Inflammation in Mice. *J Innate Immun* (2018) 10:106–18. doi: 10.1159/000485850

Conflict of Interest: The authors declare that the research was conducted in the absence of any commercial or financial relationships that could be construed as a potential conflict of interest.

Publisher's Note: All claims expressed in this article are solely those of the authors and do not necessarily represent those of their affiliated organizations, or those of the publisher, the editors and the reviewers. Any product that may be evaluated in this article, or claim that may be made by its manufacturer, is not guaranteed or endorsed by the publisher.

Copyright © 2022 Peng, Wang, Song, Huang, Hua, Wang, Xu, Ma, Gao, Zhao, Nong, Huang and Liang. This is an open-access article distributed under the terms of the Creative Commons Attribution License (CC BY). The use, distribution or reproduction in other forums is permitted, provided the original author(s) and the copyright owner(s) are credited and that the original publication in this journal is cited, in accordance with accepted academic practice. No use, distribution or reproduction is permitted which does not comply with these terms.

Advantages of publishing in Frontiers



OPEN ACCESS

Articles are free to read
for greatest visibility
and readership



FAST PUBLICATION

Around 90 days
from submission
to decision



HIGH QUALITY PEER-REVIEW

Rigorous, collaborative,
and constructive
peer-review



TRANSPARENT PEER-REVIEW

Editors and reviewers
acknowledged by name
on published articles

Frontiers

Avenue du Tribunal-Fédéral 34
1005 Lausanne | Switzerland

Visit us: www.frontiersin.org

Contact us: frontiersin.org/about/contact



REPRODUCIBILITY OF RESEARCH

Support open data
and methods to enhance
research reproducibility



DIGITAL PUBLISHING

Articles designed
for optimal readership
across devices



FOLLOW US

@frontiersin



IMPACT METRICS

Advanced article metrics
track visibility across
digital media



EXTENSIVE PROMOTION

Marketing
and promotion
of impactful research



LOOP RESEARCH NETWORK

Our network
increases your
article's readership